



**US Army Corps
of Engineers**
Waterways Experiment
Station

Site Characterization Investigations in Support of UXO Technology Demonstrations, Jefferson Proving Ground, Indiana

*by José L. Llopis, Janet E. Simms, Dwain K. Butler, John O. Curtis,
Harold W. West, WES*

Steven A. Arcone, Norbert E. Yankielun, CRREL



Approved For Public Release; Distribution Is Unlimited

The contents of this report are not to be used for advertising, publication, or promotional purposes. Citation of trade names does not constitute an official endorsement or approval of the use of such commercial products.

The findings of this report are not to be construed as an official Department of the Army position, unless so designated by other authorized documents.



PRINTED ON RECYCLED PAPER

Site Characterization Investigations in Support of UXO Technology Demonstrations, Jefferson Proving Ground, Indiana

by José L. Llopis, Janet E. Simms, Dwain K. Butler, John O. Curtis, Harold W. West

U.S. Army Corps of Engineers
Waterways Experiment Station
3909 Halls Ferry Road
Vicksburg, MS 39180-6199

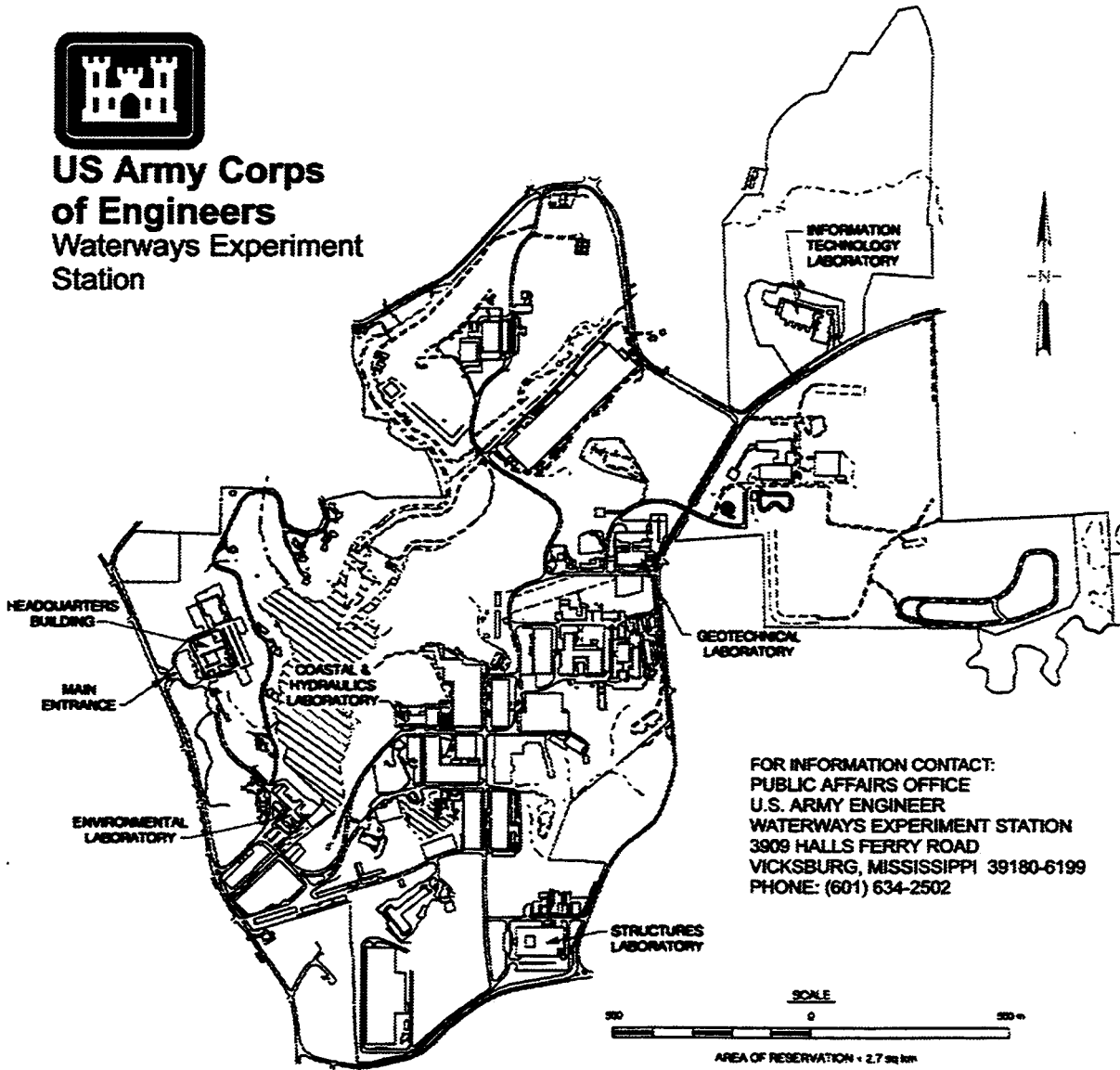
Steven A. Arcone, Norbert E. Yankielun
U.S. Army Corps of Engineers
Cold Regions Research and Engineering Laboratory
72 Lyme Road
Hanover, NH 03755

Final report

Approved for public release; distribution is unlimited



**US Army Corps
of Engineers**
Waterways Experiment
Station



Waterways Experiment Station Cataloging-in-Publication Data

Site characterization investigations in support of UXO technology demonstrations, Jefferson Proving Ground, Indiana / by Jose L. Llopis ... [et al.]; prepared for U.S. Army Environmental Center.

321 p. : ill. ; 28 cm. — (Technical report ; GL-98-20)

Includes bibliographic references.

1. Explosive ordnance disposal. 2. Explosives, Military. 3. Ordnance testing. 4. Jefferson Proving Ground (Ind.) I. Llopis, Jose L. II. United States. Army. Corps of Engineers. III. U.S. Army Engineer Waterways Experiment Station. IV. Geotechnical Laboratory (U.S. Army Engineer Waterways Experiment Station) V. U.S. Army Environmental Center. VI. Series: Technical report (U.S. Army Engineer Waterways Experiment Station) ; GL-98-20.

TA7 W34 no.GL-98-20

Contents

Preface	vi
Conversion Factor, Non-SI to SI Units of Measurement	vii
1—Introduction	1
Background Information	1
Scope of Report	3
2—Geology	7
Physiographic Setting	7
General Site Description	7
40-acre site	7
80-acre site	7
1-hectare site	12
Soils Description	12
40-acre site	12
80-acre site	16
1-hectare site	18
Bedrock Description	18
3—Summary of Original Site Characterization Efforts	20
Geotechnical Investigation	20
Soil thickness	20
Soil sampling	23
Environmental Sampling	23
Geophysical Testing	26
Magnetic surveys	26
Electrical resistivity surveys	26
4—Supplemental Site Characterization	27
Preliminary Activities	27
Gridding the 40- and 80 acre sites	27
Selection of the 1-hectare site	27

Soil Sampling and Testing Plan	28
40- and 80-acre sites	28
1-hectare site	28
Geophysical Test Principles, Equipment, and Field Procedures	32
40- and 80-acre sites	32
Test principles and equipment	32
Electrical resistivity soundings	32
Electromagnetic surveys	33
Ground penetrating radar surveys	34
Additional electrical properties	37
Field procedures	37
40-acre site	37
Electrical resistivity soundings	37
EM31 surveys	37
Ground penetrating radar surveys	37
DICON probe measurements	38
80-acre site	38
Electrical resistivity soundings	38
EM31 surveys	38
DICON probe measurements	38
1-hectare site	38
Test principles and equipment	38
Magnetic surveys	38
Ground penetrating radar surveys	39
Field procedures	41
5—Soils Investigations	42
Introduction	42
40-and 80-acre Sites	42
Physical properties	42
XRD analysis	48
Dielectric properties	49
1-hectare Site	56
Summary and Conclusions from Soils Analysis	56
6—Geophysical Test Results and Interpretation	59
40-acre Site	59
Electrical resistivity soundings	59
DICON probe measurements	59
EM31 surveys	65
Ground penetrating radar surveys	69
Postprocessing and display of data	69
Profile interpretation	69
Results and discussion	70
Control studies	70
Grid survey: 300 MHz	74

Grid survey: 600 MHz	77
Distribution of ϵ'	85
Theoretical discussion	85
80-acre Site	90
Electrical resistivity soundings	90
DICON probe measurements	93
EM31 surveys	94
1-hectare Site	94
Electrical resistivity soundings	104
EM31 surveys	104
Magnetic surveys	104
Ground penetrating radar surveys	105
Summary and Conclusions from Geophysical Testing	114
 7—Summary and Conclusions	 115
 References	 117
 Appendix A: Soil Gradation Curves: 40-acre Site	 A1
Appendix B: Soil Gradation Curves: 80-acre Site	B1
Appendix C: Laboratory Dielectric Soil Properties: 40- and 80-acre Sites	C1
Appendix D: Soil Gradation Curves: 1-hectare Site	D1
Appendix E: Vertical Electric Sounding Curves: 40-acre Site	E1
Appendix F: Vertical Electric Sounding Curves: 80-acre Site	F1
Appendix G: Vertical Electric Sounding Curves: 1-hectare Site	G1
Appendix H: GPR Records: 1-hectare Site	H7

SF298

Preface

Site characterization investigations were conducted at Jefferson Proving Ground (JPG), Indiana, by personnel of the Geotechnical Laboratory (GL) and Environmental Laboratory (EL), U.S. Army Engineer Waterways Experiment Station (WES), and the U.S. Army Cold Regions Research and Engineering Laboratory (CRREL). The field data collection phases of the investigation occurred during August and October through December 1997 and April 1998. The investigations included measurements and surveys to determine geological, geophysical, and environmental parameters or properties and their variations with depth, lateral dimension, and time. The investigations were conducted for the U.S. Army Environmental Center (AEC), Aberdeen Proving Ground, Maryland, as part of JPG Unexploded Ordnance (UXO) Technology Demonstration, Phase IV. AEC Program Managers during this investigation were Ms Kelly Rigano and Mr. George Robitaille. Drs. Ernesto R. Cespedes, EL, and Dwain K. Butler, GL, are the WES Principal Investigators.

Report preparation was coordinated at WES by Mr. José L. Llopis with input from Drs. Dwain K. Butler, Janet E. Simms, Earthquake Engineering and Geosciences Division (EEGD), GL; Mr. Harold W. West, Natural Resources Division, and Dr. John O. Curtis, Environmental Engineering Division, EL; Dr. Paul Wolfe, Wright State University; and Dr. Steven A. Arcone, CRREL. Geophysical field work was performed by Drs. Simms and Richard Olsen and Messrs. Llopis and Thomas S. Harmon, EEGD; Dr. Arcone and Messrs. Bert Yankielun, Allan J. Delany, and Paul V. Sellmann, CRREL; and Dr. Wolfe. Soils testing and analysis were conducted by the Soil and Rock Mechanics Division, GL, along with the Environmental and Structures Laboratories, WES. Geophysical data analysis was conducted by Drs. Butler and Simms and Mr. Llopis. The work was performed under the direct supervision of Dr. Mary Ellen Hynes, Chief, Earthquake Engineering and Geophysics Branch, EEGD, and the general supervision of Drs. A. G. Franklin, Chief, EEGD, and William F. Marcuson III, Director, GL.

At the time of publication of this report, Director of WES was Dr. Robert W. Whalin. Commander was COL Robin R. Cababa, EN.

The contents of this report are not to be used for advertising, publication, or promotional purposes. Citation of trade names does not constitute an official endorsement or approval of the use of such commercial products.

Conversion Factors, Non-SI to SI Units of Measurement

Non-SI units of measurement used in this report can be converted to SI units as follows:

Multiply	By	To Obtain
acres	2.47105	hectares
feet	0.3048	meters
gamma	1.0	nanotesla
miles (U.S. statute)	1.609347	kilometers
millimho per foot	3.28	millisiemen per meter
pounds (mass)	0.4535924	kilograms
pounds per cubic feet	0.016018	grams per cubic centimeter
tons per square foot	95.76052	kilopascals

1 Introduction

Background Information

Location of buried landmines and unexploded ordnance (UXO) requires the application of surface geophysical techniques and/or very low-level airborne geophysical techniques to detect anomalies or signatures of the objects against a background. The geophysical techniques include magnetic methods, electromagnetic (EM) induction methods, ground penetrating radar (GPR) methods (wave propagation electromagnetic methods), microgravity methods, and various multi-spectral and infrared (IR) remote imaging methods. Since each of the detection methods listed respond to contrasts or changes or variations of physical properties or features, a multitude of geophysical sensor responses are a result of site characteristics. Site characteristics which produce sensor responses are called the background. The background is both site and time dependent and includes the effects of site geology, site physiography, vegetation, climatic variables, and any surface and buried cultural debris or engineered structures. Many times, much of the surface and buried cultural debris will be the metallic remains of ordnance that has performed successfully (i.e., detonated as designed). The background at a site may be such that the geophysical signatures of landmines and UXO cannot be discriminated or detected against the background signature complex. Also, particular features of the background may produce signatures that are interpreted as caused by landmines or UXO, thus producing false alarms. For example, buried metallic debris can produce magnetic and electromagnetic signatures that look similar to the signatures of UXO. Also, buried metallic debris, tree roots, and large cobbles can produce GPR signatures that look similar to UXO.

In 1993, Congress mandated that the U.S. Army conduct a program at Jefferson Proving Ground (JPG), Indiana, to demonstrate and evaluate systems and technologies that can be used to detect, identify, and remediate buried UXO. The U.S. Army Environmental Center, Aberdeen, MD, was designated as the program manager. AEC tasked the Naval Explosive Ordnance Technology Division (NAVEODTECHDIV), Indian Head, MD, with the technical lead. Two controlled test sites (40- and 80-acres) were created by emplacing inert ordnance and debris at documented but unpublished locations. The first phase of the program was completed in October 1994. This phase included demonstrations of 29 systems. The data collected from Phase I was compared to the known (baseline) target data, and a technical report was published (USAEC 1994, 1995). From May through September 1995, Phase II of the program was conducted in a similar manner as

Phase I, and 17 additional systems were demonstrated. Data collected from Phase II was again compared to the baseline targets, and a technical report was published (USAEC 1996).

AEC conducted a Phase III program during September through November 1996. It was conducted in a similar manner as Phases I and II, but the overall program goals and objectives were expanded. In Phase III, the 2 test sites were subdivided to encompass realistic UXO scenarios. The main objective was to assess system performance in the various UXO scenarios. The site layout the 40- and 80-acre sites included the following scenarios:

Scenario 1 Aerial Gunnery Range

An aerial gunnery range results from both helicopter and fixed wing aircraft aerial delivery of ordnance, ranging in size from 2.75-in rockets to 2000-lb bombs, and found at depths ranging from near surface to 3 m.

Scenario 2 Artillery and Mortar Range

A typical artillery and mortar range contains assorted types of conventional ground ordnance fired at fixed hardened targets, usually from a position outside the range; ordnance typically ranges in size from 60-mm mortars to 8-in projectiles and is found at depths ranging from near surface to 1.2 m.

Scenario 3 Grenades and Submunitions Range

The grenades and submunitions range represents a portion of a conventional impact area that has been set aside for sensitive-fuzed submunitions firing. These submunitions are delivered by aircraft and field artillery. The purpose of Phase III demonstrations was to detect only submunitions and grenades at depths shallower than 0.5 m.

Scenario 4 Interrogation and Burial Area

The interrogation area represents a conventional impact area. At this area, demonstrators were given target location and required to classify and precisely position targets. The target type, size, orientation, and depth of ordnance were not provided. The targets used in this area were aerial weapon systems ranging from 2.75-in rockets to 2000-lb bombs as well as conventional ground weapons ranging from 60-mm mortars to 8-in projectiles. Burn or burial sites may be present in this impact area as well as fragments from exploded munitions and other ordnance components, such as mortar fins and empty illumination rounds. Ordnance was buried at depths ranging from near surface to 2 m.

Results of the Phase III program were published in April 1997 (USAEC 1997).

For UXO remediation/cleanup based on geophysical surveys for UXO detection and location, the current levels of false alarms are a major limiting factor (effort and cost). Recent Technology Demonstrations (TDs) at JPG illustrated the problems caused by the site background and associated false alarms in degrading the capability for landmine and UXO detection (Altshuler et al. 1995; Sparrow et al.

1995). In JPG Phase I (Sparrow et al. 1995), only one demonstrator had an ordnance detection ratio in excess of 60 percent. The best performance in terms of ordnance detection ratio in Phase II was 85 percent, but that demonstrator had 4.7 false alarms per ordnance item detected. Much of the improved performance from Phase I to Phase II can be attributed to repeat demonstrators' improved knowledge of site conditions and generally improved navigation (positioning) capability. Magnetic and electromagnetic induction systems were the most successful at JPG. GPR systems performed extremely poorly at JPG, both in terms of poor ordnance detection and high false alarm rates. Airborne systems were totally ineffective at JPG for both Phases I and II, with ordnance detection results statistically indistinguishable from random location (Altshuler et al. 1995).

JPG is located approximately 5 miles north of Madison, Indiana, in the southeastern portion of the state (Figure 1). JPG is approximately 19 miles long and 3 to 6 miles in width and lies within Jefferson, Ripley, and Jennings Counties (Figure 2). The 40-acre test site is located in the northwest quarter of Section 36, Township 6 North, Range 10 East. The 80-acre site is located at the center of Section 14, Township 5 North, Range 10 East. Both areas are located near the north-south perimeter road on the eastern side of JPG.

An additional 1-hectare (approximately 2.5 acres) site was established approximately 150 ft north of the 40-acre site. This site was set-up to complement four sites established as part of the Defense Advanced Research Program Agency's (DARPA) Backgrounds Characterization Program (Simms et al. 1997). The purpose of the DARPA Program is to collect background and clutter data in a variety of geologic and geographic conditions. A simple site classification scheme, that used sand and clay as generic particle size and soil type classifiers and moist and dry as soil moisture and climatic classifiers, was used to locate potential test sites. The DARPA 1-hectare sites are located at Fort Carson, CO, and Fort A.P. Hill, VA. Figure 3 shows how each DARPA test site location fits a simple soil particle size and moisture regime classification scheme.

The JPG 1-hectare site is shown as completing the simple site classification matrix, as a moist clay site. This initial classification, based on published soil classifications and documented poor GPR performance, is shown to be somewhat erroneous, as a result of site characterization work documented in this report.

Scope of Report

The purpose of this report is to present archival documentation of geological, geophysical, environmental, and geotechnical site characterization of the JPG UXO Technology Demonstration Sites. This documentation supports:

- a. Phase IV demonstrator planning and results assessment,
- b. Additional assessments of Phase I-III
- c. Future use of JPG sites,
- d. Comparisons of the JPG sites with other UXO and landmine test sites and cleanup sites.

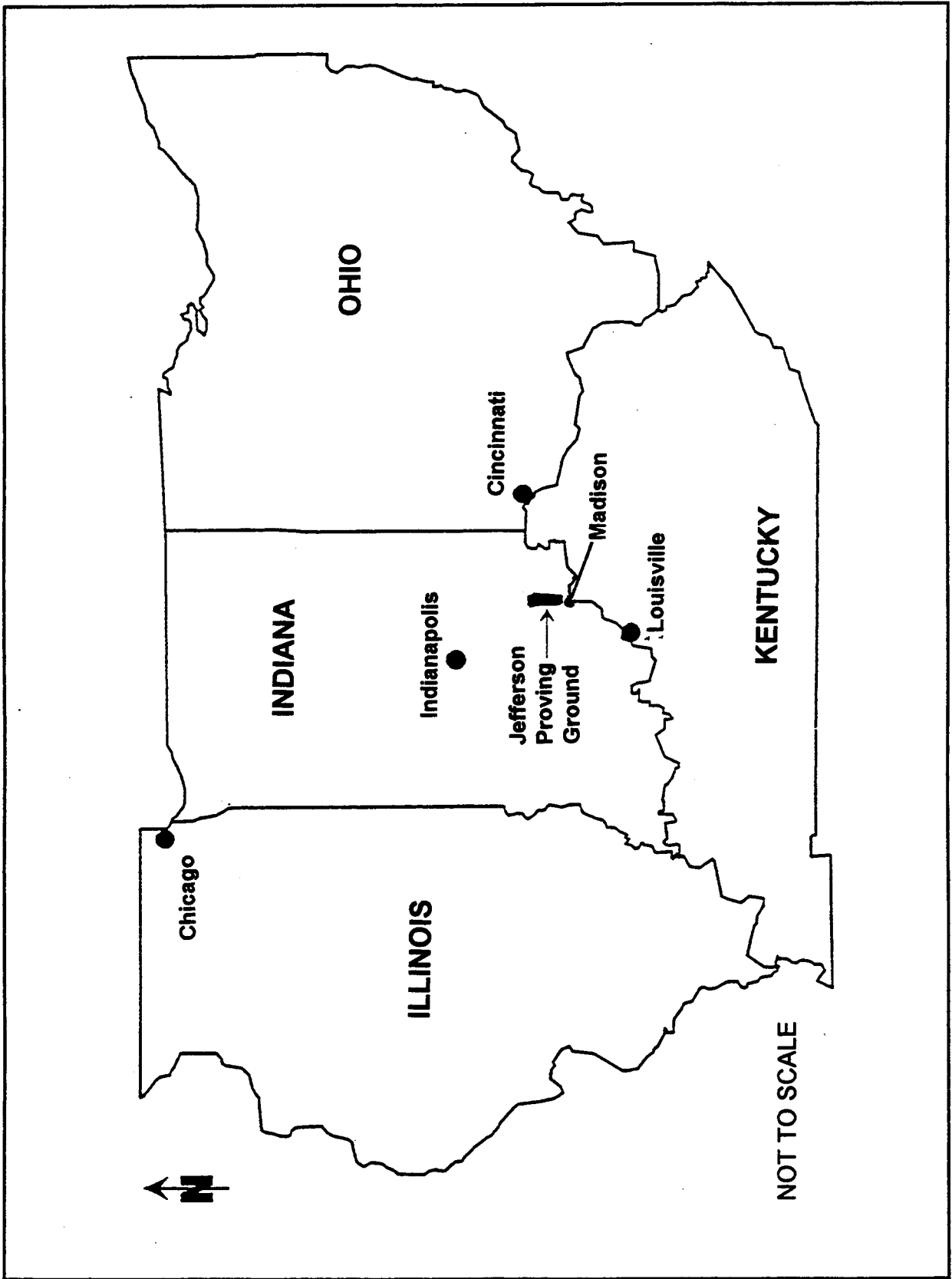


Figure 1. Vicinity map

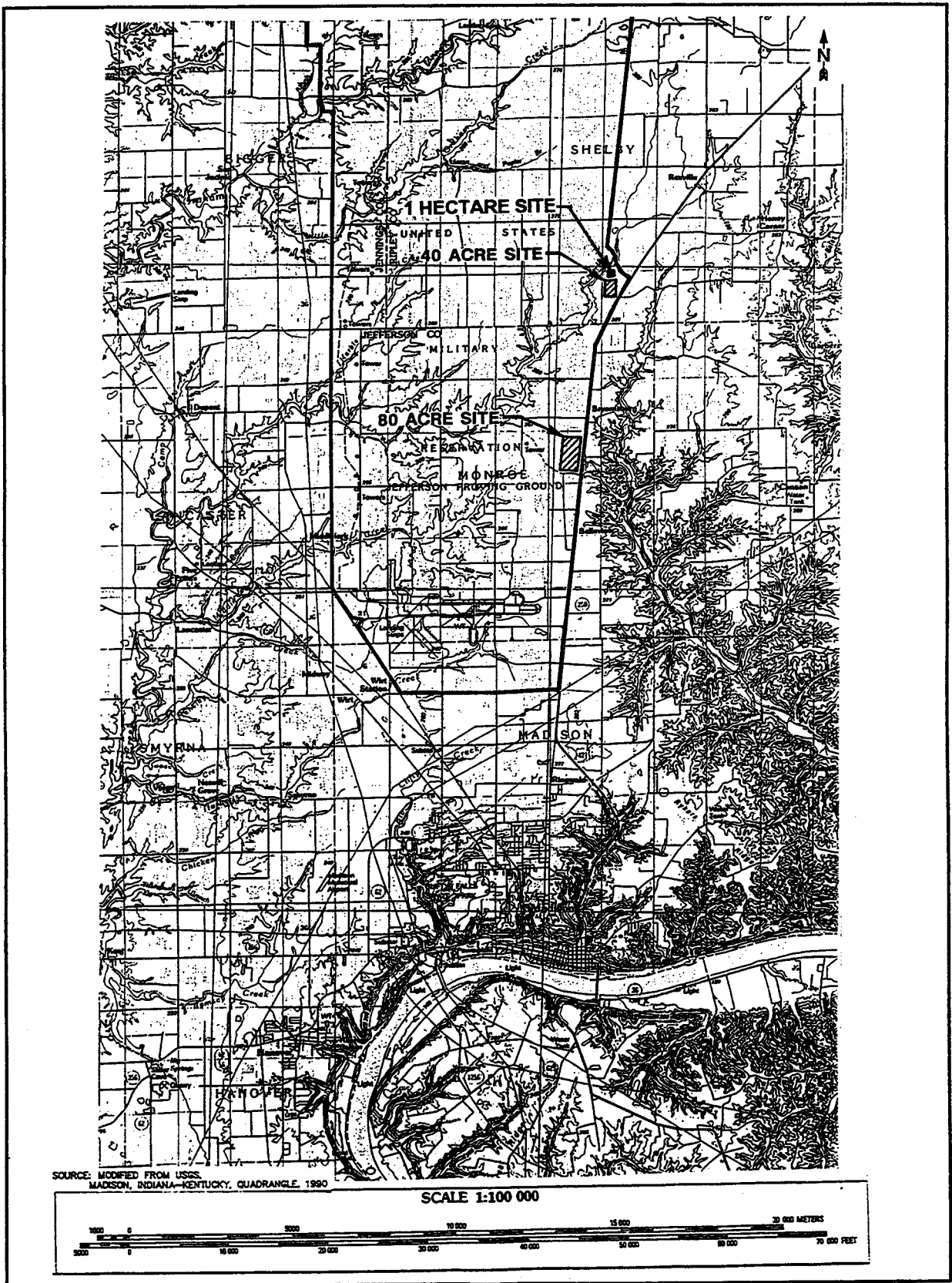


Figure 2. Site map

Chapter 2 of this report describes the general geology of the JPG tests sites including soils and bedrock descriptions. A summary of 1993 geotechnical, environmental, and geophysical testing results conducted at the test sites is presented in Chapter 3. Chapter 4 describes the soil sampling and testing plan, and also geophysical survey concepts and field procedures employed at the test sites to supplement the 1993 site characterization information. Chapters 5 presents the results of the soils investigation whereas, Chapter 6 presents the results and interpretation of the geophysical surveys.

SAND	FORT A.P. HILL, VA (Firing Points 20 and 21)	FORT CARSON, CO (Turkey Creek Site)
	JEFFERSON PROVING GROUND, IN	FORT CARSON, CO (Seabee Site)
CLAY		
	MOIST	DRY

Figure 3. Simplified soil particle size and moisture regime classification for DARPA 1-hectare sites

2 Geology

Physiographic Setting

JPG is located in the Muscatatuck Regional Slope physiographic unit of southeastern Indiana. The development of modern surface features have been controlled by normal degradational processes such as weathering, stream erosion, entrenchment, and mass movement (Schneider 1966). This physiographic unit lies within the Glaciated Outer Bluegrass section of the interior Low Plateau Province (Fenneman 1938 and Ray 1974). Although a northern portion of the Muscatatuck Regional Slope was glaciated during the Wisconsin Age, the entire unit was covered by glacial ice in the early Pleistocene Epoch. Stream valleys cut into the upper portions of underlying limestones and dolomites. Upland areas between drainages are typically broad and nearly flat to undulating, indicating that the region is still in a youthful state of landform development (Schneider 1966).

General Site Description

40-acre site

The 40-acre site is a grassy field with scattered trees and measures 1320 ft by 1320 ft. A topographic map, based on a local datum, is shown in Figure 4. The topographic map is based on elevations taken at 202 grid points. The topographic map shows a broad plain gently dipping to the southwest. An east-west trending gully is seen in the northern portion of the site. Figure 5 shows the X-Y locations and elevations of three benchmarks established at the 40-acre site.

80-acre site

The 80-acre site, also a grassy field with scattered trees, measures 2600 ft by 1400 ft. The long axis of the site is oriented approximately north-south. A topographic map, based on a local datum, shows that the site dips gently to the east and exhibits a depression along the southern perimeter (Figure 6). The topographic map is based on elevations taken at 202 grid points. The locations of four benchmarks showing their X-Y positions and elevations is presented in Figure 7.

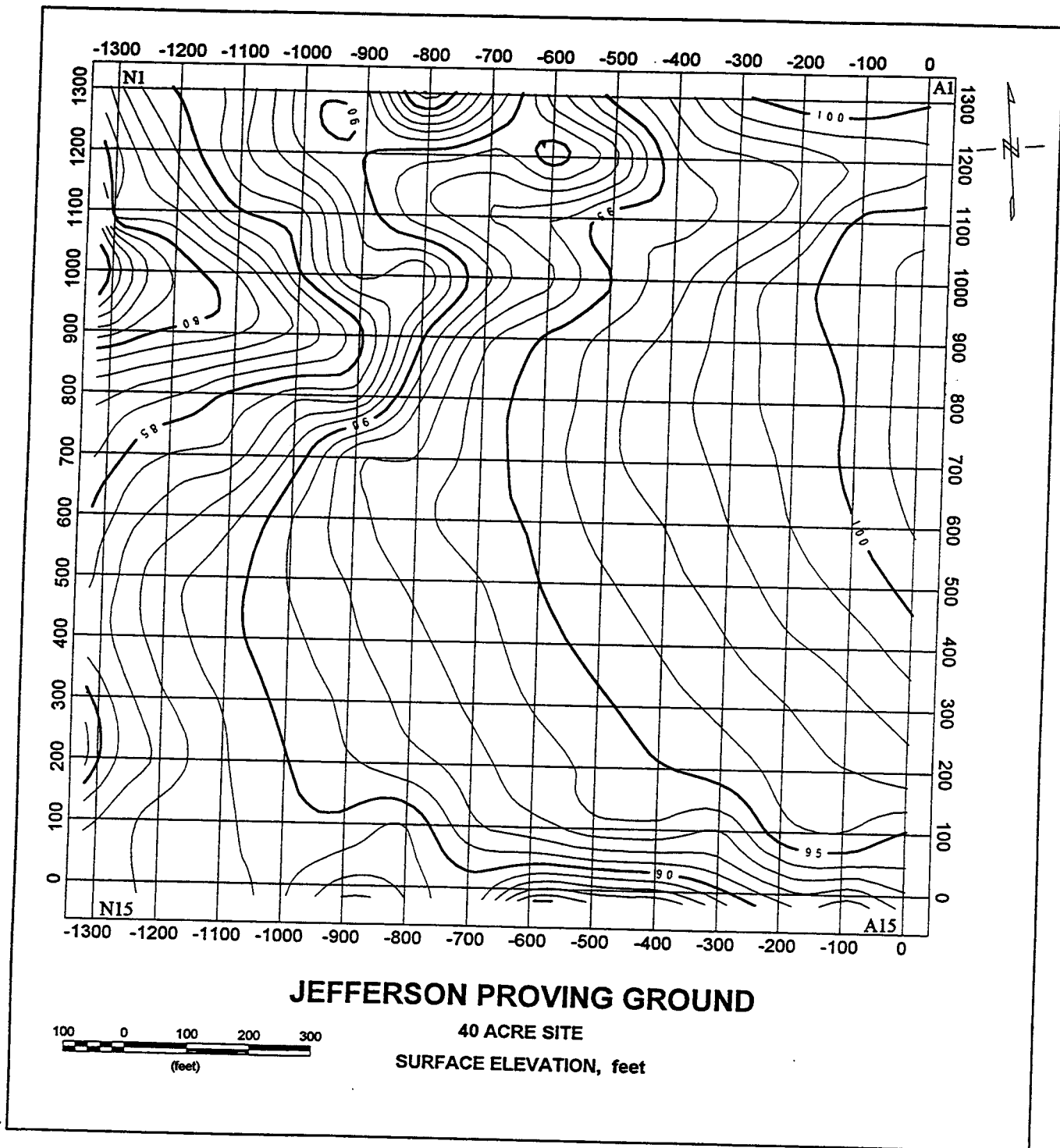


Figure 4. Topography map, 40-acre site

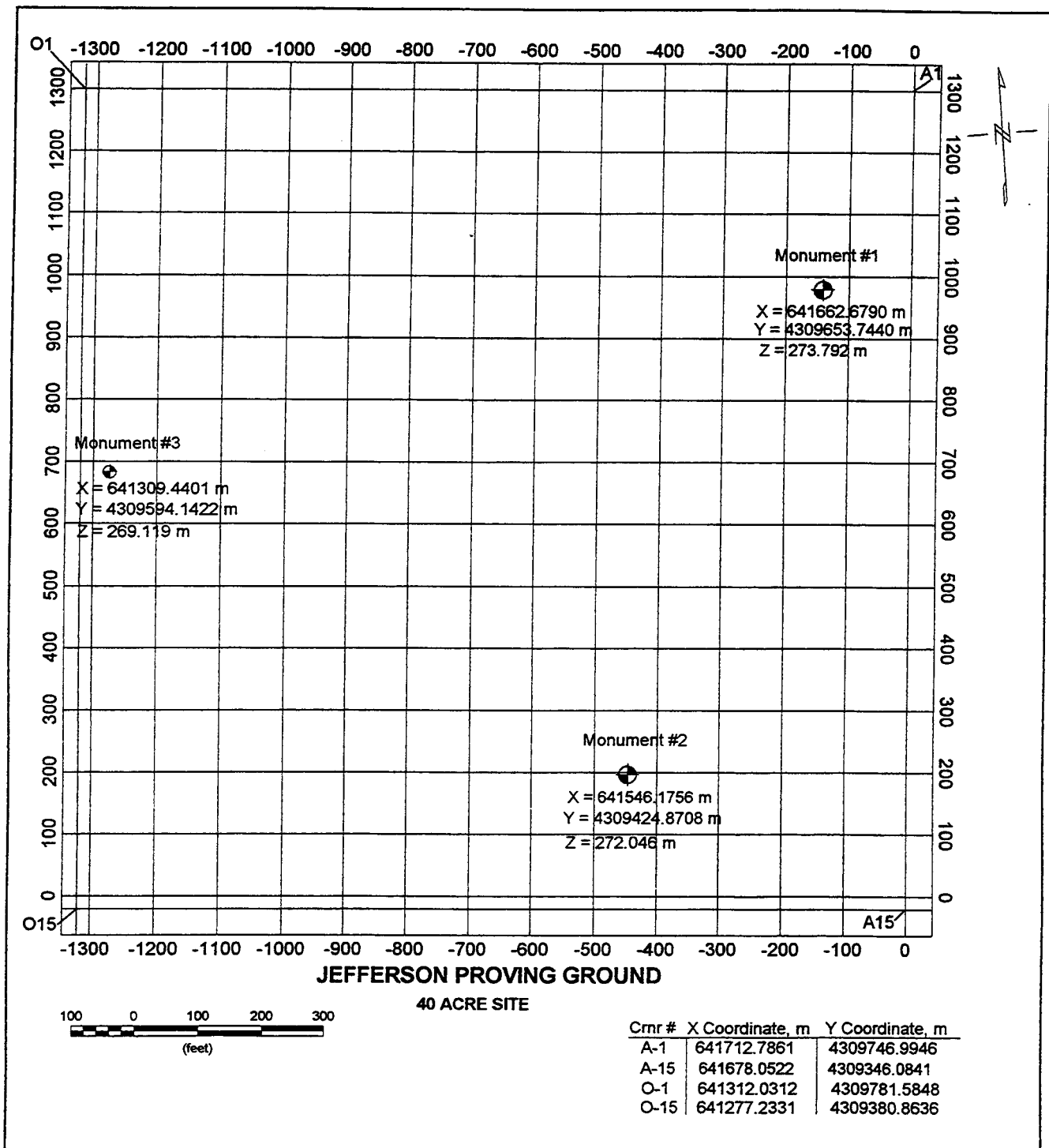


Figure 5. Survey benchmark locations, 40-acre site

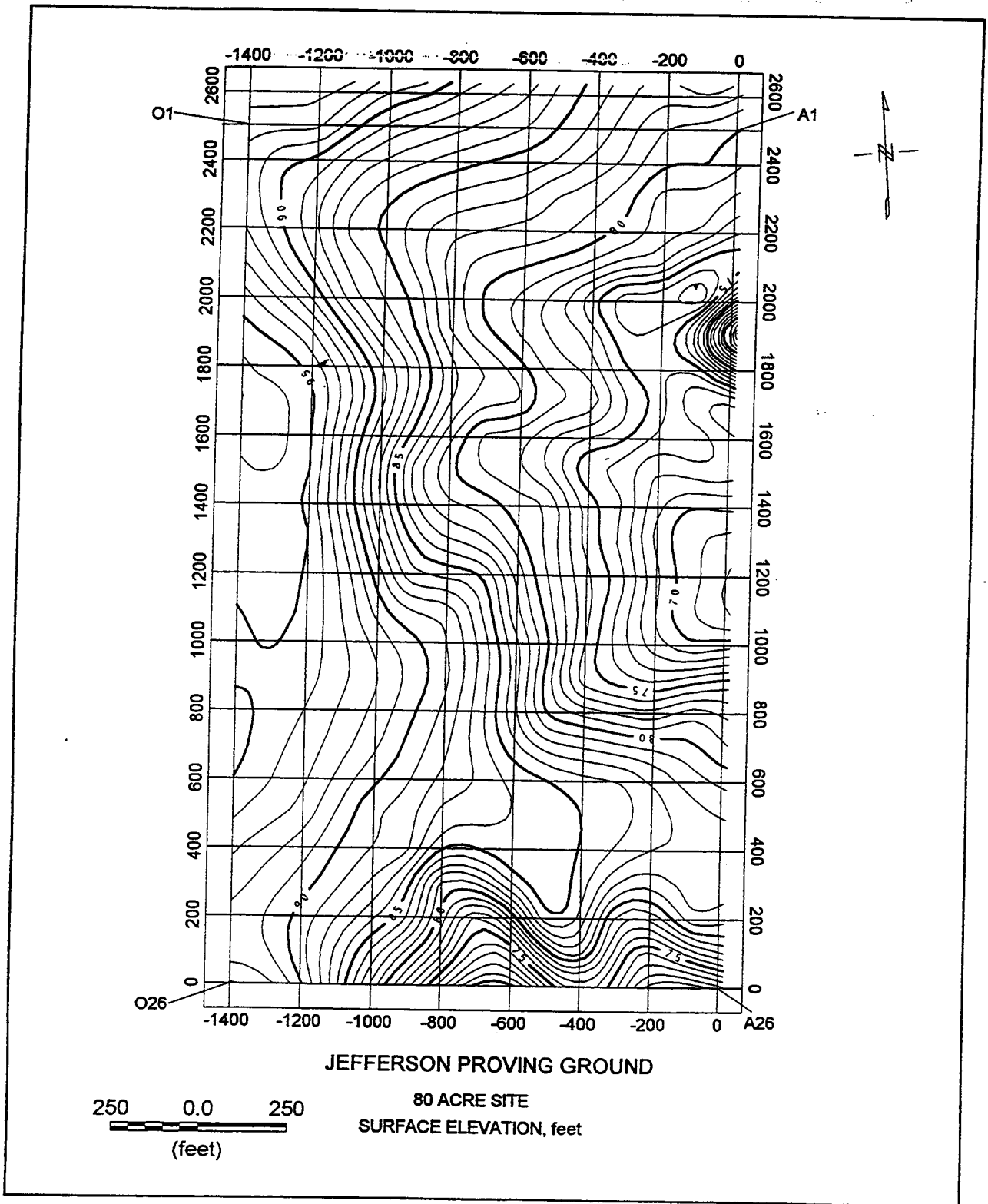


Figure 6. Topography map, 80-acre site

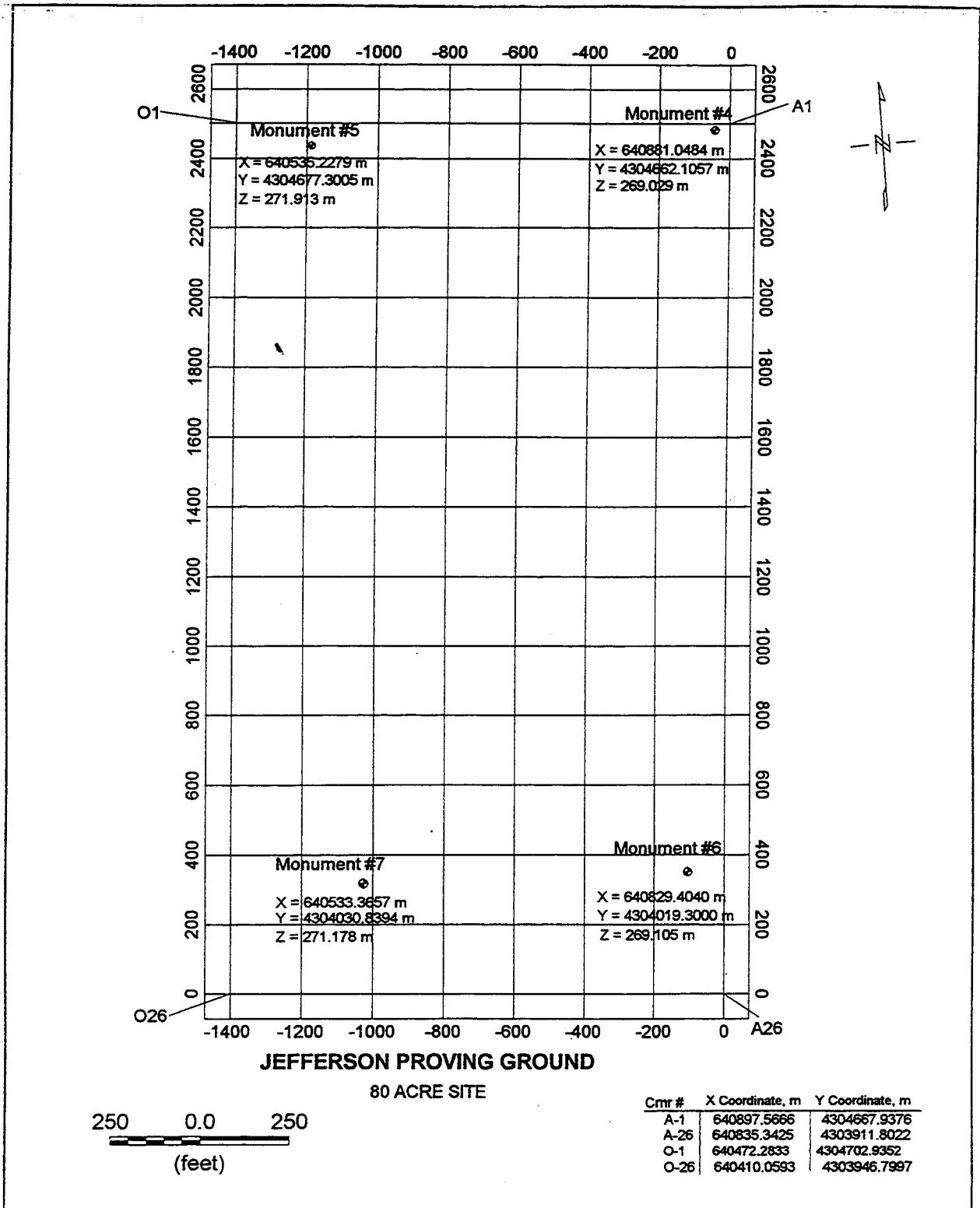


Figure 7. Survey benchmark locations, 80-acre site

1-hectare site

The 1-hectare UXO backgrounds characterization test site, as previously mentioned, is located approximately 150 ft north of the northern boundary of the 40-acre site (Figure 8). The test site is 125 m long in the east-west direction and 100 m long in the north-south direction. The topographic map of the site (Figure 9) reveals a relatively flat (less than 2 percent slope) surface. The site has a dip of approximately 1.5 percent to the northwest. The site is covered chiefly with grass and also with a few small shrubs.

Soils Description

40-acre site

The soils within the 40-acre site are mapped by McWilliams (1985) as Avonburg, Cincinnati, Cobbsfork, and Rossmoyne silt loam soils (Figure 10). General characteristics of each soil are discussed below.

AvA—Avonburg silt loam, 0 to 2 percent slopes. The Avonburg soils occur on uplands of glacial drift plains and have either gently sloping or nearly level topographic features. Drainage is poor, as Avonburg soils have low permeability. The soils were formed from a thin mantle of loess and underlying glacial drift. Avonburg soils have a dark grayish brown color within the upper 10 inches. Avonburg subsoils are friable and mottled. The upper subsoil horizon generally consists of a yellowish brown silt loam and light brownish gray friable silt loam about 17 inches thick. The lower part to a depth of 80 inches is a fragipan generally mottled, light brownish gray in color, firm and very firm silty clay loam and silt loam.

CcC3—Cincinnati silt loam, 6 to 12 percent slopes, severely eroded. The Cincinnati silt loam soils are formed on 6 to 12 percent slopes. They are deep, well drained soil found on the side slopes in uplands. The surface layer is yellowish brown silt loam about 7 inches thick. The upper horizon of the subsurface is light yellowish brown, mottled, friable silt loam about 3 inches thick. The middle horizon consists of a mottled yellowish brown and gray, firm silty clay loam fragipan. This horizon extends to approximately 29 inches. The horizon below the fragipan extends to a depth of about 80 inches. It is, in sequence downward, yellowish brown, mottled firm silty clay loam; mottled light olive gray and yellowish brown, firm clay; and dark yellowish brown, mottled, firm clay. In places, the fragipan occurs at the surface.

Cm—Cobbsfork silt loam. The Cobbsfork soils are formed from loess and silty glacial drift found on uplands. Cobbsfork soil is deep and poorly drained and has low permeability (0.06 to 0.2 in/hr). This soil is subject to ponding. The Cobbsfork soil has a 10-inch surface layer consisting of a silt loam that is dark grayish-brown. Generally 80 inches of subsoil is found with the Cobbsfork soil of which the upper horizon is a friable and firm mottled light gray silt loam. The middle horizon is gray and light-gray, mottled, firm silty clay loam. The deepest horizon consists of a yellowish brown and dark yellowish brown, mottled, very firm silt loam.

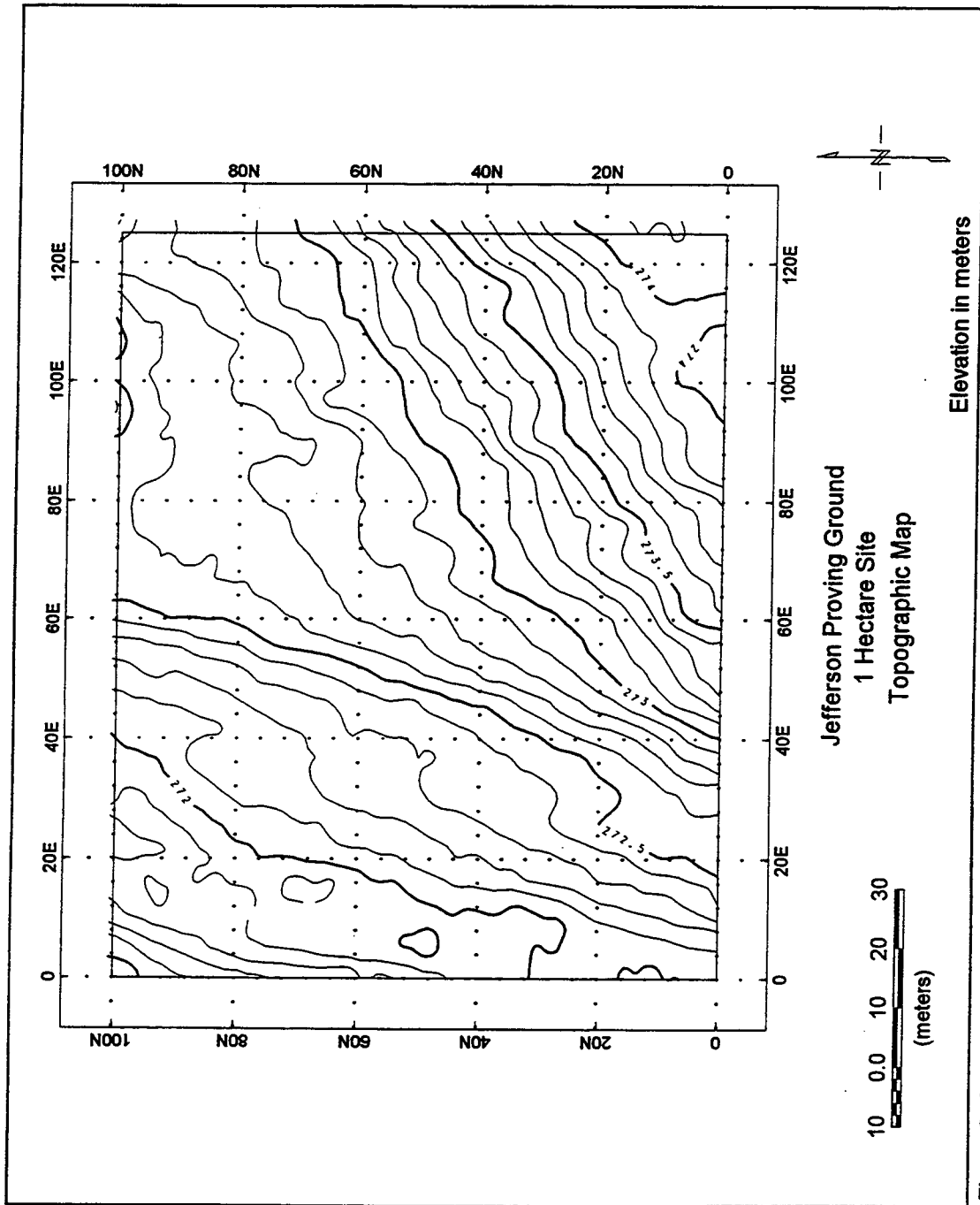


Figure 9. Topography map, 1-hectare site

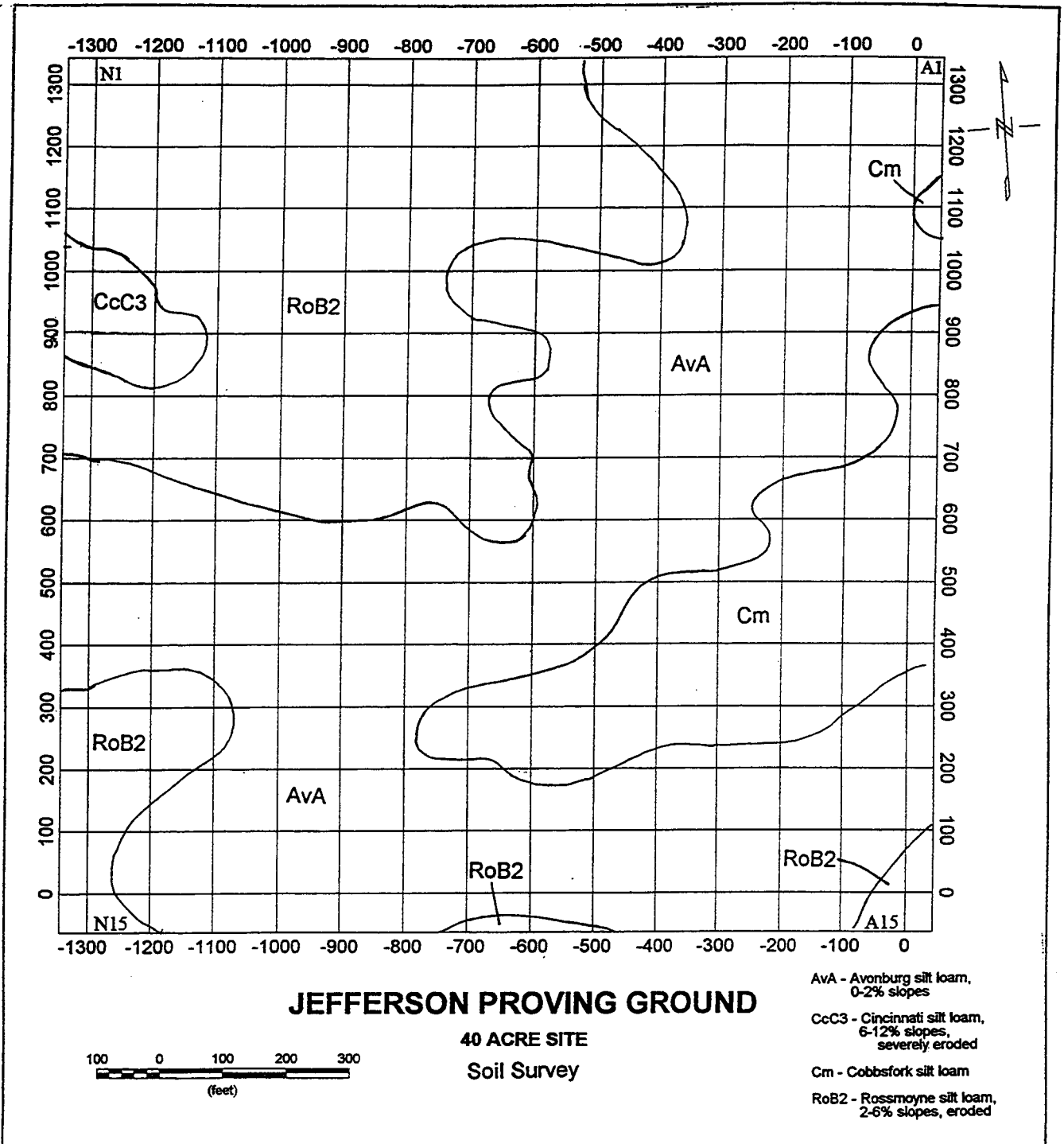


Figure 10. Soil map, 40-acre site

Source: McWilliams, K. M., 1985. "Soil Survey of Ripley County and Part of Jennings County, Indiana," United States Department of Agriculture, Soil Conservation Service, Washington, D.C.

RoB2—Rossmoyne silt loam, 2 to 6 percent slopes, eroded. The Rossmoyne silt loam forms on 2 to 6 percent slopes. It is deep, moderately well drained soil found on uplands. It appears on the northwest portion of the 40-acre site, encompassing about one-third of the parcel. Permeability is low in this soil and a perched seasonal high water table is at a depth of 1.5 to 3.0 ft in winter and early spring. A 9-inch thick brown silt loam makes up the surface layer. The subsurface of the Rossmoyne soil extends to a depth of 28 inches and consists of a light brownish yellow, friable silt loam in the upper horizon and a friable, mottled, yellowish brown, silt loam in the lower horizon. Below this horizon to a depth of about 80 inches is a fragipan that is light gray, mottled, very firm silt loam and silty clay loam.

80-acre site

The soils found at the 80-acre site, according to Nickell (1985), are the Avonburg, Cincinnati, Cobbsfork, Rossmoyne, and Ryker silt loams and are shown in Figure 11. The Avonburg soil at the 80-acre site is the same as described for the 40-acre site.

CnB2—Cincinnati silt loam, 2-6 percent slopes, eroded. The Cincinnati eroded silt loam formed on 2 to 6 percent slopes. This soil is formed from loess and underlying glacial drift. Cincinnati soils appear on summits, shoulder slopes, and in uplands. Cincinnati Soils are well drained and deep; however, its permeability is low. The Cincinnati surface layer is 6 inches deep with a mixture of yellowish and dark brown silt loams. The subsoil extends to a depth of 80 inches and may be underlain with interbedded limestone, calcareous shale, or black shale bedrock. The upper subsoil horizon is mottled yellowish-brown, firm clay loam. The middle horizon is a mottled yellowish-brown very firm clay loam fragipan. The lower horizon of the subsoil is firm clay loam. A seasonal high perched water table is found in the Cincinnati soil.

CO—Cobbsfork silt loam. The Cobbsfork soils are poorly drained, have a seasonal high water table and are subject to ponding. In a typical profile the surface layer is grayish brown silt loam about 6 inches thick. The subsurface layer is also about 6 inches of grayish brown silt loam. The subsoil extends to a depth of about 80 inches. It is, in sequence downward, light gray and light brownish gray, mottled silt loam; light brownish gray and yellowish brown, mottled, firm and brittle silt loam; and strong brown, firm clay loam.

RoA—Rossmoyne silt loam, 0 to 2 percent slopes. This soil is formed from a thin layer of loess and underlain by glacial drift. The Rossmoyne is well drained in places, nearly level, deep and appears on narrow summits in the uplands. A perched seasonal high water table is at a depth of 1.5 to 3.0 feet in winter and spring. A dark brown silt loam 7 inches thick is typical of the Rossmoyne surface layer. Generally, 80 inches of subsoil is found with Rossmoyne soil. The subsoil is a yellowish brown. It is, in sequence downward, friable silt loam; mottled, friable silt loam; a mottled, very firm silt loam, loam, and clay loam fragipan; and mottled, firm clay loam. The Rossmoyne soil only exists on narrow strips at the northeast and southeast corners of the 80-acre site.

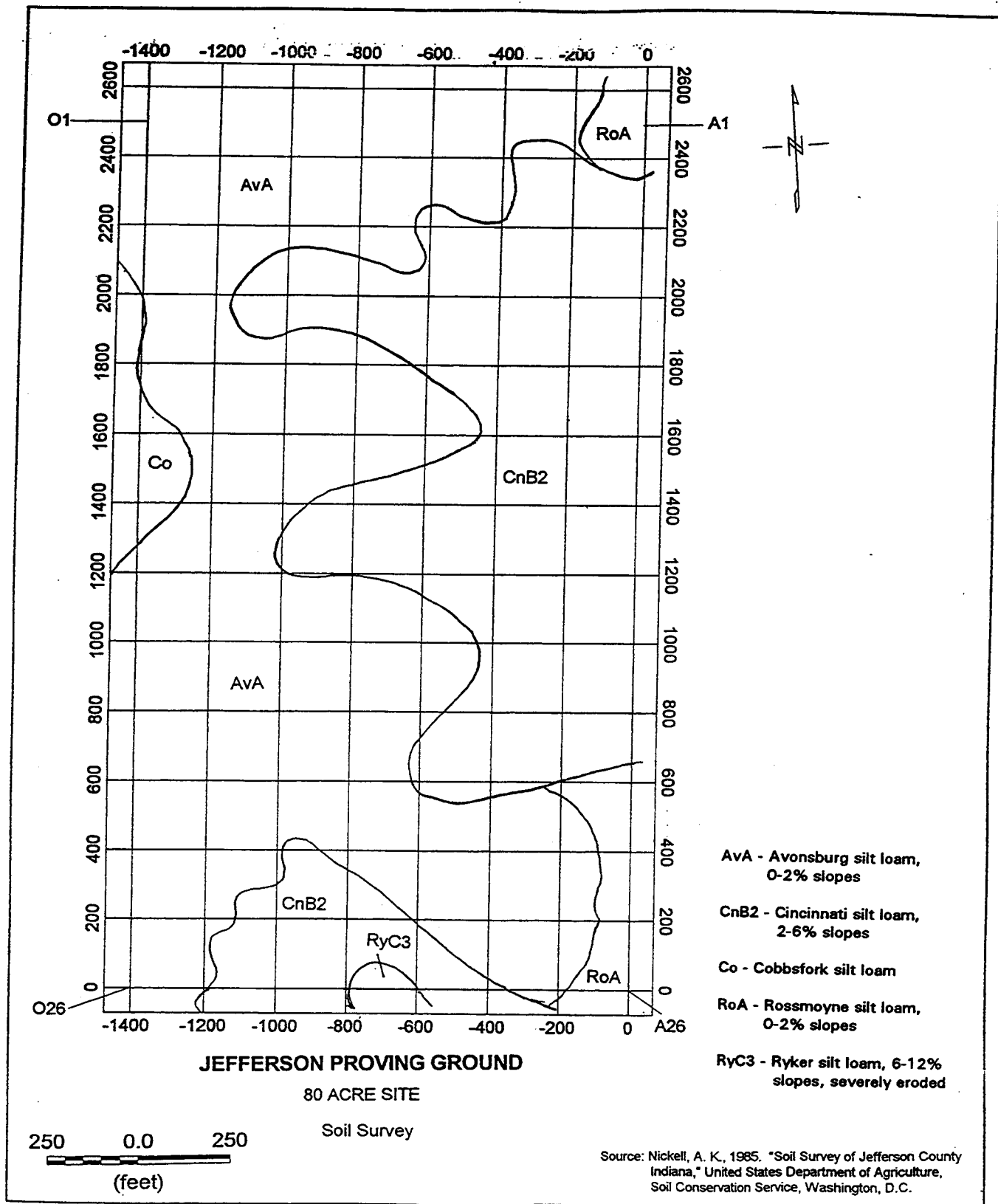


Figure 11. Soil map, 80-acre site

RyC3—Ryker silt loam, 6 to 12 percent slopes, severely eroded. This moderately sloping, deep, well drained soil is on summits, shoulder slopes, and back slopes in uplands. Permeability is moderate (0.6 to 2.0 in/hr) in the Ryker soil. The surface layer is about 7 inches thick consisting of yellowish red silt loam mixed with a small amount of dark brown silt loam. The subsoil extends to about 80 inches in depth. The upper part is yellowish red, firm silty clay loam, and the lower part is yellowish red clay loam.

1-hectare site

The soils mapped by McWilliams (1985) at the 1-hectare site, are the Avonburg and Rossmoyne silt loam soils (Figure 12). The Avonburg (AvA) and Rossmoyne (RoB2) soils found at the 1-hectare site are the same as described for the 40-acre site.

Bedrock Description

The bedrock beneath the 40- and 80-acre and 1-hectare sites is Laurel Dolomite. The Silurian aged Laurel Dolomite, approximately 45 ft thick, caps the uplands throughout much of the area. The Laurel Dolomite is described as gray, cherty, dolomitic limestone (Nickell 1985). The residuum of this dolomite is rich in chert nodules, which are abundant in the subsoils that formed on this bedrock. Underlying the Laurel Dolomite are 300 to 400 feet of interbedded shales and limestone of the Silurian and Ordovician age.

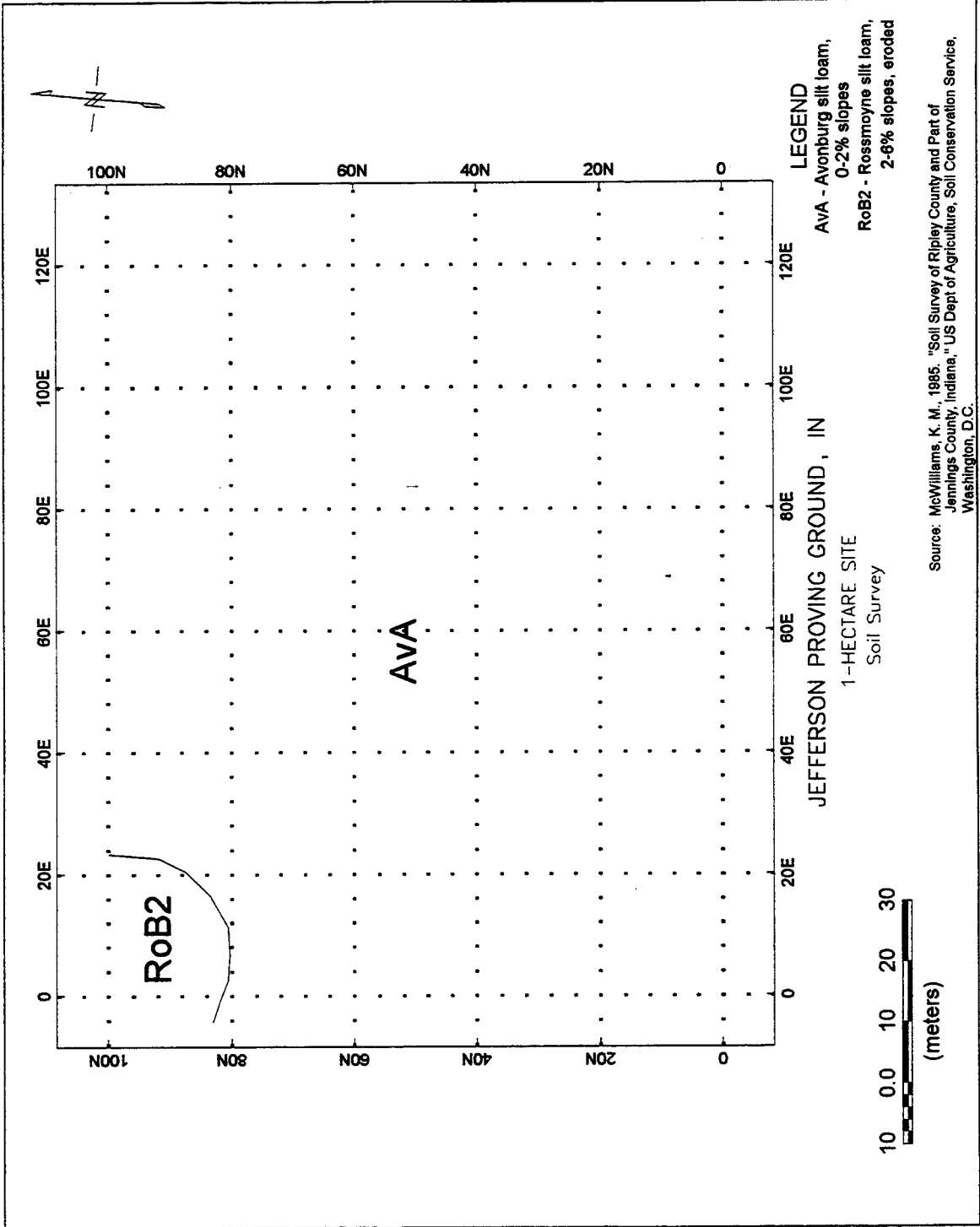


Figure 12. Soil map, 1-hectare site

3 Summary of Original Site Characterization Efforts

In 1993 NAVEODTECHDIV tasked Tetra Tech, Inc. (formerly PRC Environmental Management, Inc.) to conduct a geotechnical investigation and to collect environmental samples from the 40- and 80-acre sites. Also, as part of the field investigation Tetra Tech conducted limited geophysical testing. The data was gathered to (1) determine if the 2 sites were appropriate for demonstrations, (2) to help Tetra Tech and JPG personnel decide where to emplace UXO items, and (3) to help technology developers calibrate their equipment prior to the demonstrations. The results of these investigations along with soil descriptions of the 40- and 80-acre sites were provided to technology demonstrators.

Prior to any testing at the sites a topographic survey was conducted to establish vertical control and to locate grid nodes. Grid nodes were established on 100-ft by 100-ft square pattern and each node marked with 2-in by 2-in stakes. Permanent vertical control points were installed at the 40- and 80-acre sites for future reference.

Geotechnical Investigation

The geotechnical investigation conducted by Tetra Tech consisted of determining soil thickness and collecting soil and water samples for physical and chemical analysis.

Soil thickness

Soil thickness at the 40- and 80-acre sites was determined by using a hydraulic Geoprobe® to push molybdenum steel rods into the soil at selected grid nodes until refusal was observed. Refusal is defined as a penetration rate less than 2.5 cm/min, while operating the geoprobe on high power (Tetra Tech EM, Inc 1998).

Tetra Tech probed the soil at 202 nodes at the 40-acre site. Refusal depths ranged from 3.5 to 23.8 ft below ground surface (bgs) with an average refusal depth of 12.8 ft bgs. Figure 13 shows the top of rock elevation, based on a local datum, while Figure 14 shows the depth to bedrock for the 40-acre site. Tetra Tech also

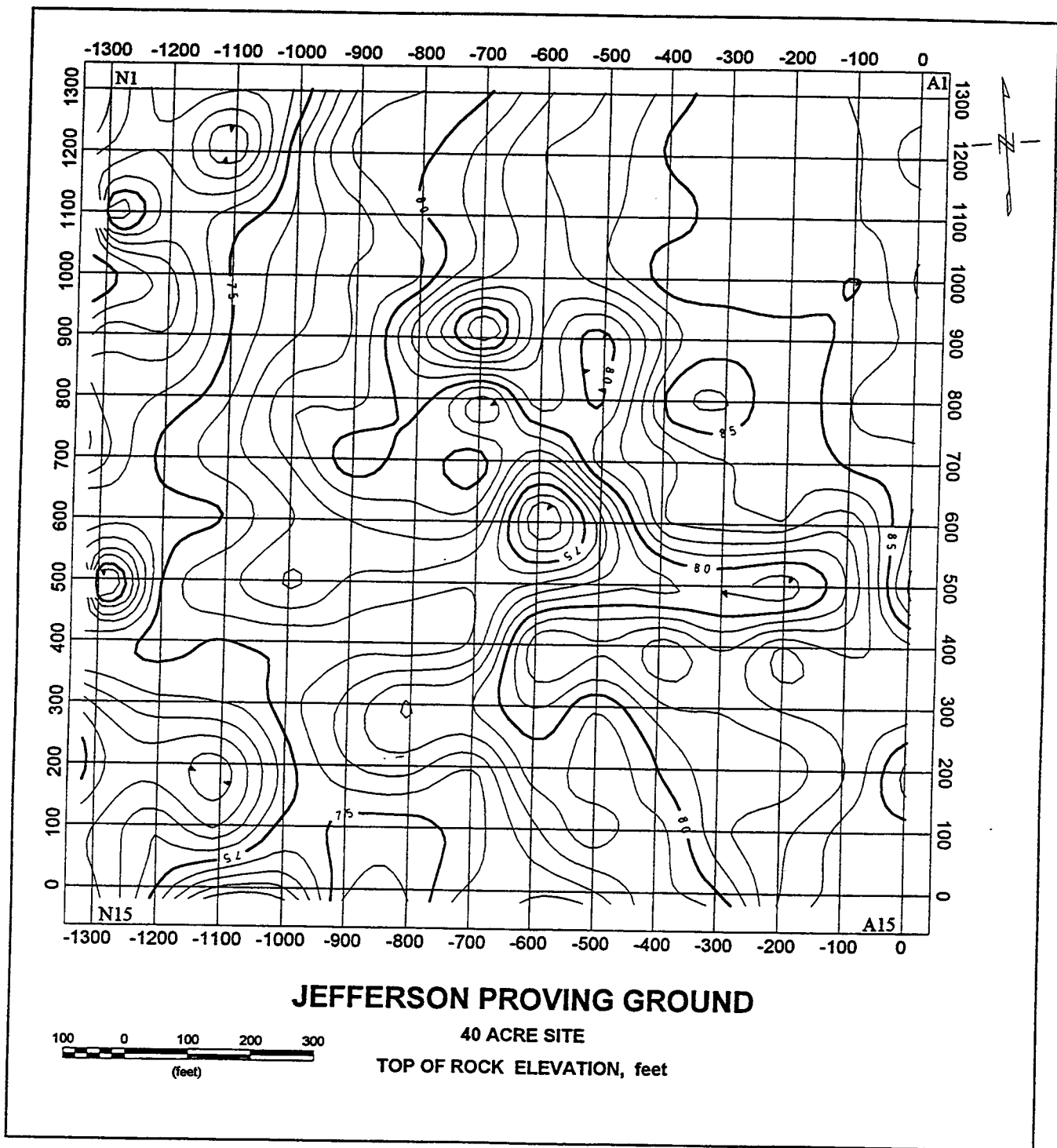


Figure 13. Top of rock elevation, 40-acre site

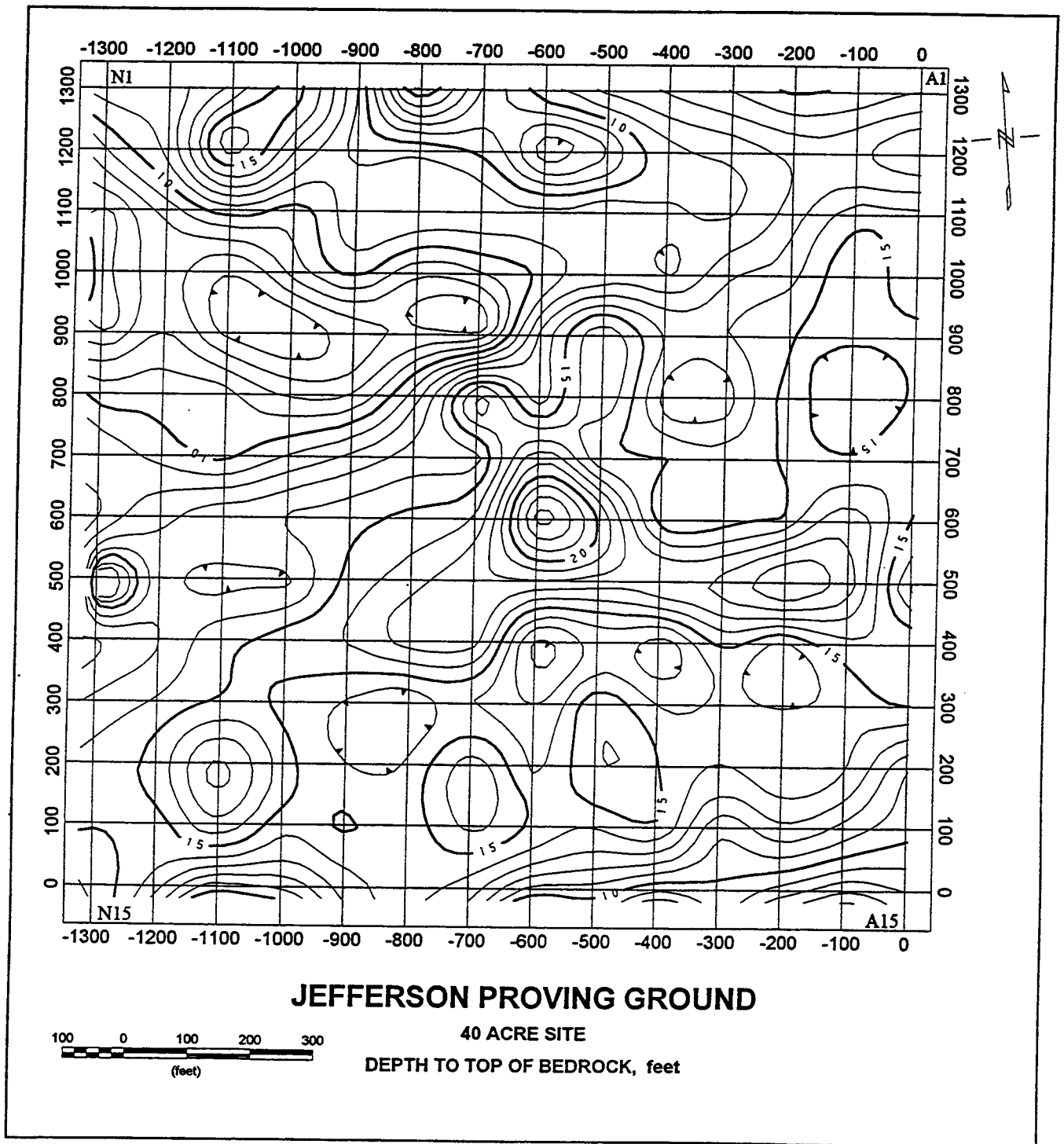


Figure 14. Depth to rock, 40-acre site

probed 202 locations at the 80-acre site and had refusal depths ranging between 2.8 and 23.7 ft with an average depth of refusal of 10.3 ft bgs. The top of rock elevation, referenced to a local datum, and depth to bedrock for the 80-acre site are presented in Figures 15 and 16, respectively. At each site, depth and rate of penetration was fairly uniform and predictable. At some locations, penetration was not as deep as expected, probably because of the presence of scattered large rocks in the subsurface above the bedrock surface (Tetra Tech EM, Inc 1998).

Soil sampling

Twenty soil samples were collected at the test sites for geotechnical characterization. Borings were placed at three locations at the 40-acre site and at five locations at the 80-acre site. The following laboratory tests were run on the samples:

- Grain size
- Moisture content
- Hydraulic conductivity
- Swell test
- Natural density

The grain size analysis of the 20 samples indicated that 80 to 90 percent of the soil matrix is in the silt- or clay-size fraction. The soil moisture content of the 20 soil samples, in general, ranged between 20 to 25 percent. The unit dry weight of the 20 soil samples ranged from 90 to 111 pounds per cubic foot (pcf) (1.44 to 1.78 g/cm³). The lone exception was a sample collected at B-26 (80-acre site) which was measured as 74 pcf (1.18 g/cm³). This sample also exhibited the highest moisture content (45 percent) of all the samples. Eleven samples were tested for swell pressure and free swell. Swell pressure ranged between 0.03 and 1.00 tons per square foot (2.87 and 95.76 kilopascals) whereas free swell ranged from 0.3 to 3.46 percent. Typical free swell values generally were less than 1 percent. Triaxial permeability tests run on eight samples showed a permeability range of 1×10^{-6} to 1×10^{-8} cm/sec with an average value of 1×10^{-7} cm/sec. Boring logs and test data sheets for the above soil analysis are given in PRC Environmental Management, Inc. (1994a.)

Environmental Sampling.

Environmental samples were collected at the 40- and 80-acre sites to assess the presence of volatile organic compounds (VOCs), semivolatile organic compounds (SVOCs), metals, and explosives. Three soil and one groundwater sample was collected at each site. The sampling was conducted to assess the potential risks to workers during the demonstrations and during the placement of UXOs.

The analytical results from the groundwater and soil samples indicated that VOCs, SVOCs, metal, and explosives contamination had no impact on the test sites. It was concluded that no environmental hazards existed at the sites. A description of sampling and testing procedures and laboratory analysis reports are given in PRC Environmental Management, Inc. (1994a).

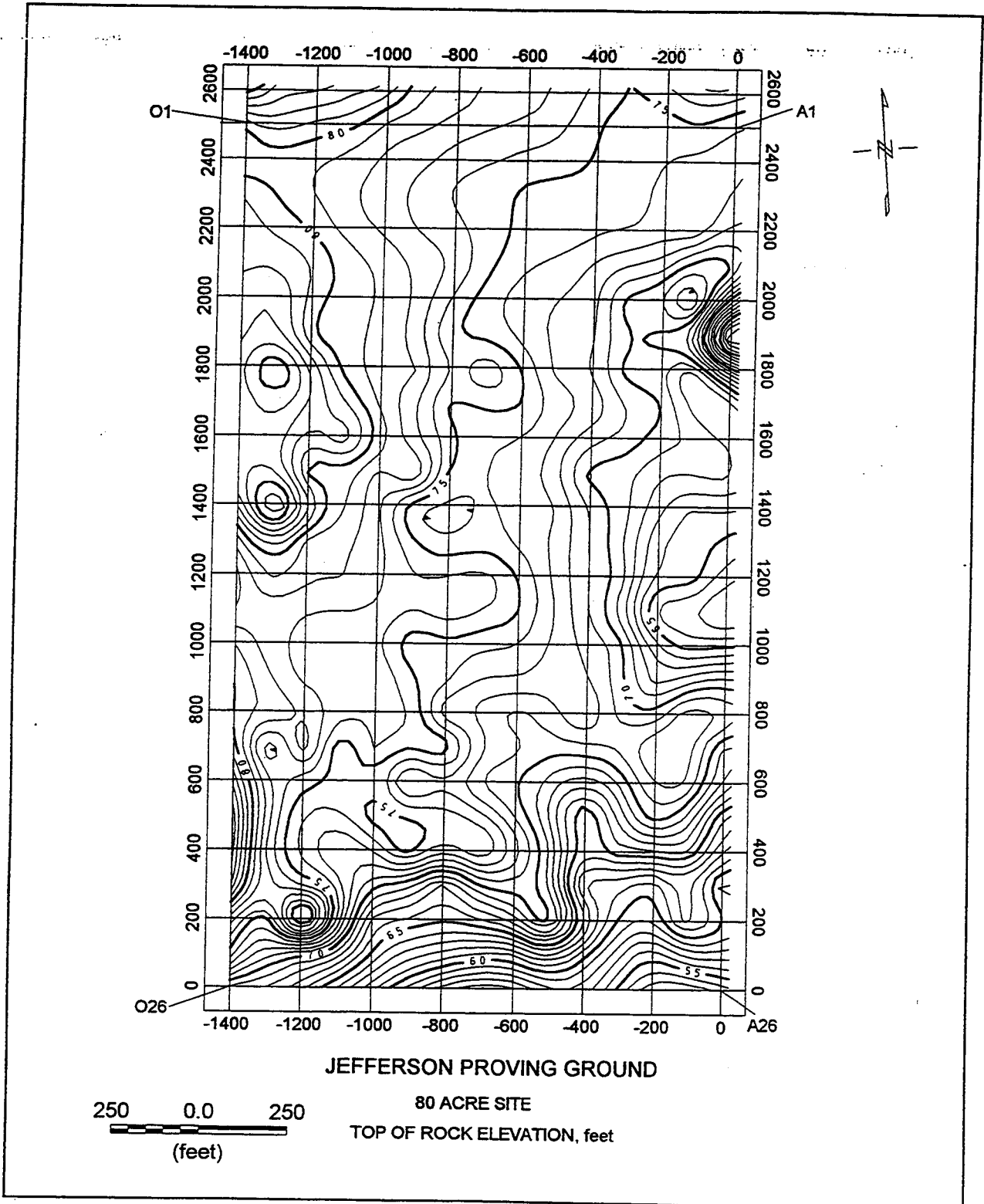


Figure 15. Top of rock elevation, 80-acre site

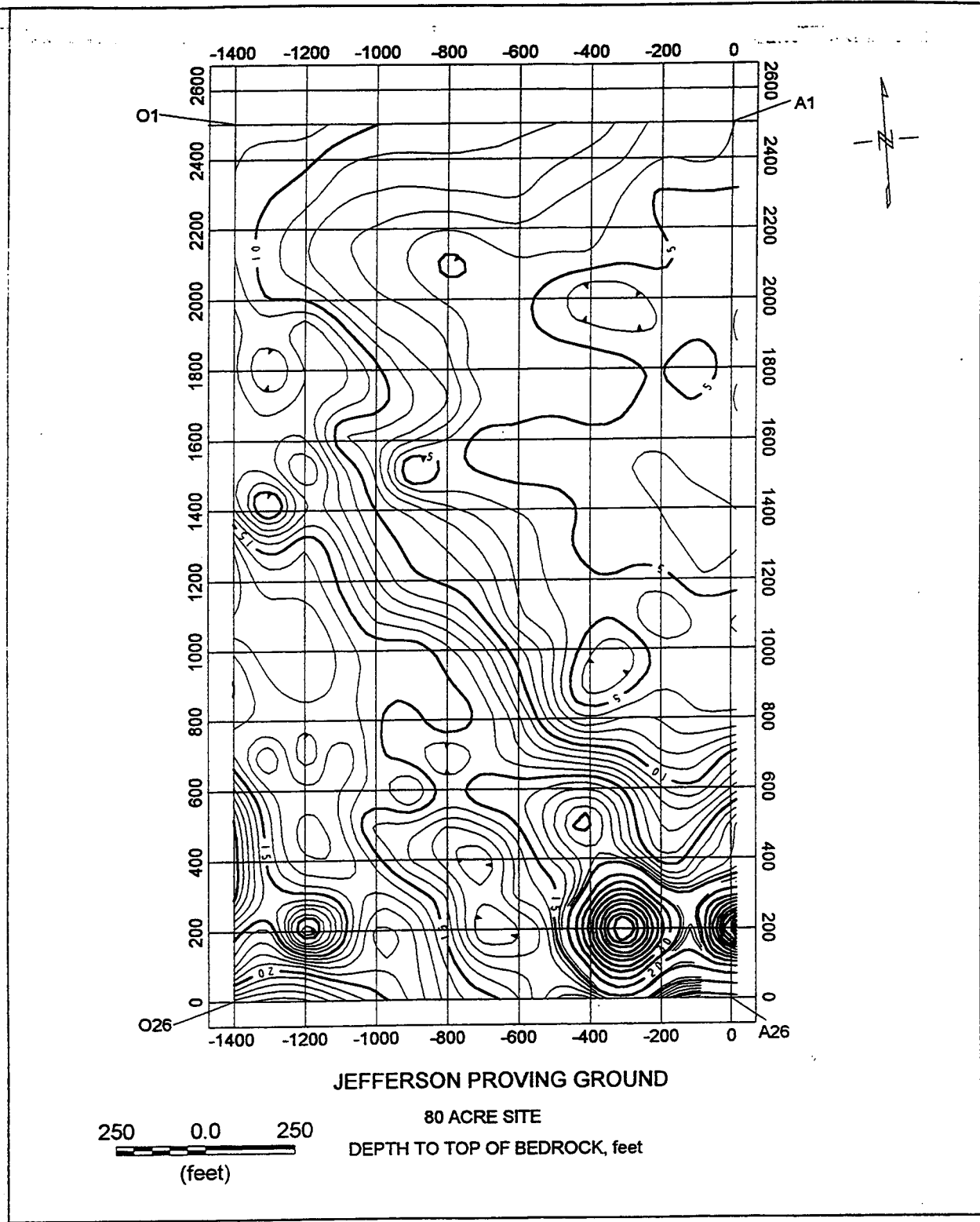


Figure 16. Depth to rock, 80-acre site

Geophysical Testing

A total magnetic field, electrical resistivity, and GPR survey were conducted at the test sites to establish baseline geophysical parameters. The geophysical survey results are provided in PRC Environmental Management, Inc. (1994b). Even though the report describes the GPR technique and equipment used, no data is presented.

Magnetic surveys

Total magnetic field readings were collected at 100-ft intervals both in the east-west and north-south directions at the demonstration sites. The 40-acre site results show numerous anomalies along the length of the western edge of the site and they are attributed to the presence of a barbed wire fence. Anomalously low readings are also noted approximately 150 ft on either side of a north-south trending line located 500 ft from the eastern edge of the site. The cause of this linear anomaly is unknown and it is presumed to be caused by a geologic feature. The range of magnetic readings, with the exception of the anomalous values caused by the fence, ranged between 54,510 and 54,622 nanoTeslas (nT).

The 80-acre site was also surveyed on a 100 ft by 100 ft grid layout. Anomalies were detected along the length of the eastern edge of the site. These anomalies are caused by the north-south trending asphalt perimeter road located within 50 ft of the site and which runs along the site's entire eastern boundary. A localized anomalous area was also noted in the southwestern corner of the site which was caused by nearby metal racks. The rest of the site was reported to have fairly uniform magnetic readings ranging between 54,615 to 54,630 nT.

Electrical resistivity surveys

Vertical electrical resistivity surveys were conducted at three locations at the 40-acre site and at four locations at the 80-acre site. A Wenner array was used to conduct the soundings. A-spacings of 0.91, 1.52, 2.13, and 30.48 m were used for the surveys. One location at the 40-acre site had A-spacings of 0.91, 1.52, and 2.13 m. However, there were not enough data points collected at any of the survey locations to adequately determine layer thicknesses or corresponding layer resistivities of the underlying materials. It was reported that apparent resistivities generally decreased with depth and was probably caused by an increase in moisture and or clay content. It was also reported that several soundings indicated increasing resistivity with depth probably caused by the underlying bedrock.

4 Supplemental Site Characterization

Preliminary Activities

Gridding the 40- and 80-acre sites

Wooden stakes, planted 100 feet apart, were used to mark the perimeter and the grid nodes of the 40 and 80-acre sites. The approximately 4-ft high stakes aided in survey location and navigation. The grid nodes are designated with a letter followed by a number for example, A1. The "A" indicates the node is on north-south trending line "A" and the "1" indicates that the node is on east-west trending line 1. The north-south trending lines are designated with a letter and increase in alphabetical order from east to west whereas the east-west trending lines are designated with numbers that increase in value from north to south. Therefore, for the 40-acre site the northeast corner is designated as A1 and the other 3 corners are A15, O15, and O1 moving in a clockwise manner. Similarly, the four corners for the 80-acre site are designated, from the northeast corner and proceeding in a clockwise fashion, A-1, A-26, O-26, and O1.

A local Cartesian coordinate system was established for geophysical surveying at the 40- and 80-acre sites. The origin of the 40-acre site (0E,0N) is located at grid node A14 near the southeast corner. The northwest corner, grid node O1, has coordinates of (-1320E,1320N). The origin of the 80-acre site has coordinates of (0E,0N) at grid node A26 and coordinates of (-1400E,2500N) at the northwest grid node, O1.

Selection of the 1-hectare site

The 1-hectare test site was established using the same guidelines as those mandated for the 1-hectare UXO backgrounds characterization sites established at Fort Carson, CO, and Fort A. P. Hill, VA (Simms et al. 1997). A local Cartesian coordinate system was also established for this site. The origin is located at the southwest corner and is designated (0E,0N) and the northwest corner is designated (125E,100N). Three 125-m east-west trending lines located along line 0N (southern boundary), 55N, and 100N (northern boundary) were marked with plastic

flags at 2-m intervals. Flags were also planted every 10 m along 100-m long north-south trending lines. The north-south lines were laid-out every 20 m between line 0E and 120E.

Soil Sampling and Testing Plan

40- and 80-acre sites

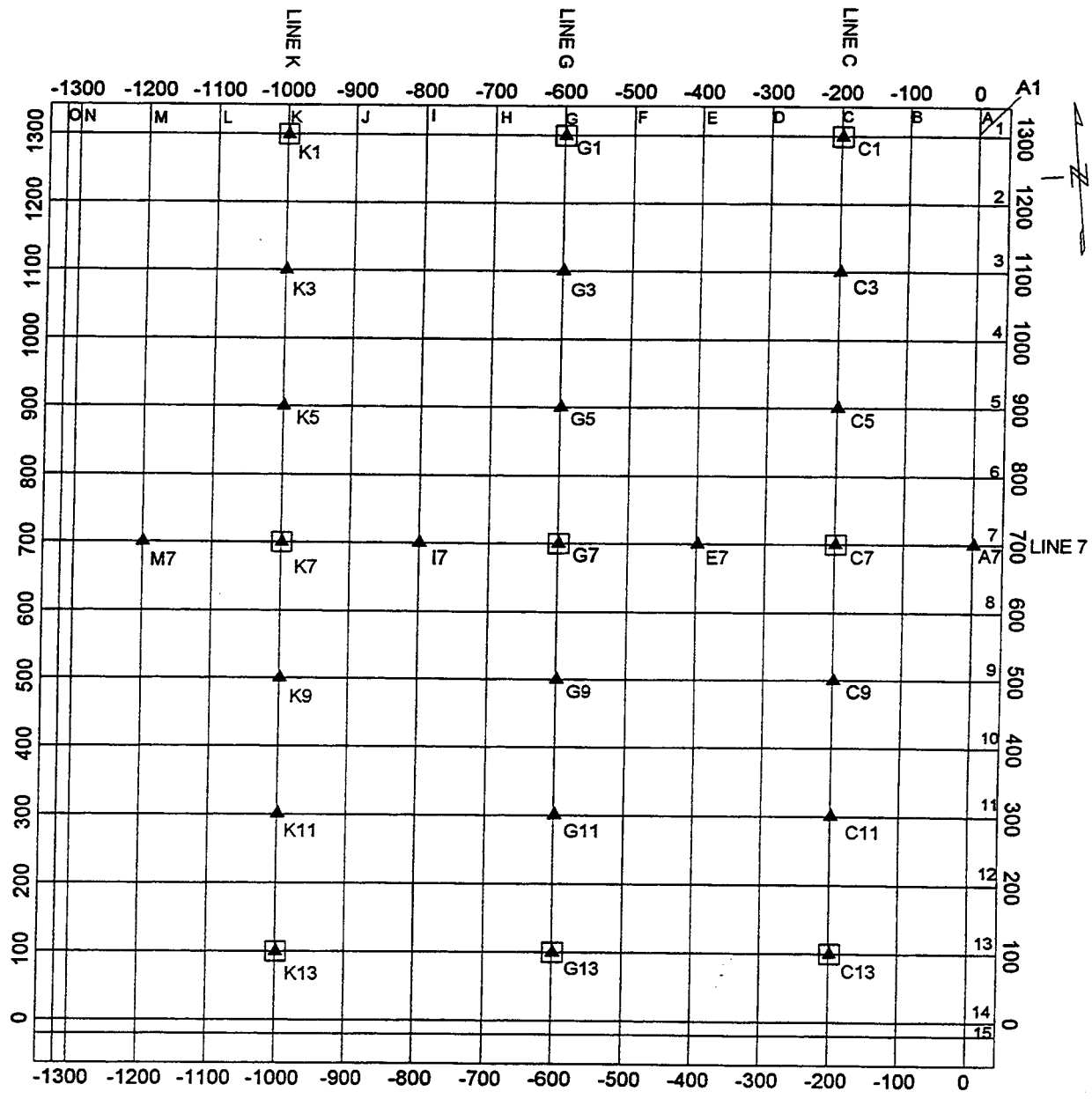
Soil samples were collected on August 3, 1997 at 9 locations at the 40-acre site and at 5 locations at the 80-acre site. The sampling locations are shown in Table 1 and in Figures 17 and 18.

Table 1 Soil Sampling Locations, 40- and 80-acre Sites	
Site	Soil Sampling Locations
40-acre	C1,C7,C13,G1,G7,G13,K1,K7,K13
80-acre	A13,H1,H13,H26,O13

Soil samples were collected at depths of 10, 50, and 100 cm at each location with the exception of locations K1 and K7, 40-acre site, where no samples were collected at the 100 cm depth. A hand-held power auger was used to advance the hole to the sampling depth and a hand auger used to collect the sample. The samples were placed in double, sealed, plastic bags. The samples were stored in ice chests in a humid room to minimize desiccation. Visual classification, moisture content, and complex dielectric properties were determined for each sample in the laboratory. In addition, grain-size gradation, Atterberg limits, specific gravity, organic content, and classification based on the Unified Soil Classification System (USCS) (USAEWES 1982) were determined for eleven soil samples collected from locations C7, G7, and K7 at the 40-acre site and from location A13 at the 80-acre site. Qualitative X-ray diffraction (XRD) tests to determine the mineralogy and estimate the quantity of each mineral present were also run on the eleven samples.

1-hectare site

Soil samples were collected at the 1-hectare site in October, 1997. A total of 15 samples were collected from seven locations as shown in Figure 19. The coordinates of the sampling locations are as follow; (27.5E, 73N), (65E, 10.5N), (122E, 8N), (123E, 97N), (40E, 23N), (52.5E, 85.5N) and (77.5E, 60.5N). Sampling depths ranged from 0 to 1 m. Visual classification, moisture content, grain-size gradation, and Atterberg limits, were determined for each sample.



JEFFERSON PROVING GROUND
TEST LOCATIONS

LEGEND

- SOIL BORING LOCATIONS
- ▲ VES AND DICON PROBE LOCATIONS

100 0 100 200 300
(feet)

Figure 17. Soil sampling locations and geophysical test layout, 40-acre site

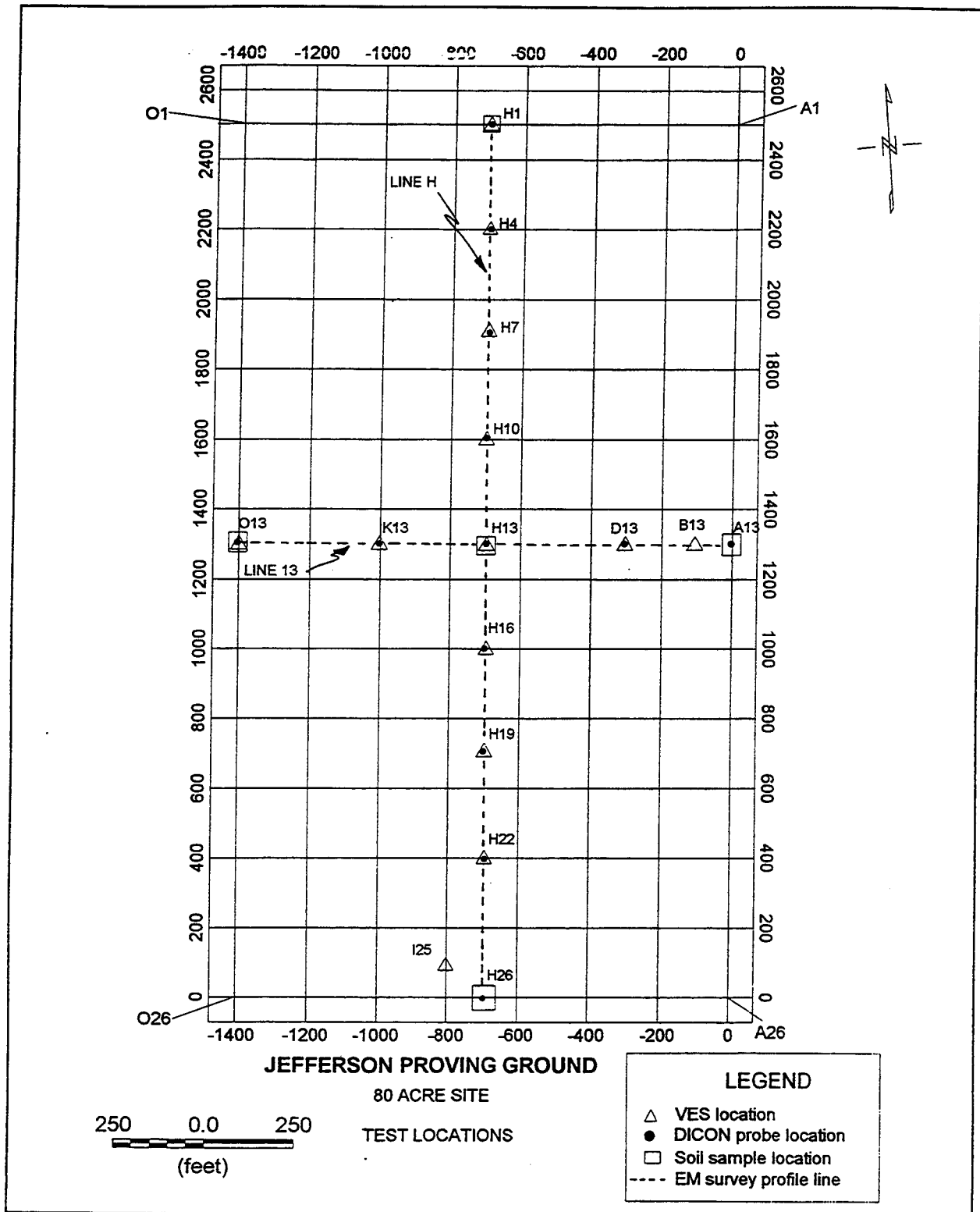


Figure 18. Soil sampling locations and geophysical test layout, 80-acre site

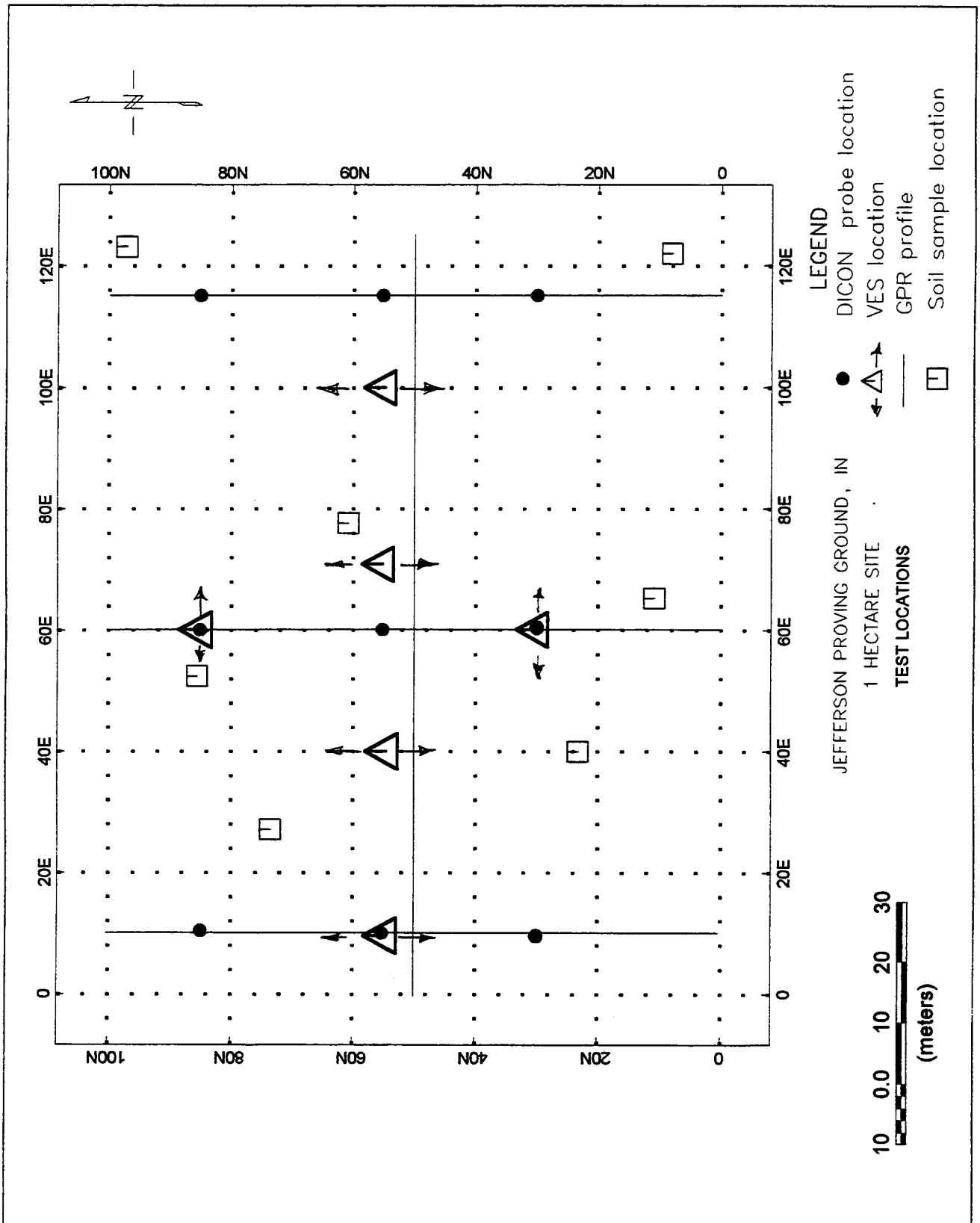


Figure 19. Soil sampling locations and geophysical test layout, 1-hectare site

Geophysical Test Principles, Equipment, and Field Procedures

This section details the site characterization plan, concepts of the geophysical methods, and field procedures. Electrical resistivity, EM induction, and GPR were the geophysical methods chosen to supplement the original geophysical surveys mentioned in Chapter 3. The electrical resistivity and EM techniques are complimentary and provide 1) both detailed and larger scale subsurface stratigraphy and 2) electrical resistivity and conductivity of the soil. GPR is used to determine the depth and attitude of subsurface stratigraphy, detection of anomalies and to characterize the electromagnetic properties of soils.

40- and 80-acre sites

Test principles and equipment

Electrical resistivity soundings. Electrical resistivity is a measure of how well the soil conducts an electrical current. Resistivity values can vary over several orders of magnitude depending on the type of earth material and on the degree of compaction. Major factors influencing the resistivity measurement are the amount of pore fluid present, the salinity of the pore fluid, and the presence of conductive minerals. An increase in any of these factors will cause the resistivity to decrease. A linear array of four metal rods or electrodes is generally used in an electrical resistivity survey. The array consists of two outer current electrodes and two inner potential electrodes. Current is introduced into the ground through one current electrode (positive electrode) and flows through the subsurface to the other current electrode (negative electrode). The subsurface material acts as a natural resistor and a potential difference is generated across the two potential electrodes. Knowing the amount of current injected into the ground, the electrode separation, and the potential difference, an apparent resistivity can be computed.

There are two types of resistivity surveys, horizontal profiling and vertical electrical sounding (VES). The profiling technique is used to identify lateral variations for a given depth of investigation, whereas the VES method gives variations in resistivity as a function of depth at a particular surface location. The VES method employing a Schlumberger array was used in this study. When performing a VES, the potential (center) electrodes remains fixed and electrical resistance measurements are taken at increasing current (outer) electrode spacings; the greater the current electrode spacing, the greater the depth of investigation. The VES data represent the subsurface resistivity structure below the center point of the array. A general rule of thumb is that the depth of investigation is equal to 0.2–0.5 the spacing between current electrodes, depending on the actual values of the material resistivities. The measured resistance reading is multiplied by a factor, based on the array geometry, to obtain an apparent resistivity value. A VES curve is obtained by plotting apparent resistivity versus electrode spacing (typically log-axes). The resistivity, thickness, and number of subsurface layers can be estimated from the shape of the VES curve. The unit of electrical resistivity is the ohm-meter ($\Omega\text{-m}$). Resistivity is the reciprocal of electrical conductivity, which can be measured in an electromagnetic survey. To convert from resistivity, in ohm-meters,

to conductivity, in millisiemen per meter, divide 1000 by the resistivity value. An Atlas Copco ABEM Terrameter SAS 300B and a STING resistivity meter were used at the 40- and 80-acre sites, respectively. An inverse modeling computer program, RESIX Plus (Interpex Ltd. 1988), was used to interpret the VES data in terms of a layered earth model.

Electromagnetic surveys. A frequency domain EM induction method is commonly used to measure an apparent terrain conductivity. The conductivity of a material is dependent on the degree of water saturation, the types of ions in solution, porosity, the chemical constituents of the soil, and the physical nature of the soil. Because of these factors, conductivity values can range over several orders of magnitude.

The EM system consists of a transmitter and receiver coil separated by a fixed distance. An alternating current, commonly in the 1 to 20 kilohertz range, is passed through the transmitter coil, thus generating a primary time varying magnetic field. This primary field induces eddy currents in subsurface conductive materials. The induced eddy currents are the source of a secondary magnetic field which is detected by the receiver coil along with the primary field. Under a fairly wide range of conditions, the measured component that is ninety degrees out of phase (quadrature component) with the primary field is linearly related to the terrain conductivity (Keller and Frischknecht 1982, Dobrin 1960, Telford et al. 1976). Conductivity is measured in units of millisiemen per meter (mS/m).

Two components of the induced magnetic field are measured by the EM system. The first is the quadrature phase component, sometimes referred to as the out-of-phase or imaginary component. An apparent ground terrain conductivity is determined from the quadrature component. Disturbances in the subsurface caused by compaction, soil removal and fill activities, or buried objects may produce conductivity readings different from that of the background values, thus indicating anomalous areas. The second component is the inphase or real component. The inphase component is primarily used for calibration purposes, however, it is also very sensitive to metallic objects and therefore useful when looking for buried metal (Geonics Ltd. 1984). The inphase component is measured relative to an arbitrarily set level and assigned units of parts per thousand (ppt).

A Geonics EM31 terrain conductivity meter was used for this investigation. The EM31 has a transmitter-receiver coil separation of 12 ft (3.7 m) and an effective depth of investigation of approximately 20 ft (6.1 m) (Geonics Ltd. 1984). The EM31 meter reading is a volume weighted average of the earth's conductivity; half of the instrument's readings result from features shallower than about 9 ft (2.7 m), and the remaining half from below that depth (Bevan 1983). When the EM31 is carried at a height of approximately 3 ft (0.9 m), it is most sensitive to features at a depth of about 1 ft (0.3 m). Carrying the instrument about 3 ft (0.9 m) above the ground surface reduces the meter reading by 12 percent, however, the instrument has been calibrated to read correctly when carried at this height (Geonics Ltd. 1984). The instrument can be operated in both a horizontal and vertical dipole orientation, each having different depths of investigation. The instrument is normally operated with the dipoles vertically oriented (coils oriented horizontally and co-planar) which gives the maximum depth of penetration.

Ground penetrating radar surveys. The radar detectability of a subsurface target strongly depends on the EM wave speed, v , and attenuation rate, β , of the soil. The speed determines the shape of the antenna beam pattern, and β determines how far the waves can penetrate and return to the surface with enough intensity to be detected. These quantities are related to the relative complex permittivity of soil, ϵ_s^* , such that

$$v = c / \text{Real}(\epsilon_s^{*1/2}), \quad (1)$$

and

$$\beta(\text{dB/m}) = 20 \log [\exp(-i\omega / c(\text{Imag}(\epsilon_s^{*1/2})))] \quad (2)$$

where $i = (-1)^{1/2}$, ω is frequency in radians/s, and $c = 3 \times 10^8$ m/s is the wave speed in free space. The quantity ϵ_s^* is determined by the Debye relaxation permittivity (Debye 1929), ϵ_{rel} , and a contribution from the very-low-frequency soil conductivity, σ (Siemens/m, or S/m) such that

$$\epsilon_s^* = \epsilon_{\text{rel}} - i\sigma / \omega\epsilon_0, \quad (3)$$

where

$$\epsilon_{\text{rel}} = \epsilon_{\infty} + (\epsilon_x - \epsilon_{\infty}) / (1 + i f/f_{\text{rel}}), \quad (4)$$

ϵ_0 is the dielectric permittivity of free space (a constant), ϵ_x is the low frequency, “static,” value of the relative soil permittivity, ϵ_{∞} is the very-high-frequency value, $f = 2\pi\omega$ is the wave frequency in Hertz (Hz), or frequency component for a radar wavelet, and f_{rel} is the soil relaxation frequency. The quantity ϵ_{rel} determines the dipole moment density induced in a material by a passing wave. The quantity f_{rel} is a characteristic frequency above which the induced dipoles no longer stay in phase with the incident wave. These dipoles then generate interference which effectively slows and attenuates the incident radiation. This process is dispersive, which means that different frequencies within the incident wavelets propagate at different speeds and attenuation (Stratton 1941, Brillouin 1960, and Feynman et al. 1964).

Values of ϵ_x are directly related to the water content for clay-(non-mineralogic) and silt-sized materials (Topp et al. 1980) and generally equal ϵ_s^* for $f < 600$ MHz. Above about 600 MHz laboratory investigations (Hoekstra and Doyle 1971; Hoekstra and Delaney 1974) show that the adsorbed water on the particle surfaces of the silt-clay fraction (Tice et al. 1982) strongly influences the dielectric properties. The adsorption process lowers both the very high dielectric constant (81) of the normally free water, and the free water relaxation frequency (22 GHz) to about 1–3 GHz. Values of ϵ_{∞} are generally related to the dry soil density, range from about 2.5–3.5, and equal ϵ_s^* at frequencies above about 100,000 MHz. For JPG soils and the radar frequencies used, σ is large enough to also influence attenuation.

The resulting values of ϵ_s^* for silty and clay-rich soils at frequencies above about 100 MHz provide high values of β and wave speeds lower than would be expected for sandy soils with the same volumetric water content. The β values (a

quantitative discussion is given later) increase as f approaches, and then exceeds, f_{rel} , and are orders of magnitude greater than attenuation rates caused by the geometric spreading of the radiation energy. At frequencies below about 1000 MHz, the real part, $\epsilon' = \epsilon_{\text{sp}}$, often referred to as the dielectric constant, determines the wave speed v through the relation

$$v = c / \epsilon'^{1/2} \quad (5)$$

for a variety of frozen and unfrozen silts and (non-mineralogic) clay-sized materials (Hoekstra and Delaney 1974; Topp et al. 1980; Delaney and Arcone 1984).

A GSSI (Geophysical Survey Systems, Inc.) SIR system model 2 and models 3207 (100 MHz), 5103 (300 MHz), and 101C (600 MHz) antenna transducers were used in this study. The control unit was used to set the time range (in nanoseconds, ns) for the echo traces, the data acquisition rate (48 or 64 traces/s), the sampling density (512 samples per trace), trace sample density (16-bit) and time variable gain (TVG) across the traces. The settings were calibrated with the antennas set over emplaced targets. The resulting reflections required a large amount of gain, ranging up to 65 dB, at time ranges of only 50 (300 MHz) and 30 ns (600 MHz). The short time ranges were sufficient to capture target responses throughout the site, but were also necessary to limit radiowave interference which beat with the radar returns at the high-gain time ranges. The high gain had the negative effect of amplifying small antenna impedance mismatches and low amplitude clutter (unwanted events), which probably originated from radiation which leaked on to the antenna housing and cables. These events usually arrive at constant time delay and are usually alleviated with a horizontal “background removal” filter. However, in this case where short time ranges were used, electronic jitter and erratic movement of the antenna may have caused these events to arrive at variable amplitude and so they were not consistently reduced by filtering.

The antennas are resistively loaded dipoles. The smaller, 300- and 600-MHz antennas are shielded with semi-cylindrical housings to alleviate above-surface clutter. These frequencies are “local” (also known as “instantaneous”) values, which correspond with the dominant periods and lie approximately at the center of the received wavelet spectrum. They are considerably below manufacturer’s specifications for these antennas (400 and 900 MHz, respectively), which generally apply to operation in air, or on ground with lower values of dielectric permittivity and loss than encountered at JPG. Their transmitters do not exceed 8 W (peak power) in order to protect the nearby receiver. Data was also acquired using 100-MHz antennas but are not discussed because the direct coupling between these antennas, which lasts approximately 30–50 ns, obliterated any near surface returns. The antenna directivity, becomes increasingly confined beneath the antenna as ϵ' increases (Arcone 1995). The typical shape of a transmitted GPR wavelet for either the 300- or 600-MHz antenna system is shown in Figure 20. The phase polarity sequence of the half-cycles defines the wavelet phase (Arcone 1995).

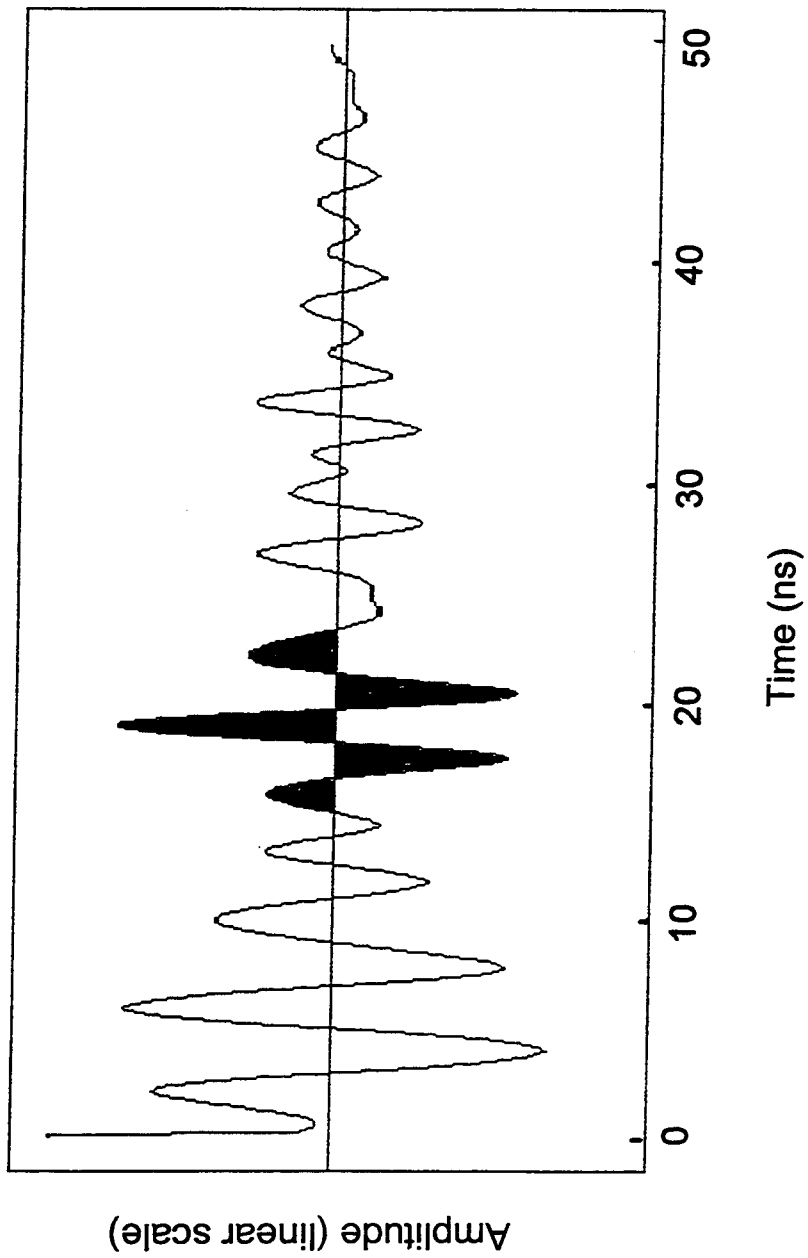


Figure 20 Typical form of a radiated GPR wavelet

Additional electrical properties. A DICON probe was used to take in situ point measurements of the electrical properties of the soil. The following information describing the DICON probe is extracted from Miller et al. (1992). The DICON (DIelectric/CONductivity) probe measures the conductivity and dielectric constant of the soil at a frequency of 60 MHz. Each DICON probe unit consists of two separate pieces of equipment, a probe assembly and a reflectometer. The probe head consists of two half-cylindrical-shaped brass plates attached to an insulating body of polytetrafluoroethylene (Teflon®), with a small gap between the plates. The brass plates on the probe head represent two capacitors; one internal to the probe with the Teflon as the dielectric and the other external with the soil as the dielectric. The plates behave as a simple capacitor with the soil in their immediate vicinity as the dielectric with virtually no electromagnetic radiation outside of the plates. The reflectometer houses the electronics of the DICON probe. A voltmeter placed on the top face of the reflectometer displays the real (R) and imaginary (I) components of the complex reflection coefficient.

Prior to making any measurements the probe is calibrated following a standard procedure (Miller et al. 1992). Readings are taken by inserting the probe head to the desired depth into a one inch diameter augered hole. The displayed real and imaginary components of the complex reflection coefficient are used to calculate the electrical conductivity and relative dielectric permittivity.

Field procedures

40-acre site

Electrical resistivity soundings. The locations of the 25 Schlumberger resistivity soundings are shown in Figure 17. All of the soundings were oriented east-west with the exception of soundings located at M7, I7, E7, and A7, which were oriented north-south. The minimum current electrode spacing was 1.0 m and the maximum spacing was 200 m, allowing a depth of investigation of at least 25 m.

EM31 surveys. EM31 data were collected along north-south oriented lines A-O spaced 100 ft apart (Figure 17). The EM31 was programmed to collect readings every 2 seconds along each survey line or approximately 1 reading for every 6 ft. The EM31 was placed approximately 3 ft from the ground surface on a non-metallic cart and hand-towed along each survey line. Conductivity and inphase readings were collected at each survey location. Fiducial markers were marked in the data at 100 ft intervals while collecting the data along each line for position reference. A data logger connected to the EM31 was used to store the data during the surveys and at the conclusion of each survey the data were transferred to a field computer for later processing.

Ground penetrating radar surveys. Profiles were run along established transects and electronic event markers entered on the profiles at previously established, 100-foot (30-m) distance marks. The transects generally deviated 1–2 m from a straight line, but sometimes as much as 5 m to avoid isolated bushes, trees and tire ruts. Consequently, the position along the lines cannot be reconstructed exactly, and errors may occur in the interpretation of distance between markers. The antennas were dragged by vehicle at less than 1 m/s speed for long

distances, and by hand for the small surveys over emplaced targets. All antennas were polarized perpendicular to the transect direction. It was determined that vehicle reflections were not in the data by comparing profiles recorded with and without the vehicle. The smaller antennas were placed in a fiberglass box to alleviate erratic antenna to ground coupling. However, the uneven towing speed over the rough ground also degraded the appearance of the profiles.

DICON probe measurements. DICON probe measurements were taken at 25 stations as shown in Figure 17. The readings were taken at depths of 0.1 and 0.5 m. The locations of the DICON probe measurements corresponded to the center of an electrical resistivity survey line.

80-acre site

Electrical resistivity soundings. The locations of the 14 Schlumberger resistivity soundings are shown in Figure 18. Soundings located at B13, D13, H13, K13, and H1 were oriented east-west and the remaining soundings oriented north-south. In addition a sounding at H13 was conducted using a north-south line orientation. The minimum current electrode spacing was 0.5 m and the maximum spacing was 98 m, allowing a maximum depth of investigation of about 25 m.

EM31 surveys. EM31 data were collected along north-south Line H and along east-west Line 13 as shown in Figure 18. The EM31 was programmed to collect readings every 2 seconds along each survey line or approximately 1 reading every 6 ft. The EM31 was placed approximately 3 ft from the ground surface on a non-metallic cart and hand-towed along each survey line. Conductivity and inphase readings were collected at each survey location. Fiducial markers were marked in the data at 100 ft intervals while collecting the data along each line for position reference. A data logger connected to the EM31 was used to store the data during the surveys and at the conclusion of each survey the data were transferred to a field computer for later processing.

DICON probe measurements. DICON probe measurements were taken at 13 stations as shown in Figure 18. The readings were taken at depths of 0.1 and 0.5 m. The locations of the DICON probe measurements generally corresponded to the center of an electrical resistivity survey line.

1-hectare site

Test principles and equipment

Five types of geophysical data were collected at this site: terrain conductivity, magnetometer, electrical resistivity, GPR, and DICON probe. Terrain conductivity, electrical resistivity, and DICON probe measurements were collected using the same instrumentation as used at the 40- and 80-acre sites. The magnetometer and GPR system used at the 1-hectare site are described below.

Magnetic surveys. A magnetic survey measures changes in the earth's total magnetic field caused by variations in the magnetic mineral content of near surface rocks and soils or ferrous objects. These variations are generally local in extent.

The magnetic response is attributed both to induction by the earth's magnetic field and to remanent magnetization. Remanent magnetization is permanent magnetization and depends on the thermal and magnetic history of the body; it is independent of the field in which it is measured (Breiner 1973). Induced magnetization is temporary magnetization that disappears if the material is removed from the inducing field. Generally, the induced magnetization is parallel with and proportional to the inducing field (Barrows and Rocchio 1990).

A GEM GST-19T proton precession magnetometer with an accuracy of 1 nanotesla (nT) was used to collect the magnetic survey data. This magnetometer is equipped with a sensor that contains a hydrogen-rich fluid as a source for the protons. The proton precession magnetometer is based on the principle that protons will precess freely in the presence of the earth's magnetic field. The hydrogen-rich fluid is subjected to an external magnetic field applied in a direction approximately perpendicular to the earth's field. The proton's moment will align in the direction of the resultant field between that of the external magnetic field and earth magnetic field. When the external field is removed, the magnetic moment of the proton will precess about the earth's field until it returns to its original alignment with the earth's magnetic field. The proton precesses at an angular frequency which is proportional to the magnetic field. Therefore, by measuring the frequency at which the protons precess the strength of the local magnetic field can be determined.

Any material or object having a magnetic susceptibility will contribute to the total magnetic field measured by the magnetometer. If an object is present such that its magnetization is great enough to perturb the ambient magnetic field, then it will appear as an anomaly on the magnetic data plot. The size, depth of burial, magnetic susceptibility, and remanent magnetization of the object determine the magnitude of the anomaly and thus affect the ability of the magnetometer to detect the object. For a given susceptibility and remanent magnetization, as the size of the object decreases and depth of burial increases, the magnitude of the anomaly decreases; eventually the anomaly will be undetectable.

Ground penetrating radar surveys. A thorough discussion on GPR principles is given in the 40- and 80-acre Site - Test Principles section presented above. Although a different GPR unit was used at the 1-hectare site than was used at the 40-acre site, basic GPR principles remain the same. A Sensors & Software, Inc. modified pulseEKKO IV system was used to collect the GPR data at the 1-hectare site. The pulseEKKO IV is a low frequency antenna system (12.5–200 MHz). The nominal center-frequencies of the antennas used in this investigation were 50, 100, 200 MHz. Both reflection profiling and velocity sounding GPR surveys were performed. In reflection mode, the transmitter and receiver antennas are kept a fixed distance apart and both antennas are simultaneously moved along the survey line. The time (in nanoseconds) required for the EM wave to travel through the subsurface and return to the receiver is recorded at each sample station. The received signal is plotted against two-way travel time at each sample station along the survey line. Figure 21 illustrates the reflection mode concept and the corresponding GPR response for the hypothetical anomaly shown. The common-midpoint (CMP) technique is used to perform the velocity sounding. The transmitter and receiver antennas are initially placed a given distance apart, and then moved

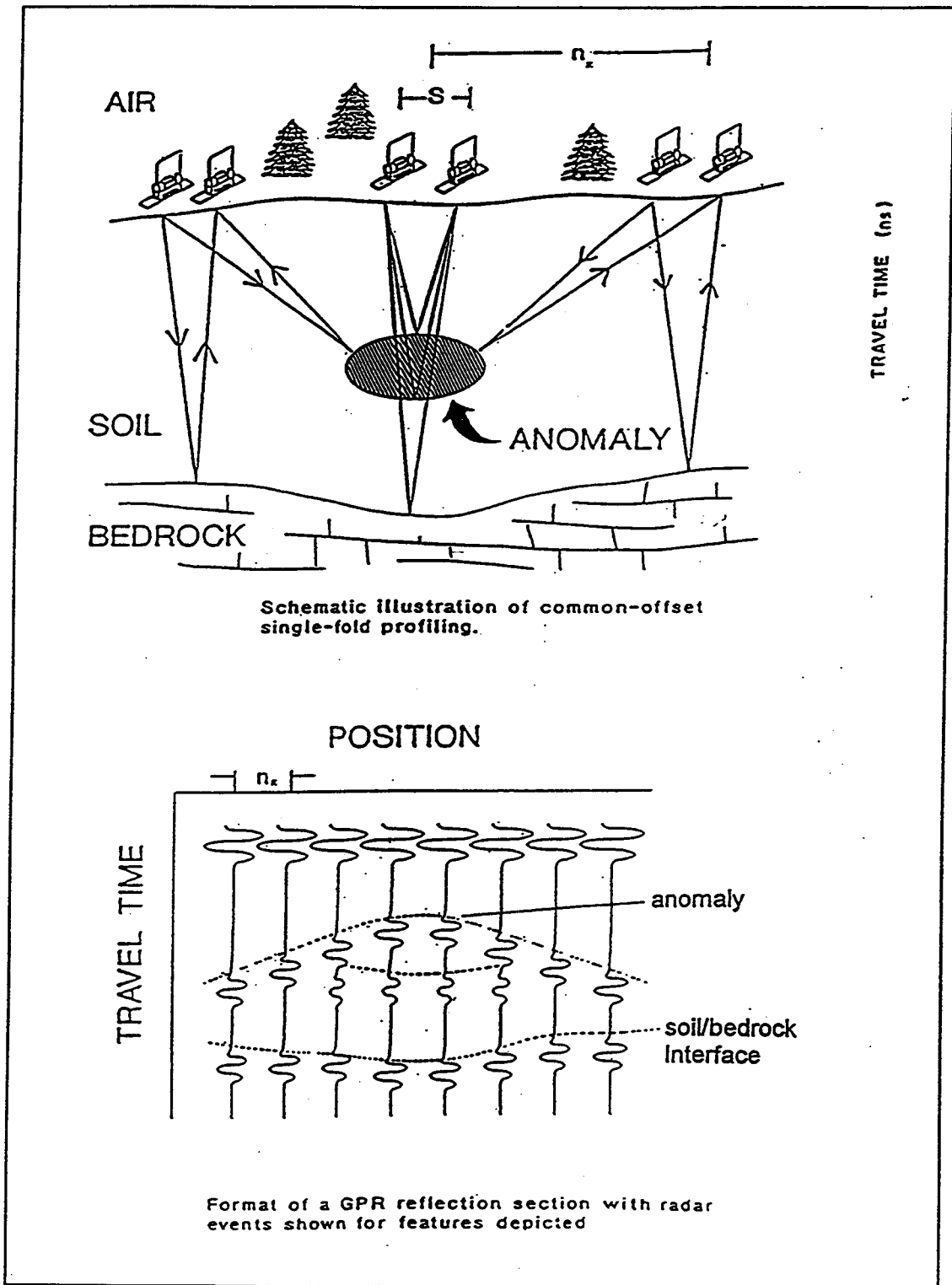


Figure 21. Illustration of a reflected mode GPR survey and corresponding radar section for anomaly shown (adapted from Annan 1992)

outward from the center at small, equal increments. By plotting antenna separation versus time, the various EM wavefronts can be identified and an approximate radar wave velocity obtained.

Field procedures

The survey grid was flagged at 2 m intervals along the north and south perimeter, and at 5 m intervals along the east and west perimeter. Additional flagged lines (2 m flag intervals) were placed at 20 m intervals in both the north-south and east-west directions. The emplaced flags were used to as a navigation aid during data collection. The terrain conductivity data were collected along 2 m spaced survey lines with a measurement acquired at 1.0 second intervals, providing one reading per meter. The magnetometer sensor was mounted on a backpack worn by the operator and positioned approximately 1.5 m above the ground surface. These data were acquired at 0.5 seconds intervals along 1 m spaced survey lines, which resulted in one reading per meter. Fiducial markers were placed in the data at 5 m intervals for position reference while collecting the data. A data logger connected to the conductivity meter was used to store the data during the surveys and at the conclusion of each survey the data were transferred to a field computer for later plotting. The magnetometer data were stored internally in the unit's control console and later transferred to a field computer. Schlumberger resistivity soundings were performed along selected survey lines, which included both north-south and east-west oriented lines. A minimum of five measurements per logarithmic decade were taken, with the electrode spacings approximately equally spaced on a logarithmic scale. The minimum current electrode spacing was 1 m and the maximum spacing was 120 m, allowing a depth of investigation of at least 15 m.

GPR reflection and CMP data were collected along both north-south and east-west oriented profile lines. For the reflection GPR surveys, the distance between the 50, 100, and 200 MHz transmitter and receiver antennas were kept at a constant spacing of 2.0, 1.0, and 0.5 m, respectively, and oriented normal to the survey direction. The data were collected in high speed data acquisition mode at sampling intervals of 0.25 m (50, 100 MHz) and 0.1 m (200 MHz). The data were recorded on a field computer for later processing. When performing the CMP surveys, the transmitter and receiver antennas were initially spaced at the respective antenna spacing used during the reflection survey, and then each antenna is moved outward in increments of 0.1 m (50, 100 MHz) or 0.05 m (200 MHz) relative to the center point. An average EM wave velocity of the medium was determined based on the CMP data.

DICON probe measurements were taken at nine stations within the grid and at three depths (0.1, 0.3 and 0.5 m) at each station. The location of a DICON probe measurement corresponds to the center of a resistivity sounding or a position along a GPR profile.

The locations of the electrical resistivity soundings, GPR profiles and DICON probe measurements are shown in Figure 19. The arrows in the symbol denoting a resistivity sounding indicate the direction of expansion of the array.

5 Soils Investigations

Introduction

Prior to the present study, investigators held the distinct impression that soils at JPG were predominantly clay. This impression about the JPG soils was so strong that it was the basis for the decision to establish a 1-hectare site at JPG to complement the four DARPA Backgrounds Program sites (Figure 3). Descriptions from the original JPG site characterization (field boring logs and soils laboratory testing results) indicated that the soils were clayey-silts, silty-clays, and clays. Visual soil classifications were OL-ML for depths less than 0.15 to 0.2 m and CL-CH for depths greater than 0.2 m (soil classifications are described below), and particle-size gradation of the samples was 80 to 90 percent silt- and clay-sized materials (PRC Environmental Management, Inc. 1994a). Additionally, GPR is known, based on both ground-based and airborne GPR demonstrations at the sites, to perform very poorly; high GPR signal attenuation is reported. The poor GPR performance is consistent with the soils descriptions as clays.

The present work includes (1) visual classification, (2) laboratory geotechnical properties determinations (including water content, Atterberg limits, organic content, specific gravity, and particle size gradation), (3) laboratory EM properties determinations, and (4) laboratory XRD analysis (to determine soils mineralogy and clay identification).

40- and 80-acre Sites

Physical properties

The soils analysis indicate that the soils from the 40- and 80-acre sites are very similar. All the soils are classified either as CL or CH with the exception of the 10 cm sample collected at location G7 at the 40-acre site which is classified as an ML. The grain-size analysis for the 40-acre site indicates that 85 percent of each soil sample, *on average*, passed the No. 200 sieve (0.075 mm opening) whereas 94 percent passed the No. 200 sieve for the 80-acre site samples. The average specific gravity and organic content values for the 40-acre site samples are 2.63 and 2.6 percent, respectively, and 2.67 and 3.3 percent, respectively, for the 80-acre site. The *average* natural water contents, in percent, for the 10, 50, and 100 cm deep

samples for the 40-acre site are 12.6, 19.6, and 18.8, respectively, and 14.6, 18.2, and 22.5, respectively, for the 80-acre site. Tabulated results of the laboratory analysis for 40- and 80-acre sites are presented in Tables 2 and 3, respectively. Appendixes A and B present the soil gradation curves for the soil samples collected at the 40- and 80-acre sites, respectively.

As mentioned in Chapter 4, the soils are classified according to the USCS, where the classifications CL and CH refer to low (L) and high (H) plasticity clays (C) and ML refers to low plasticity silts and very fine grained sands. A way to view the classification scheme is a plot of liquid limit (LL) versus plasticity index (PI), where LL and PI are Atterberg limits index properties of soils. Figure 22 adapted from Means and Parcher (1963) and Casagrande (1947), illustrates the soil classification scheme and shows the JPG soils (data from Tables 2 and 3). The JPG soils are problematic in terms of classification in that they are very near the “A-Line”, that typically separates organic (below the A-Line) from inorganic soils, and are in a region of the classification chart where soils can be either clays, sandy-clays, and silty-clays, or silts and very fine-grained silty-sands

Table 2
Summary of Soils Laboratory Analysis, 40-Acre Site

Location	Depth m	Classification	% Gravel	% Sand	% Fines	Liquid Limit	Plastic Limit	Plasticity Index	Natural Water Content, %	Specific Gravity	Organic Content, %
C1	0.10	Sandy clay (CL), gray; with organic roots	N/A	N/A	N/A	N/A	N/A	N/A	10.7	N/A	N/A
	0.50	Sandy clay (CH), grayish brown*	N/A	N/A	N/A	N/A	N/A	N/A	19.0	N/A	N/A
	1.00	Sandy clay (CH), brown*	N/A	N/A	N/A	N/A	N/A	N/A	19.9	N/A	N/A
C7	0.10	Sandy silty clay (CL), gray	0.5	18.9	80.6	25	21	4	12.0	2.65	2.5
	0.50	Clay (CL), brown; with sand	0.0	9.8	90.2	36	20	16	20.8	2.63	1.9
	1.00	Sandy clay (CL), brown	1.6	18.9	79.4	31	18	13	17.2	2.61	1.8
C13	0.10	Sandy clay (CL), gray; with organic roots*	N/A	N/A	N/A	N/A	N/A	N/A	12.8	N/A	N/A
	0.50	Sandy clay (CH), grayish brown*	N/A	N/A	N/A	N/A	N/A	N/A	14.6	N/A	N/A
	1.00	Sandy clay (CH), brown*	N/A	N/A	N/A	N/A	N/A	N/A	16.7	N/A	N/A
G1	0.10	Sandy clay (CL), gray; with organic roots*	N/A	N/A	N/A	N/A	N/A	N/A	14.5	N/A	N/A
	0.50	Sandy clay (CH), brown*	N/A	N/A	N/A	N/A	N/A	N/A	21.1	N/A	N/A
	1.00	Sandy clay (CH), brown*	N/A	N/A	N/A	N/A	N/A	N/A	20.3	N/A	N/A
G7	0.10	Sandy clayey silt (ML), gray	0.0	17.3	82.7	30	23	7	13.3	2.65	2.8
	0.50	Sandy clay (CL), brown	0.0	13.0	87.0	30	20	10	18.0	2.68	1.9
	1.00	Sandy clay (CL), brown	2.7	14.6	82.7	35	18	17	19.5	2.58	2.2

(Continued)

Location	Depth m	Classification	% Gravel	% Sand	% Fines	Liquid Limit	Plastic Limit	Plasticity Index	Natural Water Content, %	Specific Gravity	Organic Content, %
G13	0.10	Sandy clay (CL), gray; with organic roots*	N/A	N/A	N/A	N/A	N/A	N/A	12.0	N/A	N/A
	0.50	Sandy clay (CH), brown*	N/A	N/A	N/A	N/A	N/A	N/A	18.1	N/A	N/A
	1.00	Sandy clay (CH), brown*	N/A	N/A	N/A	N/A	N/A	N/A	18.0	N/A	N/A
K1	0.10	Sandy clay (CL), brown; with trace of organic roots*	N/A	N/A	N/A	N/A	N/A	N/A	13.4	N/A	N/A
	0.50	Sandy clay (CH), brown*	N/A	N/A	N/A	N/A	N/A	N/A	23.6	N/A	N/A
K7	1.00	Sandy silty clay (CL), gray	0.0	15.8	84.2	38	24	14	11.7	2.60	5.3
	0.50	Clay (CL), brown; with sand	0.0	5.8	94.2	44	21	23	20.6	2.67	2.0
K13	0.10	Sandy clay (CL), gray; with organic roots*	N/A	N/A	N/A	N/A	N/A	N/A	12.6	N/A	N/A
	0.50	Sandy clay (CH), brown*	N/A	N/A	N/A	N/A	N/A	N/A	20.2	N/A	N/A
	1.00	Sandy clay (CH), brown*	N/A	N/A	N/A	N/A	N/A	N/A	19.8	N/A	N/A

* Visual classification

Table 3
Summary of Soils Laboratory Analysis, 80-Acre Site

Location	Depth m	Classification	% Gravel	% Sand	% Fines	Liquid Limit	Plastic Limit	Plasticity Index	Natural Water Content, %	Specific Gravity	Organic Content, %
A13	0.10	Silty clay (CL), brown; with sand	0.0	5.9	94.1	45	28	19	18.4	2.64	4.3
	0.50	Clay (CL), brown; trace of sand	0.0	3.2	96.8	38	21	17	17.6	2.66	2.4
	1.00	Clay (CL), brown; with sand	0.0	8.9	91.1	52	23	29	22.2	2.70	3.1
H1	0.10	Sandy clay (CL), brown; with organic roots*	N/A	N/A	N/A	N/A	N/A	N/A	16.7	N/A	N/A
	0.50	Sandy clay (CH), brown; with trace of organic roots*	N/A	N/A	N/A	N/A	N/A	N/A	21.6	N/A	N/A
	1.00	Clay (CH), gray*	N/A	N/A	N/A	N/A	N/A	N/A	25.8	N/A	N/A
H13	0.10	Sandy clay (CL), brown; with organic roots*	N/A	N/A	N/A	N/A	N/A	N/A	11.8	N/A	N/A
	0.50	Sandy clay (CH), brown; with organic roots*	N/A	N/A	N/A	N/A	N/A	N/A	19.0	N/A	N/A
	1.00	Clay (CH), brownish gray*	N/A	N/A	N/A	N/A	N/A	N/A	25.0	N/A	N/A
H26	0.10	Sandy clay (CL), brown; with organic roots*	N/A	N/A	N/A	N/A	N/A	N/A	15.1	N/A	N/A
	0.50	Sandy clay (CH), brown; with organic roots*	N/A	N/A	N/A	N/A	N/A	N/A	17.5	N/A	N/A
	1.00	Clay (CH), brown*	N/A	N/A	N/A	N/A	N/A	N/A	18.4	N/A	N/A
O13	0.10	Sandy clay (CH), gray; with organic roots*	N/A	N/A	N/A	N/A	N/A	N/A	11.2	N/A	N/A
	0.50	Sandy clay (CH), brownish gray*	N/A	N/A	N/A	N/A	N/A	N/A	15.3	N/A	N/A
	1.00	Clay (CH), brown*	N/A	N/A	N/A	N/A	N/A	N/A	21.1	N/A	N/A

* Visual classification

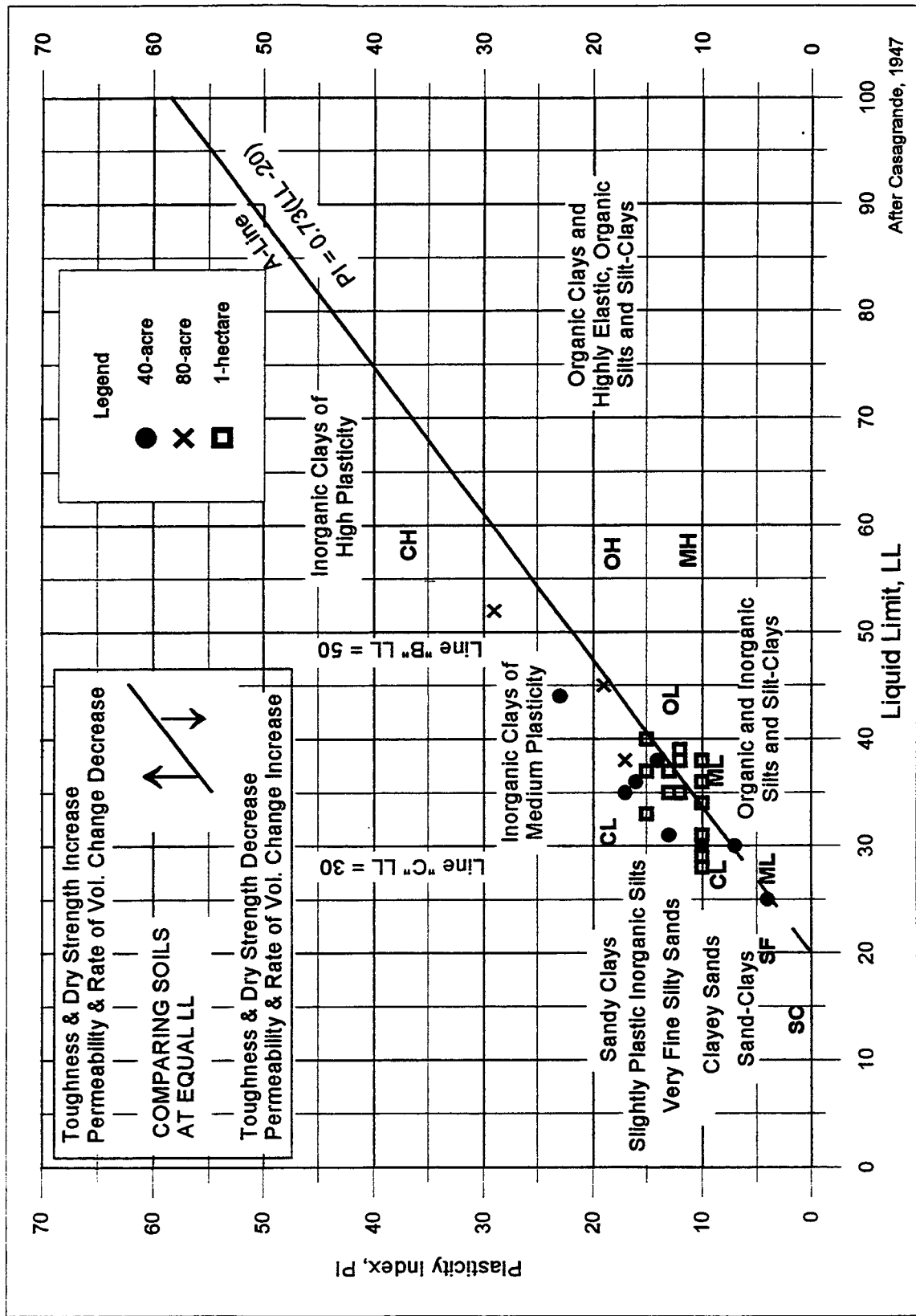


Figure 22. Plasticity chart

XRD analysis

Eleven soil samples were tested to determine the bulk mineralogy and clay minerals present by XRD. A list of the sample locations is shown in Table 4.

Site	Soil Sample Location
40-acre	C7, G7, K7
80-acre	A13

Soil samples were tested from depths of 10, 50, and 100 cm with the exception of location K7 which had samples from depths of 10 and 50 cm, only.

In preparation for the XRD analysis of the bulk samples, a portion of each sample was ground in a mortar and pestle to pass a 45 μ m (No. 325) mesh sieve. For subsequent analysis of the clay-size fraction a slurry of the powder with water was made, suspended on a substrate, and allowed to dry overnight. An XRD pattern was collected on these resultant oriented samples. These samples were then placed in an ethylene glycol atmosphere overnight at room temperature, and a XRD diffraction pattern was collected for each sample.

Bulk sample random powder mounts were analyzed using XRD to determine the mineral constituents present in each sample. All samples had similar mineralogies which included mostly quartz, and Na- and K-feldspar. Quartz was the predominant mineral in all the samples. Na- and K-feldspar were also common constituents in each sample. The patterns also indicate the samples have a small, but finite amount of phyllosilicates present.

To determine the type of phyllosilicate present, oriented samples of the <1 μ m size fraction of each sample were prepared and XRD patterns obtained. It was observed that the <1 μ m size fraction of each sample still contains a dominantly large proportion of quartz and Na- and K-feldspar. Other phases present in minor or trace amounts in most samples include kaolinite, illite or mica, chlorite, a hydroxy-interlayered smectite, and/or smectite. To determine if there was a any expandable component in these fractions, each oriented sample was exposed to an ethylene glycol atmosphere. Smectite, if present, in the sample will expand to 1.7 nm (17 \AA). Chlorites and hydroxy-interlayered smectites will not expand upon exposure to this compound. The data indicate that there is a very small amount of expandable clays present in each sample. Table 5 lists representative chemical compositions for the minerals found in the samples. The stoichiometries of the minerals present in the samples will probably vary from these values (Weiss 1998).

Table 5 Idealized Phase Compositions for Minerals Found at the 40- and 80-acre Sites	
Mineral	Composition
Quartz	SiO ₂
Na-feldspar	NaO _{.8} CaO.1AlSi ₃ O ₈
K-feldspar	KAISi ₃ O ₈
Kaolinite	Al ₄ Si ₄ O ₁₀ (OH) ₈
Illite/Mica	K ₂ Al ₄ (Si ₆ Al ₂)O ₂₀ (OH) ₄
Chlorite	[(R ₂₊ ,R ₃₊) ₆ (Si,Al) ₈ O ₂₀ (OH) ₄][(R ₂₊ ,R ₃₊) ₆ (OH) ₁₂]
Hydroxy-interlayered smectite	Variable composition
Smectite	Variable composition

Dielectric Properties

Laboratory experiments were conducted on soil samples collected from the 40- and 80-acre sites to determine their dielectric properties. These properties control the subsurface propagation of electromagnetic energy and are thus important in assessing and predicting the effectiveness of GPR for detecting UXOs. The electromagnetic wave attenuation values and velocities measured in the laboratory can be used to predict a particular GPR antenna's depth of penetration and to estimate depths to targets or anomalies.

The same samples used for the physical laboratory soil analysis performed above were used to measure the dielectric properties and are again listed below.

<u>Site</u>	<u>Sample Location</u>
40-acre	C1,C7,C13,G1,G7,G13,K1,K7,K13
80-acre	A13,H1,H13,H26,O13

The samples were tested at three times, once at the natural water content, once after air drying, and once at near-saturation conditions. Testing was conducted in a stepped-frequency sweep (5 MHz steps) over the range of 45 MHz to 4.045 GHz. From the complete set of data, EM properties as a function of volumetric moisture content were extracted at frequencies of 100, 200, 495, and 1015 MHz, typical GPR antenna frequencies. A more thorough discussion of electromagnetic theory and laboratory procedures along with a complete data set and a discussion of results are presented in Appendix C.

Jefferson Proving Ground, Phase IV Properties at 200 MHz, All Depths

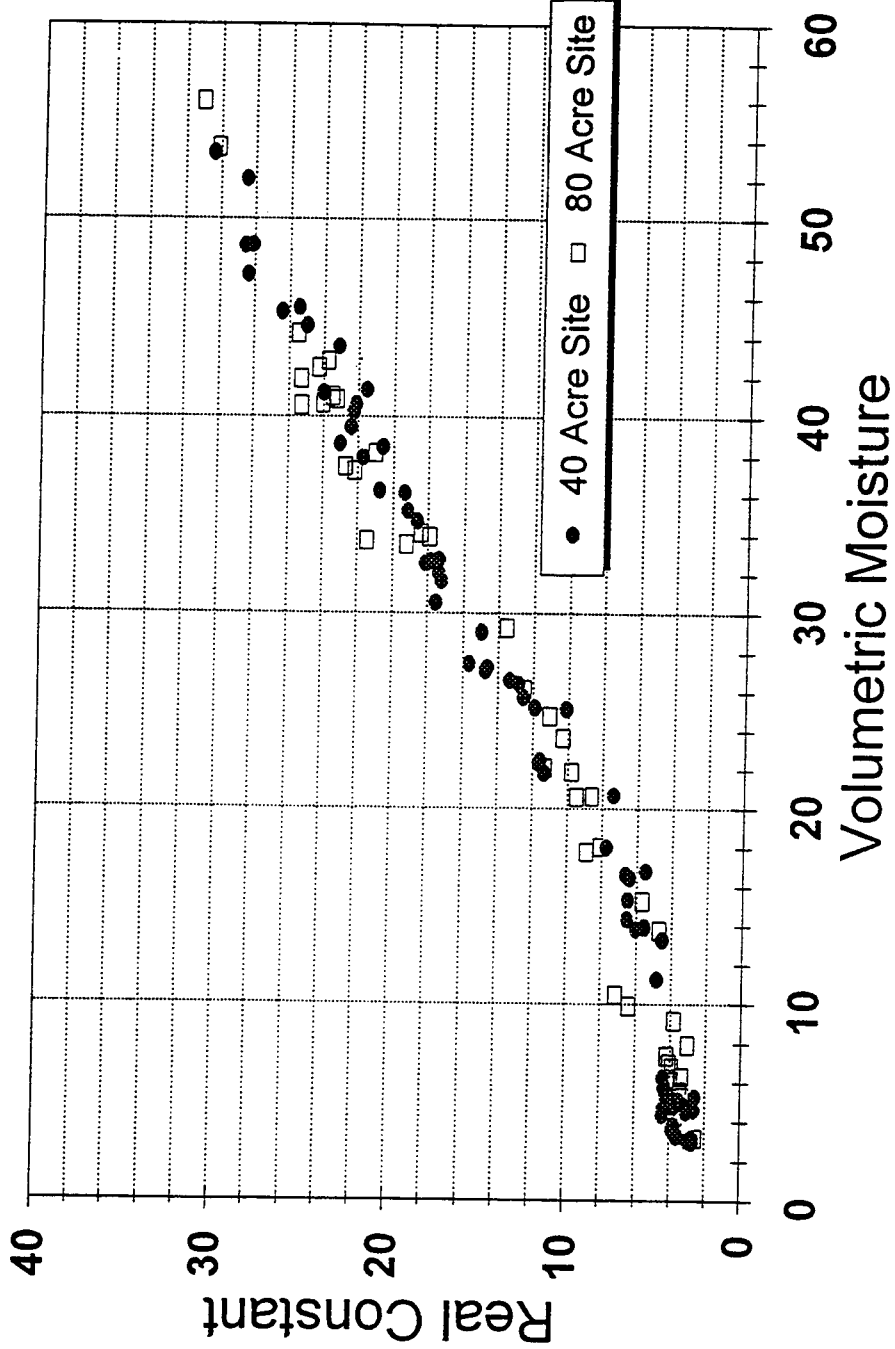


Figure 23. Volumetric moisture versus real constant, 200 MHz, 40- and 80-acre sites

Jefferson Proving Ground, Phase IV

Properties at 200 MHz, All Depths

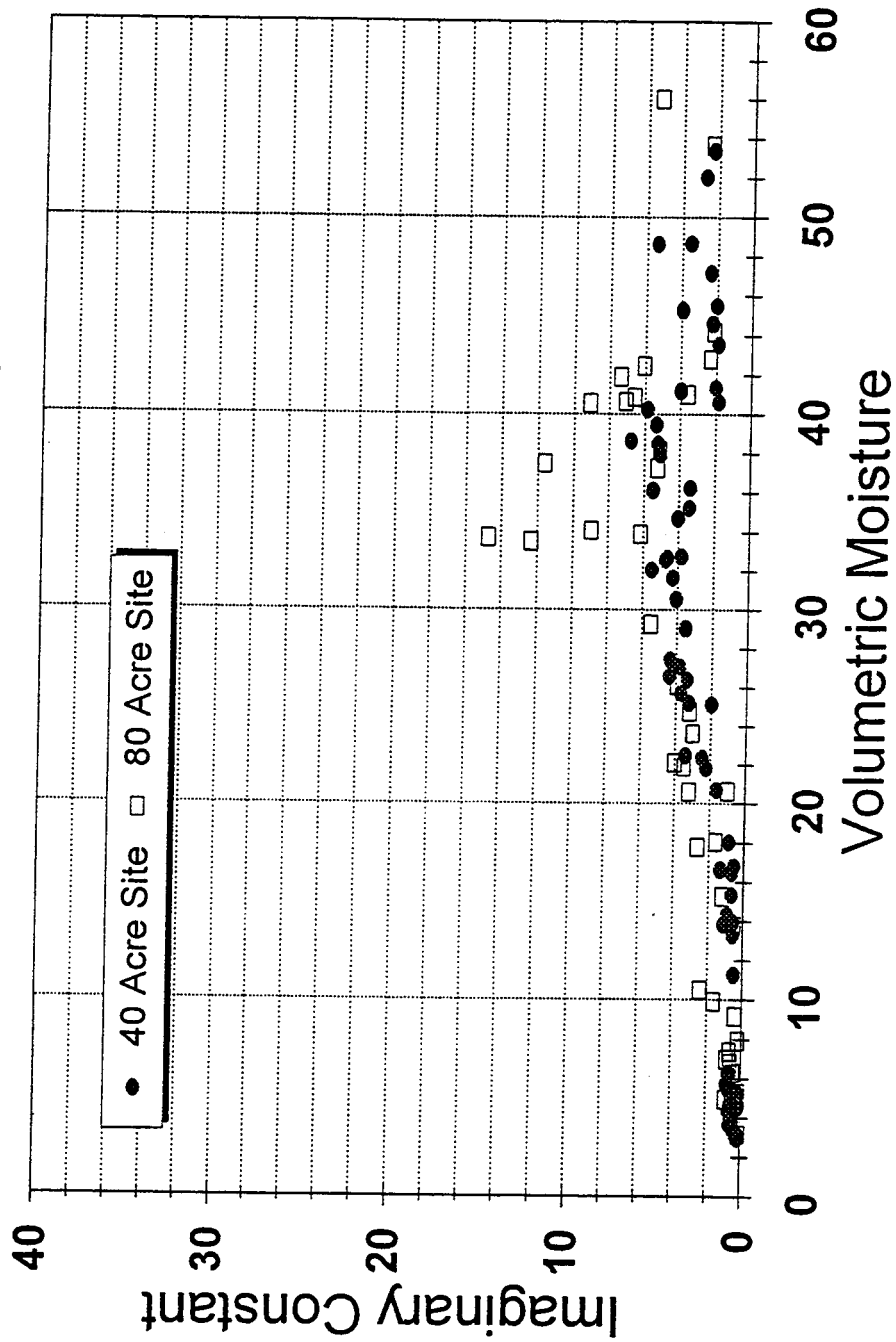


Figure 24. Volumetric moisture versus imaginary constant, 200 MHz, 40- and 80-acre sites

Jefferson Proving Ground, Phase IV Properties at 200 MHz, All Depths

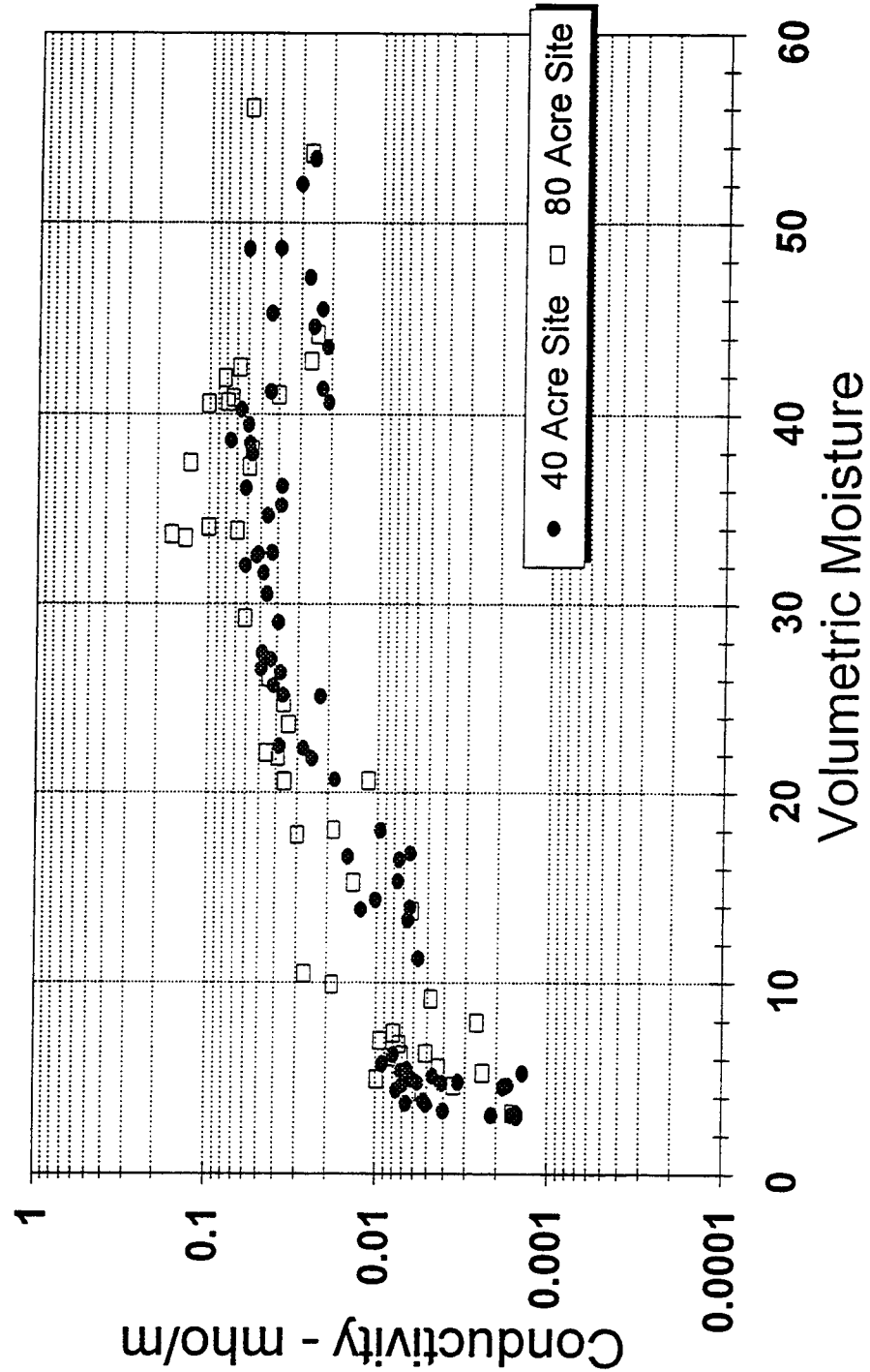


Figure 25. Volumetric moisture versus conductivity, 200 MHz, 40- and 80-acre sites

Jefferson Proving Ground, Phase IV Properties at 200 MHz, All Depths

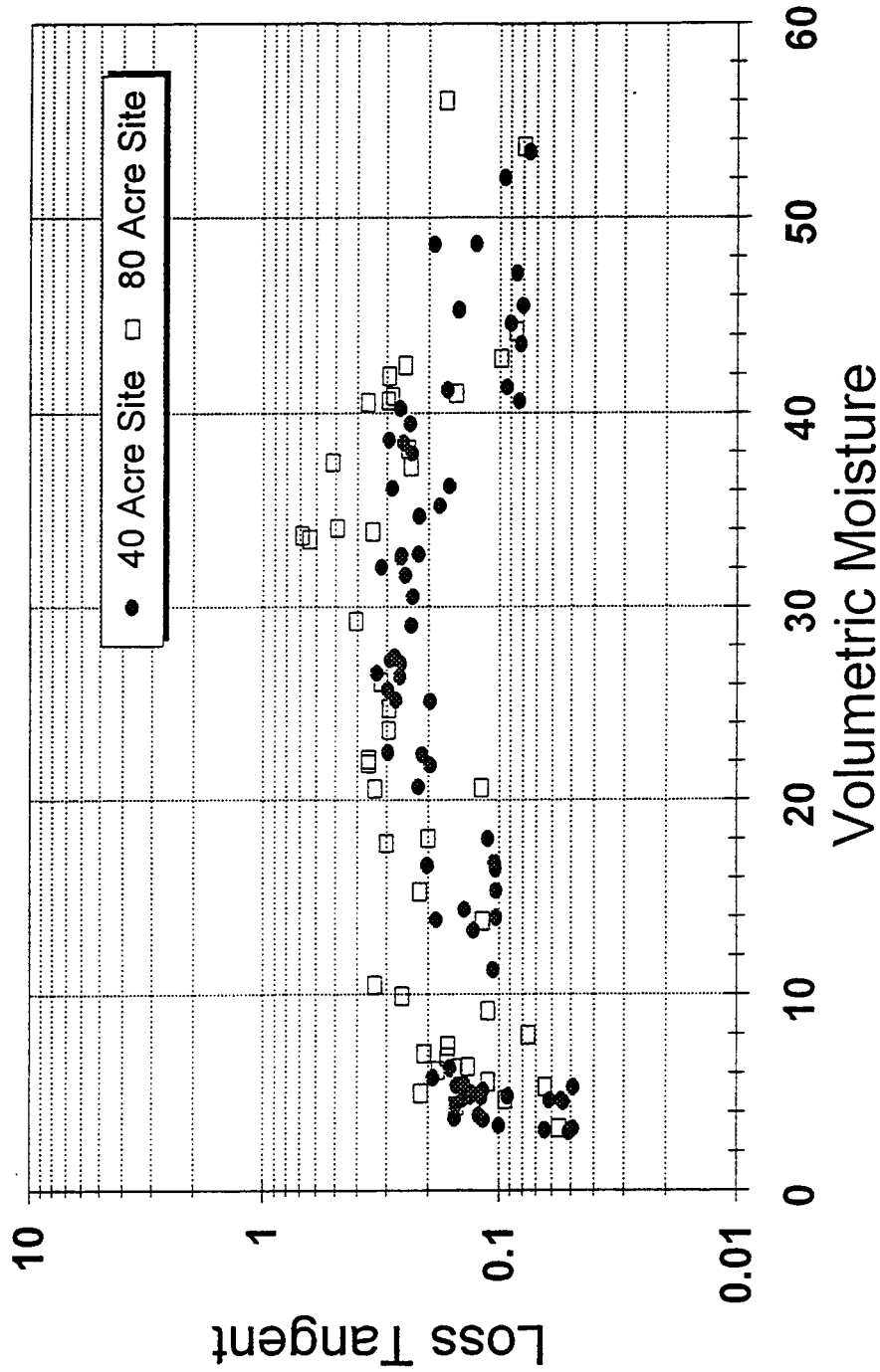


Figure 26. Volumetric moisture versus loss tangent, 200 MHz, 40- and 80-acre sites

Jefferson Proving Ground, Phase IV Properties at 200 MHz, All Depths

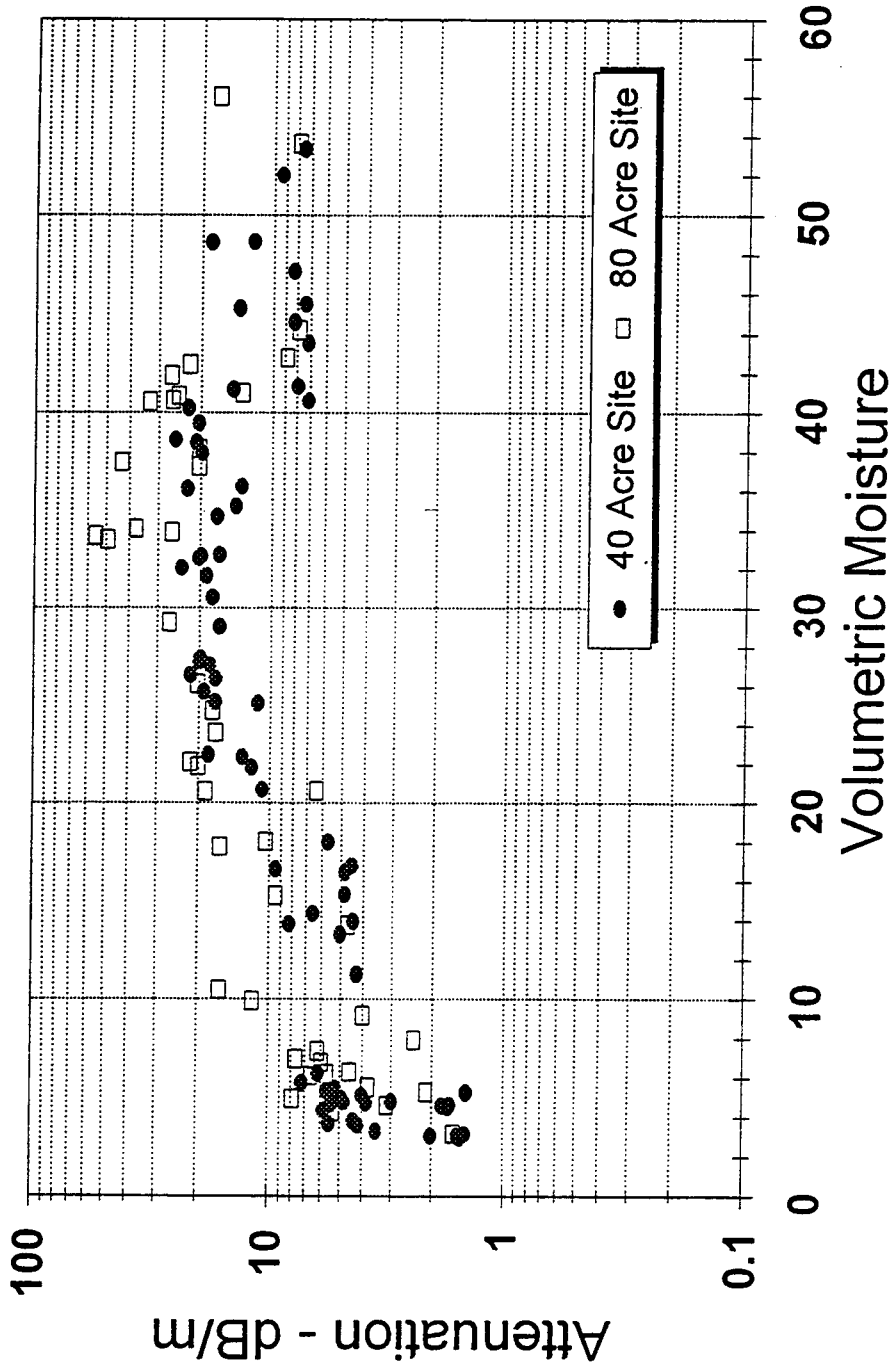


Figure 27. Volumetric moisture versus attenuation, 200 MHz, 40- and 80-acre sites

Jefferson Proving Ground, Phase IV

Properties at 200 MHz, All Depths

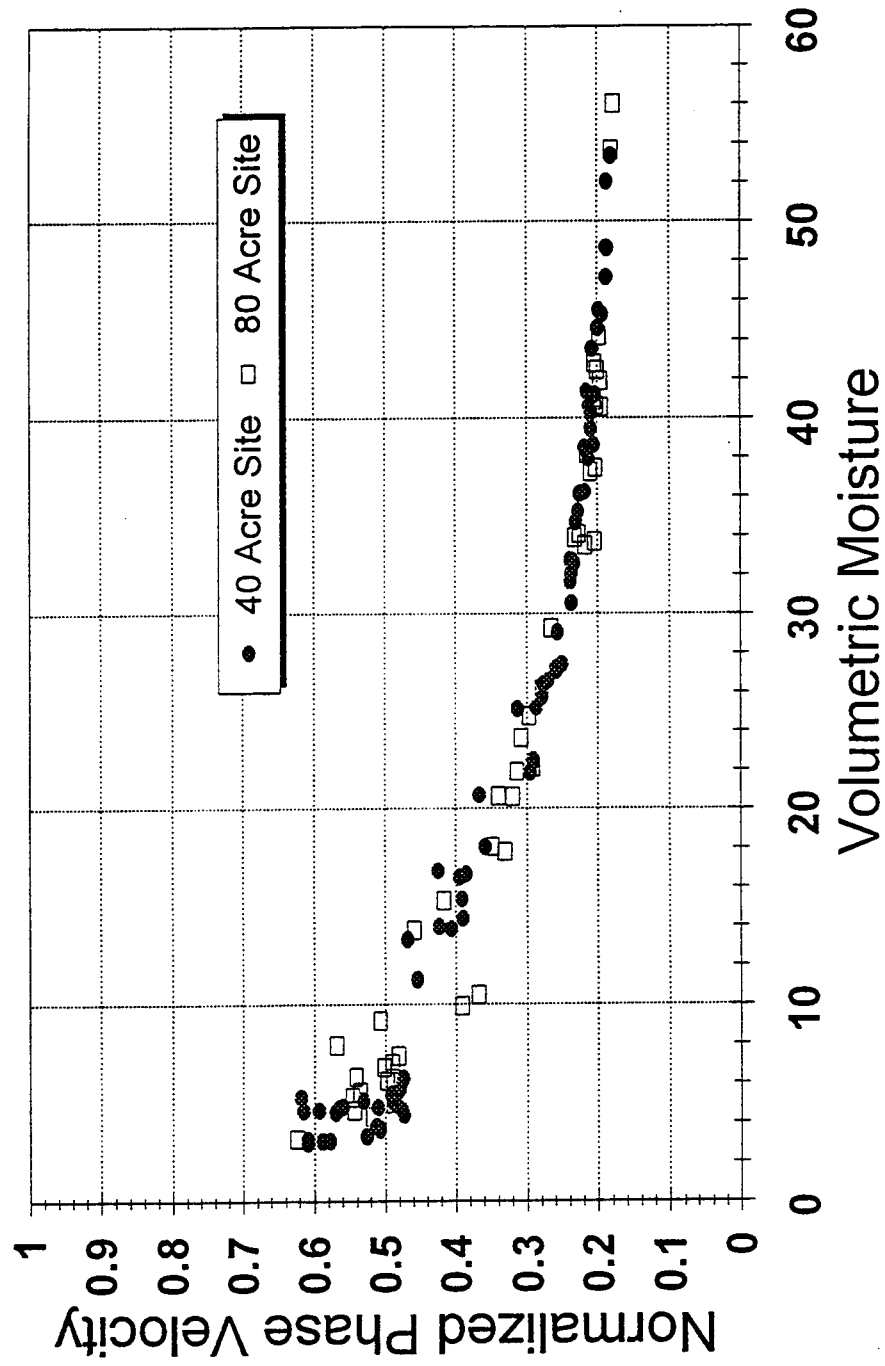


Figure 28. Volumetric moisture versus normalized phase velocity, 200 MHz, 40- and 80-acre sites

Figures 23 through 28 present plots of the real constant (dielectric permittivity), imaginary constant, conductivity, loss tangent, attenuation, and normalized phase velocity each plotted as a function of volumetric moisture for all depths at the 40- and 80- acre sites at 200 MHz, a typical GPR antenna frequency. For an average soil water content of 25 percent the dielectric permittivity of the soil samples is approximately 11. The plot of volumetric moisture versus signal attenuation shows that at a water content of 25 percent the signal attenuation about 20 dB/m.

1-hectare Site

A summary of the 1-hectare site soil properties is provided in Table 6. The 0.1 m deep samples are classified as silt with clay and/or silt and the 0.5 and 1 m deep samples are classified as sandy or silty clay. None of the samples contain gravel-size particles. The samples, on average, contain 81 percent fines (silt and clay-size); and eliminating the samples from location (122E,8N), which are anomalous compared to all other samples, the 1-hectare samples contain an average of 88 percent fines. Figure 22 shows a plot of LL versus PI for the 1-hectare soils and how they compare with the 40- and 80-acre soil samples. The soil water content generally ranges between 20 and 36 percent, the exception being the samples collected at (122E,8N) with a water content of 13-18 percent and at (123E,97N), 1 m depth, with a water content of 18.6 percent. The soil gradation curves for samples collected at the 1-hectare site are provided in Appendix D.

Summary and Conclusions from Soils Analysis

Laboratory analysis indicate that the soils at the 40- and 80-acre sites are very similar in terms of classification. All of the soil samples, with the exception of one, are classified as either (CH) or (CL) and in general are characterized as clays or sandy clays. The one exception was the sample collected at the 40-acre site at depth of 0.1 m at location G7 which is classified as ML, sandy clayey silt. Plotted on a plasticity chart, the soil samples are very near the A-line and exhibit little plasticity. Average water contents, even under very dry environmental conditions, show an increase with depth and range from 13.9 percent at a depth of 0.1 m to 20.3 percent at a depth of 1 m.

The samples are characterized as clays or sandy clays according to the USCS. This classification is based in part on grain size and not mineralogy. In the USCS, soil particles passing the No. 200 sieve are considered silt or clay. However, in the case of the JPG soils XRD analysis show that these soils contain little or no clay minerals. The XRD analysis indicate that these soils consist chiefly of very fine grained (silt or clay-sized) quartz particles. This finding is consistent with other studies of loess in the southern United States (Rodbell et al. 1997), which show a predominant amount of quartz, and also with studies in the interior of Alaska (Péwé 1955).

The general results of the laboratory EM properties show that the dielectric permittivity values of the soil samples collected at the 40- and 80-acre sites are relatively high. For the range of frequencies tested, 100 to 1015 MHz, the values

range between approximately 10 and 12. The soils also exhibit high signal attenuation at typical field soil water contents. For 200 MHz and typical water content conditions, the attenuation approaches 20 dB/m.

The 1-hectare site soils exhibit similar characteristics as those of the 40- and 80- acre site with the exception of water content. Generally, the 1-hectare site water contents are higher than those found at the 40- and 80-acre sites. The average water content of the 1-hectare site soils, for all depths, is 27.6 percent. However, the 1-hectare site samples were collected in October, while soil conditions were wet, versus August, when samples were collected at the 40-and 80-acre site, and soil conditions at the sites were drier.

Table 6
Summary of Soils Laboratory Analysis, 1-hectare Site

Location	Depth m	Classification	% Gravel	% Sand	% Fines	Liquid Limit	Plastic Limit	Plasticity Index	Natural Water Content, %
27.5E, 73N	0.10	Sandy clayey silt (ML), brown	0	12.9	87.1	34	24	10	26.6
	0.50	Silty clay (CL), brown	0	10.5	89.5	31	21	10	24.4
	1.00	Sandy clay (CL), brown	0	22.1	77.9	33	18	15	20.7
65E, 10.5N	0.10	Clayey silt (ML), brown	0	5.7	94.3	36	26	10	30.7
	0.50	Silty clay (CL), brown	0	6.1	93.9	40	25	15	30.7
	1.00	Silty clay (CL), brown	0	11.6	88.4	35	23	12	29.0
122E, 8N	Surface	Sandy clayey silt (ML), brown	0	41.2	58.8	35	22	13	17.4
	0.50	Sandy clay (CL), brown	0	56.3	43.7	31	21	10	13.1
	0.10	Clay (CL), brown	0	47.0	53.0	29	19	10	15.1
123E, 97N	Surface	Silty clay (CL), brown	0	9.1	90.9	37	24	13	31.3
	0.50	Clay (CL), brown	0	8.1	91.9	37	22	15	24.7
	0.10	Sandy clay (CL), brown	0	19.4	80.6	28	18	10	18.6
40E, 23N	0.10	Clayey silt (ML), brown	0	11.0	89.0	38	26	12	33.0
52.5E, 85.5N	0.10	Sandy clayey silt (ML), brown	0	13.6	86.4	39	27	12	35.5
77.5E, 60.5N	0.10	Sandy silt (ML), brown	0	16.4	83.6	38	28	10	33.6

6 Geophysical Test Results and Interpretation

40-acre Site

Electrical resistivity soundings

The results of the Schlumberger resistivity soundings conducted at the 40-acre site are summarized in Figures 29 through 32. Figures 29 through 31 show the sounding results obtained along north-south lines C, G, and K, respectively, whereas Figure 32 shows the results of the data obtained along east-west trending line 7. Generalized results indicate a 3- or 4-layer model. The 2 models are similar with the exception that an intermediate layer is interpreted between the surface layer and the low resistivity layer for the 4-layer model. The top layer in both models is relatively thin, less than 1 m in thickness, and has a relatively high resistivity ranging between about 150 and 1000 $\Omega\text{-m}$ (1-7 mS/m). The intermediate layer interpreted in the 4-layer model is about 1.4 m thick and has a resistivity of approximately 110 $\Omega\text{-m}$ (9 mS/m). The upper and intermediate layers appear to consist primarily of silts with the amount of clay and/or moisture increasing with depth. Both models indicate an underlying very low resistivity layer, exhibiting a resistivity of about 35 $\Omega\text{-m}$ (29 mS/m) and a thickness of 3.5 m. This low resistivity layer is presumed to correspond to a moist to wet soil with a high clay content. The deepest layer interpreted for both models has a relatively high resistivity of approximately 1250 $\Omega\text{-m}$ (<1 mS/m) and is found at depths ranging between 1.9 and 7.0 m. This layer is interpreted to be the limestone/dolomite bedrock. The sounding curve and model for each resistivity sounding are presented in Appendix E.

DICON probe measurements

The results of the DICON probe measurements are shown in Table 7. The range of values for the relative dielectric permittivity, conductivity, and wave speed are 8.6 to 35.3, 7.1 to 98.4 mS/m, and 0.051 to 0.102 m/ns, respectively. The average values for the relative dielectric permittivity, conductivity, and wave speed for the 10 cm depth samples are 14.4, 14.2 mS/m, and 0.081 m/ns, respectively. The average values for the relative dielectric permittivity, conductivity, and wave speed for the 50 cm depth samples are 24.2, 37.4 mS/m, and 0.064 m/ns, respectively.

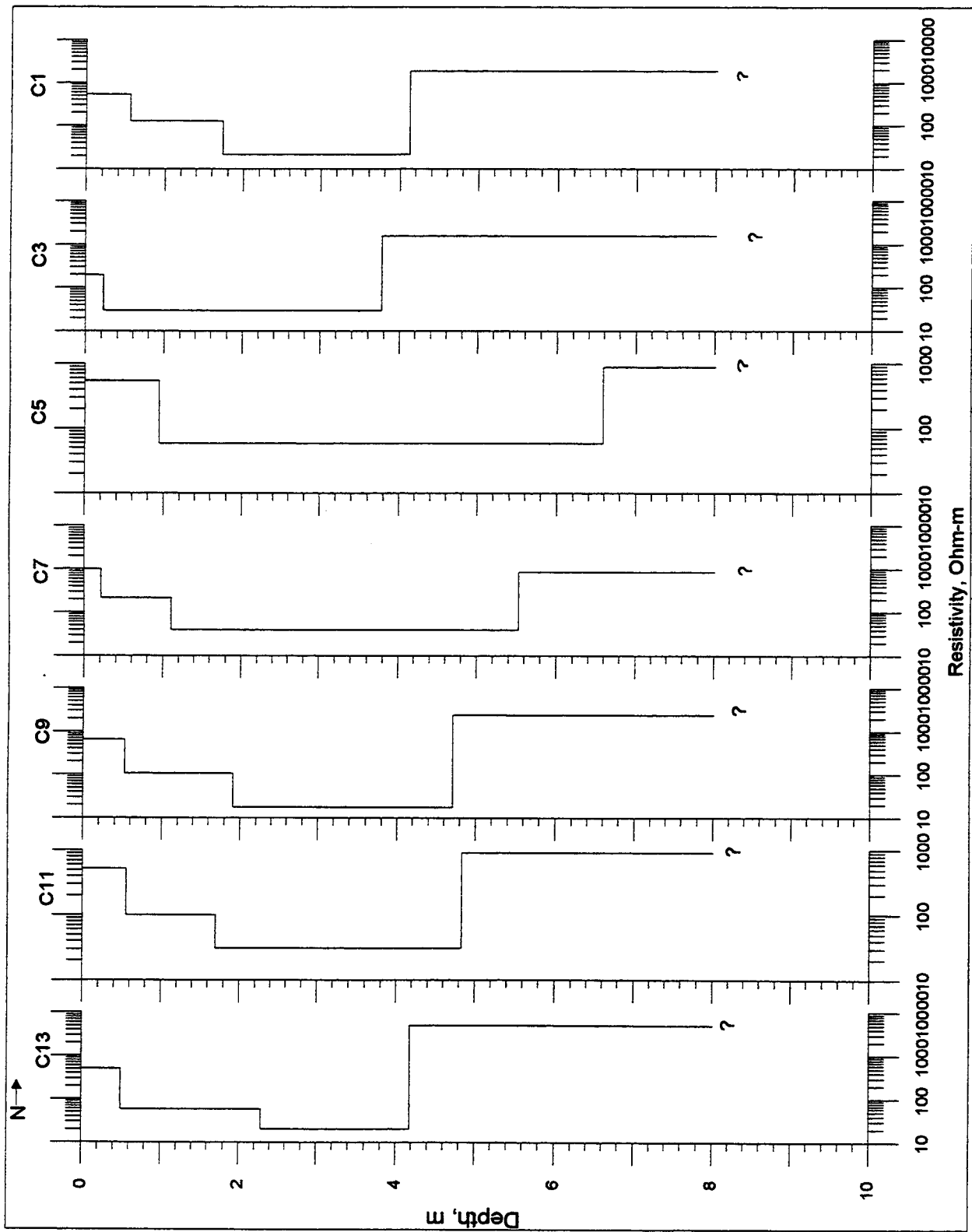


Figure 29. VES modeling results, Line C (north-south), 40-acre site

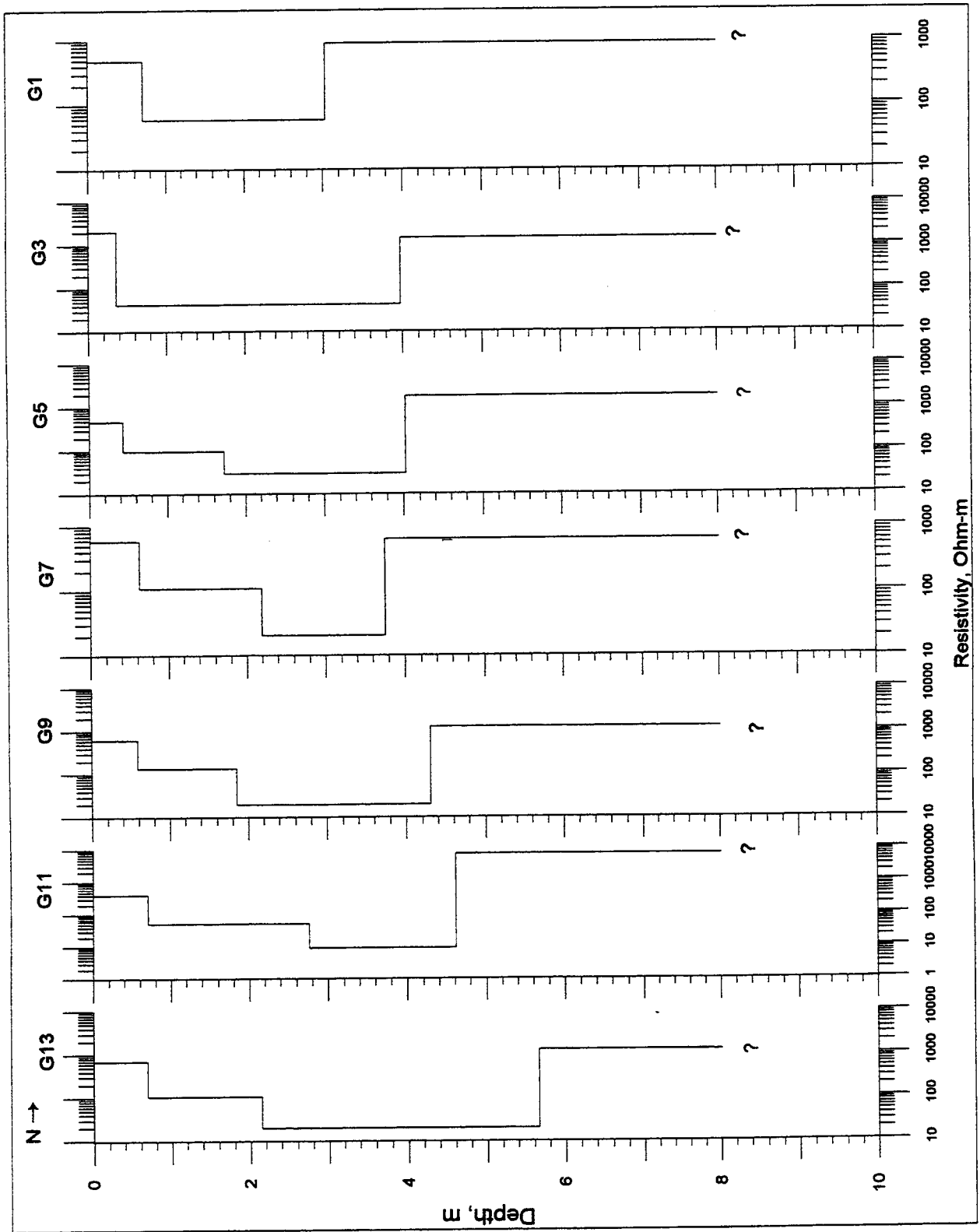


Figure 30. VES modeling results, LineG (north-south), 40-acre site

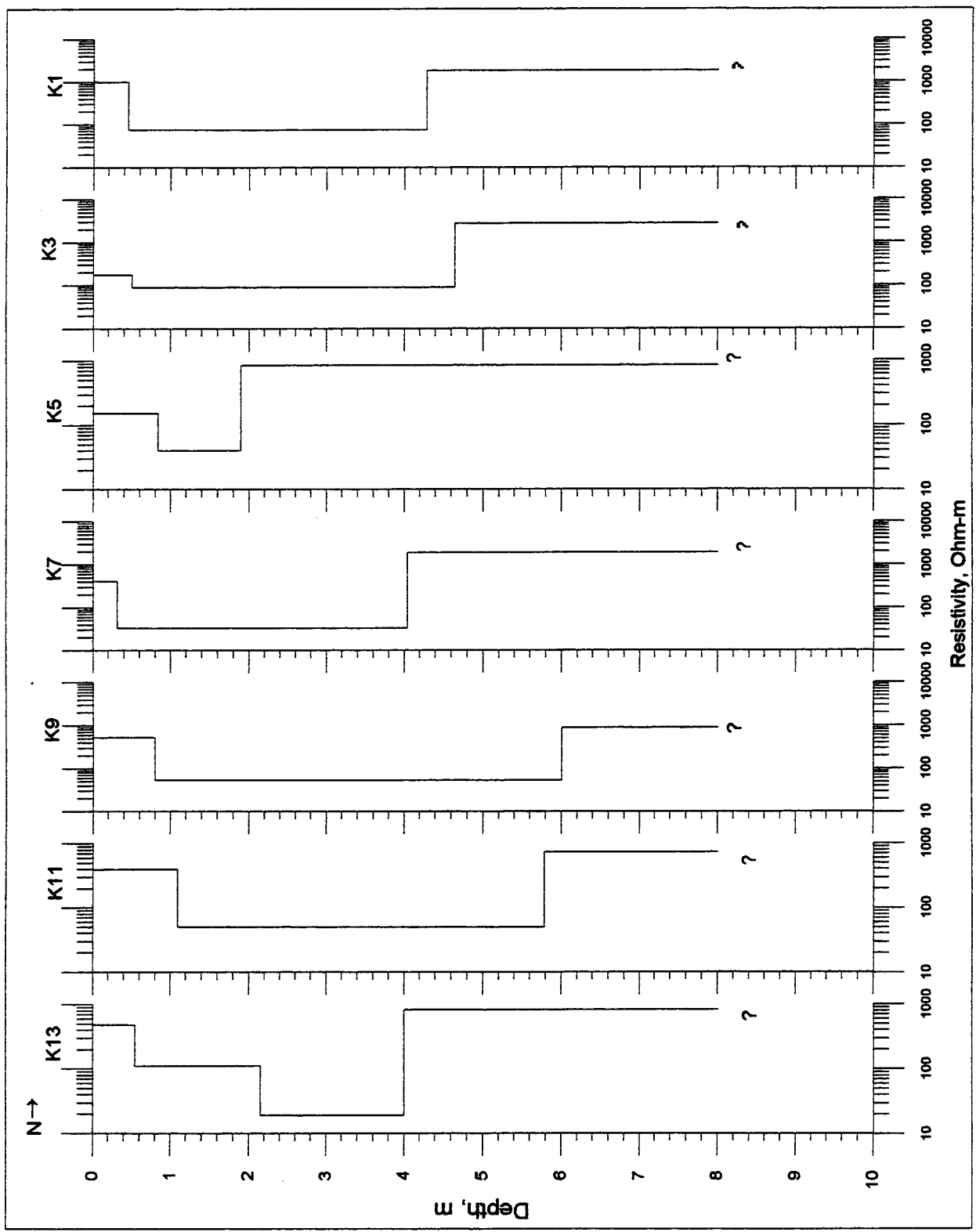


Figure 31. VES modeling results, Line K (north-south), 40-acre site

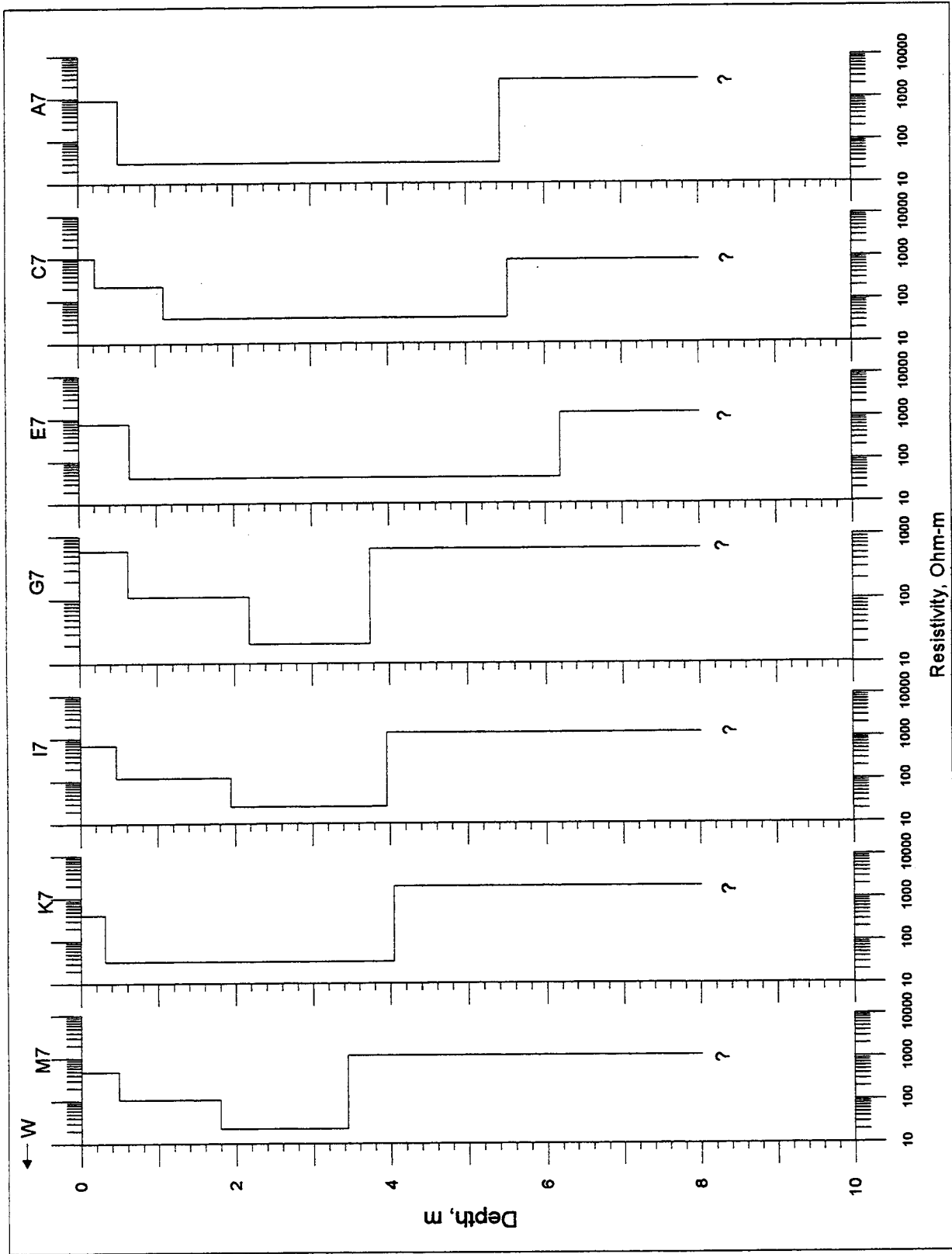


Figure 32. VES modeling results, Line 7 (east-west), 40-acre site

Table 7 DICON Probe Data, 40-acre Site				
Location	Depth, m	Relative Dielectric Permittivity	Conductivity mS/m	Wave Speed m/ns
C1	0.10	16.0	13.9	0.075
	0.50	25.6	36.1	0.059
C3	0.10	17.5	22.6	0.072
	0.50	30.9	98.4	0.054
C5	0.10	23.5	21.9	0.062
	0.50	24.1	28.5	0.061
C7	0.10	14.7	11.2	0.078
	0.50	29.2	44.6	0.056
C9	0.10	9.7	10.5	0.096
	0.50	21.0	24.5	0.066
C11	0.10	14.1	16.0	0.080
	0.50	17.2	18.1	0.072
C13	0.10	10.0	12.8	0.095
	0.50	13.0	14.9	0.083
G1	0.10	10.9	10.7	0.091
	0.50	21.4	27.9	0.065
G3	0.10	13.1	11.5	0.083
	0.50	29.9	55.4	0.055
G5	0.10	15.2	15.4	0.077
	0.50	31.5	55.8	0.054
G7	0.10	18.5	14.6	0.070
	0.50	26.1	35.4	0.059
G9	0.10	18.1	19.0	0.071
	0.50	23.3	29.6	0.062
G11	0.10	17.9	20.2	0.071
	0.50	22.4	29.4	0.063
G13	0.10	12.3	13.1	0.086
	0.50	22.4	29.4	0.063
K1	0.10	13.1	11.5	0.083
	0.50	28.9	47.3	0.056
K3	0.10	16.3	17.9	0.074
	0.50	26.1	44.7	0.059
K5	0.10	13.5	18.4	0.082
	0.50	19.0	30.2	0.069

(Continued)

Table 7 (Concluded)				
Location	Depth, m	Relative Dielectric Permittivity	Conductivity mS/m	Wave Speed m/ns
K7	0.10	11.6	12.5	0.088
	0.50	35.3	96.5	0.051
K9	0.10	19.1	12.7	0.069
	0.50	29.2	40.1	0.056
K11	0.10	12.3	12.4	0.086
	0.50	21.4	24.1	0.065
K13	0.10	8.6	11.0	0.102
	0.50	20.3	27.9	0.067
A7	0.10	8.8	7.1	0.101
	0.50	22.4	22.6	0.101
E7	0.10	17.9	17.3	0.071
	0.50	23.6	32.2	0.062
I7	0.10	14.3	11.6	0.079
	0.50	17.5	18.7	0.072
M7	0.10	12.1	10.6	0.086
	0.50	23.2	22.5	0.062
Average	0.10	14.4	14.2	0.081
	0.50	24.2	37.4	0.064

EM31 surveys

Figures 33 and 34 respectively, present the results of the conductivity and inphase surveys conducted at the 40-acre site. The conductivity values generally range between 10 and 30 mS/m (33 and 100 Ω -m). The average conductivity value obtained from the DICON probe falls within this range of values. The EM31 conductivity results (10 to 30 mS/m) agree with the resistivity sounding values (approximately 17 mS/m) for the upper 4-6 m. The lowest conductivity values are found at the north central part of the site in a topographically low area. A wide, high conductivity lobe extends from approximately (-400E,600N) to (-850E,-20N); no visible topographic features are correlated with this high conductivity zone. The inphase results generally range between -0.9 and 0.8 ppt and show considerable variability across the site. Since the inphase readings are sensitive to metallic objects it is possible that the high degree of variability in the inphase values may be attributed to the large amount of buried metal at the site.

Figure 35 shows the 40-acre soils map with the superimposed EM31 conductivity results. The figure shows the correlation of soil type and conductivity.

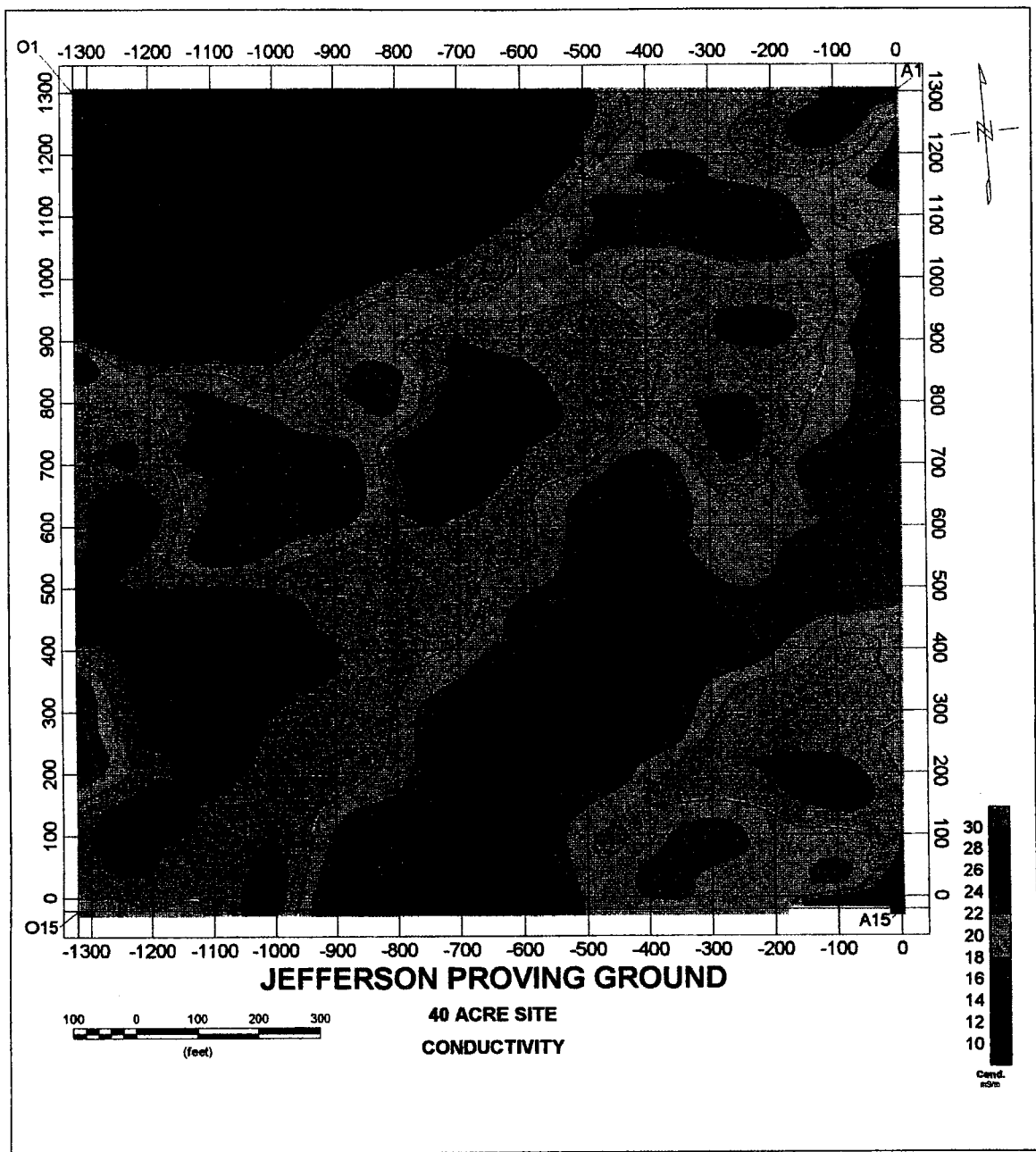


Figure 33. Conductivity survey results, 40-acre site

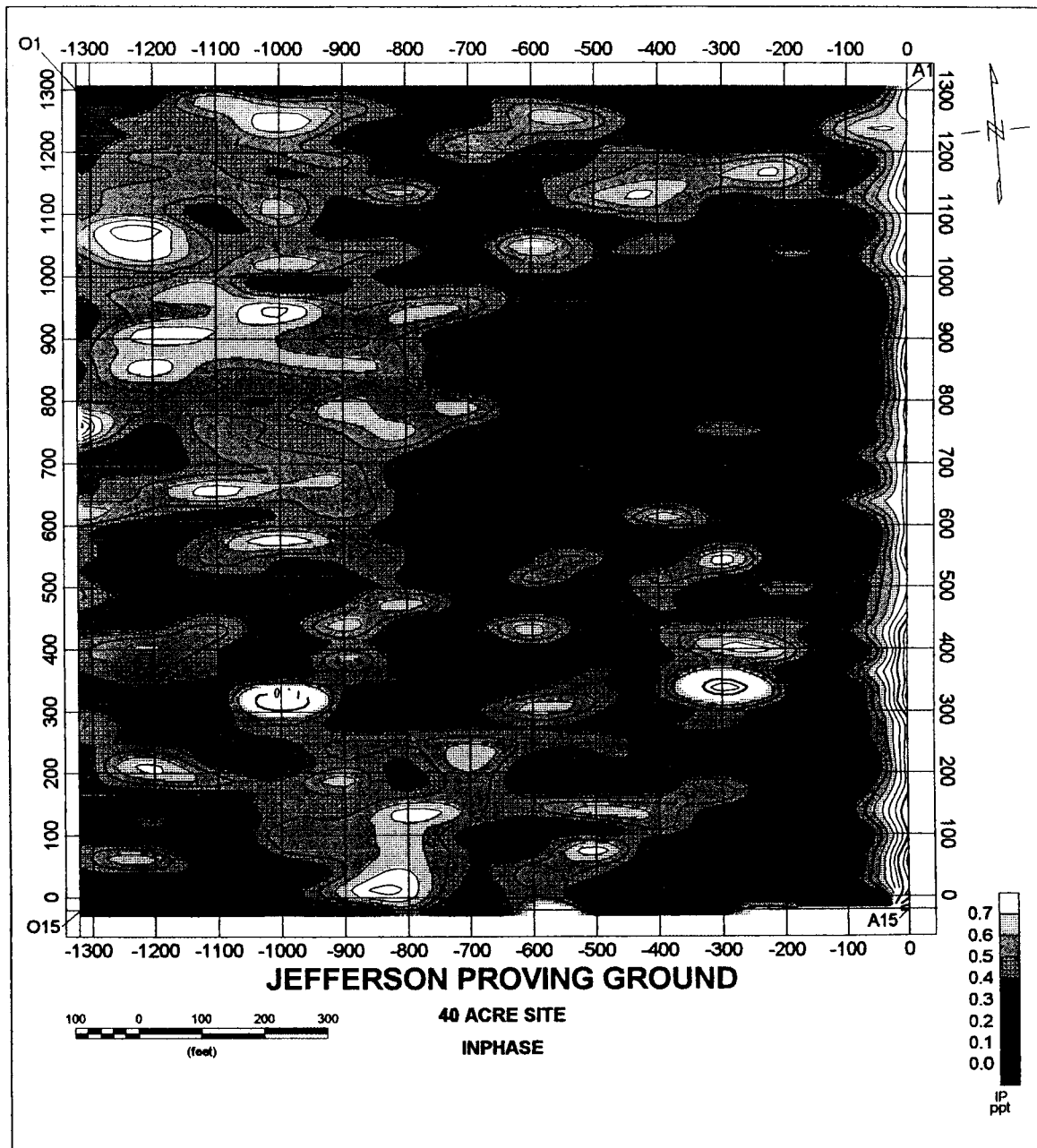


Figure 34. Inphase survey results, 40-acres site

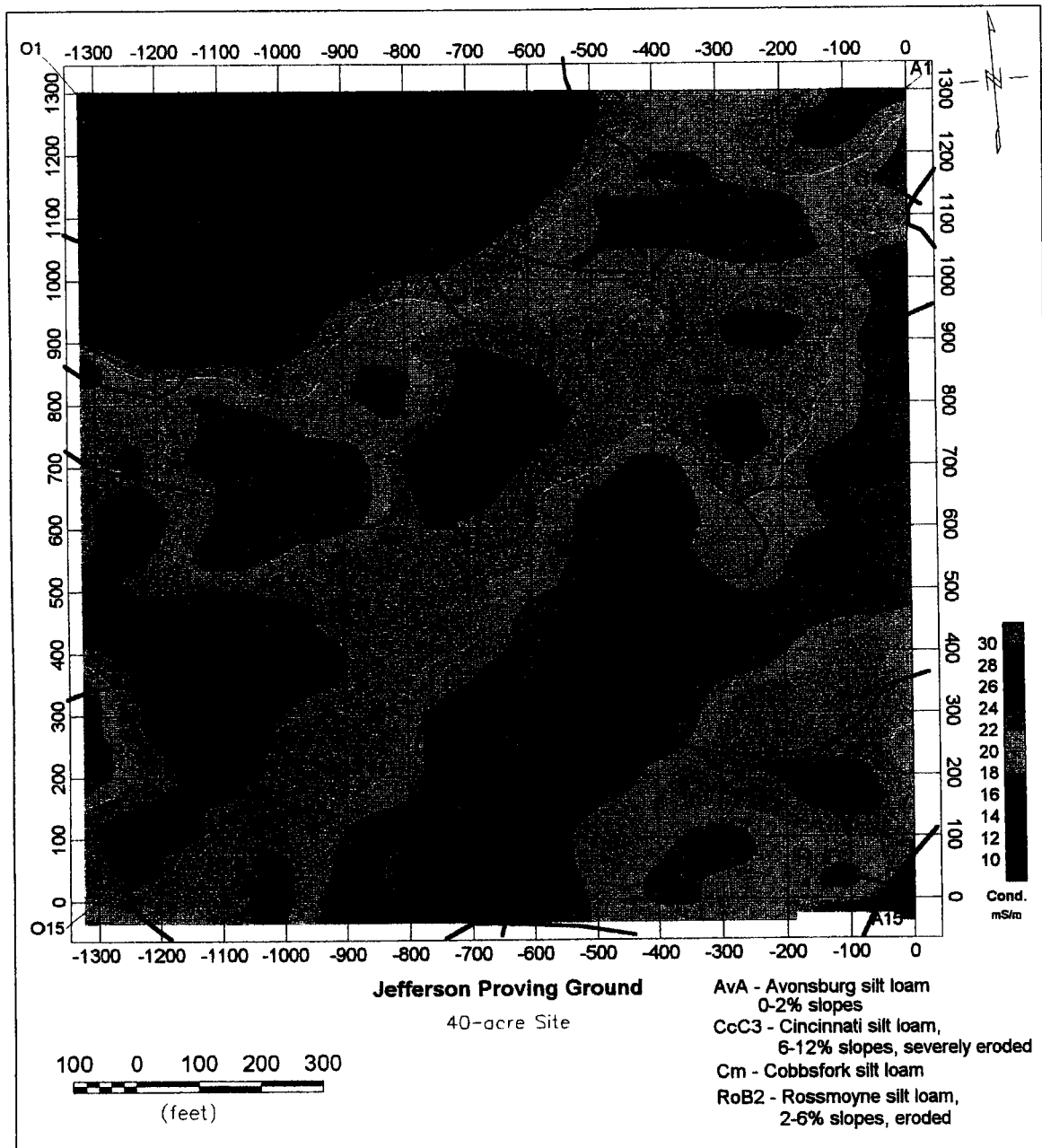


Figure 35. Conductivity results superimposed on soils map, 40-acre site

Ground penetrating radar surveys

Postprocessing and display of data

The recorded data was first band-pass-filtered (very wide settings; e.g. 50-600 MHz for the Model 5103 antenna) to alleviate high-frequency electronic noise and low-frequency, above-surface, clutter. The number of data traces between event markers over the emplaced targets were normalized to compensate for changes in dragging speed. The longer profiles with the 100-foot marker spacing are not normalized because vehicle speed varied between any two markers.

Both linear and nonlinear gray-scale formats were used to indicate signal strength. An amplitude format was used to display the profiles for the buried control targets. In this format, positive phase is indicated by lighter tones and negative phase by darker tones. An intensity format was used to display the profiles of the permanent targets at JPG. In this format, which is insensitive to phase, strength is indicated by the intensity of the darker tones.

Profile interpretation

The main objectives of the profile analysis are to determine a range of ϵ' values for the site soil and if ordnance targets had been detected. The permittivity analysis uses the diffractions caused by radar scattering from targets. In this method, the hyperbolic shape of the diffractions is matched with theoretical hyperbolas for a given value of ϵ' (Jezek et al. 1979; Clarke and Bentley 1994; Arcone et al. 1998). The main disadvantages of this approach are (1) the hyperbolas can actually be responses to linear soil inclusions, in which case the hyperbolas are actually the distorted reflections that result when the transect obliquely intersects the inclusion direction (Jezek et al. 1979) and are thus, artificially wide; and (2) an erratic towing speed, which would distort the hyperbolic image. Item (1) was not considered important because of the depositional process of the soil (glacial drift and loess) and because of probable historical tilling. Number (2) is a concern and for this reason a statistical study is presented.

Target detection depends on the presence of either or both diffractions and reflections, and also on their phase polarity. Both the strength and phase polarity of a reflected/diffracted event depend on the reflectivity of a target, which is determined by its Fresnel reflection coefficient R , where

$$R = (\epsilon_s^{*1/2} - \epsilon_t^{1/2}) / (\epsilon_s^{*1/2} + \epsilon_t^{1/2}), \quad (6)$$

and ϵ_t is the complex permittivity for the target medium (Wait 1970). Although this formula applies to plane wave incidence upon large flat reflectors, its use is invoked because of the small *in situ* wavelengths (30 cm at 300MHz) and large nature of some of the targets known to be buried at JPG and because it predicts the correct

phase polarity. For a metal target, assumed to be ordnance, ϵ_r is orders of magnitude higher than ϵ_r^* and produces a wavelet with a phase structure opposite to that produced when ϵ_r is lower than ϵ_r^* .

It is unlikely that any profiled geologic or organic inhomogeneity in the soil had a higher ϵ_r than that of the soil itself. Consistent horizons were virtually absent in the data, which means that electrically important changes, such as in moisture content, were gradational. The soil-limestone interface is likely not detectable, since ϵ_r' of limestone is generally between 8 and 10 (Parkhomenkho 1967), which is near that of the soil and resulting in R being approximately equal to 0. Also, the limestone is generally too deep (see Chapter 3), considering the high EM attenuation (see Chapter 4 and Appendix C).

Results and discussion

Control studies. The objectives for the control studies were to obtain profile responses and wavelet forms for buried metal reflectors, as well as soil moisture and conductivity profiles. The studies were conducted either outside or along the perimeter of the 40-acre site (Figure 36). Two, 9-inch (23 cm) diameter metal disks were buried at depths of 11 (28 cm) and 23 (58 cm) inches. The removed soil was highly compact and did not appear to have excess moisture. Therefore, it is presumed that no significant soil drying took place between removal and reburial. The 300- and 600-MHz diffraction profiles from the deeper target (Figure 37) (the response to the more shallow target is not sufficiently separated from the direct coupling between antennas to facilitate analysis) best fit theoretical diffraction hyperbolas for $\epsilon_r' = 9.3$ and 8.6 at 300- and 600- MHz, respectively. The values of ϵ_r' , computed from the wavelet round-trip travel time when the antennas are over the center of the targets, are 9.5 and 8.7, respectively. In accordance with the measurements, dielectric dispersion theory (eq. 4, and discussed below) predicts that the 600-MHz value should be slightly less than the 300-MHz value

The accompanying profiles in Figure 37, whose positions within the traces are indicated by arrows, show the forms of the scattered wavelets within the diffractions. The wavelets have a negative-positive-negative sequence to the phase polarity of the dominant half-cycles. This sequence is typical for the relative polarity wiring of GSSI antennas and is characteristic of targets whose wave impedance (eq. 6) is higher than that of the surrounding media. Targets characterized by an ϵ_r' value less than that of the soil matrix would produce a similar wavelet, but with opposite phase polarity of the individual half-cycles. The local frequency is indicated for the wavelets.

The amplitude along the 600-MHz hyperbolic asymptotes in Figure 37 rapidly fades with distance from the target. This indicates a very high soil attenuation rate per meter; the change in antenna directivity with angle to the target (discussed later) is an insignificant loss factor. Commercial GPR systems at these frequencies commonly have a performance figure of about 100–120 dB and a dynamic range (the amplitude range visible in any particular trace) of about 60–70 dB. This latter range is consistent with the gain added before recording and with soil attenuation rates discussed later.

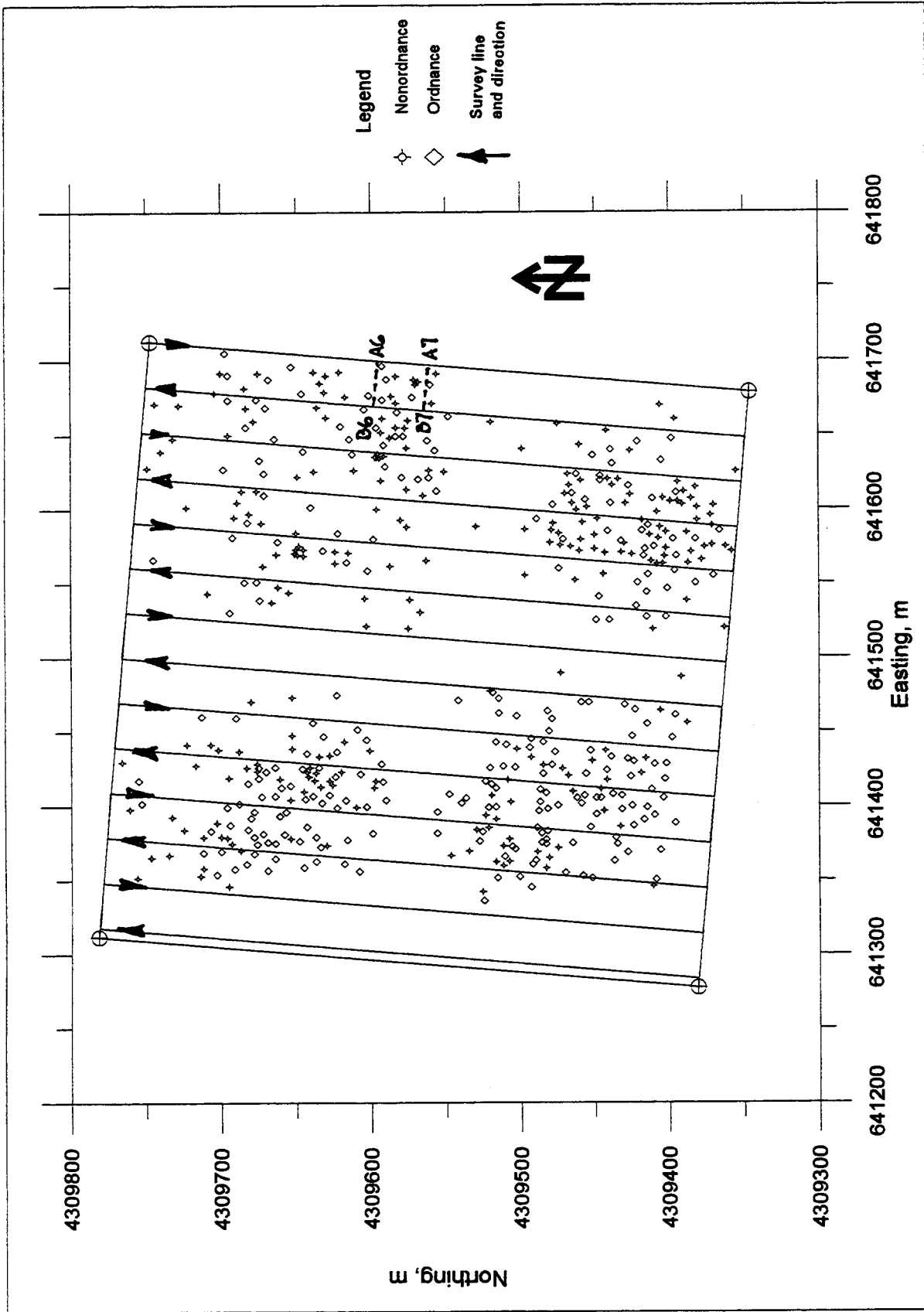


Figure 36. Location and distribution of ordnance and non-ordnance items, 40-acre site (continued)

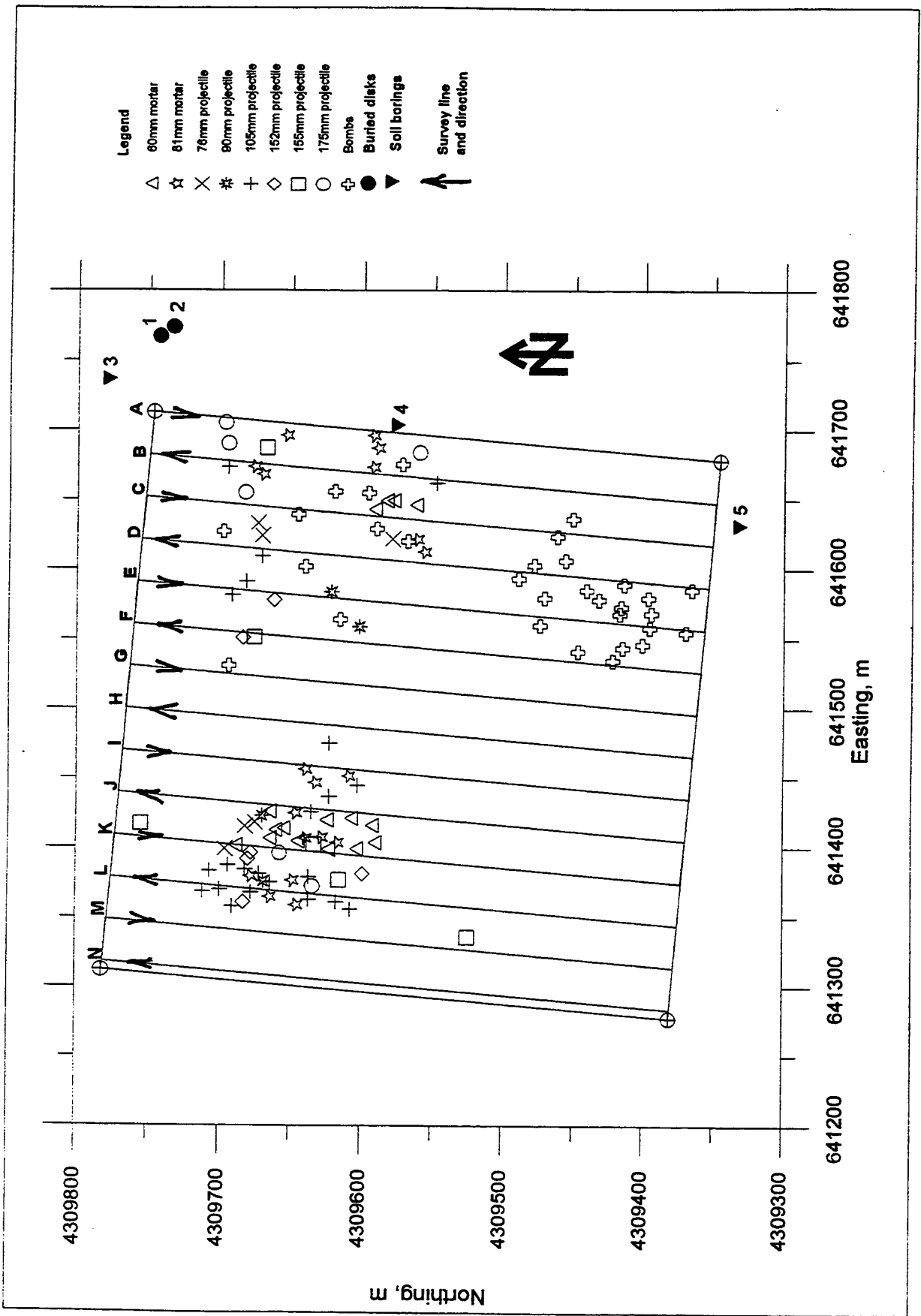


Figure 36. Location and distribution of ordnance and non-ordnance items, 40-acre site (concluded)

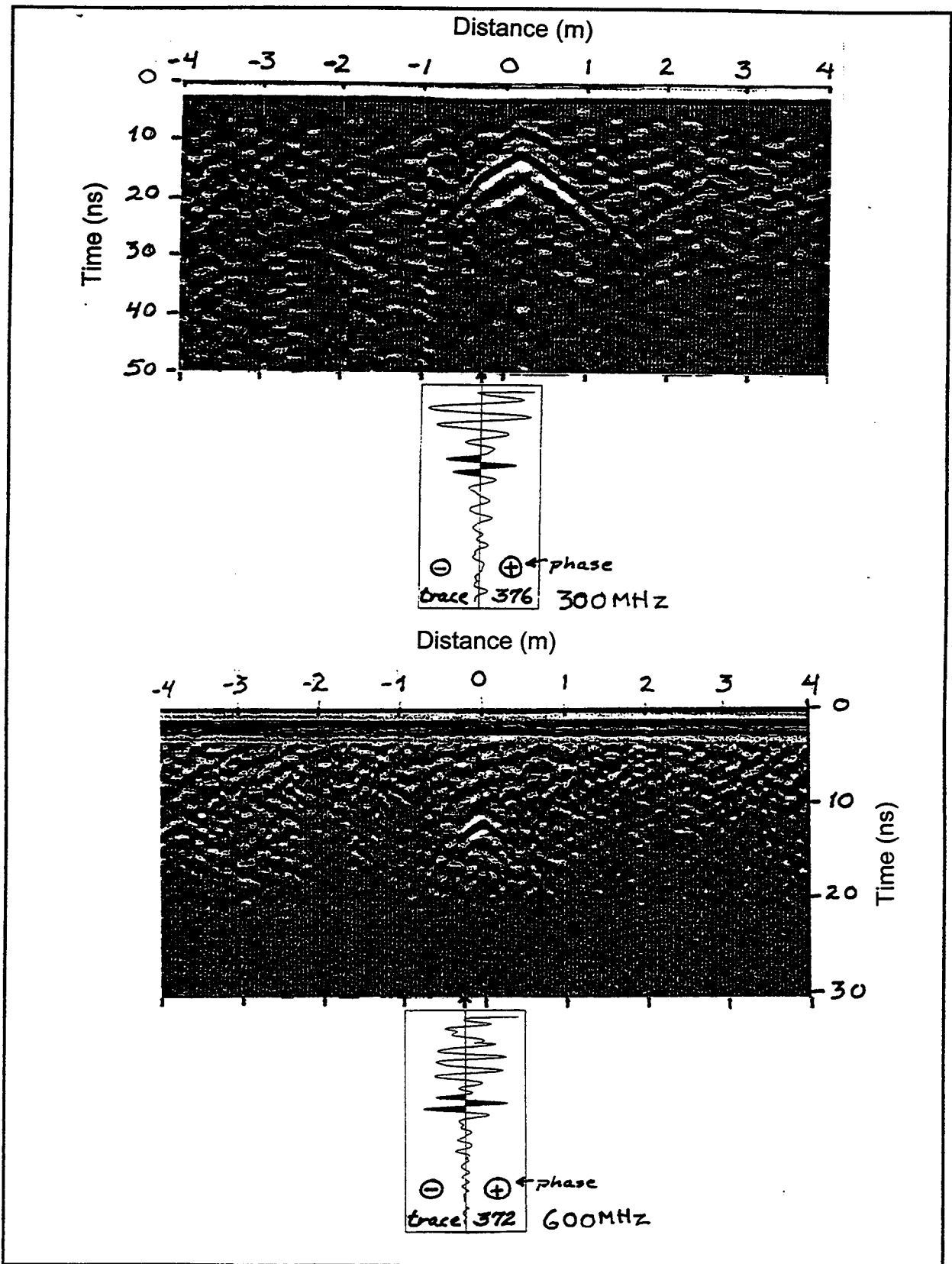


Figure 37. Diffraction profile and waveform response of 300 and 600 MHz antennas to a metal disk buried 23 inches deep, 40-acre site
 Chapter 6 Geophysical Test Results and Interpretation

The volumetric water content profiles of soil core samples (obtained before rain occurred) show values ranging from about 15% at the surface to as high as 40% at 30–180 cm in depth (Figure 38). The water contents within the profile of the core obtained about 24 hours after steady rain had begun ranged from 23%–45%, the latter of which is at about saturation for this type of soil. The core obtained above the 58 cm deep target showed a moisture content that varied from 15% at 15 cm depth to 24% at 50–70 cm depth. According to Topp et al. (1980), these water contents correspond with ϵ' values ranging from about 7 (15%), to 12 (25%), which agrees well with values of 8.6–9.5 obtained for this soil column. A time-of-flight analysis, in which the appropriate ϵ' was ascribed to the 10-cm soil increments and then calculated the time delay in each increment, gives an effective ϵ' value of 9.5 (Figure 38, profile 2).

The soil conductivity values measured at the site strongly influence EM wave attenuation below about 400 MHz, while the imaginary part of ϵ^* , ϵ'' , influences attenuation above 400 MHz (discussed later). Although ϵ'' was not measured or determined from the field surveys, the high amount of gain used for the radar measurements indicates a high attenuation rate for this soil and is consistent with the above range of σ and the high ϵ'' values and high attenuation observed in the laboratory EM properties measurements.

Grid survey: 300 MHz. The transect lines on the 40-acre site are superimposed on maps of target and ordnance distribution in Figure 36. The lines surveyed are designated as transects A, B, C, etc. and are 1300 feet (396 m) long. The class of target (ordnance or non-ordnance) is indicated on the map. Additional information regarding exact location, type of target, target depth, and approximate orientation are available. All ordnance are metal.

Figure 39 shows a typical 300-MHz profile segment before and after horizontal background removal filtering. Intensity is linearly proportional to signal amplitude in the profile. The time range is 50 ns, beyond which noise became severe, corresponds to about 2.3 m of penetration for $\epsilon' = 10.4$, the average value obtained at JPG (discussed later). The direct coupling between antennas occupies about 8 ns of the record and masks part of the responses to some of the targets. The noise bands between about 30 and 40 ns are probably caused by radiation leakage onto the cables that reflected back to the receiver, and internal system mismatch reflections caused by either the high value of ϵ' at the surface or poor system design. In both cases, erratic ground contact, caused by uneven topography and jerks in the towing, cause the amplitude of these bands to vary and precluded the efficacy of horizontal filtering. No distinct and extended horizons indicative of soil stratification or a bedrock interface appear within the 2-3 m of radar penetration along any of the profiles.

Arrows are used to identify several targets of anomalously high amplitude in the unfiltered profile of Figure 39. These targets are characterized by both hyperbolic diffractions (between 859 ft and 865 ft) and short reflection segments. Although the background filtering reduces the noise bands and the direct coupling, it also

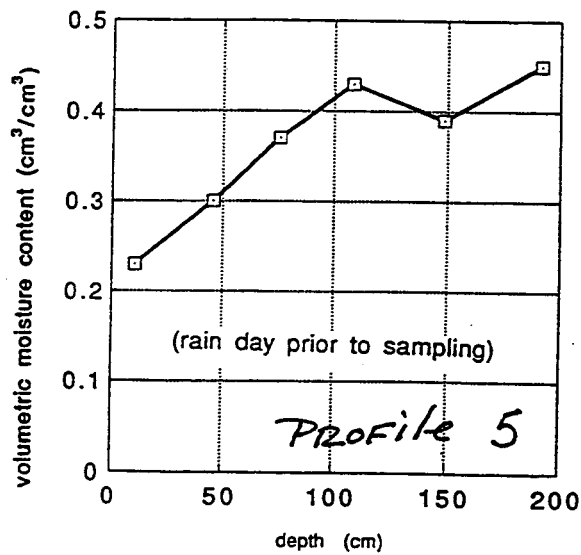
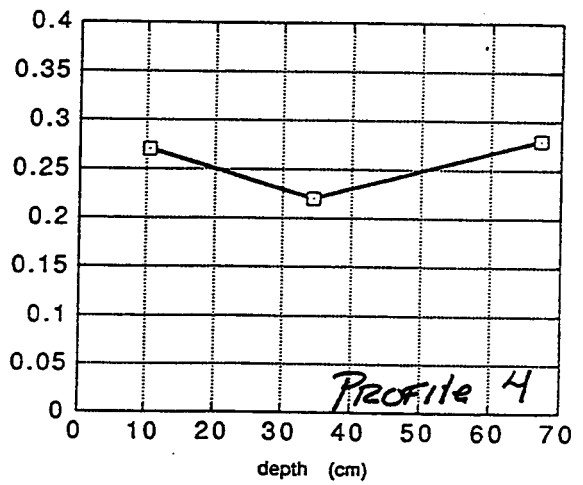
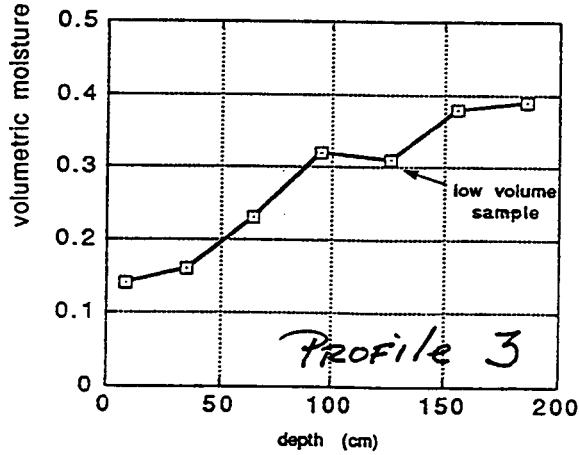
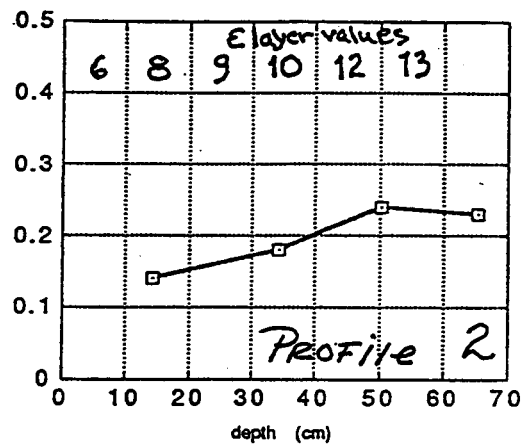
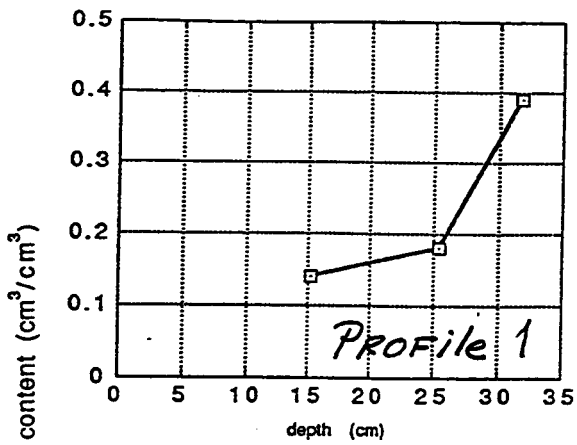


Figure 38. Soil moisture profiles for five locations, 40-acre site

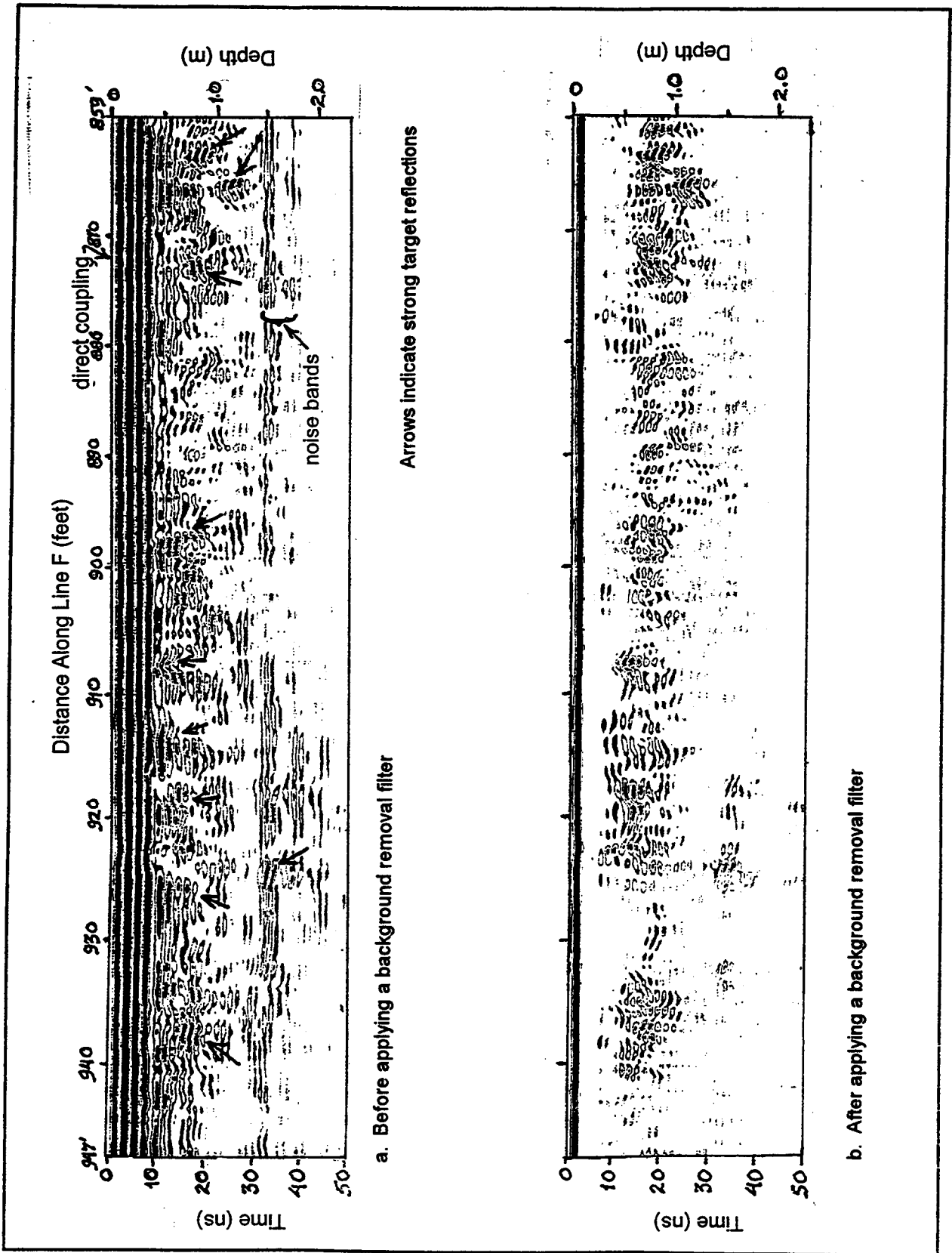


Figure 39. Sample segment of a 300 MHz profile, 40-acre site

attenuates many target responses, especially those characterized by short reflection segments such as occur near 926 ft, 915 ft and 900 ft. The use of more traces (i.e., a wider “window”) in the background filter would retain these reflection responses but at the expense of less noise reduction.

In general, a total of 30 high amplitude targets were detected along all 14 lines, of which eight responses are shown within segments of these profiles in Figure 40. The phase structure of several of the target wavelets (transects C, left; G, left; K, left; and I, left) identifies them as being of higher impedance than the surrounding soil matrix. Therefore, they are probably metal. Other target wavelets have a phase structure opposite to that of the metal response (transect F, both left and right; transect K, right). It is presumed that these responses are from the non- ordnance targets. Some targets exhibit waveform resonance, within which the first few half-cycles have the metal response waveform (transect C, right), while other targets exhibit resonances within the direct coupling and cannot be similarly analyzed (transect G, right; transect L, right). These latter resonances occur where targets are extremely close to the surface; i.e., where target multiple reflections occur before soil attenuation dampens them significantly. In all cases, diffraction asymptotes are so highly attenuated as to be either barely visible for small targets (transect G, left), as was seen in the control studies of Figure 37, or not visible at all where they should occur at the ends of short reflection segments recorded above more extended targets (transect C, left).

Probable interpretations to the target responses seen along transect C (left side) and along transect K (left side) are presented in Figure 41. The response along transect C is about 7 ft (2.1 m) long, which is nearly the length of a heavy bomb (1.6 m). The location of this response (533–572 ft) is marked in Figure 36b. The more complex response along transect K is about 12 ft (3.7 m) long and occurs in a section marked as having several medium-size mortars and projectiles. A JPG UXO ordnance brochure shows many of these projectiles to be about 2 ft (0.6 m) long. It is speculated that this transect segment spanned a series of closely spaced projectiles.

Grid survey: 600 MHz. This survey was conducted along four of the 14 grid lines. The profile segments containing the seven strongest target responses (Figure 42) are shown in a nonlinear format because the amplitudes of all the returns are extremely weak, hence the appearance of much more noise (gray speckle patterns) in the profiles than appeared at 300 MHz.

Small segments of diffractions are apparent in all the target responses in Figure 42; the lack of asymptotes indicates the high signal attenuation. Almost all of the responses have well-defined wavelets which exhibit the proper phase for a high-impedance target. These responses originate from depths less than about 0.5 m and would not have been resolved from the direct coupling of the 300-MHz system. Although the time range is only 30 ns, very few target responses occurred at greater than about 20-ns range. Therefore, the depth of penetration of this frequency in this soil was limited to about 1 m.

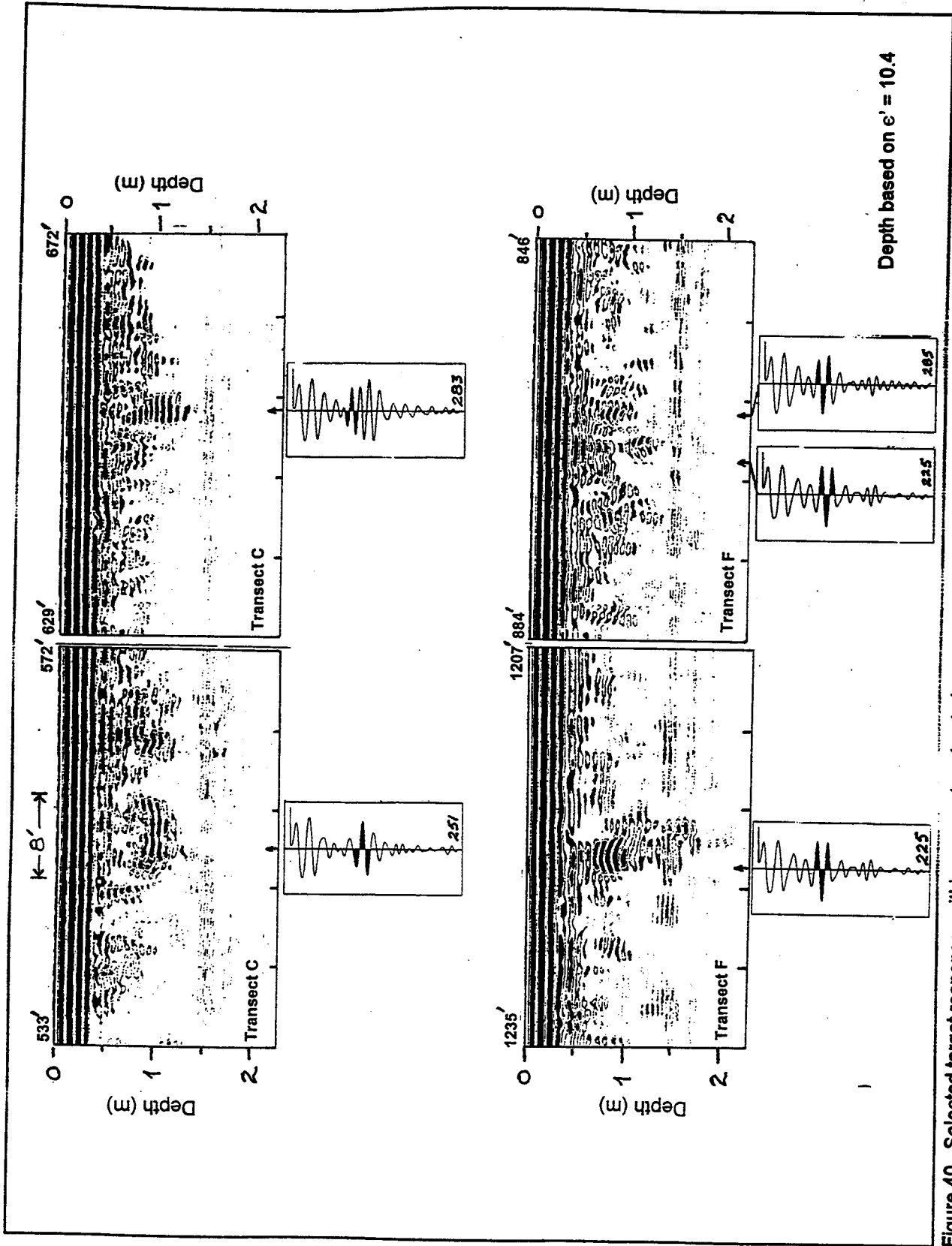


Figure 40. Selected target responses within segments extracted from 300 MHz profiles, 40-acre site (Continued)

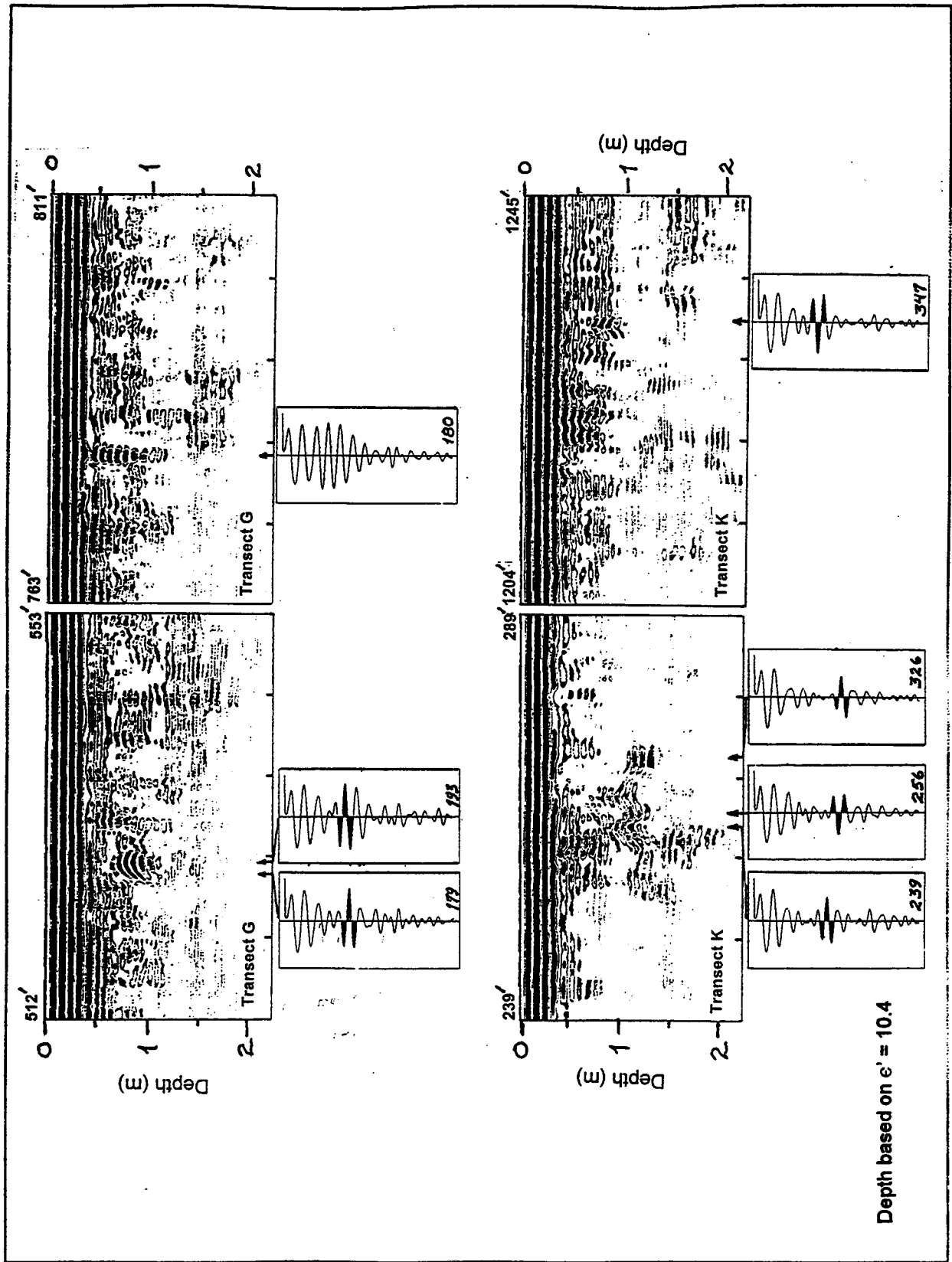


Figure 40. Selected target responses within segments extracted from 300 MHz profiles, 40-acre site (Continued)

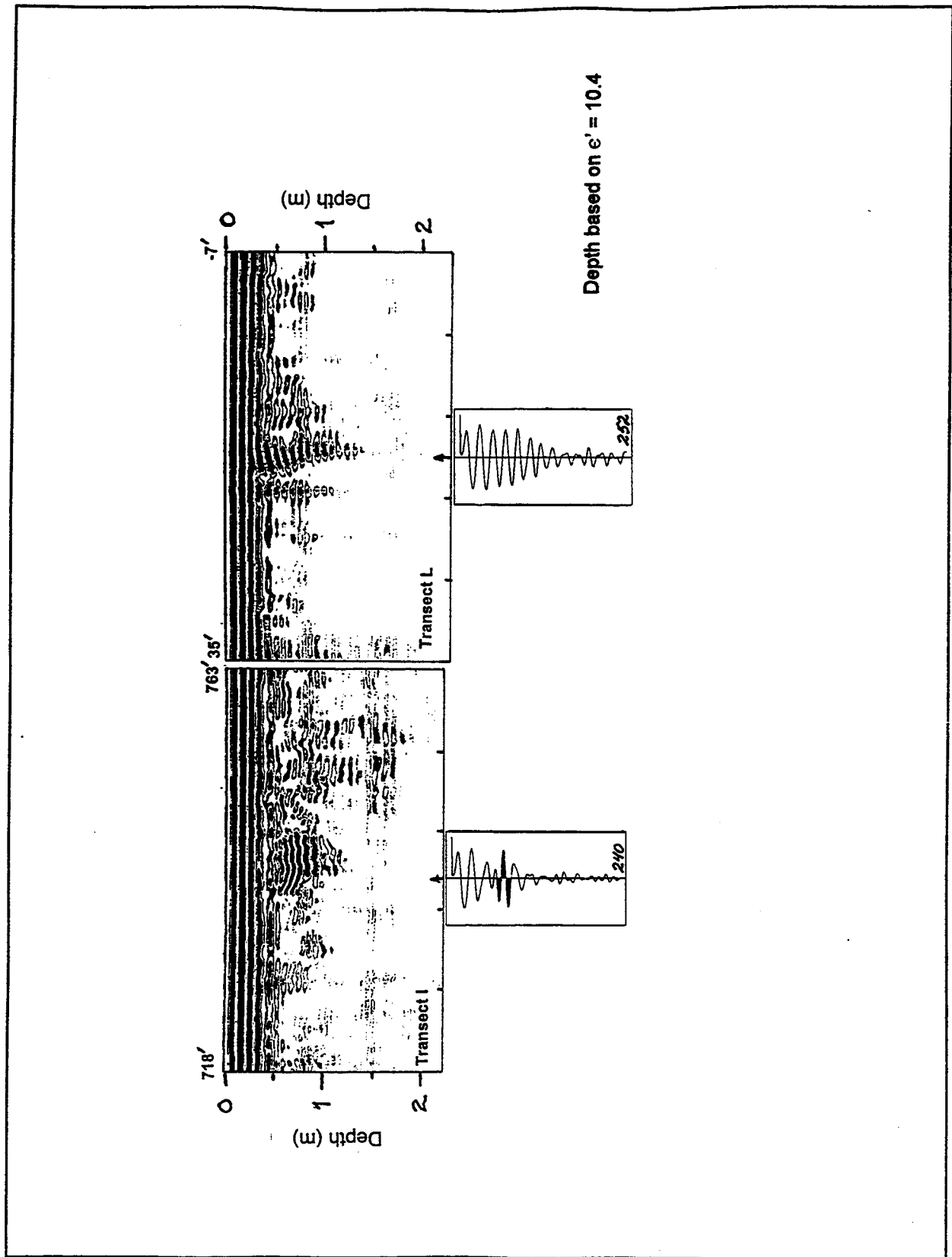


Figure 40. Selected target responses within segments extracted from 300 MHz profiles, 40-acre site (Concluded)

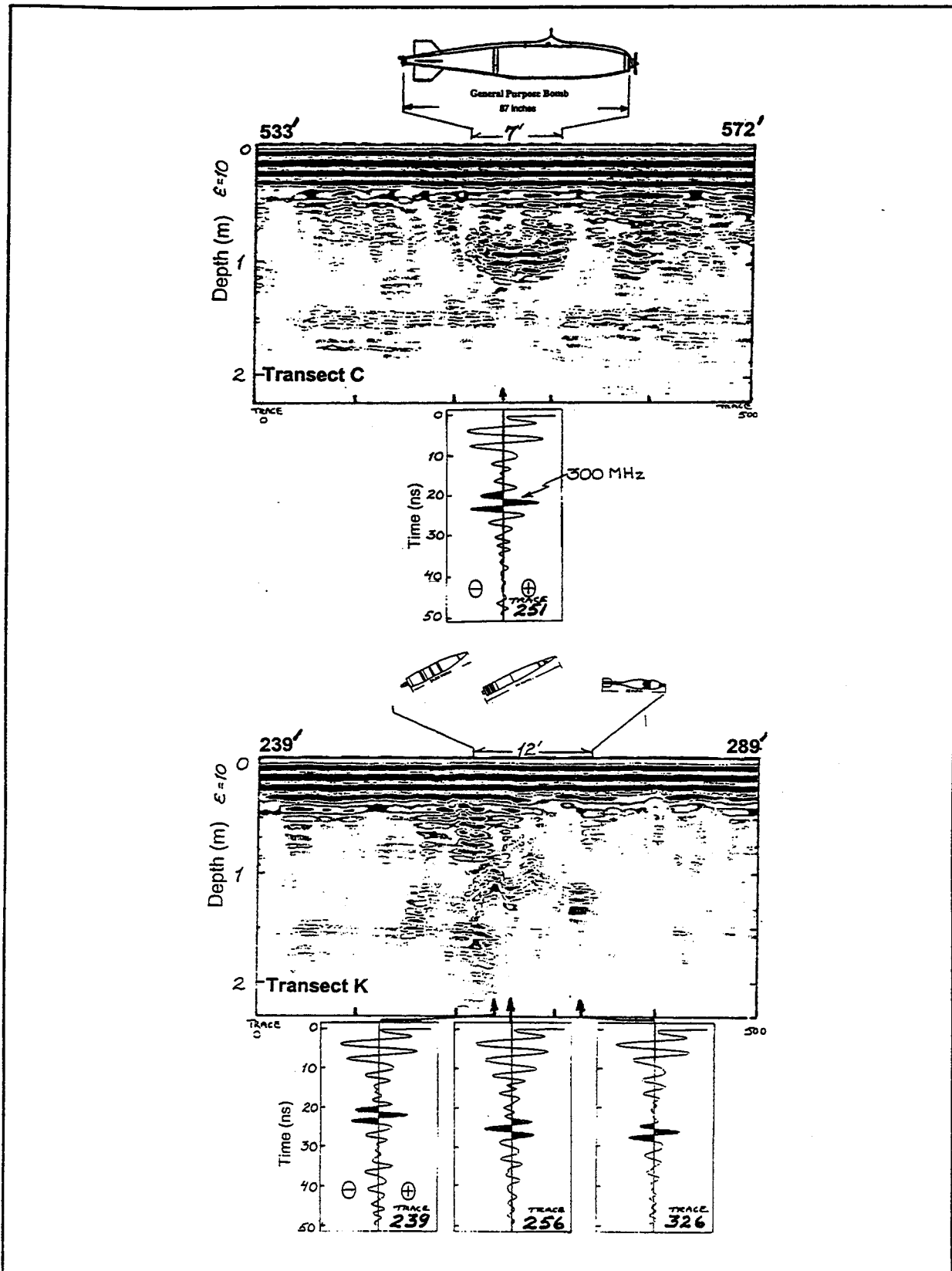


Figure 41. Interpreted results for two reposes from 300 MHz profiles, 40-acres site

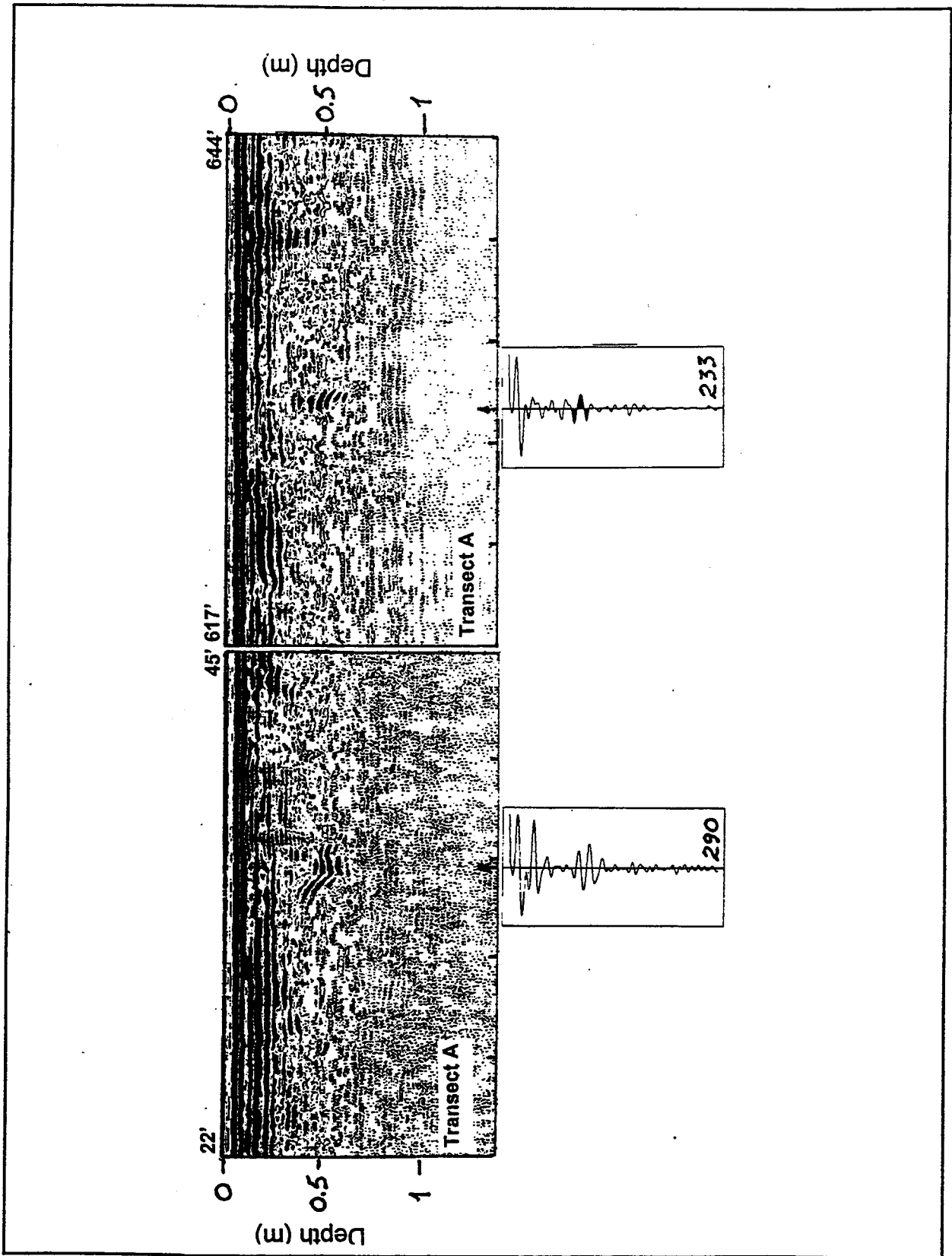


Figure 42. Selected target responses within segments extracted from 600 MHz profiles, 40-acre site (Continued)

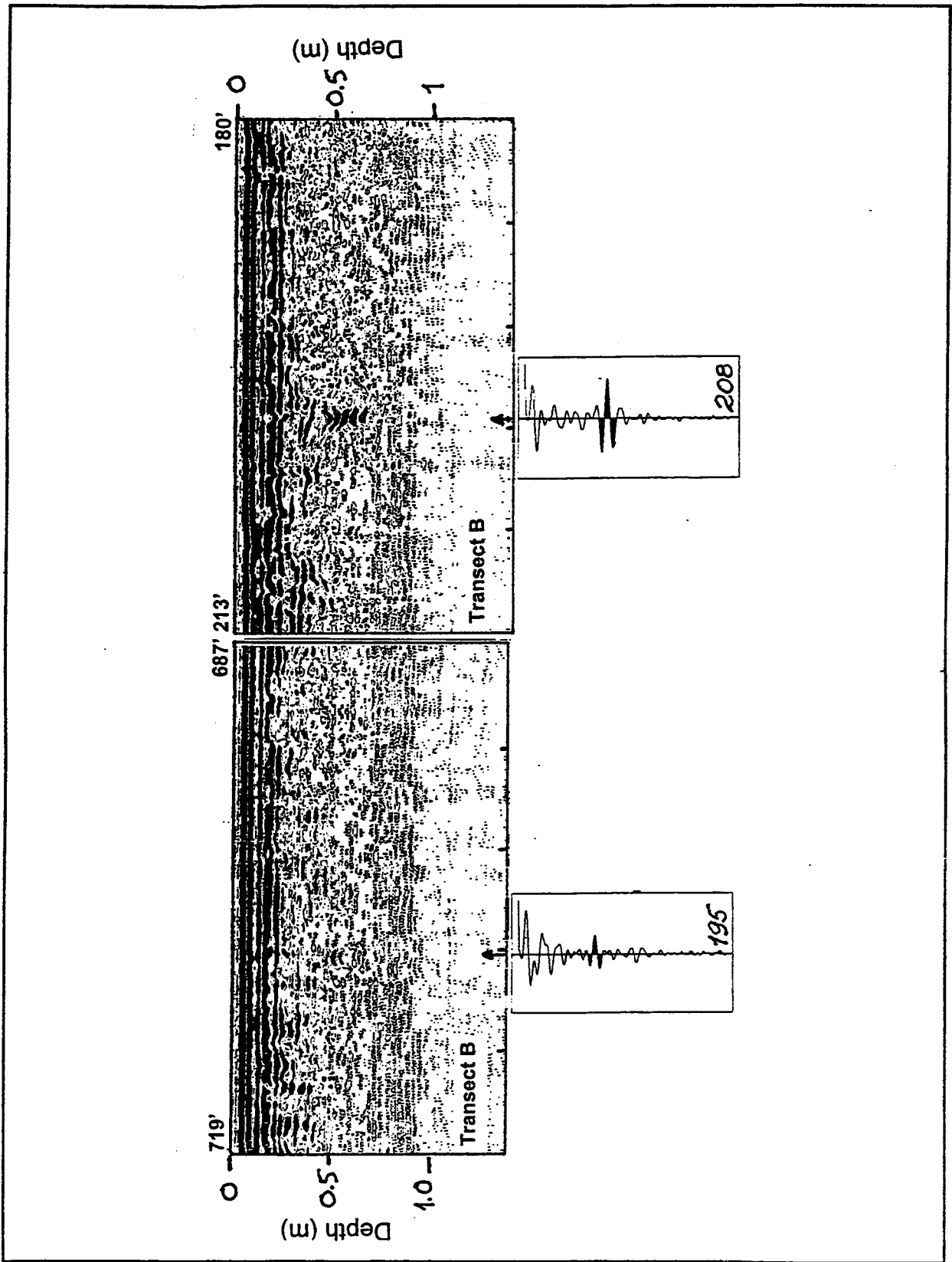


Figure 42. Selected target responses within segments extracted from 600 MHz profiles, 40-acre site (Continued)

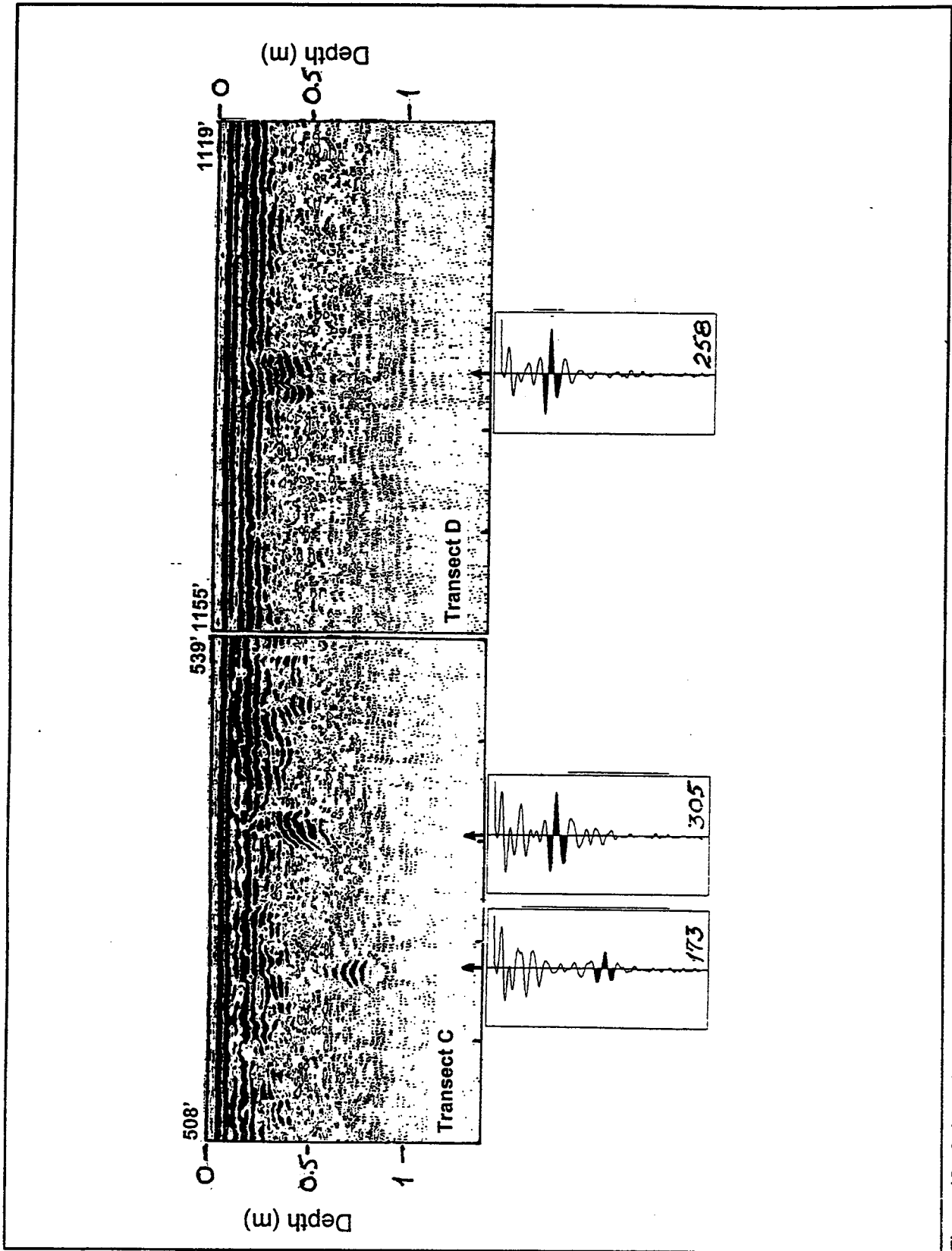


Figure 42. Selected target responses within segments extracted from 600 MHz profiles, 40-acre site (Concluded)

Distribution of ϵ' . The more prominent diffraction hyperbolas seen in both the 300- and 600-MHz surveys were compared with model hyperbolas to produce distributions of ϵ' and to compute an effective mean permittivity value for the overburden above the targets. Seventy hyperbolas were identified in the 300-MHz survey and 48 in the 600-MHz survey. A statistical approach was used to average the computational inaccuracies caused by the minor differences in distance scale that resulted from inconsistent towing speeds. Seventy hyperbolas were clear enough in the 300-MHz profiles and 48 in the 600-MHz profiles. Both distributions (Figure 43) exhibit nearly the same average value and similar standard deviations (s.d.), although their distributions are slightly different. The 300-MHz distribution is more bimodal, which may reflect different orientations of deeper targets; extended targets whose axial direction crosses that of the transect produce hyperbolic reflections rather than diffractions, with values of ϵ' reduced by the sine of the intersection angle (Jezek et al. 1979). The 600-MHz distribution may reflect less target orientation because it was limited to only lines A–D and to shallower depths.

Theoretical discussion

The average values of ϵ' , the range of σ , the fact that ϵ' may be slightly less at 600 MHz than at 300, and the high radar gain and faded diffraction asymptotes, both of which indicate high attenuation rates, allows for the estimation of the soil dielectric properties at JPG (Figure 44) and to theorize their effect upon antenna beamwidth and waveform. It is assumed that f_{rel} is about 3 GHz (Hoekstra and Delaney 1974); if it was any lower, then ϵ' at 600 MHz would be distinctly lower than it is at 300 MHz. A value of 3 was chosen for ϵ_{∞} , which is characteristic of dry soils and applies to frequency values where water is non-dispersive. The σ values at JPG strongly influence β below about 400 MHz, while ϵ_{rel} is the dominant factor above about 400 MHz (Figure 44b). Unfrozen mineralogic clays can exhibit even stronger absorption and may preclude any radar penetration at these frequency ranges and above (Hoekstra and Doyle 1971).

The effects of the soil properties upon the round trip propagation of both a model of the 300-MHz wavelet used in this survey and an ideal monocycle type waveform were computed and are shown in Figure 45. A monocycle is the shortest possible pulse an antenna can radiate and may be nearly achieved with unshielded antennas. It therefore has a wider bandwidth than the system model used in this study, and would provide the highest possible target resolution. Both wavelets start propagation with a local frequency of 400 MHz (Figure 45a), which is that of antenna model 5103 used in this study, when used on low permittivity (e.g., $\epsilon' = 4$) material. Both wavelets then experience strong attenuation caused by conductivity alone (Figure 45b), but maintain their original form in this case and show no shift in local frequency. However, Figure 45 c-d shows that shifts in local frequency will occur when the dielectric relaxation is considered. Despite the shift, the wavelet form is changed little.

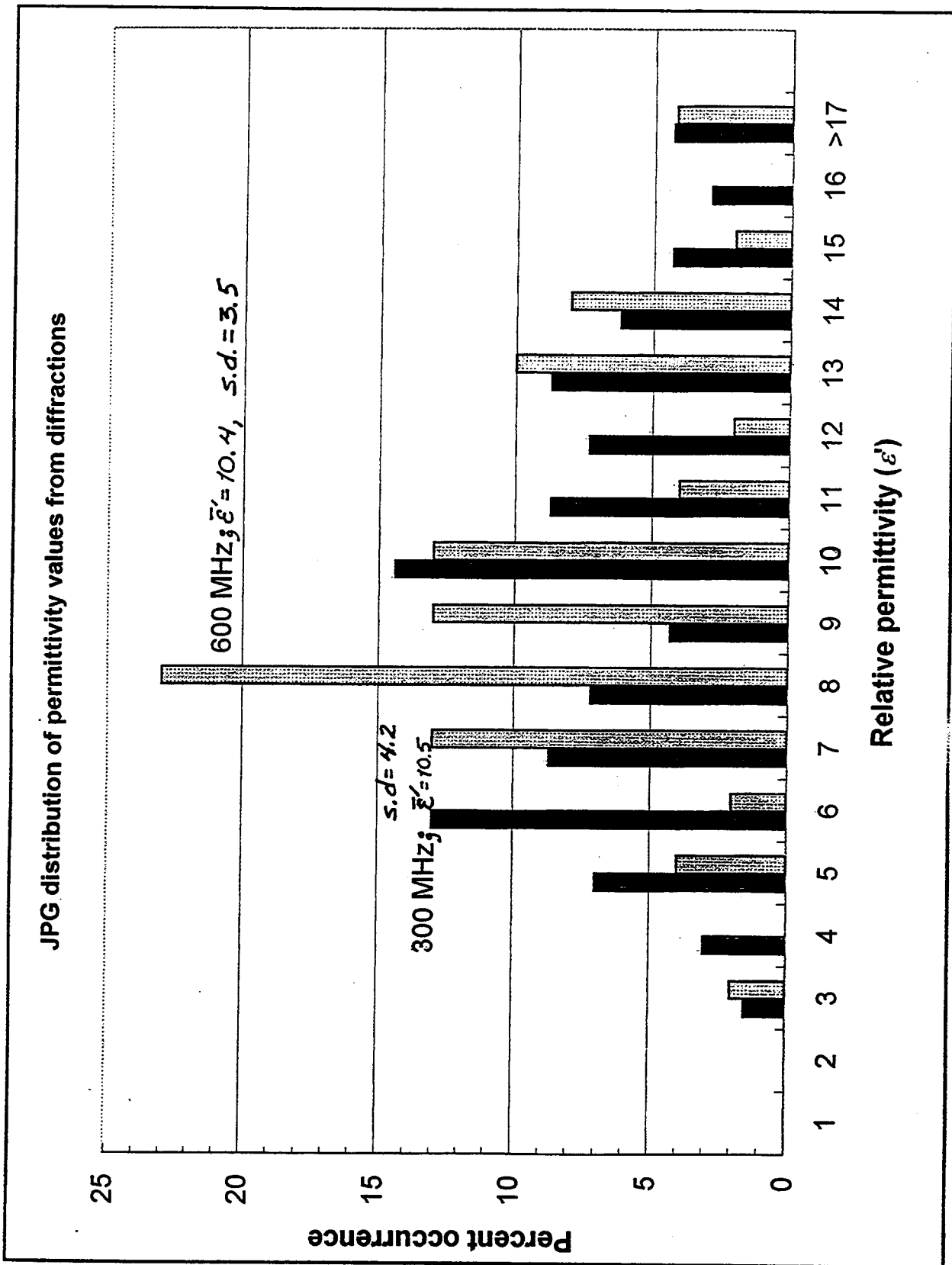


Figure 43. Relative permittivity (ϵ') distribution from 300 and 600 MHz antennas, 40-acre site

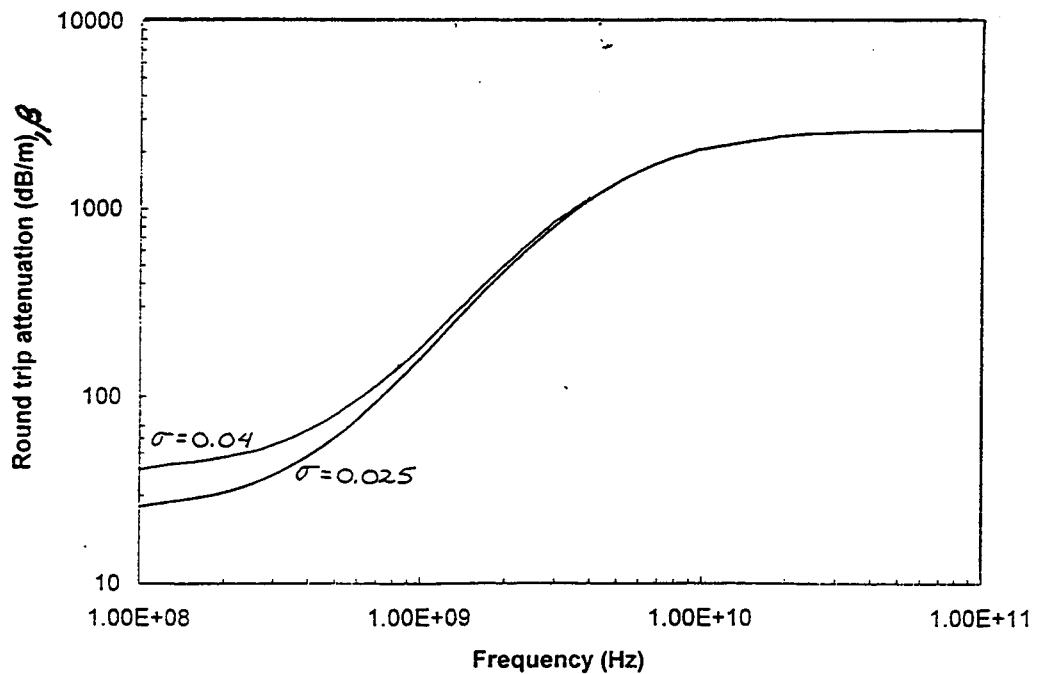
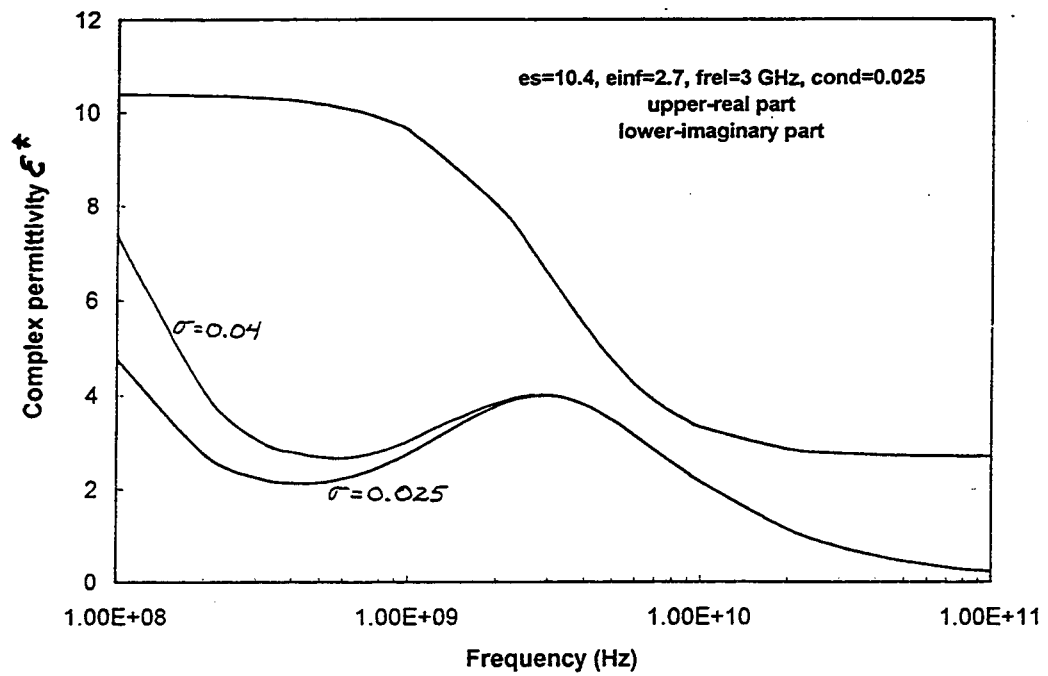


Figure 44. Dielectric permittivity curves and attenuation rates for the average ϵ' , range of σ , and probable values of f_{rel} and ϵ_{∞} , 40-acre site

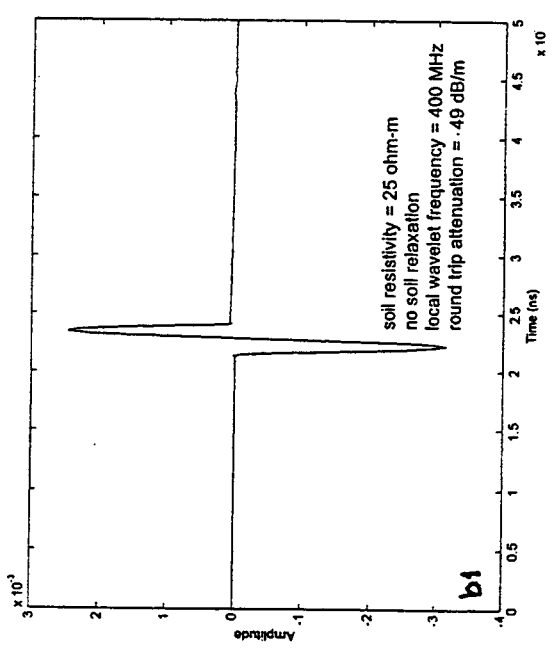
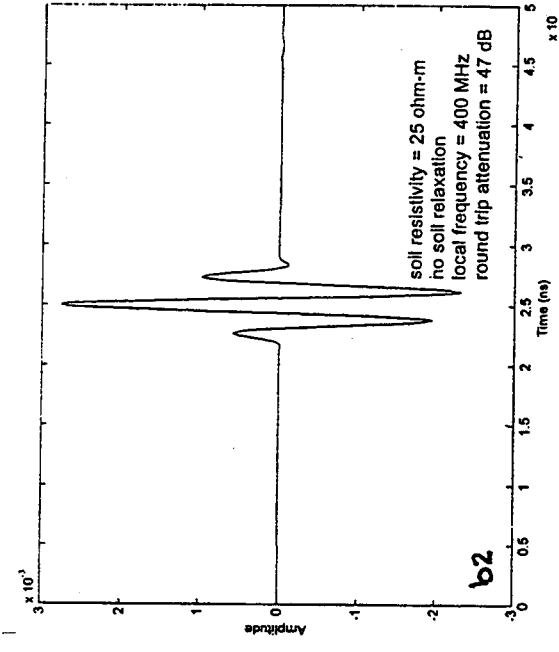
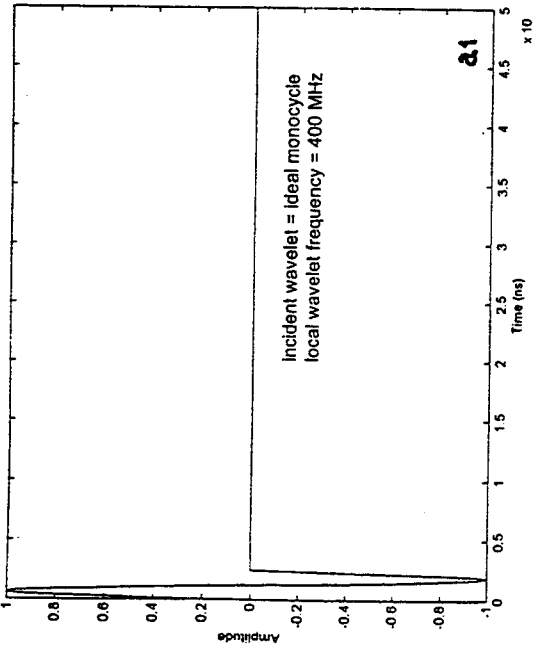
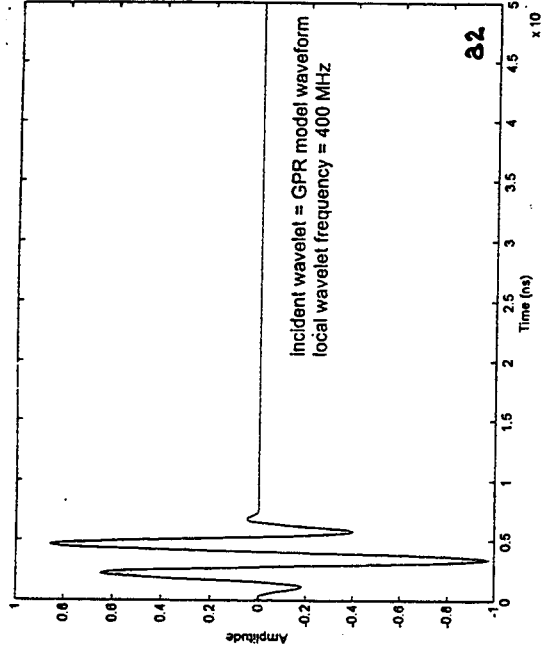


Figure 45. Modeled 400 MHz wavelets before and after round-trip propagation within one meter of ground surface (Continued)

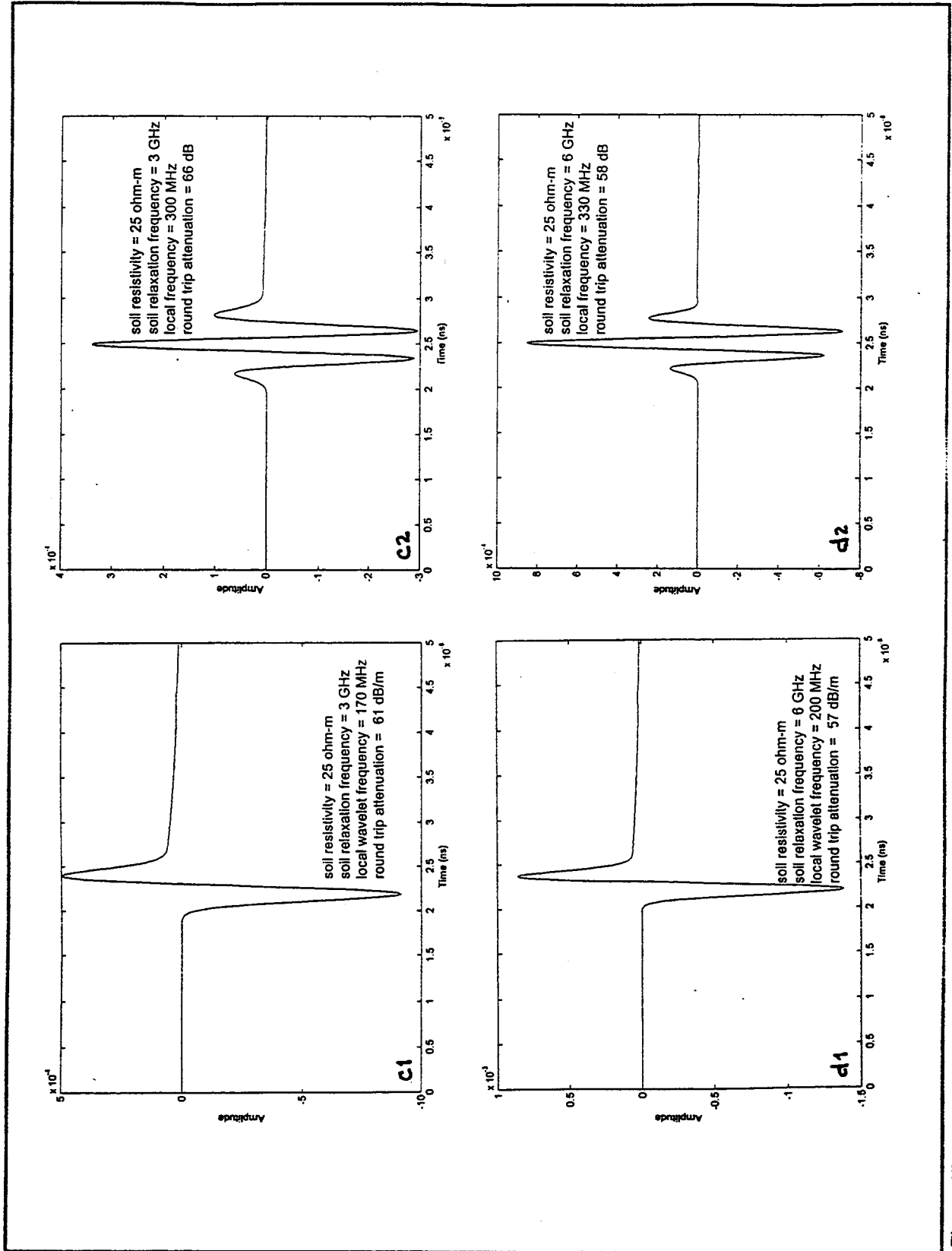


Figure 45. Modeled 400 MHz wavelets before and after round-trip propagation within one meter of ground surface (Concluded)

The value of ϵ' also determines the antenna directivity (Arcone 1995). Horizontal dipoles on the ground surface show a greater concentration of energy within the subsurface vertical plane that includes the antenna axis than in the plane perpendicular to the axis (Figure 46). As ϵ' increases, the radiation will become more confined within the plane containing the antenna axis. This means that the profiles in this study were mainly sensitive to the ground directly beneath the transects. The greater width of the pattern perpendicular to the axis (and along the surveyed transects) shows that the rapid fading observed within diffraction asymptotes was due to soil attenuation and not radiation directivity.

Figure 47 shows a histogram of the DICON probe permittivities sampled at depths of 0.1 m and 0.5 m. The histogram shows that the DICON probe permittivities have higher average values and than those derived from the GPR. Possible reasons for this difference may be caused by the different testing frequencies used by the DICON probe (60 MHz) versus the GPR (300 and 600 MHz). Also, permittivities determined using the DICON probe are point samples whereas, the GPR permittivities are obtained over a larger volume. Table 8 shows the 40-acre permittivity values obtained from laboratory EM tests, GPR surveys, and DICON probe measurements. The reported EM laboratory values were estimated from curves of water content versus real constant at a water content of 25 percent for frequencies ranging between 100 and 1015 MHz. The table shows that the GPR and laboratory acquired permittivity values agree well. The DICON probe uses a frequency of 60 MHz which is lower than the frequencies used by the GPR and laboratory instrumentation. The table shows that the permittivity values tend to increase with lower frequencies.

Test Type	Frequency, MHz	Permittivity
Laboratory	100	13
	200	11
	495	11
	1015	10
GPR	300	10.5
	600	10.4
DICON probe	60	19.2

80-acre Site

Electrical resistivity soundings

The results of the Schlumberger resistivity soundings conducted at the 80-acre site are summarized in Figures 48 and 49. Figure 48 shows the results obtained

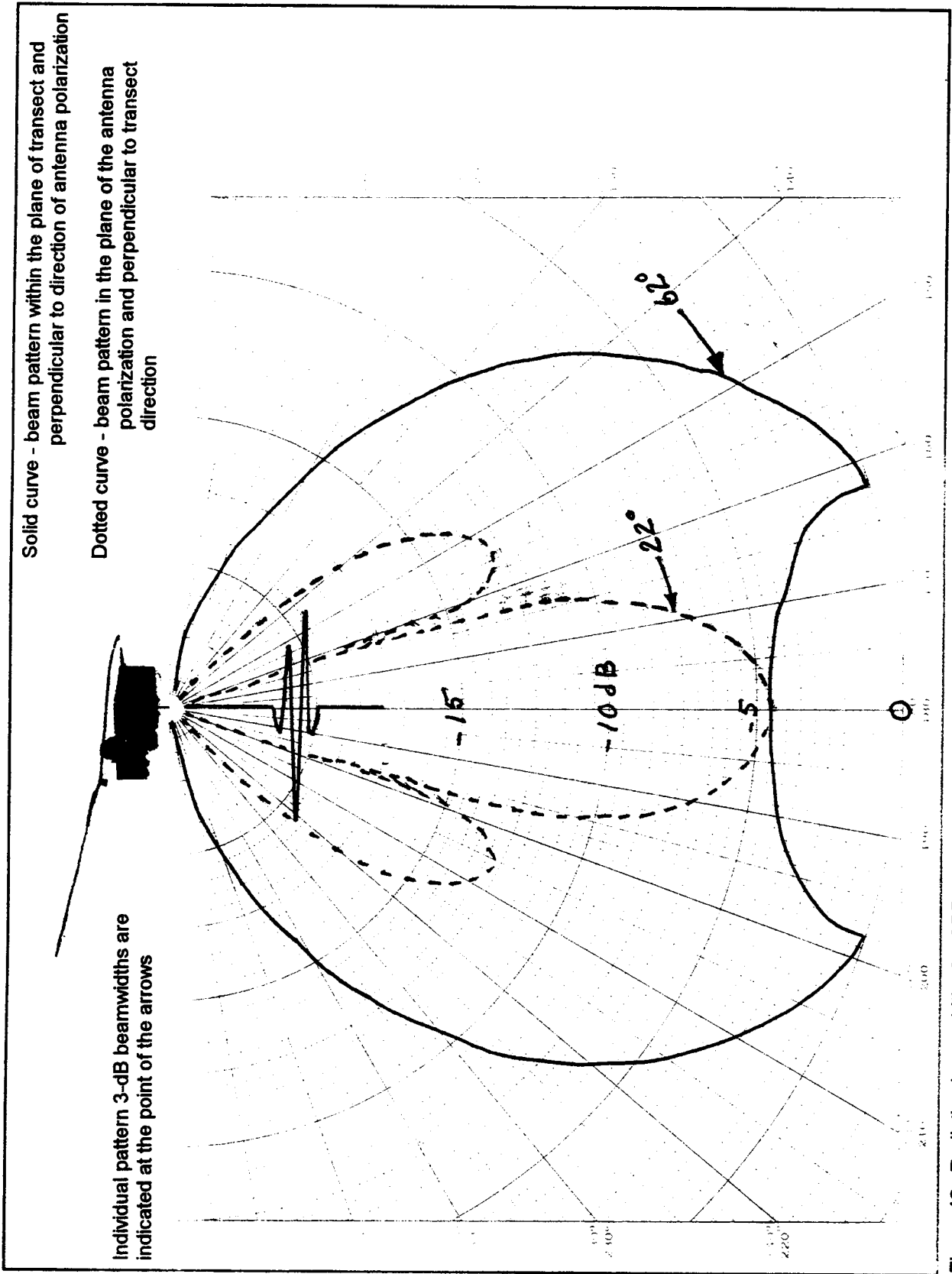


Figure 46. Radiation beamwidths for GPR antennas using an average $e' = 10.4$, 40-acre site

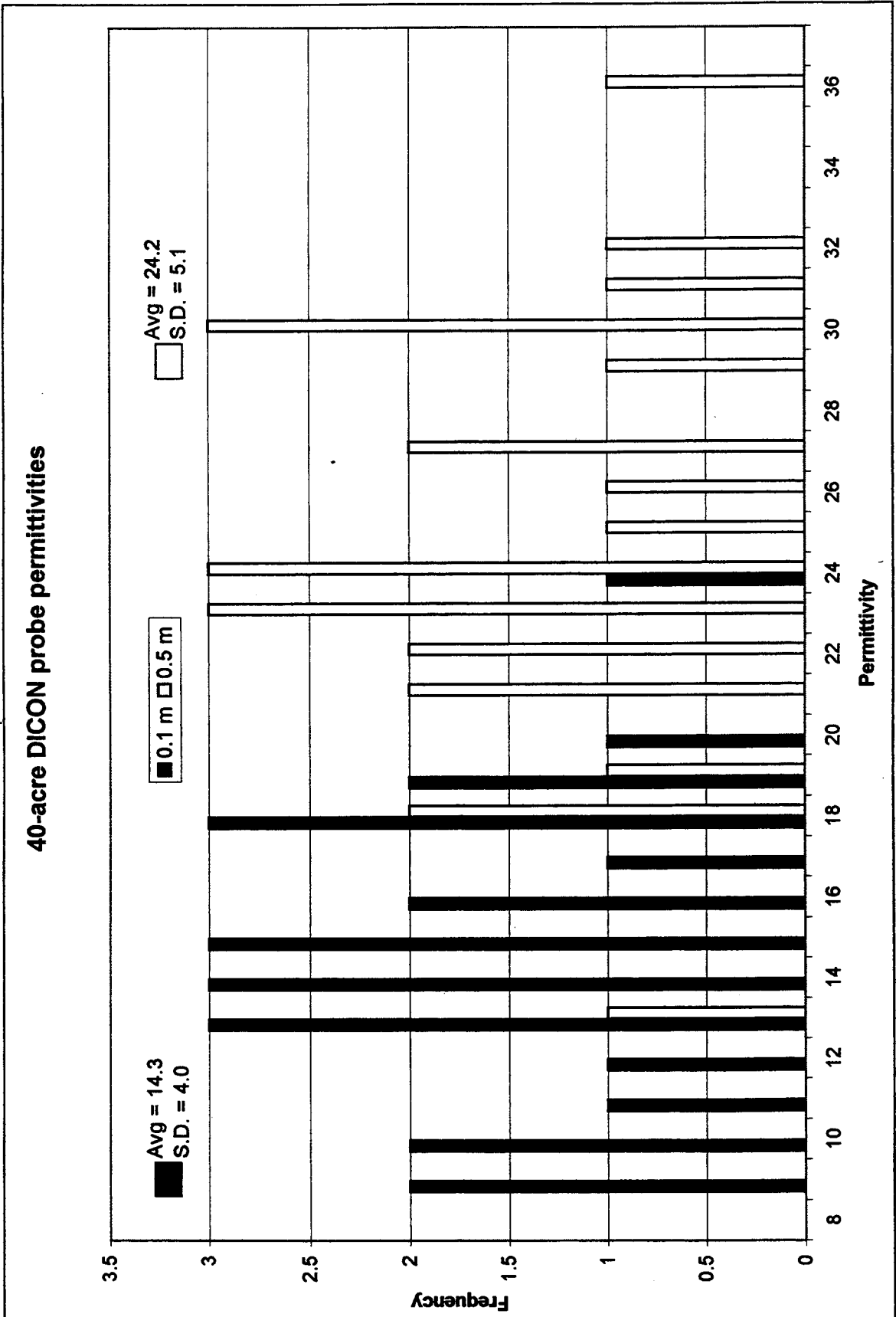


Figure 47. DICON probe dielectric permittivity histogram, 40-acre site

along north-south Line H whereas Figure 49 shows the results of the data obtained along east-west Line 13. The interpreted resistivity model indicates a 3-layer model. The surface layer is thin with an average thickness of about 0.5 m, and relatively resistive with an average resistivity of about 420 Ω -m (2 mS/m) and with a range of 154 to 996 Ω -m (1 to 7 mS/m). This layer is underlain by a layer with a resistivity ranging between 5 and 78 Ω -m (13 to 200 mS/m) and an average resistivity of about 30 Ω -m (33 mS/m). The thickness of this layer varies between 0.4 and 6.4 m with the average being 2.3 m. The upper 2 layers correspond to silt-clay materials. The low resistivity layer is probably indicative of an increase in the clay and/or moisture content. The deepest layer has an interpreted depth ranging between 0.7 and 7.2 m. The average depth to this layer is about 3.2 m. This layer is very resistive with a resistivity ranging between 574 and 6325 Ω -m (less than 2 mS/m) and a median resistivity of about 700 Ω -m (1 mS/m). This layer is interpreted to correspond with the dolomite/limestone bedrock. The sounding curve and model for each resistivity sounding are presented in Appendix F.

DICON probe measurements

The results of the DICON probe measurements are presented in Table 9. The range of values for the relative dielectric permittivity, conductivity, and wave speed are 8.7 to 33.9, 11 to 80.3 mS/m, and 0.052 to 0.102 m/ns, respectively. The average values for the relative dielectric permittivity, conductivity, and wave speed for the 10 cm depth are 13.8, 17.0 mS/m, and 0.082 m/ns, respectively. The average values for the relative dielectric permittivity, conductivity, and wave speed for the 50 cm depth are 26.8, 51.4 mS/m, and 0.058 m/ns, respectively. These results are very similar, with the exception of the 50 cm conductivity value, to the 40-acre DICON probe results. Also, the range of conductivity values agree with the results of the resistivity soundings.

Location	Depth, m	Relative Dielectric Permittivity	Conductivity mS/m	Wave Speed m/ns
H1	0.10	17.3	15.4	0.072
	0.50	33.9	80.3	0.052
H4	0.10	14.6	20.2	0.079
	0.50	26.6	34.2	0.058
H7	0.10	18.4	27.4	0.070
	0.50	30.3	71.1	0.055
H10	0.10	14.2	13.5	0.080
	0.50	28.8	49.6	0.056
H13	0.10	8.7	11	0.102
	0.50	26.9	49.9	0.058

(Continued)

Table 9 (Concluded)				
Location	Depth, m	Relative Dielectric Permittivity	Conductivity mS/m	Wave Speed m/ns
H16	0.10	16.6	19.8	0.074
	0.50	27.3	53.8	0.057
H19	0.10	9.9	13.6	0.095
	0.50	24.6	44.6	0.060
H22	0.10	11.3	11	0.089
	0.50	25.4	47.5	0.060
H26	0.10	10.9	16.2	0.091
	0.50	25.1	44	0.060
A13	0.10	13.7	25.4	0.081
	0.50	27	70.6	0.058
D13	0.10	12.5	17.7	0.085
	0.50	21.3	40.8	0.065
K13	0.10	15.7	15.4	0.076
	0.50	28.3	45.8	0.056
O13	0.10	15.7	14.6	0.076
	0.50	23.6	35.4	0.062
Average	0.10	13.8	17.0	0.082
	0.50	26.8	51.4	0.058

EM31 surveys

Figures 50 and 51 present the results of the conductivity surveys conducted along profile Lines H and 13, respectively, at the 80-acre site. The conductivity values generally range between 10 and 34 mS/m. The average conductivity value obtained from the DICON probe is slightly higher than the average value obtained from the EM31. The conductivity values vary considerably along Line H and have an average value of approximately 20 mS/m. The conductivity values along Line 13 show a general increase from approximately 10 mS/m to 26 mS/m from east to west. The inphase results for Lines H and 13 are shown in Figures 52 and 53, respectively. Both inphase profile lines show considerable variability across the site. Since the inphase readings are sensitive to metallic objects it is possible that the high degree of variability in the inphase values may be caused by the large amount of buried metal at the site.

1-hectare Site

The data presented include electrical resistivity sounding data, electrical conductivity and inphase data collected in the vertical dipole mode, magnetic total field data, GPR profile data, and DICON probe measurements. The resistivity data are displayed as log-log plots of apparent resistivity versus electrode spacing with a corresponding interpreted resistivity versus depth profile; conductivity and magnetometer data are presented as contour plots; GPR data are shown as profiles

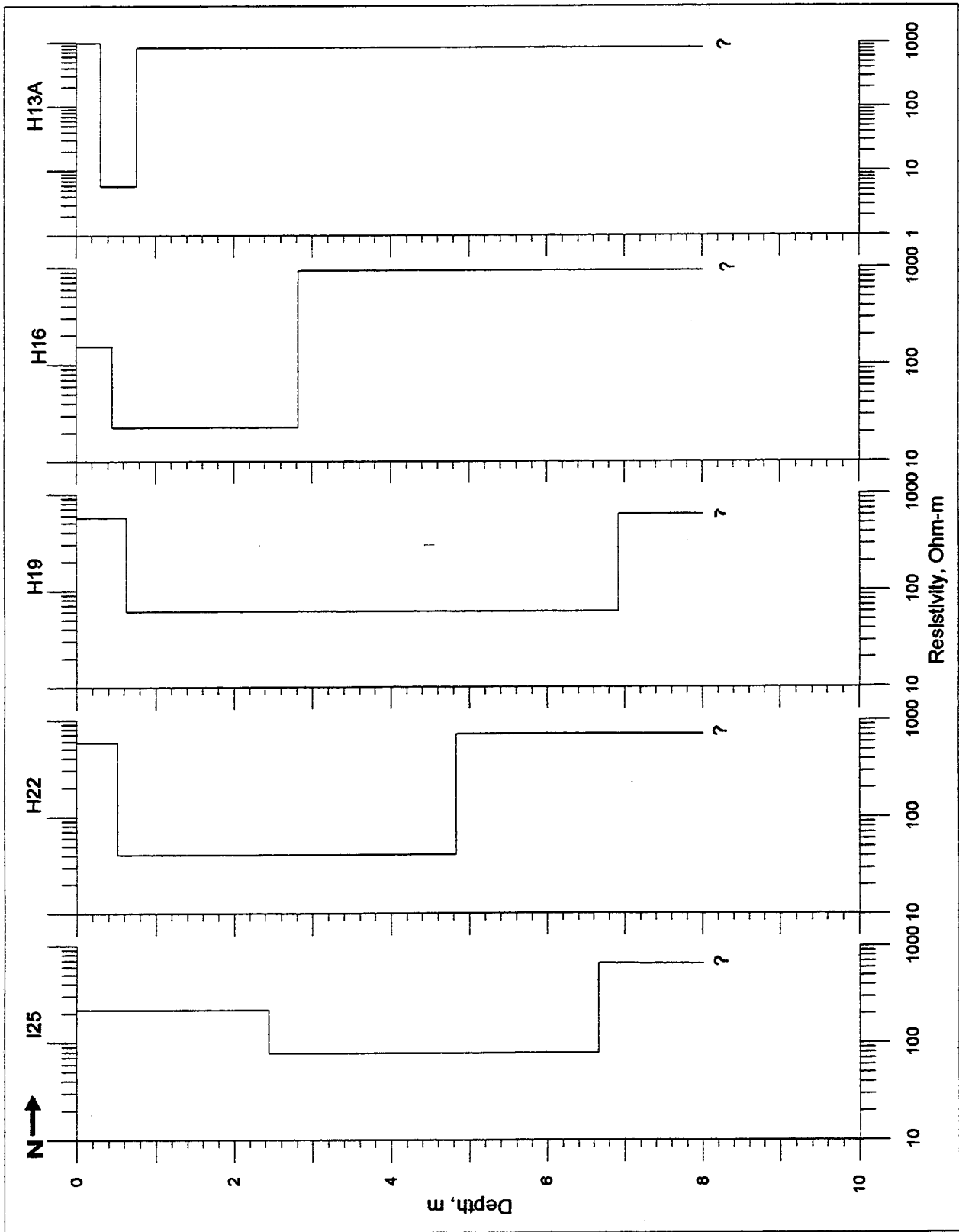


Figure 48. VES modeling results, Line H (north-south), 80-acre site (Continued)

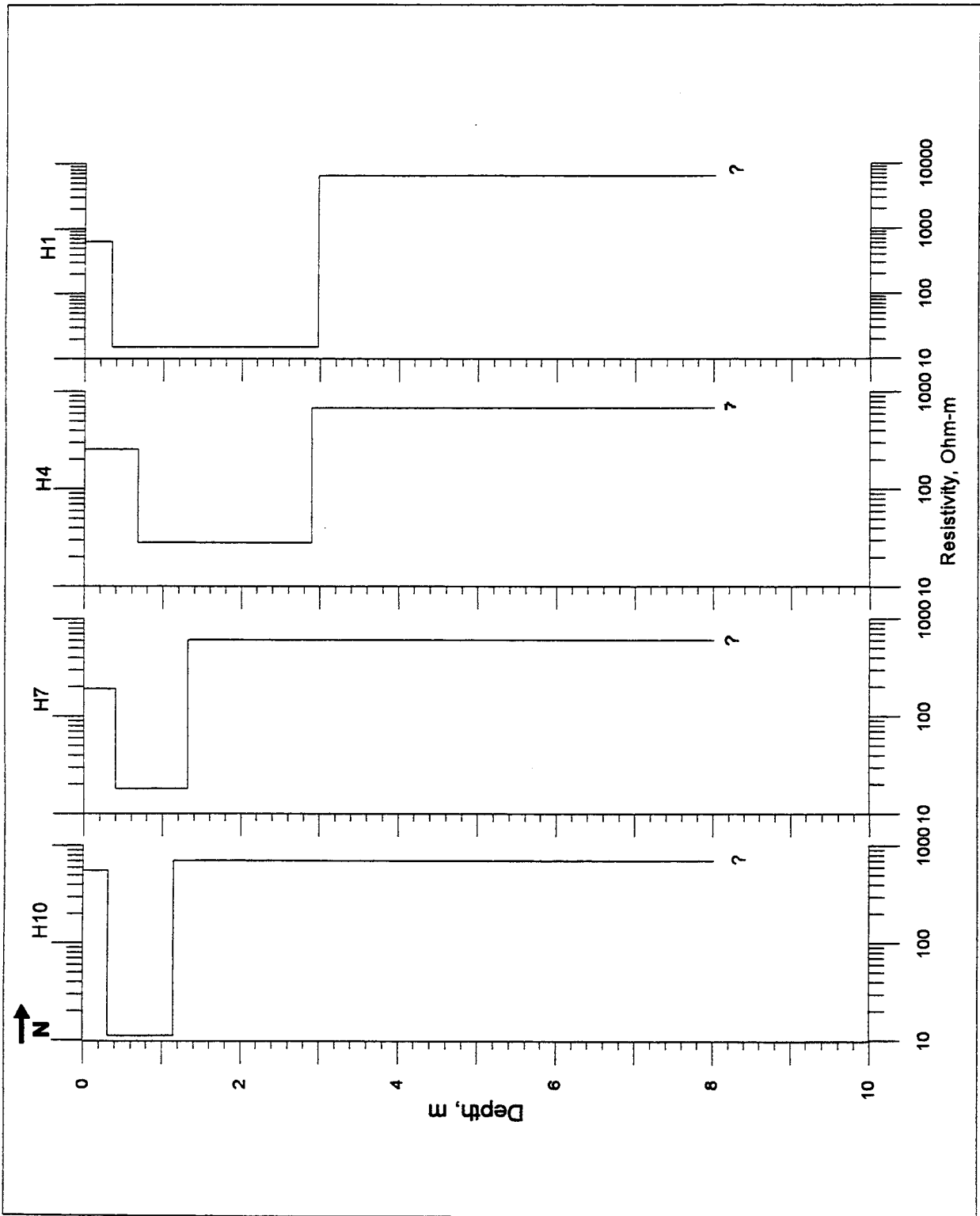


Figure 48. modeling results, Line H (north-south), 80-acre site (Concluded)

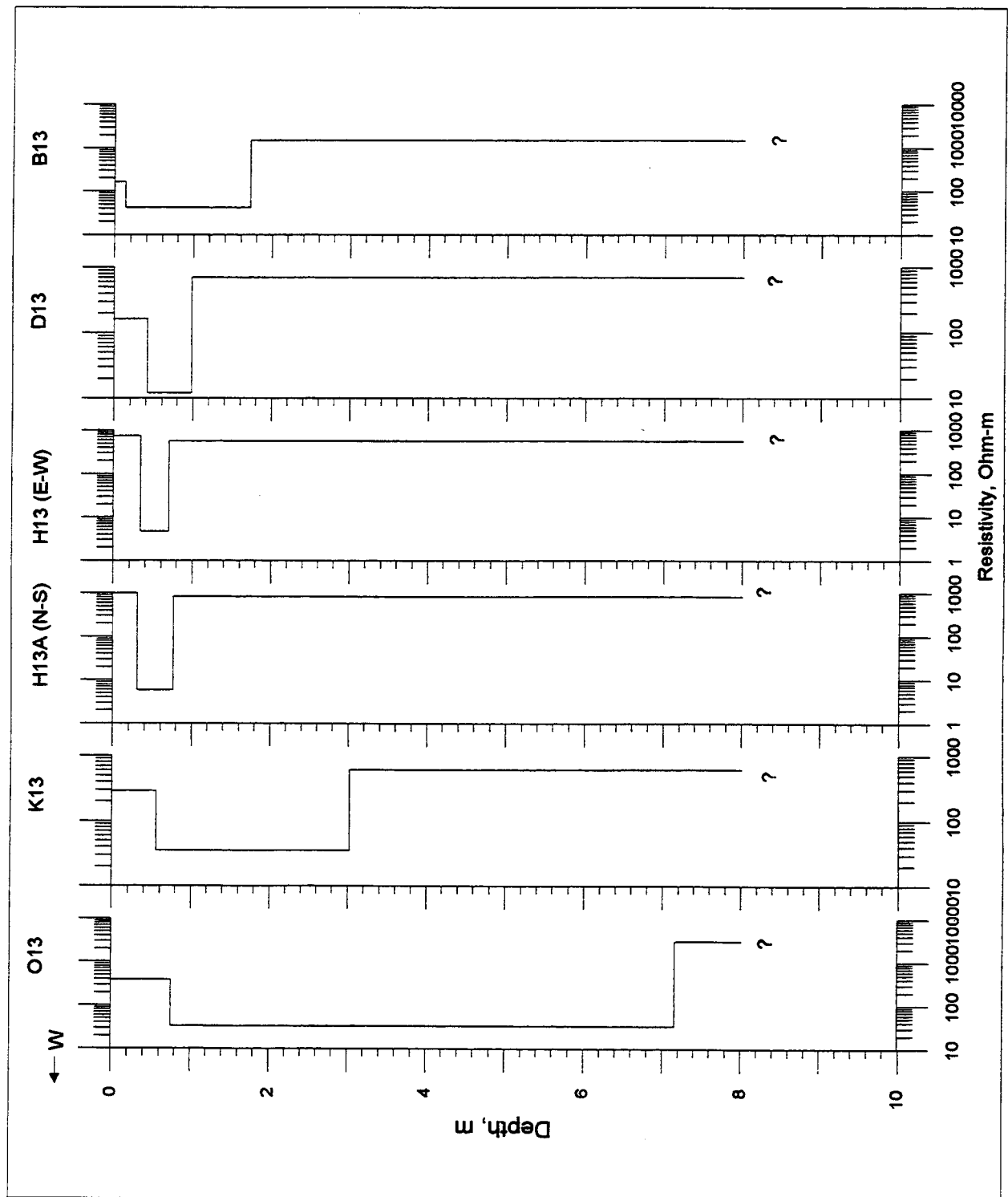


Figure 49. VES modeling results, Line 13 (east-west), 80-acre site

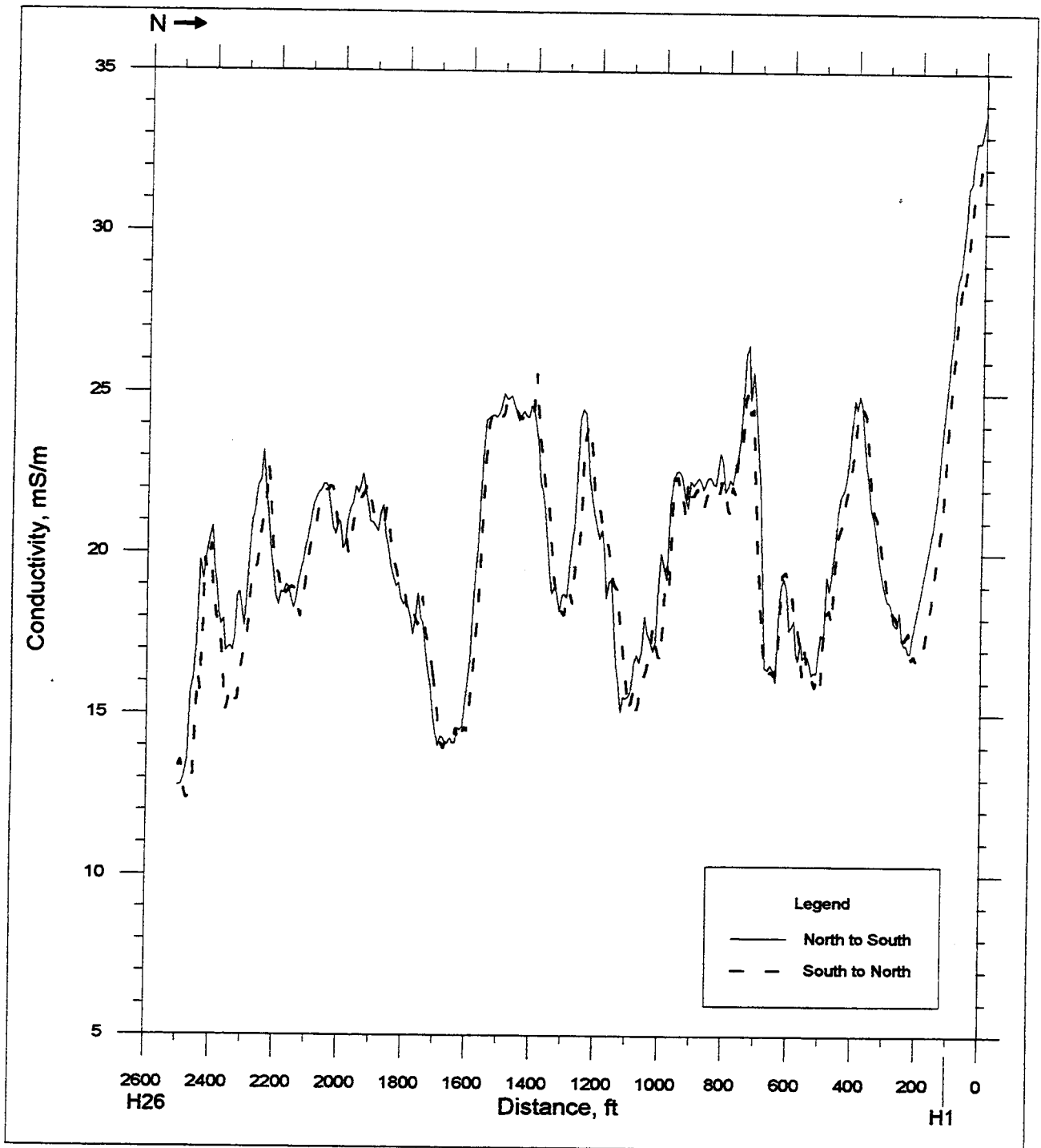


Figure 50. Conductivity survey results, Line H (north-south), 80-acre site

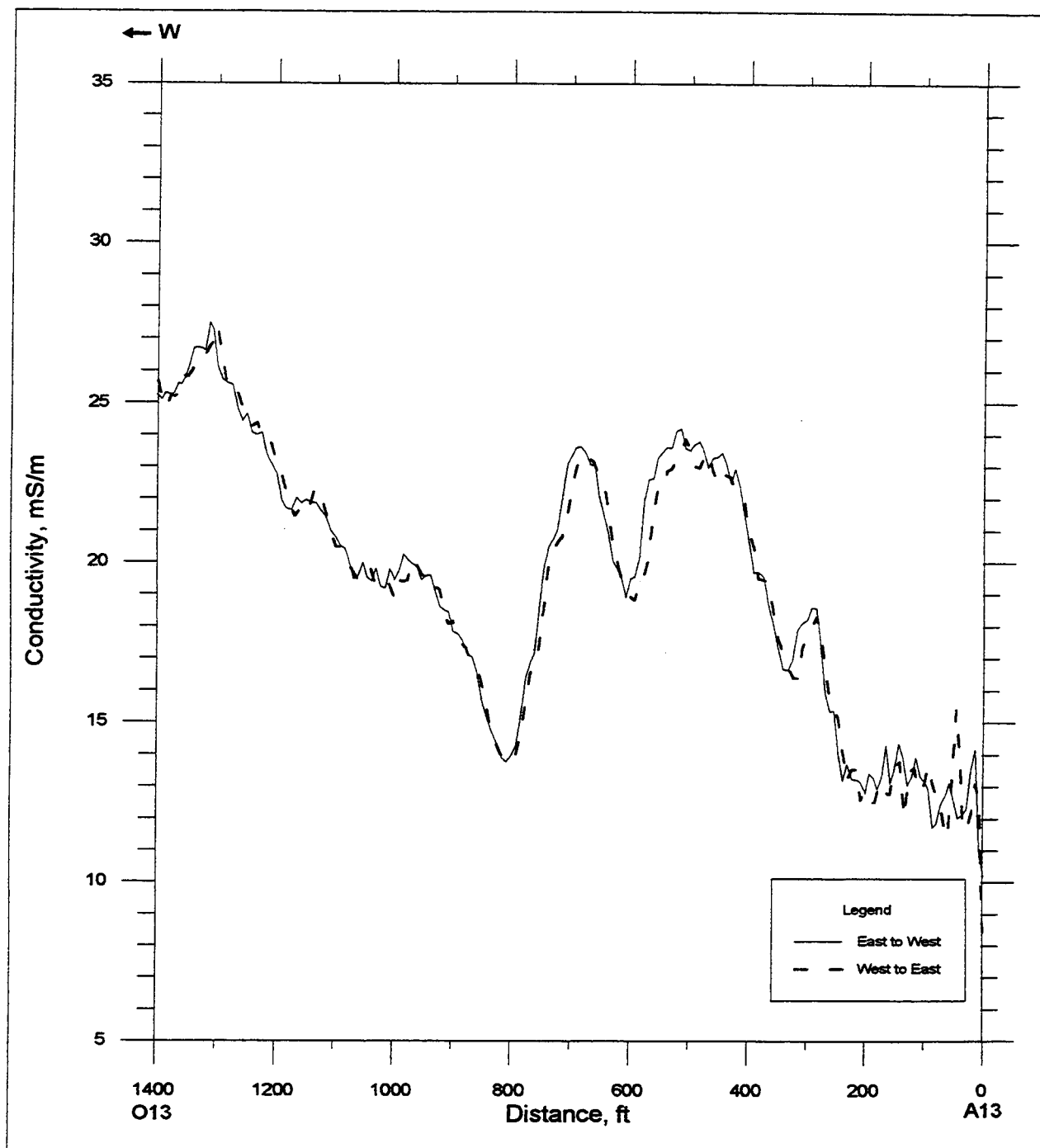


Figure 51. Conductivity survey results, Line 13 (east-west), 80-acre site

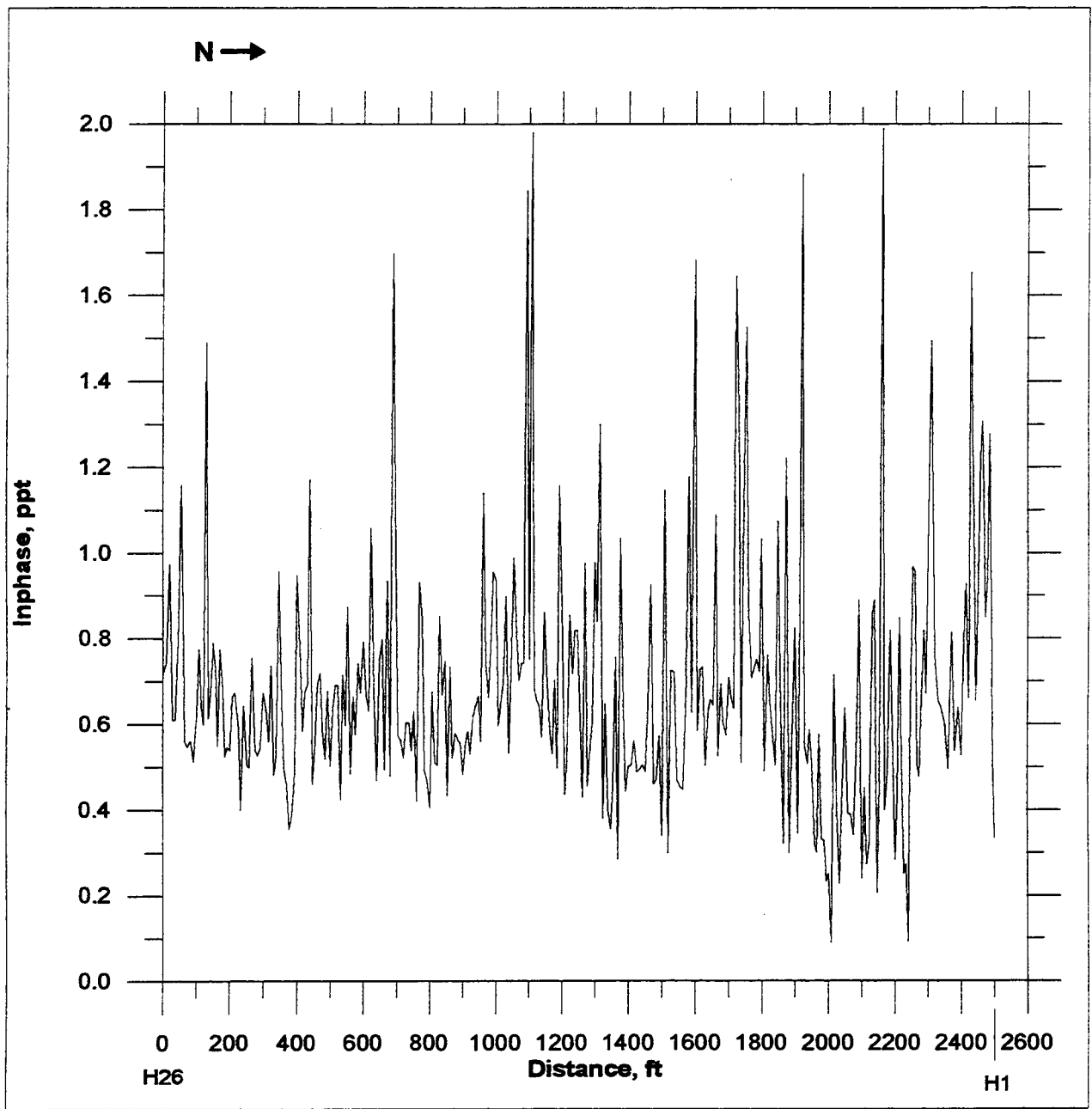


Figure 52. Inphase survey results, Line H (north-south), 80-acre site

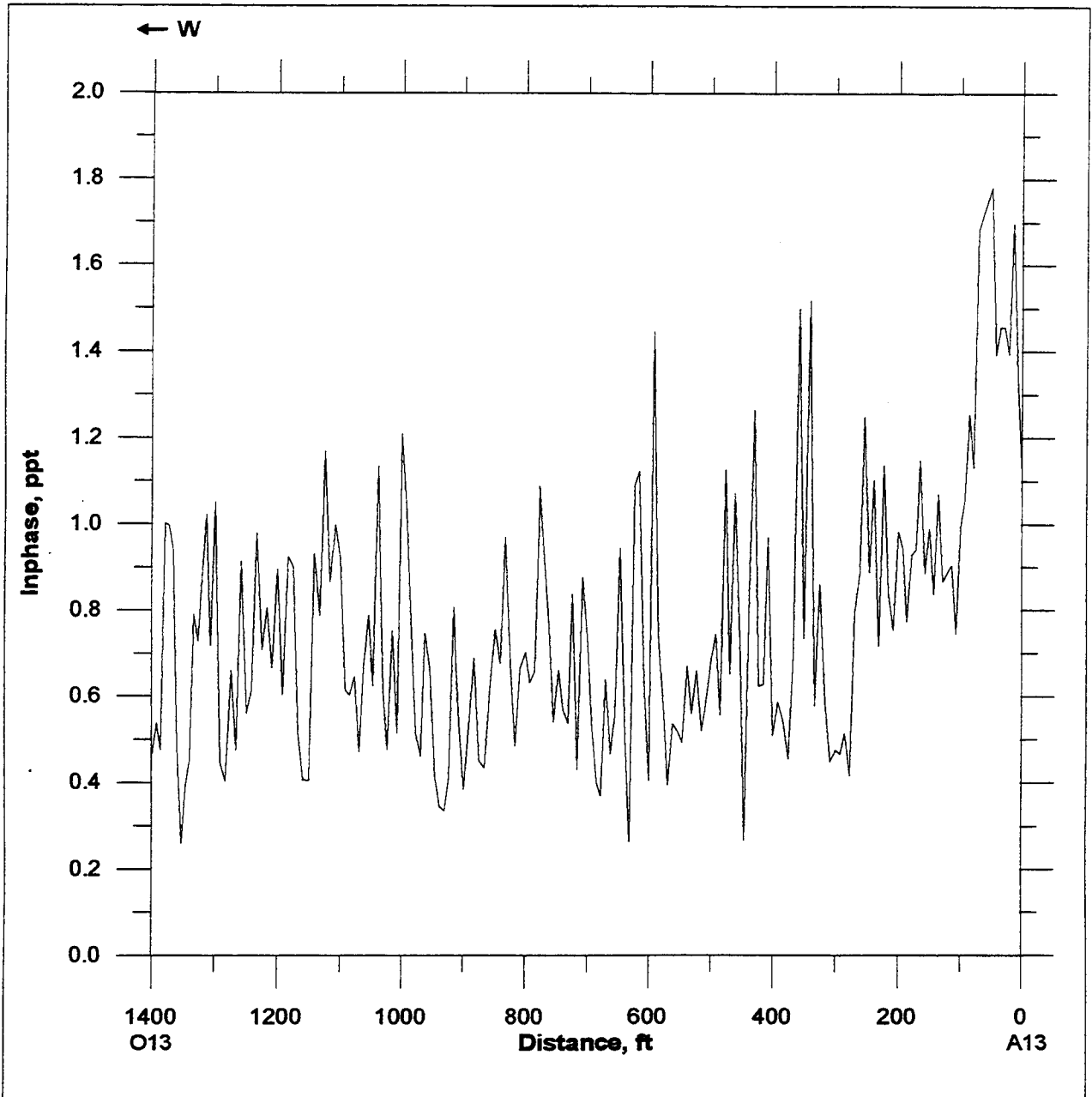
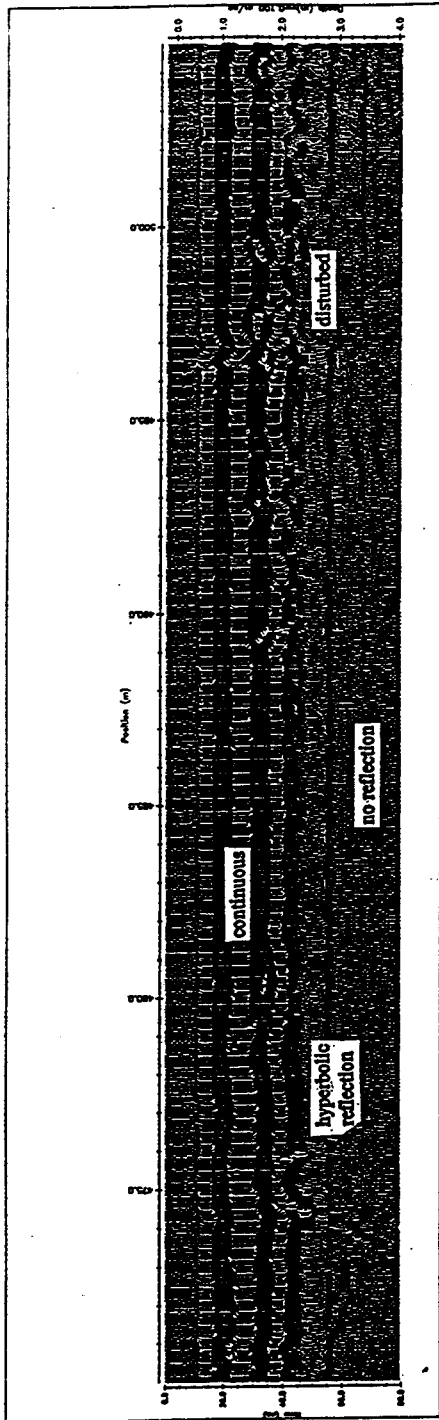


Figure 53. Inphase survey results, Line 13, (east-west), 80-acre site

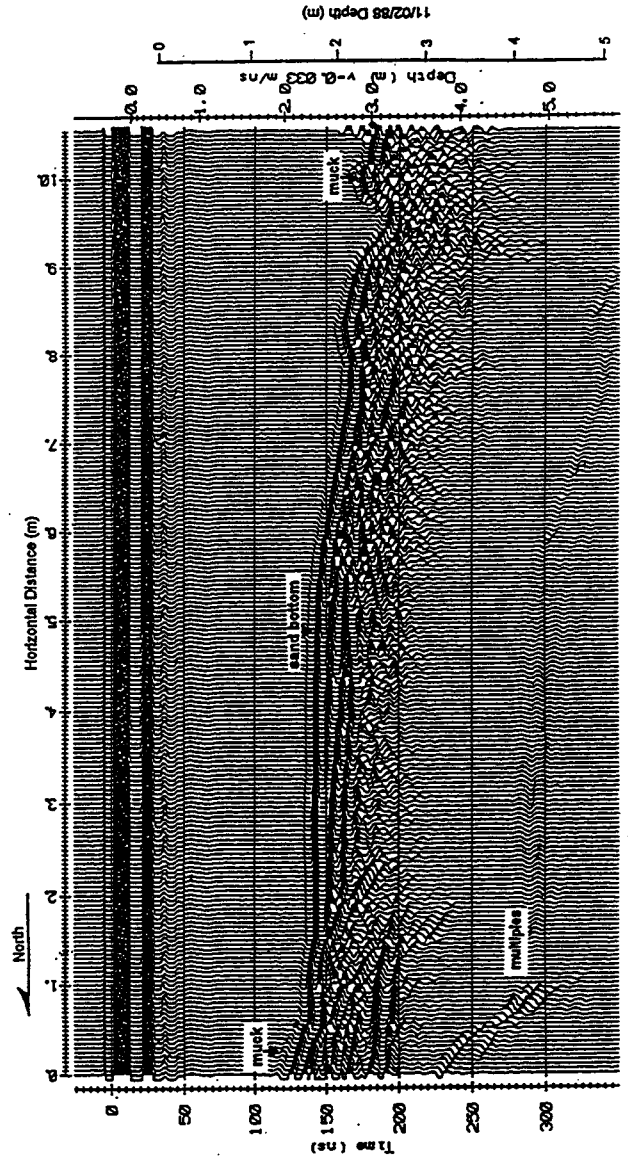
with distance along survey line plotted against time and depth (both increasing downward); DICON probe data are in tabular form giving the measured conductivity and relative dielectric permittivity, and calculated EM wave velocity. The resistivity sounding data show general variations in soil resistivity with depth. Anomalies on the conductivity and magnetic contour plots are identified as areas that differ significantly in value from the average or background value, and can be identified by a concentration of contour lines. On the GPR profile plots, anomalous areas are indicated by an interruption in reflector continuity. Anomaly detection is dependent not only on the type and size of material and the depth of burial, but also on the contrast between the soil and buried material.

The GPR data are presented as travel time versus distance along survey line. The time axis, in nanoseconds, is located on the left side of the plot and depth, in meters, is on the right. The depth scale is based on a subsurface radar velocity determined by analysis of the CMP data. There are two aspects of the GPR field data plot that require some explanation. The first notable feature is the lack of coincidence between zero time and zero depth (for example, see Figure 54). This offset is due to the separation of the transmitter and receiver antenna. The first arrival at the receiver is the reflection from the direct wave traveling from the transmitter to the receiver, not the reflection from the ground surface. The time span between zero time and zero depth is the one-way travel time of the direct wave between the transmitter and the receiver. The second point of initial confusion is the depth scale, in particular at very shallow depths where the scale is obviously nonlinear. The depth is determined based on the velocity of the media. Because the transmitter and receiver antenna are separated by a finite distance and the transmitted pulse has a lobe-shaped radiation pattern, the ray of the transmitted pulse that arrives at the receiver does not strike the subsurface interface at normal incidence, but at an acute angle. The depth scale is corrected for non-normal incidence of the transmitted ray path.

There are six common features which can often be identified in a GPR record: continuous reflector, discontinuous reflector, chaotic or disturbed reflection, no reflection, hyperbolic reflection, and multiple (Figure 54). A continuous reflector identifies a relatively smooth and uninterrupted boundary, whereas a discontinuous reflector represents a rough and intermittent boundary. A chaotic reflection is caused by a disturbance of the subsurface material, such as soil that has been removed and then backfilled, or rapid deposition. An area of no reflection on the radar record represents a loss of signal strength caused by a highly conductive or magnetic material, or system power limitations. In addition, no reflections will be observed for regions with no discontinuities or abrupt changes in dielectric properties. Hyperbolic reflection patterns are generated by the radar signal reflecting off a localized buried object (natural or man-made) as the antenna (which are located on the surface) pass over the object. A multiple is not a true reflection surface, but is generated by the transmitted pulse traversing an indirect path between the transmitter, a given reflection surface, and receiver (reflecting off multiple internal boundaries prior to reaching the receiver). Multiple reflections can travel various paths depending on the number of true subsurface reflectors, and the



(Simms 1996)



(Llopi and Sharp 1997)

Figure 54. Common features found on a GPR record

travel time of the multiple will always be greater than the reflection travel time of the true reflector. The reflection characteristics described above are used to qualitatively interpret the radar record and identify anomalous areas.

The DICON probe data are used to obtain very near surface conductivity data and to aid in estimating velocities used in presenting the GPR data. The data are also used as an index property indication of spatial variation in EM properties.

Electrical resistivity soundings

Six electrical resistivity soundings were performed. The center of each sounding and direction of expansion is depicted in Figure 8. Plots of the field data (Appendix G) suggest a (near surface) three layer earth structure having a high-low-high resistivity pattern. Graphical results of the inverse modeling are shown in Figure 55. A three or four layer model best fits the data. When a fourth layer is present, it has an intermediate resistivity value between the initial high-low. The upper, high resistivity layer ranges in thickness from 0.2 to 0.8 meters with resistivity varying between 460 and 880 ohm-m (1-2 mS/m). The middle layer exhibits little variation in both resistivity, 50-70 ohm-m (14-20 mS/m), and thickness, 4.2-5.2 m. The lower-most resistive layer is detected at depths of 4.7-5.5 m and ranges in resistivity from 1300 to 9000 ohm-m (<1 mS/m). The three interpreted layers can be associated with a thin silt layer underlain by a thicker moist to saturated silt or clayey-silt unit, which overlies limestone bedrock. The estimated depth to bedrock determined from the resistivity soundings (4.7-5.5 m) is comparable to the 1.8-6.0 m depth of refusal encountered during soil sampling at the 40-acre site (PRC Environmental Management, Inc. 1994a).

EM31 surveys

The conductivity data show a general increase in conductivity from north to south (Figure 56). Average background values range from 15 to 20 mS/m. The northwest corner and northeast portion of the grid exhibit slightly lower values (11-15 mS/m). Conductivity values greater than 18 mS/m are found within the southern half of the survey grid, with values increasing toward the southwest and southeast corners. The most conductive area exists between (104-118E, 0-10N) where values exceed 24 mS/m.

Little variation is seen in the inphase data (Figure 57), with typical background values ranging from 0.4 to 0.8 ppt. Several small, weak and shallow isolated anomalies are located at (10E, 39N), (14E, 1N), (14E, 31N), (14E, 47N), (16E, 12N), (20E, 31N), and (78E, 14N).

Magnetic surveys

The results of the magnetic survey are presented in Figure 58. A nonlinear filter was applied to the data to remove spikes caused by spurious noise. The data show no apparent trends. The magnetic data have a nominal background value of

53,997 nT with an average variation of ± 6 nT. Two moderate anomaly highs are located at (74E,40N) and (102E,32N) and a small low anomaly is located at (69E, 1N).

Ground penetrating radar surveys

Figure 8 shows the location of the GPR profiles. The profile data collected using the 50, 100, and 200 MHz antennas are given in Appendix H. A velocity of 0.07 m/ns, determined using both the CMP and DICON probe measurements, was used for estimating depth of investigation. The DICON probe data are tabulated in Table 10.

An investigation depth of about 3.5 m was obtained with the 50 MHz antenna (Appendix H). Figure 59 shows a typical profile collected at this site using the 50 MHz antenna. At this frequency, two prominent reflectors are resolved and are seen to extend across the site along each line profiled. These layers, at depths of 0.5-0.7 m and 1.6-2 m, are continuous and relatively flat. A third layer having a discontinuous and intermittent reflection boundary is at a depth of approximately 3.2 m. A broad, hyperbolic reflection is evident in the east-west profile data acquired along line 50N at position 88 (Figure 59). This reflection has a calculated wave velocity of about 0.3 m/ns, that of an EM wave in air, indicating the reflection is caused by an object located on or above the ground surface.

The 100 MHz profiles (Appendix H) also image the two prominent reflectors identified in the 50 MHz data. The lower reflector (depth 1.5-2 m) is at the investigation depth limit for this frequency. The 100 MHz antenna detects a rough, discontinuous and intermittent reflector located between the other two layers at a depth of 0.9-1.2 m. A series of small, hyperbolic reflections is observed in profile line 50N between stations 90-115 at a depth of 1.5 m. Depth of investigation decreases but resolution of the shallower layers improves at the higher antenna frequencies. This is seen in a comparison of the 50 and 100 MHz profiles along line 115E (Figure 60). Note the uplifting of the reflector at 1.5 m depth between stations 45-71 in the 50 MHz profile. Greater detail is seen in the 100 MHz profile at this location, where small, sharp hyperbolic reflections from individual sources can be identified.

An approximate depth of investigation of 1 m was obtained with the 200 MHz antenna. The roughness of the shallow soil boundaries can be seen in the data (Appendix H). The shallowest reflector imaged is at a depth of 0.3-0.4 m; two deeper layers are seen at 0.8 m and 0.9 m depth. An anomaly is apparent in the 60E profile line at position 64 and at a depth of 1.0 m (Figure 61).

**Table 10
DICON Probe Data, 1-hectare Site**

Location	Depth, m	Relative Dielectric Permittivity	Conductivity mS/m	Wave Speed m/ns
10E, 30N	0.10	22.3	15.4	0.062
	0.30	23.9	27.7	0.061
	0.50	25.0	28.9	0.060
10E, 55N	0.10	17.5	8.8	0.072
	0.30	19.1	18.5	0.069
	0.50	28.0	40.6	0.057
10E, 85N	0.10	13.9	6.4	0.061
	0.30	14.6	7.6	0.079
	0.50	24.6	29.6	0.061
60E, 30N	0.10	21.7	11.4	0.064
	0.30	22.7	14.2	0.063
	0.50	24.7	24.5	0.060
60E, 55N	0.10	19.0	9.6	0.069
	0.30	19.9	15.1	0.067
	0.50	22.3	23.2	0.064
60E, 85N	0.10	19.9	9.7	0.067
	0.30	20.1	16.0	0.067
	0.50	27.0	34.3	0.058
115E, 30N	0.10	21.0	15.4	0.066
	0.30	27.7	34.9	0.057
	0.50	28.0	40.6	0.057
115E, 55N	0.10	25.4	16.2	0.060
	0.30	22.6	25.4	0.063
	0.50	26.7	29.2	0.058
115E, 85N	0.10	21.6	12.9	0.065
	0.30	23.1	16.1	0.062
	0.50	25.2	21.8	0.060
Average	0.10	14.4	11.8	0.067
	0.30	21.5	19.5	0.065
	0.50	25.7	30.3	0.059

JPG -- 1 Hectare Site

Electrical Resistivity Results

LEGEND

-  Array Center
-  Array Expansion Direction

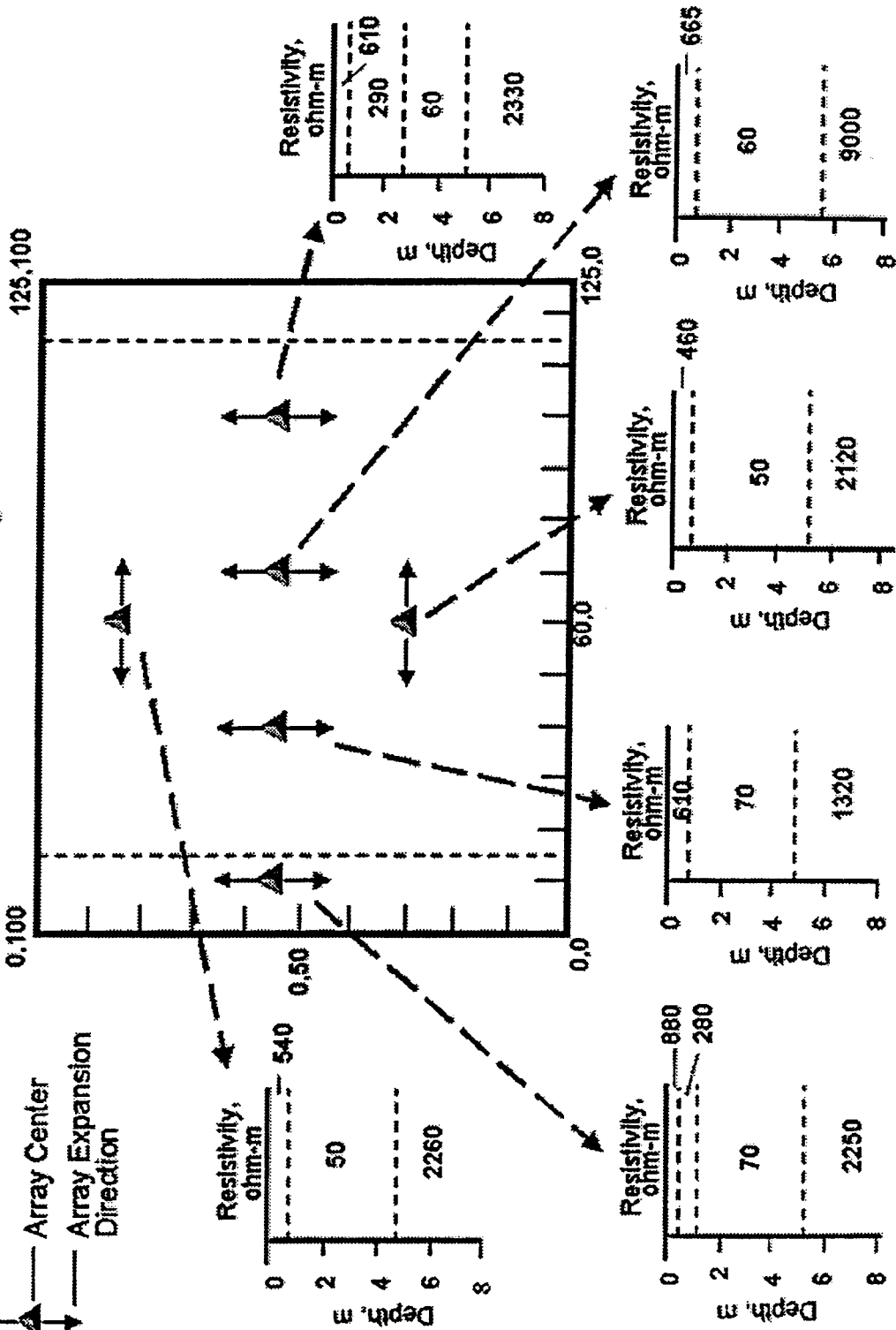


Figure 55. VES modeling results, 1-hectare site

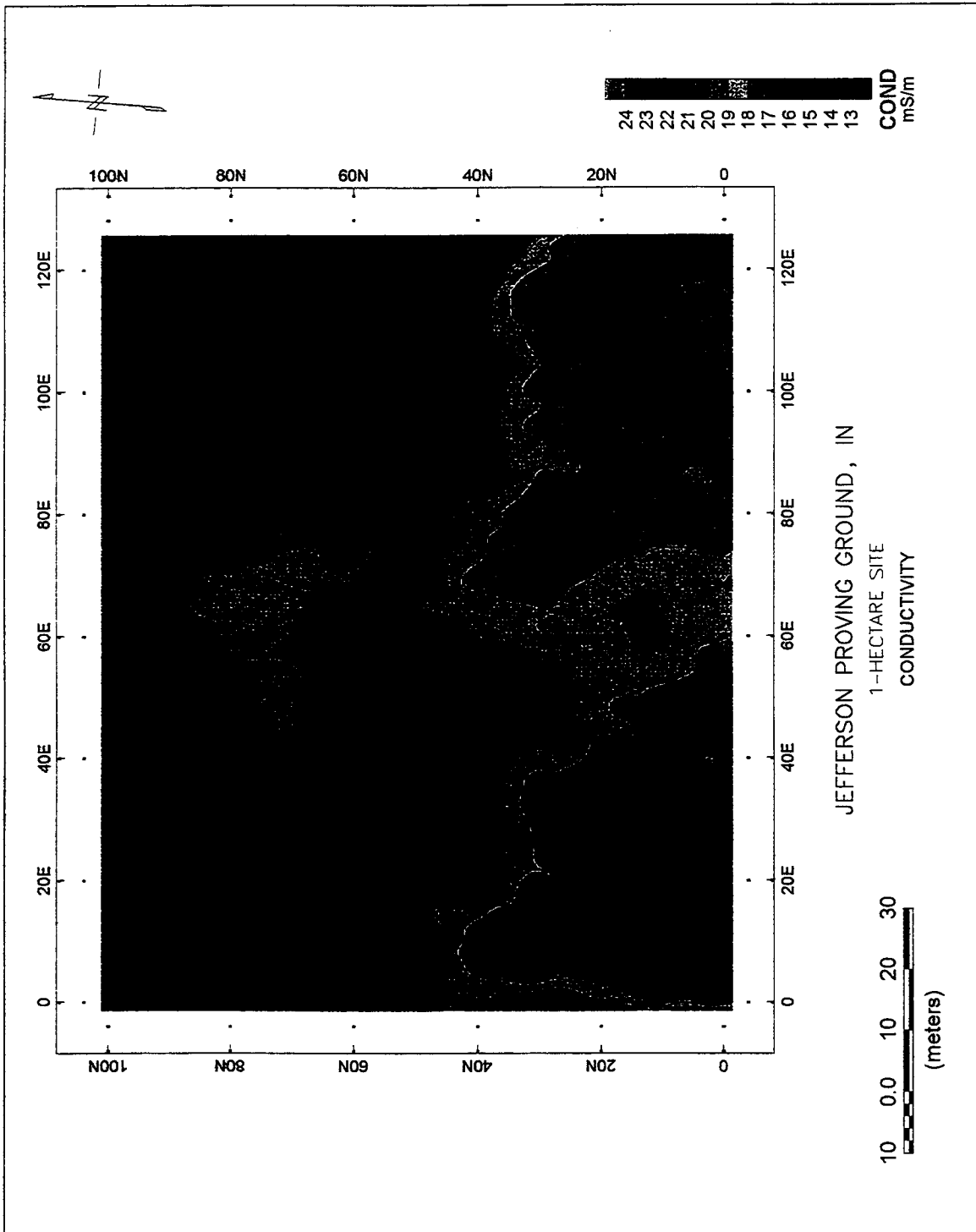


Figure 56. Conductivity survey results, 1-hectare site

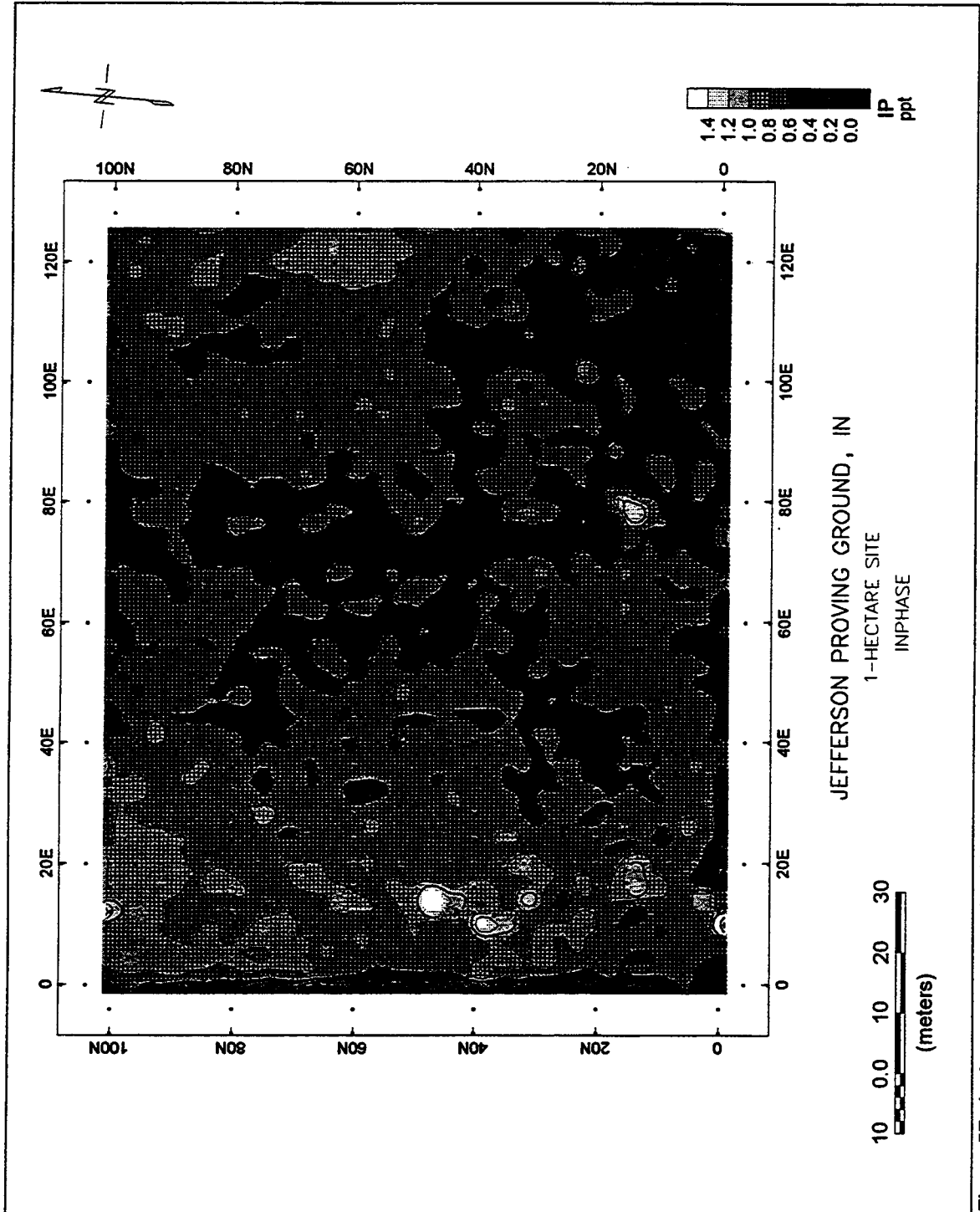


Figure 57. Inphase survey results, 1-hectare site

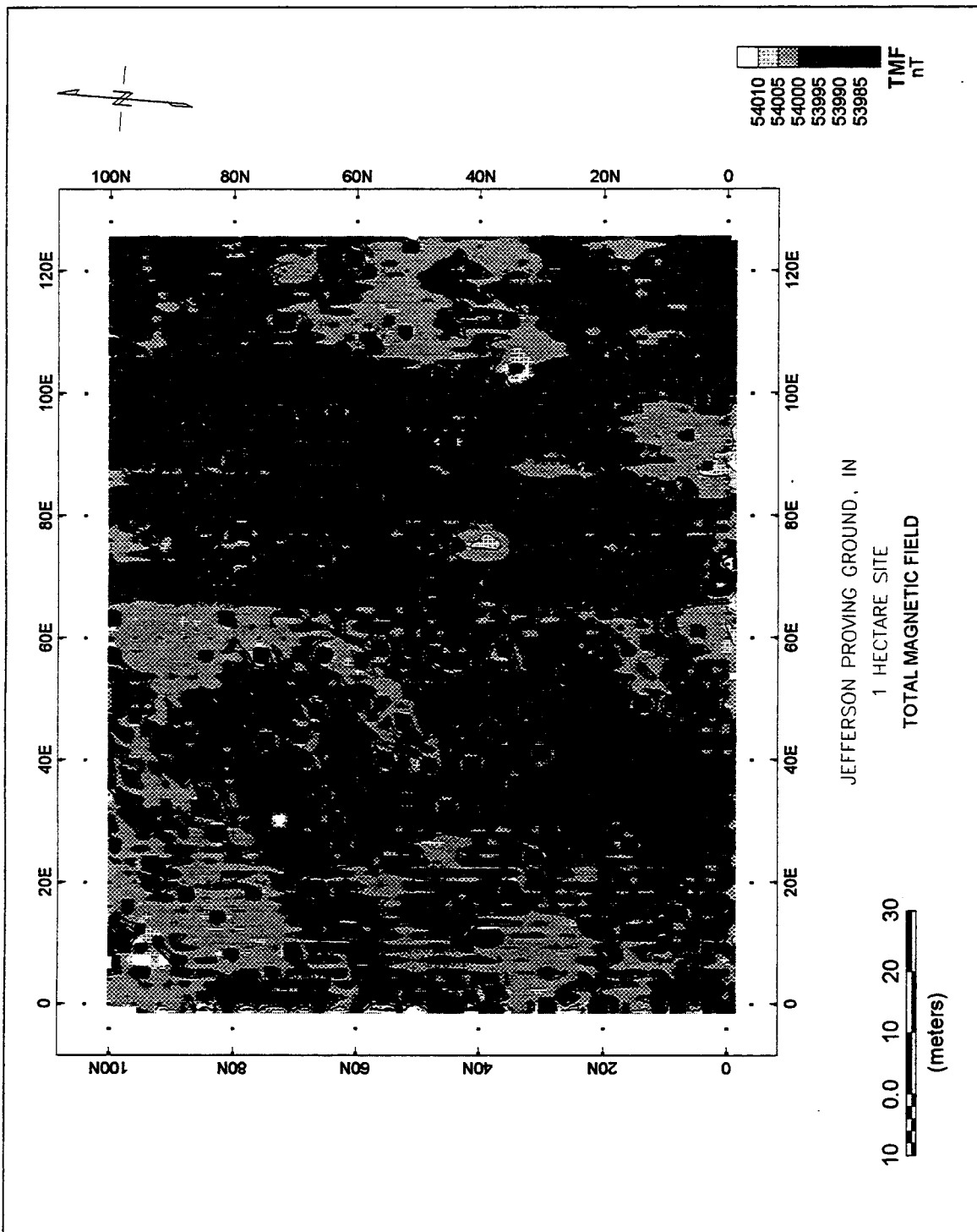


Figure 58. Magnetometer survey results, 1-hectare site

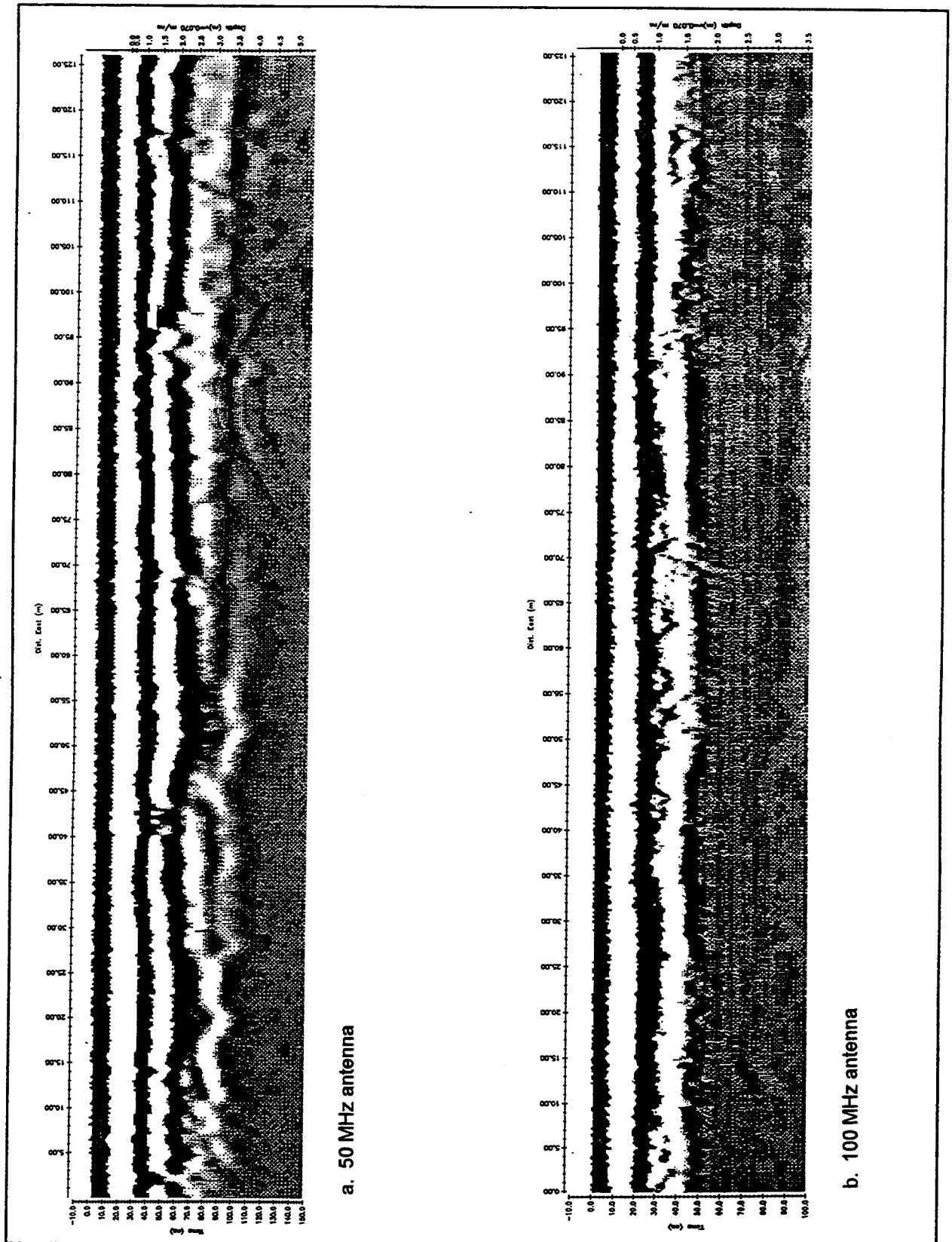
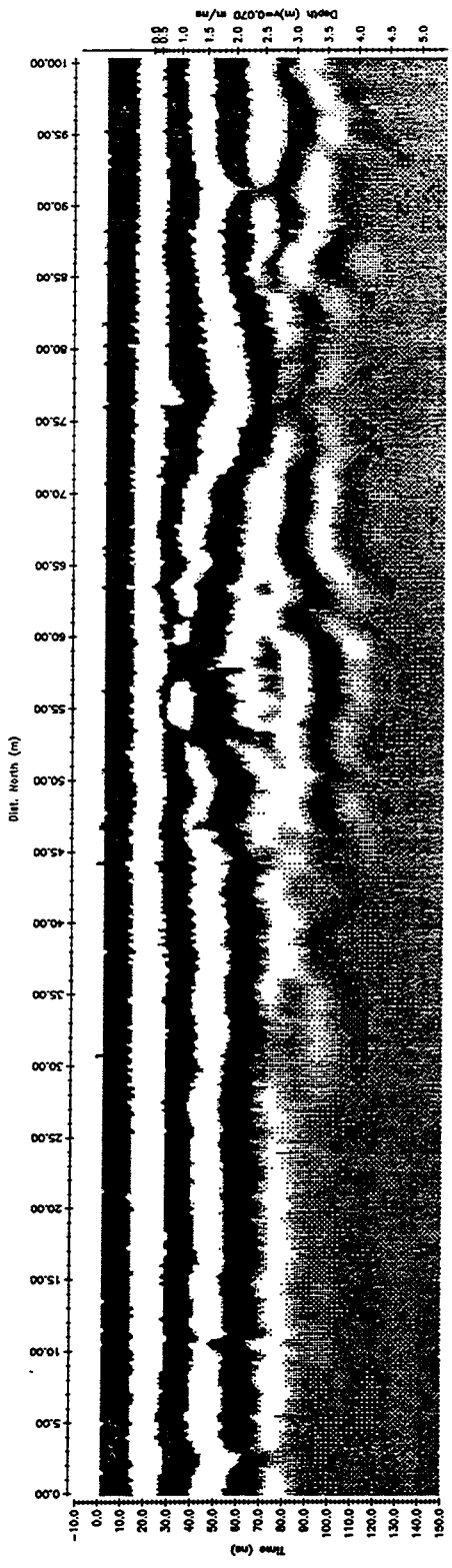
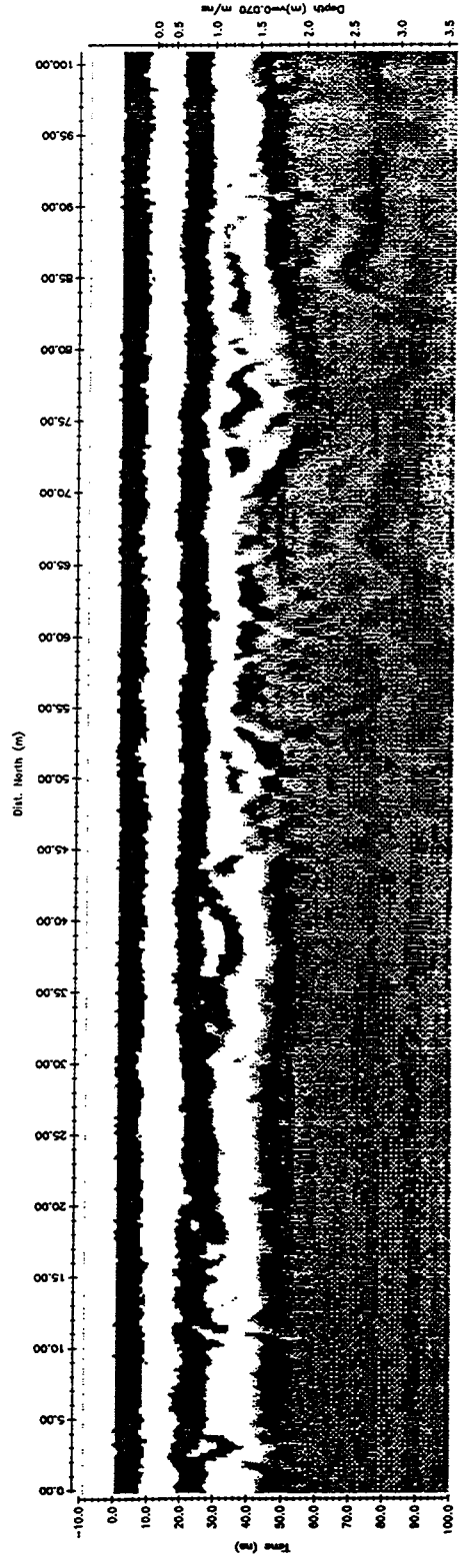


Figure 59. GPR profile lines collected along Line 50N (east-west), 1-hectare site



a. 50 MHz antenna



b. 100 MHz antenna

Figure 60. GPR profile lines collected along Line 115E (north-south), 1-hectare site

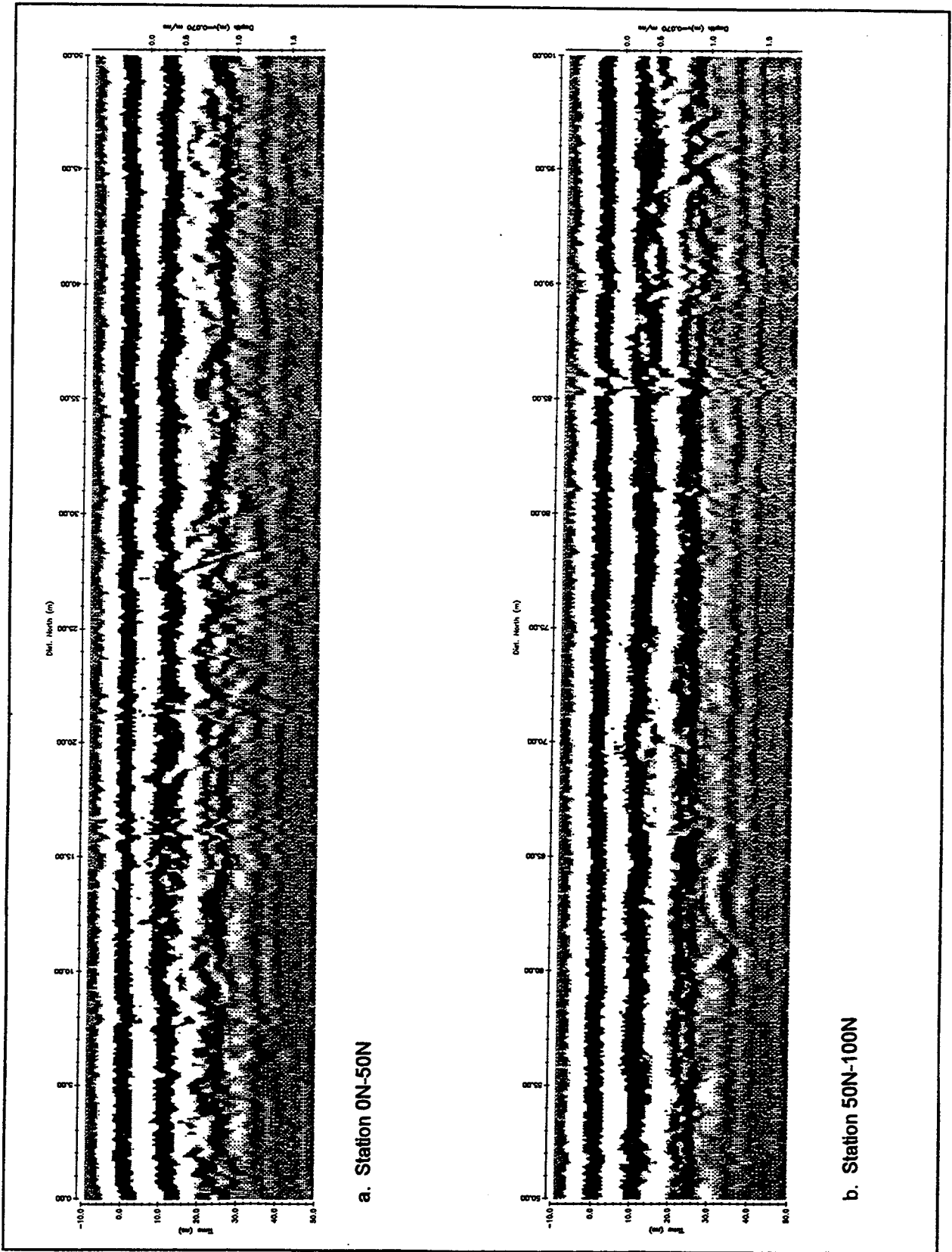


Figure 61. GPR profile line collected along Line 60E (north-south), 200 Mhz, 1-hectare site

Summary and Conclusions from Geophysical Testing

Geophysical survey results at JPG indicate that similar site conditions exist at the 40- and 80-acre and 1-hectare sites. The resistivity data generally indicate a three layer model. The top layer, corresponding to dry silty material, is usually on the order of 0.5 -1.0 m in thickness with an average resistivity of about 500-600 Ω -m (1-2 mS/m). The second layer is about 4 m thick and has an average range of resistivities of about 30 to 60 Ω -m (17-30 mS/m). This layer probably corresponds to silty material with increasing percentages of clay and/or moisture. The deepest layer detected is found at depths ranging between 2 and 7 m. This layer has a resistivity range of between approximately 600 and 9000 Ω -m (<1 to 2 mS/m), but more typically about 1800 Ω -m (1 mS/m). This layer is presumed to correspond with limestone bedrock. The EM31 derived conductivities for the upper 4-6 m generally range between about 15 and 25 mS/m and agree with the values from the resistivity surveys.

The average dielectric permittivities obtained from the DICON probe at the three test sites for depths of 0.1 and 0.5 m are 16.2 and 25.6, respectively, and are slightly higher than the GPR derived dielectric permittivity value of 10.4 obtained at the 40-acre test site.

The GPR surveys conducted at the 40-acre site using a 300 and 600 MHz antennas indicate high soil attenuations which agrees with the results of the laboratory EM tests. The high attenuation limited the depth of investigation to about 2 m. The dielectric permittivity of about 10 predicts a narrow beam pattern which means that the GPR antenna would have to be directly above a target in order to detect it. GPR surveys were conducted at the 1-hectare site using antenna frequencies of 50, 100, and 200 MHz. The maximum depth of investigation was about 3.5 m using the 50 MHz antenna.

7 Summary and Conclusions

This report details the geological, geophysical, environmental and geotechnical characterization of three UXO test sites at Jefferson Proving Ground, IN. The purpose of the site characterization is to support:

- a. Phase IV demonstrator planning and results assessment,
- b. Additional assessments of Phase I-III
- c. Future use of JPG sites,
- d. Comparisons of the JPG sites with other UXO and landmine test sites and cleanup sites.

Laboratory analysis indicate that the soils at the 40- and 80-acre sites are very similar in terms of classification. The soil samples were collected at depths of 0.10, 0.50 and 1 m depths and all samples, with the exception of one, are classified as either CH or CL and in general are characterized as clays or sandy clays. Plotted on a plasticity chart, the soil samples are very near the A-line and exhibit little plasticity. Average water contents, even under very dry environmental conditions, show an increase with depth and range from 13.9 percent at a depth of 0.10 m to 20.3 percent at a depth of 0.10 m. The seven locations from which soil samples were collected at the 1-hectare site are visually classified as silt with clay and/or sand or as sandy or silty clay ML and CL.

The samples from the 40- and 80-acre site as mentioned above are characterized as clays or sandy clays according to the USCS. This classification is based in part on grain size and not mineralogy. In the USCS, soil particles passing the No. 200 sieve are considered silt or clay. However, in the case of the JPG soils XRD analysis show that these soils contain little or no clay minerals. The XRD analysis indicate that these soils consist chiefly of very fine grained (silt or clay-sized) silica particles. No XRD analysis were performed on the 1-hectare soils. It is presumed that the 1-hectare soils have a similar mineralogical makeup as those of the 40-acre site because of their similar soil classifications and proximity.

The general results of the laboratory EM properties show that the dielectric permittivity of the soil samples collected at the 40- and 80-acre sites are relatively high, ranging between approximately 10 and 12. The soils also exhibit high signal attenuation at

typical field soil water contents. For the 200 MHz test and at typical water content conditions the attenuation approaches 20 dB/m which is similar to the value for wet soil conditions. No laboratory EM tests were performed on the 1-hectare site soils.

Geophysical survey results at JPG indicate that similar site conditions exist at the 40- and 80-acre and 1-hectare sites. The resistivity data generally indicate a three layer model. The top layer, corresponding to dry silty material, is usually on the order of 0.5 -1.0 m in thickness with an average resistivity of about 500-600 Ω -m (1-2 mS/m). The second layer is about 4 m thick and has an average range of resistivities of about 30 to 60 Ω -m (17-30 mS/m). This layer probably corresponds to silty material with increasing percentages of clay and/or moisture. The deepest layer detected is found at depths ranging between 2 and 7 m. This layer has a resistivity range of between approximately 600 and 9000 Ω -m (<1 to 2 mS/m), but more typically about 1800 Ω -m (1 mS/m). This layer is presumed to correspond with limestone bedrock. The EM31 derived conductivities for the upper 4-6 m generally range between about 15 and 25 mS/m and agree with the values from the resistivity surveys and generally correlate to soil type.

The average dielectric permittivities obtained from the DICON probe at the three test sites for depths of 0.1 and 0.5 m are 16.2 and 25.6, respectively, and are slightly higher than the GPR derived dielectric permittivity value of 10.4 obtained at the 40-acre test site.

The GPR surveys conducted at the 40-acre site using a 300 and 600 MHz antennas indicate high soil attenuations which agrees with the results of the laboratory EM tests. The high attenuation limited the depth of investigation to about 2 m. The dielectric permittivity of about 10 predicts a narrow beam pattern which means that the GPR antenna would have to be directly above a target in order to detect it. GPR surveys were conducted at the 1-hectare site using antenna frequencies of 50, 100, and 200 MHz. The maximum depth of investigation was about 3.5 m using the 50 MHz antenna. An EM velocity of 0.7 m/ns was used for depth estimations.

References

- Altshuler, T. W., Andrews, A. M., Dugan, R. E., George, V., Mulqueen, M. P., and Sparrow, D. A. (1995). "Demonstrator performance at the Unexploded Ordnance Technology Demonstration at Jefferson Proving Ground (Phase I) and implications for UXO clearance," IDA Paper P-3114, Institute for Defense Analysis, Alexandria, VA.
- Annan, A. P. (1992). *Ground penetrating workshop notes*. Sensors & Software, Inc., Mississauga, Ontario, Canada.
- Arcone, S. A. (1995). "Numerical studies of the radiation patterns of resistively loaded dipoles," *Journal of Applied Geophysics*, 33, 39-52.
- Arcone, S. A., Lawton, D. E., Delaney, A. J., Strasser, J. C. and Strasser, J. D. (1998). "Ground-penetrating radar reflection profiling of groundwater and bedrock in an area of discontinuous permafrost," *Geophysics*, in prep.
- Barrows, L. And Rocchio, J. E. (1990). Geophysical surveying for buried metallic objects," *Ground Water Monitoring Review* 10(3), 204-211
- Bevan, B.W. (1983). "Electromagnetics for mapping buried earth features," *Journal of field archaeology* 10.
- Breiner, S. (1973). "Applications manual for portable magnetometers," Geometrics, Sunnyvale, CA.
- Brillouin, L. (1960). *Wave propagation and group velocity*. Academic Press: New York.
- Casagrande, A. (1947). "Classification and identification of soils." Proc. ASCE, June, pp 783-810.
- Clarke, T. S., and Bentley, C. R. (1994). "High-resolution radar on Ice Stream B2, Antarctica: Measurements of electromagnetic wave speed in firm and strain history from buried crevasses," *Annals of Glaciology*, 20, 153-159.

- Delaney, A. J. and Arcone, S. A. (1984). "Dielectric measurements of frozen silt using time domain reflectometry," *Cold Regions Science and Technology*, 9, 39-46.
- Debye, P. (1929). *Polar molecules*. Dover Pub., Mineola, New York.
- Dobrin, M. B. (1960). *Introduction to geophysical prospecting*. 2nd ed., McGraw-Hill, New York.
- Fenneman, N. M. (1938). *Physiography of the Eastern United States*. McGraw Hill, New York.
- Feynman, R. P., Leighton, R. B. and Sands, M. (1964). *The Feynman Lectures on Physics, Vol. II*. Addison Wesley: Reading, MA.
- Geonics Limited (1984). "Operating manual for EM31-D non-contacting terrain conductivity meter," Geonics Limited, Mississauga, Ontario, Canada.
- Hoekstra, P. and Delaney, A. J. (1974). "Dielectric properties of soils at UHF and microwave frequencies," *Journal of Geophysical Research*, 79, 1699-1708.
- Hoekstra, P. and Doyle, W. T. (1971). "Dielectric relaxation of surface adsorbed water," *Journal of Colloid and Interface Science*, 36, 513-521.
- Interpex Ltd. (1988). "RESIX Plus DC resistivity data interpretation software" (computer program), Interpex Ltd., Golden, CO.
- Jezek, K. C., Bentley, C. R., and Clough, J. W. (1979). "Electromagnetic sounding of bottom crevasses on the Ross Ice Shelf, Antarctica," *Journal of Glaciology*, 24, 321-330.
- Keller, G. V., and Frischknecht, F. C. (1982). *Electrical methods in geophysical prospecting*. Pergamon Press, New York.
- Llopis, J. L. And Sharp, M. K. (1997). A feasibility study on the use of waterborne ground penetrating radar to profile the bottom of the Kissimmee River, Florida," Letter Report, submitted to The South Florida Water Management District, Palm Beach, FL, prepared by U.S. Army Engineer Waterways Experiment Station, Vicksburg, MS.
- McWilliams, K. M. (1985). "Soil survey of Ripley County and part of Jennings County, Indiana," U.S. Department of Agriculture, Soil Conservation Service, Washington, D.C.
- Means, R. E. and Parcher, J. V. (1963). *Physical properties of soils*. Charles E. Merrill Publishing Co., Columbus, OH.

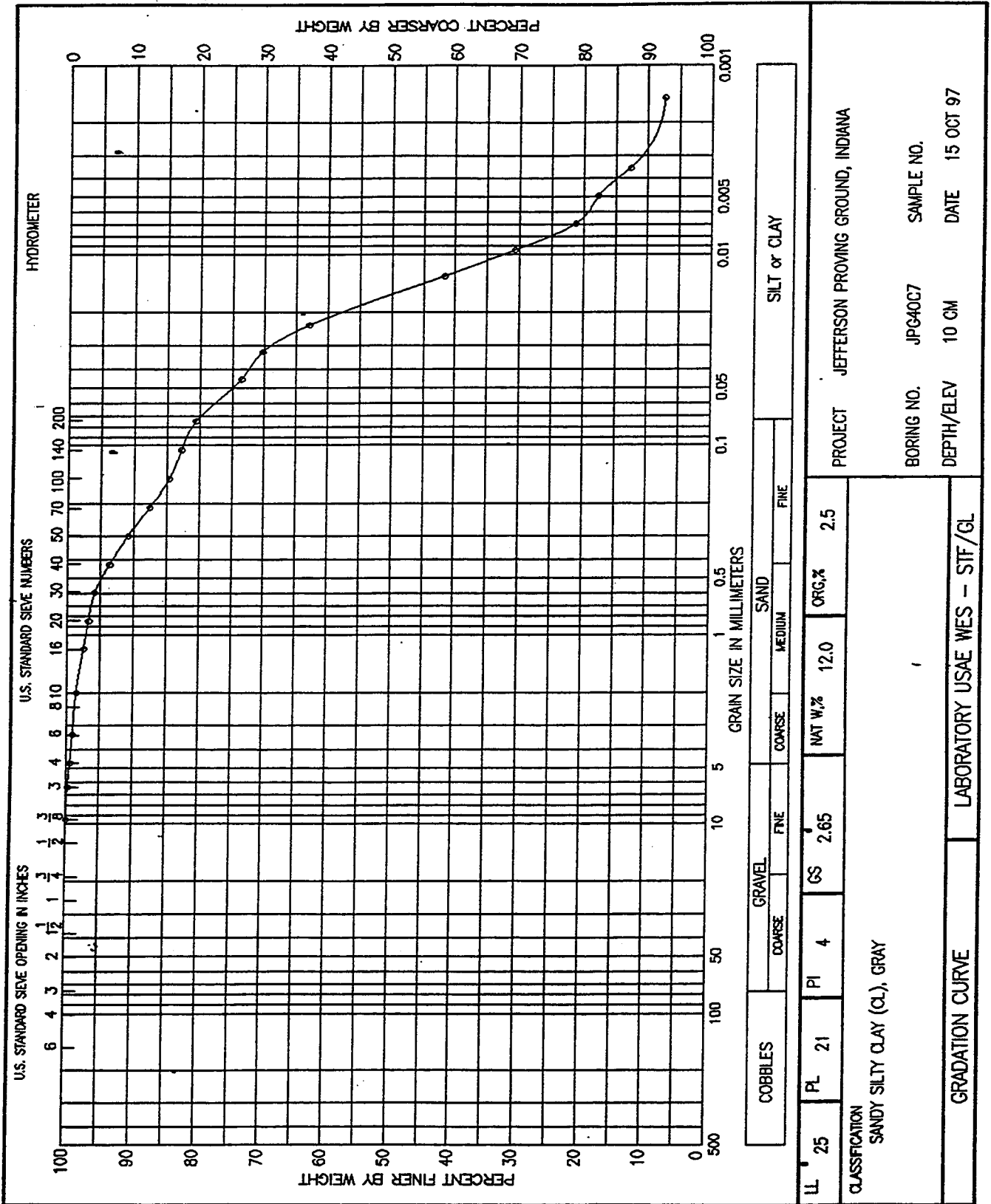
- Miller, C. A., Malone, C. R., and Blount, C. B. (1992). "Guide for the conduct of predeployment site characterization surveys for the AN/GSS-34 (V) Ported Coaxial Cable Sensor (PCCS)," Instruction Report EL-92-1, U.S. Army Engineer Waterways Experiment Station, Vicksburg, MS.
- Nickell, A. K. (1985). "Soil survey of Jefferson County, Indiana," U.S. Department of Agriculture, Soil Conservation Service, Washington, D.C.
- Parkhomenko, E. I. (1967). *Electrical properties of rocks*. Plenum Press: New York.
- Péwé, T. L. (1955). "Origin of the upland silt near Fairbanks, Alaska," *Geological Society of America Bulletin*, 67, 699-724.
- PRC Environmental Management, Inc (1994a). "Geotechnical investigation report (Draft)," Task 3: Preparation of demonstration site, Jefferson Proving Ground Madison, Indiana.
- PRC Environmental Management, Inc (1994b). "Geophysical investigation report (Draft)," Task 3: Preparation of demonstration site, Jefferson Proving Ground Madison, Indiana.
- Ray, L. L. (1974). "Geomorphology and quaternary geology of the glaciated Ohio River Valley: A reconnaissance survey," U.S. Geological Survey. Professional Paper 826.
- Rodbell, D. T., Forman, S. L., Pierson, J. and Lynn, W. C. (1997). "Stratigraphy and chronology of Mississippi Valley loess in western Tennessee," *Geological Society of America Bulletin*, 109, 1134-1148.
- Schneider, A. F. (1966). "Physiography." *Natural features of Indiana*. A. A. Lindsey, ed., Indiana Academy of Science. Indianapolis, IN.
- Simms, J. E. (1996). "Geophysical investigation at the Upatoi village archaeological site (9ME395), Fort Benning, Georgia," Draft Report, U.S. Army Engineer Waterways Experiment Station, Vicksburg, MS.
- Simms, J. E., Llopis, J. L., Butler, D. K., and Smith, L. M. (1997). "Geophysical site characterization for UXO Backgrounds Study at Fort Carson, Colorado and Fort A.P. Hill, Virginia," Letter Report, U.S. Army Engineer Waterways Experiment Station, Vicksburg, MS.
- Sparrow, D. A., Andrews, A. M., and Dugan, R. E. (1995). "Evaluation of individual demonstrator performance at the Unexploded Advanced Technology Program at Jefferson Proving Ground (Phase I)," SFIM-AEC-ET-CR-95033, U.S. Army Environmental Center, Aberdeen Proving Ground, MD.

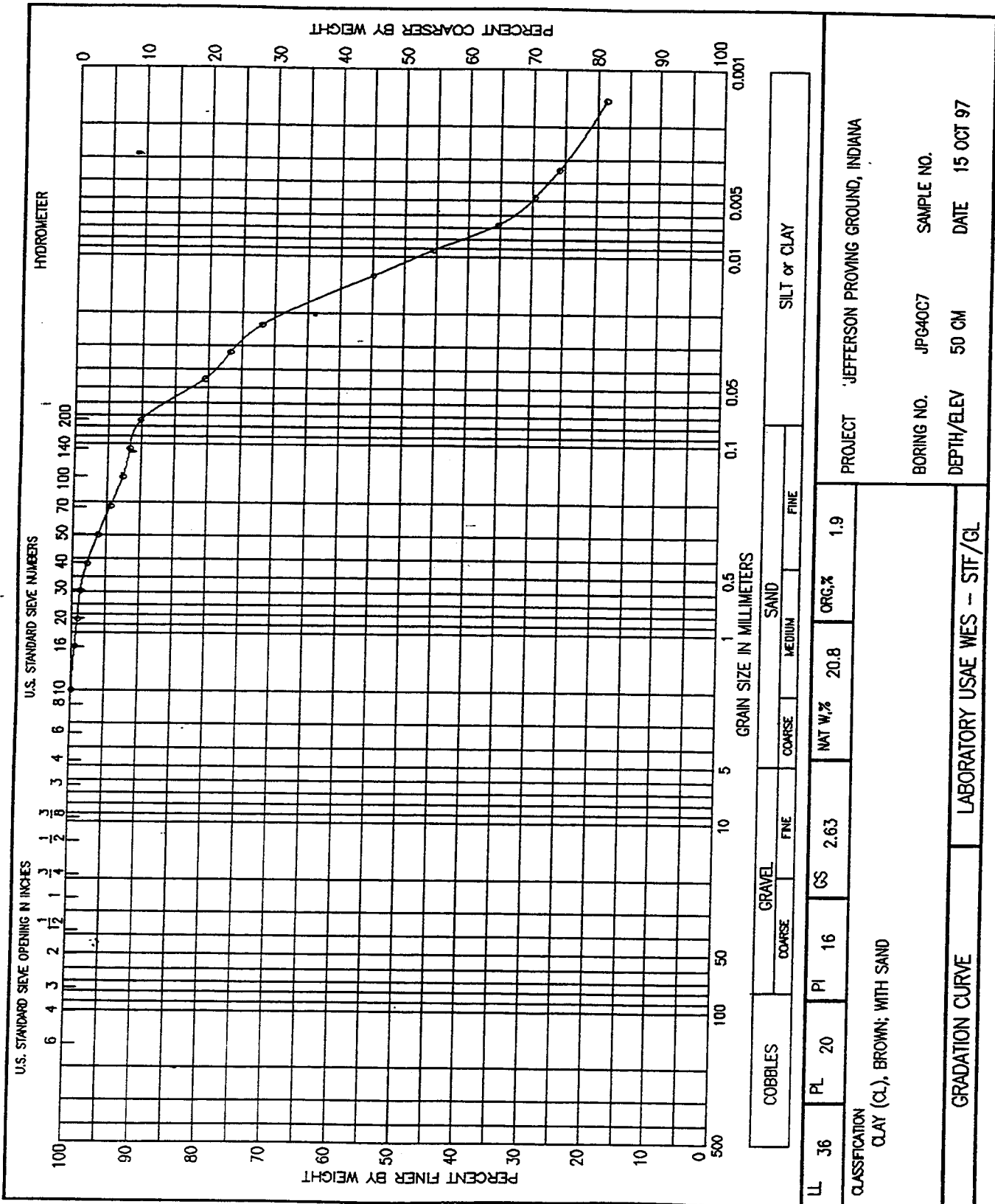
- Stratton, J. (1941). *Electromagnetic theory*. McGraw-Hill: New York.
- Telford, W. M., Geldhart, L. P., Sheriff, R. E., and Keys, D. A. (1976). *Applied geophysics*. Cambridge University Press, New York.
- Tetra Tech EM, Inc. (1998). "Demonstration work plan (draft). Phase IV controlled site advanced technology demonstrations at Jefferson Proving Ground, Indiana," Tetra Tech EM, Inc., Brookfield, WI.
- Tice, A. R., Oliphant, J. L., Nakano, Y. and Jenkins, T. F. (1982). "Relationship between the ice and unfrozen water phases in frozen soil as determined by pulsed nuclear magnetic resonance and physical desorption data," CRREL Report 82-15, U. S. Army Cold Regions Research and Engineering Laboratory, Hanover, NH, 8 pp.
- Topp, G. C., Davis, J. L. and Annan, A. P. (1980). "Electromagnetic determination of soil water content: measurements in coaxial transmission lines," *Water Resources Research*, 16, 574-582.
- USAEC (1994). "Unexploded Ordnance Advanced Technology Demonstration Program at Jefferson Proving Ground (Phase I)," Report No. SFIM-AEC-ET-CR-94120, U.S. Army Environmental Center, Aberdeen Proving Ground, MD.
- USAEC (1995). "Evaluation of individual demonstrator performance at the Unexploded Ordnance Advanced Technology Demonstration Program at Jefferson Proving Ground (Phase I)," Report No. SFIM-AEC-ET-CR-95033, U.S. Army Environmental Center, Aberdeen Proving Ground, MD.
- USAEC (1996). "Unexploded Ordnance Advanced Technology Demonstration Program at Jefferson Proving Ground (Phase II)," Report No. SFIM-AEC-ET-CR-96170, U.S. Army Environmental Center, Aberdeen Proving Ground, MD.
- USAEC (1997). "Unexploded Ordnance Advanced Technology Demonstration Program at Jefferson Proving Ground (Phase III)," Report No. SFIM-AEC-ET-CR-97011, U.S. Army Environmental Center, Aberdeen Proving Ground, MD.
- USAEWES (1982). "The Unified Soil Classification System," Technical Memorandum No. 3-357, U.S. Army Engineer Waterways Experiment Station, Vicksburg, MS.
- Wait, J. R. (1970). *Electromagnetic waves in stratified media*, 2nd Ed. Pergamon Press, New York.
- Weiss, C. A., Jr. (1998). "Clay mineral identification of eleven soils from Jefferson Proving Ground, Indiana, by X-ray diffraction (XRD) analysis," Memorandum For Dr. Dwain Butler (CEWES-GG), U.S. Army Engineer Waterways Experiment Station, Vicksburg, MS.

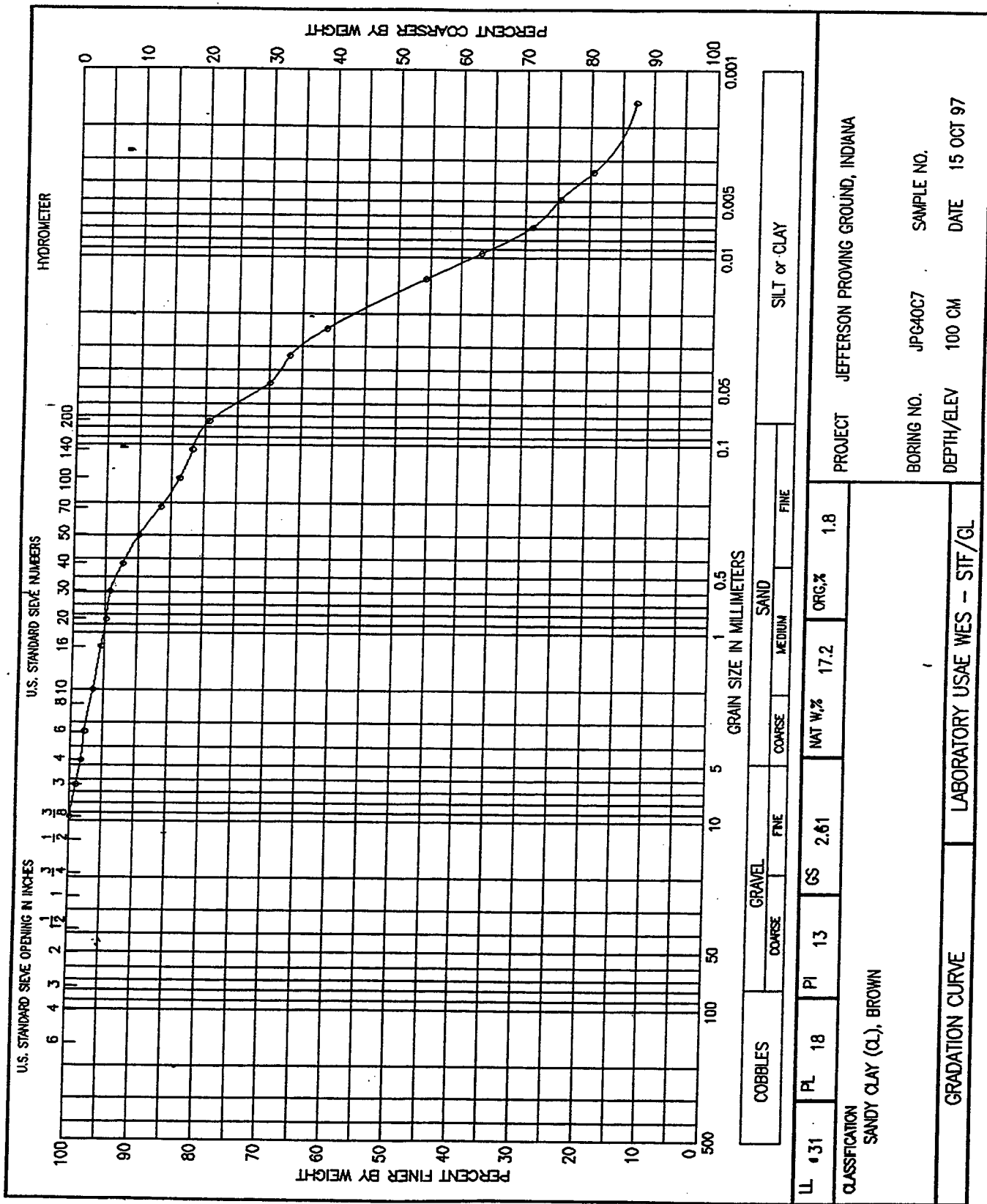
Appendix A

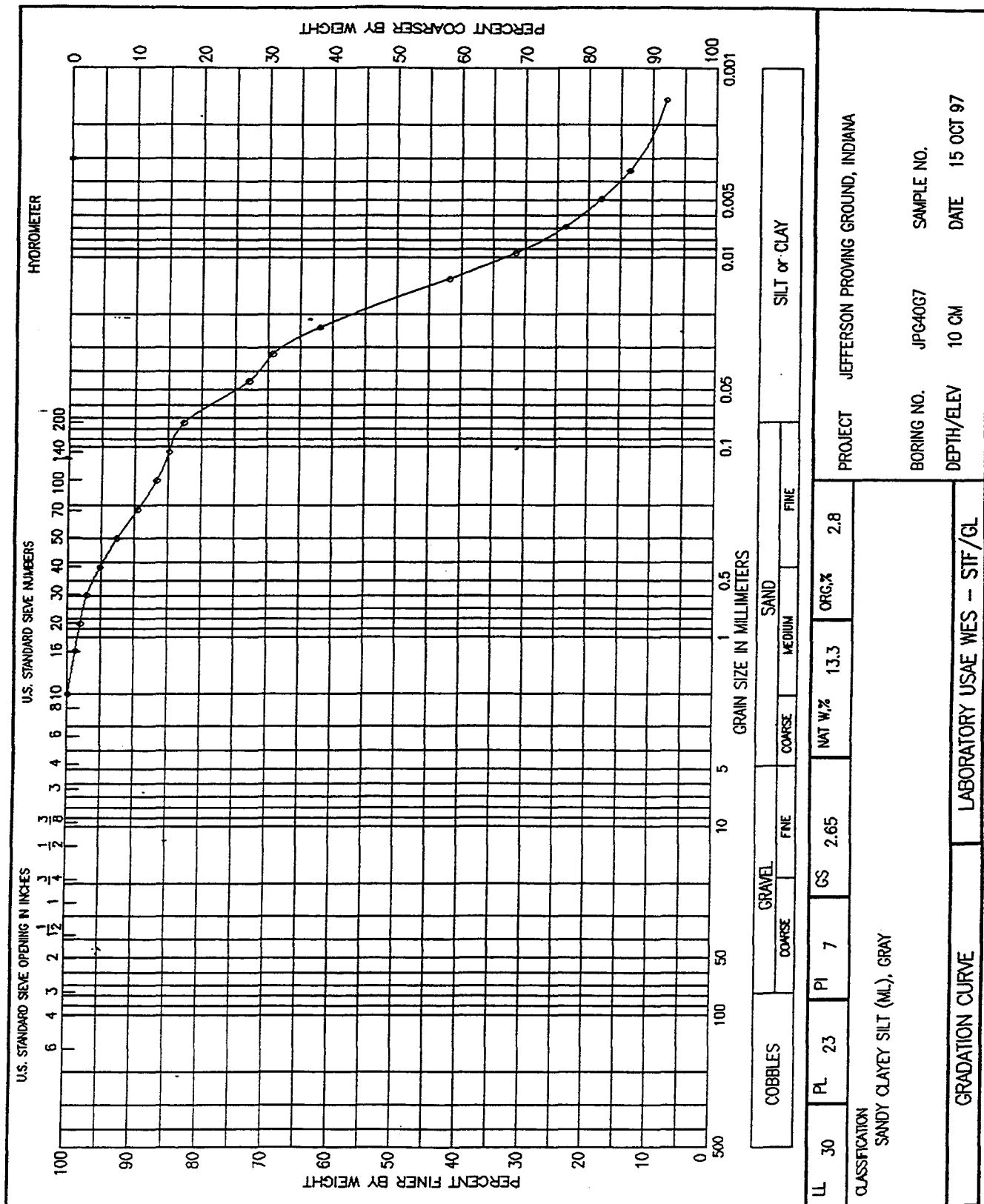
Soil Gradation Curves:

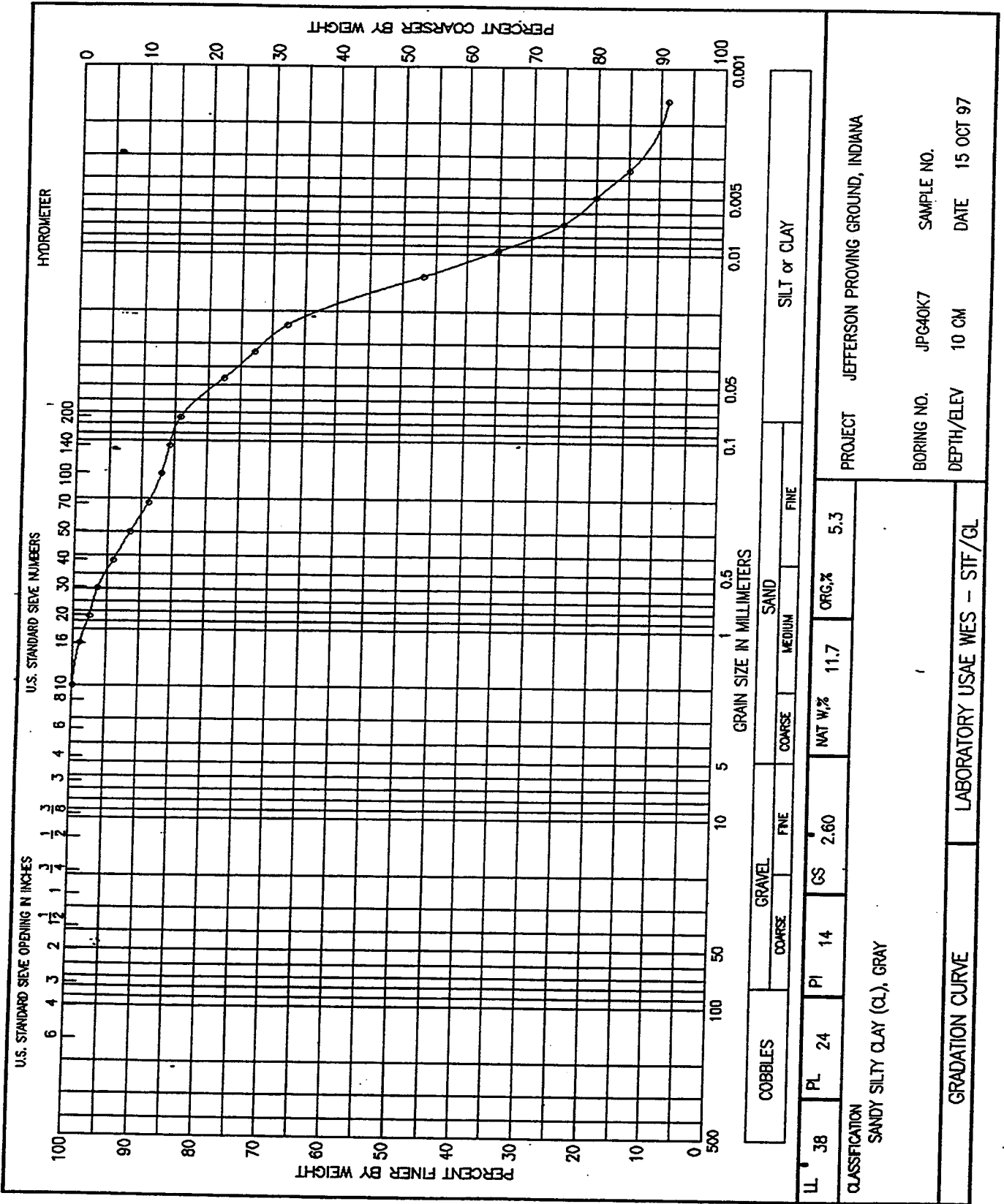
40-acre Site

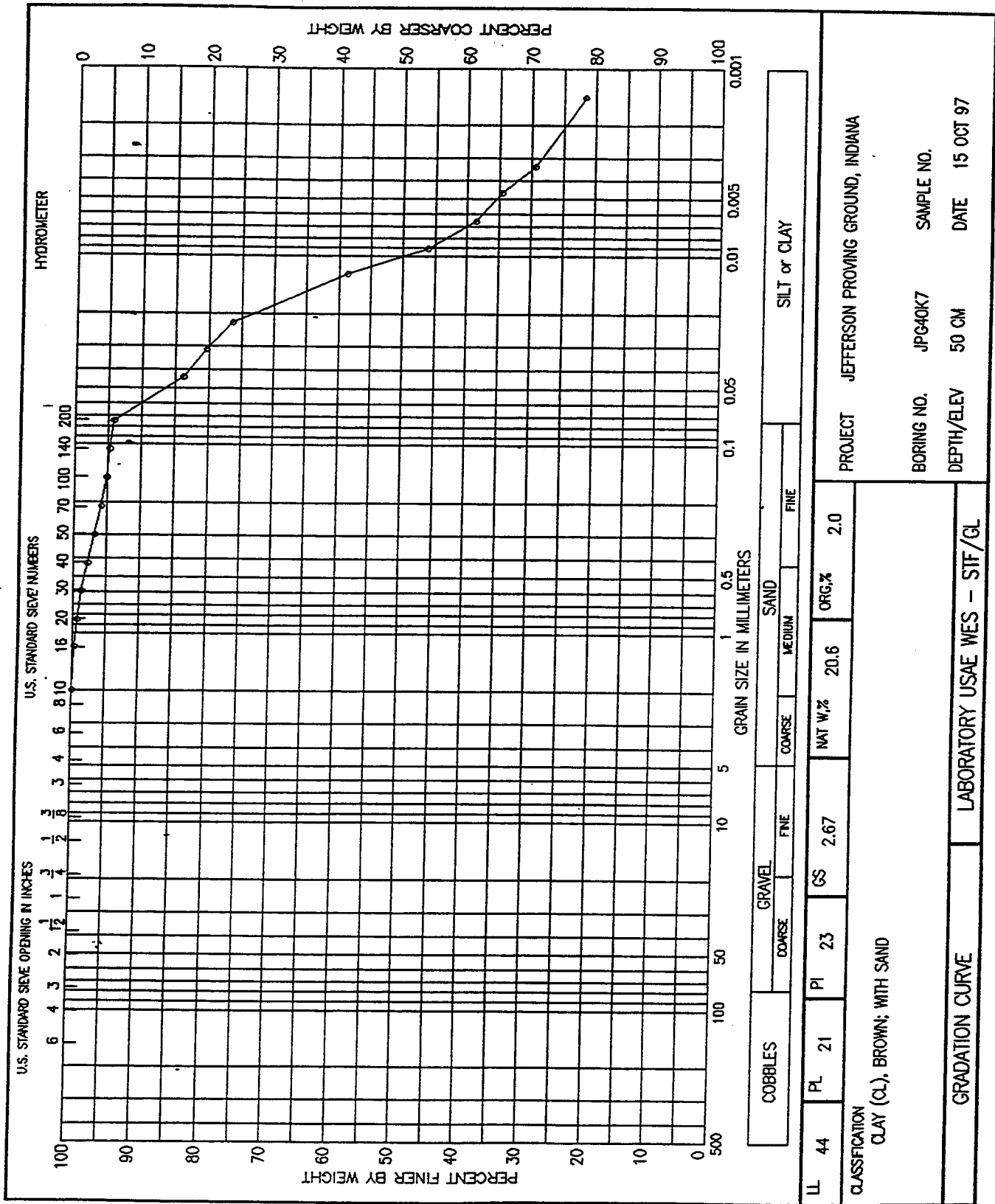








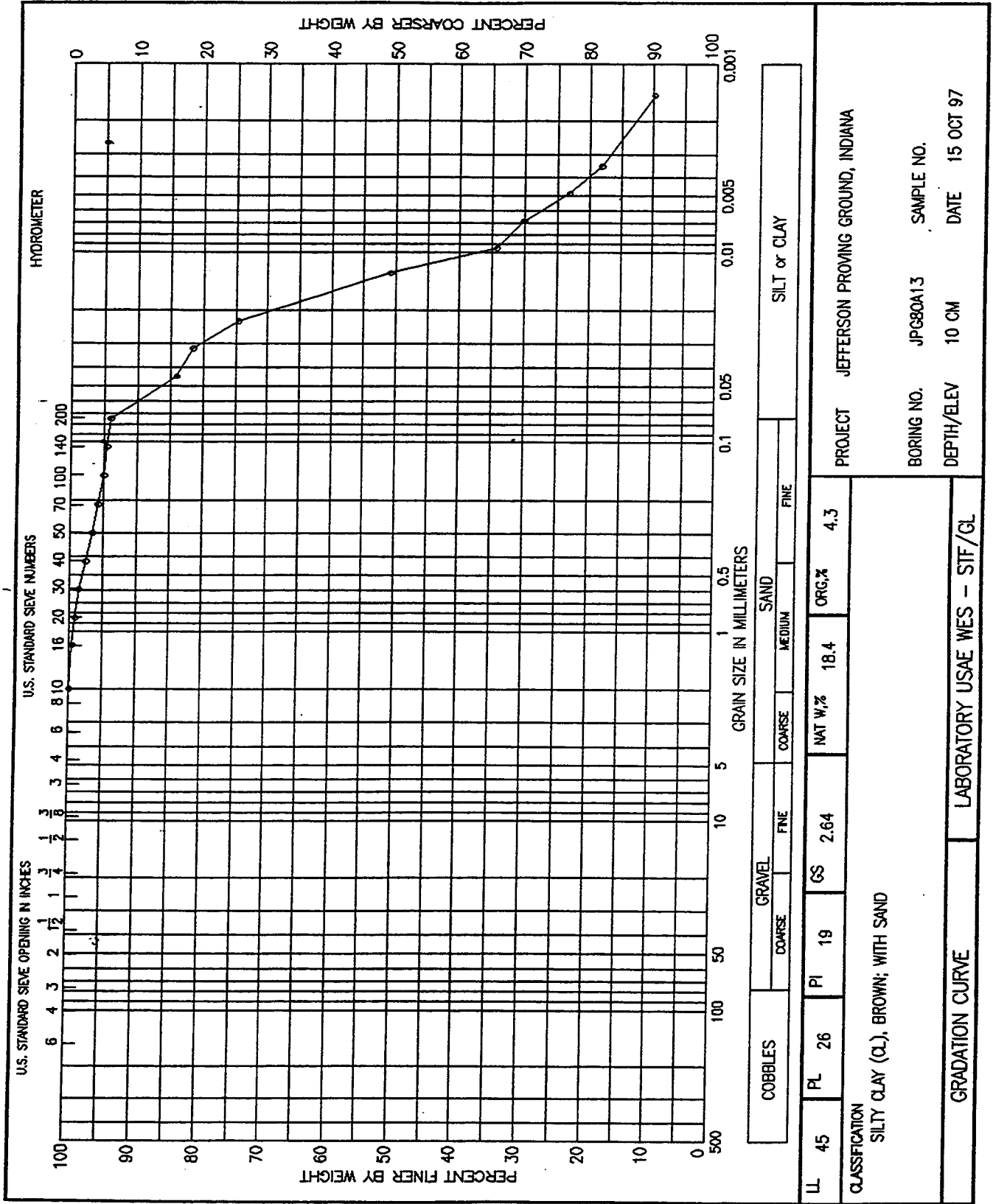


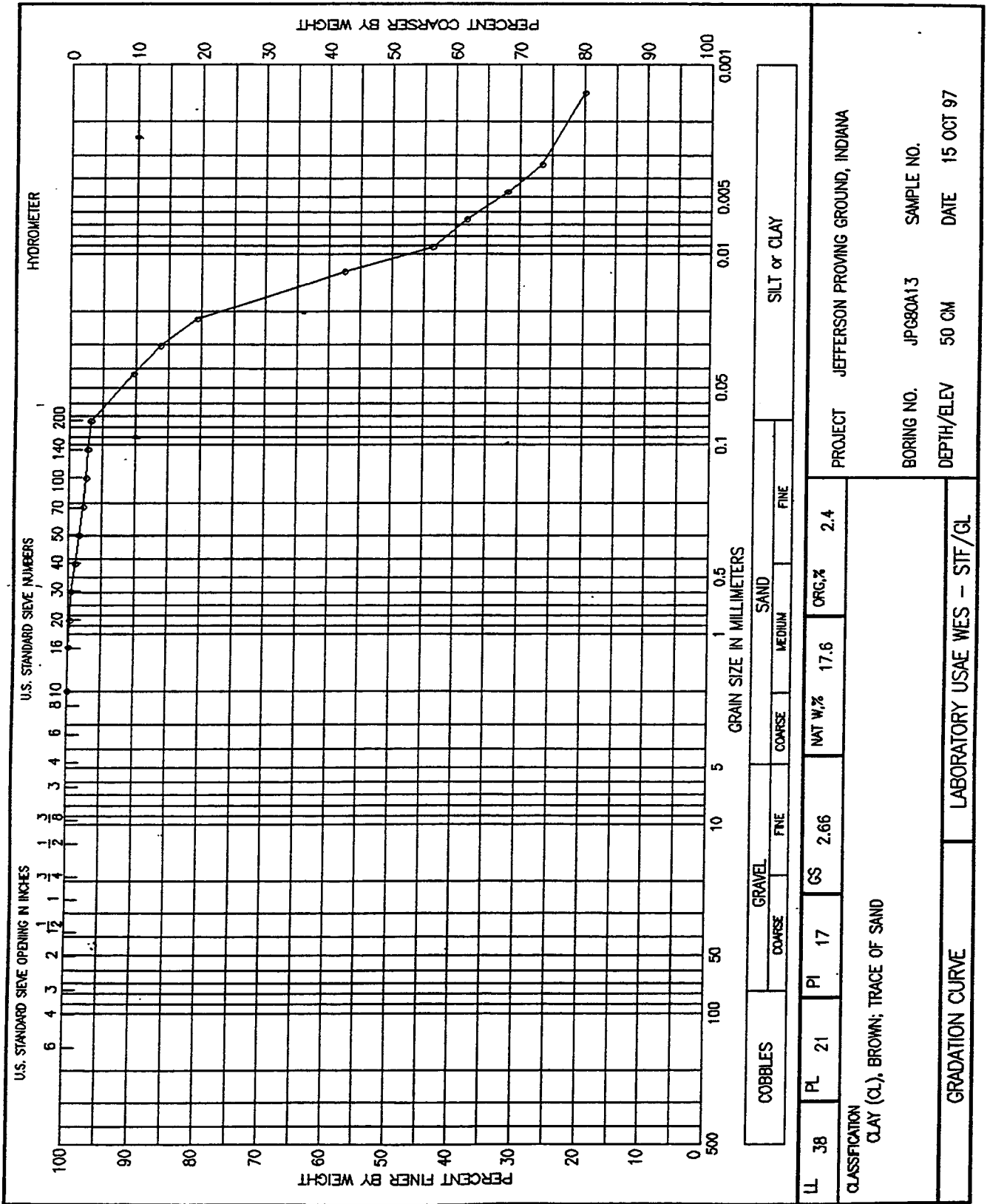


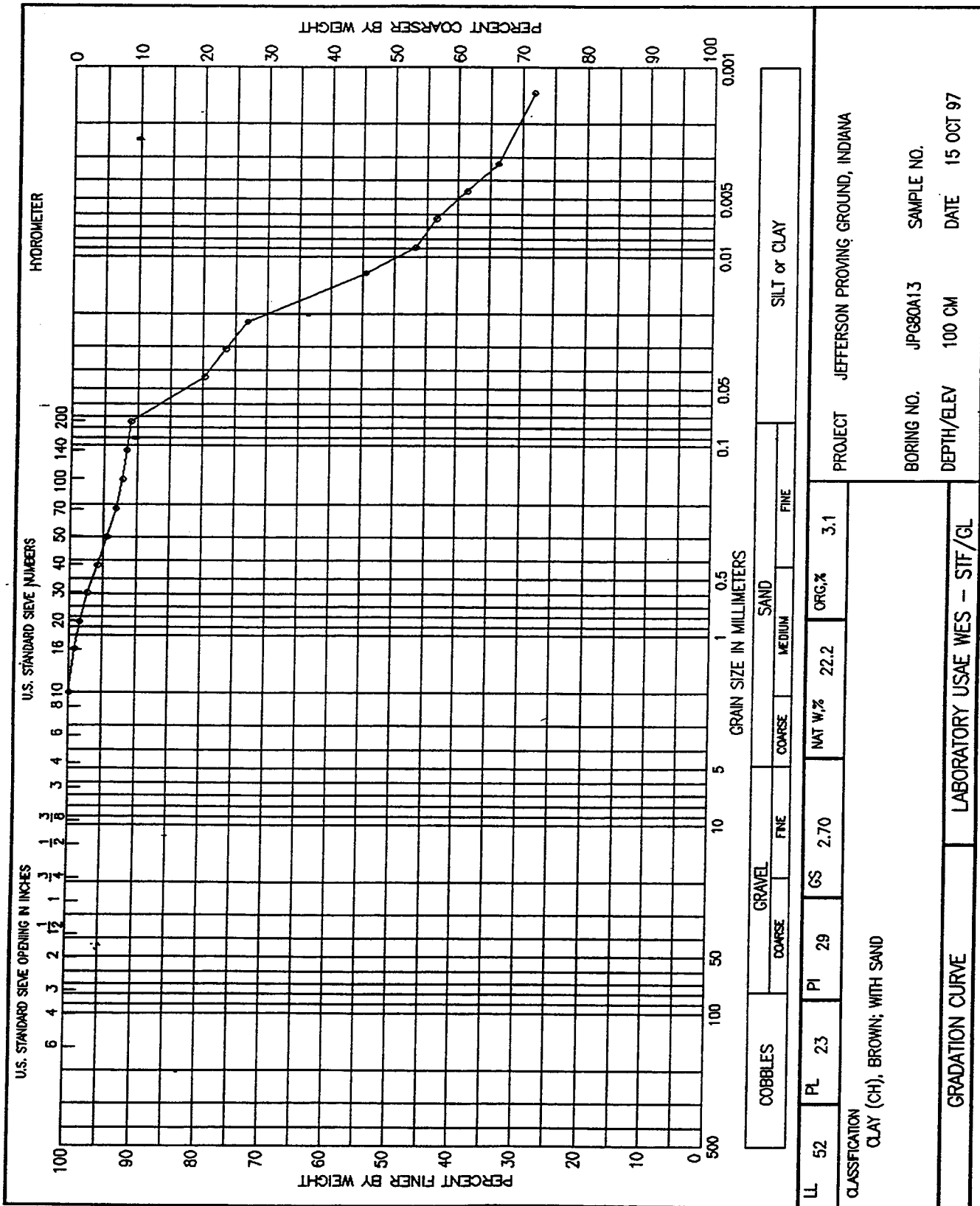
Appendix B

Soil Gradation Curves:

80-acre Site







Appendix C

Laboratory Dielectric Soil Properties: 40- and 80-acre Sites

Data Report

Dielectric Properties of Soils

Jefferson Proving Ground , IN

Prepared for: Dwain K. Butler
Earthquake Engineering and Geosciences Division
U.S. Army Engineer Waterways Experiment Station
3909 Halls Ferry Road
Vicksburg, MS 39180

Prepared by: John O. Curtis
Environmental Engineering Division
U.S. Army Engineer Waterways Experiment Station
3909 Halls Ferry Road
Vicksburg, MS 39180

Table of Contents

Introduction	1
Source of Soil Samples	1
Experimental Procedures	1
Fundamental Relationships	2
Theoretical Loss Tangent Effects	4
Observations on Data	8
Frequency Dependence	8
Moisture Dependence at Selected Frequencies	9
Data Tables and Graphs	10
Frequency Dependence - Sample JPG_80_O13_0.1_D	11
Frequency Dependence - Sample JPG_80_H13_1.0	14
Moisture Dependence, Tabulations, 100 MHZ	17
Moisture Dependence, Graphs, 100 MHZ, All Data	20
Moisture Dependence, Graphs, 100 MHZ, 40 Acre Site, By Depth	26
Moisture Dependence, Graphs, 100 MHZ, 80 Acre Site, By Depth	32
Moisture Dependence, Tabulations, 200 MHZ	38
Moisture Dependence, Graphs, 200 MHZ, All Data	41
Moisture Dependence, Graphs, 200 MHZ, 40 Acre Site, By Depth	47
Moisture Dependence, Graphs, 200 MHZ, 80 Acre Site, By Depth	53
Moisture Dependence, Tabulations, 495 MHZ	59
Moisture Dependence, Graphs, 495 MHZ, All Data	62
Moisture Dependence, Graphs, 495 MHZ, 40 Acre Site, By Depth	68
Moisture Dependence, Graphs, 495 MHZ, 80 Acre Site, By Depth	74
Moisture Dependence, Tabulations, 1015 MHZ	80
Moisture Dependence, Graphs, 1015 MHZ, All Data	83
Moisture Dependence, Graphs, 1015 MHZ, 40 Acre Site, By Depth	89
Moisture Dependence, Graphs, 1015 MHZ, 80 Acre Site, By Depth	95

Introduction

This report contains dielectric property measurement results for soils. The original data were collected in the form of the real and imaginary parts of the complex dielectric constant versus frequency utilizing a Hewlett-Packard 8510C Vector Network Analyzer System with an S-Parameter Test Set and a coaxial sample holder. Software developed at the U.S. Army Engineer Waterways Experiment Station was used to convert S-parameter measurements at selected frequencies into a complex dielectric constant. The soils were assumed to be nonmagnetic. Other useful electromagnetic properties were calculated from the dielectric constant and frequency, including an equivalent electrical conductivity, the loss tangent, power attenuation, and a normalized phase velocity. The section entitled, "Fundamental Relationships," contains the formulae used to calculate these properties. Additional physical parameters of the soil samples that are included in the report include their dry density, volumetric moisture content, and temperature.

Measurement results and calculated parameters are listed and/or graphically displayed either as a function of frequency for representative soil samples or as a function of volumetric moisture content at selected frequencies. The intent of presenting data in the latter way is to demonstrate the experimental observation that the real part of the dielectric constant, as well as the normalized phase velocity are strong functions of volumetric moisture and reasonably independent of soil texture. Other parameters are clearly dependent on soil texture, and, given enough data from several different types of soils, their graphs versus moisture content would show a great deal of scatter. The four frequencies chosen for data presentation span the range of frequencies normally associated with ground penetrating radars.

For additional details on how the data were collected, please contact the author at the U.S. Army Engineer Waterways Experiment Station (WES), Vicksburg, MS, (voice: 601-634-2855, FAX: 601-634-2732, e-mail: curtisj@ex1.wes.army.mil).

Source of Soil Samples

Soil samples were obtained from two test areas at Jefferson Proving Ground, IN, by Dr. Paul Wolfe, Department of Physics and Geological Sciences, Wright State University, Dayton, OH, and several of his graduate students during the early part of August, 1997. Samples were drawn out of an auger device at depths of about 10 cm, 50 cm and 100 cm below the surface from numerous holes at the test sites, one site being referred to as the 40 Acre Site and the other as the 80 Acre Site. 40 samples in sealed plastic bags were provided to this laboratory.

Experimental Procedures

The experimental procedure used to collect electrical property data at WES normally consists of the following steps. First of all, soil is taken from the source container and packed into a brass coaxial sample holder using small spoons and other utensils. The holders used in these measurements have a square cross section whose dimension is 0.75 cm and are either 5 cm or 10 cm in length, resulting in total sample volumes of about 2.88 cm³ and 5.78 cm³, respectively. These volumes were measured by filling the sample holders with water, noting the mass increase, and using a mass density of 1 g/cc. The samples are packed as tightly as possible at whatever moisture content they retained in the bags. Hence, there is no control over sample dry

density. It is highly unlikely, however, that the densities achieved by this sample preparation technique will ever exceed *in situ* densities.

After enclosing the sample in the holder with a brass cover plate, the holder is placed in a temperature control device and connected to the S-parameter test set. After the sample has reached the desired temperature, data are collected over the selected range of frequencies. Following removal of the sample holder from the temperature control apparatus, the cover plate is removed, and the sample is allowed to air dry (usually for a twenty-four hour period). After the collected of a second set of data at nominally-dry conditions, the sample is wetted to near saturation by the careful addition of distilled, deionized water. After allowing some time for the added moisture to fully penetrate the soil structure (usually about an hour), the electrical properties are once again measured. Therefore, each sample is tested three times, once as is, once after air drying, and once at near-saturation conditions. The addition of water would not work for a sample that contained a large amount of swelling clay minerals, as the sample would expand too far out of the sample holder to allow a measurement to be made. Similarly, such samples crack severely when dried.

Sample masses are recorded prior to each measurement. Following the last data collection, the soil is scraped and flushed from the sample holder and dried in an oven to obtain its dry mass, which, by virtue of knowing the sample volume, leads to the sample dry density and the calculation of sample volumetric moisture contents for each measurement. Of course, these data can also be used to calculate the commonly used weight-based moisture content as well.

Fundamental Relationships

Assuming plane harmonic wave propagation in a lossy, non-magnetic, unbounded medium, the wave amplitude function may be written:

$$e^{i(kx - \omega t)}$$

where

$$k = \beta + i\alpha = \omega N/c$$

k is the complex propagation constant,

β is the phase constant,

α is the amplitude attenuation factor,

ω is the radial frequency,

N is the complex index of refraction,

c is the velocity of light in a vacuum,

I is the symbol designating an imaginary quantity = $\sqrt{-1}$,

x is a space coordinate, and

t is time.

Furthermore,

$$N^2 = \epsilon = \epsilon' + \epsilon''$$

where ϵ is the relative complex dielectric constant, which, along with the electrical conductivity from Ohm's Law, represents the electrical properties of the medium. The interpretation of these properties as used in this study is that the conductivity, σ , accounts for current due to free charged particle motion, while the imaginary part of the complex dielectric constant, ϵ'' , accounts for displacement current losses (those due to the electric polarization of the medium). When both conduction and displacement currents are considered, one finds two terms in Ampere's law for current flow that represent losses (or a shift in phase), one containing the electrical conductivity and one containing the imaginary part of the dielectric constant. While these two terms account for different loss mechanisms, most researchers use only one term or the other to identify losses, with many users preferring to deal with the concept of electrical conductivity. In MKS units, the relationship between the two quantities is taken to be

$$\sigma = \epsilon''\epsilon_0\omega$$

where the units of conductivity are mhos/meter (or siemens/meter) and ϵ_0 is the permittivity of free space (8.85×10^{-12} farads/meter).

Squaring the expression for the complex propagation constant, substituting the expression for the square of the complex index of refraction, and equating real and imaginary components, one obtains two algebraic equations that relate the amplitude attenuation factor and phase constant to the complex dielectric constant:

$$\beta^2 - \alpha^2 = \frac{\omega^2}{c^2}\epsilon'$$

and

$$\alpha\beta = \frac{\omega^2\epsilon''}{2c^2}$$

Solving these equations for the amplitude attenuation factor and for the phase constant results in the

following expressions:

$$\alpha = \frac{\omega}{c} \left(\frac{\epsilon'}{2} \left(\sqrt{1 + \left(\frac{\epsilon''}{\epsilon'} \right)^2} - 1 \right) \right)^{1/2}$$

and

$$\beta = \frac{\omega}{c} \left(\frac{\epsilon'}{2} \left(\sqrt{1 + \left(\frac{\epsilon''}{\epsilon'} \right)^2} + 1 \right) \right)^{1/2}$$

The ϵ''/ϵ' ratio is also referred to as the loss tangent. Some researchers prefer to work with the electrical conductivity in place of the dielectric loss term.

Monochromatic plane waves will propagate with a velocity

$$v = \frac{\omega}{\beta} = c \left(\frac{\epsilon'}{2} \left(\sqrt{1 + \left(\frac{\epsilon''}{\epsilon'} \right)^2} + 1 \right) \right)^{-1/2}$$

This phase velocity is not necessarily the speed with which the energy of an electromagnetic wave containing a range of frequency components propagates through a medium. The latter is referred to as the group velocity and can be calculated as the rate of change of radial frequency with respect to the phase constant. However, as long as the phase velocity is relatively constant over the range of frequencies of interest, then there is little difference between phase velocity and group velocity.

The power intensity of the plane electromagnetic wave decreases exponentially with depth of penetration by the factor, $e^{-2\alpha x}$, or, in one unit of distance traveled, a decrease of $e^{-2\alpha}$. Power attenuation expressed in decibels per meter can then be written as:

$$PL = -8.6859 \frac{\omega}{c} \left(\frac{\epsilon'}{2} \left(\sqrt{1 + \left(\frac{\epsilon''}{\epsilon'} \right)^2} - 1 \right) \right)^{1/2}$$

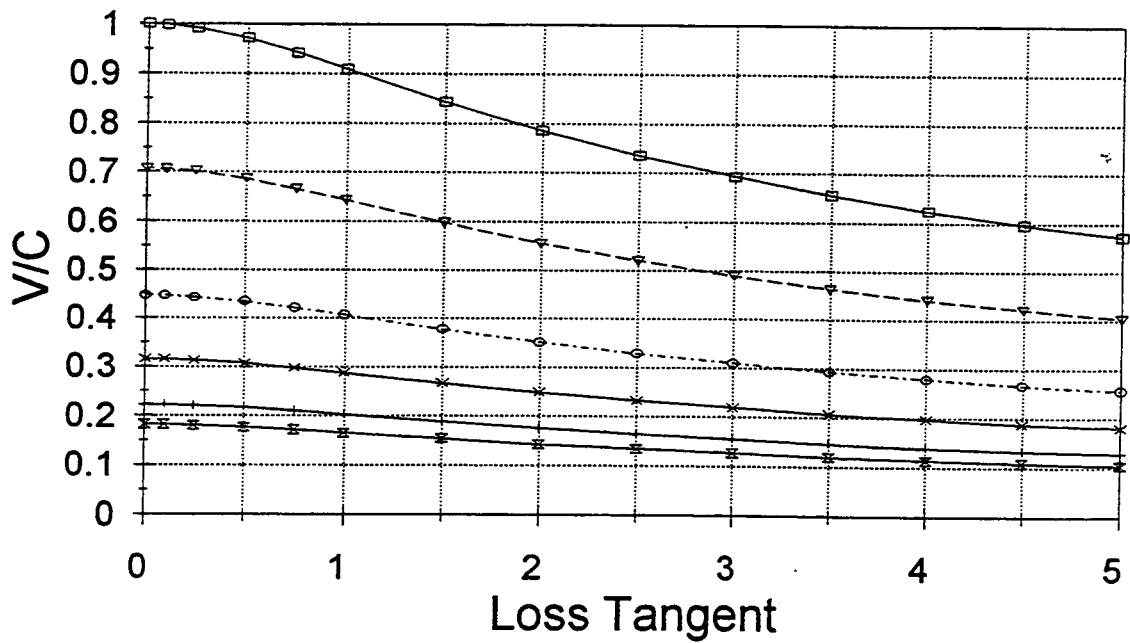
Theoretical Loss Tangent Effects

The design of a ground-penetrating radar data collection effort and subsequent analysis of those data would require estimates of the speed with which a radar signal will propagate through the terrain and the rate at which the power level of the signal will be attenuated. The former provides the locations of subsurface anomalies, while the latter controls the depth to which meaningful data can be collected.

Many designers and analysts choose to assume that the material through which an electromagnetic wave is propagating is relatively lossless. The first figure that follows is a plot of normalized phase velocity (v/c) for selected values of the real part of the complex dielectric constant (often referred to as the permittivity of the material) against values of the loss tangent. The permittivity values easily span the range of values found in most soils. The figure clearly demonstrates that as long as the loss tangent is relatively small (say, less than 0.5), the lossless material assumption is a good one. However, a loss tangent of 1.0, which is not uncommon, will result in a phase velocity that is about ten percent smaller than that calculated from the lossless assumption.

As for signal power attenuation, obviously the lossless material assumption is meaningless. One can see from the second plot that follows that the rate at which the power level of an electromagnetic wave decreases when traveling through the soil is very sensitive to the value of the loss tangent and to the frequency at which the signal is being propagated.

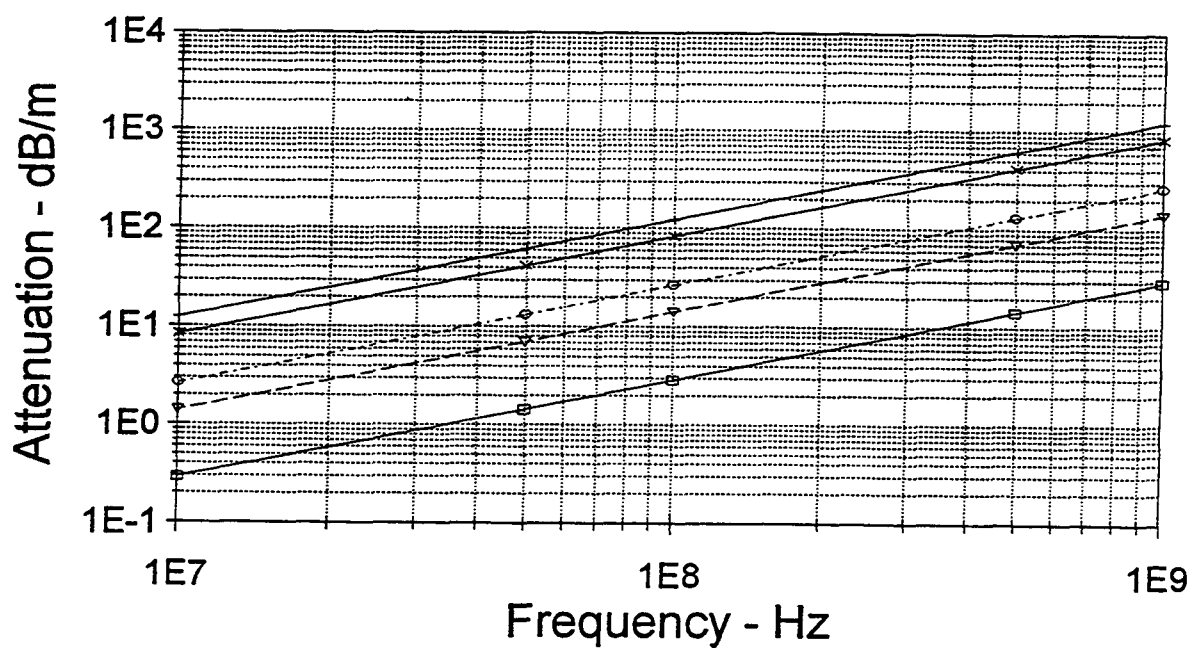
Loss Tangent Effects Normalized Phase Velocity



—□— epsilon = 1
-▽- epsilon = 2
-◇- epsilon = 5
-×- epsilon = 10
-+- epsilon = 20
-≡- epsilon = 30

Loss Tangent Effects

Attenuation (Permittivity = 10)



—□— Loss Tangent = .1 -◇- Loss Tangent = .5 -◇- Loss Tangent = 1
 -x- Loss Tangent = 5 -+— Loss Tangent = 10

Observations on Data

The following pages contain a sample of the electrical property data gathered in this study. They include tables and charts in which properties are displayed as a function of frequency for individual samples, as a function of volumetric moisture for all samples at selected frequencies, and also as a function of volumetric moisture for which sample depth is highlighted.

Frequency Dependence

Data plotted vs frequency for two samples that bound the observed behaviors of JPG soils are shown in this section. The label on the first sample, JPG_80_O13_0.1_D, indicates that it was obtained at a depth of 10 cm (0.1 meters) from the 80 Acre Site at a location identified as O13. Furthermore, the "D" designation means that this sample had been air-dried before data were collected. If the sample identifier had included a "W" instead of "D", this would indicate that the sample had been wetted to near-saturation conditions before testing. No letter designation as the end of the identifier means that the soil came straight from the sample bag. Other information on the first set of graphs reveal that the volumetric moisture for JPG_80_O13_0.1_D was computed to be 3.2%, and its dry density was calculated as 1.143 g/cc. Plot labels and legends should make the data self-explanatory.

The apparent anomalous behavior at about 950 MHz and at other later frequencies is actually due to a resonant condition existing within the sample holder. Such conditions exist whenever there are a multiple of half wavelengths being supported in the sample. The complex algebra calculations, particularly for the imaginary part of the complex dielectric constant, become somewhat unstable for low-loss materials such as this sample. Given a permittivity of about 2.6 and a frequency of 950 MHz, the resulting wavelength in this sample is about 19.5 cm, and the sample holder used for these measurements had an effective length of about 9.9 cm. Therefore, at this frequency, a half wavelength was being sustained. Obviously, since the other electrical properties are all a function of the imaginary component of the dielectric constant, they too will exhibit some instability.

Frequency-domain data from another sample, JPG_80_H13_1.0, are shown next. This was a soil that was very moist and sticky and, when air dried, showed some cracking, indicating the possible presence of swelling clay minerals. The volumetric moisture content of this sample, 33.7%, is the moisture content of the field sample; no water was added prior to measurements. This soil is clearly not a low-loss material; one doesn't see the apparent anomalous behavior which, for this sample, should first appear at about 300 MHz. Furthermore, this sample shows the classical low-frequency conduction current loss mechanism as evidenced by the straight line plot of the imaginary component of the complex dielectric constant when plotted on a log-log scale. Had data been collected at higher frequencies, the displacement current loss mechanism (dipole relaxation of the free water molecules) would have been evident as a hump on the imaginary component graph centered at about 18 GHz.

Care should be taken in comparing the measured and calculated properties for these two samples. Note that the vertical scales may be different for the two in order that the data can best be visualized. Nevertheless, these data clearly demonstrate how different the electrical behavior of soils can be at one site due to differences in chemistry, moisture content and sample density. For example, consider a mid-range GPR frequency of 500 MHz. Attenuation of signal power for the wet, sticky sample is about 80 dB/meter; whereas, for the dry, near-surface sample it is only about 3 dB/meter. Similarly, monochromatic wave speed for the wet sample is about 25% of the speed of light; whereas, the dry sample speed is about 65% of the

speed of light. Obviously, this is useful information for system designers and data processors.

Moisture Dependence at Selected Frequencies

Another format used to display these data is to plot results versus moisture content at selected frequencies. The frequencies chosen for this report are 100, 200, 495, and 1015 MHz, and were chosen to be representative of the normal operating frequencies of ground penetrating radar systems.

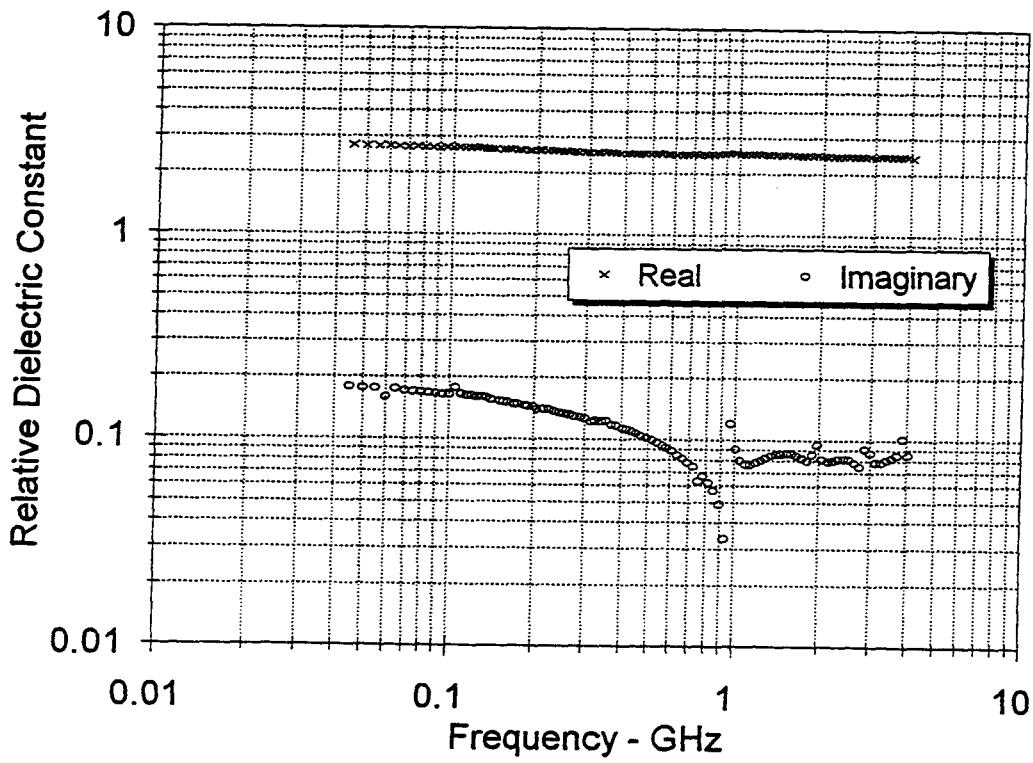
At each frequency, the data are presented in the following way. First of all, one will find a table of measured and calculated parameters. The first column of each page provides the location and depth code, while the second column lists the volumetric moisture content (in percent) of that particular sample. The third column contains the dry density (in grams per cubic centimeters) of the sample that was tested. The last six columns list the real and imaginary components of the measured relative complex dielectric constant, the equivalent conductivity (in mhos per meter), the loss tangent, the power attenuation factor in decibels per meter, and the normalized phase velocity.

Each table is followed by several plots of parameters versus volumetric moisture. Experience from previous data collection efforts with many different types of soils has shown that the permittivity and the normalized phase velocity are very strong functions of volumetric moisture and virtually independent of soil type. These data confirm those previous observations and further show that at Jefferson Proving Ground, permittivity and phase velocity are independent of test site.

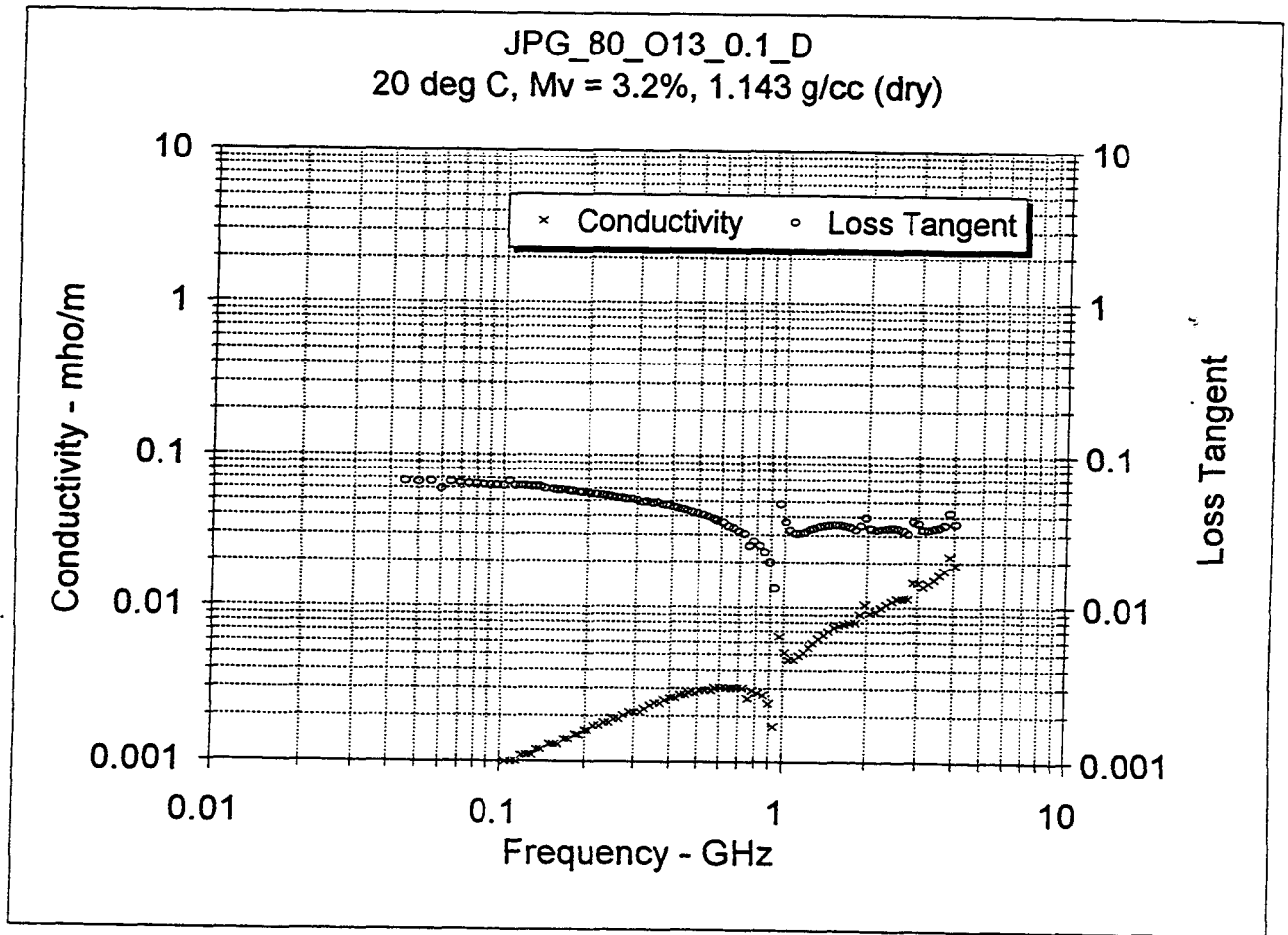
The data also show that loss terms are not site-independent. This is most evident at the lower frequencies and can clearly be seen on the dielectric constant imaginary component graphs. Cross-checking the tabulated values shows that the high-loss soils come from the 80 Acre Site at a depth of one meter. The graphs of properties in which data are labeled according to which test site they came from are followed by two other sets of graphs, one from the 40 Acre Site and one from the 80 Acre Site in which the data are labeled according to sample depth. They further confirm that something is quite different about the 80 Acre, one meter depth sample response. This report does not attempt to explain this anomalous behavior. Suffice it to say that while previous studies have shown that dry density plays some part in controlling the electromagnetic response of soils, it is most likely that soil chemistry is the overriding factor in determining the losses in moist soils.

Data Tables and Graphs

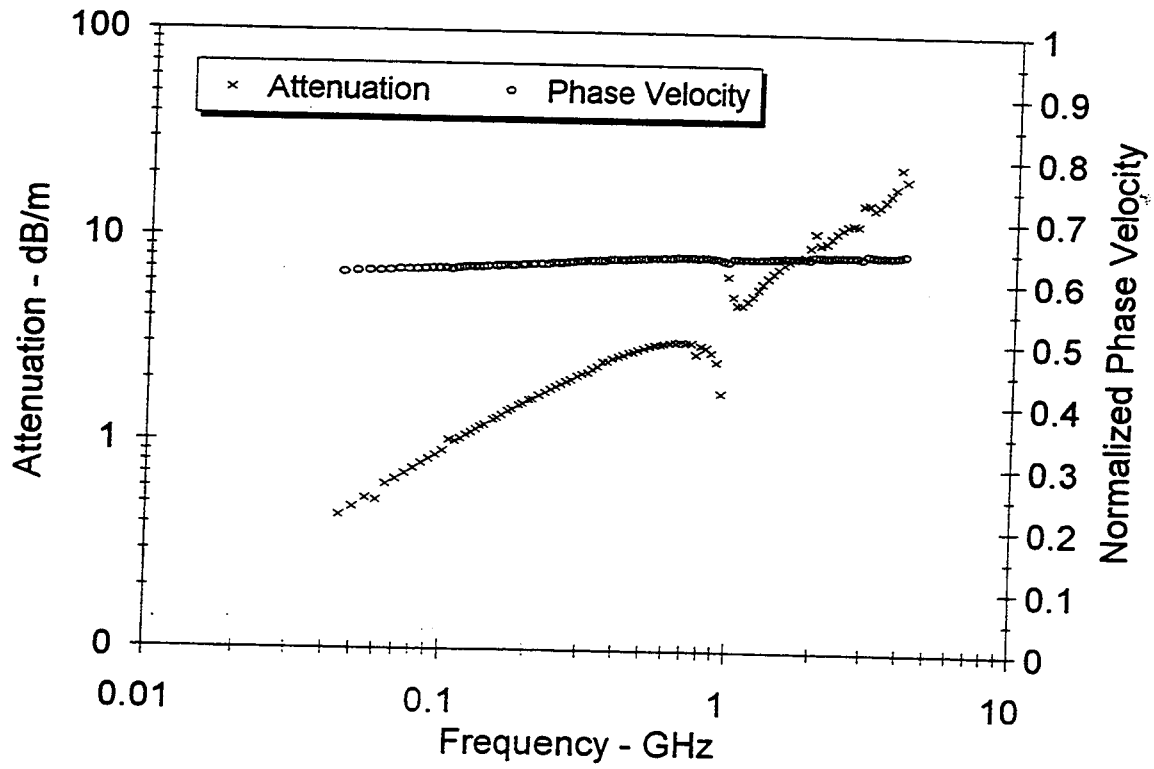
JPG_80_O13_0.1_D
20 deg C, Mv = 3.2%, 1.143 g/cc (dry)

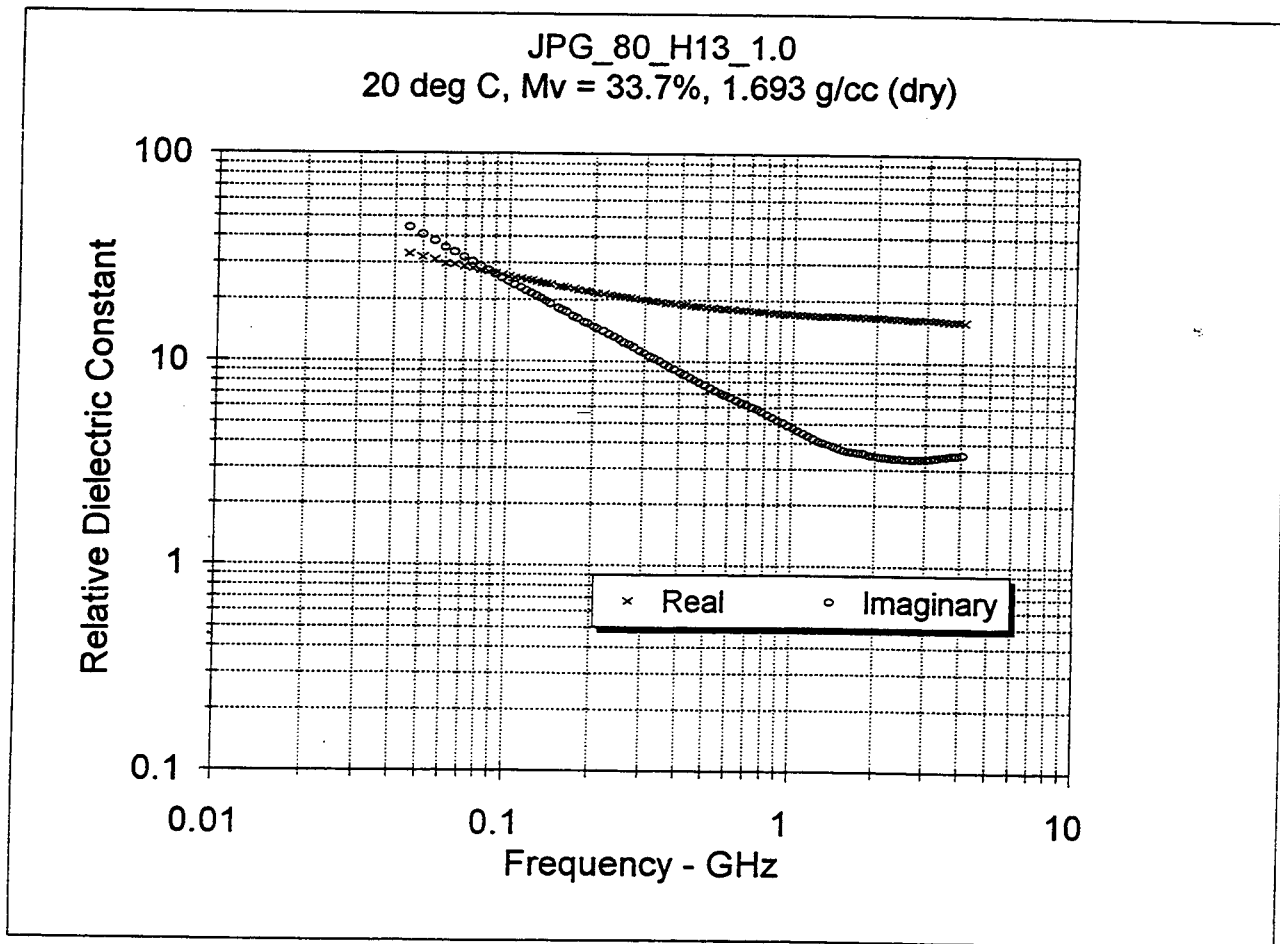


JPG_80_O13_0.1_D
20 deg C, Mv = 3.2%, 1.143 g/cc (dry)

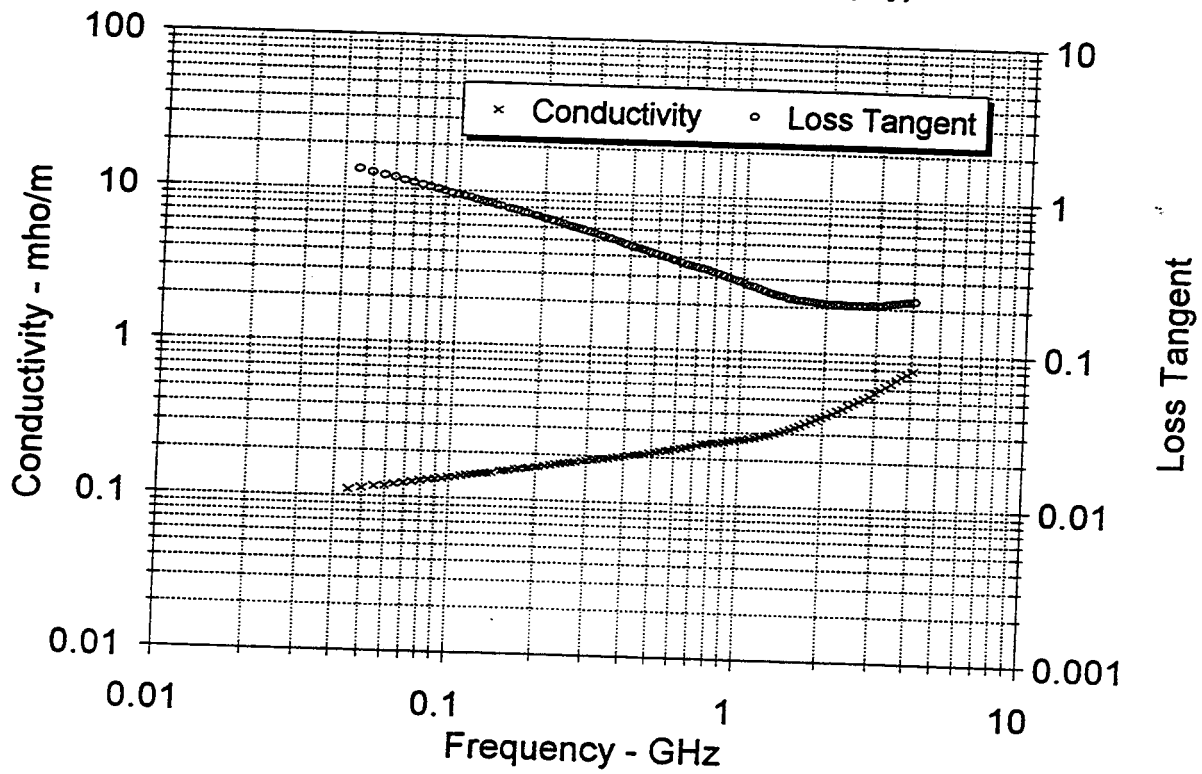


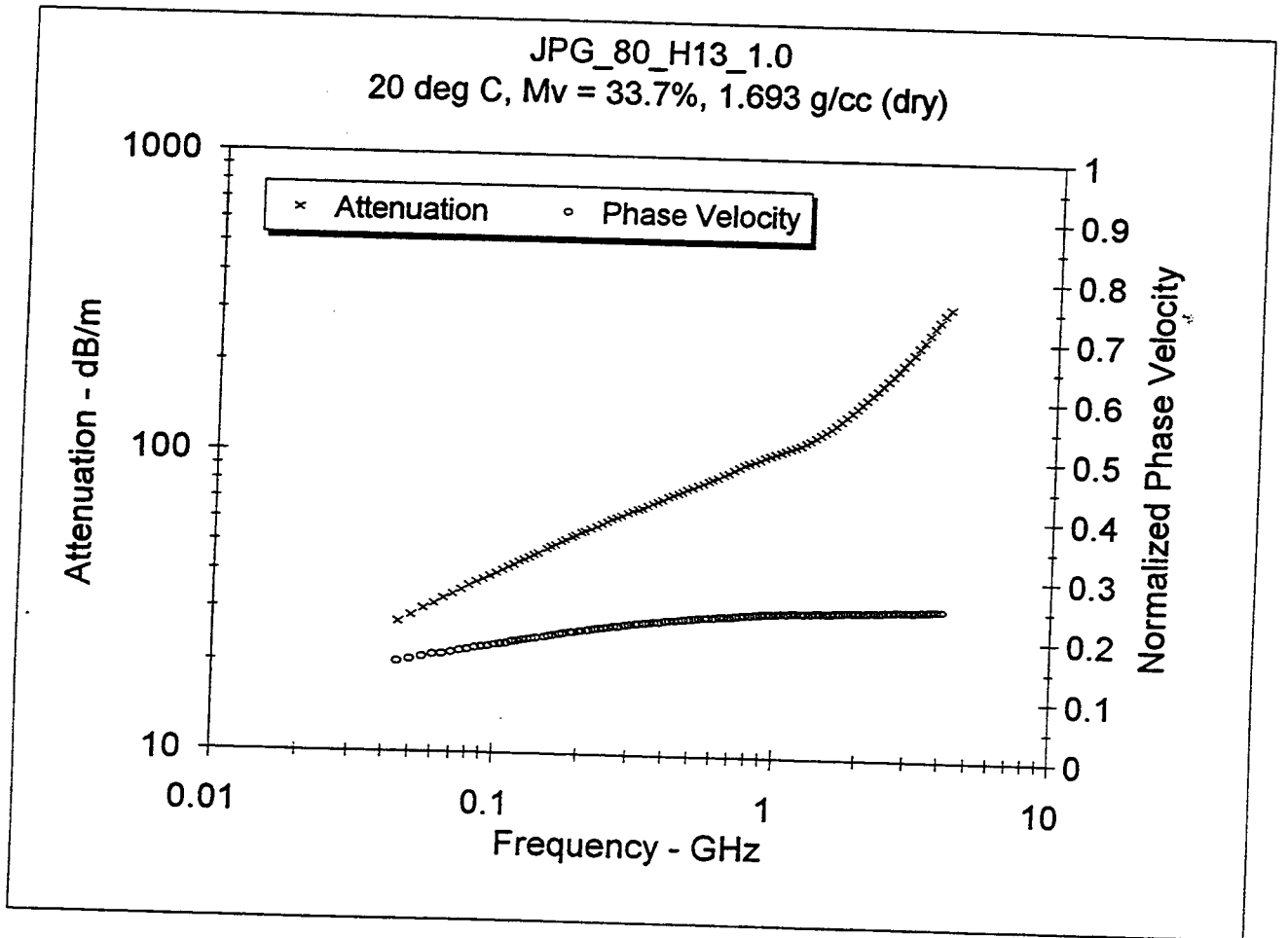
JPG_80_O13_0.1_D
20 deg C, Mv = 3.2%, 1.143 g/cc (dry)





JPG_80_H13_1.0
20 deg C, Mv = 33.7%, 1.693 g/cc (dry)





JPG , Phase IV , 40 Acre Site , 100 MHz

Sample	Vol Moist (%)	Dry Dens (g/cc)	Re(eps) (rel)	Im(eps) (rel)	Cond (mho/m)	Loss Tan	Attn (dB/m)	Ph Vel (rel)
JPG_40_C1_0.1	11.31	1.197	5.02	0.73	0.0041	0.146	2.97	0.445
JPG_40_C1_0.1_D	3.17	1.197	2.74	0.16	0.0009	0.058	0.88	0.604
JPG_40_C1_0.1_W	47.20	1.197	28.87	3.02	0.0168	0.105	5.11	0.186
JPG_40_C1_0.5	25.21	1.401	13.21	5.04	0.0280	0.381	12.39	0.270
JPG_40_C1_0.5_D	4.81	1.401	4.04	0.64	0.0036	0.159	2.90	0.496
JPG_40_C1_0.5_W	39.52	1.401	24.39	8.03	0.0446	0.329	14.59	0.200
JPG_40_C1_1.0	26.42	1.512	14.10	5.27	0.0293	0.374	12.55	0.262
JPG_40_C1_1.0_D	5.50	1.512	4.36	0.76	0.0042	0.175	3.32	0.477
JPG_40_C1_1.0_W	38.01	1.512	23.65	7.88	0.0438	0.333	14.55	0.203
JPG_40_C7_0.1	18.06	1.421	8.03	1.29	0.0071	0.160	4.11	0.352
JPG_40_C7_0.1_D	4.55	1.421	3.14	0.20	0.0011	0.064	1.03	0.564
JPG_40_C7_0.1_W	40.69	1.421	22.62	2.63	0.0146	0.116	5.02	0.210
JPG_40_C7_0.5	29.10	1.547	16.27	5.36	0.0298	0.329	11.93	0.245
JPG_40_C7_0.5_D	3.88	1.547	3.99	0.58	0.0032	0.146	2.65	0.499
JPG_40_C7_0.5_W	34.76	1.547	20.09	6.16	0.0342	0.307	12.36	0.221
JPG_40_C7_1.0	27.08	1.634	16.11	5.94	0.0330	0.369	13.24	0.245
JPG_40_C7_1.0_D	5.00	1.634	4.38	0.70	0.0039	0.160	3.04	0.476
JPG_40_C7_1.0_W	31.70	1.634	18.75	6.66	0.0370	0.355	13.78	0.228
JPG_40_C13_0.1	14.39	1.359	6.89	1.36	0.0076	0.197	4.69	0.379
JPG_40_C13_0.1_D	3.13	1.359	3.06	0.24	0.0013	0.079	1.25	0.571
JPG_40_C13_0.1_W	41.40	1.359	22.28	3.22	0.0179	0.145	6.19	0.211
JPG_40_C13_0.5	16.64	1.377	7.14	2.00	0.0111	0.280	6.75	0.371
JPG_40_C13_0.5_W	45.31	1.377	27.79	5.82	0.0324	0.210	10.00	0.189
JPG_40_C13_1.0	22.51	1.524	12.86	5.28	0.0294	0.411	13.14	0.273
JPG_40_C13_1.0_D	3.70	1.524	4.10	0.79	0.0044	0.192	3.52	0.492
JPG_40_C13_1.0_W	32.73	1.524	19.59	6.98	0.0388	0.356	14.12	0.223
JPG_40_G1_0.1	16.84	1.126	5.63	0.83	0.0046	0.147	3.17	0.420
JPG_40_G1_0.1_D	5.28	1.126	2.63	0.16	0.0009	0.061	0.90	0.616
JPG_40_G1_0.1_W	53.37	1.126	30.62	2.95	0.0164	0.096	4.84	0.181
JPG_40_G1_0.5	25.14	1.440	10.84	2.93	0.0163	0.270	8.02	0.301
JPG_40_G1_0.5_D	5.14	1.440	3.70	0.54	0.0030	0.145	2.53	0.518
JPG_40_G1_0.5_W	41.22	1.440	25.35	5.65	0.0314	0.223	10.15	0.197
JPG_40_G1_1.0	30.59	1.621	19.08	6.39	0.0355	0.335	13.12	0.226
JPG_40_G1_1.0_D	4.69	1.621	4.63	0.79	0.0044	0.171	3.33	0.463
JPG_40_G1_1.0_W	32.80	1.621	18.82	5.65	0.0314	0.301	11.73	0.228
JPG_40_G7_0.1	15.35	1.339	6.74	0.98	0.0055	0.146	3.43	0.384
JPG_40_G7_0.1_D	3.13	1.339	2.91	0.18	0.0010	0.061	0.94	0.586
JPG_40_G7_0.1_W	45.54	1.339	25.92	2.78	0.0155	0.107	4.97	0.196
JPG_40_G7_0.5	21.87	1.494	12.16	3.39	0.0189	0.279	8.77	0.284
JPG_40_G7_0.5_D	3.32	1.494	3.77	0.45	0.0025	0.118	2.09	0.514
JPG_40_G7_0.5_W	36.30	1.494	21.99	5.03	0.0280	0.229	9.70	0.212
JPG_40_G7_1.0	27.28	1.599	16.12	6.65	0.0370	0.413	14.77	0.244
JPG_40_G7_1.0_D	5.38	1.599	4.49	0.86	0.0048	0.193	3.69	0.470
JPG_40_G7_1.0_W	38.51	1.599	22.51	8.19	0.0455	0.364	15.45	0.208
JPG_40_G13_0.1	13.96	1.271	5.74	0.84	0.0047	0.147	3.19	0.416
JPG_40_G13_0.1_D	3.01	1.271	2.75	0.19	0.0010	0.069	1.04	0.603
JPG_40_G13_0.1_W	44.65	1.271	25.37	2.62	0.0145	0.103	4.72	0.198
JPG_40_G13_0.5	22.39	1.560	12.59	3.79	0.0211	0.301	9.62	0.279
JPG_40_G13_0.5_D	3.63	1.560	4.05	0.58	0.0032	0.144	2.63	0.495
JPG_40_G13_0.5_W	35.29	1.560	20.40	5.14	0.0286	0.252	10.27	0.220

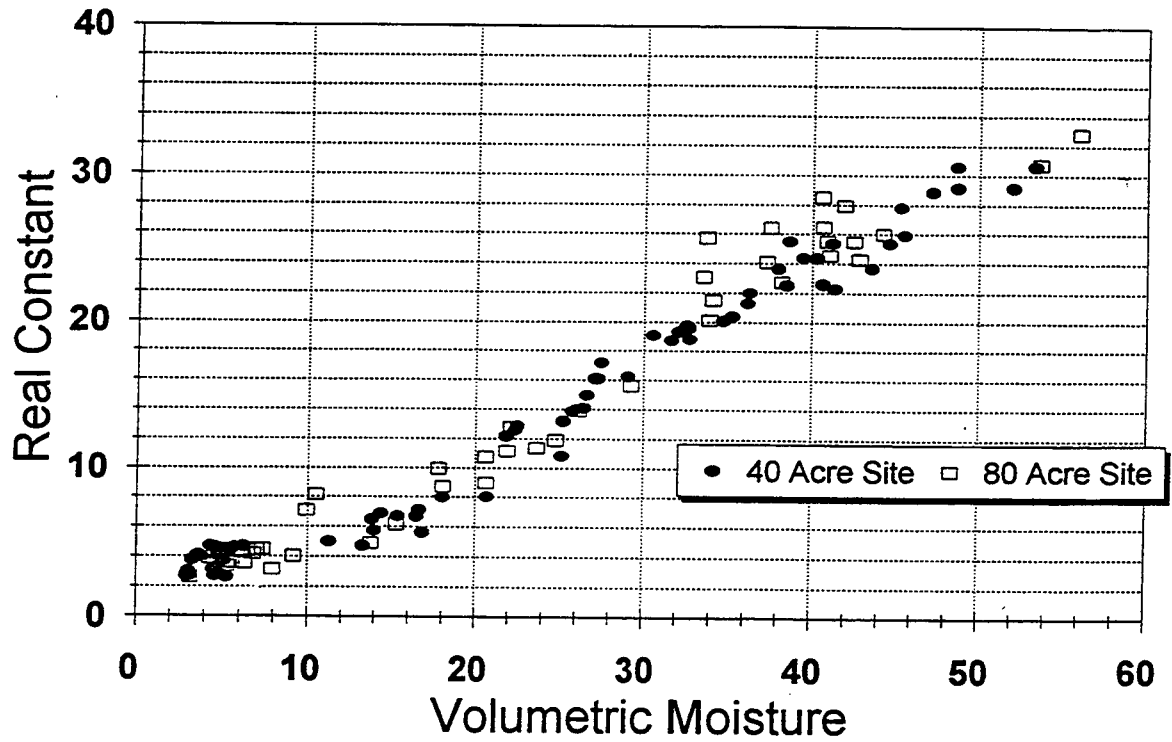
17

JPG_40_G13_1.0	27.49	1.673	17.20	6.94	0.0386	0.404	14.94	0.237
JPG_40_G13_1.0_D	4.39	1.673	4.70	0.91	0.0050	0.193	3.79	0.459
JPG_40_G13_1.0_W	32.60	1.673	19.78	7.28	0.0405	0.368	14.65	0.221
JPG_40_K1_0.1	16.49	1.217	6.70	0.94	0.0052	0.141	3.30	0.386
JPG_40_K1_0.1_D	4.65	1.217	2.88	0.18	0.0010	0.063	0.98	0.589
JPG_40_K1_0.1_W	43.58	1.217	23.66	2.56	0.0142	0.108	4.77	0.205
JPG_40_K1_0.5	32.12	1.467	19.34	8.39	0.0467	0.434	16.98	0.222
JPG_40_K1_0.5_D	6.28	1.467	4.70	0.90	0.0050	0.192	3.76	0.459
JPG_40_K1_0.5_W	36.18	1.467	21.31	8.23	0.0458	0.386	15.93	0.213
JPG_40_K7_0.1	13.85	1.228	6.49	1.63	0.0090	0.251	5.76	0.389
JPG_40_K7_0.1_D	4.83	1.228	3.31	0.37	0.0021	0.113	1.87	0.549
JPG_40_K7_0.1_W	48.72	1.228	29.16	5.16	0.0287	0.177	8.67	0.185
JPG_40_K7_0.5	26.59	1.447	14.97	6.80	0.0378	0.454	15.61	0.252
JPG_40_K7_0.5_D	5.78	1.447	4.64	1.12	0.0062	0.242	4.70	0.461
JPG_40_K7_0.5_W	38.67	1.447	25.49	10.29	0.0572	0.404	18.19	0.194
JPG_40_K13_0.1	13.33	1.185	4.74	0.85	0.0047	0.179	3.53	0.457
JPG_40_K13_0.1_D	4.62	1.185	2.71	0.19	0.0011	0.071	1.07	0.607
JPG_40_K13_0.1_W	52.08	1.185	29.15	3.95	0.0219	0.135	6.63	0.185
JPG_40_K13_0.5	20.73	1.266	8.03	2.38	0.0132	0.296	7.56	0.349
JPG_40_K13_0.5_D	4.76	1.266	3.29	0.47	0.0026	0.142	2.34	0.550
JPG_40_K13_0.5_W	48.65	1.266	30.57	7.72	0.0430	0.253	12.61	0.180
JPG_40_K13_1.0	25.73	1.516	13.86	5.79	0.0322	0.418	13.86	0.263
JPG_40_K13_1.0_D	5.42	1.516	4.36	0.77	0.0043	0.177	3.36	0.477
JPG_40_K13_1.0_W	40.31	1.516	24.35	8.92	0.0496	0.366	16.18	0.199

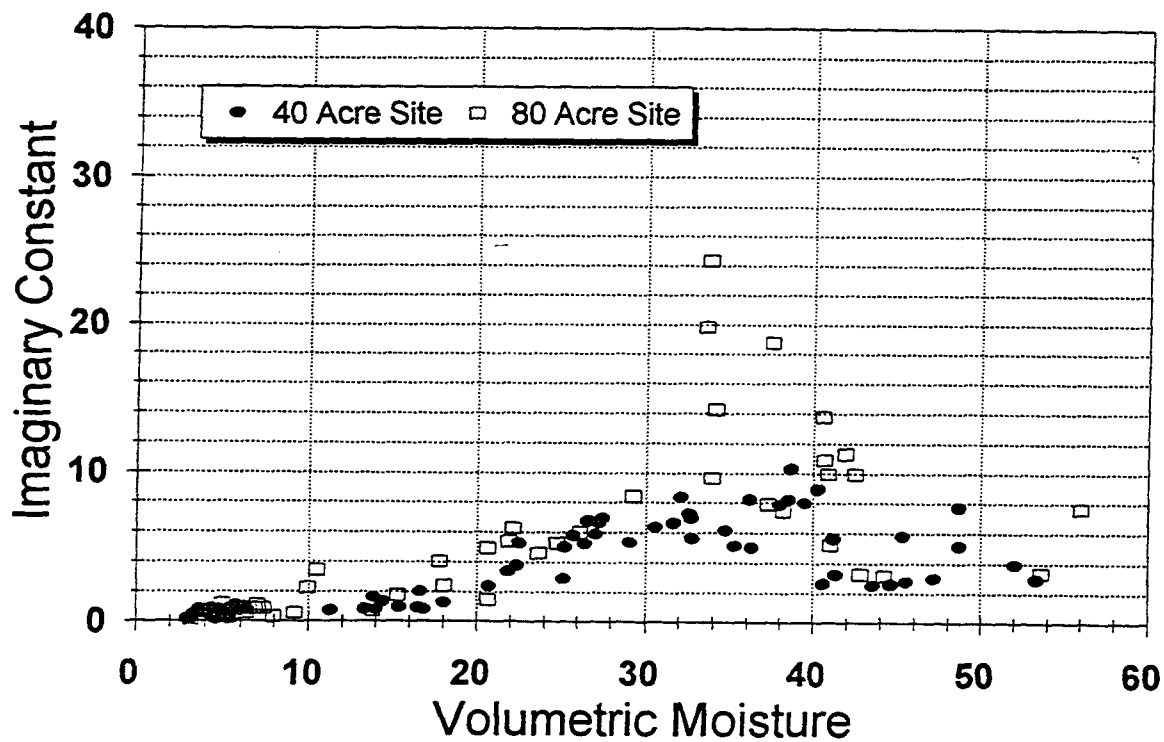
JPG , Phase IV , 80 Acre Site , 100 MHz

Sample	Vol Moist (%)	Dry Dens (g/cc)	Re(eps) (rel)	Im(eps) (rel)	Cond (mho/m)	Loss Tan	Attn (dB/m)	Ph Vel (rel)
JPG_80_A13_0.1	24.76	1.300	11.93	5.28	0.0294	0.443	13.60	0.283
JPG_80_A13_0.1_D	5.56	1.300	3.62	0.50	0.0028	0.138	2.38	0.524
JPG_80_A13_0.1_W	42.47	1.300	25.48	9.96	0.0554	0.391	17.63	0.195
JPG_80_A13_0.5	22.13	1.380	12.78	6.29	0.0350	0.492	15.56	0.272
JPG_80_A13_0.5_D	4.97	1.380	4.49	1.21	0.0067	0.270	5.16	0.468
JPG_80_A13_0.5_W	40.67	1.380	26.49	10.92	0.0607	0.412	18.92	0.191
JPG_80_A13_1.0	29.27	1.378	15.61	8.47	0.0471	0.542	18.86	0.245
JPG_80_A13_1.0_D	6.98	1.378	4.50	1.12	0.0062	0.248	4.75	0.468
JPG_80_A13_1.0_W	40.59	1.378	28.50	13.79	0.0767	0.484	22.87	0.182
JPG_80_H1_0.1	20.66	1.344	8.97	1.48	0.0082	0.165	4.48	0.333
JPG_80_H1_0.1_D	5.31	1.344	3.38	0.26	0.0014	0.077	1.28	0.543
JPG_80_H1_0.1_W	42.81	1.344	24.29	3.31	0.0184	0.136	6.09	0.202
JPG_80_H1_0.5	26.11	1.434	13.92	6.06	0.0337	0.435	14.44	0.262
JPG_80_H1_0.5_D	7.36	1.434	4.52	0.93	0.0052	0.205	3.94	0.468
JPG_80_H1_0.5_W	40.90	1.434	25.50	9.97	0.0554	0.391	17.63	0.195
JPG_80_H1_1.0	37.50	1.684	26.43	18.81	0.1046	0.712	31.53	0.184
JPG_80_H1_1.0_D	9.93	1.684	7.11	2.28	0.0127	0.321	7.68	0.371
JPG_80_H1_1.0_W	34.10	1.684	21.53	14.25	0.0792	0.662	26.64	0.206
JPG_80_H13_0.1	13.78	1.232	4.91	0.78	0.0043	0.159	3.19	0.450
JPG_80_H13_0.1_D	7.95	1.232	3.17	0.32	0.0018	0.100	1.61	0.561
JPG_80_H13_0.1_W	44.20	1.232	26.03	3.16	0.0176	0.121	5.62	0.196
JPG_80_H13_0.5	23.61	1.405	11.40	4.63	0.0257	0.406	12.22	0.291
JPG_80_H13_0.5_D	6.81	1.405	4.20	0.89	0.0049	0.211	3.92	0.485
JPG_80_H13_0.5_W	38.19	1.405	22.76	7.49	0.0416	0.329	14.09	0.207
JPG_80_H13_1.0	33.72	1.693	25.74	24.35	0.1354	0.946	40.05	0.181
JPG_80_H13_1.0_D	10.49	1.693	8.17	3.46	0.0192	0.424	10.78	0.343
JPG_80_H13_1.0_W	33.54	1.693	23.06	19.85	0.1104	0.861	34.91	0.193
JPG_80_H26_0.1	18.06	1.370	8.74	2.41	0.0134	0.276	7.35	0.335
JPG_80_H26_0.1_D	4.62	1.370	3.47	0.39	0.0021	0.111	1.88	0.536
JPG_80_H26_0.1_W	41.04	1.370	24.55	5.22	0.0290	0.213	9.53	0.201
JPG_80_H26_0.5	15.31	1.218	6.20	1.80	0.0100	0.291	6.52	0.398
JPG_80_H26_0.5_D	6.32	1.218	3.58	0.59	0.0033	0.165	2.82	0.527
JPG_80_H26_0.5_W	56.01	1.218	32.83	7.67	0.0427	0.234	12.10	0.173
JPG_80_H26_1.0	21.91	1.440	11.16	5.42	0.0301	0.486	14.36	0.291
JPG_80_H26_1.0_D	6.11	1.440	4.30	0.95	0.0053	0.220	4.12	0.480
JPG_80_H26_1.0_W	33.92	1.440	20.13	9.67	0.0538	0.481	19.09	0.217
JPG_80_O13_0.1	9.17	1.143	4.04	0.59	0.0033	0.147	2.67	0.496
JPG_80_O13_0.1_D	3.20	1.143	2.63	0.16	0.0009	0.062	0.91	0.617
JPG_80_O13_0.1_W	53.65	1.143	30.73	3.40	0.0189	0.111	5.57	0.180
JPG_80_O13_0.5	17.78	1.452	9.96	4.08	0.0227	0.410	11.54	0.311
JPG_80_O13_0.5_D	4.31	1.452	3.92	0.74	0.0041	0.188	3.37	0.503
JPG_80_O13_0.5_W	37.29	1.452	24.10	7.94	0.0442	0.330	14.53	0.201
JPG_80_O13_1.0	20.61	1.404	10.77	4.95	0.0275	0.460	13.39	0.297
JPG_80_O13_1.0_D	6.26	1.404	4.42	0.85	0.0047	0.193	3.68	0.473
JPG_80_O13_1.0_W	41.90	1.404	27.93	11.33	0.0630	0.406	19.13	0.186

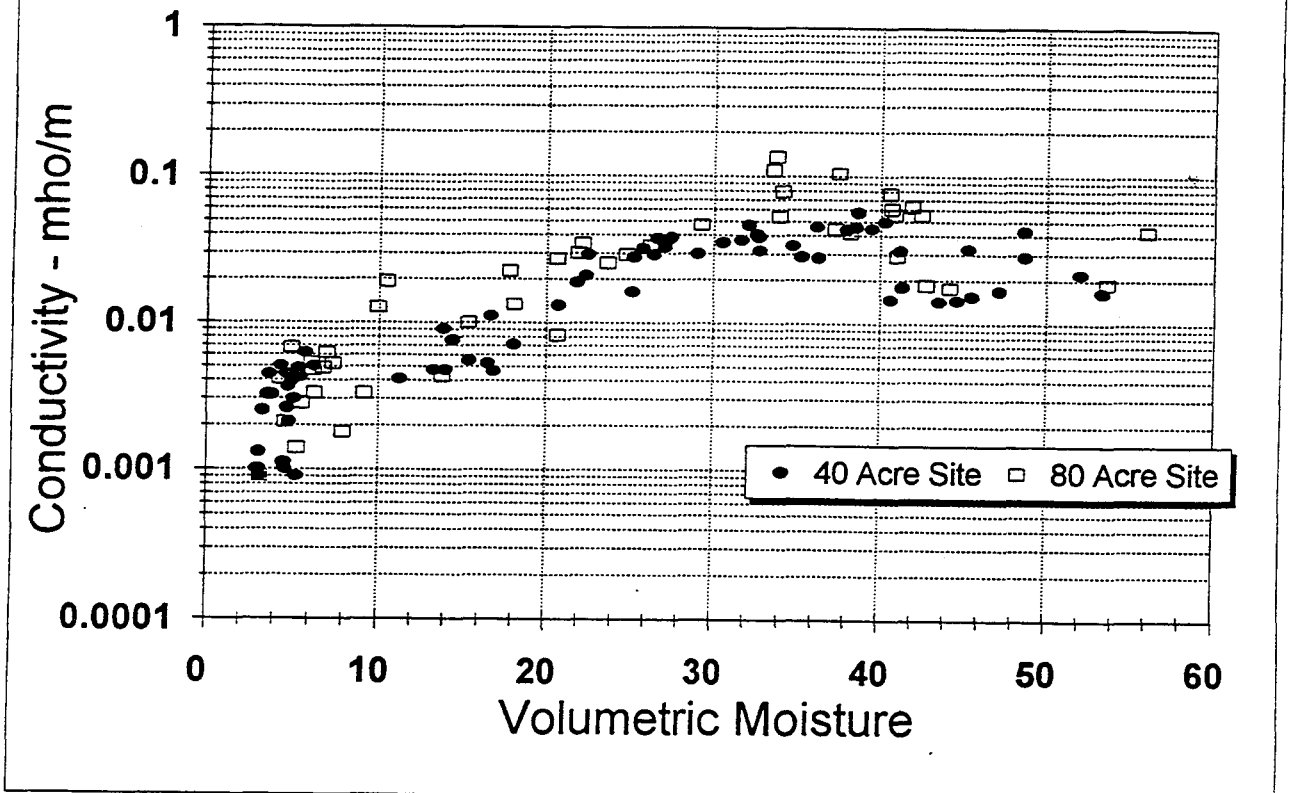
Jefferson Proving Ground , Phase IV Properties at 100 MHz , All Depths



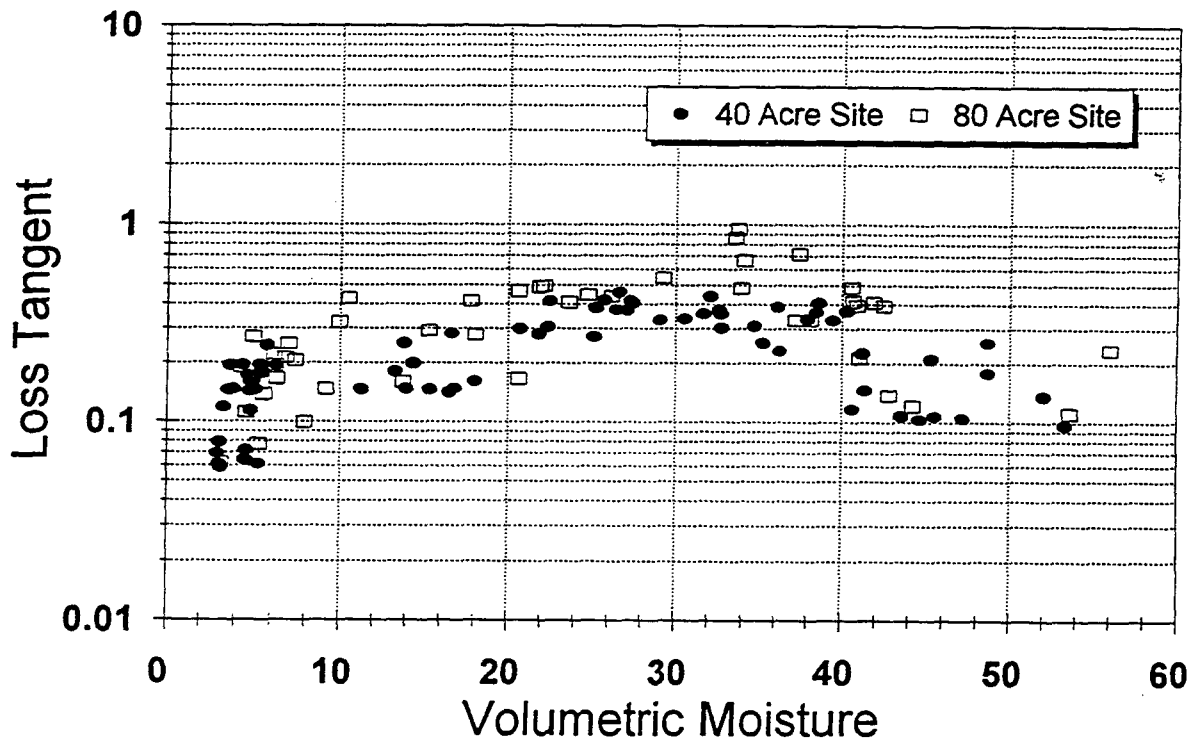
Jefferson Proving Ground , Phase IV Properties at 100 MHz , All Depths



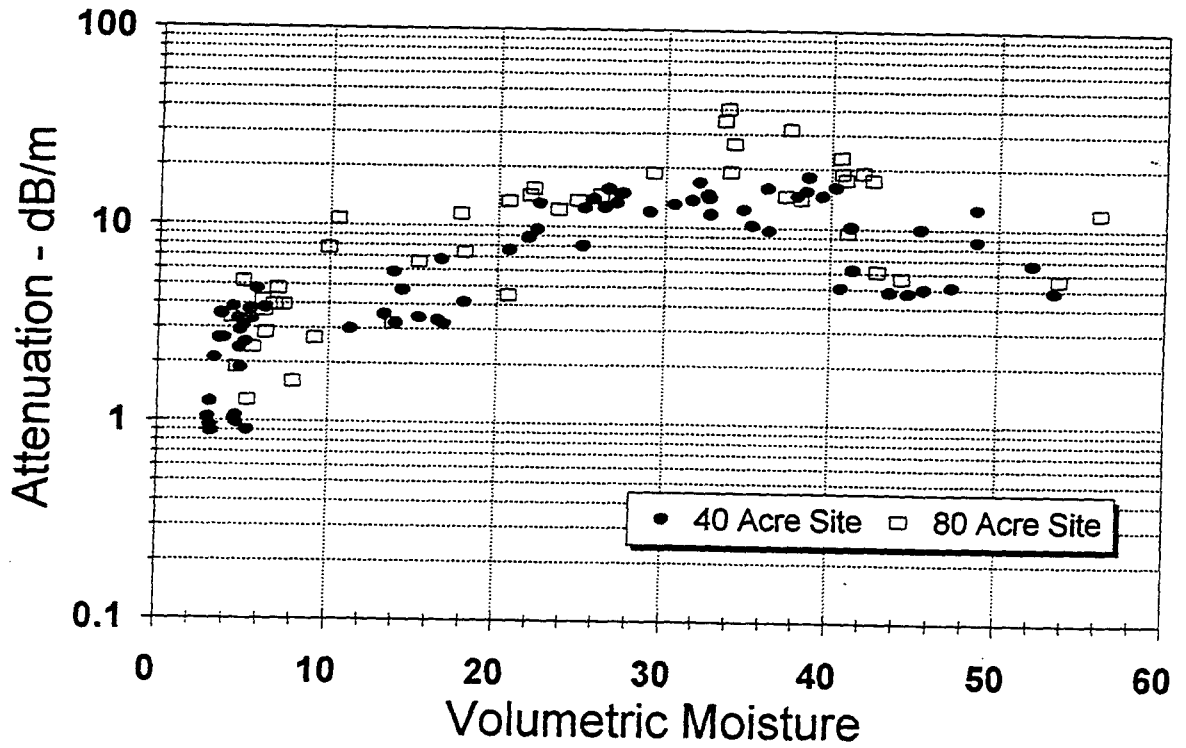
Jefferson Proving Ground , Phase IV Properties at 100 MHz , All Depths



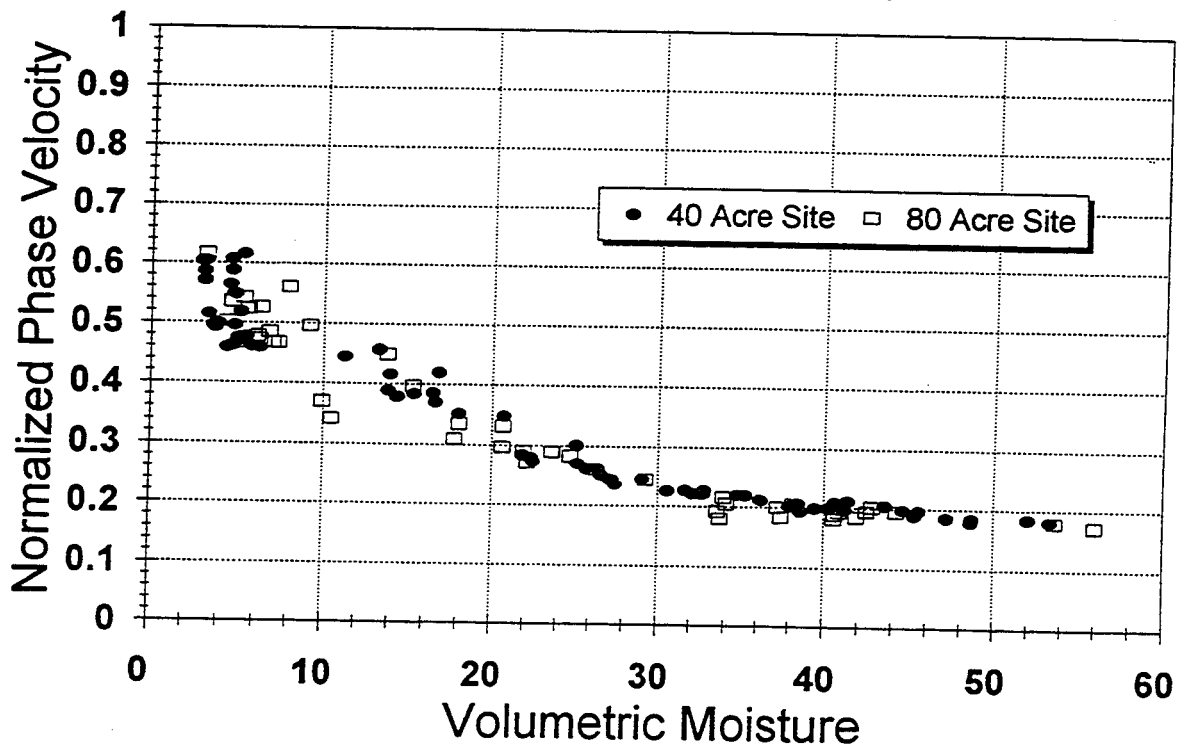
Jefferson Proving Ground , Phase IV Properties at 100 MHz , All Depths



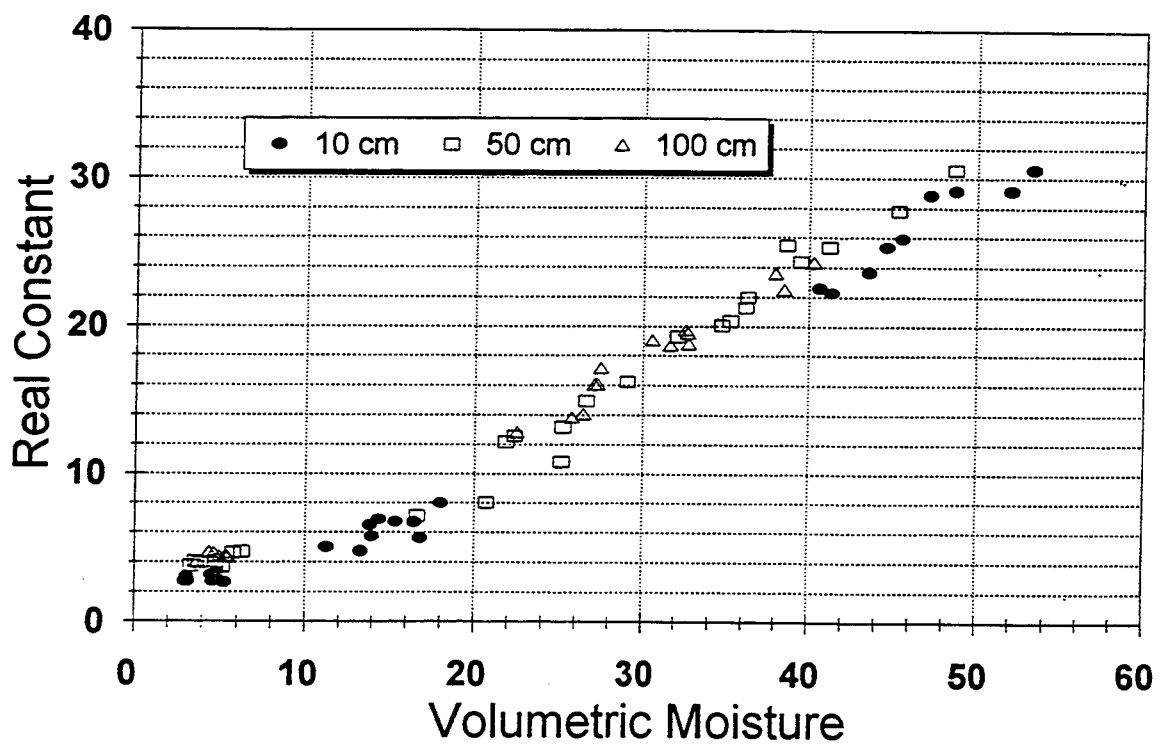
Jefferson Proving Ground , Phase IV Properties at 100 MHz , All Depths



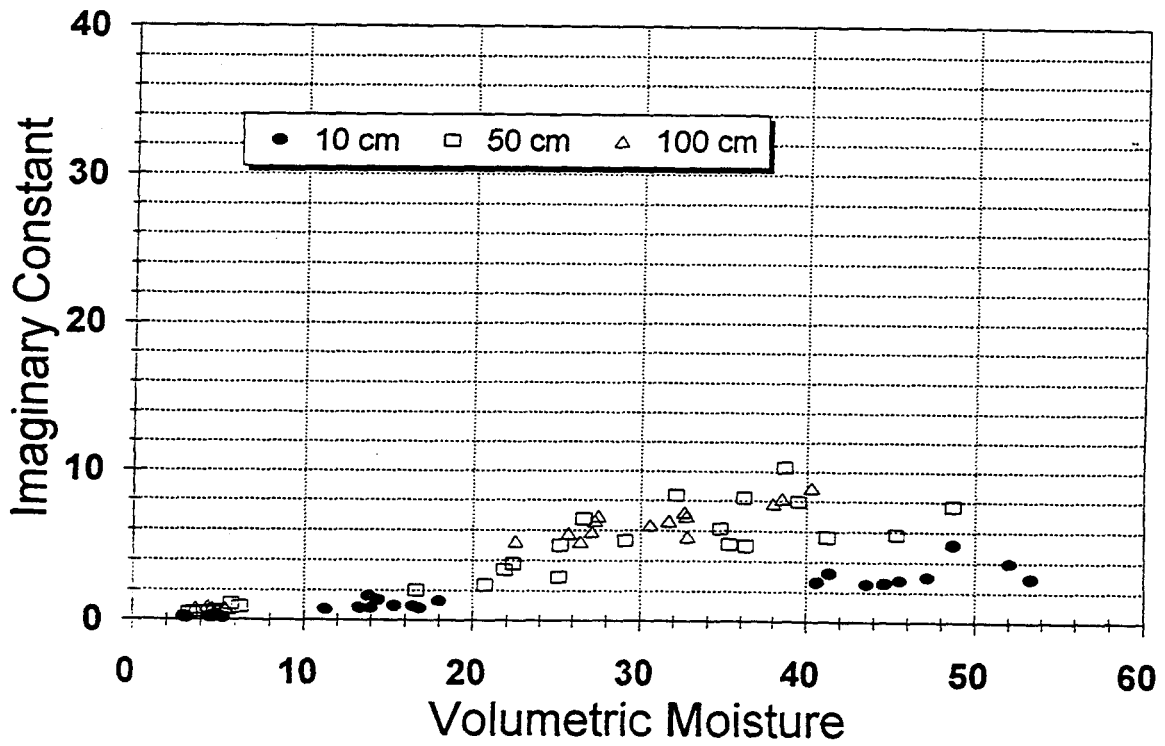
Jefferson Proving Ground , Phase IV Properties at 100 MHz , All Depths



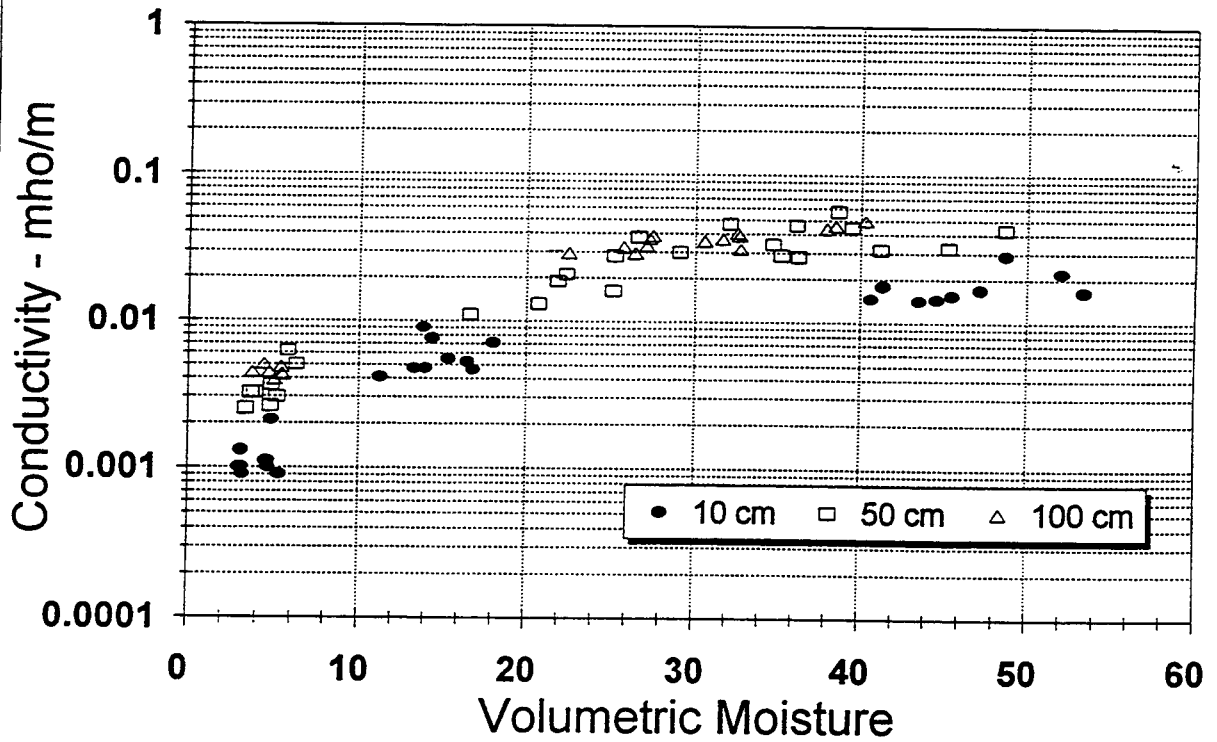
JPG , Phase IV , 40 Acre Test Site Properties at 100 MHz by Depth



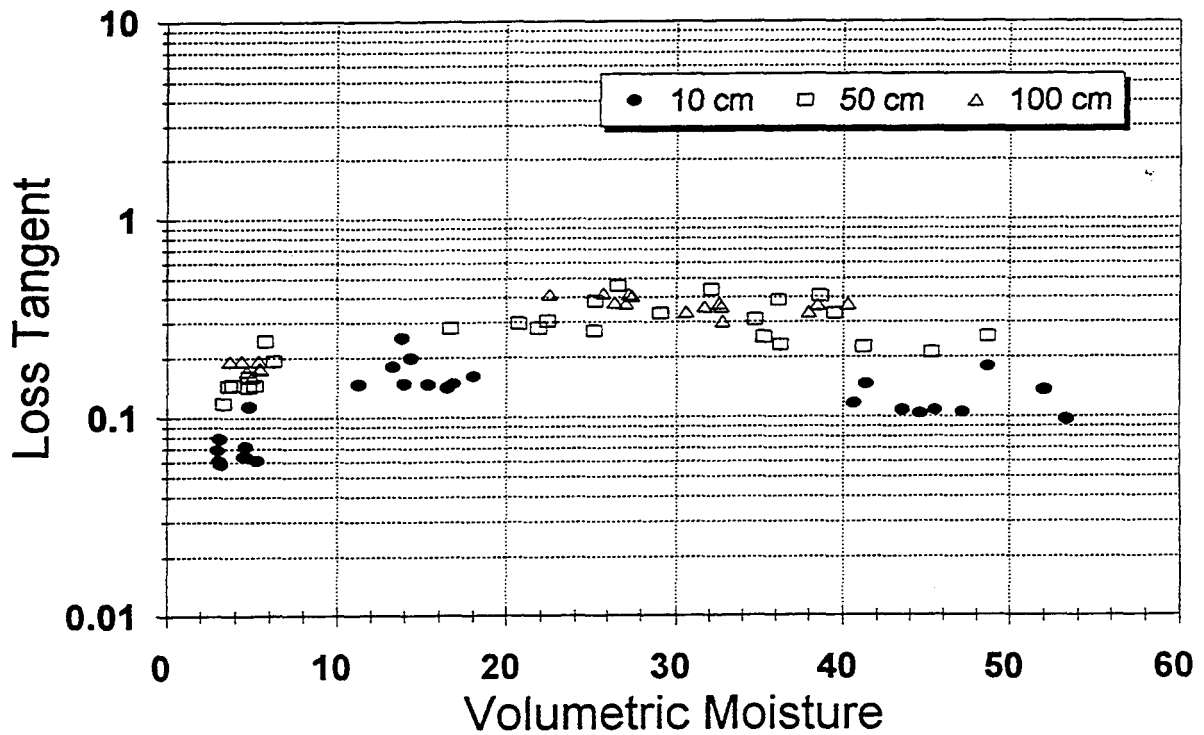
JPG , Phase IV , 40 Acre Test Site Properties at 100 MHz by Depth

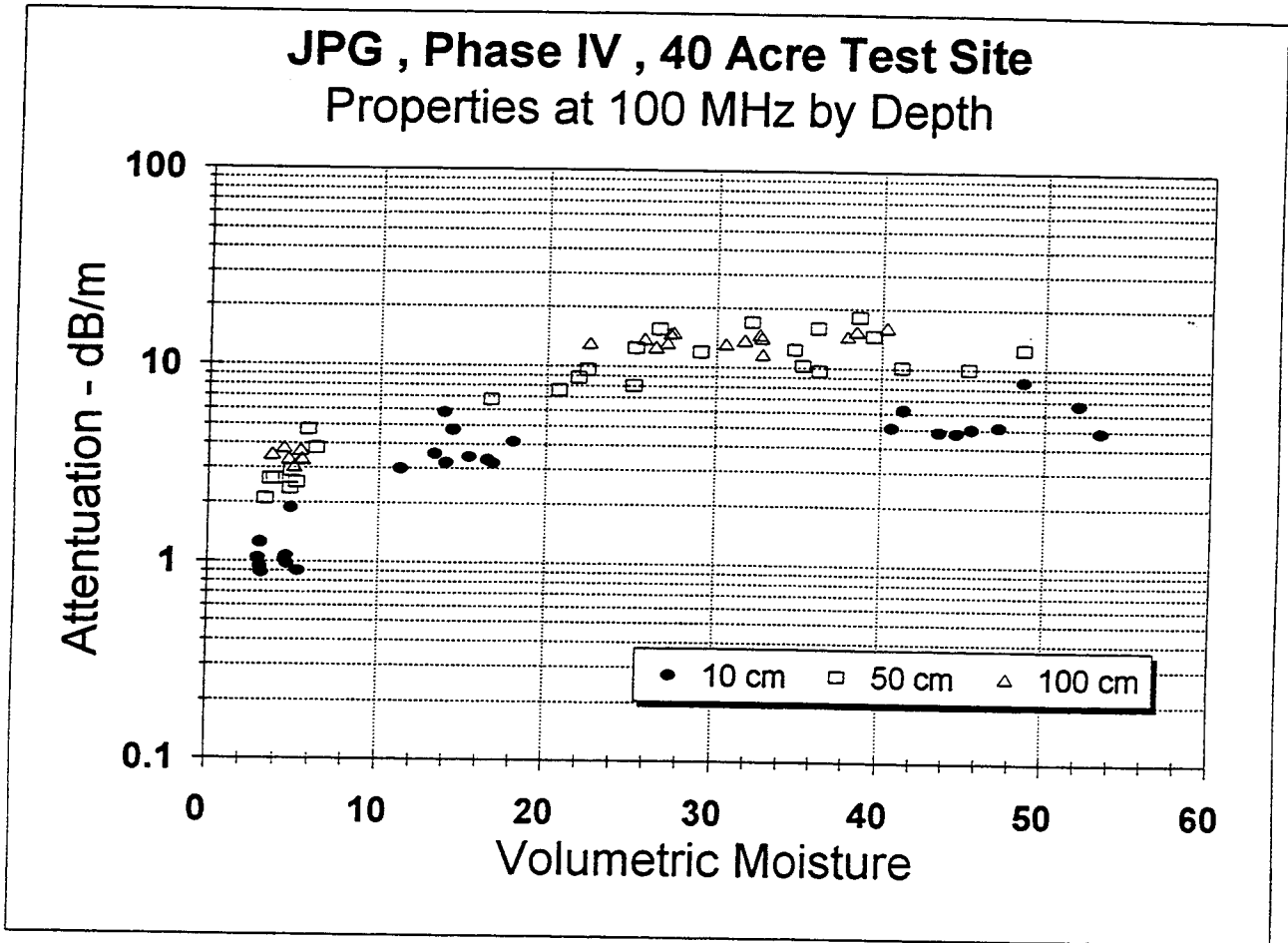


JPG , Phase IV , 40 Acre Test Site Properties at 100 MHz by Depth

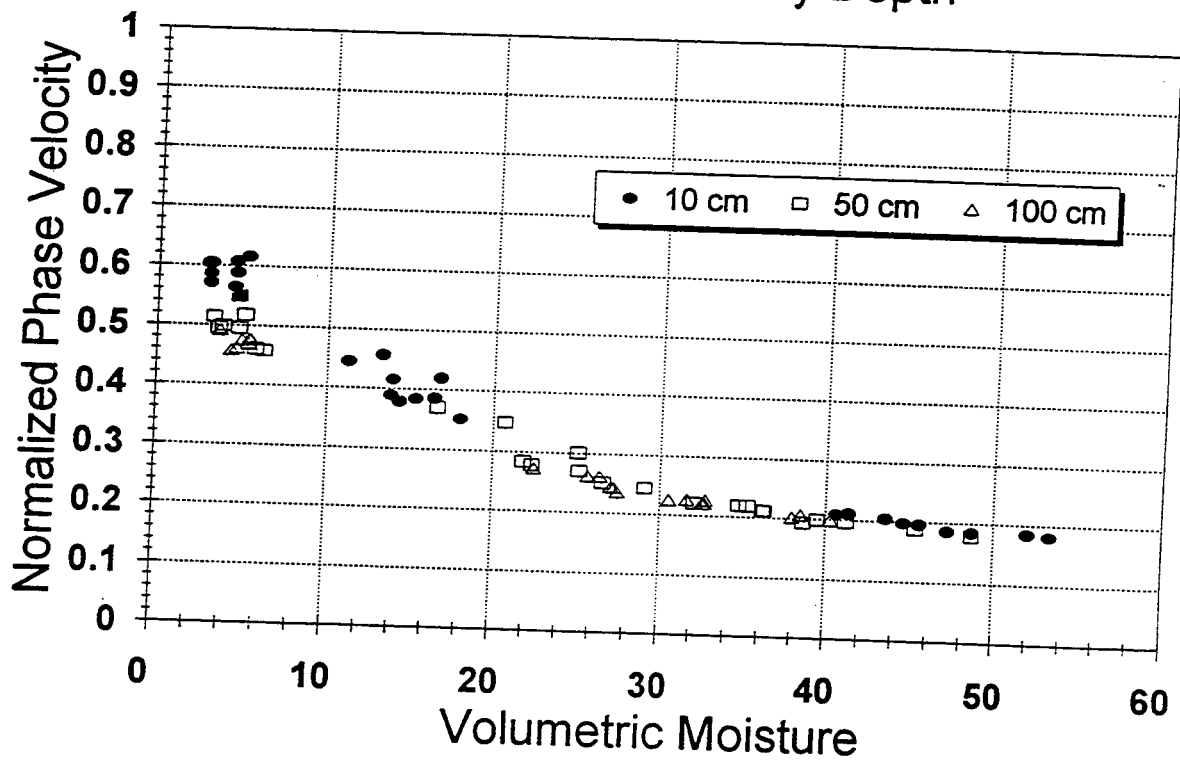


JPG , Phase IV , 40 Acre Test Site Properties at 100 MHz by Depth

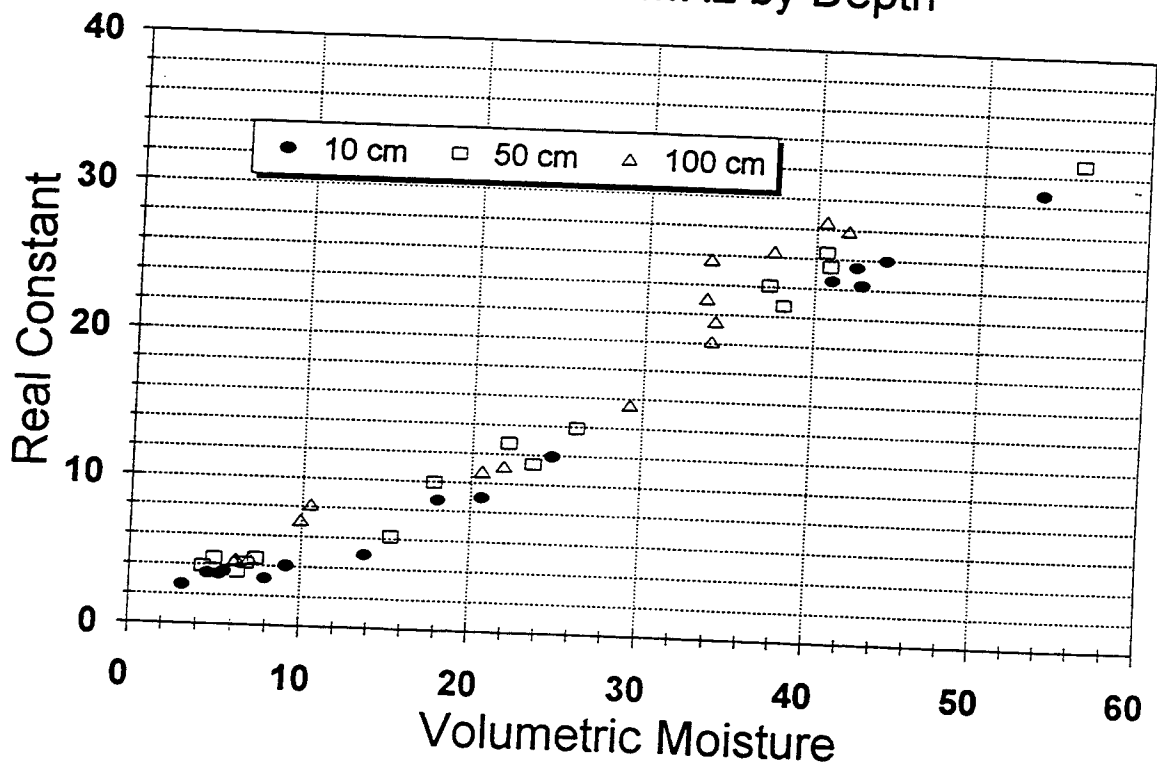




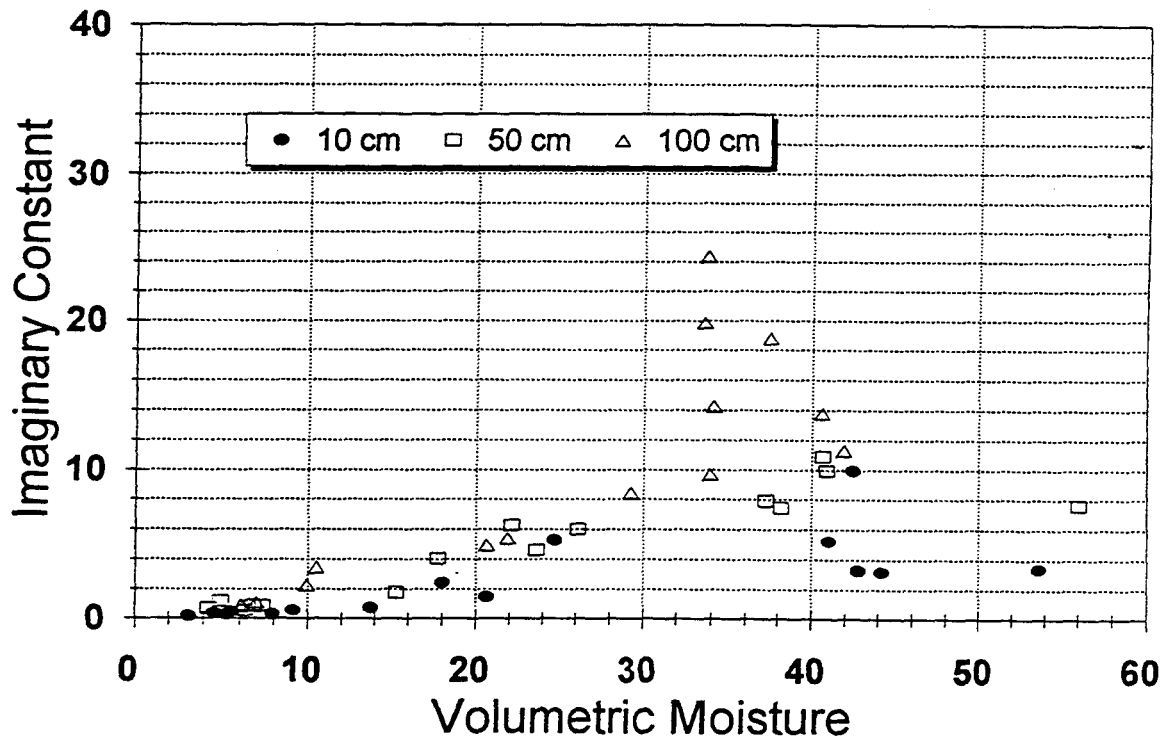
JPG , Phase IV , 40 Acre Test Site Properties at 100 MHz by Depth

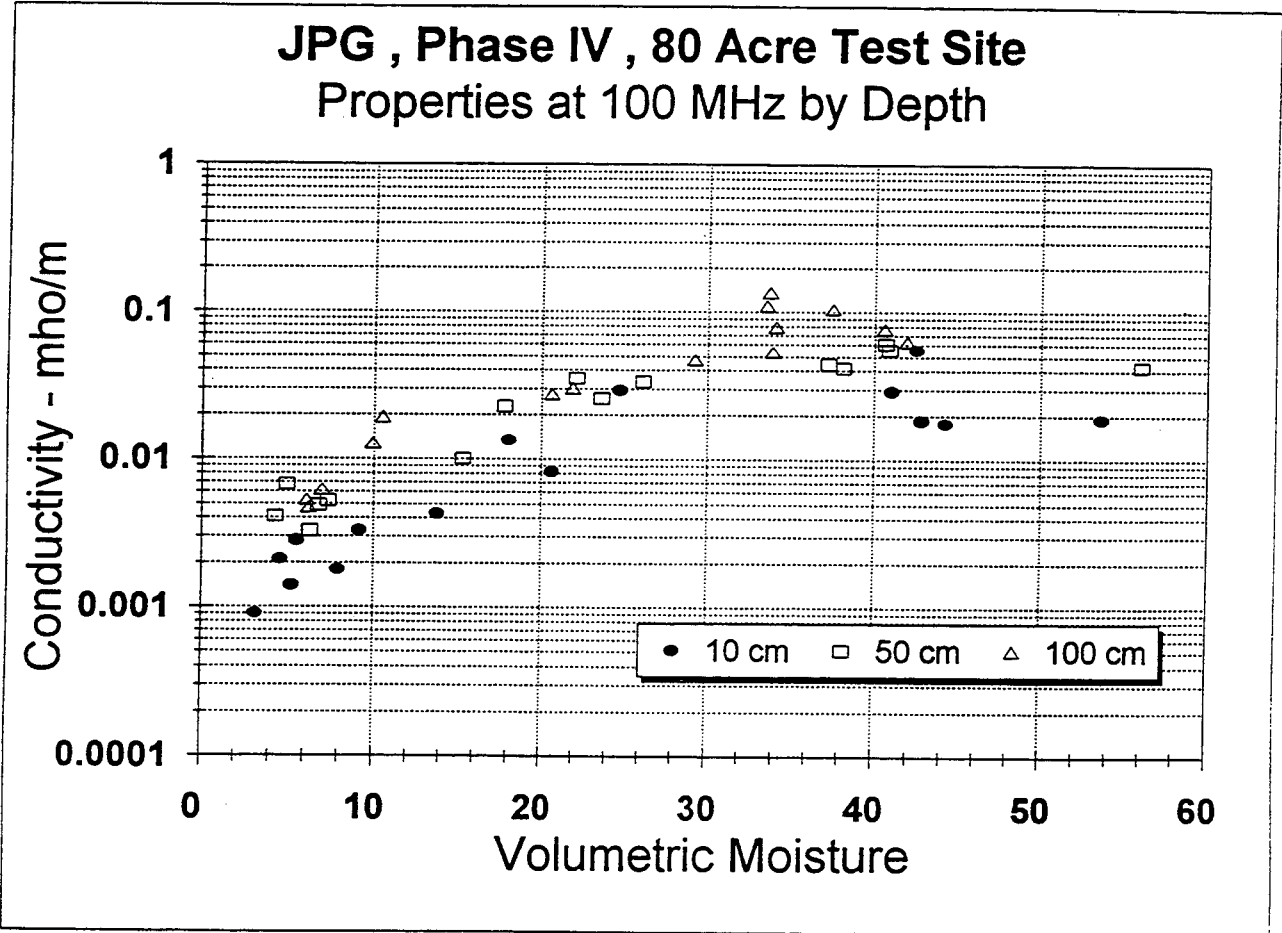


JPG , Phase IV , 80 Acre Test Site Properties at 100 MHz by Depth

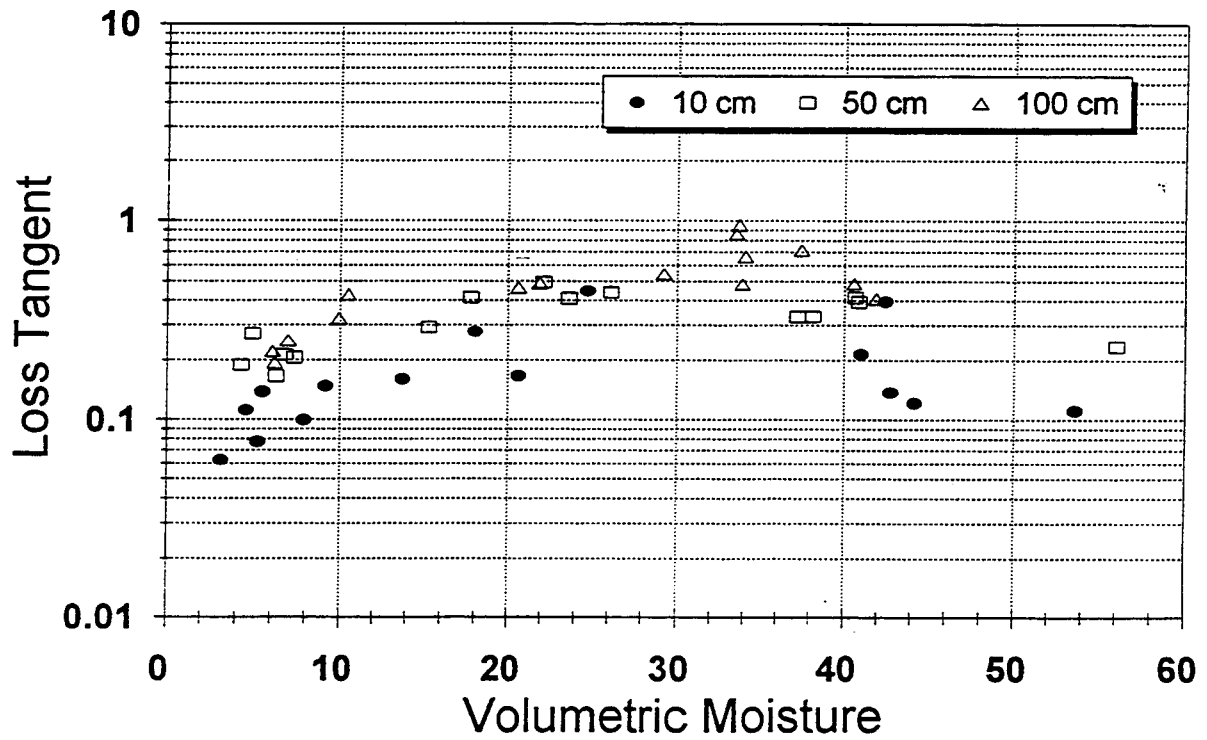


JPG , Phase IV , 80 Acre Test Site Properties at 100 MHz by Depth

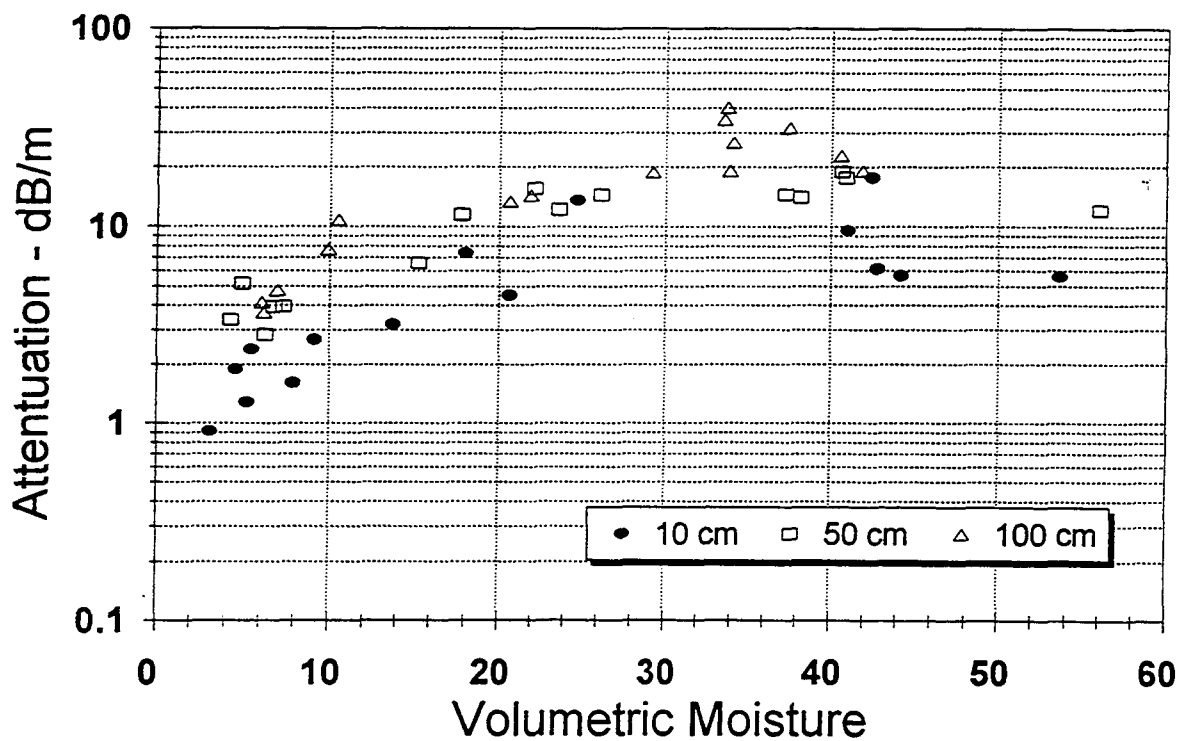




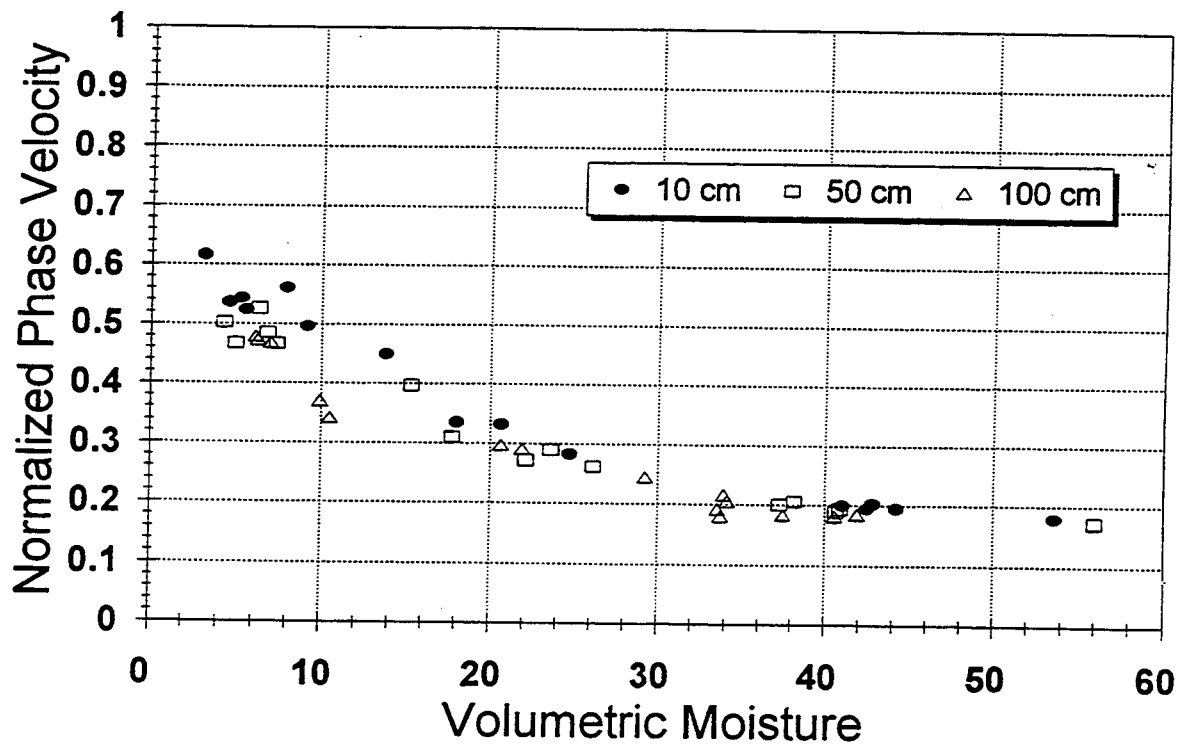
JPG , Phase IV , 80 Acre Test Site Properties at 100 MHz by Depth



JPG , Phase IV , 80 Acre Test Site Properties at 100 MHz by Depth



JPG , Phase IV , 80 Acre Test Site Properties at 100 MHz by Depth



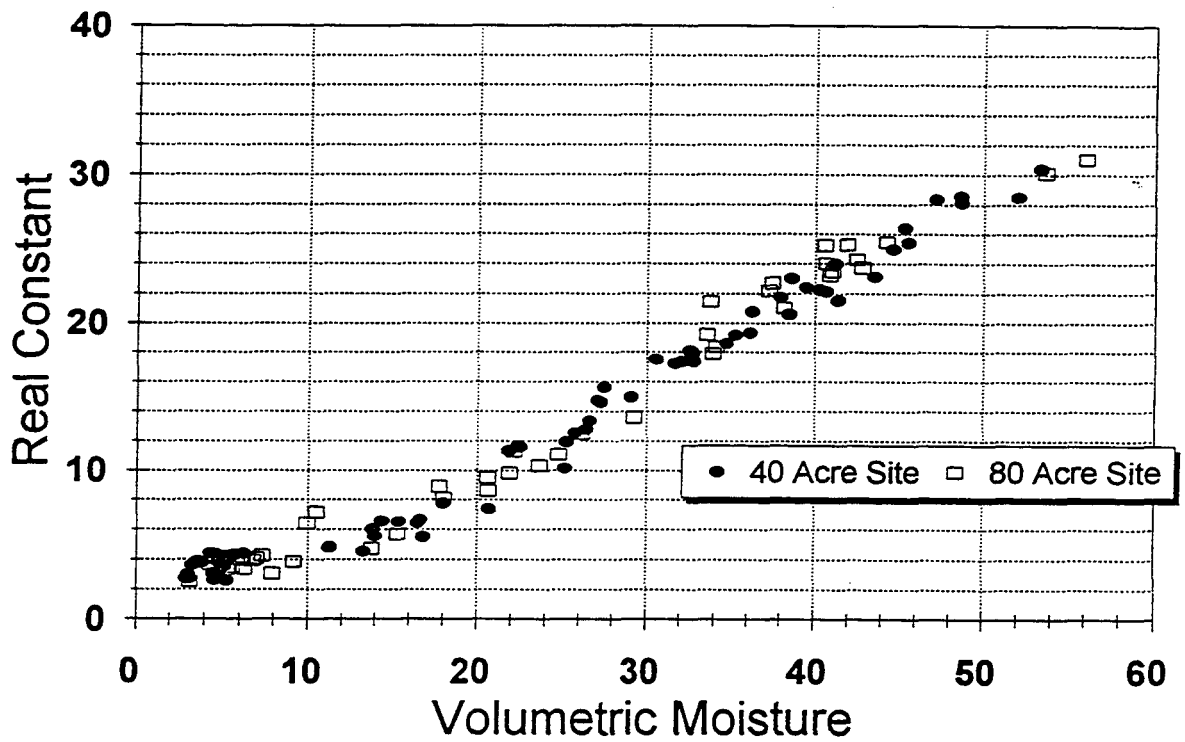
Sample	Vol Moist (%)	Dry Dens (g/cc)	Re(eps) (rel)	Im(eps) (rel)	Cond (mho/m)	Loss Tan	Attn (dB/m)	Ph Vel (rel)
JPG_40_C1_0.1	11.31	1.197	4.83	0.51	0.0057	0.106	4.24	0.454
JPG_40_C1_0.1_D	3.17	1.197	2.69	0.13	0.0015	0.049	1.45	0.609
JPG_40_C1_0.1_W	47.20	1.197	28.36	2.40	0.0267	0.085	8.20	0.188
JPG_40_C1_0.5	25.21	1.401	11.92	3.26	0.0363	0.274	17.03	0.287
JPG_40_C1_0.5_D	4.81	1.401	3.82	0.51	0.0057	0.134	4.74	0.510
JPG_40_C1_0.5_W	39.52	1.401	22.42	5.33	0.0593	0.238	20.33	0.210
JPG_40_C1_1.0	26.42	1.512	12.84	3.39	0.0377	0.264	17.08	0.277
JPG_40_C1_1.0_D	5.50	1.512	4.13	0.58	0.0065	0.141	5.20	0.491
JPG_40_C1_1.0_W	38.01	1.512	21.75	5.11	0.0568	0.235	19.80	0.213
JPG_40_C7_0.1	18.06	1.421	7.77	0.87	0.0096	0.112	5.65	0.358
JPG_40_C7_0.1_D	4.55	1.421	3.08	0.16	0.0018	0.054	1.71	0.570
JPG_40_C7_0.1_W	40.69	1.421	22.15	1.84	0.0204	0.083	7.09	0.212
JPG_40_C7_0.5	29.10	1.547	14.96	3.53	0.0392	0.236	16.48	0.257
JPG_40_C7_0.5_D	3.88	1.547	3.80	0.46	0.0052	0.122	4.33	0.512
JPG_40_C7_0.5_W	34.76	1.547	18.61	4.06	0.0451	0.218	17.01	0.231
JPG_40_C7_1.0	27.08	1.634	14.74	3.84	0.0427	0.260	18.04	0.258
JPG_40_C7_1.0_D	5.00	1.634	4.18	0.55	0.0061	0.132	4.89	0.488
JPG_40_C7_1.0_W	31.70	1.634	17.24	4.30	0.0478	0.249	18.68	0.239
JPG_40_C13_0.1	14.39	1.359	6.55	0.92	0.0102	0.140	6.50	0.390
JPG_40_C13_0.1_D	3.13	1.359	3.00	0.19	0.0021	0.064	2.02	0.577
JPG_40_C13_0.1_W	41.40	1.359	21.55	2.01	0.0223	0.093	7.86	0.215
JPG_40_C13_0.5	16.64	1.377	6.65	1.34	0.0149	0.201	9.40	0.386
JPG_40_C13_0.5_W	45.31	1.377	26.42	3.94	0.0438	0.149	13.90	0.194
JPG_40_C13_1.0	22.51	1.524	11.58	3.43	0.0381	0.296	18.14	0.291
JPG_40_C13_1.0_D	3.70	1.524	3.86	0.59	0.0066	0.154	5.49	0.507
JPG_40_C13_1.0_W	32.73	1.524	17.88	4.62	0.0514	0.259	19.72	0.235
JPG_40_G1_0.1	16.84	1.126	5.52	0.58	0.0064	0.105	4.48	0.425
JPG_40_G1_0.1_D	5.28	1.126	2.61	0.13	0.0014	0.049	1.43	0.618
JPG_40_G1_0.1_W	53.37	1.126	30.38	2.27	0.0253	0.075	7.50	0.181
JPG_40_G1_0.5	25.14	1.440	10.15	1.99	0.0221	0.196	11.32	0.313
JPG_40_G1_0.5_D	5.14	1.440	3.54	0.41	0.0046	0.117	4.01	0.531
JPG_40_G1_0.5_W	41.22	1.440	24.00	3.98	0.0442	0.166	14.71	0.203
JPG_40_G1_1.0	30.59	1.621	17.55	4.09	0.0455	0.233	17.66	0.237
JPG_40_G1_1.0_D	4.69	1.621	4.37	0.62	0.0069	0.142	5.39	0.477
JPG_40_G1_1.0_W	32.80	1.621	17.39	3.82	0.0425	0.220	16.57	0.238
JPG_40_G7_0.1	15.35	1.339	6.52	0.67	0.0075	0.103	4.79	0.391
JPG_40_G7_0.1_D	3.13	1.339	2.88	0.15	0.0016	0.050	1.56	0.589
JPG_40_G7_0.1_W	45.54	1.339	25.43	2.03	0.0225	0.080	7.30	0.198
JPG_40_G7_0.5	21.87	1.494	11.34	2.22	0.0247	0.196	11.94	0.296
JPG_40_G7_0.5_D	3.32	1.494	3.60	0.36	0.0040	0.101	3.47	0.526
JPG_40_G7_0.5_W	36.30	1.494	20.77	3.39	0.0376	0.163	13.47	0.219
JPG_40_G7_1.0	27.28	1.599	14.61	4.22	0.0470	0.289	19.90	0.259
JPG_40_G7_1.0_D	5.38	1.599	4.24	0.64	0.0071	0.152	5.66	0.484
JPG_40_G7_1.0_W	38.51	1.599	20.60	5.23	0.0581	0.254	20.79	0.219
JPG_40_G13_0.1	13.96	1.271	5.56	0.57	0.0064	0.103	4.42	0.423
JPG_40_G13_0.1_D	3.01	1.271	2.70	0.14	0.0015	0.051	1.51	0.609
JPG_40_G13_0.1_W	44.65	1.271	24.98	2.24	0.0250	0.090	8.16	0.200
JPG_40_G13_0.5	22.39	1.560	11.68	2.48	0.0276	0.213	13.14	0.291
JPG_40_G13_0.5_D	3.63	1.560	3.86	0.45	0.0050	0.116	4.16	0.508
JPG_40_G13_0.5_W	35.29	1.560	19.16	3.43	0.0381	0.179	14.19	0.228

_38

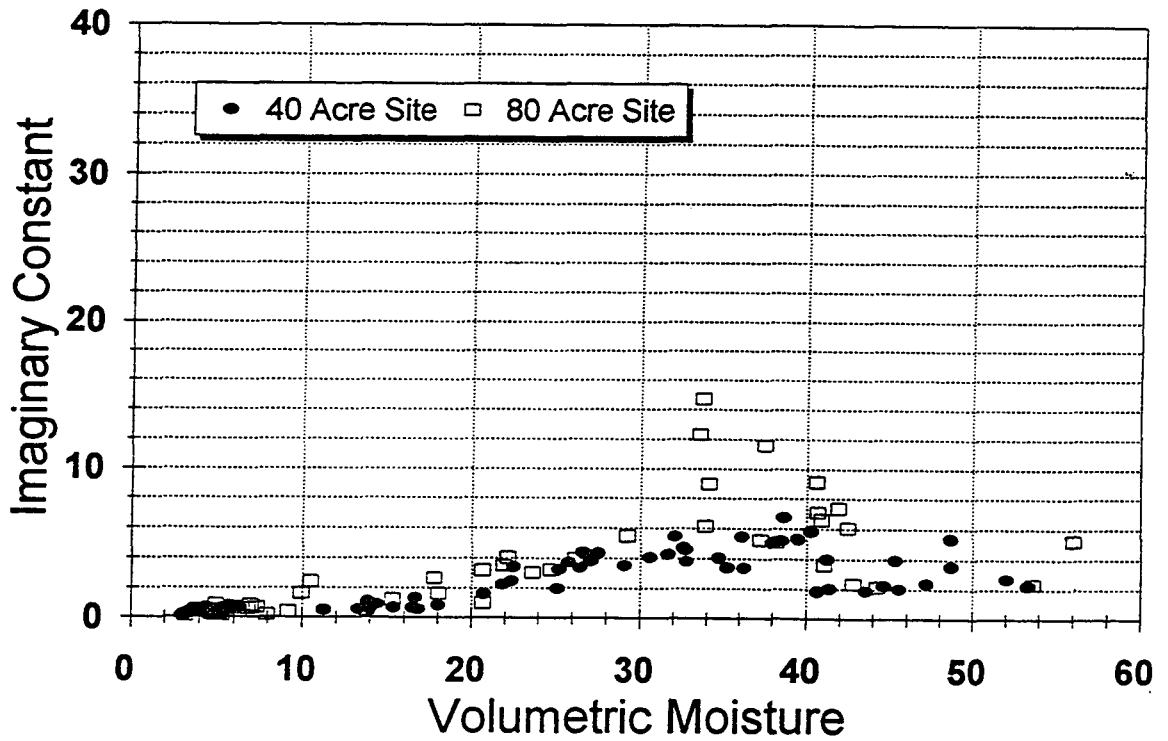
JPG_40_G13_1.0	27.49	1.673	15.64	4.34	0.0483	0.278	19.80	0.251
JPG_40_G13_1.0_D	4.39	1.673	4.43	0.67	0.0075	0.152	5.79	0.474
JPG_40_G13_1.0_W	32.60	1.673	18.10	4.72	0.0525	0.261	20.04	0.233
JPG_40_K1_0.1	16.49	1.217	6.43	0.67	0.0074	0.104	4.77	0.394
JPG_40_K1_0.1_D	4.65	1.217	2.84	0.16	0.0017	0.055	1.68	0.593
JPG_40_K1_0.1_W	43.58	1.217	23.13	1.88	0.0209	0.081	7.11	0.208
JPG_40_K1_0.5	32.12	1.467	17.39	5.48	0.0609	0.315	23.61	0.237
JPG_40_K1_0.5_D	6.28	1.467	4.41	0.71	0.0079	0.162	6.15	0.475
JPG_40_K1_0.5_W	36.18	1.467	19.32	5.50	0.0612	0.285	22.54	0.225
JPG_40_K7_0.1	13.85	1.228	6.02	1.11	0.0124	0.185	8.21	0.406
JPG_40_K7_0.1_D	4.83	1.228	3.18	0.29	0.0033	0.092	2.98	0.560
JPG_40_K7_0.1_W	48.72	1.228	28.11	3.55	0.0395	0.126	12.16	0.188
JPG_40_K7_0.5	26.59	1.447	13.35	4.39	0.0488	0.329	21.56	0.270
JPG_40_K7_0.5_D	5.78	1.447	4.32	0.83	0.0092	0.191	7.19	0.479
JPG_40_K7_0.5_W	38.67	1.447	23.03	6.75	0.0751	0.293	25.33	0.206
JPG_40_K13_0.1	13.33	1.185	4.54	0.59	0.0065	0.129	4.98	0.468
JPG_40_K13_0.1_D	4.62	1.185	2.64	0.16	0.0018	0.061	1.81	0.616
JPG_40_K13_0.1_W	52.08	1.185	28.49	2.71	0.0302	0.095	9.23	0.187
JPG_40_K13_0.5	20.73	1.266	7.38	1.62	0.0180	0.220	10.79	0.366
JPG_40_K13_0.5_D	4.76	1.266	3.12	0.37	0.0041	0.119	3.82	0.565
JPG_40_K13_0.5_W	48.65	1.266	28.56	5.38	0.0599	0.189	18.25	0.186
JPG_40_K13_1.0	25.73	1.516	12.54	3.73	0.0415	0.298	18.97	0.279
JPG_40_K13_1.0_D	5.42	1.516	4.12	0.60	0.0066	0.145	5.32	0.492
JPG_40_K13_1.0_W	40.31	1.516	22.27	5.86	0.0652	0.263	22.41	0.210

Sample	Vol Moist (%)	Dry Dens (g/cc)	Re(eps) (rel)	Im(eps) (rel)	Cond (mho/m)	Loss Tan	Attn (dB/m)	Ph Vel (rel)
JPG_80_A13_0.1	24.76	1.300	11.07	3.24	0.0360	0.293	17.54	0.297
JPG_80_A13_0.1_D	5.56	1.300	3.47	0.39	0.0043	0.112	3.79	0.536
JPG_80_A13_0.1_W	42.47	1.300	24.30	6.09	0.0677	0.250	22.29	0.201
JPG_80_A13_0.5	22.13	1.380	11.34	4.05	0.0450	0.357	21.56	0.293
JPG_80_A13_0.5_D	4.97	1.380	4.12	0.89	0.0099	0.215	7.90	0.490
JPG_80_A13_0.5_W	40.67	1.380	24.06	7.11	0.0791	0.296	26.11	0.202
JPG_80_A13_1.0	29.27	1.378	13.58	5.50	0.0612	0.405	26.64	0.266
JPG_80_A13_1.0_D	6.98	1.378	4.11	0.86	0.0095	0.208	7.63	0.491
JPG_80_A13_1.0_W	40.59	1.378	25.27	9.14	0.1017	0.362	32.57	0.196
JPG_80_H1_0.1	20.66	1.344	8.63	1.03	0.0114	0.119	6.35	0.340
JPG_80_H1_0.1_D	5.31	1.344	3.35	0.21	0.0024	0.064	2.12	0.546
JPG_80_H1_0.1_W	42.81	1.344	23.75	2.34	0.0261	0.099	8.74	0.205
JPG_80_H1_0.5	26.11	1.434	12.50	3.97	0.0442	0.318	20.20	0.279
JPG_80_H1_0.5_D	7.36	1.434	4.28	0.71	0.0079	0.165	6.20	0.482
JPG_80_H1_0.5_W	40.90	1.434	23.24	6.60	0.0734	0.284	24.65	0.205
JPG_80_H1_1.0	37.50	1.684	22.73	11.60	0.1290	0.511	42.97	0.204
JPG_80_H1_1.0_D	9.93	1.684	6.41	1.65	0.0184	0.257	11.76	0.392
JPG_80_H1_1.0_W	34.10	1.684	18.40	8.99	0.1000	0.489	37.11	0.227
JPG_80_H13_0.1	13.78	1.232	4.73	0.56	0.0062	0.118	4.66	0.459
JPG_80_H13_0.1_D	7.95	1.232	3.08	0.23	0.0026	0.076	2.41	0.569
JPG_80_H13_0.1_W	44.20	1.232	25.48	2.17	0.0242	0.085	7.82	0.198
JPG_80_H13_0.5	23.61	1.405	10.32	3.04	0.0338	0.294	17.02	0.308
JPG_80_H13_0.5_D	6.81	1.405	3.94	0.65	0.0073	0.166	5.97	0.502
JPG_80_H13_0.5_W	38.19	1.405	21.05	5.13	0.0570	0.244	20.18	0.216
JPG_80_H13_1.0	33.72	1.693	21.48	14.72	0.1637	0.685	54.94	0.205
JPG_80_H13_1.0_D	10.49	1.693	7.18	2.41	0.0268	0.336	16.14	0.368
JPG_80_H13_1.0_W	33.54	1.693	19.24	12.33	0.1371	0.641	48.90	0.218
JPG_80_H26_0.1	18.06	1.370	8.14	1.63	0.0182	0.201	10.37	0.349
JPG_80_H26_0.1_D	4.62	1.370	3.37	0.32	0.0035	0.094	3.13	0.545
JPG_80_H26_0.1_W	41.04	1.370	23.48	3.60	0.0400	0.153	13.46	0.206
JPG_80_H26_0.5	15.31	1.218	5.70	1.24	0.0138	0.218	9.40	0.417
JPG_80_H26_0.5_D	6.32	1.218	3.39	0.46	0.0051	0.136	4.54	0.542
JPG_80_H26_0.5_W	56.01	1.218	31.04	5.26	0.0585	0.169	17.10	0.179
JPG_80_H26_1.0	21.91	1.440	9.83	3.50	0.0389	0.356	20.01	0.314
JPG_80_H26_1.0_D	6.11	1.440	4.00	0.73	0.0081	0.182	6.59	0.498
JPG_80_H26_1.0_W	33.92	1.440	17.93	6.16	0.0685	0.344	26.10	0.233
JPG_80_O13_0.1	9.17	1.143	3.87	0.43	0.0048	0.112	4.00	0.508
JPG_80_O13_0.1_D	3.20	1.143	2.56	0.14	0.0016	0.056	1.63	0.625
JPG_80_O13_0.1_W	53.65	1.143	30.13	2.37	0.0264	0.079	7.86	0.182
JPG_80_O13_0.5	17.78	1.452	8.93	2.68	0.0298	0.300	16.15	0.331
JPG_80_O13_0.5_D	4.31	1.452	3.72	0.56	0.0063	0.152	5.31	0.517
JPG_80_O13_0.5_W	37.29	1.452	22.21	5.26	0.0585	0.237	20.16	0.211
JPG_80_O13_1.0	20.61	1.404	9.50	3.20	0.0356	0.337	18.65	0.320
JPG_80_O13_1.0_D	6.26	1.404	4.16	0.64	0.0071	0.154	5.69	0.489
JPG_80_O13_1.0_W	41.90	1.404	25.31	7.40	0.0823	0.293	26.50	0.197

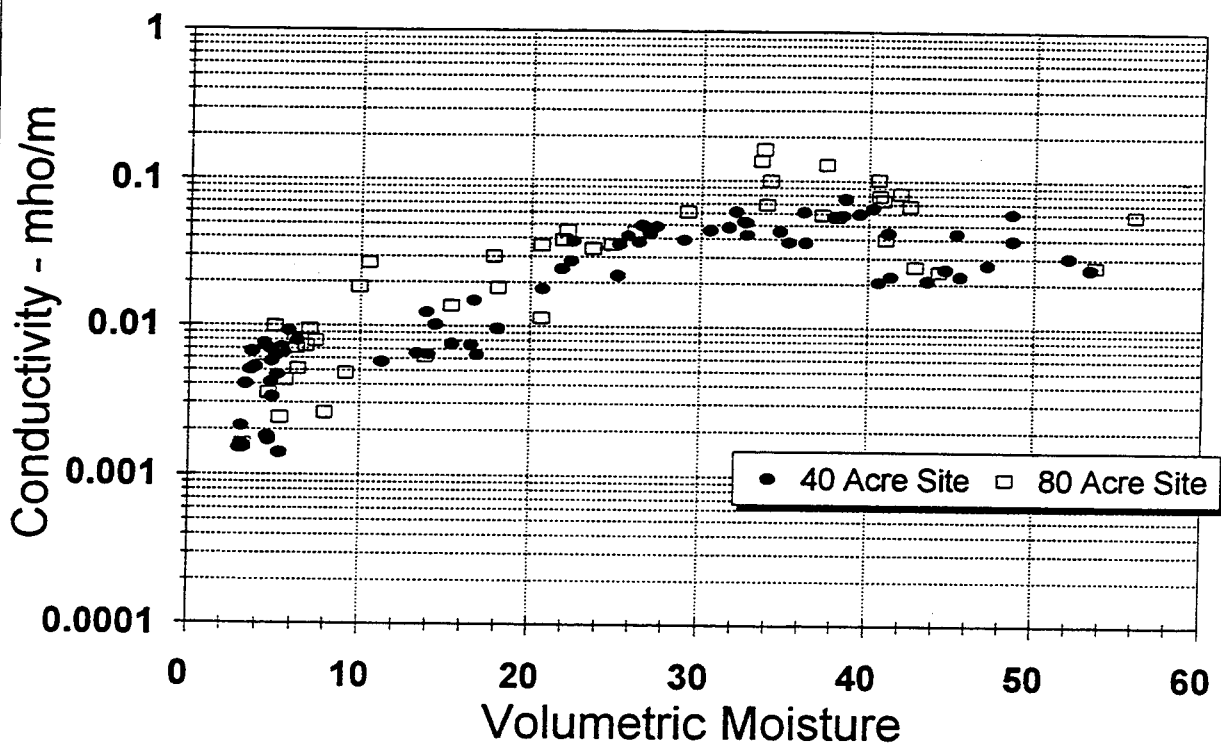
Jefferson Proving Ground , Phase IV Properties at 200 MHz , All Depths



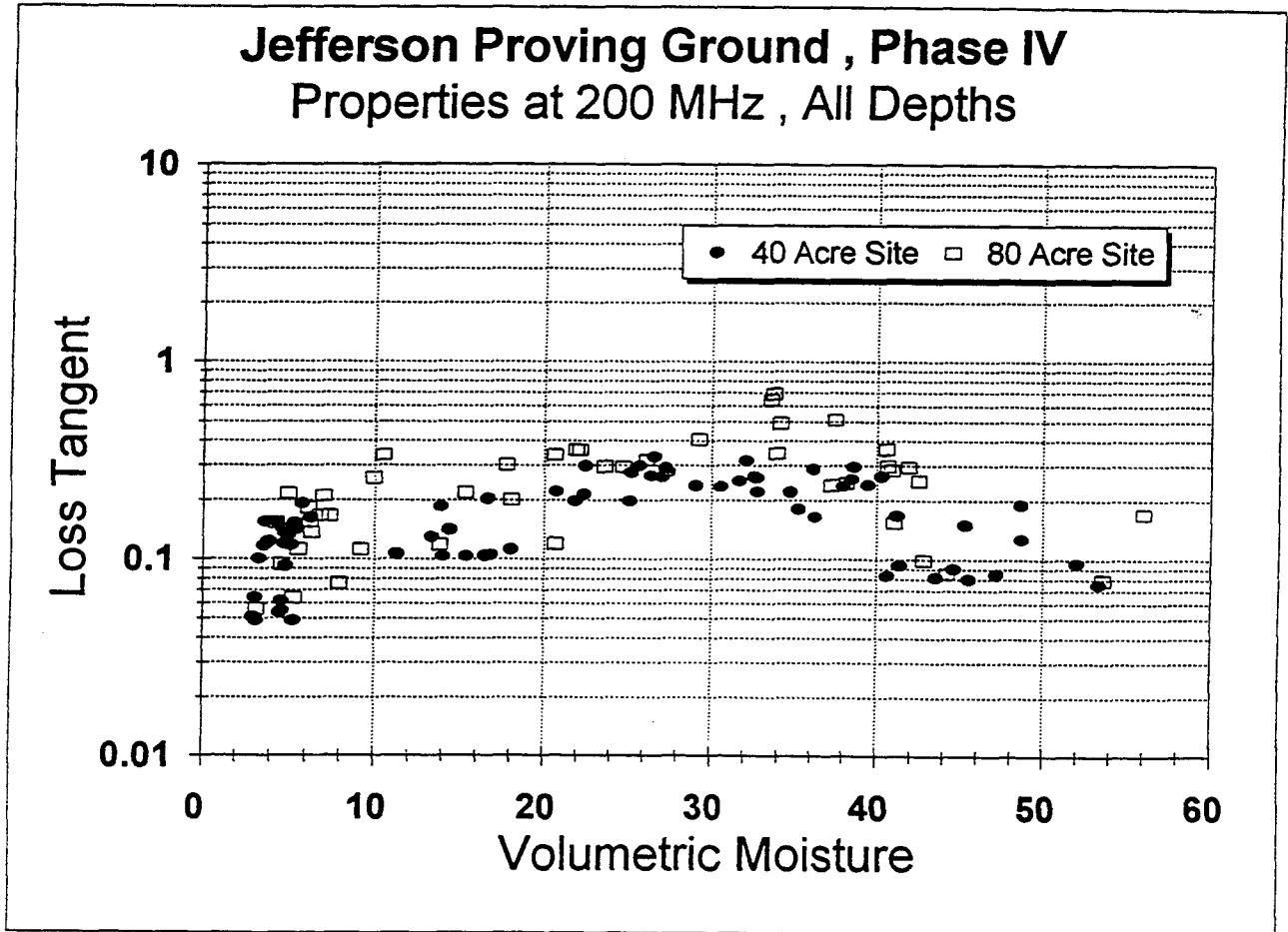
Jefferson Proving Ground , Phase IV Properties at 200 MHz , All Depths



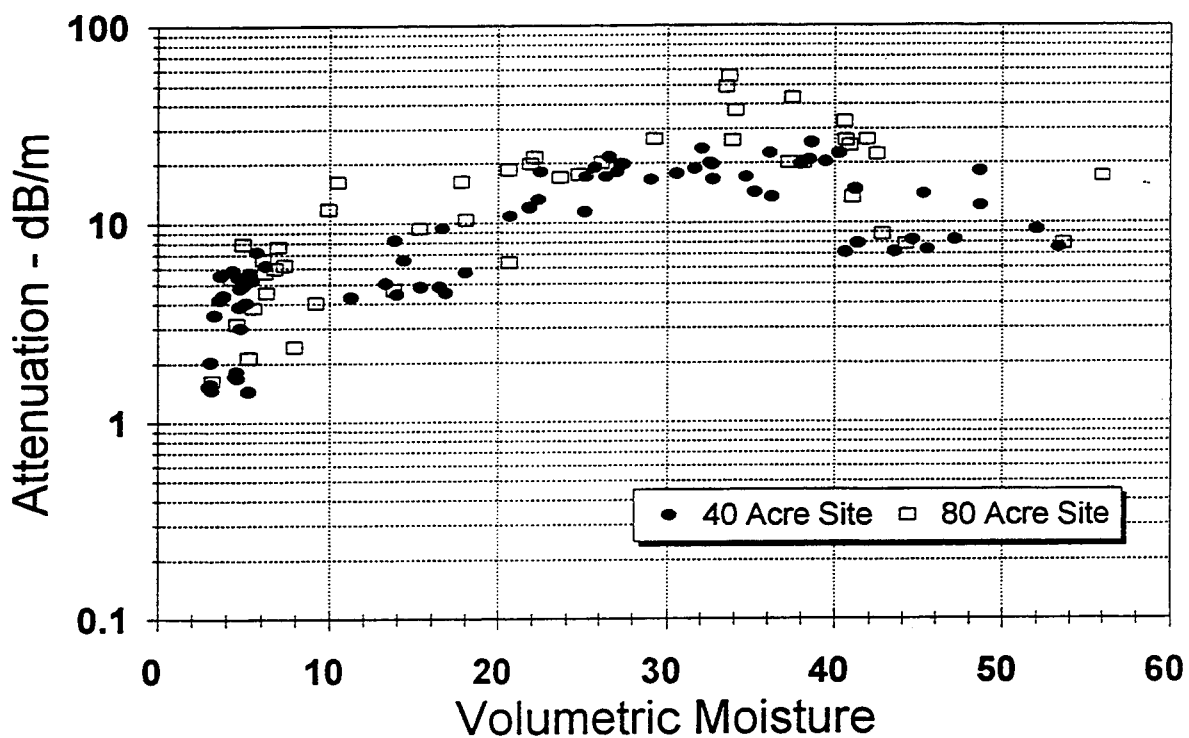
Jefferson Proving Ground , Phase IV Properties at 200 MHz , All Depths



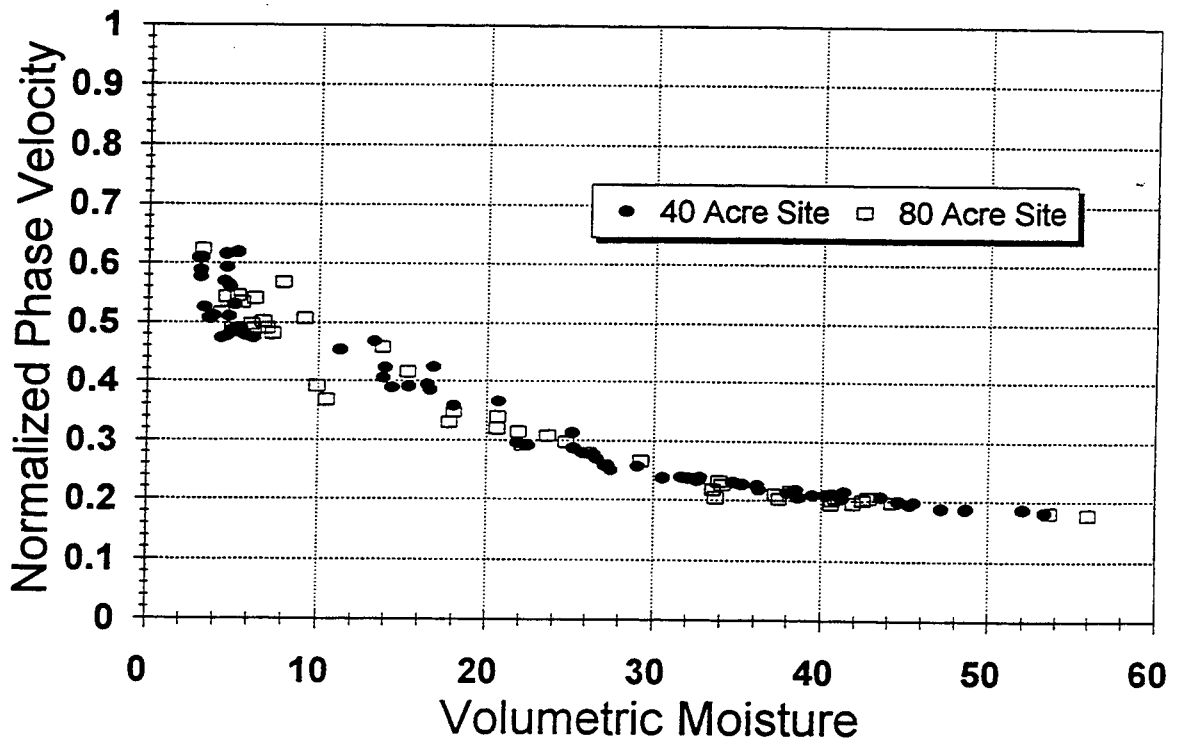
Jefferson Proving Ground , Phase IV Properties at 200 MHz , All Depths



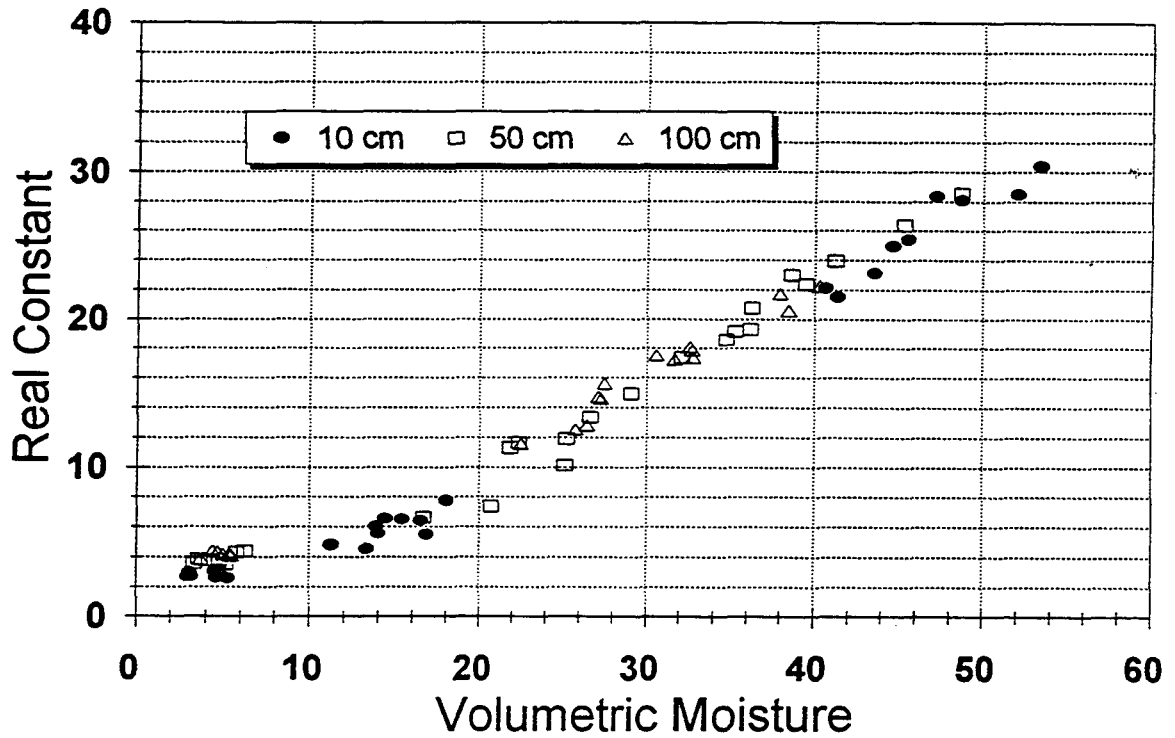
Jefferson Proving Ground , Phase IV Properties at 200 MHz , All Depths



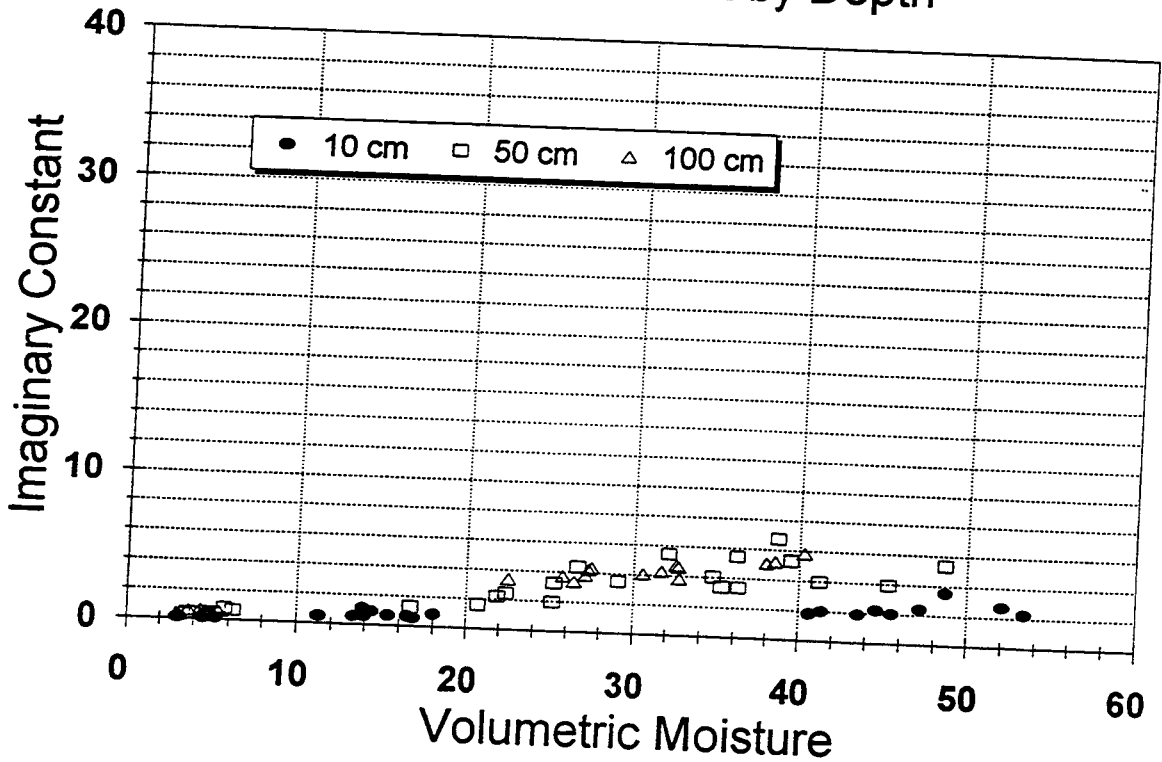
Jefferson Proving Ground , Phase IV Properties at 200 MHz , All Depths



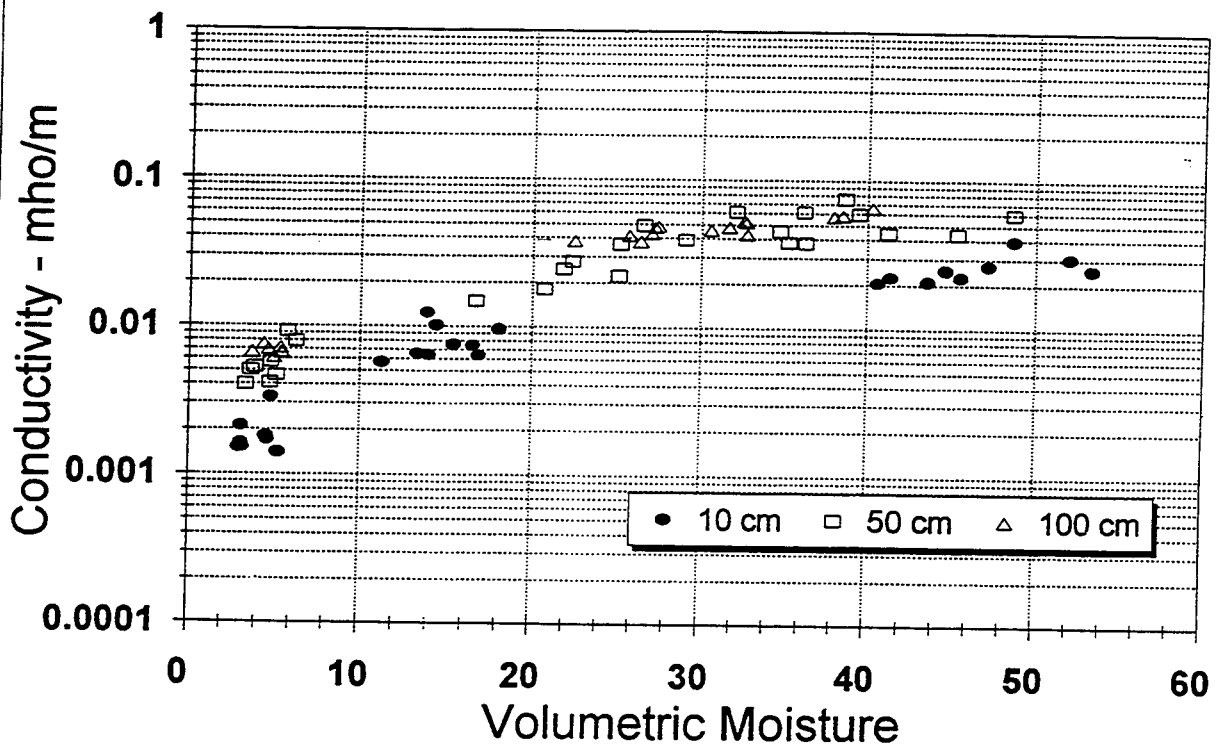
JPG , Phase IV , 40 Acre Test Site Properties at 200 MHz by Depth

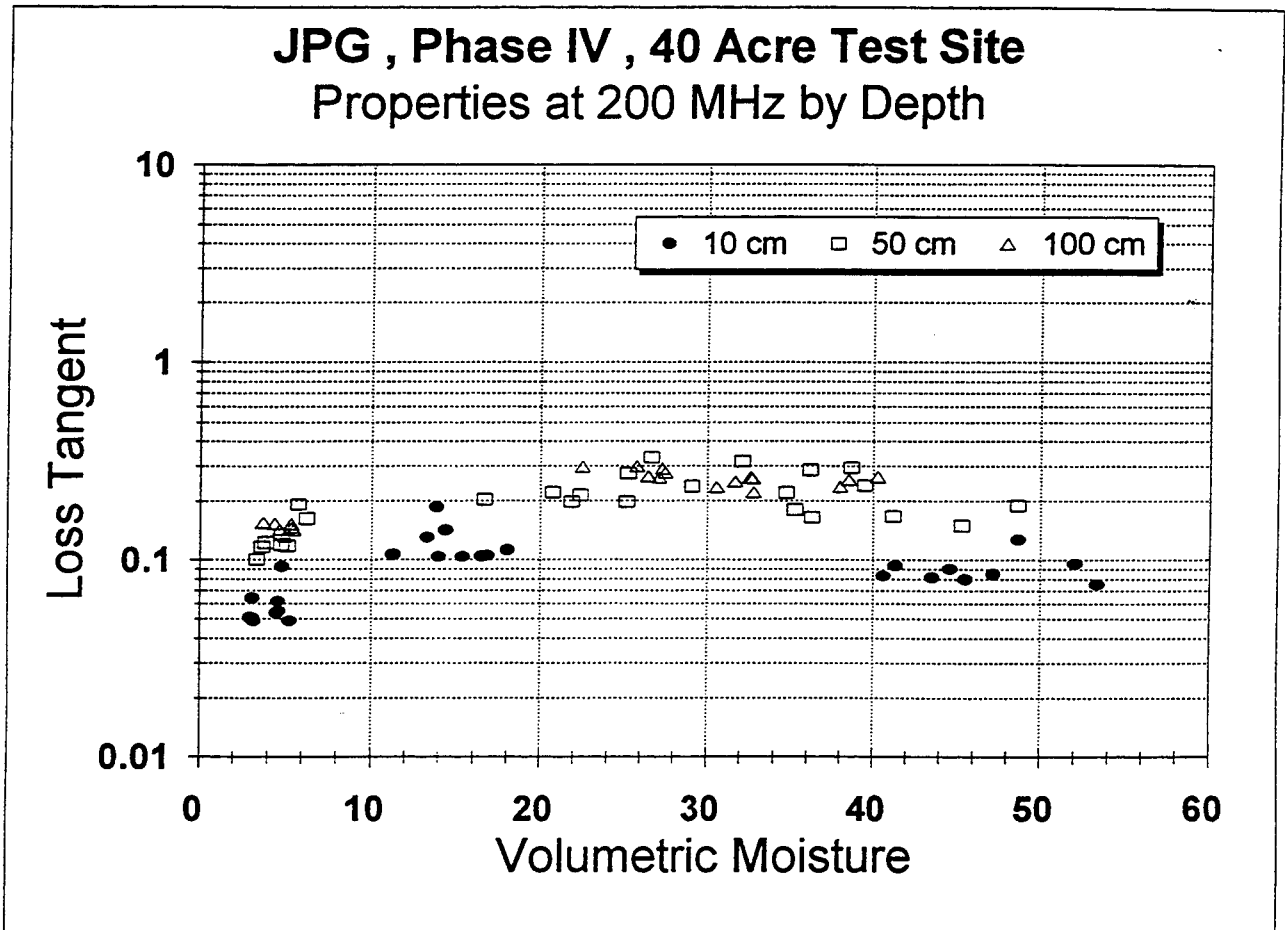


JPG , Phase IV , 40 Acre Test Site Properties at 200 MHz by Depth

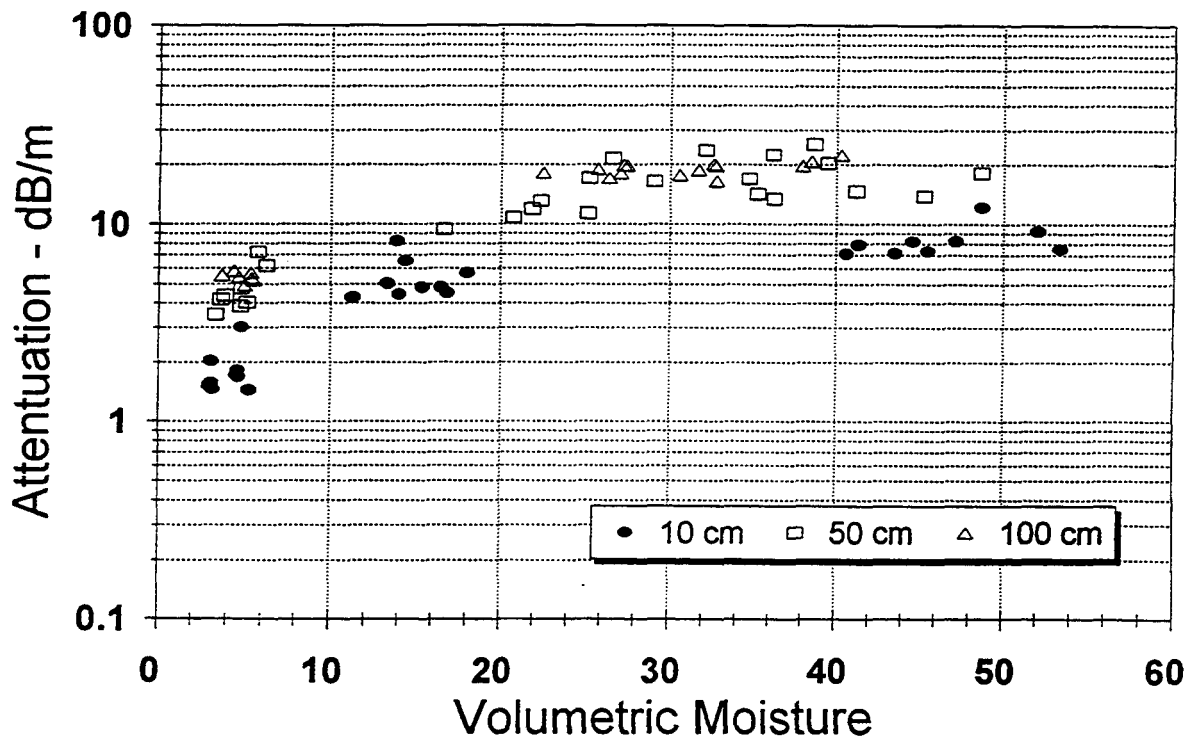


JPG , Phase IV , 40 Acre Test Site Properties at 200 MHz by Depth

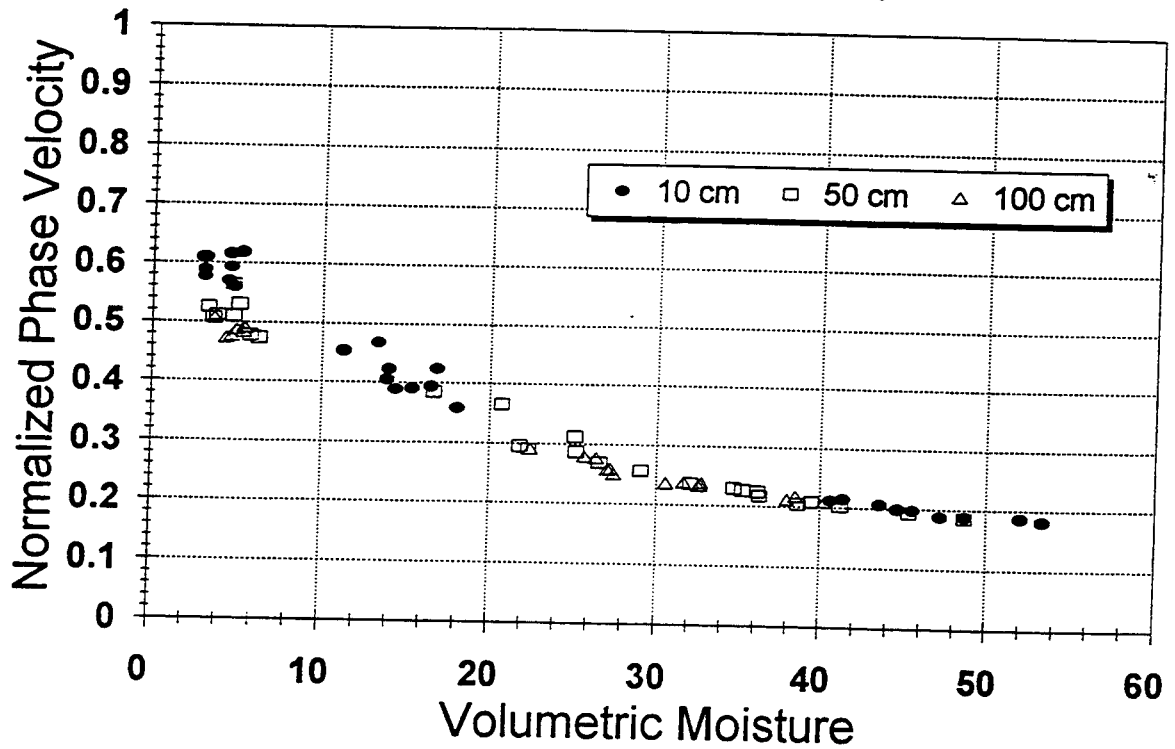




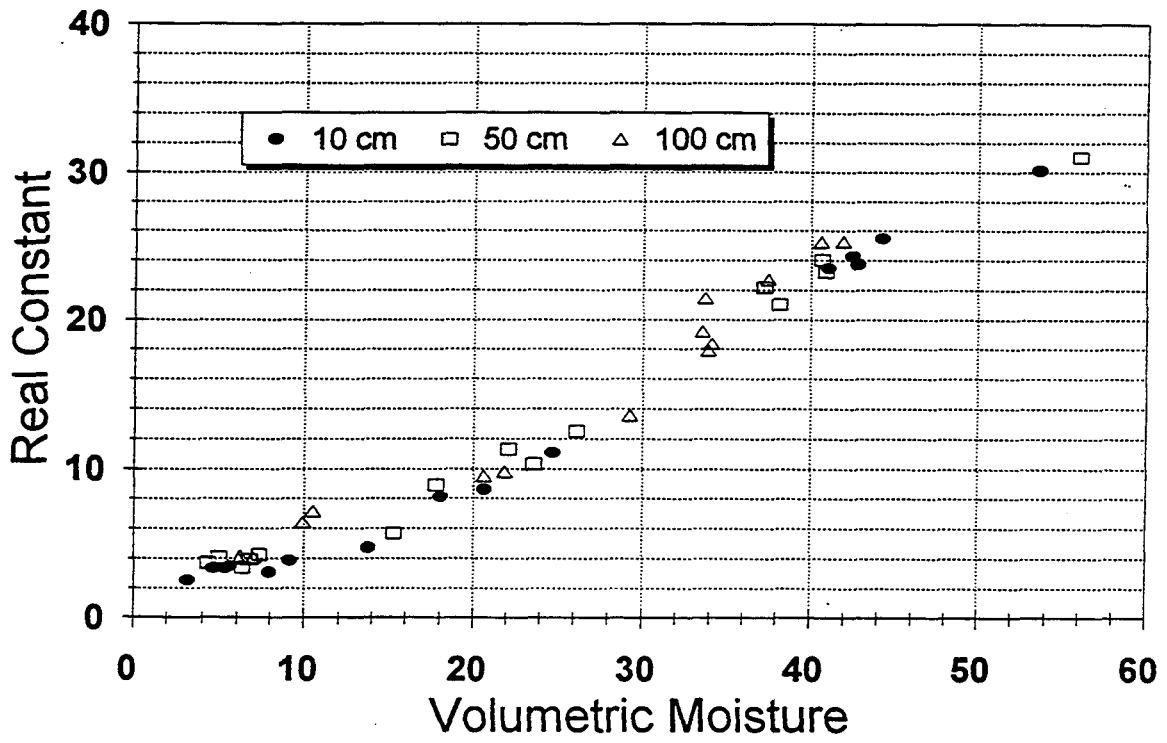
JPG , Phase IV , 40 Acre Test Site Properties at 200 MHz by Depth



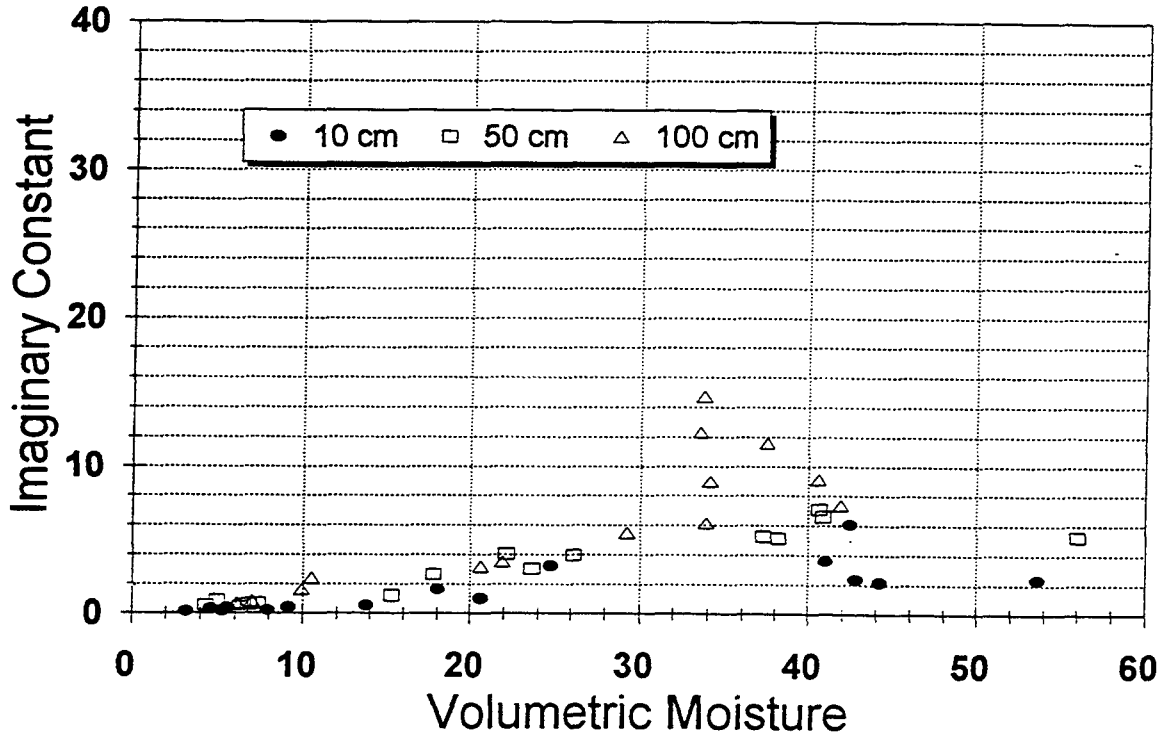
JPG , Phase IV , 40 Acre Test Site Properties at 200 MHz by Depth



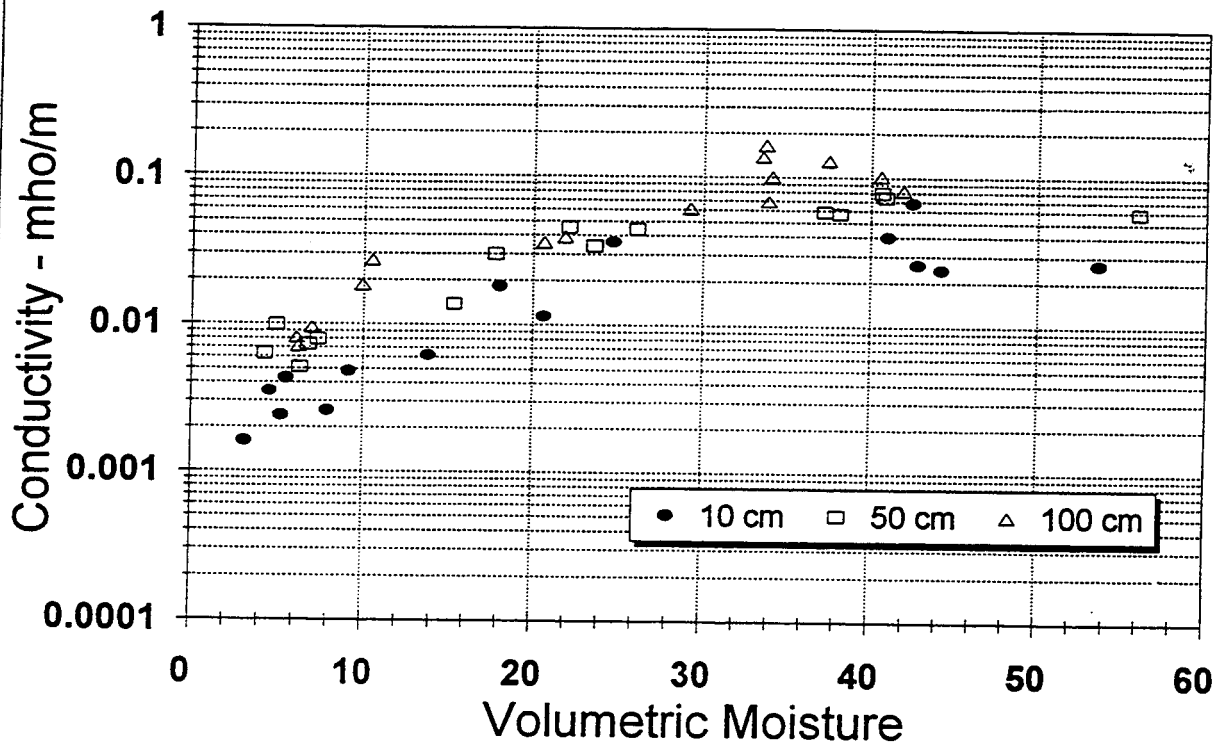
JPG , Phase IV , 80 Acre Test Site Properties at 200 MHz by Depth



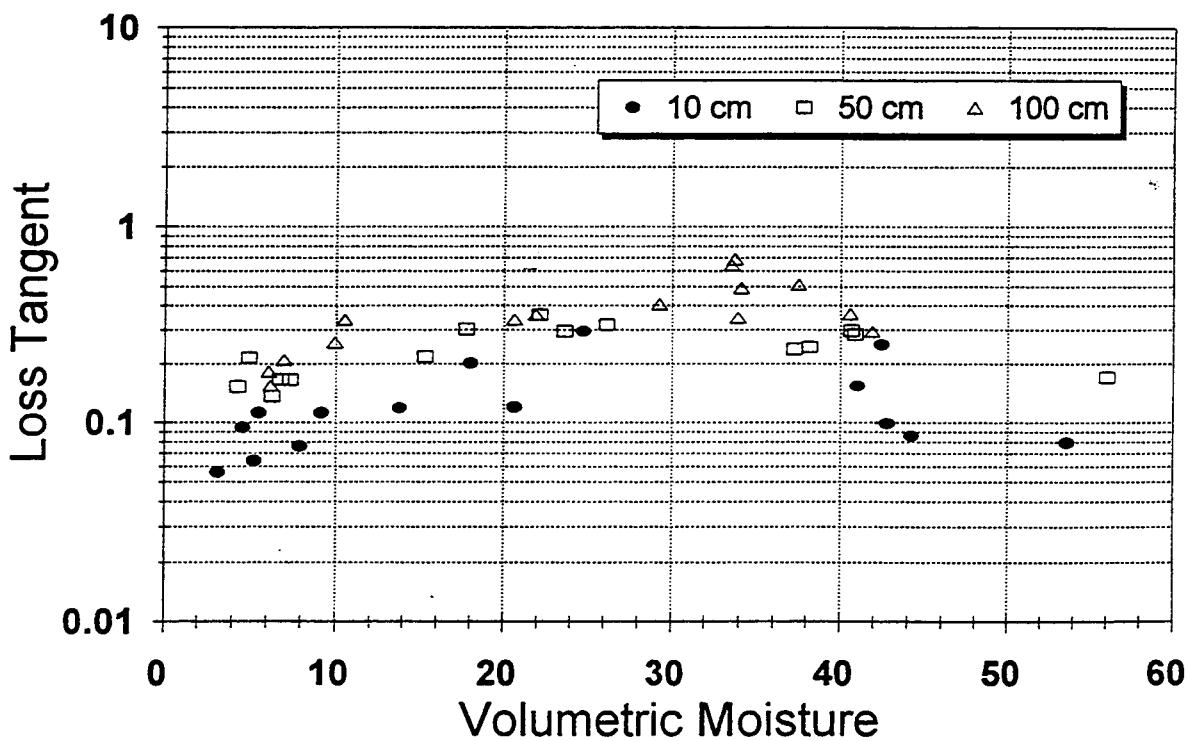
JPG , Phase IV , 80 Acre Test Site Properties at 200 MHz by Depth



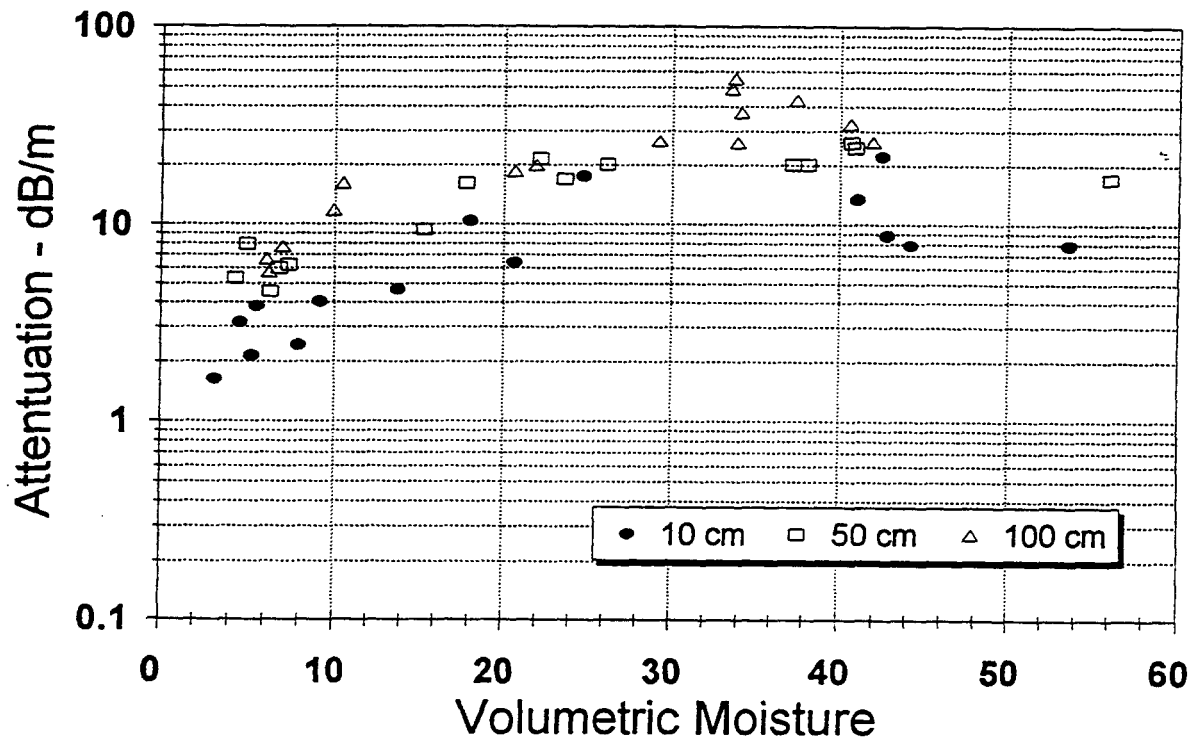
JPG , Phase IV , 80 Acre Test Site Properties at 200 MHz by Depth



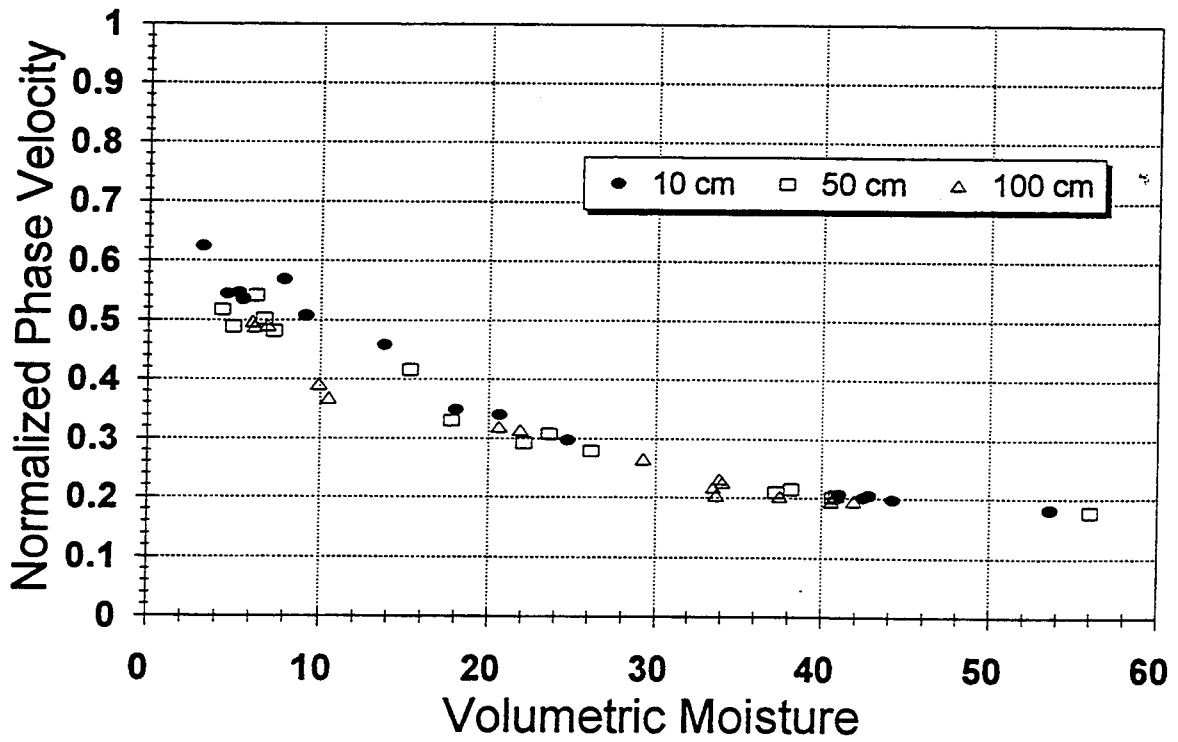
JPG , Phase IV , 80 Acre Test Site Properties at 200 MHz by Depth



JPG , Phase IV , 80 Acre Test Site Properties at 200 MHz by Depth



JPG , Phase IV , 80 Acre Test Site Properties at 200 MHz by Depth



JPG , Phase IV , 40 Acre Site , 495 MHz

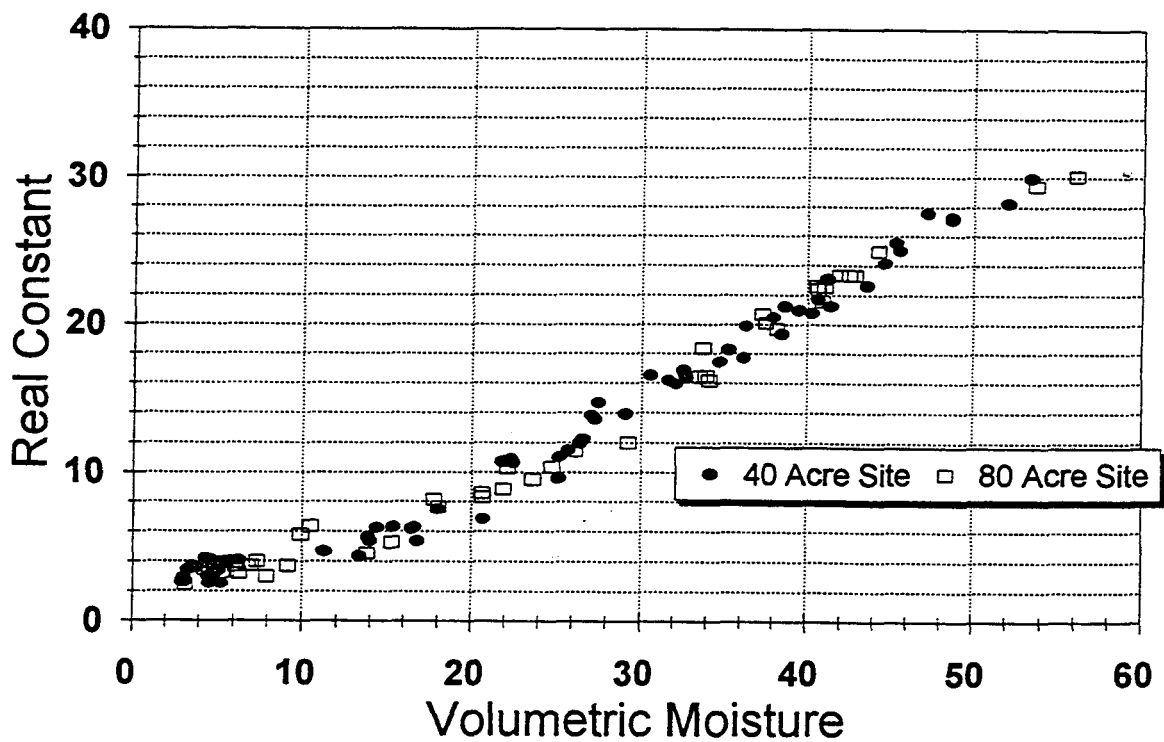
Sample	Vol Moist (%)	Dry Dens (g/cc)	Re(eps) (rel)	Im(eps) (rel)	Cond (mho/m)	Loss Tan	Attn (dB/m)	Ph Vel (rel)
JPG_40_C1_0.1	11.31	1.197	4.67	0.35	0.0096	0.075	7.29	0.463
JPG_40_C1_0.1_D	3.17	1.197	2.63	0.11	0.0030	0.041	2.98	0.616
JPG_40_C1_0.1_W	47.20	1.197	27.57	1.86	0.0511	0.067	15.90	0.190
JPG_40_C1_0.5	25.21	1.401	11.06	1.86	0.0511	0.168	25.07	0.300
JPG_40_C1_0.5_D	4.81	1.401	3.59	0.38	0.0105	0.106	9.01	0.527
JPG_40_C1_0.5_W	39.52	1.401	20.98	3.18	0.0875	0.152	31.17	0.218
JPG_40_C1_1.0	26.42	1.512	11.96	1.90	0.0524	0.159	24.69	0.288
JPG_40_C1_1.0_D	5.50	1.512	3.91	0.41	0.0112	0.104	9.25	0.505
JPG_40_C1_1.0_W	38.01	1.512	20.50	3.01	0.0830	0.147	29.89	0.220
JPG_40_C7_0.1	18.06	1.421	7.54	0.56	0.0155	0.075	9.22	0.364
JPG_40_C7_0.1_D	4.55	1.421	3.00	0.13	0.0035	0.043	3.35	0.578
JPG_40_C7_0.1_W	40.69	1.421	21.69	1.44	0.0397	0.067	13.94	0.215
JPG_40_C7_0.5	29.10	1.547	13.94	2.05	0.0563	0.147	24.61	0.267
JPG_40_C7_0.5_D	3.88	1.547	3.58	0.33	0.0090	0.092	7.79	0.528
JPG_40_C7_0.5_W	34.76	1.547	17.47	2.42	0.0666	0.139	26.02	0.239
JPG_40_C7_1.0	27.08	1.634	13.81	2.12	0.0583	0.153	25.58	0.268
JPG_40_C7_1.0_D	5.00	1.634	3.94	0.39	0.0108	0.100	8.92	0.503
JPG_40_C7_1.0_W	31.70	1.634	16.21	2.48	0.0682	0.153	27.62	0.248
JPG_40_C13_0.1	14.39	1.359	6.28	0.57	0.0157	0.091	10.21	0.399
JPG_40_C13_0.1_D	3.13	1.359	2.92	0.15	0.0041	0.051	3.92	0.586
JPG_40_C13_0.1_W	41.40	1.359	21.25	1.57	0.0432	0.074	15.33	0.217
JPG_40_C13_0.5	16.64	1.377	6.28	0.76	0.0209	0.121	13.62	0.398
JPG_40_C13_0.5_W	45.31	1.377	25.55	2.61	0.0720	0.102	23.26	0.198
JPG_40_C13_1.0	22.51	1.524	10.64	1.88	0.0518	0.177	25.88	0.305
JPG_40_C13_1.0_D	3.70	1.524	3.62	0.40	0.0111	0.111	9.49	0.525
JPG_40_C13_1.0_W	32.73	1.524	16.51	2.64	0.0727	0.160	29.19	0.245
JPG_40_G1_0.1	16.84	1.126	5.38	0.40	0.0111	0.075	7.82	0.431
JPG_40_G1_0.1_D	5.28	1.126	2.55	0.12	0.0032	0.046	3.31	0.627
JPG_40_G1_0.1_W	53.37	1.126	29.96	2.36	0.0649	0.079	19.37	0.183
JPG_40_G1_0.5	25.14	1.440	9.62	1.17	0.0322	0.122	16.95	0.322
JPG_40_G1_0.5_D	5.14	1.440	3.36	0.30	0.0082	0.089	7.32	0.545
JPG_40_G1_0.5_W	41.22	1.440	23.09	2.47	0.0681	0.107	23.14	0.208
JPG_40_G1_1.0	30.59	1.621	16.56	2.36	0.0651	0.143	26.10	0.245
JPG_40_G1_1.0_D	4.69	1.621	4.11	0.45	0.0124	0.110	9.99	0.493
JPG_40_G1_1.0_W	32.80	1.621	16.34	2.26	0.0621	0.138	25.07	0.247
JPG_40_G7_0.1	15.35	1.339	6.34	0.44	0.0121	0.070	7.88	0.397
JPG_40_G7_0.1_D	3.13	1.339	2.82	0.12	0.0034	0.044	3.30	0.595
JPG_40_G7_0.1_W	45.54	1.339	25.02	1.58	0.0435	0.063	14.21	0.200
JPG_40_G7_0.5	21.87	1.494	10.72	1.28	0.0354	0.120	17.63	0.305
JPG_40_G7_0.5_D	3.32	1.494	3.44	0.27	0.0073	0.077	6.45	0.539
JPG_40_G7_0.5_W	36.30	1.494	19.91	2.14	0.0589	0.108	21.56	0.224
JPG_40_G7_1.0	27.28	1.599	13.59	2.35	0.0646	0.173	28.58	0.270
JPG_40_G7_1.0_D	5.38	1.599	3.99	0.45	0.0124	0.113	10.17	0.500
JPG_40_G7_1.0_W	38.51	1.599	19.37	3.05	0.0839	0.157	31.08	0.227
JPG_40_G13_0.1	13.96	1.271	5.40	0.38	0.0106	0.071	7.43	0.430
JPG_40_G13_0.1_D	3.01	1.271	2.64	0.11	0.0031	0.042	3.08	0.615
JPG_40_G13_0.1_W	44.65	1.271	24.17	1.57	0.0433	0.065	14.40	0.203
JPG_40_G13_0.5	22.39	1.560	10.91	1.42	0.0390	0.130	19.26	0.302
JPG_40_G13_0.5_D	3.63	1.560	3.67	0.32	0.0088	0.087	7.52	0.521
JPG_40_G13_0.5_W	35.29	1.560	18.31	2.11	0.0582	0.116	22.21	0.233

JPG_40_G13_1.0	27.49	1.673	14.67	2.41	0.0663	0.164	28.23	0.260
JPG_40_G13_1.0_D	4.39	1.673	4.16	0.47	0.0129	0.113	10.32	0.489
JPG_40_G13_1.0_W	32.60	1.673	16.90	2.72	0.0747	0.161	29.64	0.242
JPG_40_K1_0.1	16.49	1.217	6.20	0.45	0.0125	0.073	8.22	0.401
JPG_40_K1_0.1_D	4.65	1.217	2.76	0.13	0.0035	0.045	3.39	0.602
JPG_40_K1_0.1_W	43.58	1.217	22.65	1.38	0.0379	0.061	13.02	0.210
JPG_40_K1_0.5	32.12	1.467	15.95	3.18	0.0875	0.199	35.65	0.249
JPG_40_K1_0.5_D	6.28	1.467	4.09	0.51	0.0142	0.126	11.43	0.493
JPG_40_K1_0.5_W	36.18	1.467	17.74	3.35	0.0922	0.189	35.64	0.236
JPG_40_K7_0.1	13.85	1.228	5.65	0.68	0.0188	0.121	12.94	0.420
JPG_40_K7_0.1_D	4.83	1.228	3.05	0.20	0.0056	0.067	5.24	0.573
JPG_40_K7_0.1_W	48.72	1.228	27.26	2.65	0.0729	0.097	22.82	0.191
JPG_40_K7_0.5	26.59	1.447	12.22	2.46	0.0677	0.201	31.50	0.285
JPG_40_K7_0.5_D	5.78	1.447	4.01	0.56	0.0153	0.139	12.47	0.498
JPG_40_K7_0.5_W	38.67	1.447	21.24	3.88	0.1067	0.183	37.71	0.216
JPG_40_K13_0.1	13.33	1.185	4.36	0.37	0.0102	0.085	8.01	0.479
JPG_40_K13_0.1_D	4.62	1.185	2.54	0.13	0.0035	0.051	3.63	0.627
JPG_40_K13_0.1_W	52.08	1.185	28.23	2.10	0.0578	0.074	17.78	0.188
JPG_40_K13_0.5	20.73	1.266	6.86	0.92	0.0253	0.134	15.78	0.381
JPG_40_K13_0.5_D	4.76	1.266	2.95	0.25	0.0069	0.085	6.60	0.582
JPG_40_K13_0.5_W	48.65	1.266	27.14	3.29	0.0906	0.121	28.39	0.192
JPG_40_K13_1.0	25.73	1.516	11.47	2.06	0.0566	0.179	27.24	0.294
JPG_40_K13_1.0_D	5.42	1.516	3.87	0.41	0.0114	0.107	9.48	0.508
JPG_40_K13_1.0_W	40.31	1.516	20.79	3.42	0.0941	0.164	33.65	0.219

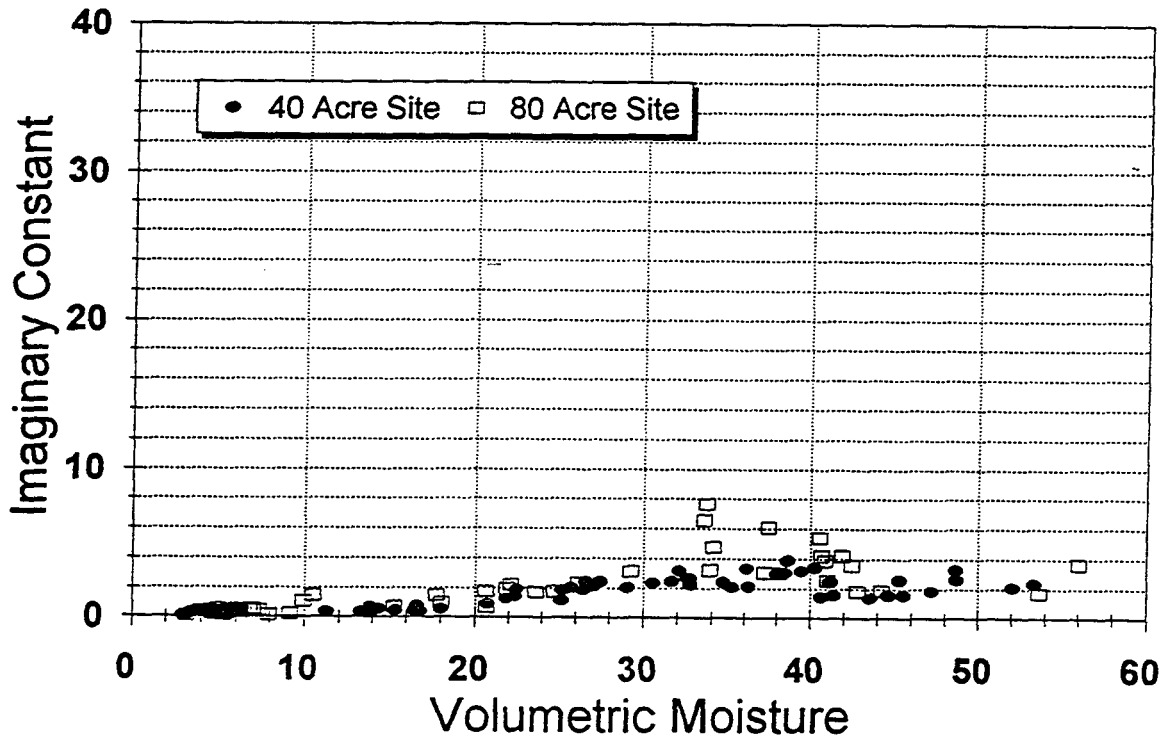
JPG , Phase IV , 80 Acre Site , 495 MHz

Sample	Vol Moist (%)	Dry Dens (g/cc)	Re(eps) (rel)	Im(eps) (rel)	Cond (mho/m)	Loss Tan	Attn (dB/m)	Ph Vel (rel)
JPG_80_A13_0.1	24.76	1.300	10.37	1.79	0.0493	0.173	24.94	0.309
JPG_80_A13_0.1_D	5.56	1.300	3.30	0.27	0.0075	0.083	6.77	0.550
JPG_80_A13_0.1_W	42.47	1.300	23.35	3.58	0.0986	0.153	33.28	0.206
JPG_80_A13_0.5	22.13	1.380	10.27	2.25	0.0619	0.219	31.40	0.310
JPG_80_A13_0.5_D	4.97	1.380	3.79	0.58	0.0159	0.153	13.35	0.512
JPG_80_A13_0.5_W	40.67	1.380	22.41	4.23	0.1163	0.189	40.02	0.210
JPG_80_A13_1.0	29.27	1.378	12.02	3.15	0.0867	0.262	40.56	0.286
JPG_80_A13_1.0_D	6.98	1.378	3.73	0.58	0.0161	0.157	13.59	0.517
JPG_80_A13_1.0_W	40.59	1.378	22.60	5.47	0.1505	0.242	51.40	0.209
JPG_80_H1_0.1	20.66	1.344	8.33	0.69	0.0190	0.083	10.76	0.346
JPG_80_H1_0.1_D	5.31	1.344	3.26	0.17	0.0048	0.054	4.35	0.554
JPG_80_H1_0.1_W	42.81	1.344	23.34	1.82	0.0501	0.078	16.94	0.207
JPG_80_H1_0.5	26.11	1.434	11.43	2.35	0.0646	0.205	31.10	0.294
JPG_80_H1_0.5_D	7.36	1.434	4.01	0.49	0.0136	0.123	11.09	0.499
JPG_80_H1_0.5_W	40.90	1.434	21.57	3.89	0.1071	0.181	37.59	0.215
JPG_80_H1_1.0	37.50	1.684	20.10	6.11	0.1682	0.304	60.70	0.221
JPG_80_H1_1.0_D	9.93	1.684	5.80	1.07	0.0295	0.185	19.93	0.414
JPG_80_H1_1.0_W	34.10	1.684	16.21	4.80	0.1321	0.296	53.08	0.246
JPG_80_H13_0.1	13.78	1.232	4.56	0.37	0.0100	0.080	7.69	0.468
JPG_80_H13_0.1_D	7.95	1.232	2.98	0.17	0.0047	0.057	4.43	0.579
JPG_80_H13_0.1_W	44.20	1.232	24.97	1.89	0.0522	0.076	17.06	0.200
JPG_80_H13_0.5	23.61	1.405	9.51	1.73	0.0477	0.182	25.18	0.323
JPG_80_H13_0.5_D	6.81	1.405	3.70	0.45	0.0123	0.121	10.46	0.519
JPG_80_H13_0.5_W	38.19	1.405	19.71	3.07	0.0845	0.156	31.05	0.225
JPG_80_H13_1.0	33.72	1.693	18.38	7.67	0.2111	0.417	78.92	0.229
JPG_80_H13_1.0_D	10.49	1.693	6.36	1.48	0.0407	0.233	26.24	0.394
JPG_80_H13_1.0_W	33.54	1.693	16.45	6.58	0.1811	0.400	71.67	0.242
JPG_80_H26_0.1	18.06	1.370	7.66	0.99	0.0274	0.130	16.15	0.361
JPG_80_H26_0.1_D	4.62	1.370	3.23	0.24	0.0066	0.074	5.99	0.556
JPG_80_H26_0.1_W	41.04	1.370	22.54	2.57	0.0707	0.114	24.32	0.210
JPG_80_H26_0.5	15.31	1.218	5.31	0.73	0.0202	0.138	14.31	0.433
JPG_80_H26_0.5_D	6.32	1.218	3.19	0.32	0.0089	0.101	8.14	0.559
JPG_80_H26_0.5_W	56.01	1.218	30.07	3.68	0.1012	0.122	30.14	0.182
JPG_80_H26_1.0	21.91	1.440	8.87	1.95	0.0535	0.219	29.24	0.334
JPG_80_H26_1.0_D	6.11	1.440	3.69	0.50	0.0138	0.136	11.70	0.520
JPG_80_H26_1.0_W	33.92	1.440	16.48	3.23	0.0890	0.196	35.69	0.245
JPG_80_O13_0.1	9.17	1.143	3.70	0.25	0.0069	0.067	5.83	0.519
JPG_80_O13_0.1_D	3.20	1.143	2.47	0.10	0.0028	0.041	2.93	0.636
JPG_80_O13_0.1_W	53.65	1.143	29.42	1.73	0.0475	0.059	14.33	0.184
JPG_80_O13_0.5	17.78	1.452	8.18	1.51	0.0416	0.185	23.67	0.348
JPG_80_O13_0.5_D	4.31	1.452	3.47	0.40	0.0109	0.114	9.57	0.536
JPG_80_O13_0.5_W	37.29	1.452	20.71	3.09	0.0850	0.149	30.45	0.219
JPG_80_O13_1.0	20.61	1.404	8.62	1.78	0.0490	0.207	27.15	0.339
JPG_80_O13_1.0_D	6.26	1.404	3.91	0.46	0.0128	0.119	10.54	0.505
JPG_80_O13_1.0_W	41.90	1.404	23.35	4.24	0.1168	0.182	39.39	0.206

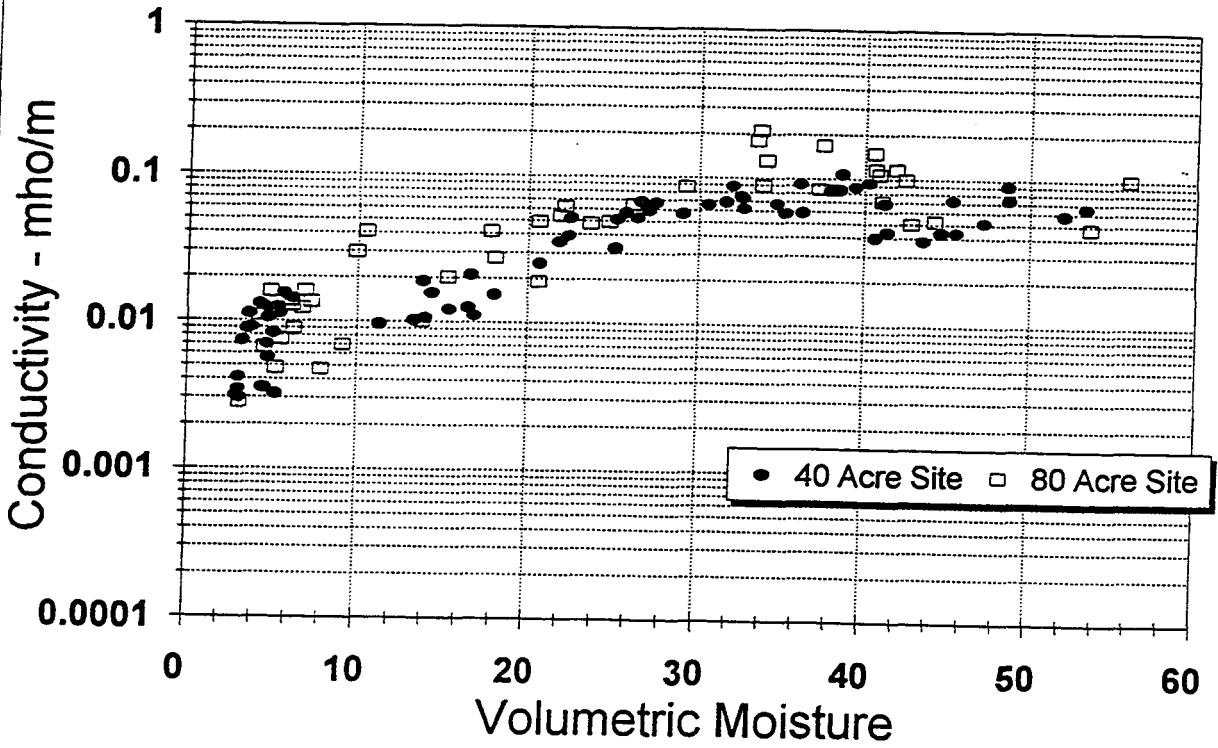
Jefferson Proving Ground , Phase IV Properties at 495 MHz , All Depths



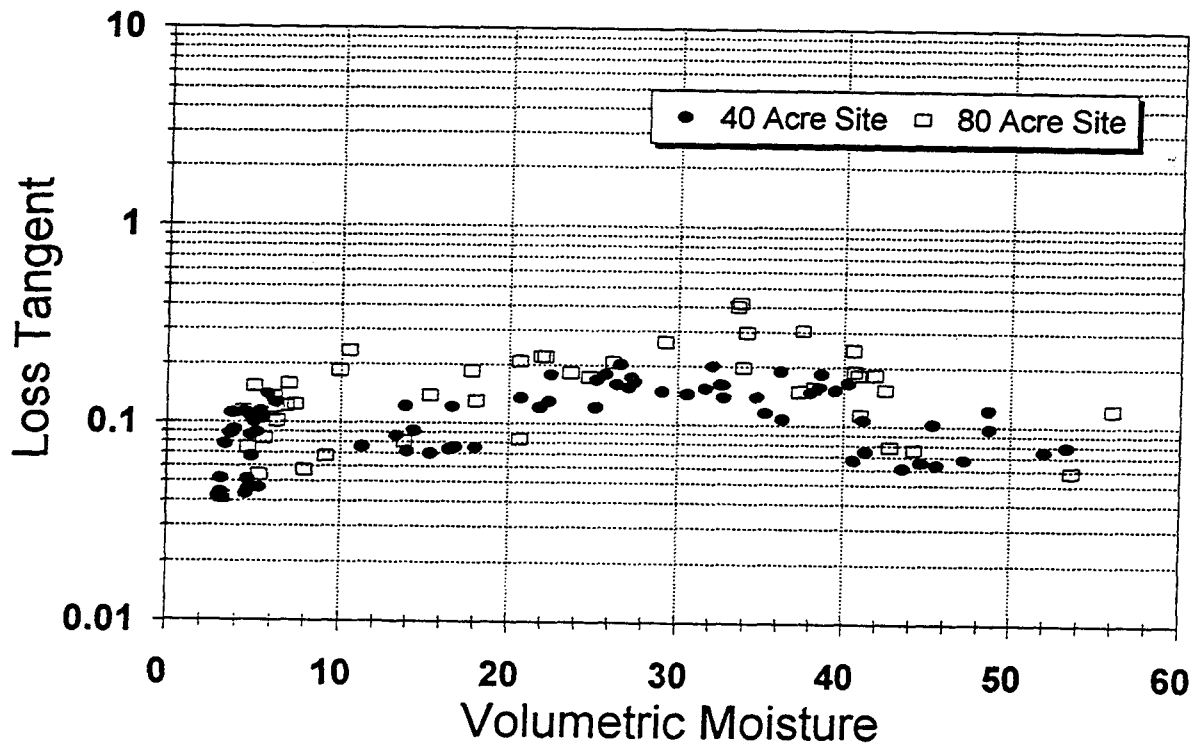
Jefferson Proving Ground , Phase IV Properties at 495 MHz , All Depths



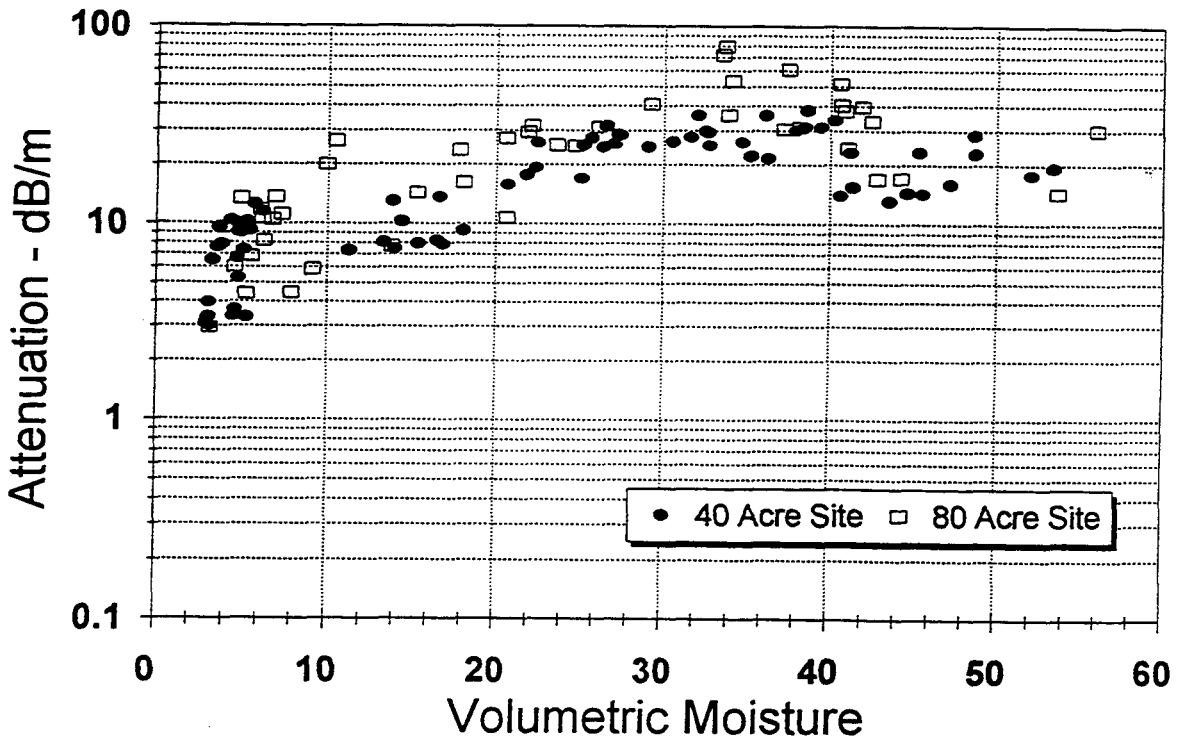
Jefferson Proving Ground , Phase IV Properties at 495 MHz , All Depths



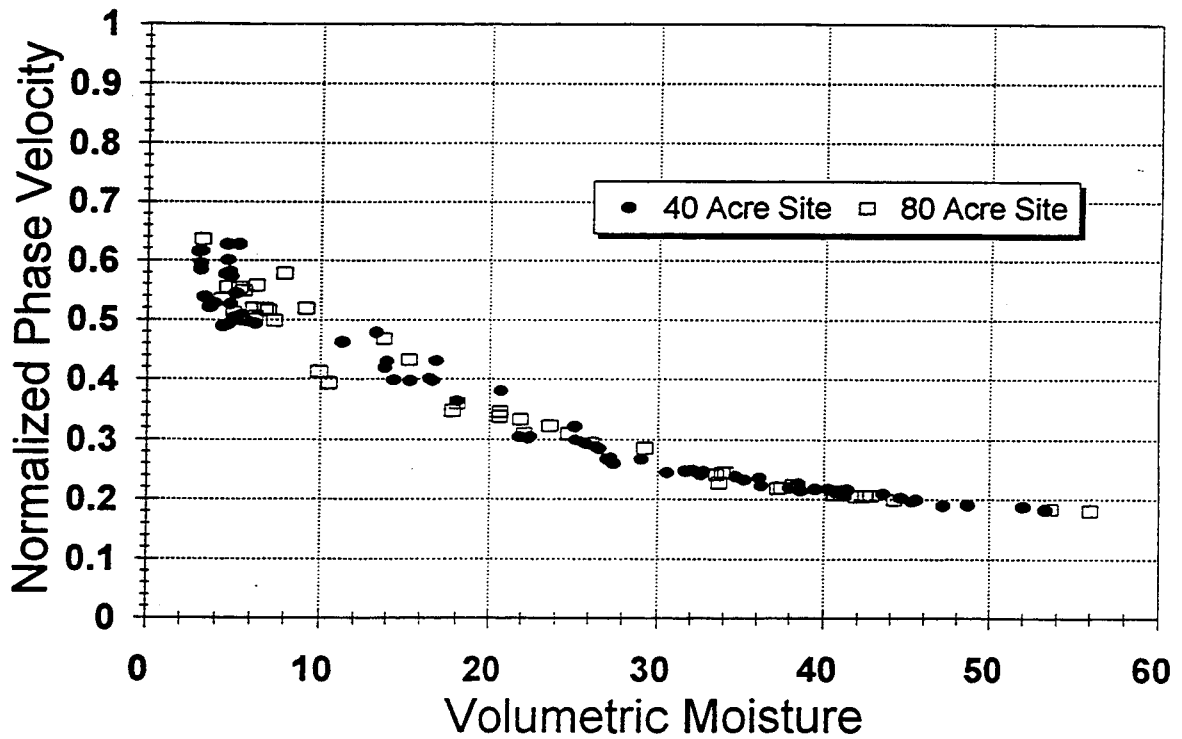
Jefferson Proving Ground , Phase IV Properties at 495 MHz , All Depths



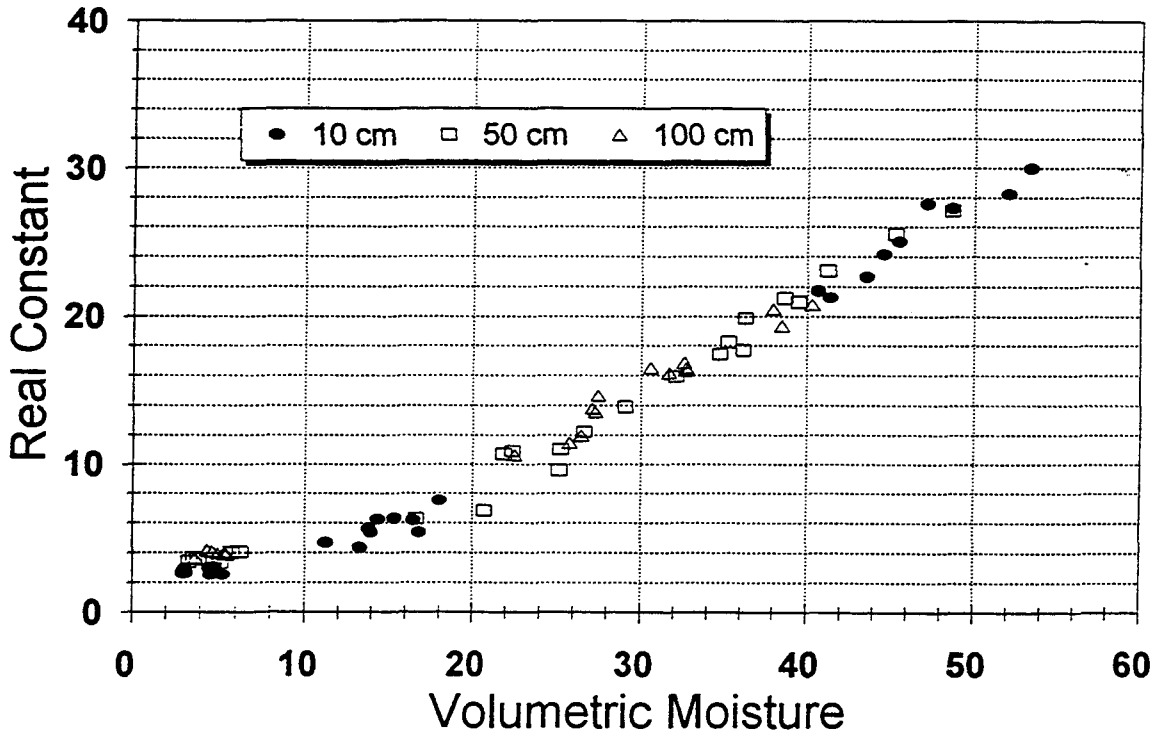
Jefferson Proving Ground , Phase IV Properties at 495 MHz , All Depths



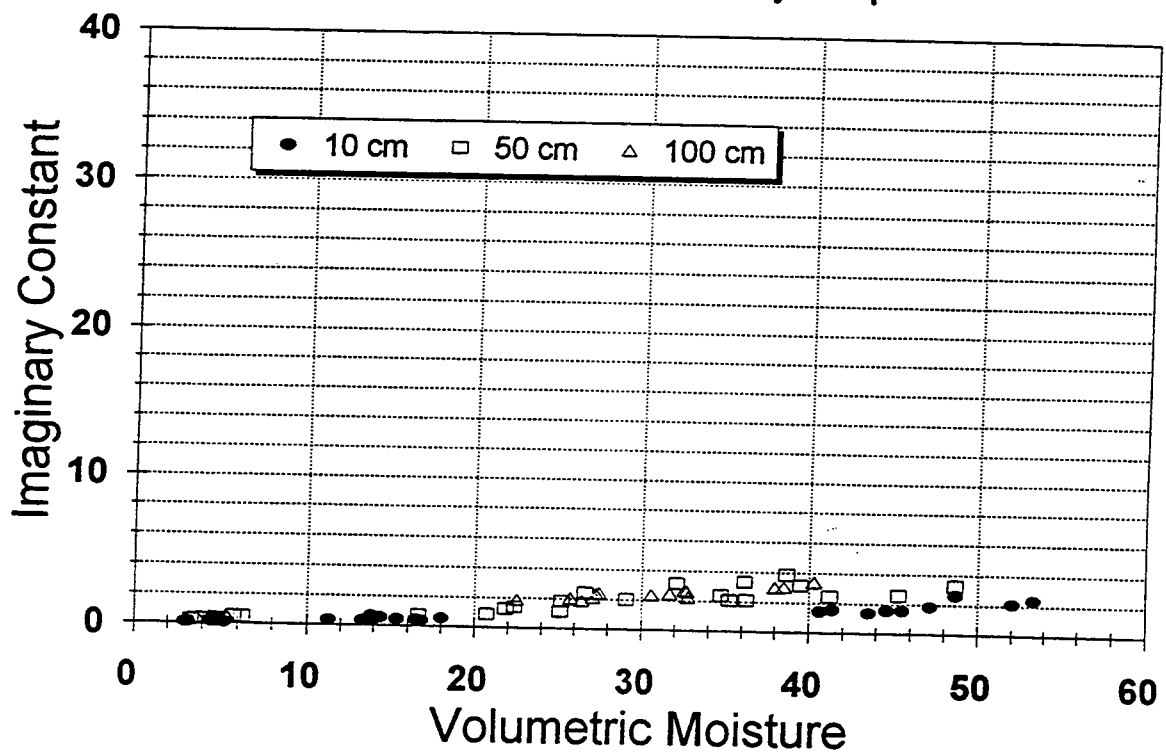
Jefferson Proving Ground , Phase IV Properties at 495 MHz , All Depths



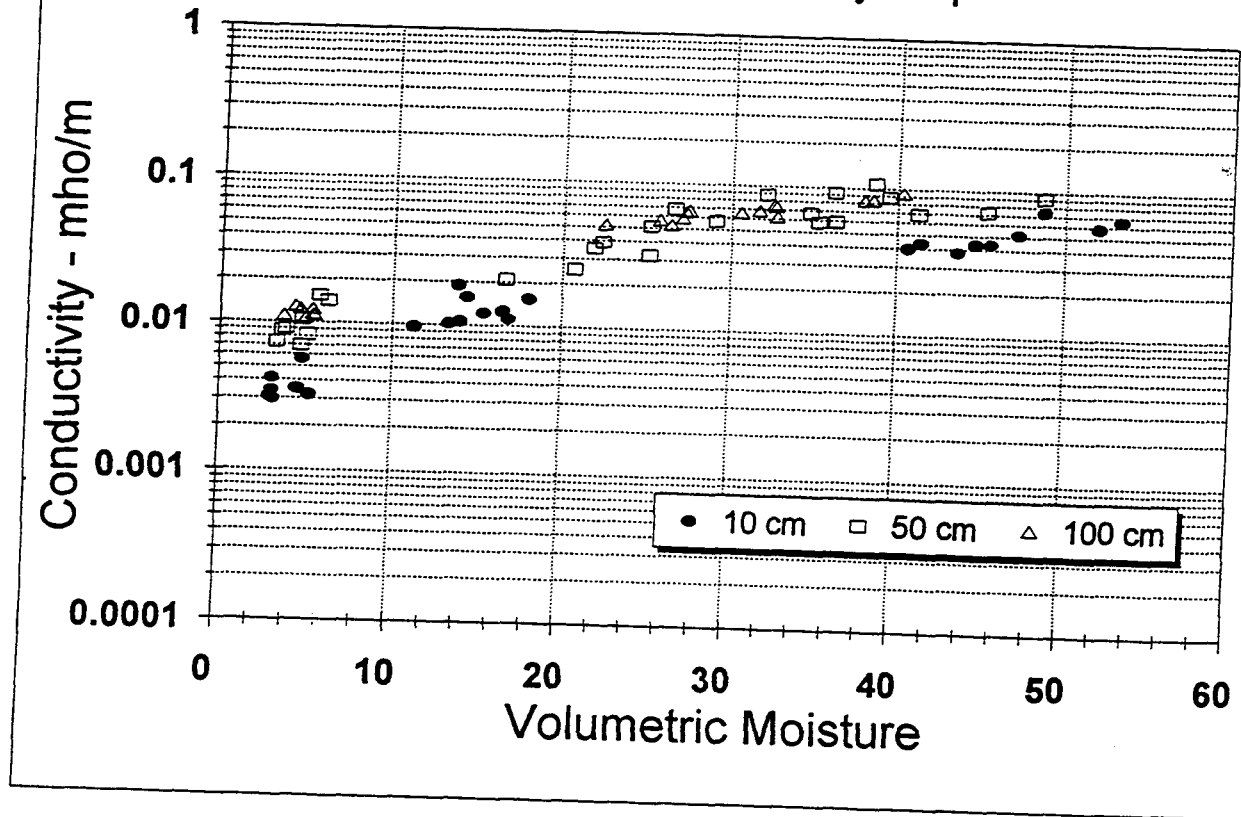
JPG , Phase IV , 40 Acre Test Site Properties at 495 MHz by Depth



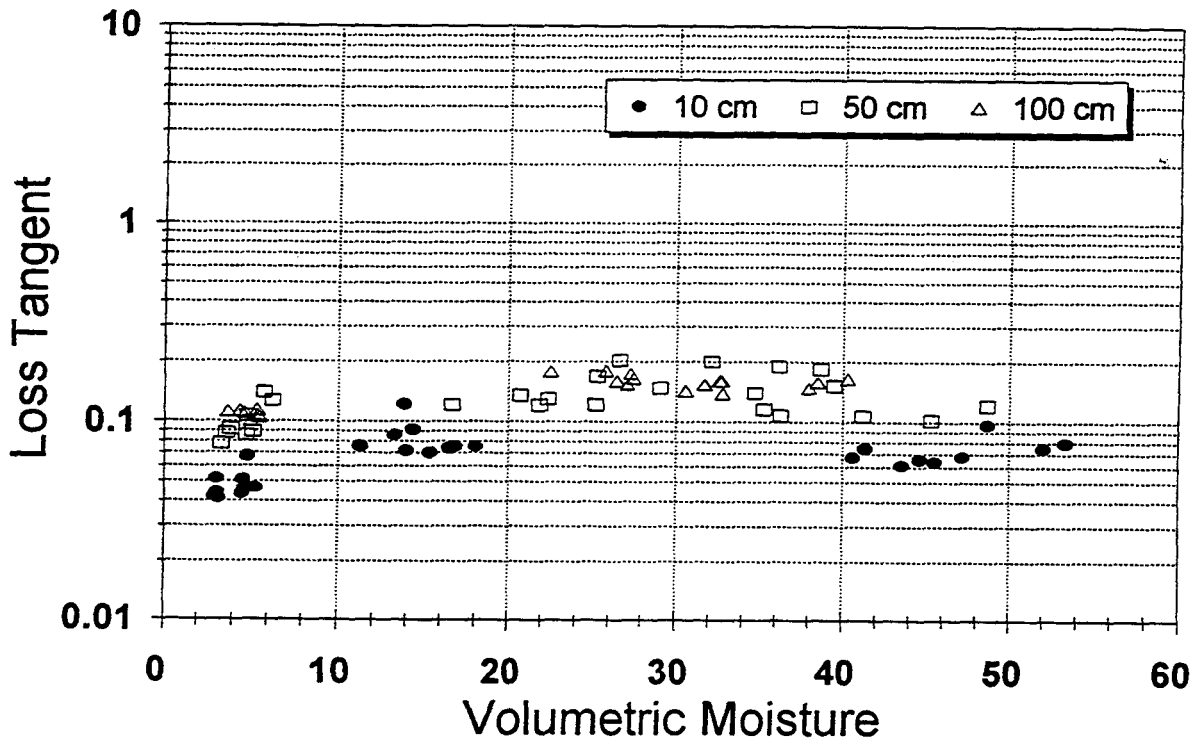
JPG , Phase IV , 40 Acre Test Site Properties at 495 MHz by Depth



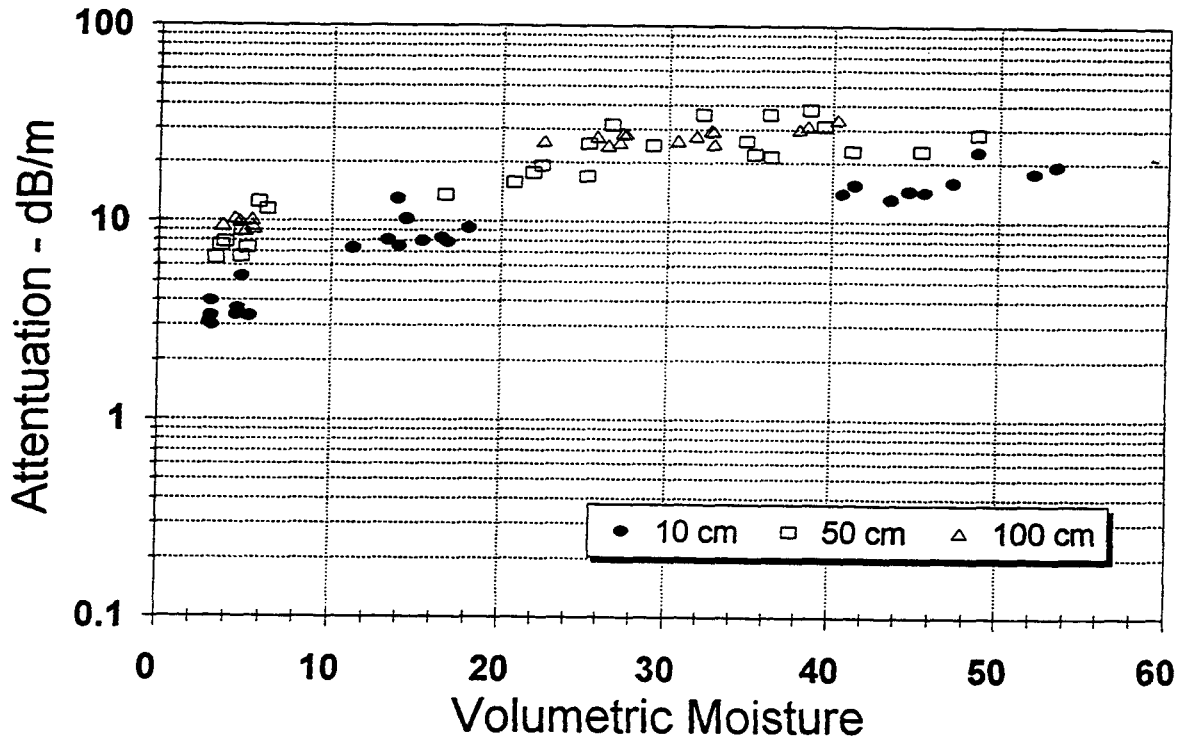
JPG , Phase IV , 40 Acre Test Site Properties at 495 MHz by Depth



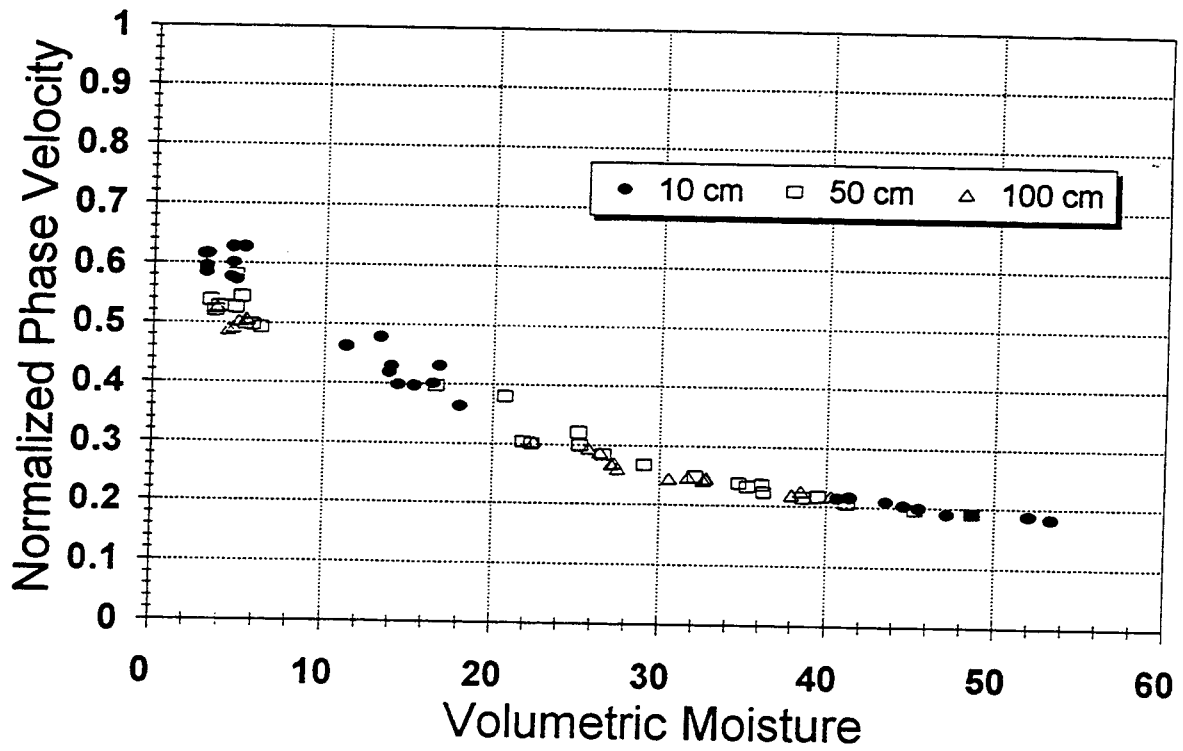
JPG , Phase IV , 40 Acre Test Site Properties at 495 MHz by Depth



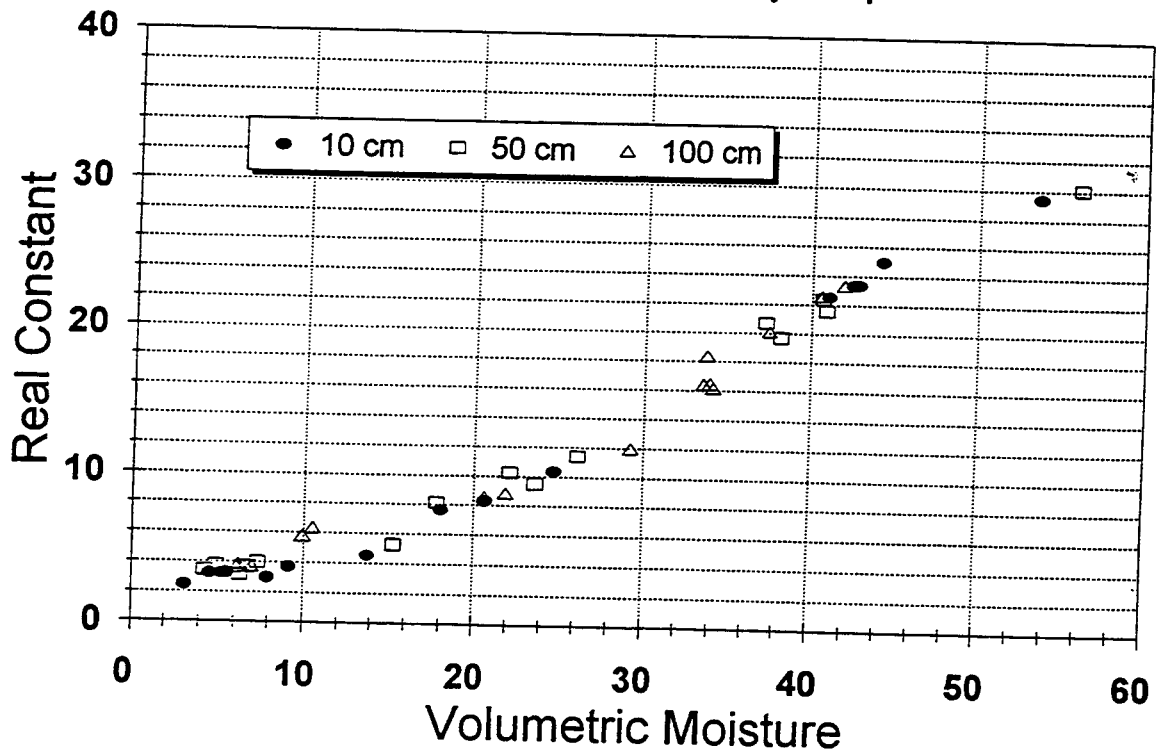
JPG , Phase IV , 40 Acre Test Site Properties at 495 MHz by Depth



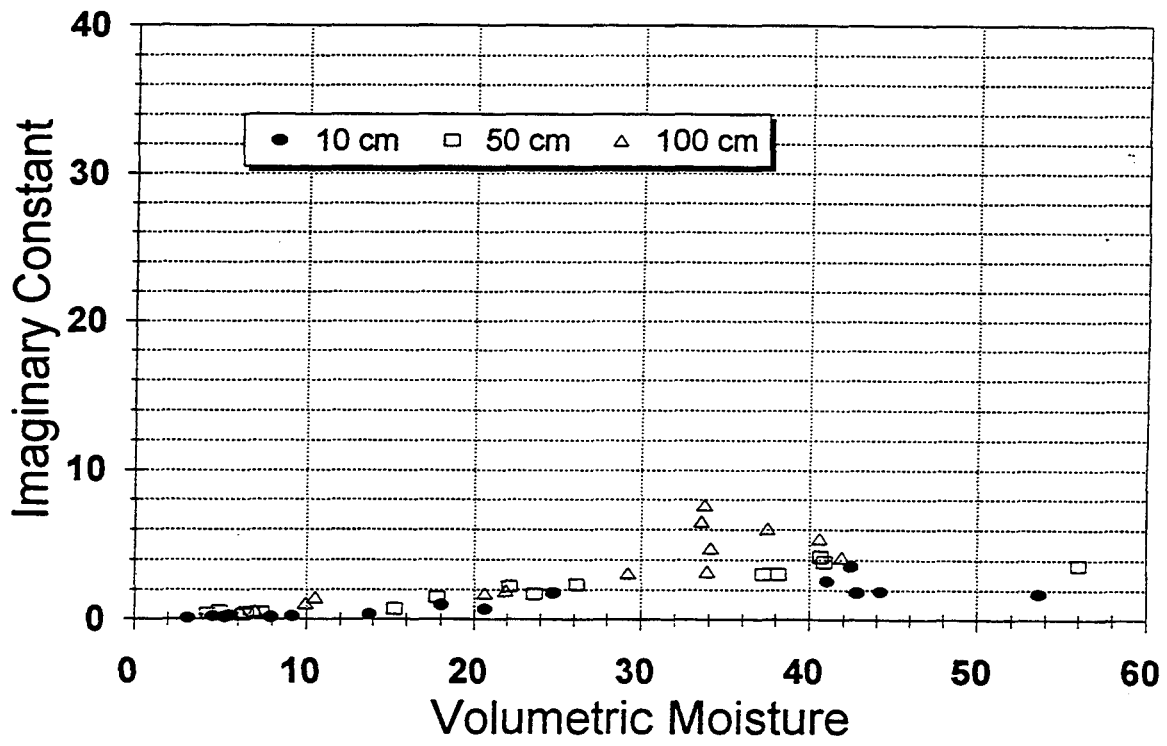
JPG , Phase IV , 40 Acre Test Site Properties at 495 MHz by Depth



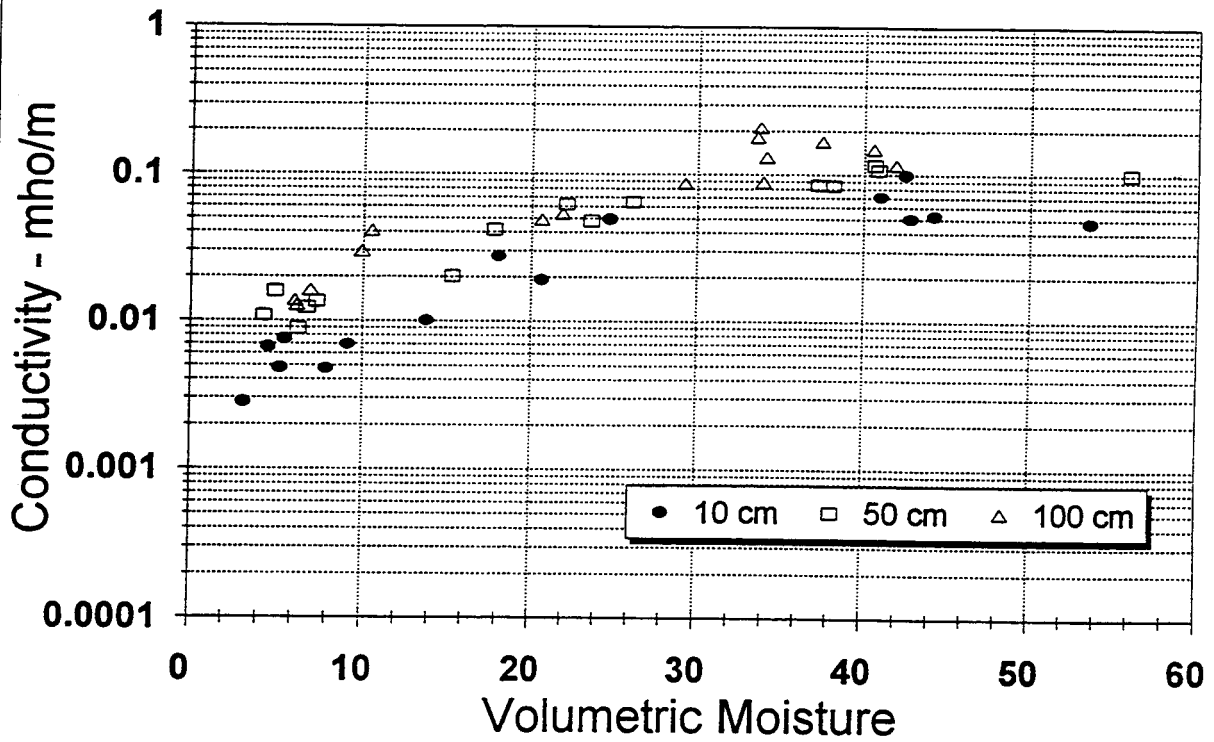
JPG , Phase IV , 80 Acre Test Site Properties at 495 MHz by Depth



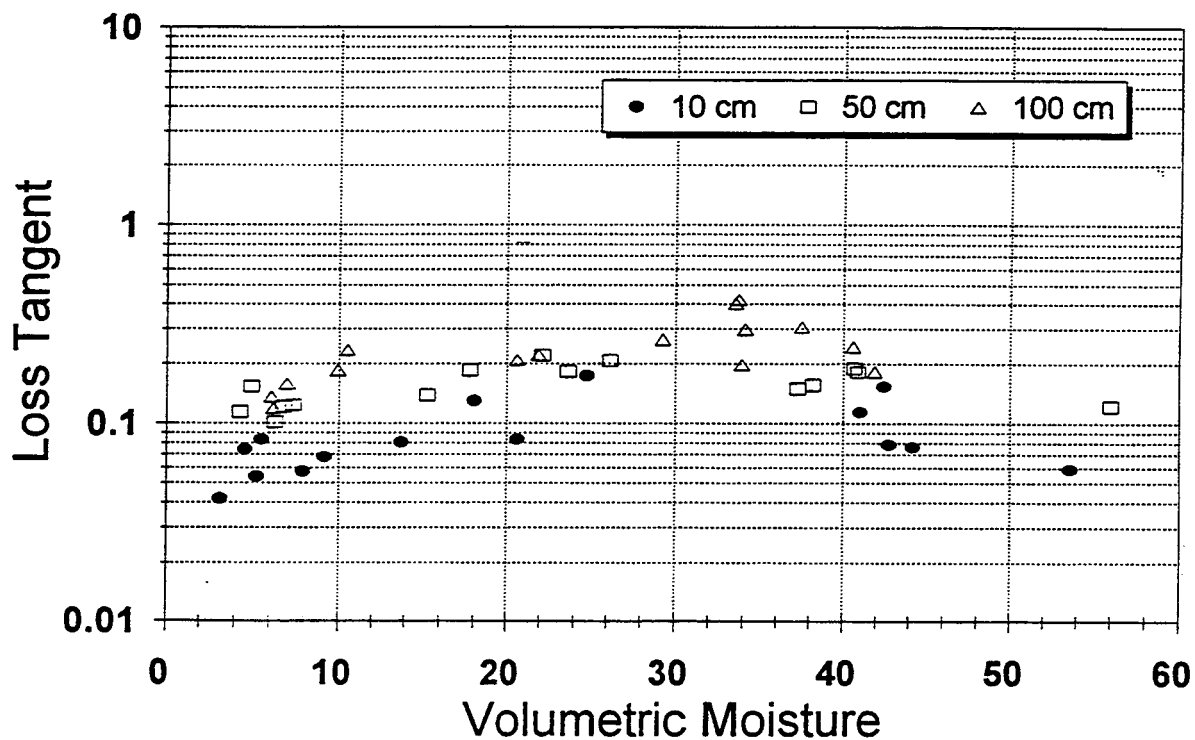
JPG , Phase IV , 80 Acre Test Site Properties at 495 MHz by Depth



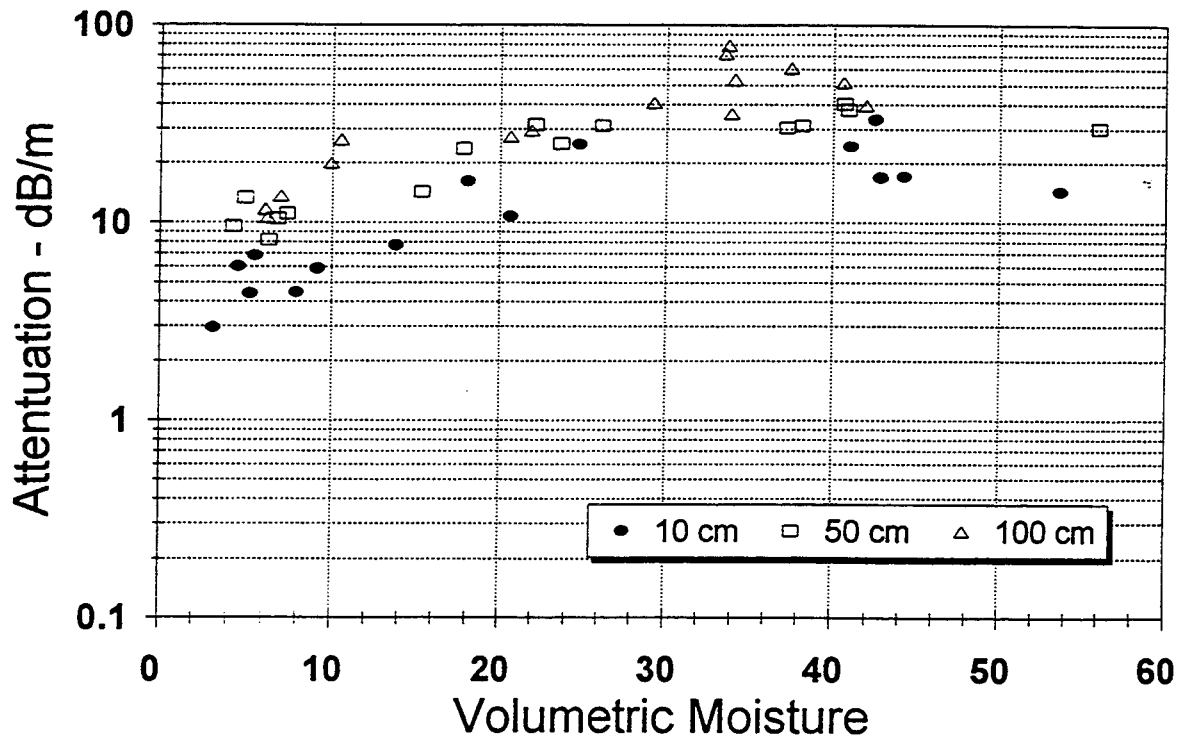
JPG , Phase IV , 80 Acre Test Site Properties at 495 MHz by Depth



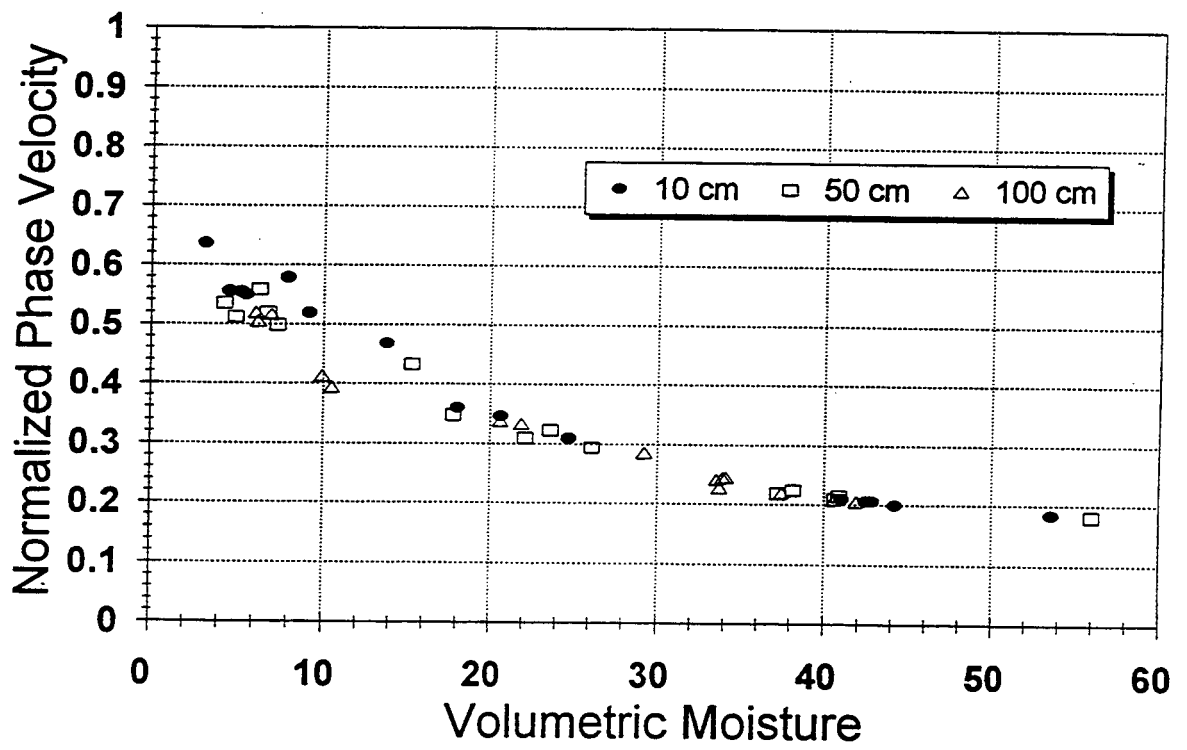
JPG , Phase IV , 80 Acre Test Site Properties at 495 MHz by Depth



JPG , Phase IV , 80 Acre Test Site Properties at 495 MHz by Depth



JPG , Phase IV , 80 Acre Test Site Properties at 495 MHz by Depth



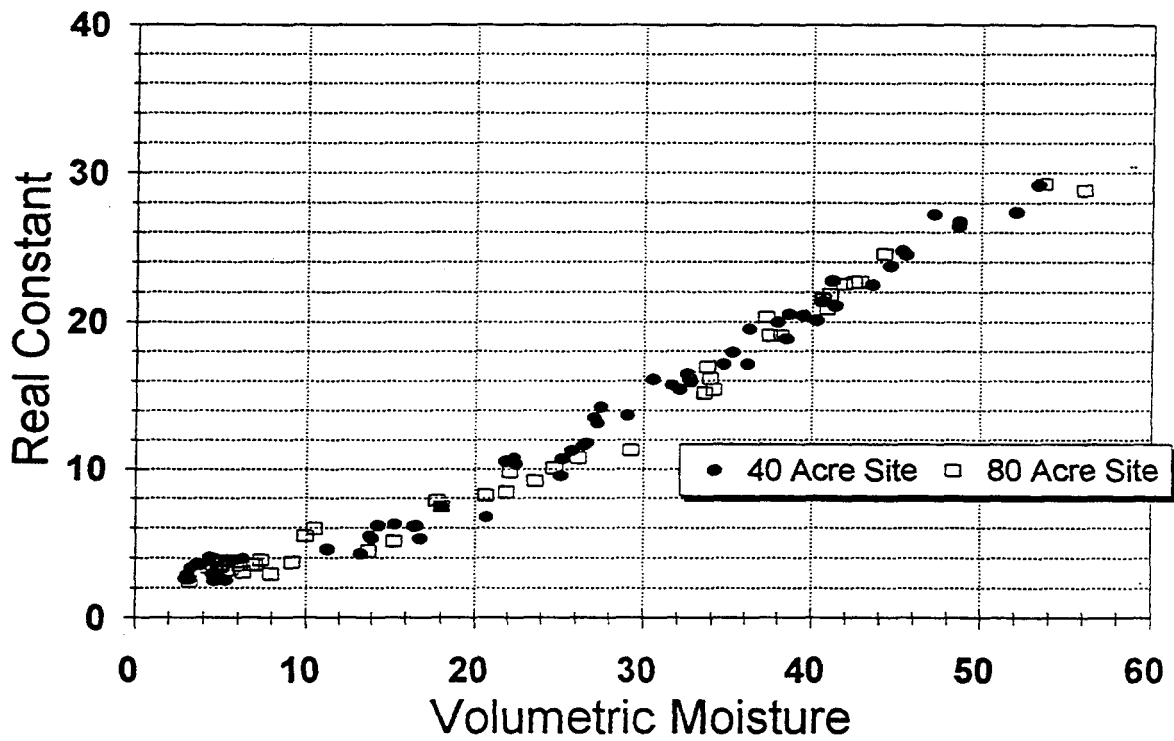
Sample	Vol Moist (%)	Dry Dens (g/cc)	Re(eps) (rel)	Im(eps) (rel)	Cond (mho/m)	Loss Tan	Attn (dB/m)	Ph Vel (rel)
JPG_40_C1_0.1	11.31	1.197	4.57	0.29	0.0163	0.063	12.50	0.468
JPG_40_C1_0.1_D	3.17	1.197	2.59	0.10	0.0058	0.039	5.86	0.621
JPG_40_C1_0.1_W	47.20	1.197	27.19	2.08	0.1173	0.076	36.76	0.192
JPG_40_C1_0.5	25.21	1.401	10.71	1.31	0.0741	0.123	36.97	0.305
JPG_40_C1_0.5_D	4.81	1.401	3.47	0.30	0.0169	0.087	14.86	0.537
JPG_40_C1_0.5_W	39.52	1.401	20.43	2.46	0.1389	0.121	50.19	0.221
JPG_40_C1_1.0	26.42	1.512	11.62	1.37	0.0775	0.118	37.11	0.293
JPG_40_C1_1.0_D	5.50	1.512	3.78	0.33	0.0186	0.087	15.60	0.514
JPG_40_C1_1.0_W	38.01	1.512	19.97	2.32	0.1308	0.116	47.80	0.223
JPG_40_C7_0.1	18.06	1.421	7.43	0.50	0.0284	0.068	17.04	0.367
JPG_40_C7_0.1_D	4.55	1.421	2.97	0.13	0.0071	0.042	6.71	0.580
JPG_40_C7_0.1_W	40.69	1.421	21.36	1.53	0.0861	0.071	30.44	0.216
JPG_40_C7_0.5	29.10	1.547	13.68	1.51	0.0852	0.110	37.65	0.270
JPG_40_C7_0.5_D	3.88	1.547	3.50	0.26	0.0147	0.074	12.84	0.534
JPG_40_C7_0.5_W	34.76	1.547	17.15	1.94	0.1098	0.113	43.28	0.241
JPG_40_C7_1.0	27.08	1.634	13.52	1.55	0.0873	0.115	38.79	0.272
JPG_40_C7_1.0_D	5.00	1.634	3.84	0.32	0.0182	0.084	15.17	0.510
JPG_40_C7_1.0_W	31.70	1.634	15.70	1.87	0.1054	0.119	43.43	0.252
JPG_40_C13_0.1	14.39	1.359	6.16	0.46	0.0261	0.075	17.20	0.403
JPG_40_C13_0.1_D	3.13	1.359	2.87	0.12	0.0069	0.042	6.63	0.590
JPG_40_C13_0.1_W	41.40	1.359	21.09	1.51	0.0851	0.072	30.28	0.218
JPG_40_C13_0.5	16.64	1.377	6.15	0.55	0.0310	0.089	20.45	0.403
JPG_40_C13_0.5_W	45.31	1.377	24.76	2.37	0.1338	0.096	43.95	0.201
JPG_40_C13_1.0	22.51	1.524	10.33	1.30	0.0734	0.126	37.27	0.311
JPG_40_C13_1.0_D	3.70	1.524	3.52	0.30	0.0167	0.084	14.53	0.532
JPG_40_C13_1.0_W	32.73	1.524	16.10	1.95	0.1101	0.121	44.81	0.249
JPG_40_G1_0.1	16.84	1.126	5.31	0.35	0.0200	0.067	14.21	0.434
JPG_40_G1_0.1_D	5.28	1.126	2.51	0.11	0.0060	0.042	6.14	0.631
JPG_40_G1_0.1_W	53.37	1.126	29.16	2.29	0.1294	0.079	39.17	0.185
JPG_40_G1_0.5	25.14	1.440	9.54	0.94	0.0530	0.098	28.03	0.323
JPG_40_G1_0.5_D	5.14	1.440	3.28	0.27	0.0152	0.082	13.72	0.552
JPG_40_G1_0.5_W	41.22	1.440	22.72	2.32	0.1307	0.102	44.79	0.210
JPG_40_G1_1.0	30.59	1.621	16.12	1.81	0.1020	0.112	41.49	0.249
JPG_40_G1_1.0_D	4.69	1.621	3.96	0.36	0.0203	0.091	16.67	0.502
JPG_40_G1_1.0_W	32.80	1.621	15.92	1.75	0.0986	0.110	40.38	0.250
JPG_40_G7_0.1	15.35	1.339	6.25	0.40	0.0226	0.064	14.79	0.400
JPG_40_G7_0.1_D	3.13	1.339	2.78	0.10	0.0059	0.038	5.78	0.600
JPG_40_G7_0.1_W	45.54	1.339	24.49	1.81	0.1021	0.074	33.73	0.202
JPG_40_G7_0.5	21.87	1.494	10.51	0.99	0.0559	0.094	28.17	0.308
JPG_40_G7_0.5_D	3.32	1.494	3.37	0.22	0.0123	0.065	10.94	0.545
JPG_40_G7_0.5_W	36.30	1.494	19.53	1.81	0.1024	0.093	37.87	0.226
JPG_40_G7_1.0	27.28	1.599	13.17	1.68	0.0949	0.128	42.71	0.275
JPG_40_G7_1.0_D	5.38	1.599	3.86	0.35	0.0195	0.090	16.26	0.509
JPG_40_G7_1.0_W	38.51	1.599	18.86	2.40	0.1352	0.127	50.83	0.230
JPG_40_G13_0.1	13.96	1.271	5.30	0.33	0.0184	0.062	13.08	0.434
JPG_40_G13_0.1_D	3.01	1.271	2.59	0.12	0.0066	0.045	6.74	0.621
JPG_40_G13_0.1_W	44.65	1.271	23.73	1.75	0.0990	0.074	33.24	0.205
JPG_40_G13_0.5	22.39	1.560	10.73	1.08	0.0607	0.100	30.27	0.305
JPG_40_G13_0.5_D	3.63	1.560	3.58	0.26	0.0147	0.073	12.68	0.528
JPG_40_G13_0.5_W	35.29	1.560	17.94	1.78	0.1003	0.099	38.68	0.236

JPG_40_G13_1.0	27.49	1.673	14.24	1.75	0.0989	0.123	42.80	0.265
JPG_40_G13_1.0_D	4.39	1.673	4.01	0.36	0.0205	0.091	16.74	0.499
JPG_40_G13_1.0_W	32.60	1.673	16.46	2.00	0.1129	0.122	45.42	0.246
JPG_40_K1_0.1	16.49	1.217	6.10	0.41	0.0231	0.067	15.29	0.405
JPG_40_K1_0.1_D	4.65	1.217	2.74	0.12	0.0069	0.045	6.85	0.604
JPG_40_K1_0.1_W	43.58	1.217	22.50	1.67	0.0944	0.074	32.55	0.211
JPG_40_K1_0.5	32.12	1.467	15.42	2.18	0.1230	0.141	51.11	0.254
JPG_40_K1_0.5_D	6.28	1.467	3.95	0.40	0.0225	0.101	18.53	0.503
JPG_40_K1_0.5_W	36.18	1.467	17.13	2.33	0.1318	0.136	51.95	0.241
JPG_40_K7_0.1	13.85	1.228	5.48	0.55	0.0311	0.101	21.73	0.427
JPG_40_K7_0.1_D	4.83	1.228	2.99	0.19	0.0110	0.065	10.39	0.578
JPG_40_K7_0.1_W	48.72	1.228	26.72	2.56	0.1443	0.096	45.62	0.193
JPG_40_K7_0.5	26.59	1.447	11.77	1.68	0.0948	0.143	45.07	0.291
JPG_40_K7_0.5_D	5.78	1.447	3.86	0.41	0.0229	0.105	19.05	0.508
JPG_40_K7_0.5_W	38.67	1.447	20.48	2.87	0.1620	0.140	58.42	0.220
JPG_40_K13_0.1	13.33	1.185	4.27	0.28	0.0161	0.067	12.72	0.484
JPG_40_K13_0.1_D	4.62	1.185	2.49	0.11	0.0062	0.044	6.44	0.633
JPG_40_K13_0.1_W	52.08	1.185	27.36	2.16	0.1219	0.079	38.08	0.191
JPG_40_K13_0.5	20.73	1.266	6.74	0.65	0.0368	0.097	23.17	0.385
JPG_40_K13_0.5_D	4.76	1.266	2.91	0.20	0.0111	0.068	10.68	0.586
JPG_40_K13_0.5_W	48.65	1.266	26.40	2.79	0.1576	0.106	50.10	0.194
JPG_40_K13_1.0	25.73	1.516	11.24	1.44	0.0810	0.128	39.43	0.298
JPG_40_K13_1.0_D	5.42	1.516	3.77	0.32	0.0178	0.084	15.01	0.515
JPG_40_K13_1.0_W	40.31	1.516	20.07	2.75	0.1552	0.137	56.53	0.223

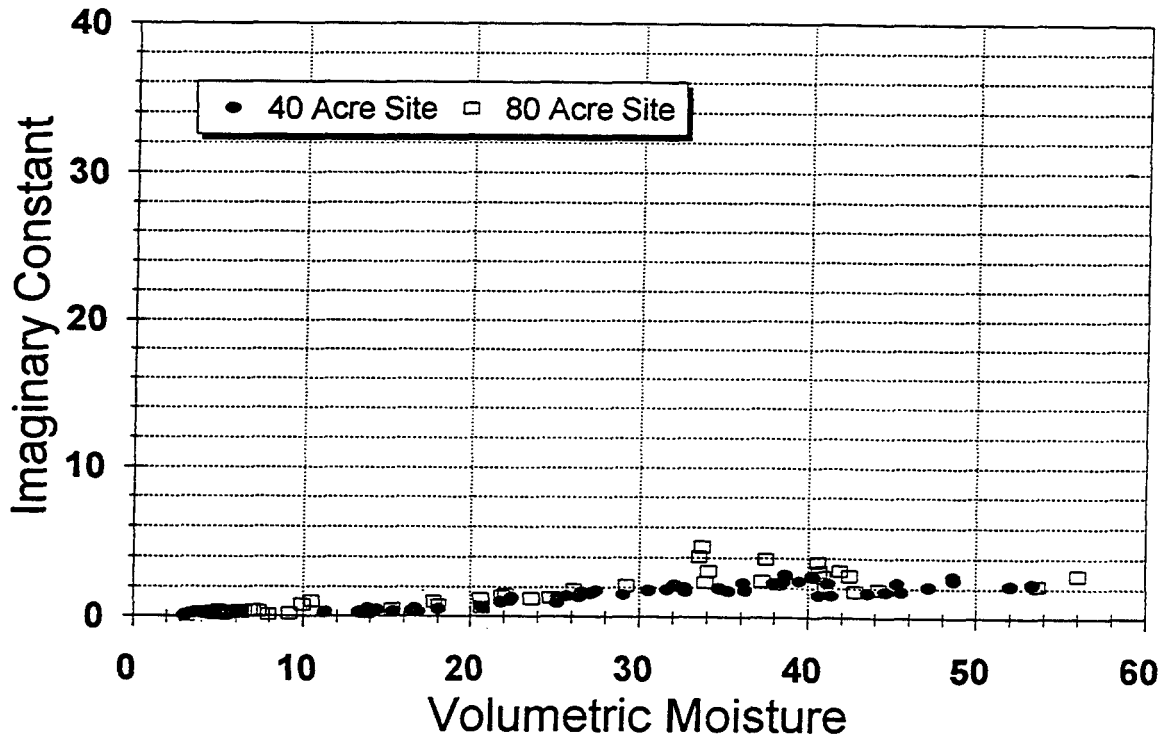
JPG , Phase IV , 80 Acre Site , 1015 MHz

Sample	Vol Moist (%)	Dry Dens (g/cc)	Re(eps) (rel)	Im(eps) (rel)	Cond (mho/m)	Loss Tan	Attn (dB/m)	Ph Vel (rel)
JPG_80_A13_0.1	24.76	1.300	10.07	1.29	0.0729	0.128	37.51	0.315
JPG_80_A13_0.1_D	5.56	1.300	3.23	0.24	0.0134	0.073	12.15	0.556
JPG_80_A13_0.1_W	42.47	1.300	22.64	2.85	0.1610	0.126	55.24	0.210
JPG_80_A13_0.5	22.13	1.380	9.82	1.53	0.0861	0.155	44.81	0.318
JPG_80_A13_0.5_D	4.97	1.380	3.61	0.43	0.0240	0.118	20.65	0.526
JPG_80_A13_0.5_W	40.67	1.380	21.46	3.12	0.1758	0.145	61.93	0.215
JPG_80_A13_1.0	29.27	1.378	11.29	2.15	0.1214	0.191	58.84	0.296
JPG_80_A13_1.0_D	6.98	1.378	3.55	0.41	0.0231	0.115	19.99	0.530
JPG_80_A13_1.0_W	40.59	1.378	21.62	3.73	0.2103	0.172	73.70	0.214
JPG_80_H1_0.1	20.66	1.344	8.21	0.63	0.0357	0.077	20.37	0.349
JPG_80_H1_0.1_D	5.31	1.344	3.21	0.17	0.0096	0.053	8.73	0.558
JPG_80_H1_0.1_W	42.81	1.344	22.69	1.79	0.1009	0.079	34.63	0.210
JPG_80_H1_0.5	26.11	1.434	10.77	1.83	0.1032	0.170	51.27	0.304
JPG_80_H1_0.5_D	7.36	1.434	3.87	0.37	0.0208	0.095	17.31	0.508
JPG_80_H1_0.5_W	40.90	1.434	20.89	2.76	0.1559	0.132	55.68	0.218
JPG_80_H1_1.0	37.50	1.684	19.11	3.96	0.2237	0.207	83.26	0.228
JPG_80_H1_1.0_D	9.93	1.684	5.50	0.79	0.0448	0.145	31.20	0.425
JPG_80_H1_1.0_W	34.10	1.684	15.43	3.14	0.1772	0.203	73.39	0.253
JPG_80_H13_0.1	13.78	1.232	4.47	0.31	0.0174	0.069	13.46	0.473
JPG_80_H13_0.1_D	7.95	1.232	2.94	0.15	0.0085	0.051	8.11	0.583
JPG_80_H13_0.1_W	44.20	1.232	24.54	1.92	0.1086	0.078	35.85	0.202
JPG_80_H13_0.5	23.61	1.405	9.21	1.23	0.0695	0.134	37.38	0.329
JPG_80_H13_0.5_D	6.81	1.405	3.58	0.35	0.0197	0.097	16.97	0.528
JPG_80_H13_0.5_W	38.19	1.405	19.09	2.31	0.1301	0.121	48.62	0.228
JPG_80_H13_1.0	33.72	1.693	16.97	4.72	0.2665	0.278	104.84	0.241
JPG_80_H13_1.0_D	10.49	1.693	5.99	1.04	0.0590	0.174	39.26	0.407
JPG_80_H13_1.0_W	33.54	1.693	15.20	4.10	0.2315	0.270	96.24	0.254
JPG_80_H26_0.1	18.06	1.370	7.45	0.76	0.0430	0.102	25.71	0.366
JPG_80_H26_0.1_D	4.62	1.370	3.18	0.21	0.0119	0.066	10.88	0.561
JPG_80_H26_0.1_W	41.04	1.370	21.86	2.18	0.1229	0.100	42.95	0.214
JPG_80_H26_0.5	15.31	1.218	5.14	0.53	0.0297	0.102	21.40	0.440
JPG_80_H26_0.5_D	6.32	1.218	3.09	0.27	0.0150	0.086	13.92	0.569
JPG_80_H26_0.5_W	56.01	1.218	28.82	2.90	0.1639	0.101	49.89	0.186
JPG_80_H26_1.0	21.91	1.440	8.46	1.39	0.0782	0.164	43.83	0.343
JPG_80_H26_1.0_D	6.11	1.440	3.56	0.38	0.0215	0.107	18.62	0.530
JPG_80_H26_1.0_W	33.92	1.440	16.17	2.37	0.1340	0.147	54.36	0.248
JPG_80_O13_0.1	9.17	1.143	3.70	0.21	0.0118	0.056	9.99	0.519
JPG_80_O13_0.1_D	3.20	1.143	2.46	0.09	0.0051	0.037	5.31	0.637
JPG_80_O13_0.1_W	53.65	1.143	29.28	2.22	0.1251	0.076	37.80	0.185
JPG_80_O13_0.5	17.78	1.452	7.89	1.02	0.0578	0.130	33.57	0.355
JPG_80_O13_0.5_D	4.31	1.452	3.37	0.30	0.0169	0.089	15.06	0.544
JPG_80_O13_0.5_W	37.29	1.452	20.34	2.48	0.1402	0.122	50.75	0.221
JPG_80_O13_1.0	20.61	1.404	8.27	1.20	0.0677	0.145	38.39	0.347
JPG_80_O13_1.0_D	6.26	1.404	3.75	0.35	0.0199	0.094	16.77	0.516
JPG_80_O13_1.0_W	41.90	1.404	22.54	3.18	0.1792	0.141	61.61	0.210

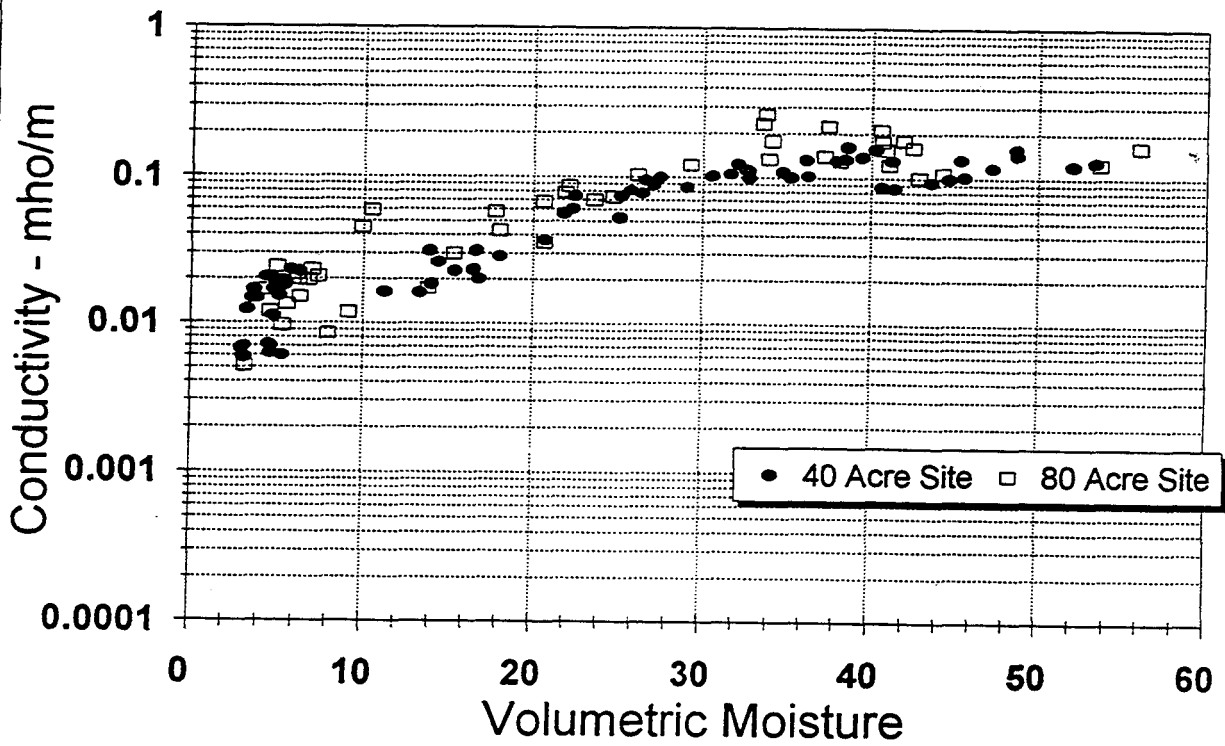
Jefferson Proving Ground , Phase IV Properties at 1015 MHz , All Depths



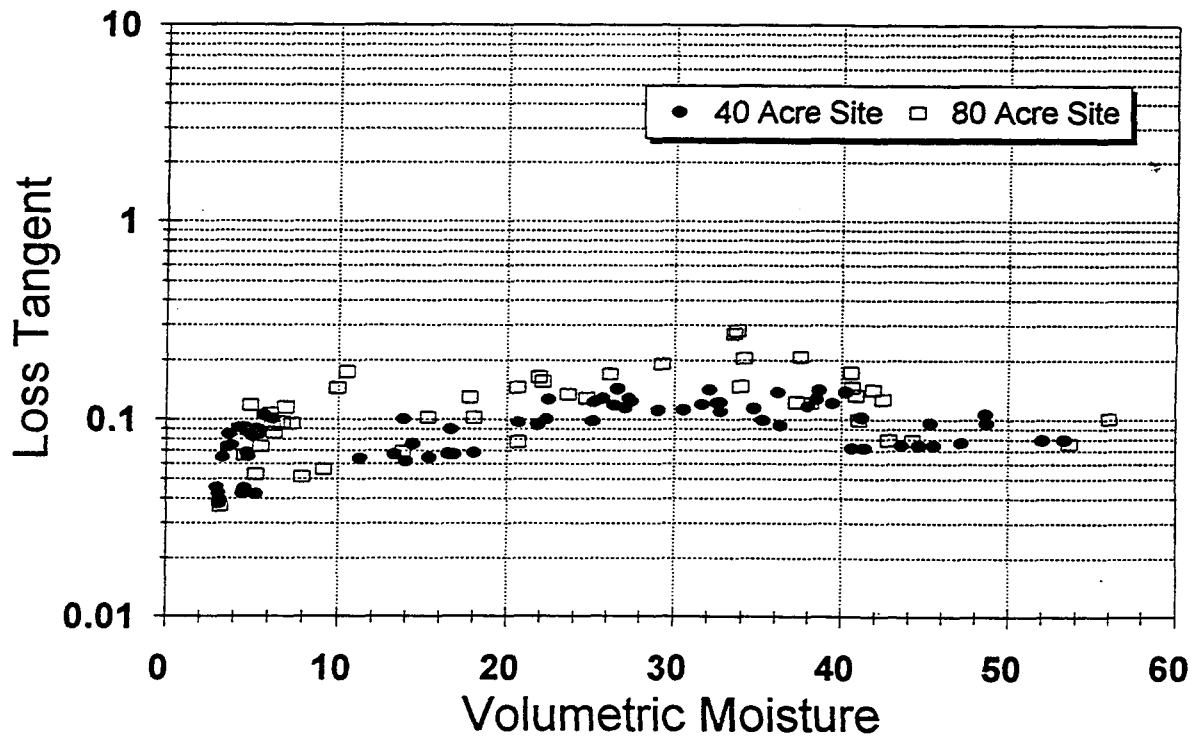
Jefferson Proving Ground , Phase IV Properties at 1015 MHz , All Depths



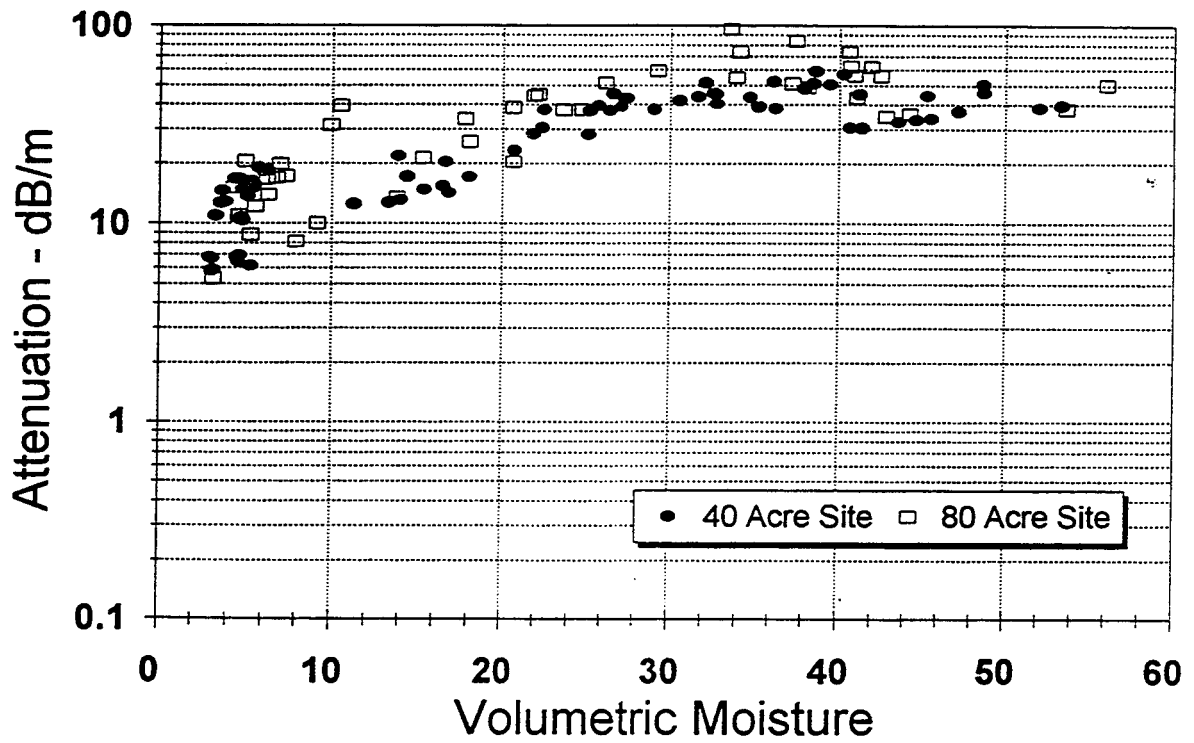
Jefferson Proving Ground , Phase IV Properties at 1015 MHz , All Depths



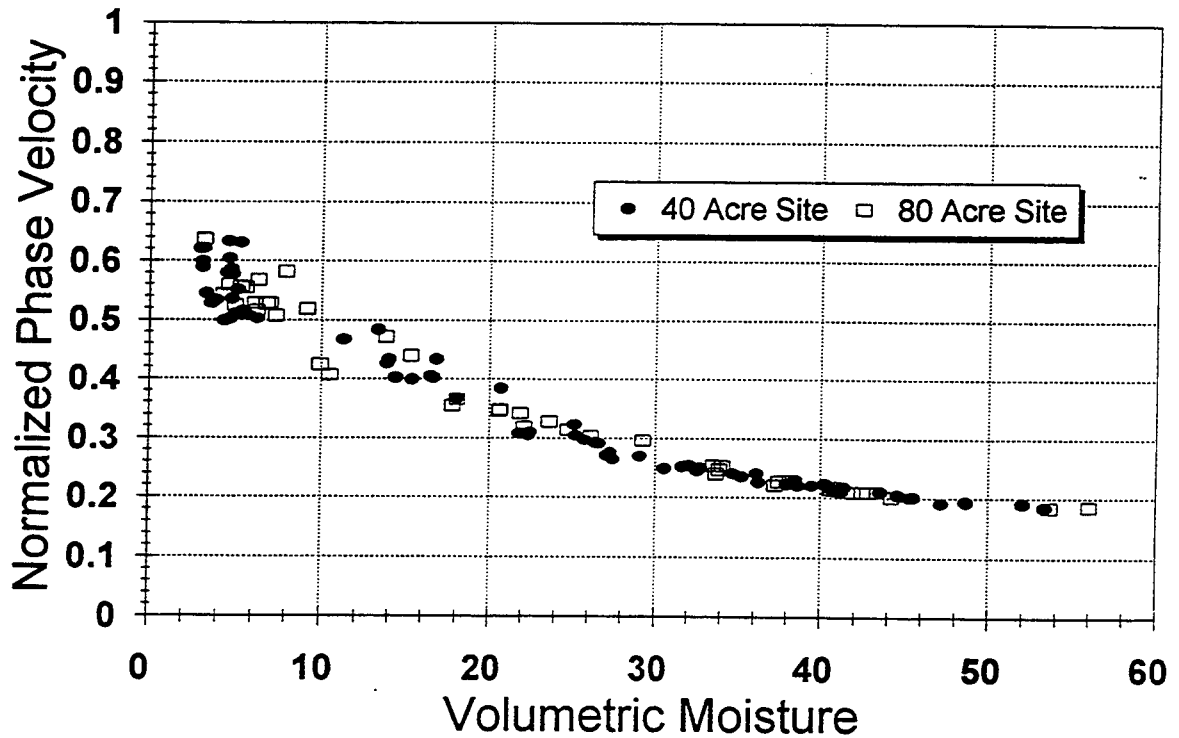
Jefferson Proving Ground , Phase IV Properties at 1015 MHz , All Depths



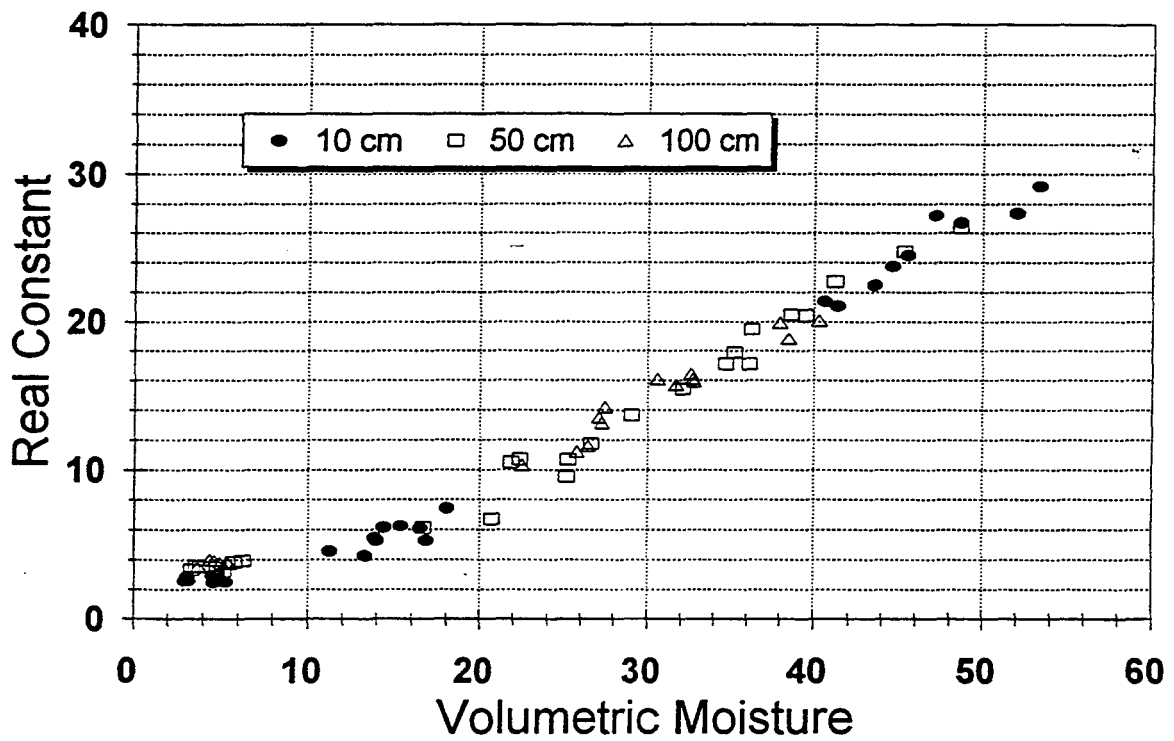
Jefferson Proving Ground , Phase IV Properties at 1015 MHz , All Depths



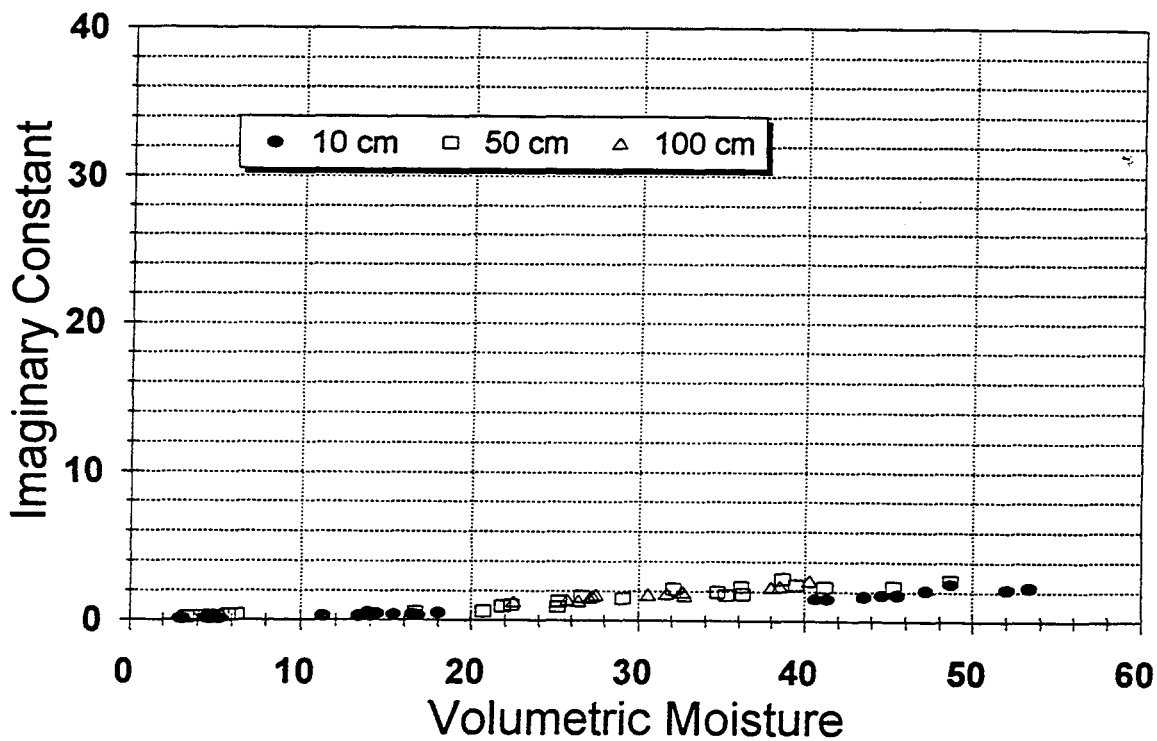
Jefferson Proving Ground , Phase IV Properties at 1015 MHz , All Depths



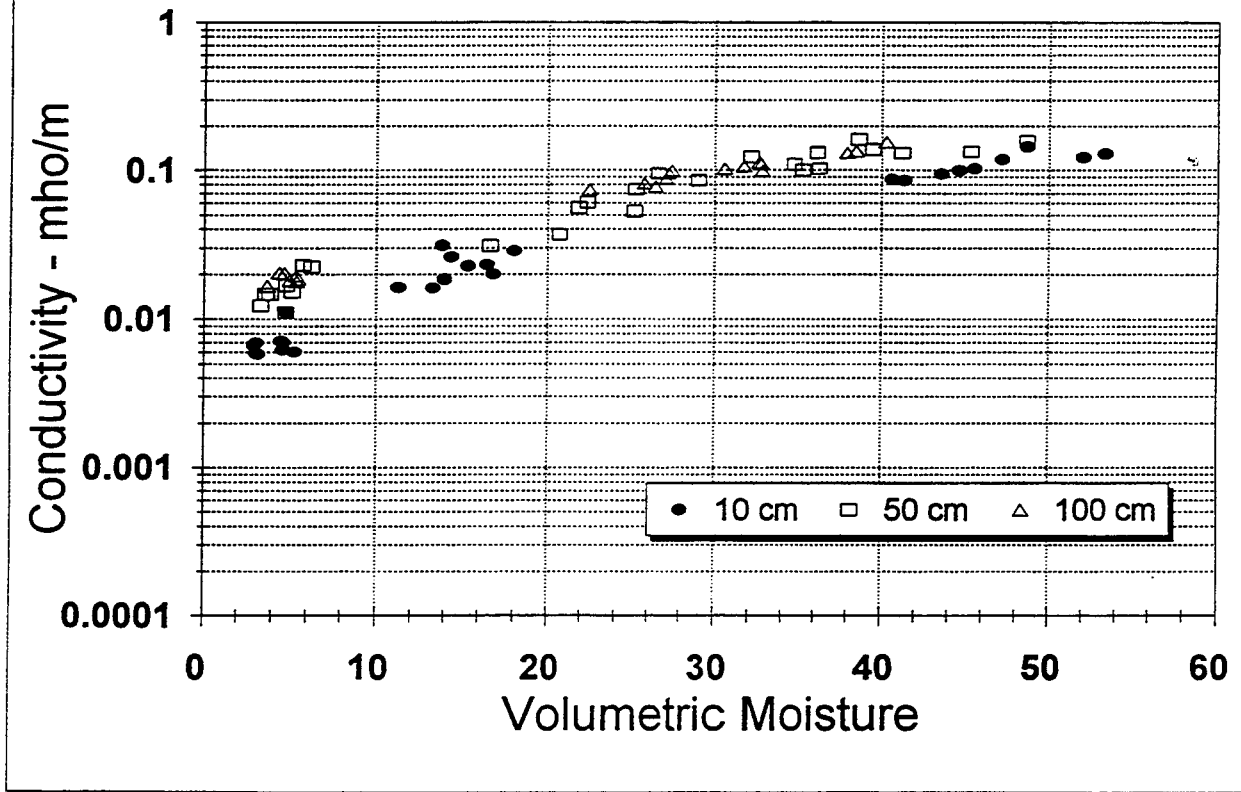
JPG , Phase IV , 40 Acre Test Site Properties at 1015 MHz by Depth



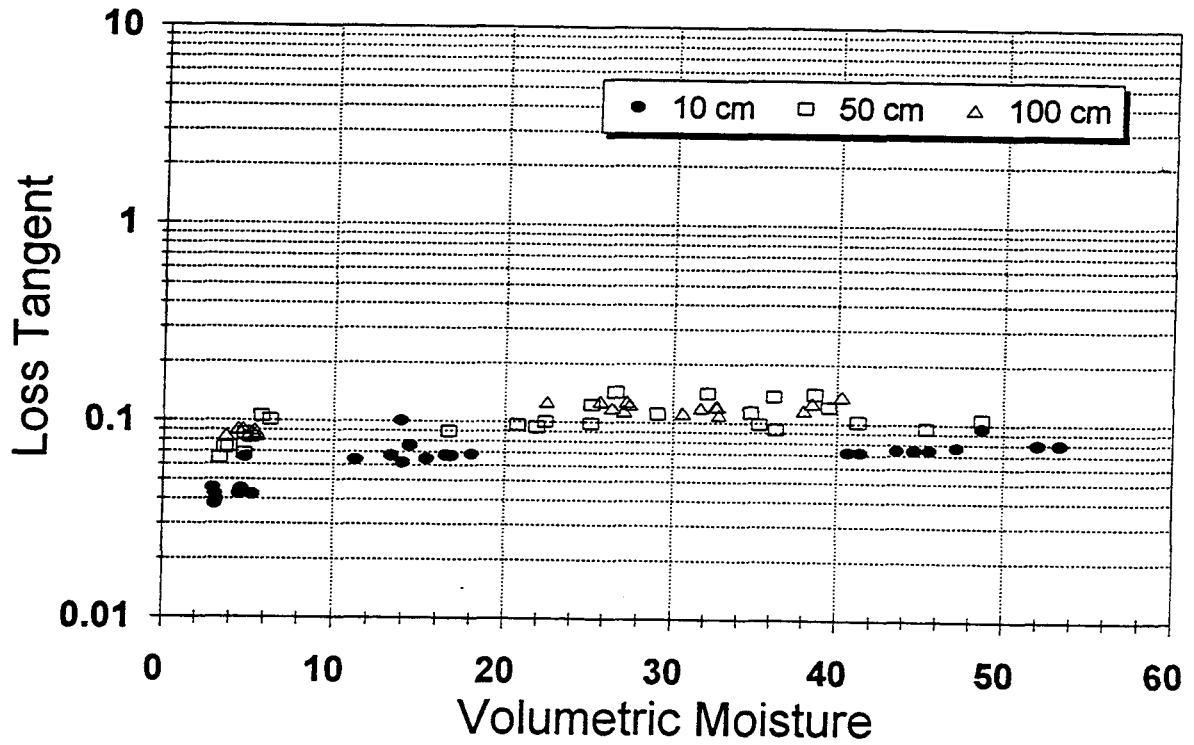
JPG , Phase IV , 40 Acre Test Site Properties at 1015 MHz by Depth



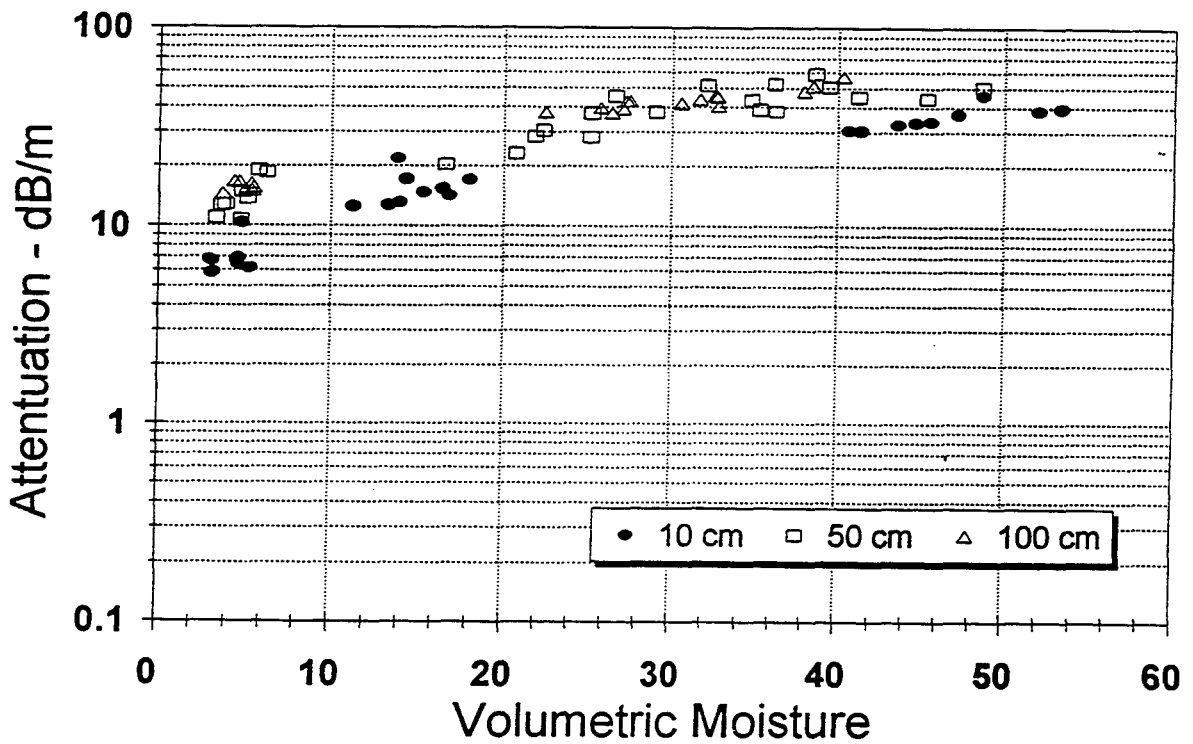
JPG , Phase IV , 40 Acre Test Site Properties at 1015 MHz by Depth



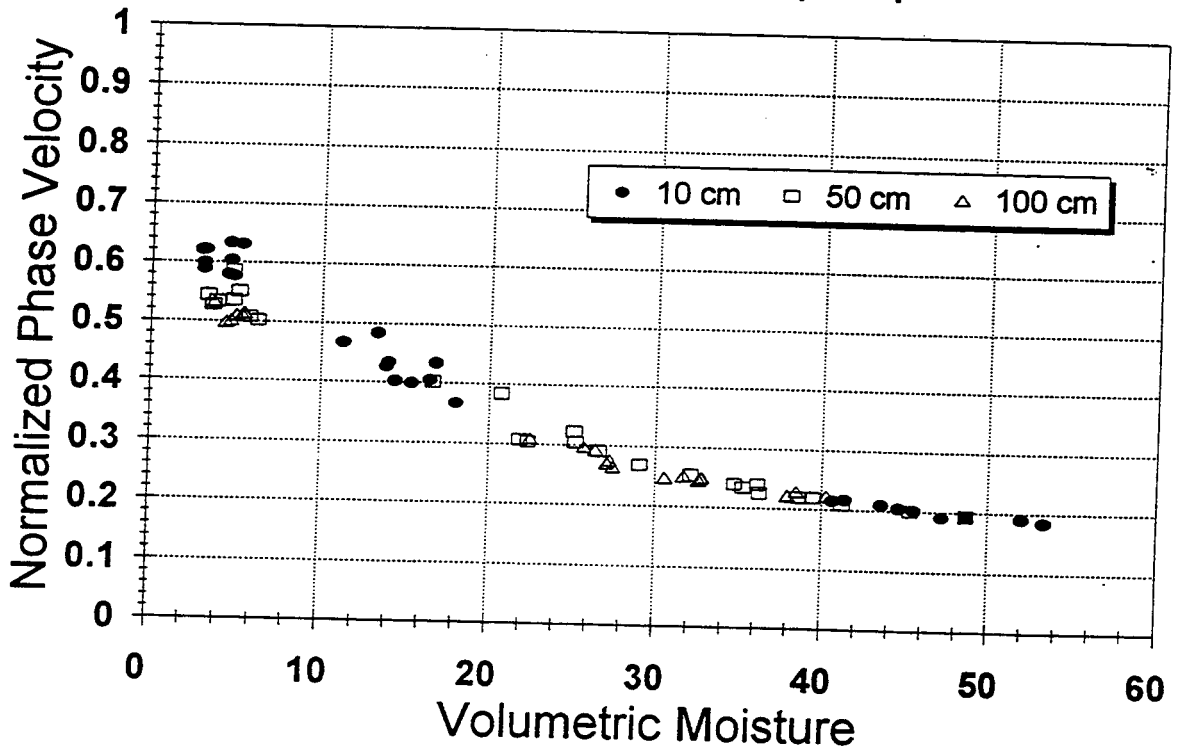
JPG , Phase IV , 40 Acre Test Site Properties at 1015 MHz by Depth



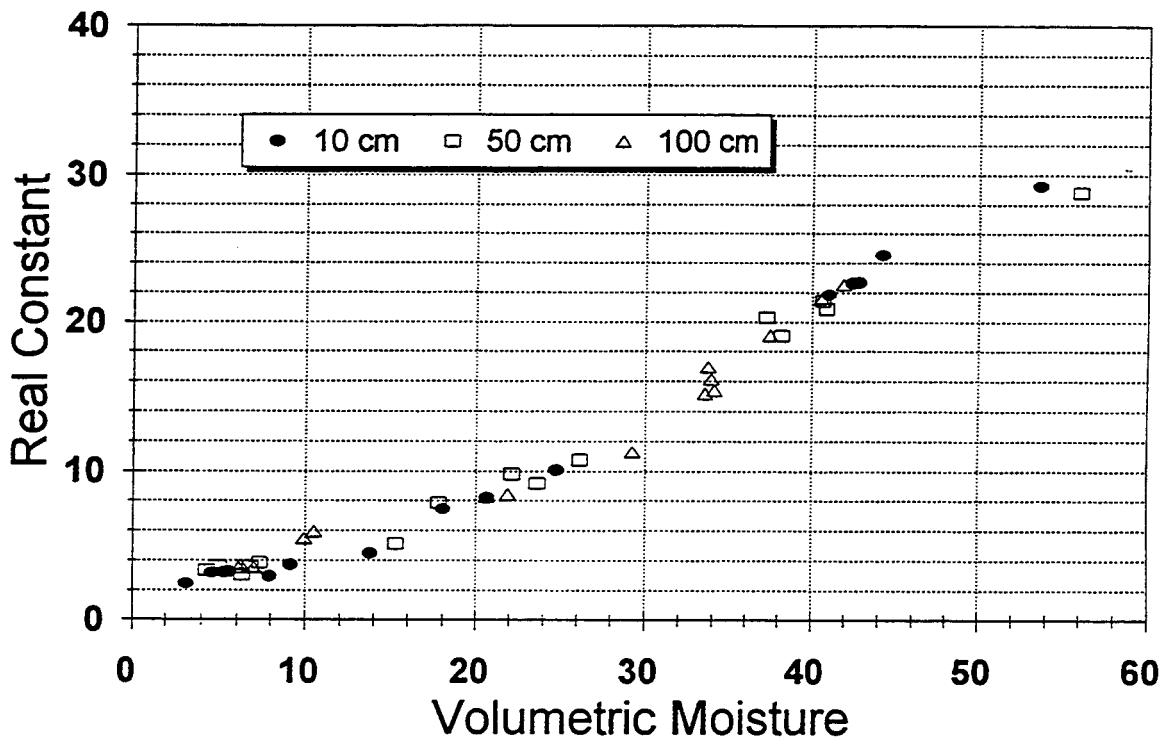
JPG , Phase IV , 40 Acre Test Site Properties at 1015 MHz by Depth



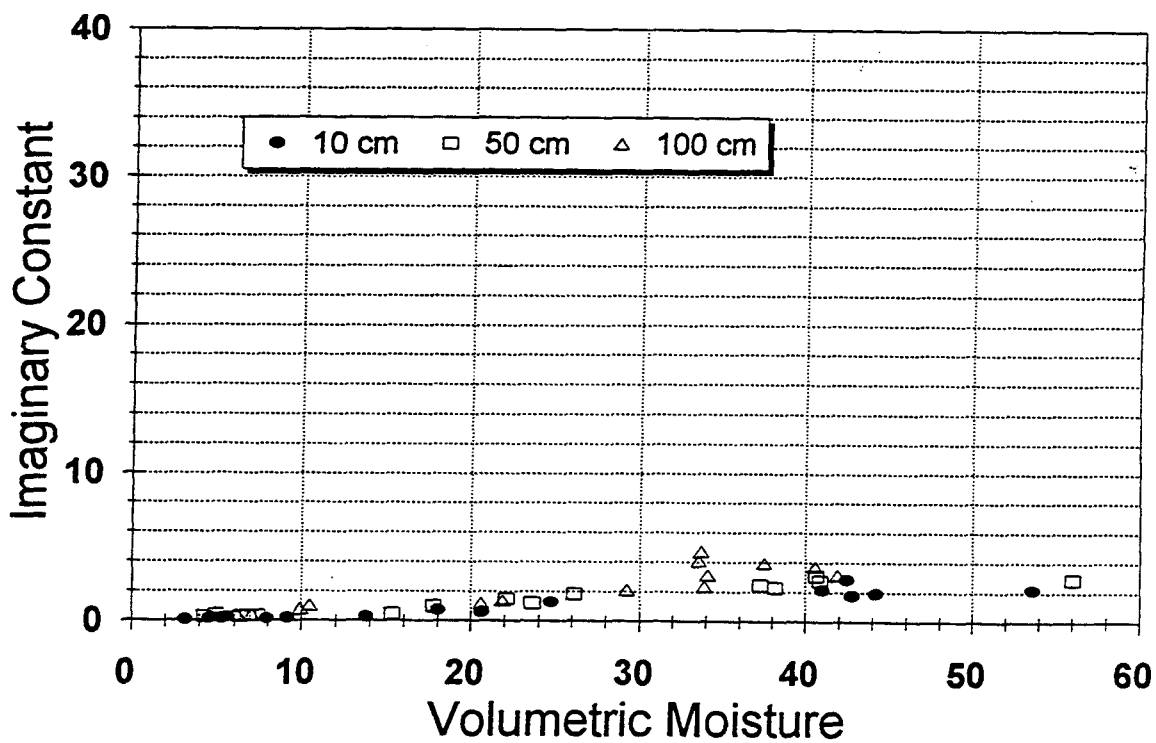
JPG , Phase IV , 40 Acre Test Site Properties at 1015 MHz by Depth



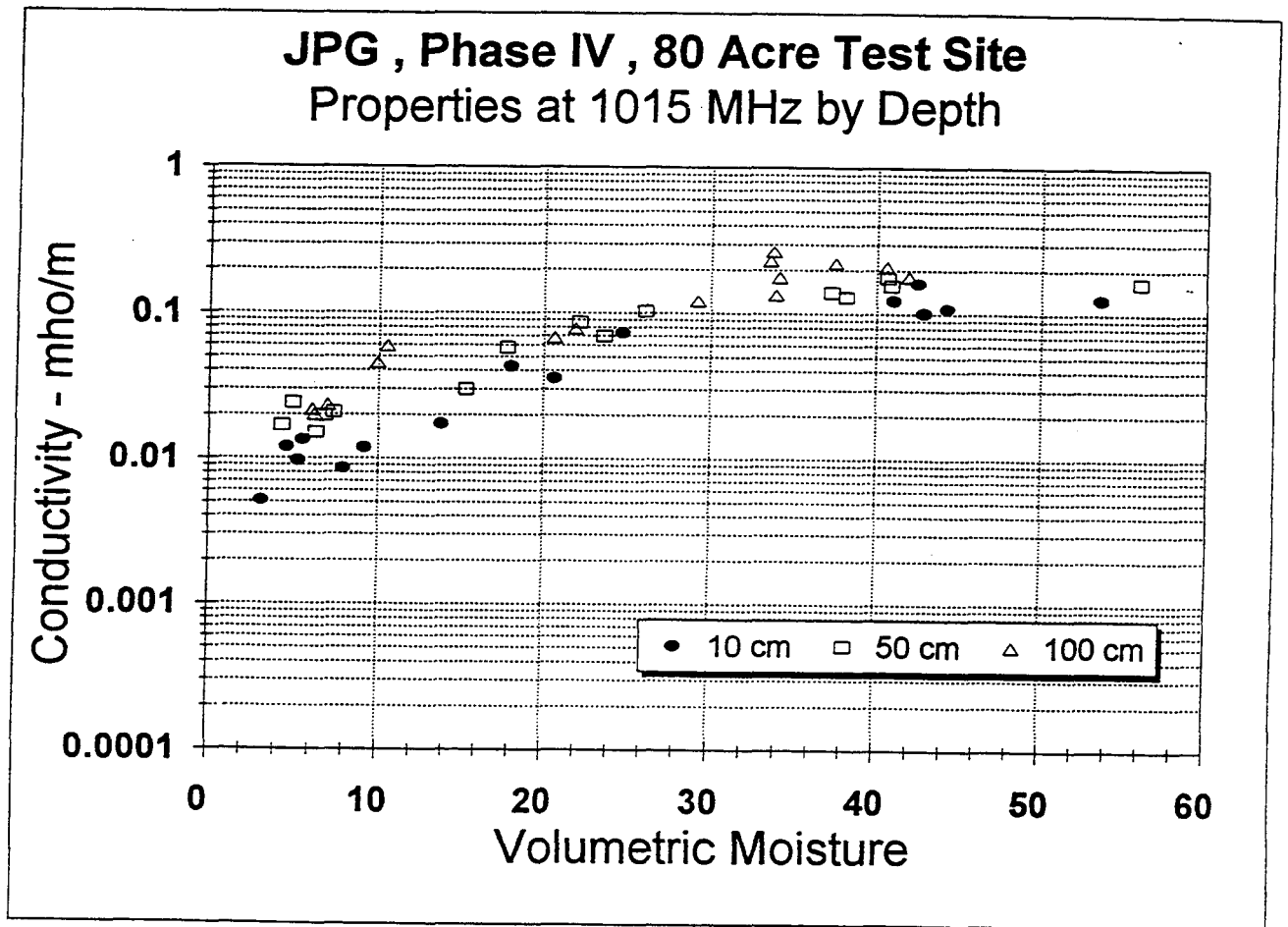
JPG , Phase IV , 80 Acre Test Site Properties at 1015 MHz by Depth



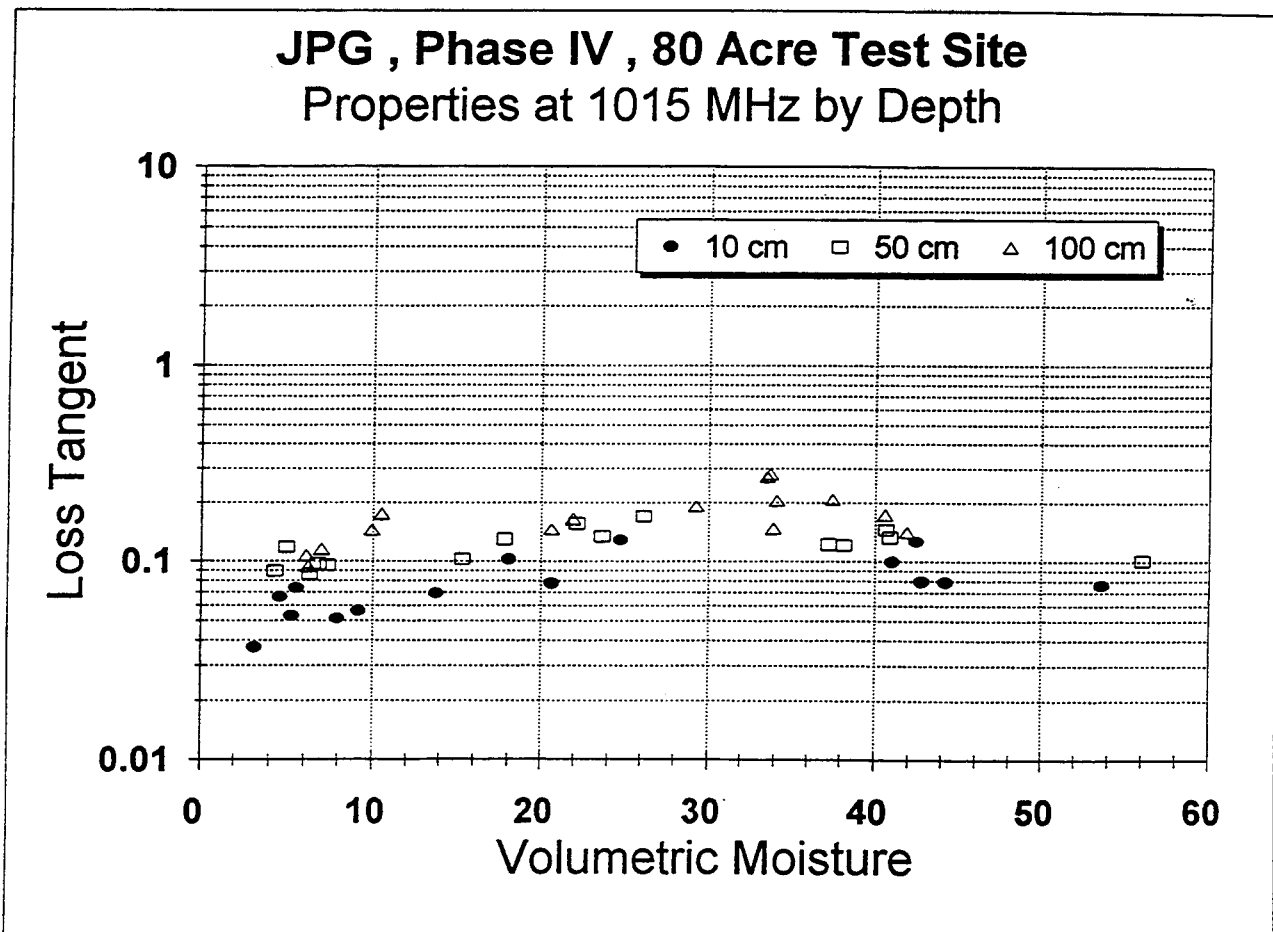
JPG , Phase IV , 80 Acre Test Site Properties at 1015 MHz by Depth



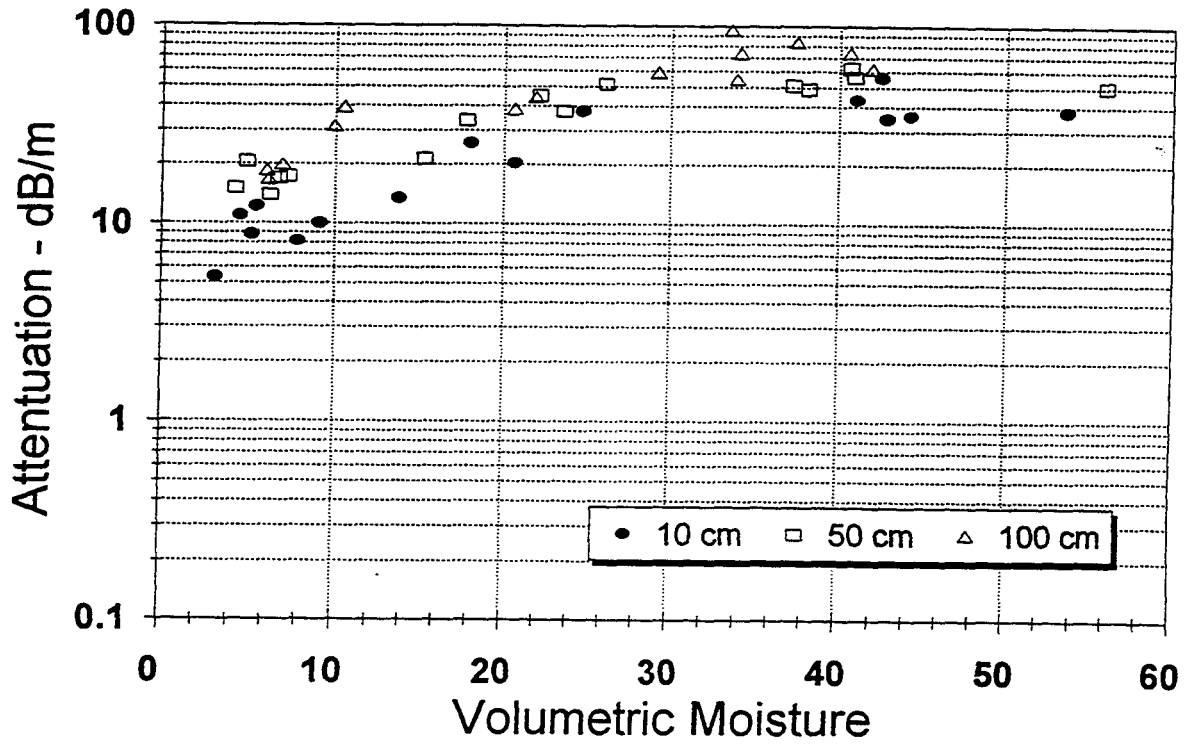
JPG , Phase IV , 80 Acre Test Site Properties at 1015 MHz by Depth



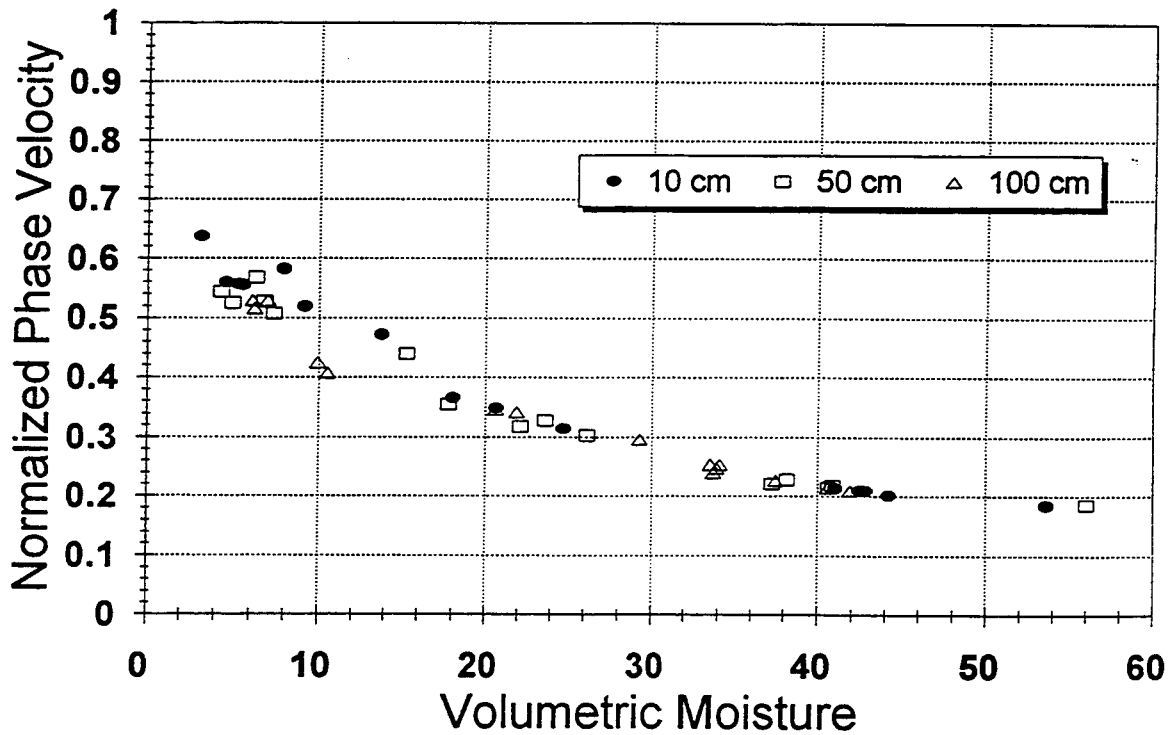
JPG , Phase IV , 80 Acre Test Site Properties at 1015 MHz by Depth



**JPG , Phase IV , 80 Acre Test Site
Properties at 1015 MHz by Depth**



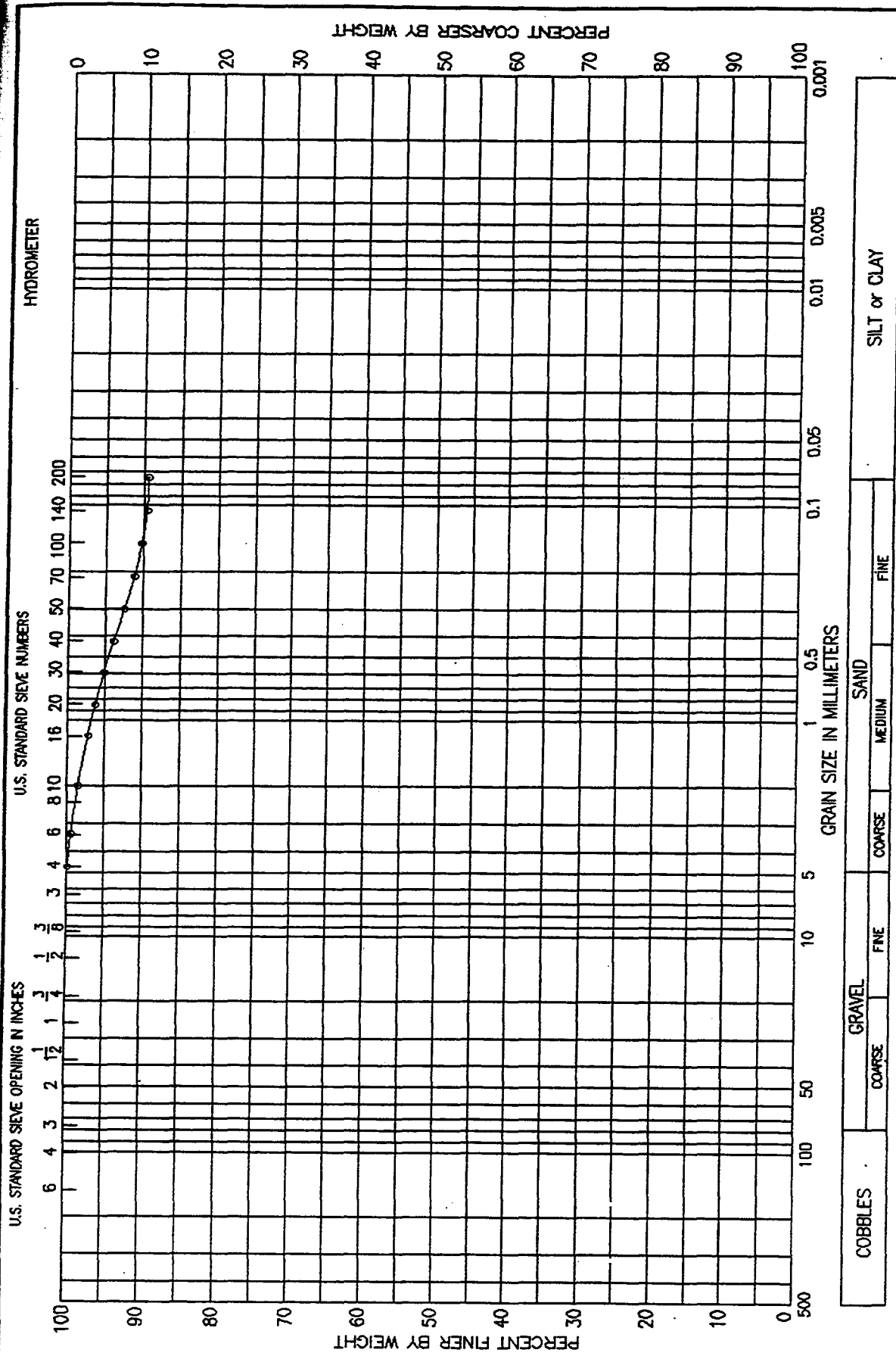
JPG , Phase IV , 80 Acre Test Site Properties at 1015 MHz by Depth



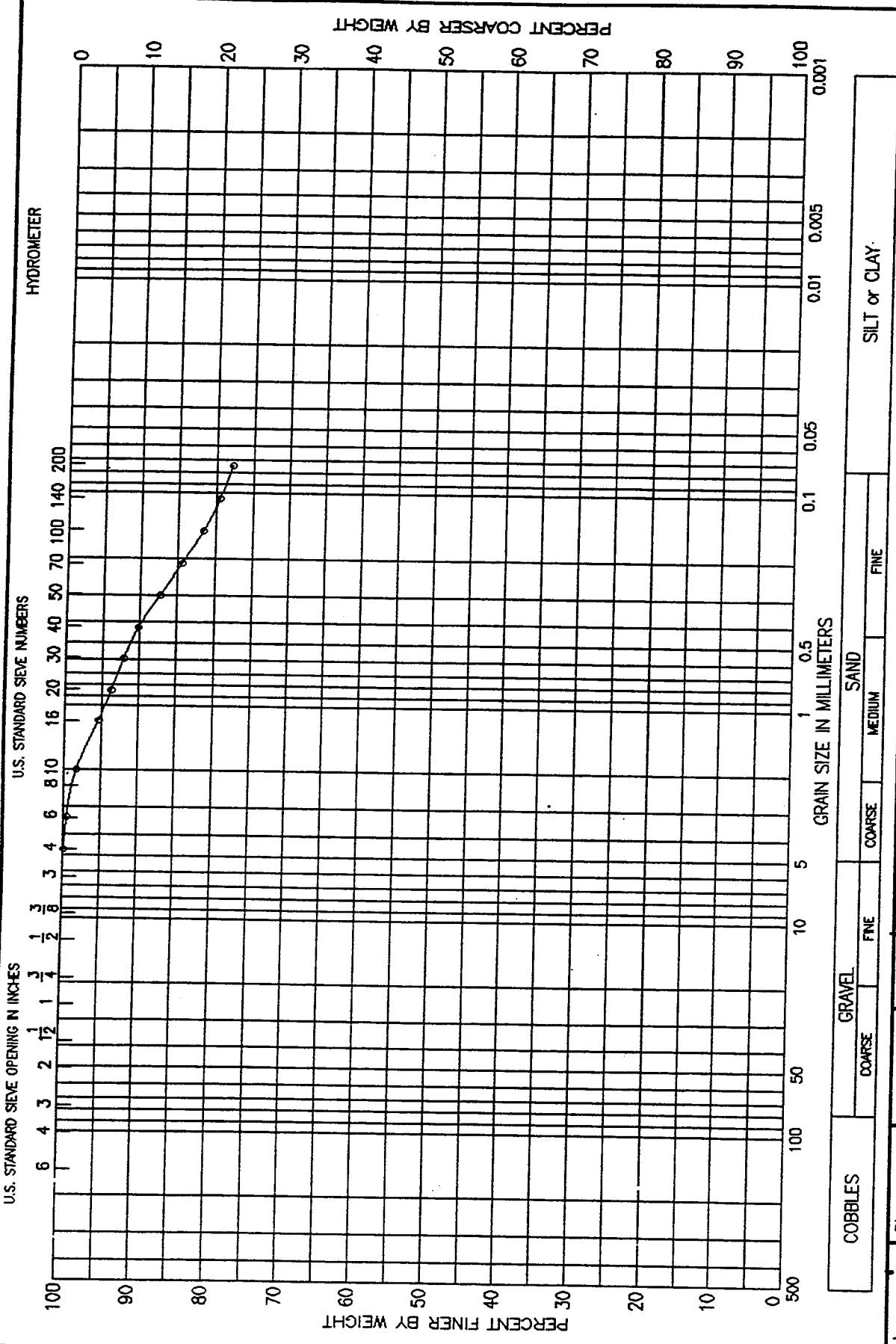
Appendix D

Soil Gradation Curves:

1-hectare Site



U.S. STANDARD SIEVE OPENING IN INCHES 100 6 4 3 2 1 1/2 1 3/4 1 1/2 3/8 1/2 3/8 3/16 1/4 3/16 1/8 3/16 1/4 3/8 1/2 3/4 1 1 1/2 2 3 4 6		U.S. STANDARD SIEVE NUMBERS 100 60 40 20 10 5 2.5 1.5 0.75 0.425 0.25 0.15 0.075		HYDROMETER 0 10 20 30 40 50 60 70 80 90 100		PERCENT FINER BY WEIGHT		PERCENT COARSER BY WEIGHT	
COBBLES PL 21		GRAVEL COARSE 10 FINE 2.79		SAND COARSE 24.4 MEDIUM 2.2 FINE 2.2		SILT or CLAY			
CLASSIFICATION SILTY CLAY (CL), BROWN; WITH SAND		LL 31 PL 21 PI 10		GS 2.79 NAT W.% 24.4 ORG.% 2.2		PROJECT JEFFERSON PROVING GROUND, IN (27.5E, 73N)		BORING NO. JPG REG 1 SAMPLE NO. 0.5M DEPTH/ELEV DATE 23 FEB 98	
GRADATION CURVE		LABORATORY USAE WES - STF/GL							

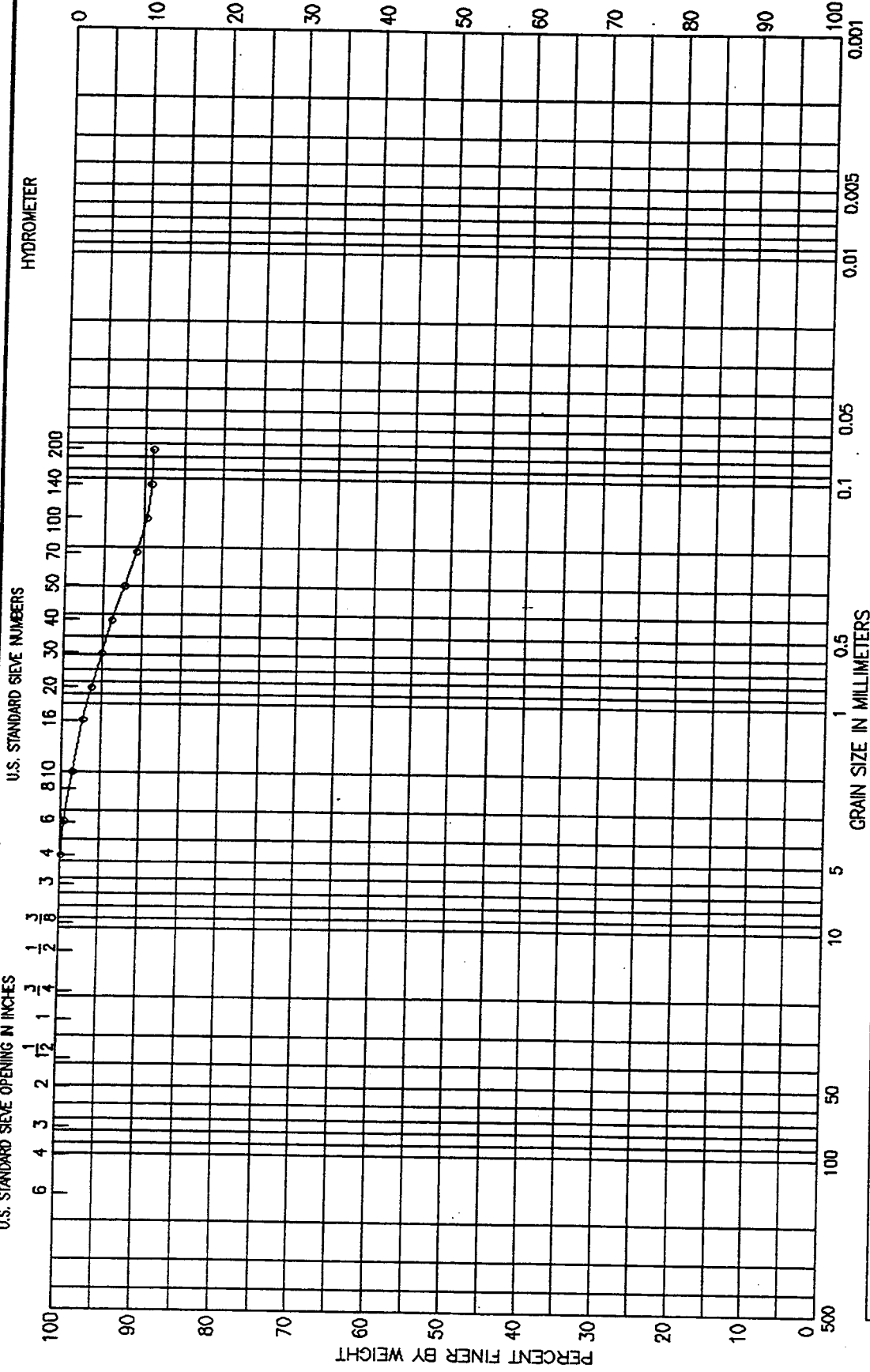


PROJECT		JEFFERSON PROVING GROUND, IN	
BORING NO.		(27.5E, 73N)	
DEPTH/ELEV		JPG REG 1	SAMPLE NO. 1.0M
DATE		23 FEB 98	
CLASSIFICATION		SANDY CLAY (CL), BROWN	
LL	33	PI	18
		CS	15
		NAT W.%	20.7
		ORG.%	2.2
GRADATION CURVE		LABORATORY USAE WES - STF/GL	

U.S. STANDARD SIEVE OPENING IN INCHES

U.S. STANDARD SIEVE NUMBERS

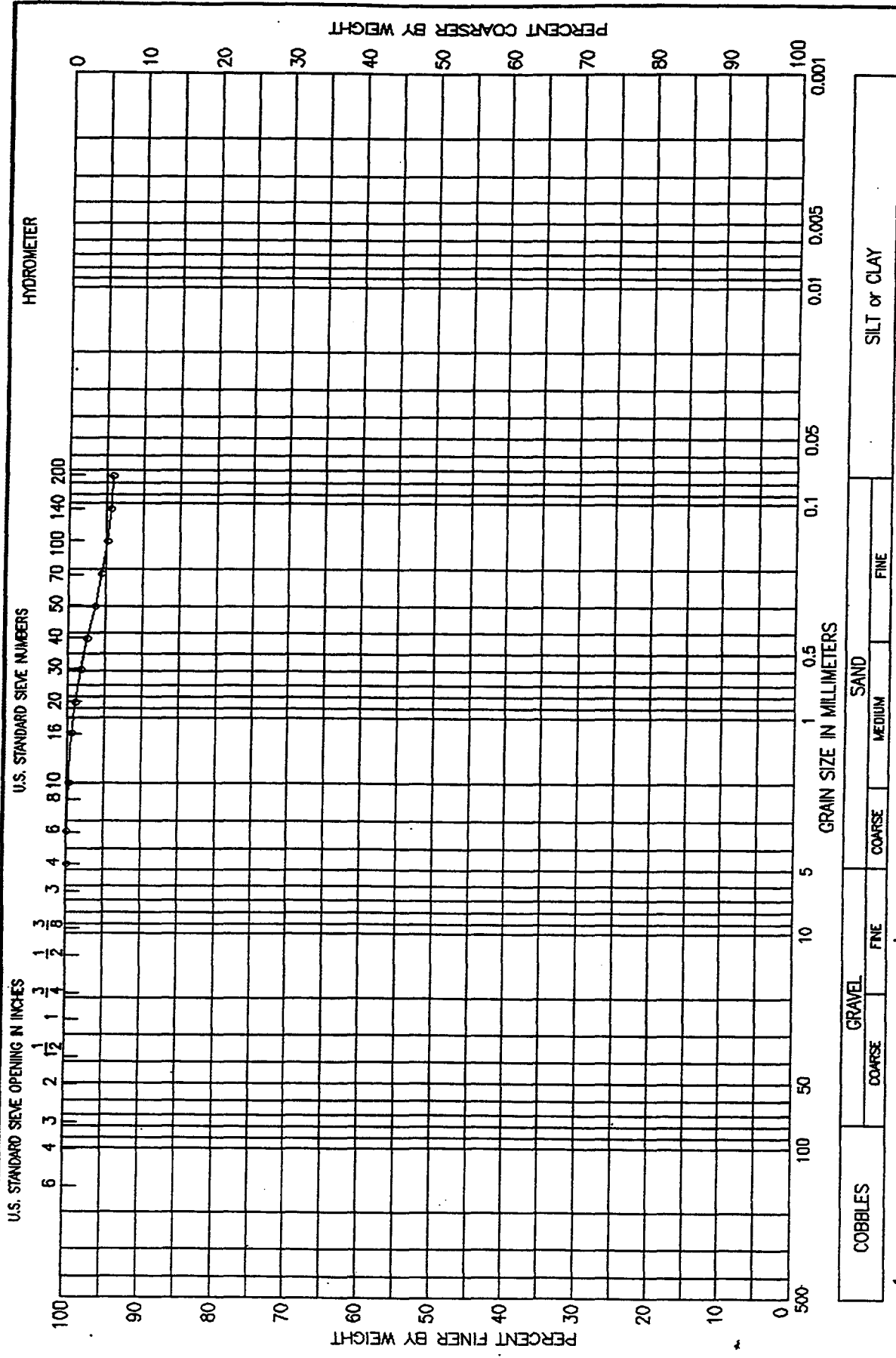
U.S. STANDARD SIEVE OPENING IN INCHES



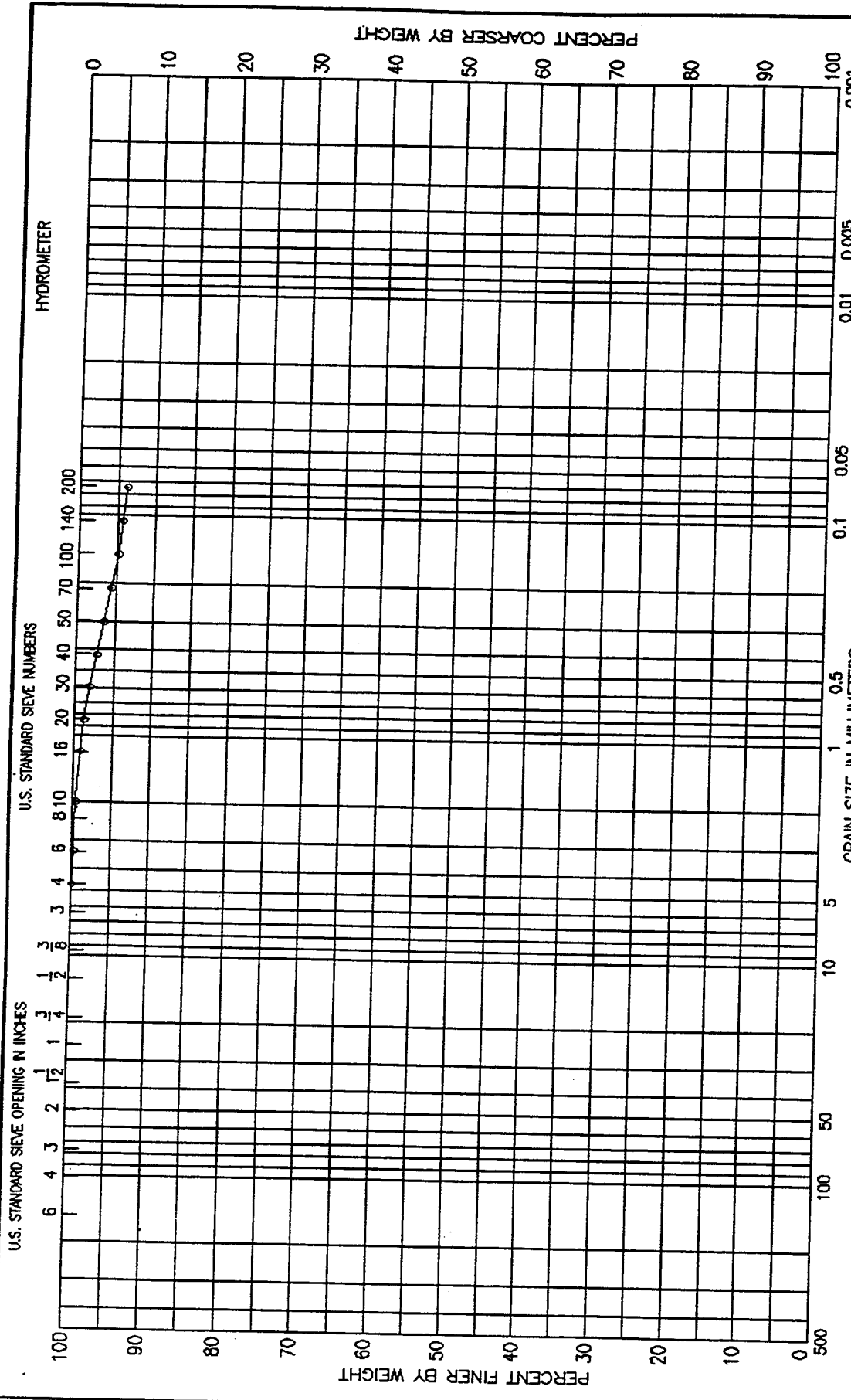
COBBLES		GRAVEL		SAND			SILT or CLAY	
		COARSE	FINE	COARSE	MEDIUM	FINE		

LL	38	PL	26	PI	12	GS	2.73	NAT W, %	33.0	ORG, %	3.7
CLASSIFICATION											
CLAYEY SILT (ML), BROWN; WITH SAND											
GRADATION CURVE						LABORATORY USAE WES - SIF/GL					

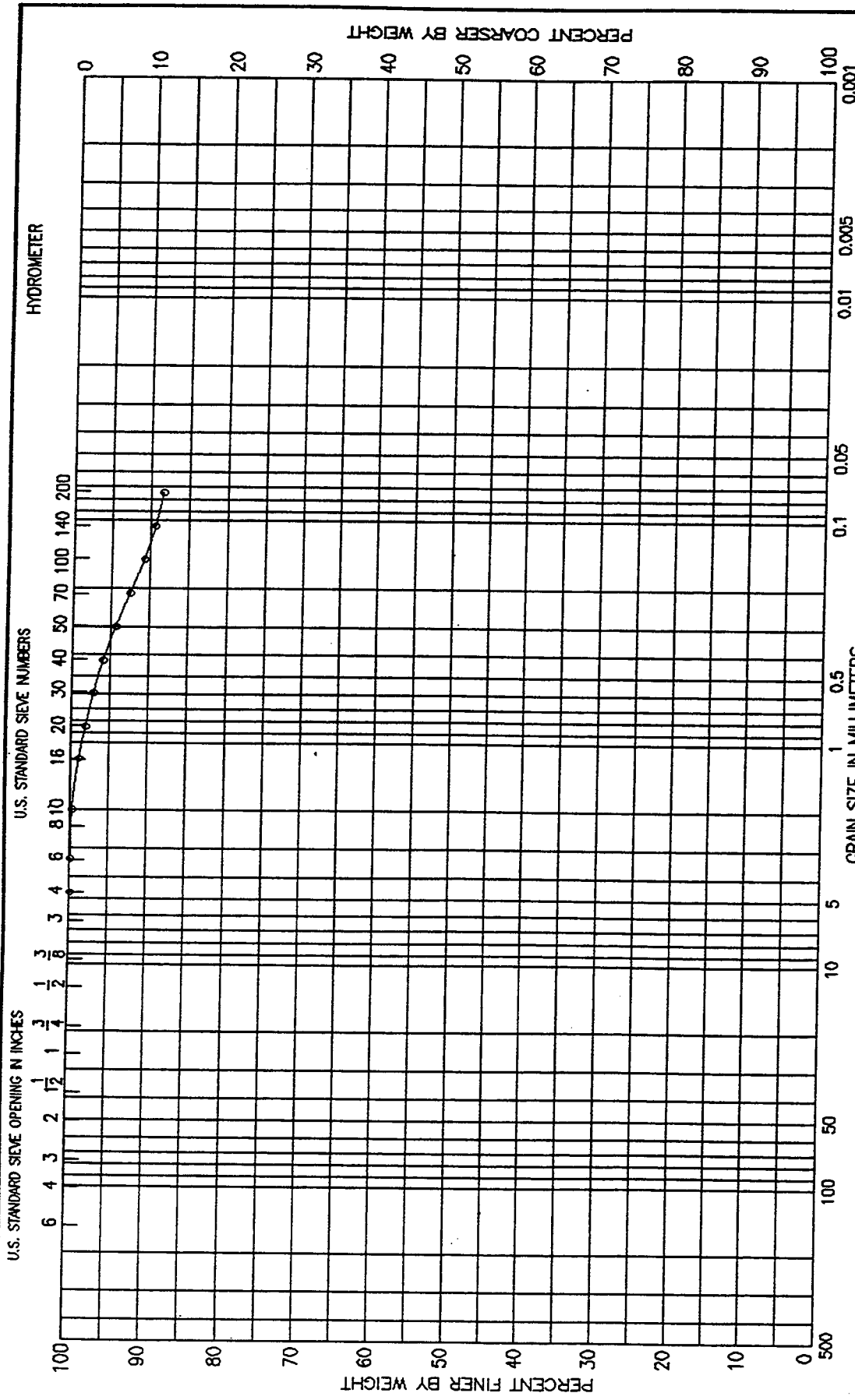
PROJECT JEFFERSON PROVING GROUND, IN
 BORING NO. (40E, 23A) JPG REG 2 SAMPLE NO. 10CM
 DEPTH/ELEV DATE 23 FEB 98



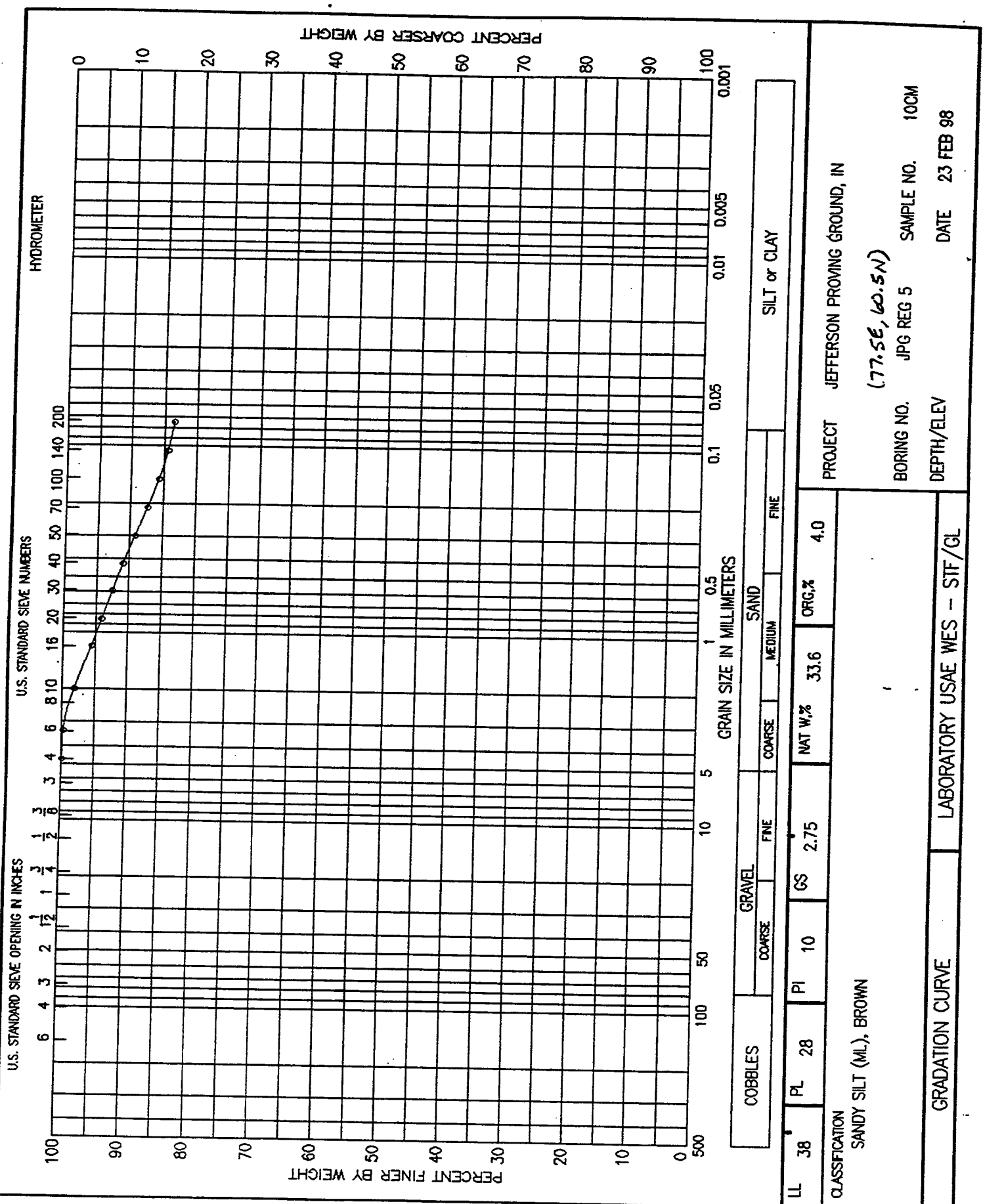
COBBLES	GRAVEL	SAND		SILT or CLAY
COARSE	FINE	COARSE	MEDIUM	FINE
LL 36	PL 26	PI 10	GS 2.76	ORG.% 3.3
CLASSIFICATION CLAYEY SILT (ML), BROWN; WITH SAND				
GRADATION CURVE		LABORATORY USAE WES - STF/GL		
PROJECT		JEFFERSON PROVING GROUND, IN		
BORING NO.		(105E, 10.57A)		
DEPTH/ELEV		SAMPLE NO. 10CM		
		DATE 23 FEB 98		

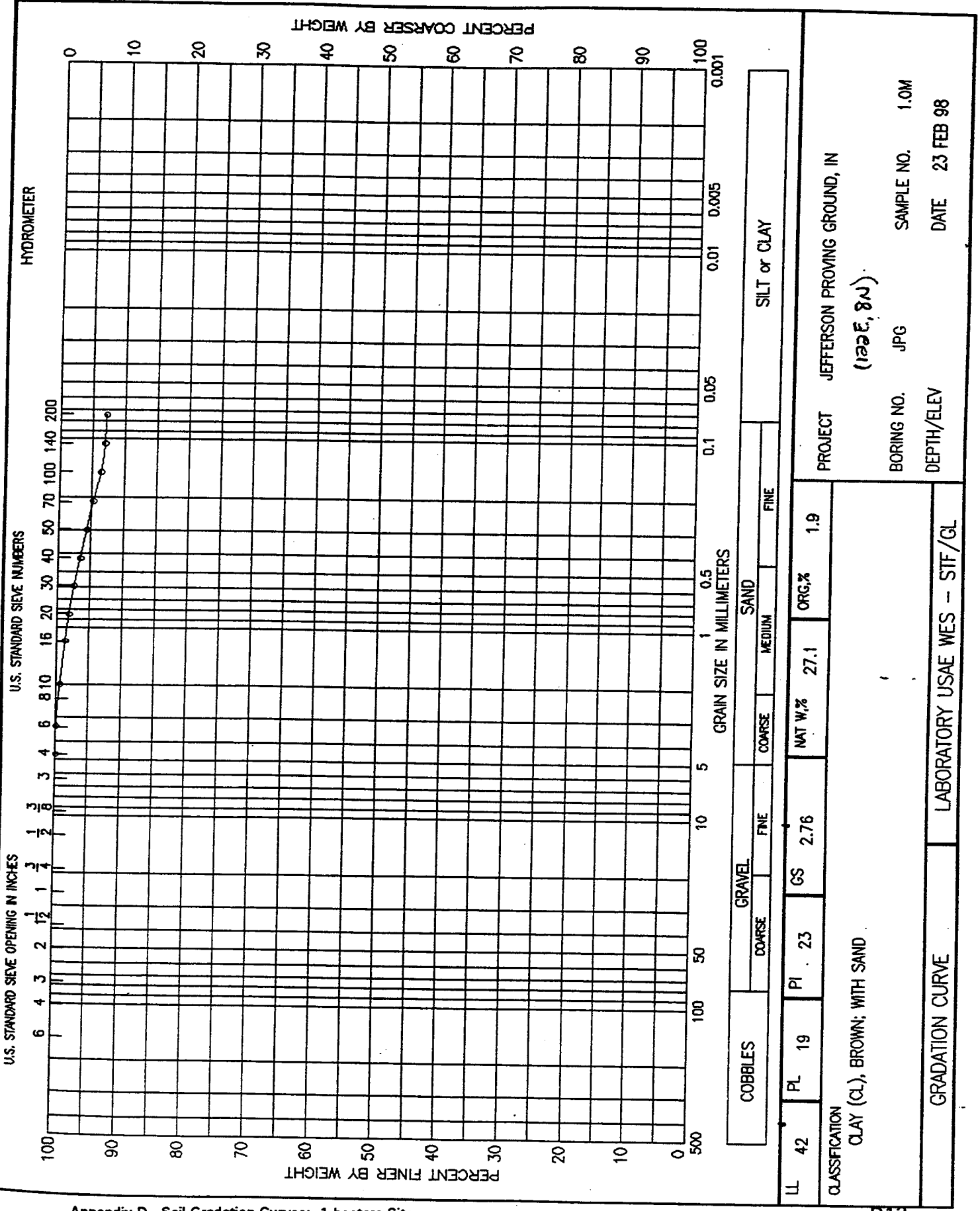


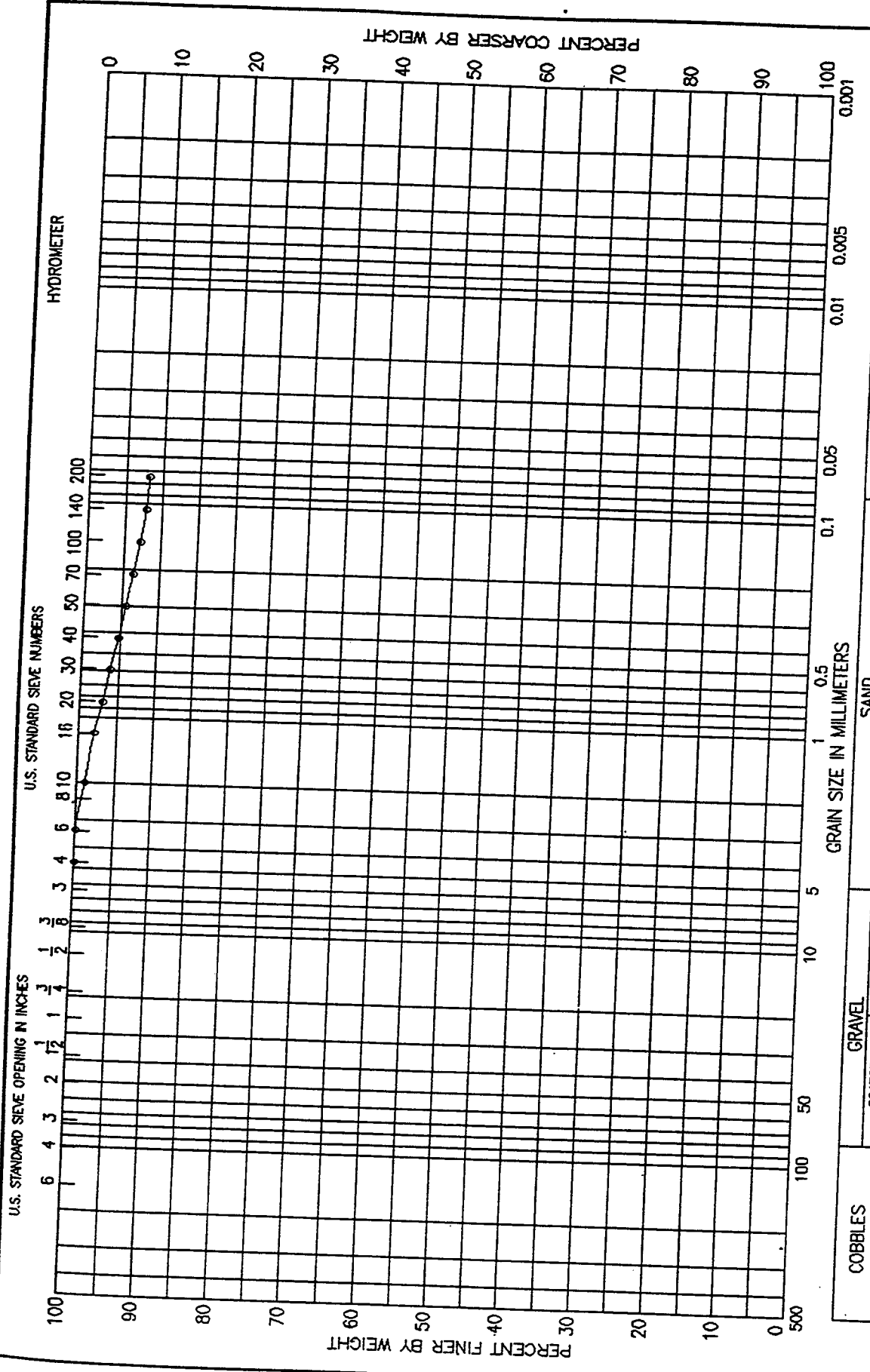
COBBLES	GRAVEL	SAND		SILT or CLAY	
COARSE	FINE	COARSE	MEDIUM	FINE	
LL 40	PL 25	PI 15	GS 2.81	NAT W.% 30.7	ORG.% 2.6
CLASSIFICATION SILTY CLAY (CL), BROWN; WITH SAND					
GRADATION CURVE			LABORATORY USAE WES - STF/GL		
PROJECT		JEFFERSON PROVING GROUND, IN			
BORING NO.		(655, 10.5M)		SAMPLE NO. 0.5M	
DEPTH/ELEV		JPG REG 4		DATE 23 FEB 98	



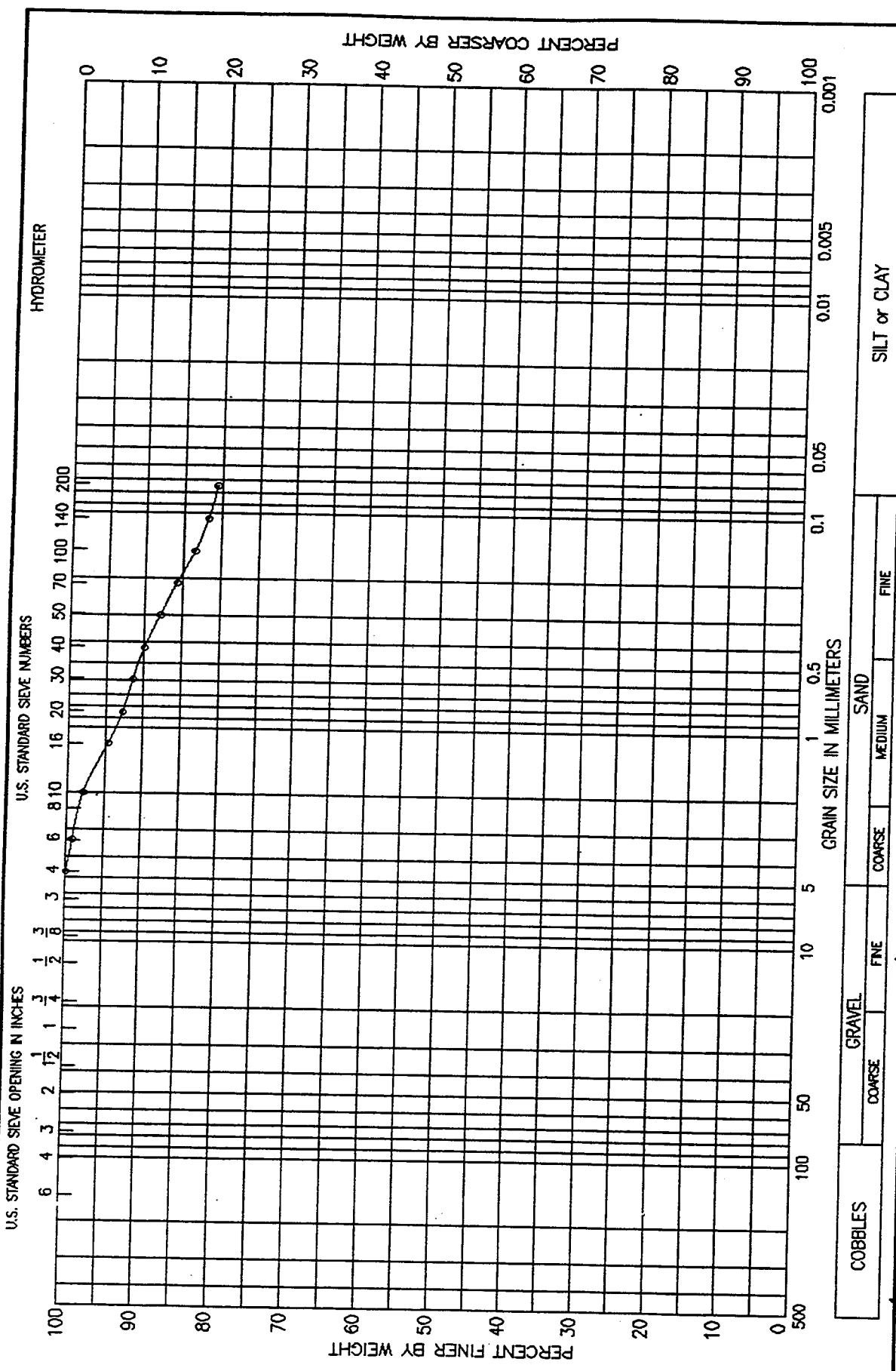
COBBLES	GRAVEL COARSE	GRAVEL FINE	SAND COARSE	SAND MEDIUM	SAND FINE	SILT or CLAY
LL 35	PL 23	PI 12	GS 2.71	NAT W.% 29.0	ORG.% 2.6	
CLASSIFICATION SILTY CLAY (CL), BROWN; WITH SAND						
GRADATION CURVE			LABORATORY USAE WES -- STF/GL			
PROJECT			JEFFERSON PROVING GROUND, IN			
BORING NO.			(65E, 10.5N)		JPG REG 4	
DEPTH/ELEV			SAMPLE NO.		DATE	
			1.0M		23 FEB 98	







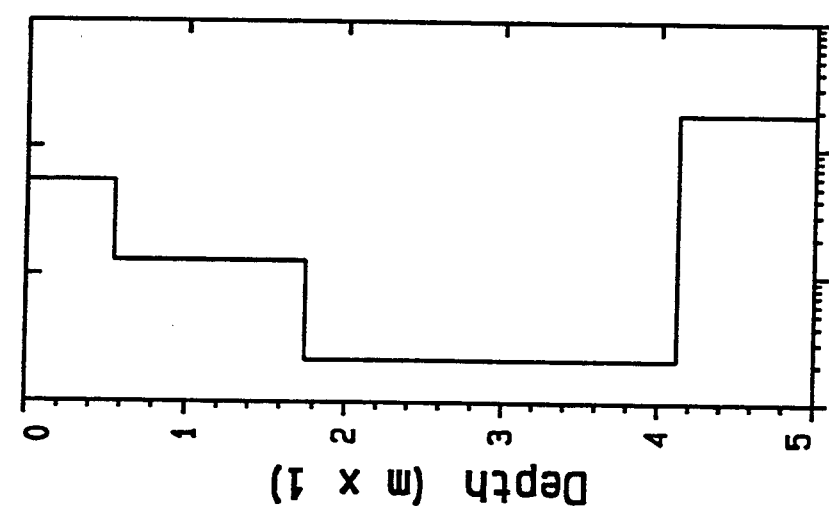
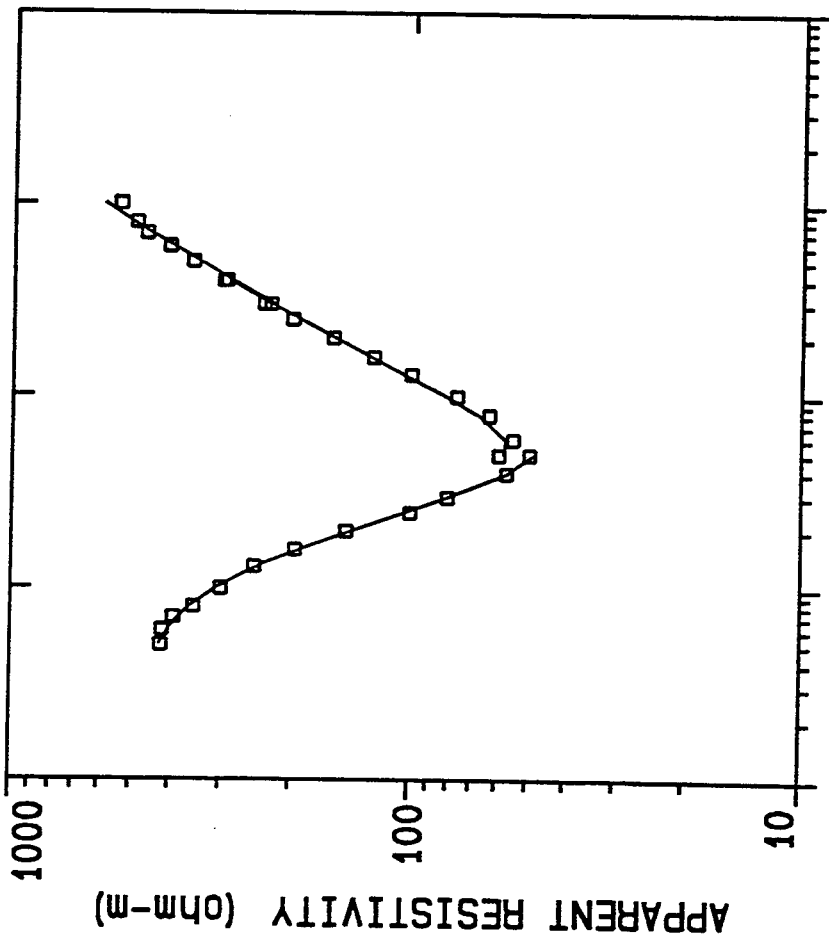
LL 37	PL 22	PI 15	GS 2.78	NAT W.% 24.7	ORG.% 2.1
CLASSIFICATION CLAY (CL), BROWN; WITH SAND					
GRADATION CURVE					
LABORATORY USAE WES - STF/GL					
PROJECT JEFFERSON PROVING GROUND, IN (123 E, 97 N)			BORING NO. JPG		
DEPTH/ELEV			SAMPLE NO. 0.5M		
			DATE 23 FEB 98		



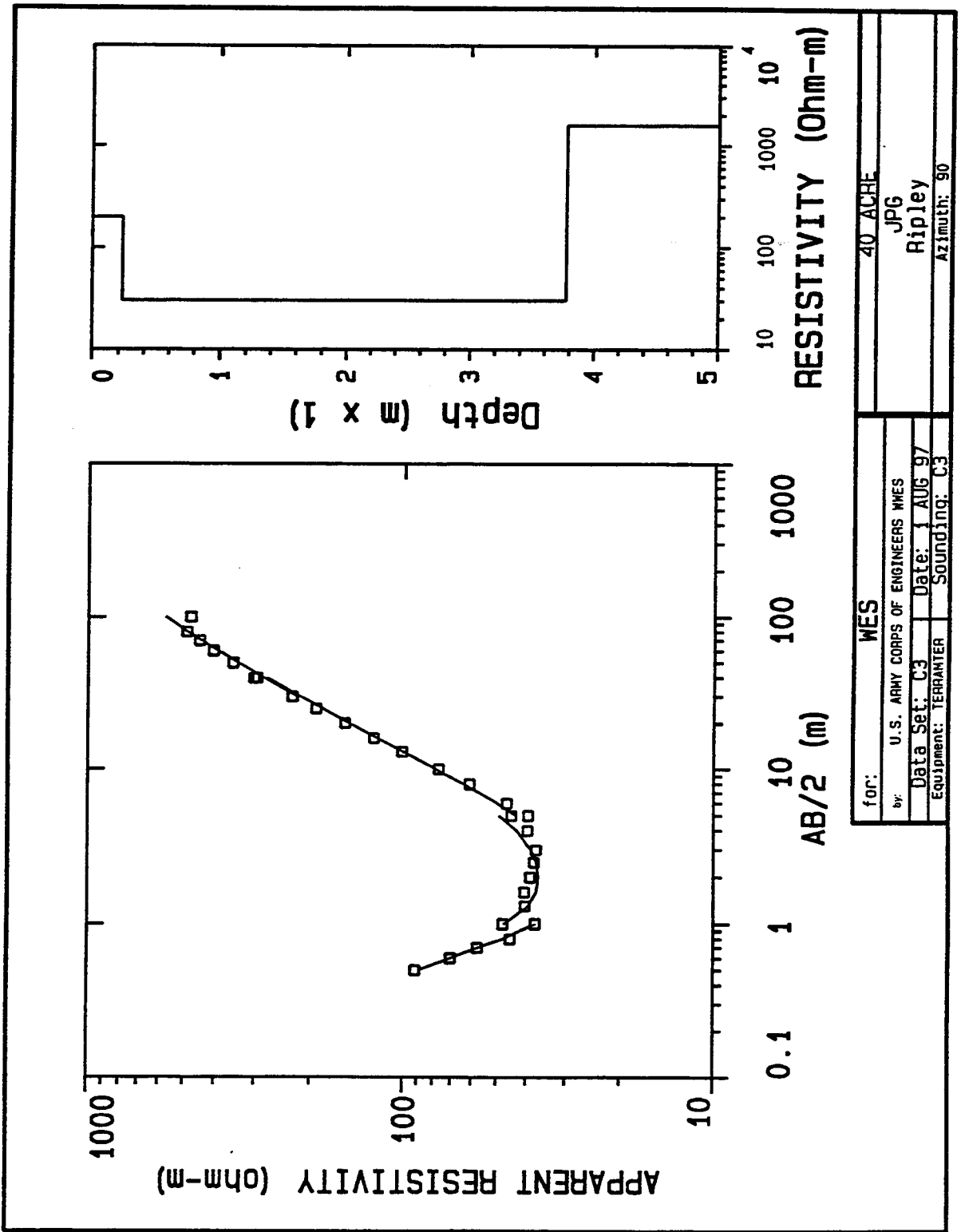
Appendix E

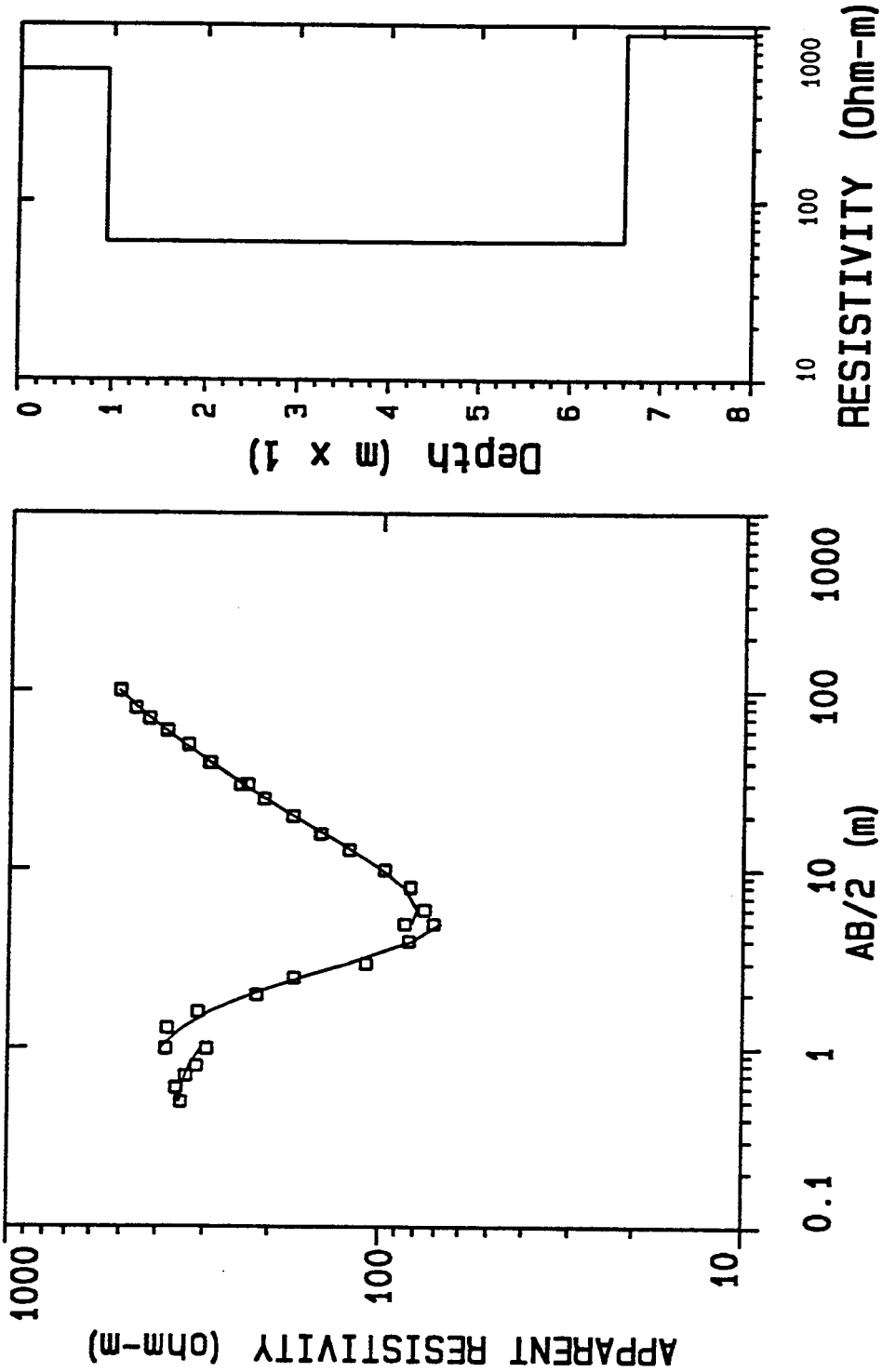
Vertical Electric Sounding

Curves: 40-acre Site

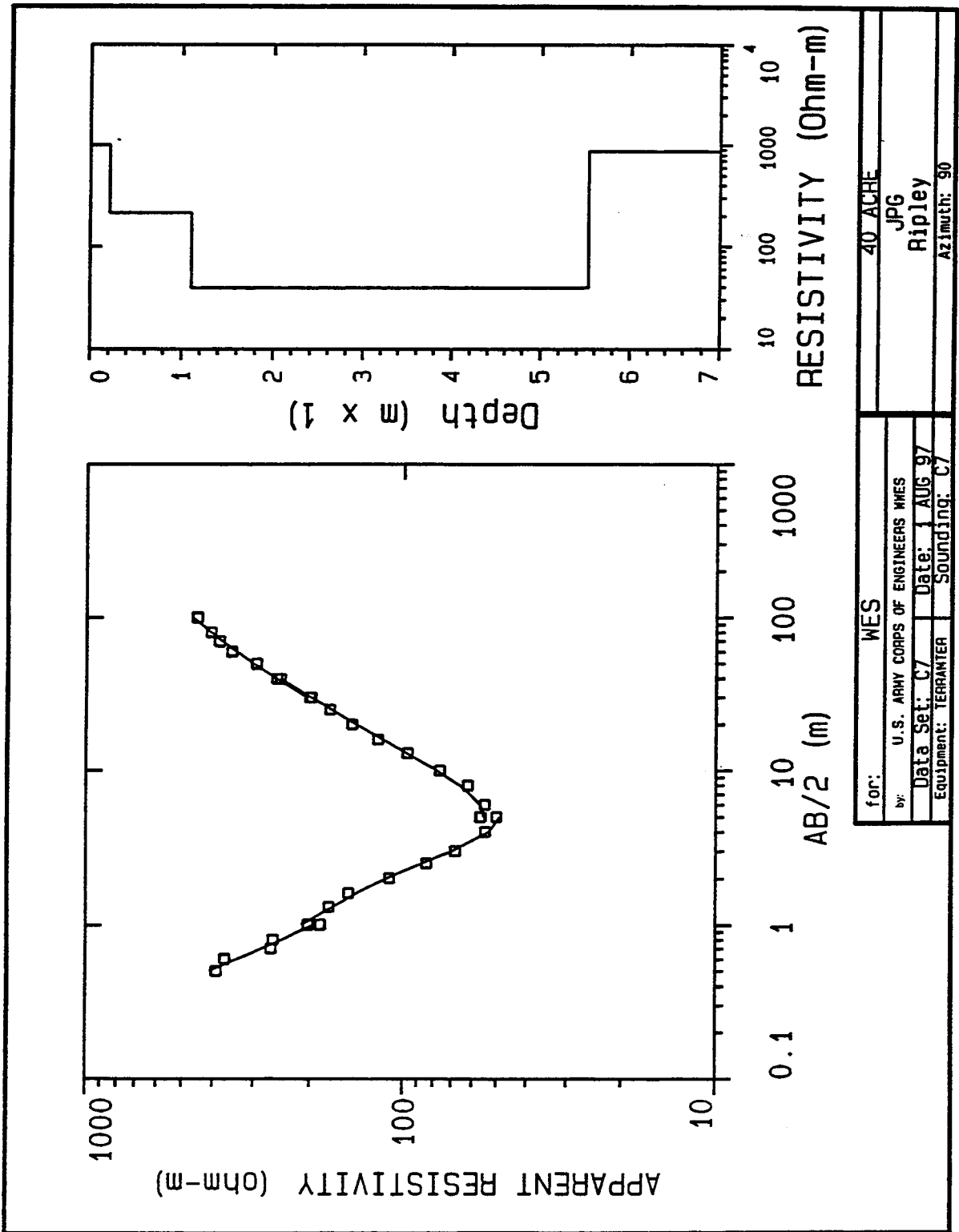


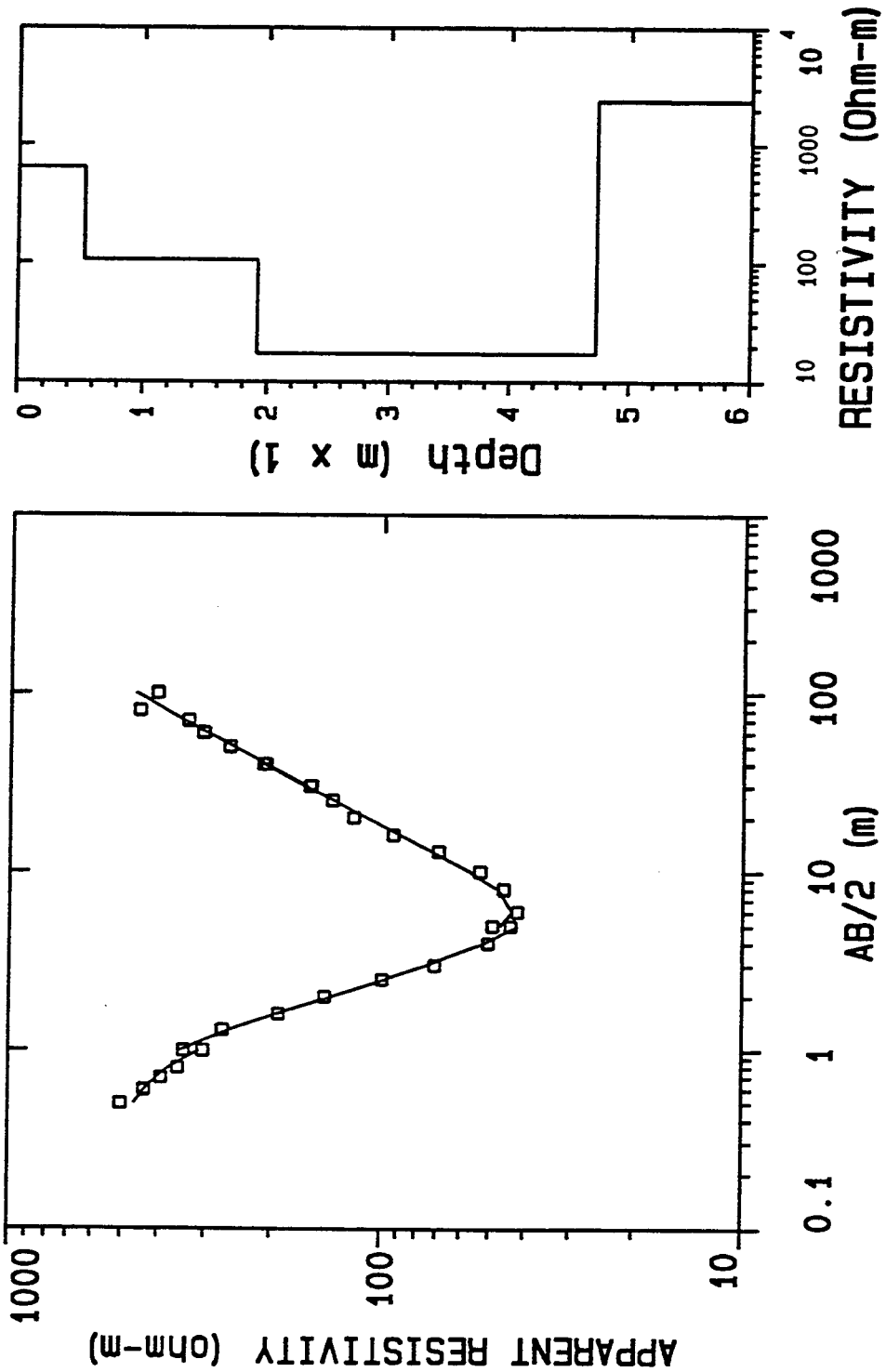
for:	WES	40 ACRE
by:	U.S. ARMY CORPS OF ENGINEERS WNES	JPG
Date Set:	C1	Date: 31 JULY 97
Equipment:	TERRAMETER	Sounding: C1
		Azimuth: 90



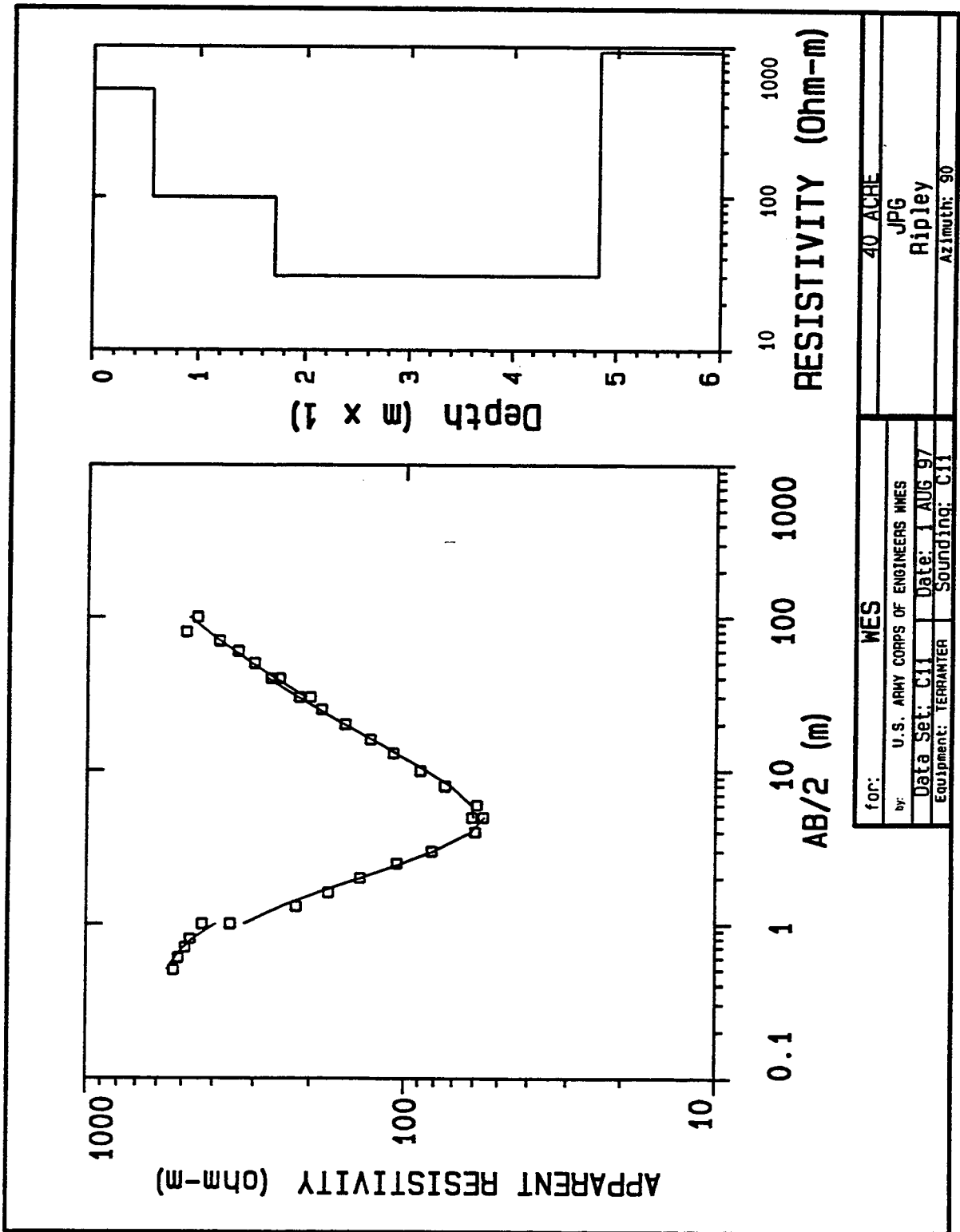


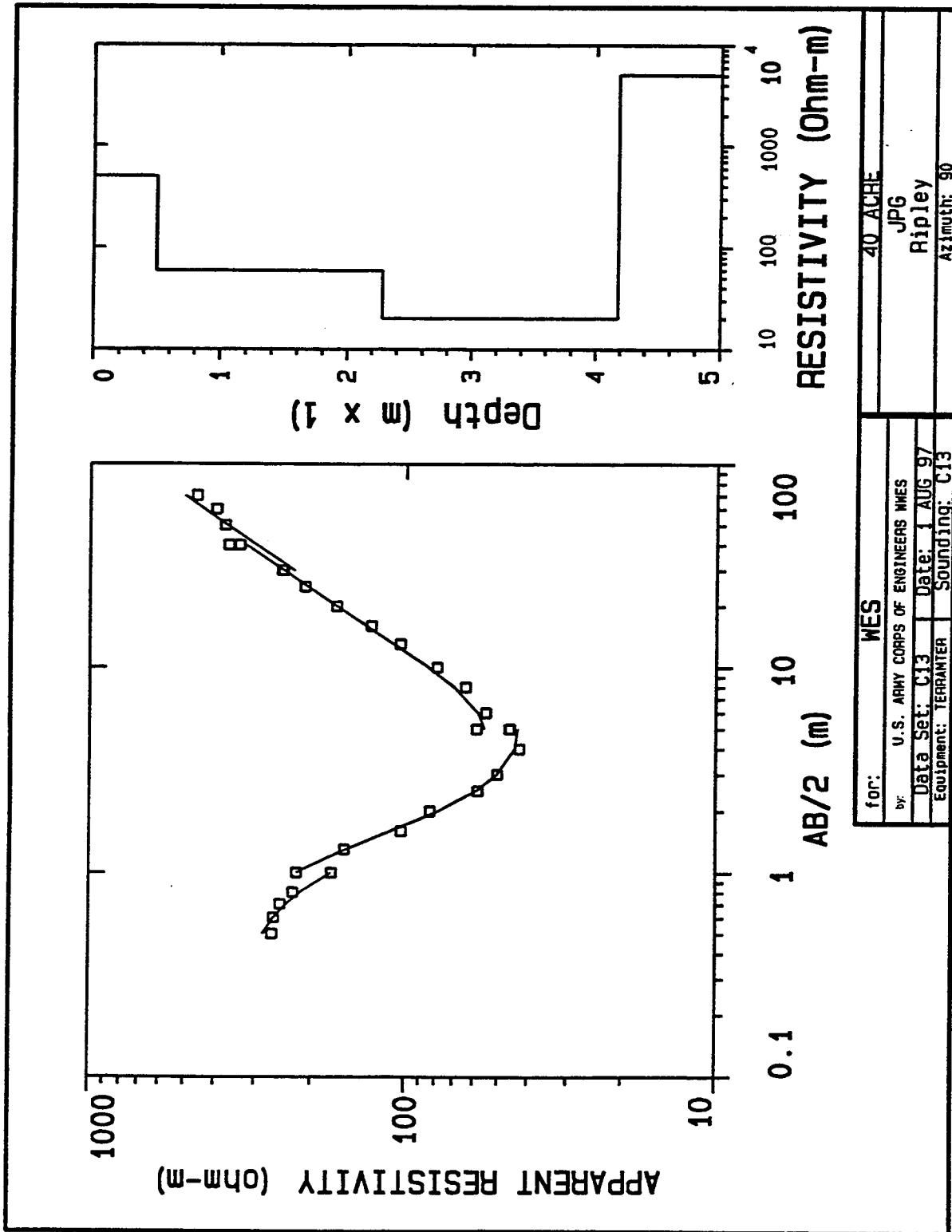
for:	WES	40 ACRE
by:	U.S. ARMY CORPS OF ENGINEERS MMS	JPG
Date Set:	C5	?
Equipment:	TERRAMETER	Sounding: C5
		Azimuth: 90

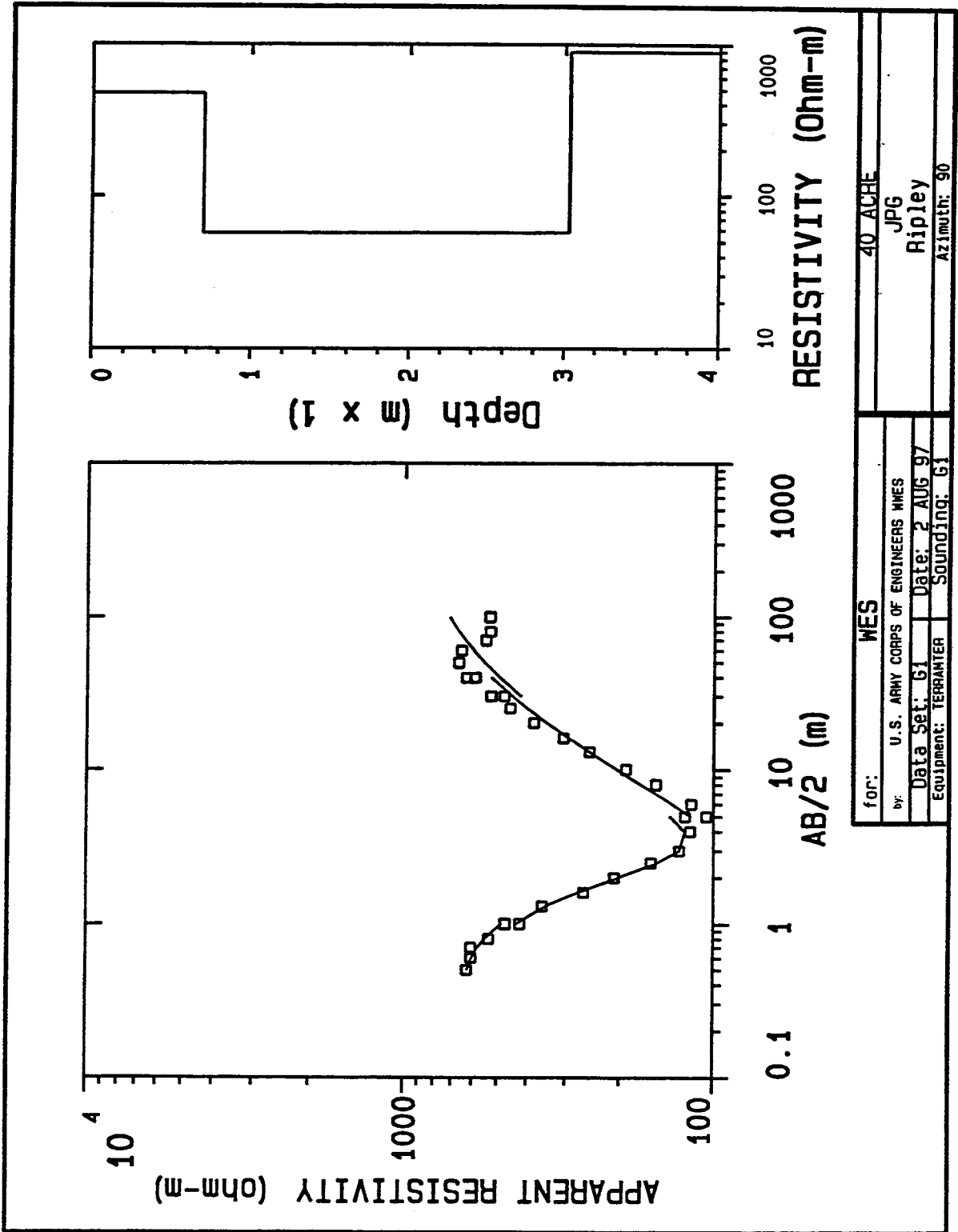


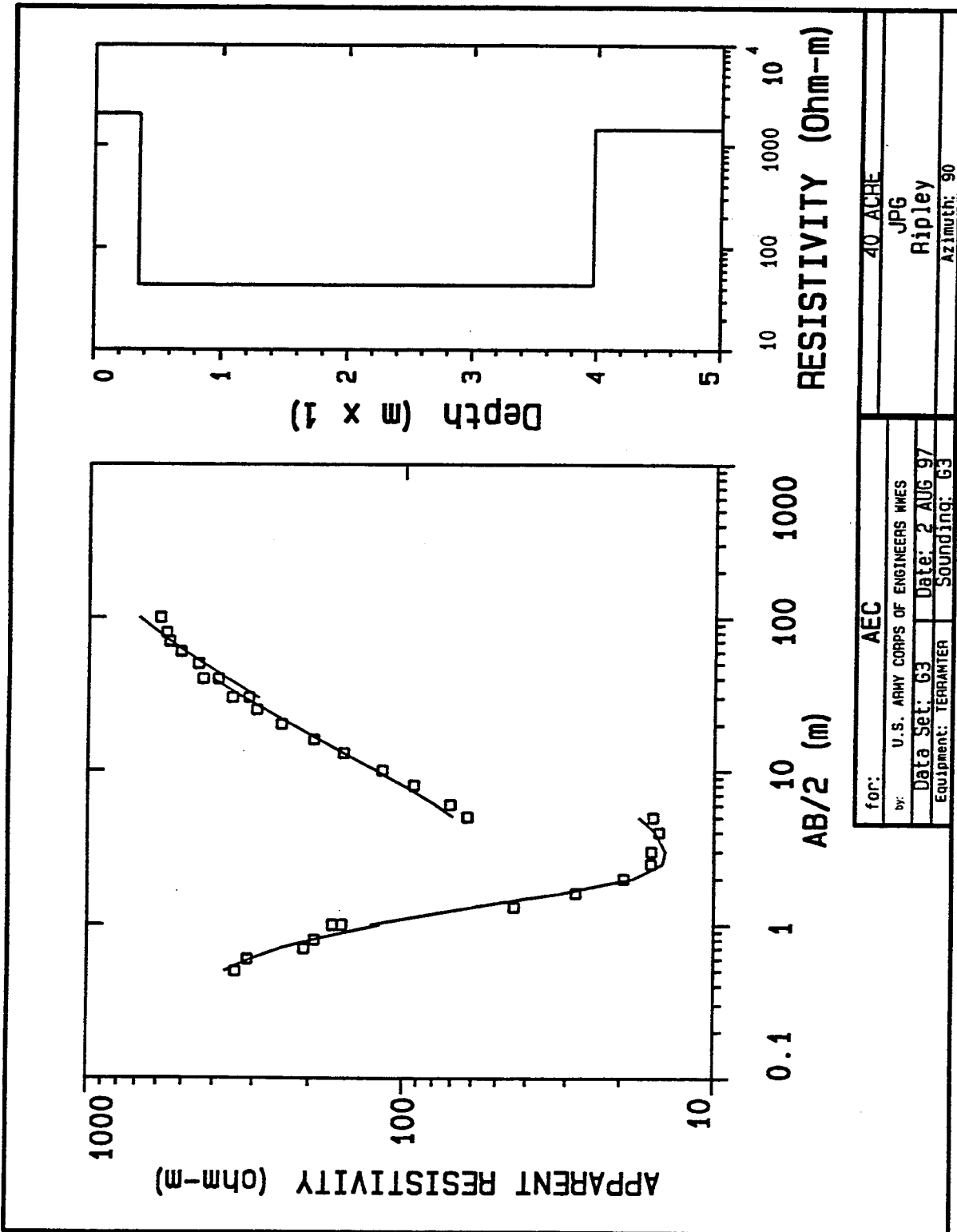


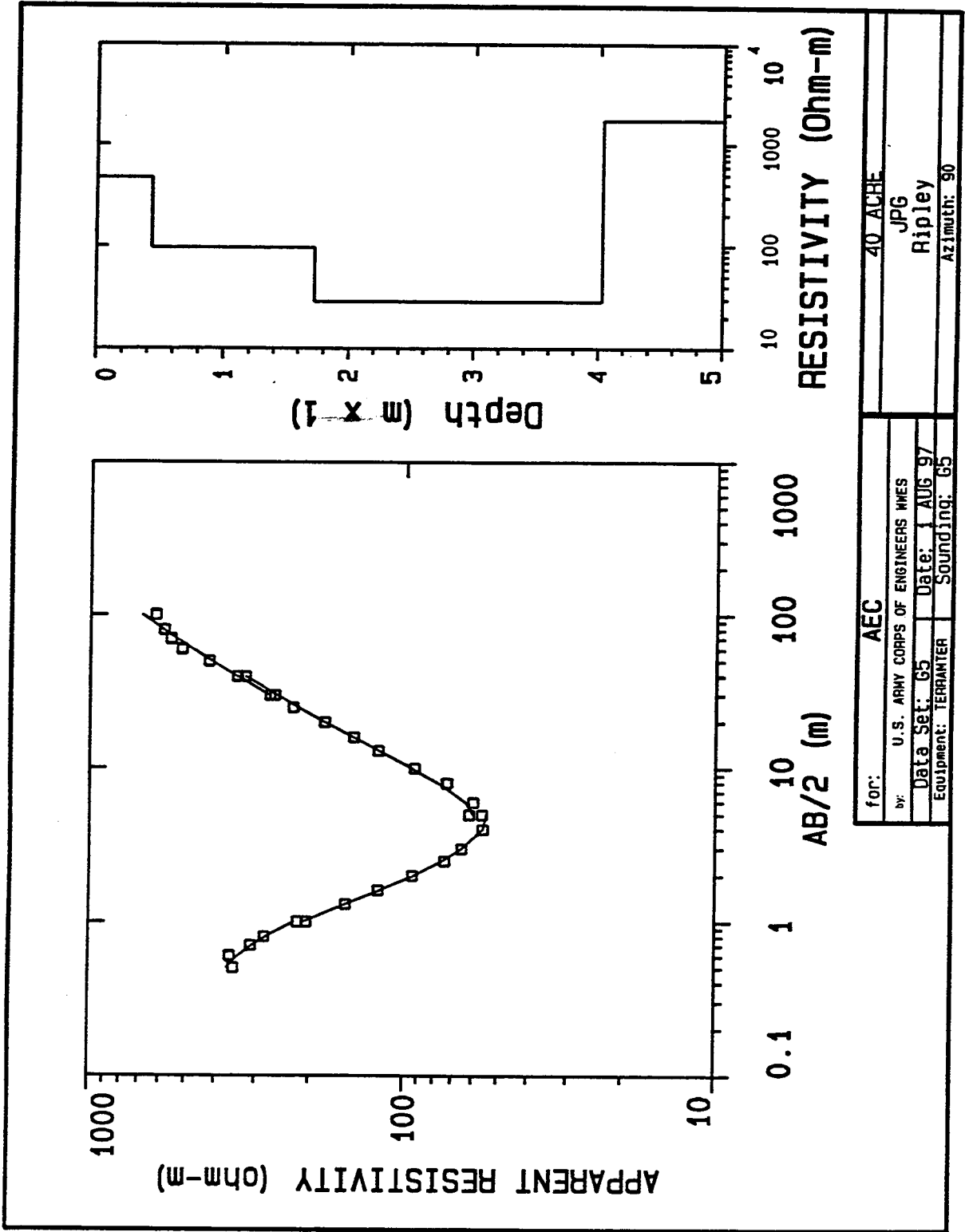
for:	WES		
by:	U.S. ARMY CORPS OF ENGINEERS MHES		
Date Set:	C9	Date:	
Equipment:	TERRANTER	Sounding:	C9
	40 ACRE	JPG	Ripley
			Azimuth: 90

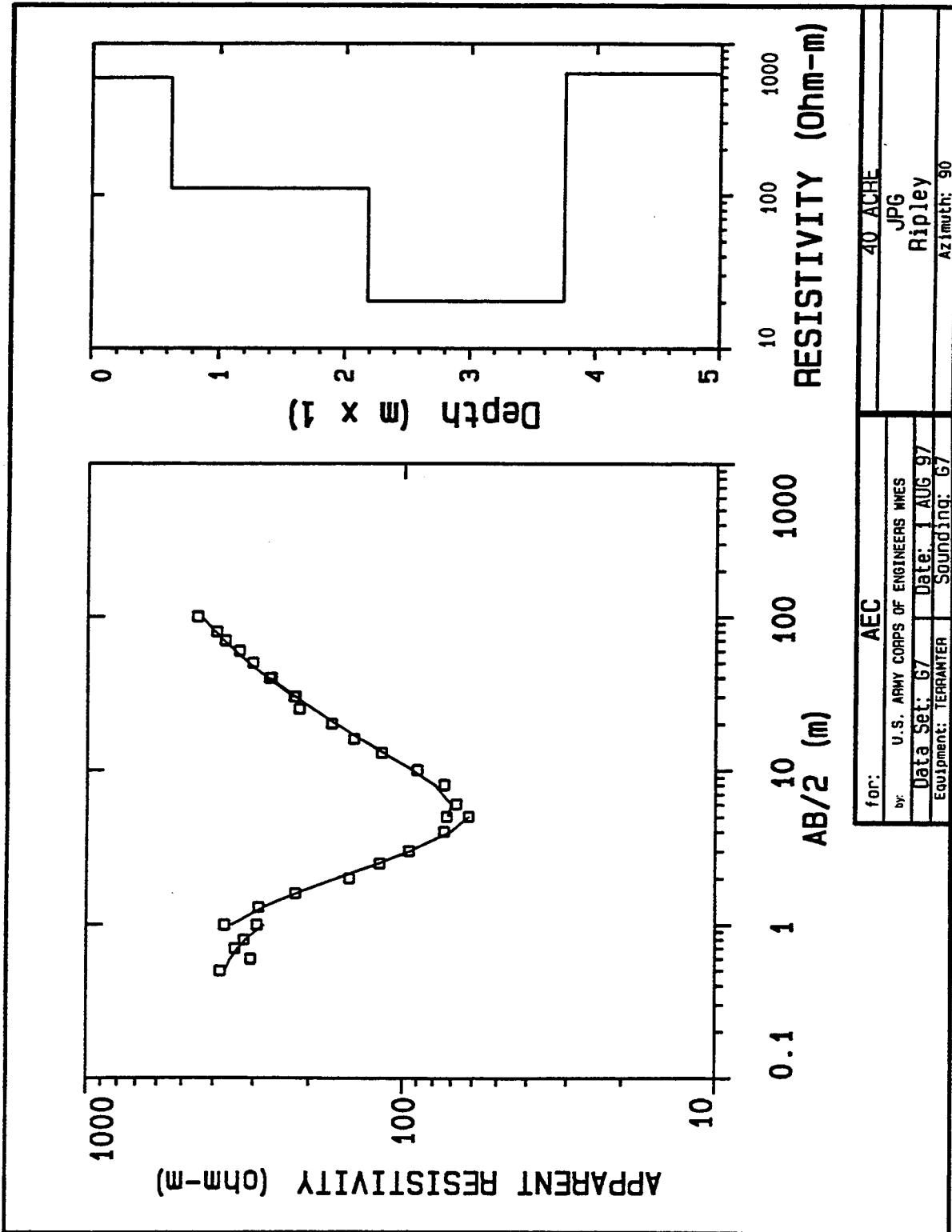




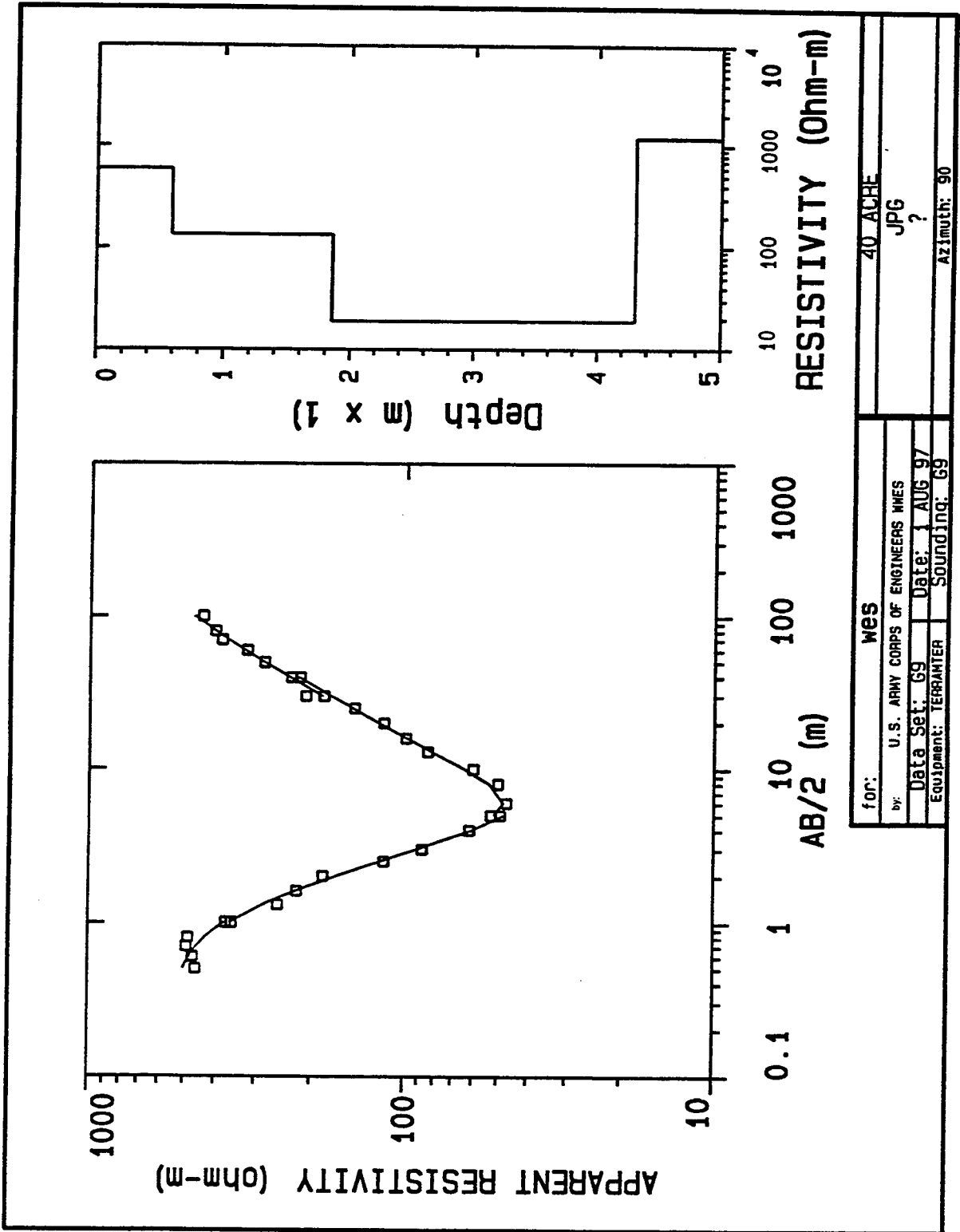


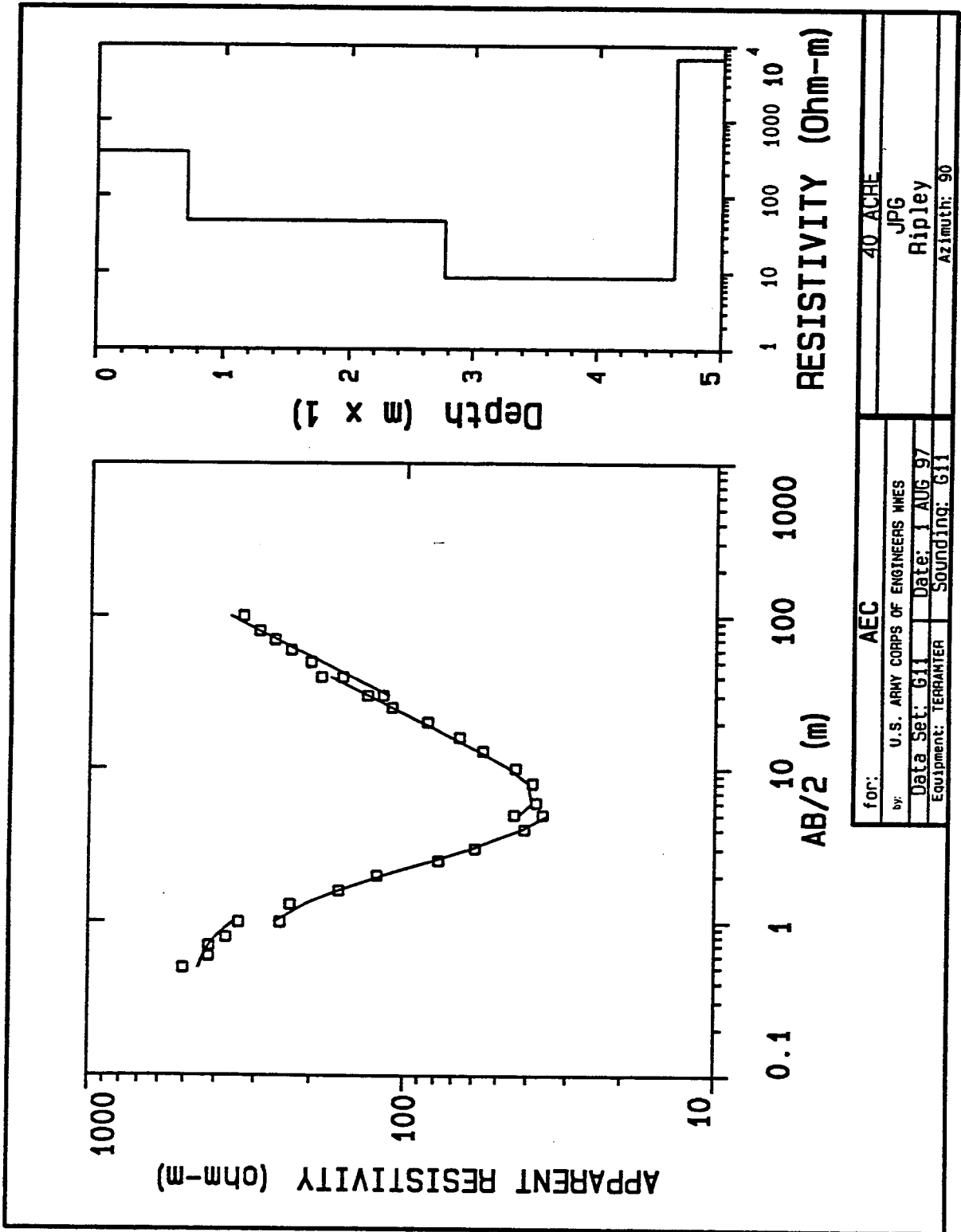


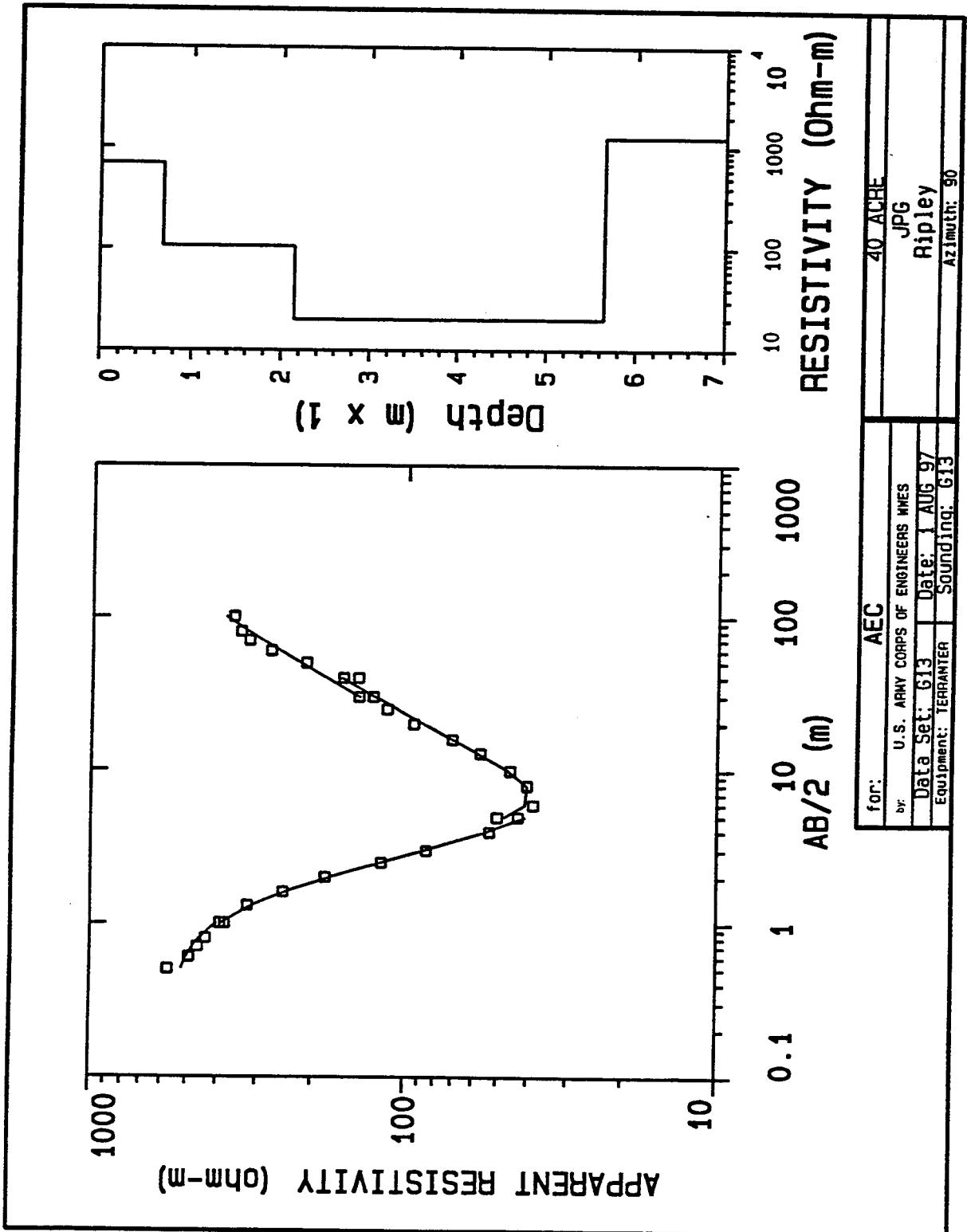


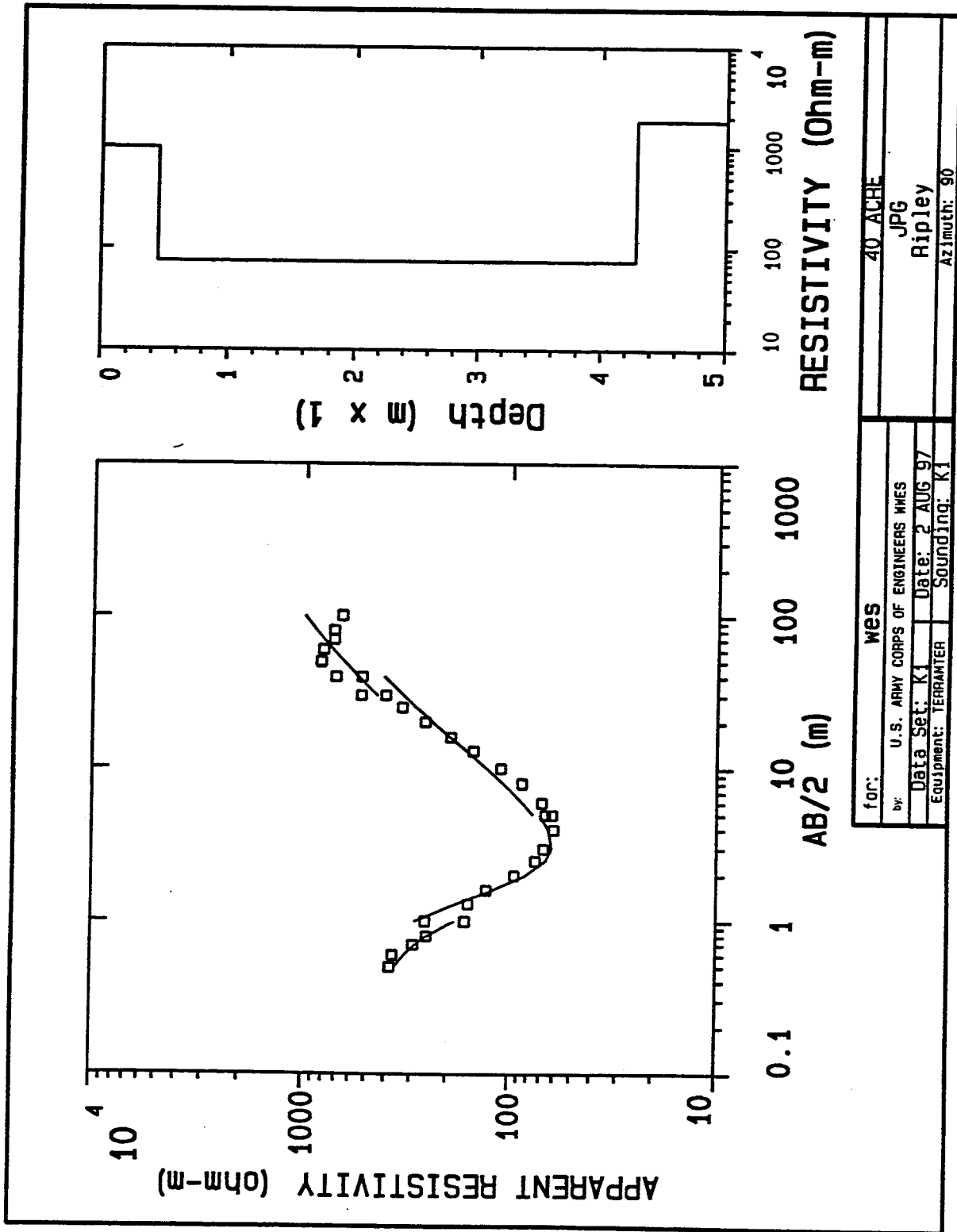


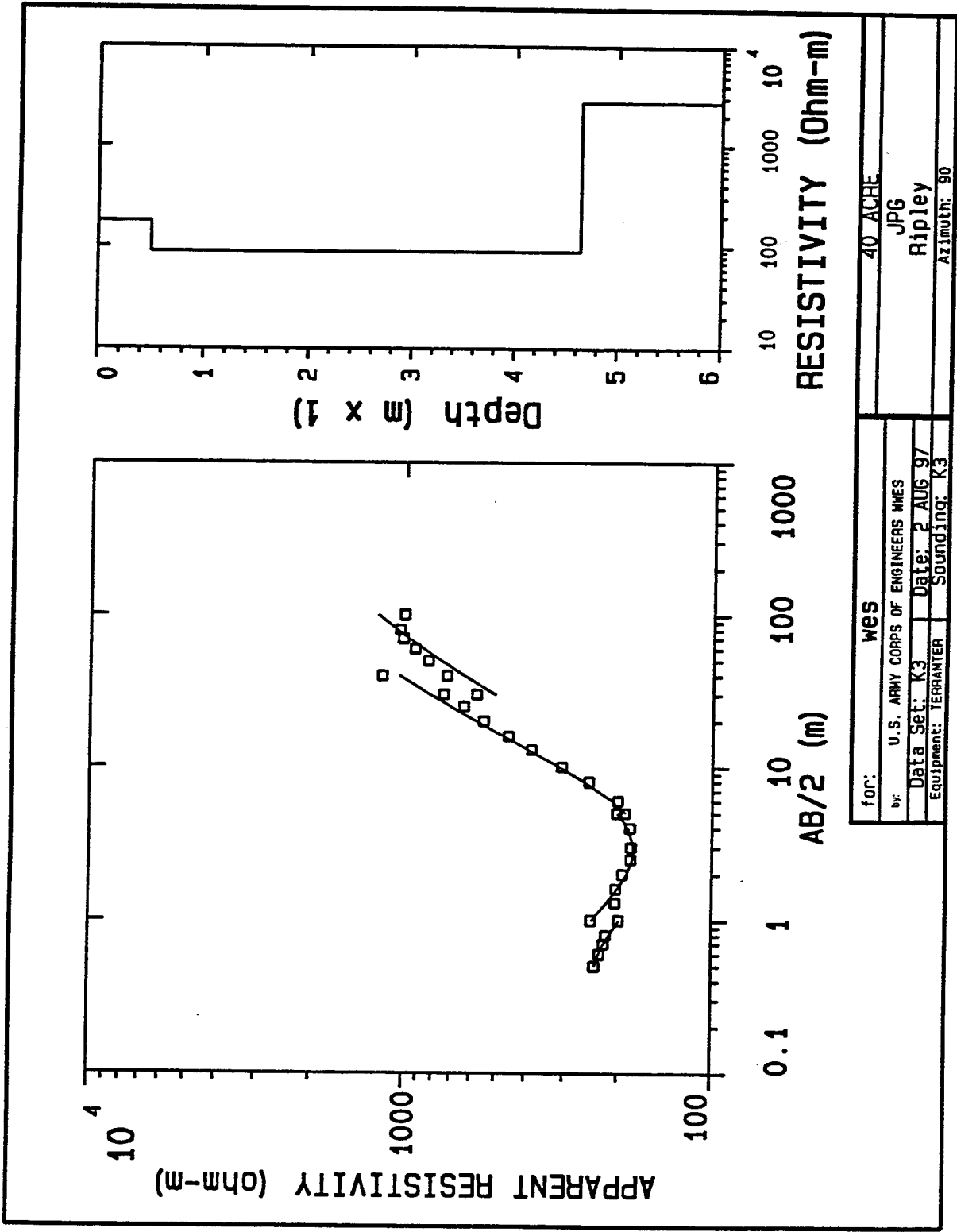
for: **AEC**
 U.S. ARMY CORPS OF ENGINEERS WNES
 by: **JPG**
Ripley
 Date: **1 AUG 97**
 Equipment: **TERRAMETER** Sounding: **G7**
 Azimuth: **90**
 for: **40 ACRE**

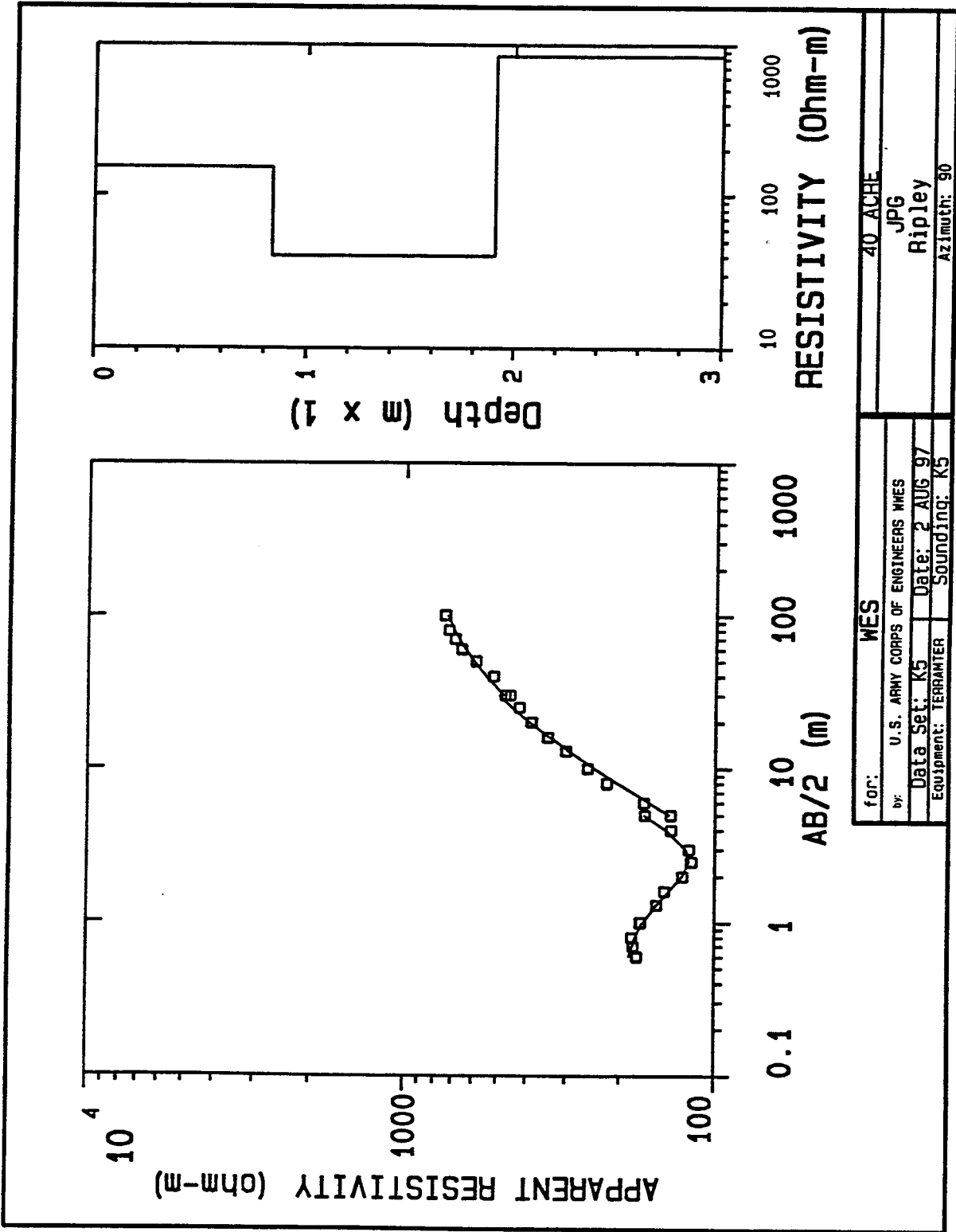


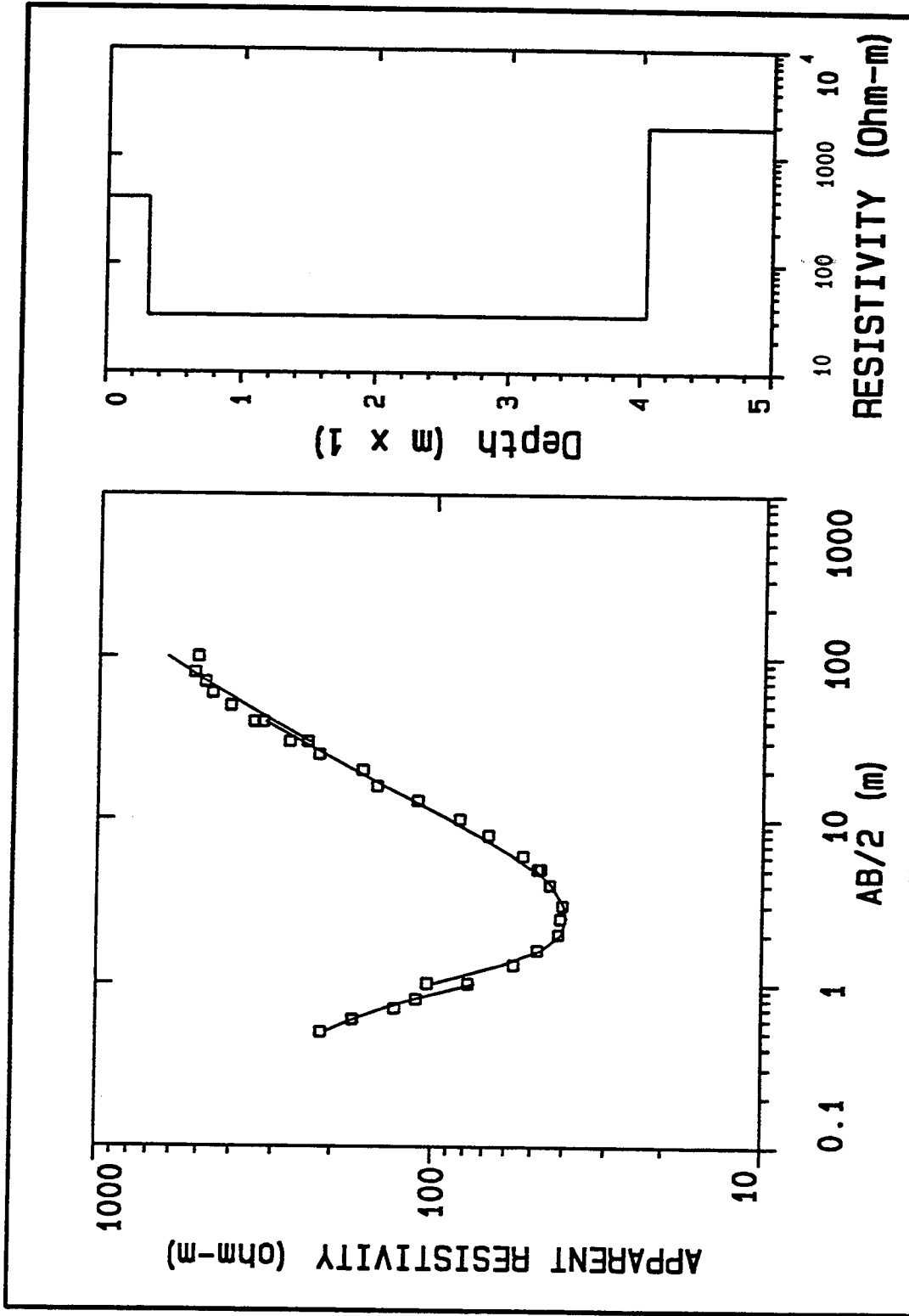




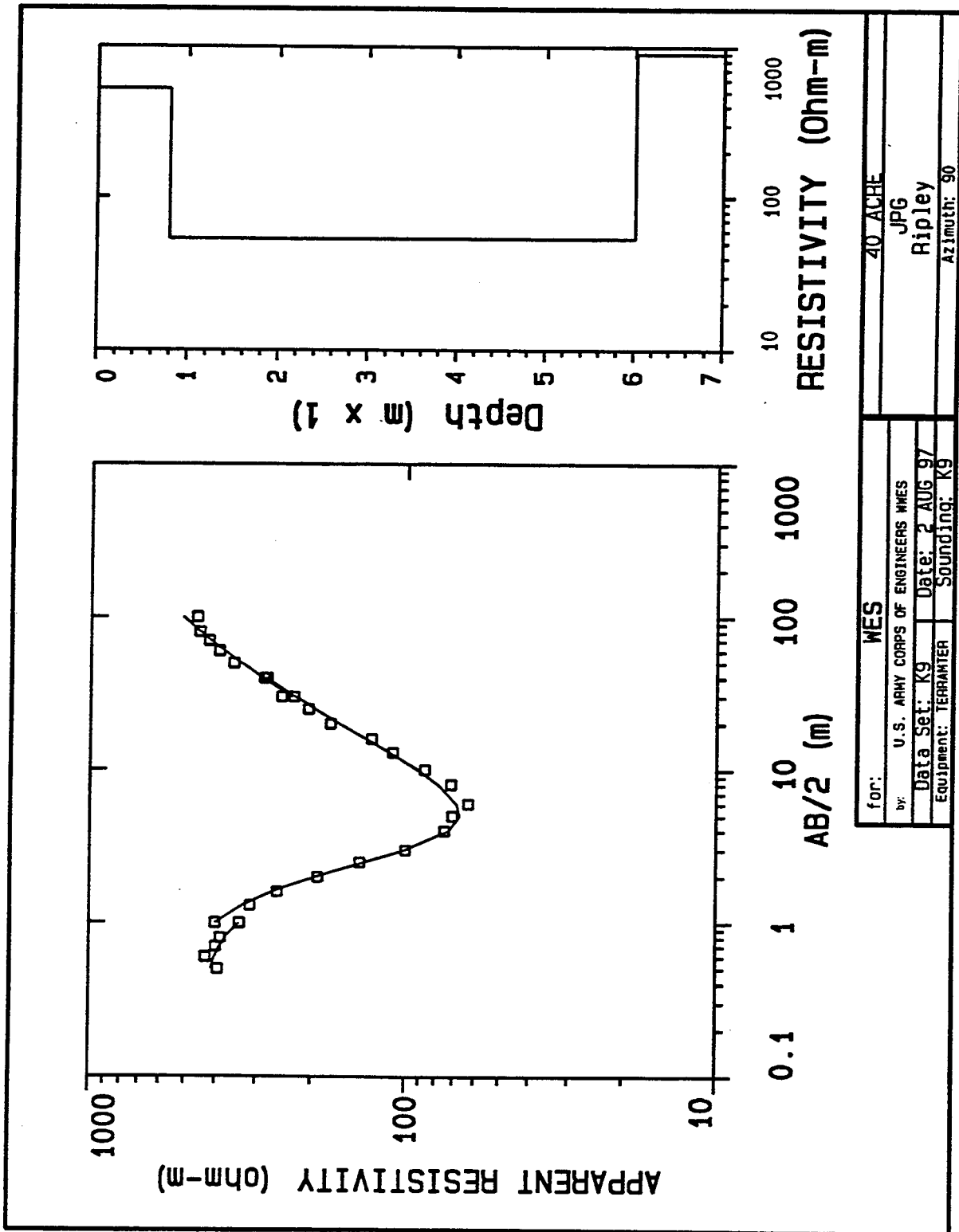


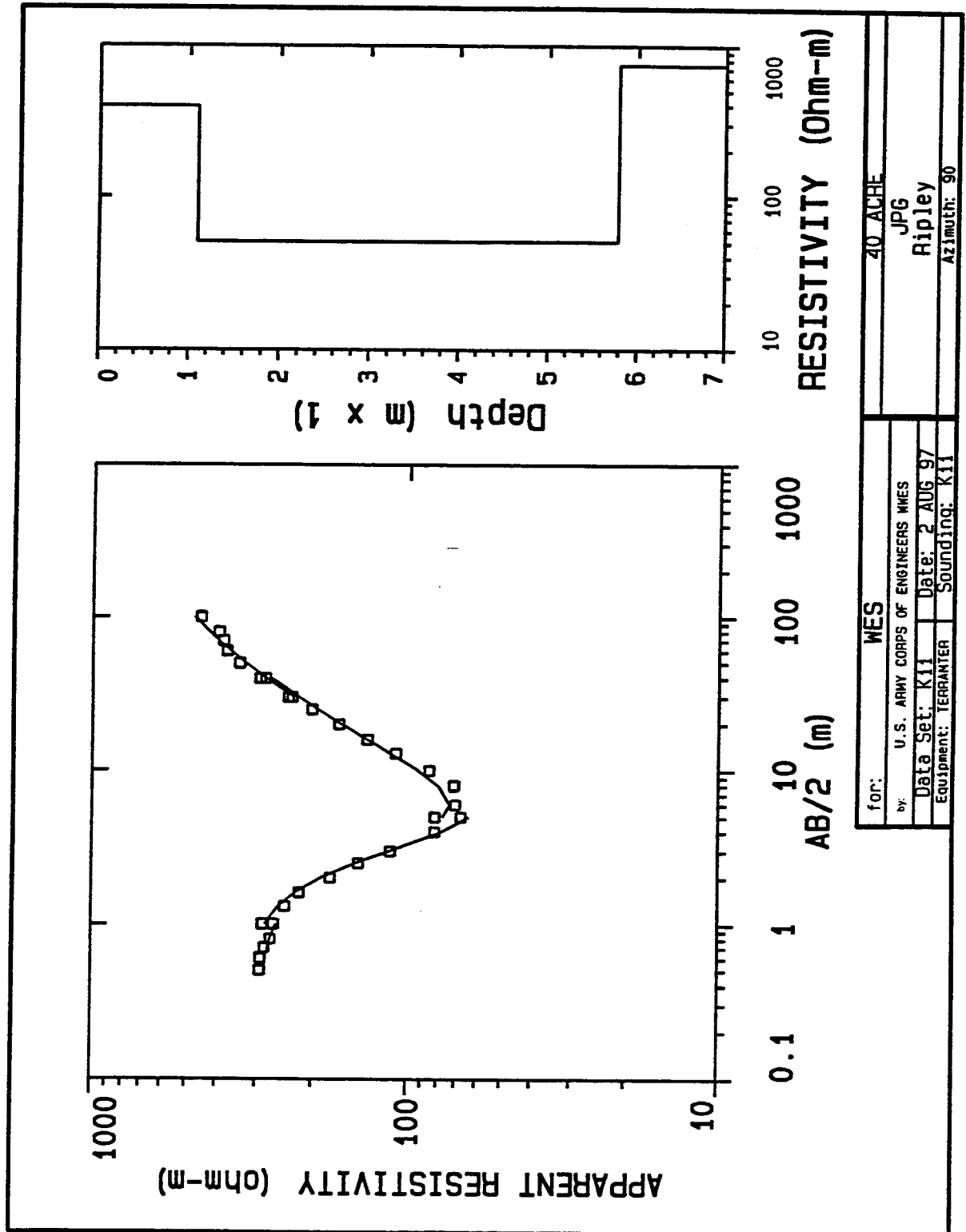


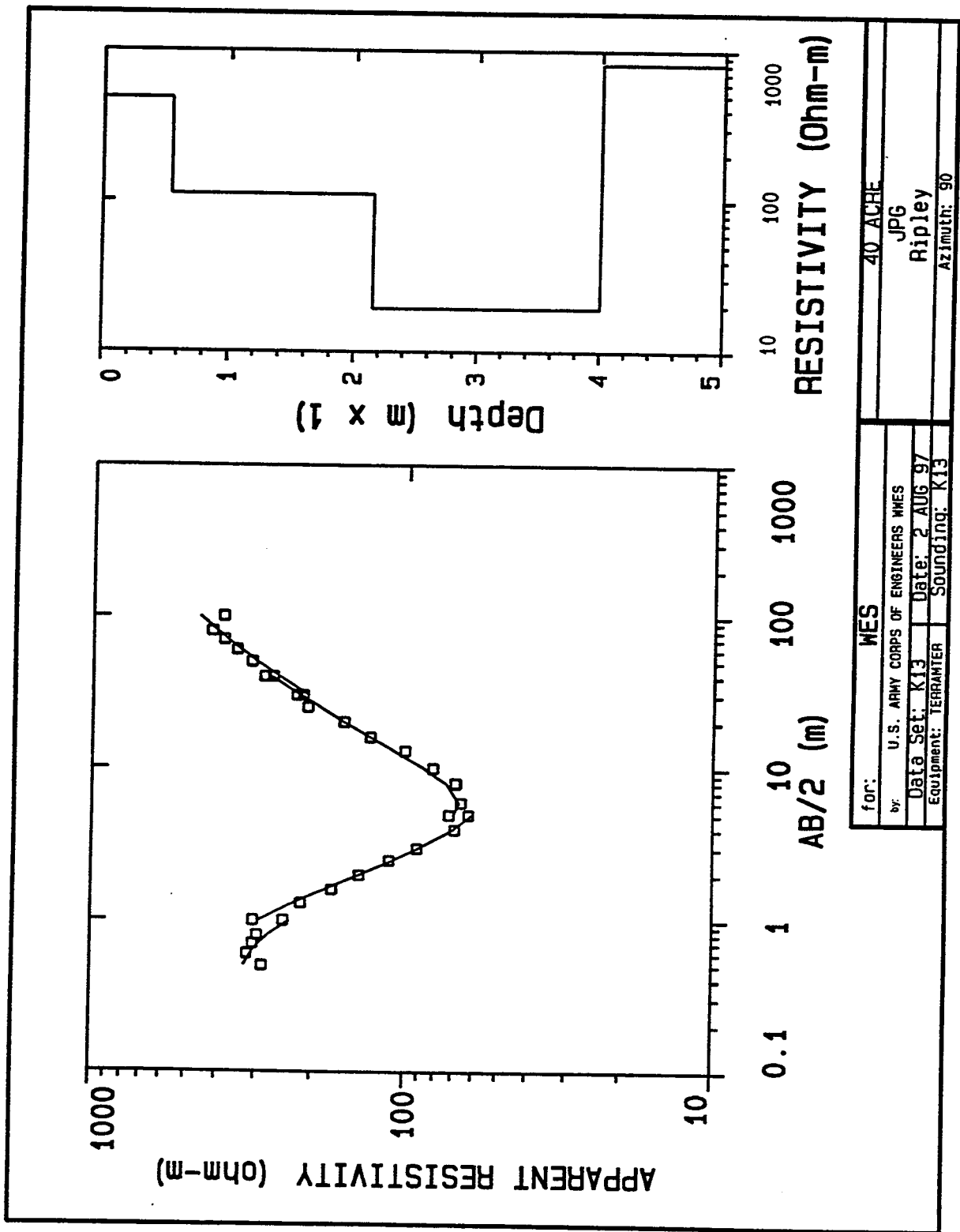


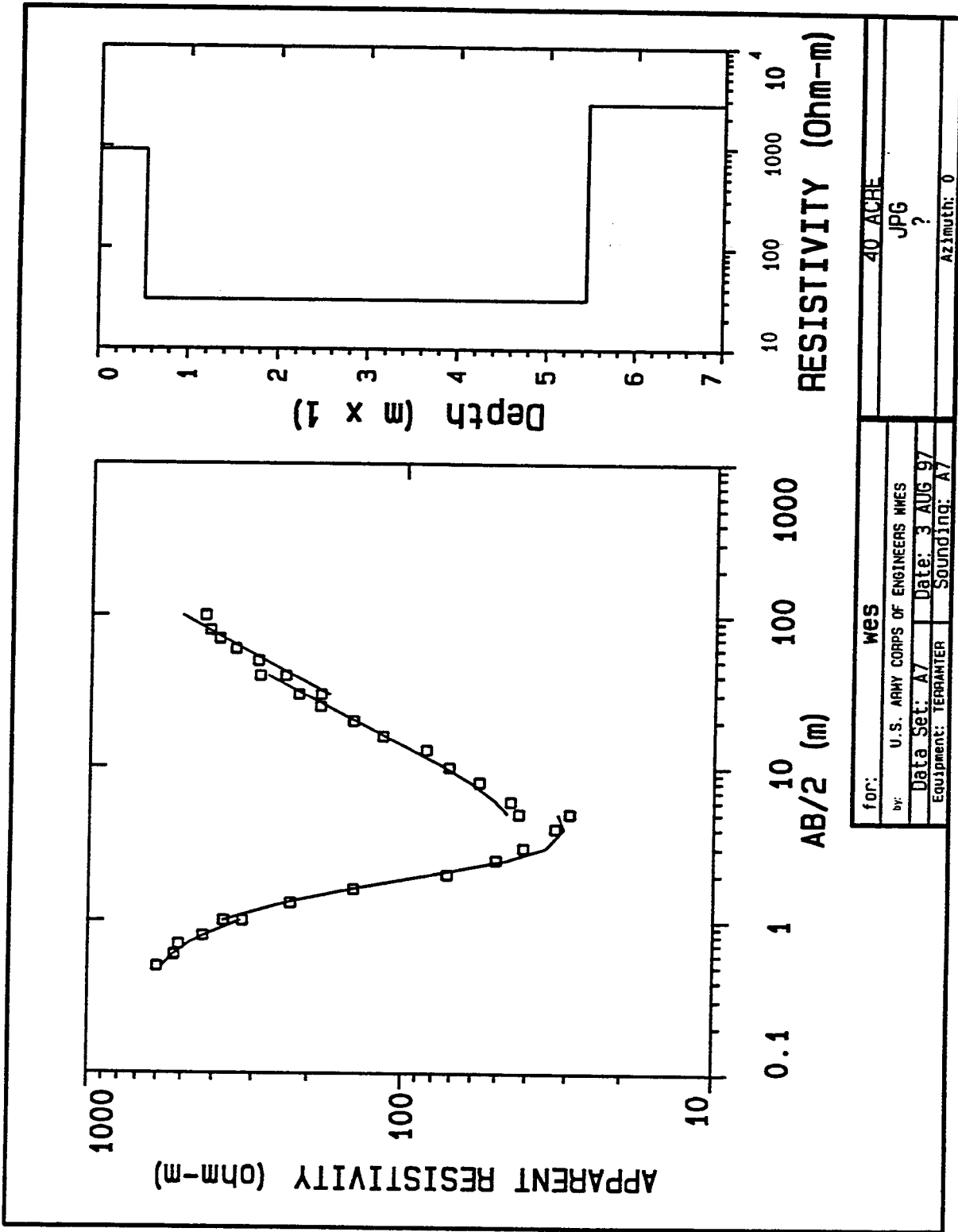


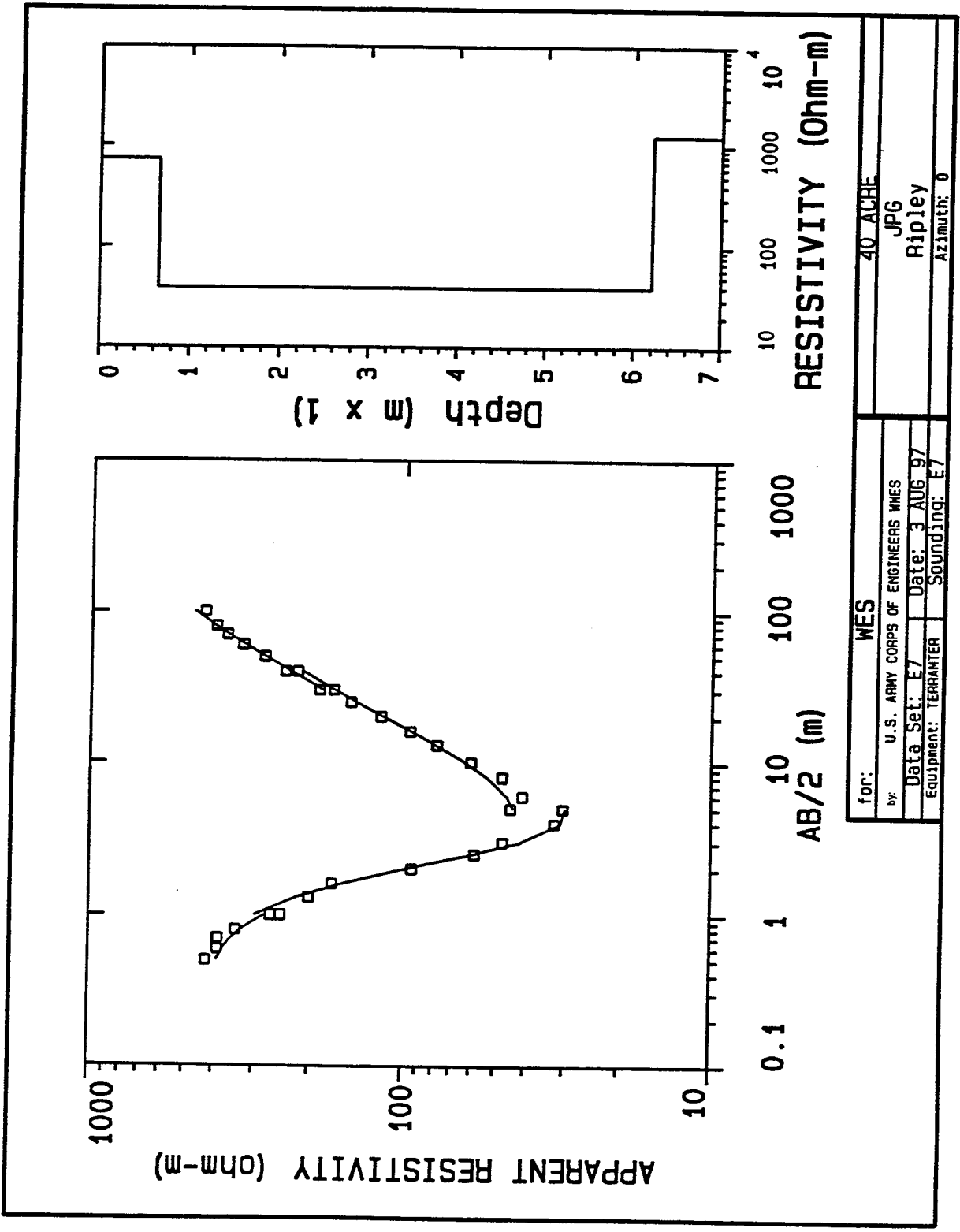
for: WES		40 ACRE	
by: U.S. ARMY CORPS OF ENGINEERS WES		JPG	
Data Set: K7	Date: 2 AUG 97	Ripley	
Equipment: TERRAMETER	Sounding: K7	Azimuth: 90	



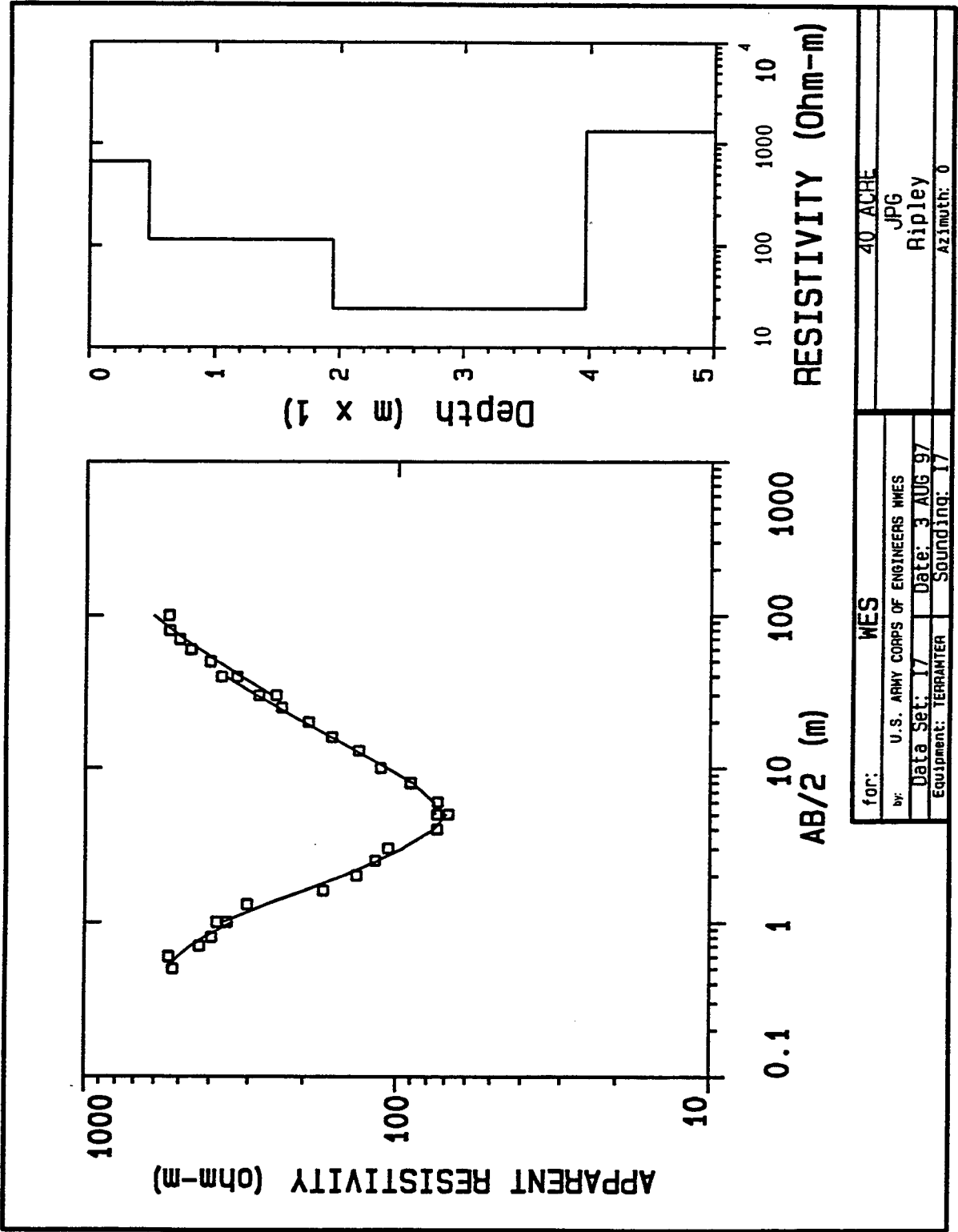


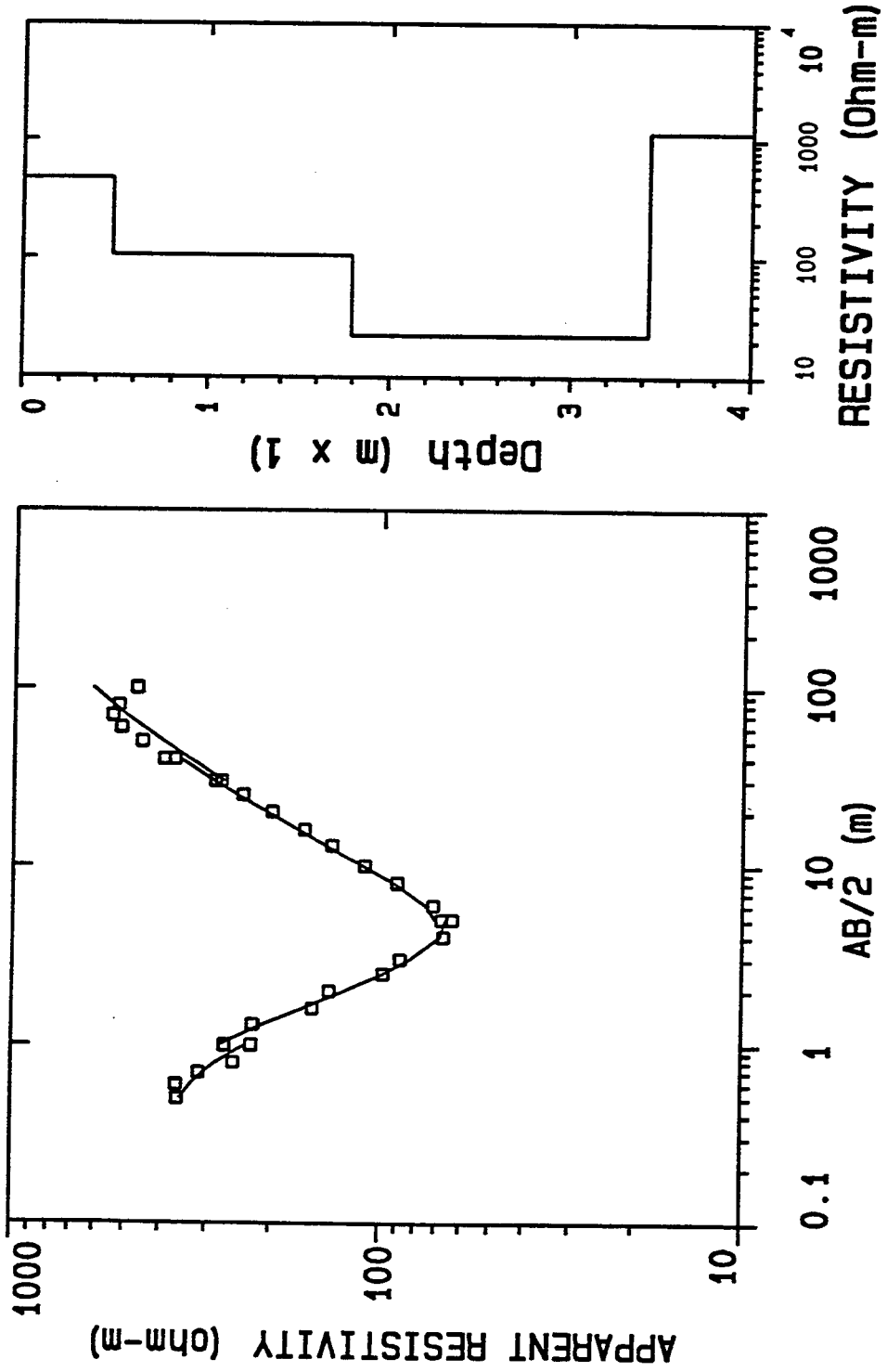






for:	MES	
by:	U.S. ARMY CORPS OF ENGINEERS WMS	
Data Set:	E7	Date: 3 AUG 97
Equipment:	TERRANTER	Sounding: E7
	40 ACRE	JPG
		Ripley
		Azimuth: 0



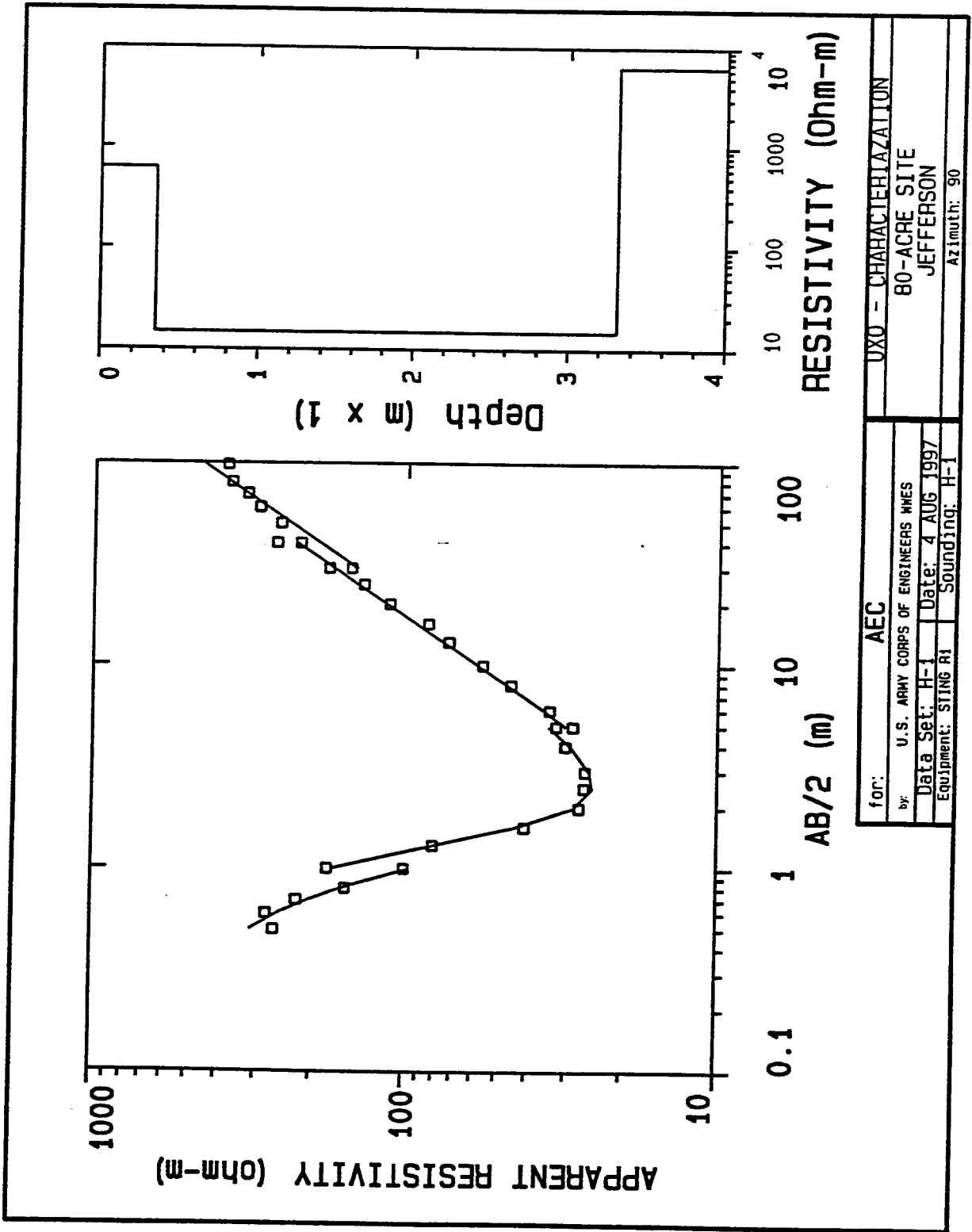


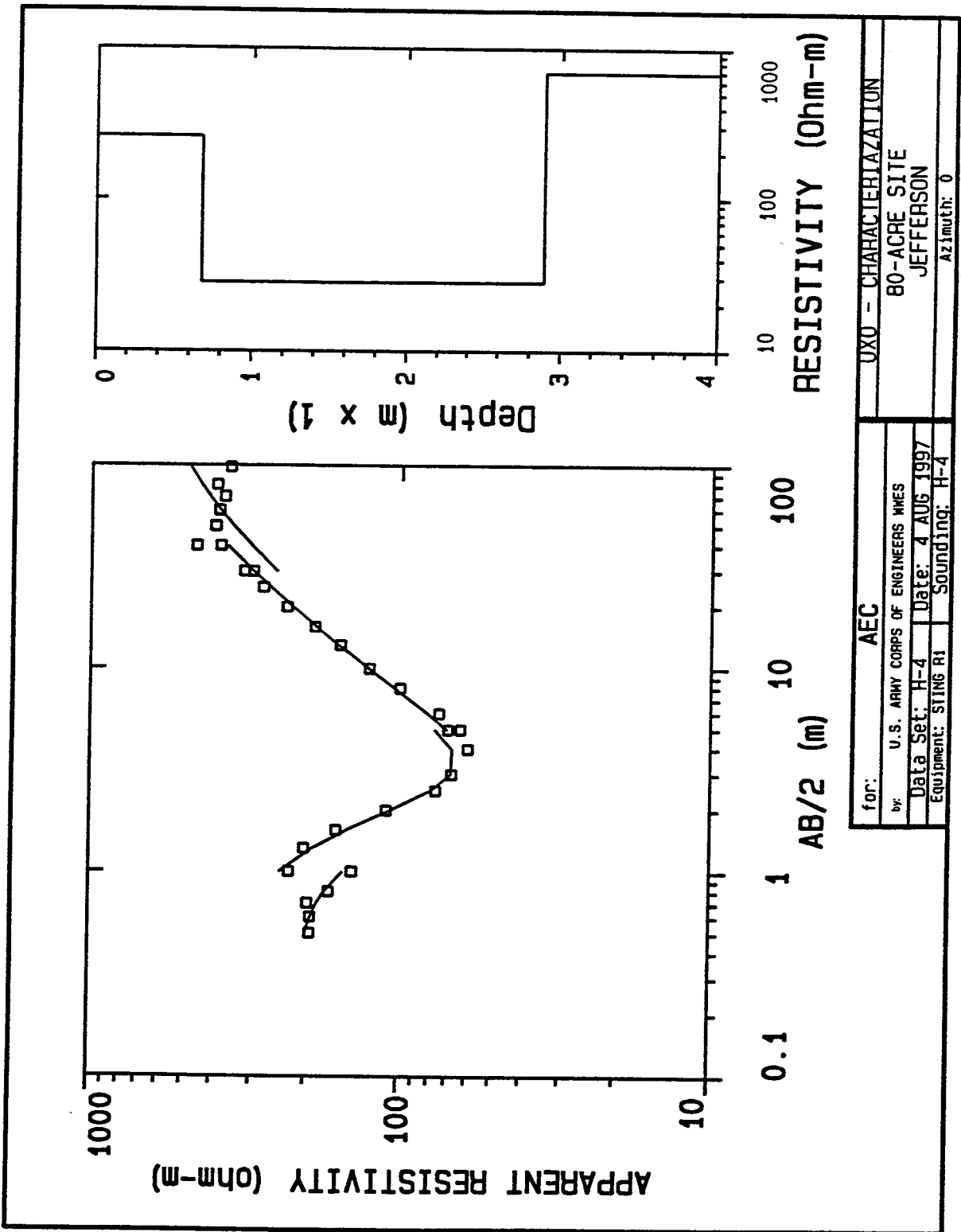
for:	WES		
by:	U.S. ARMY CORPS OF ENGINEERS WES		
Data Set:	M7	Date:	3 AUG 97
Equipment:	TERRAMETER	Sounding:	M7
	40 ACRE	JPG	ripley
			Azimuth: 0

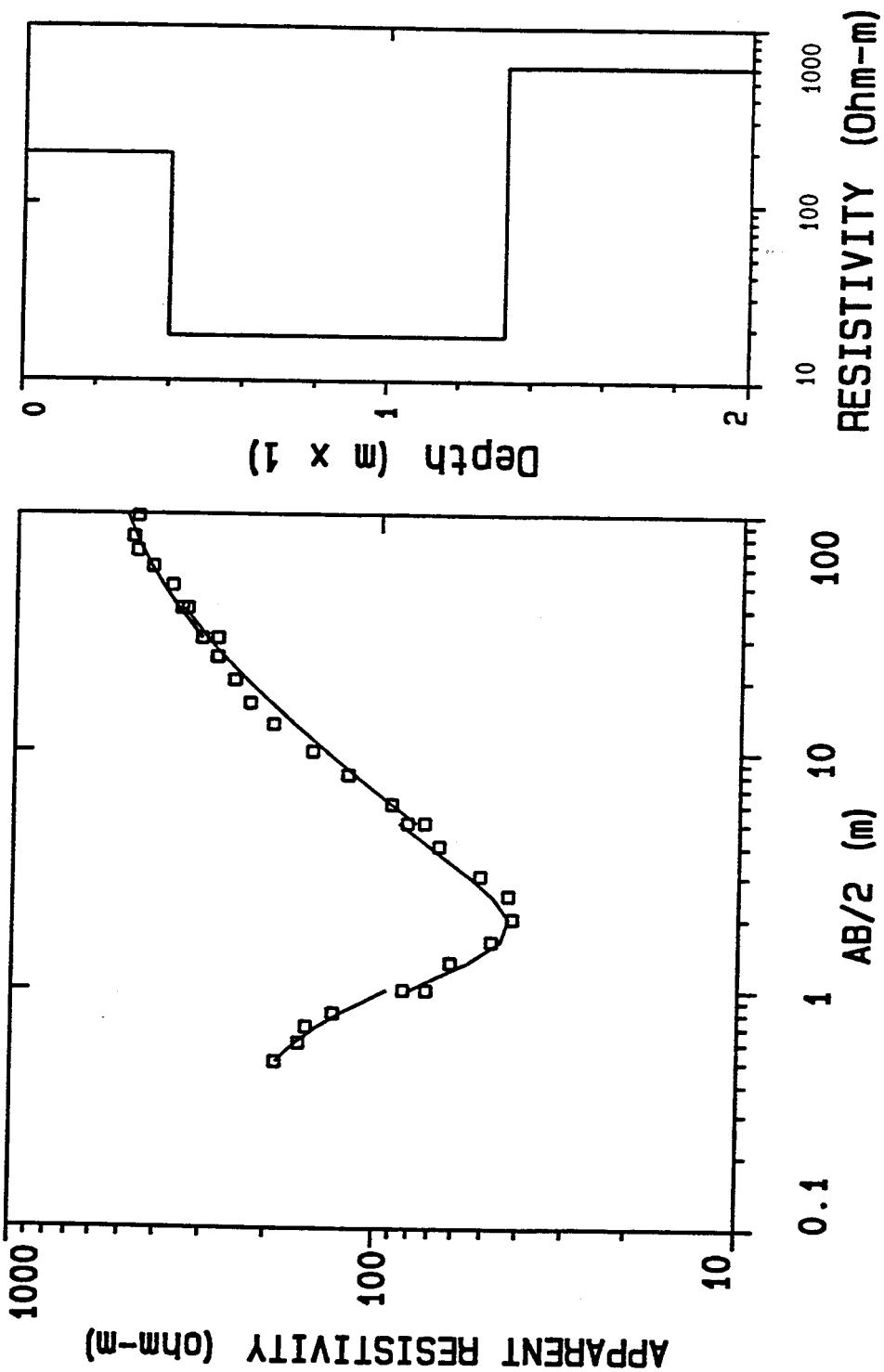
Appendix F

Vertical Electric Sounding

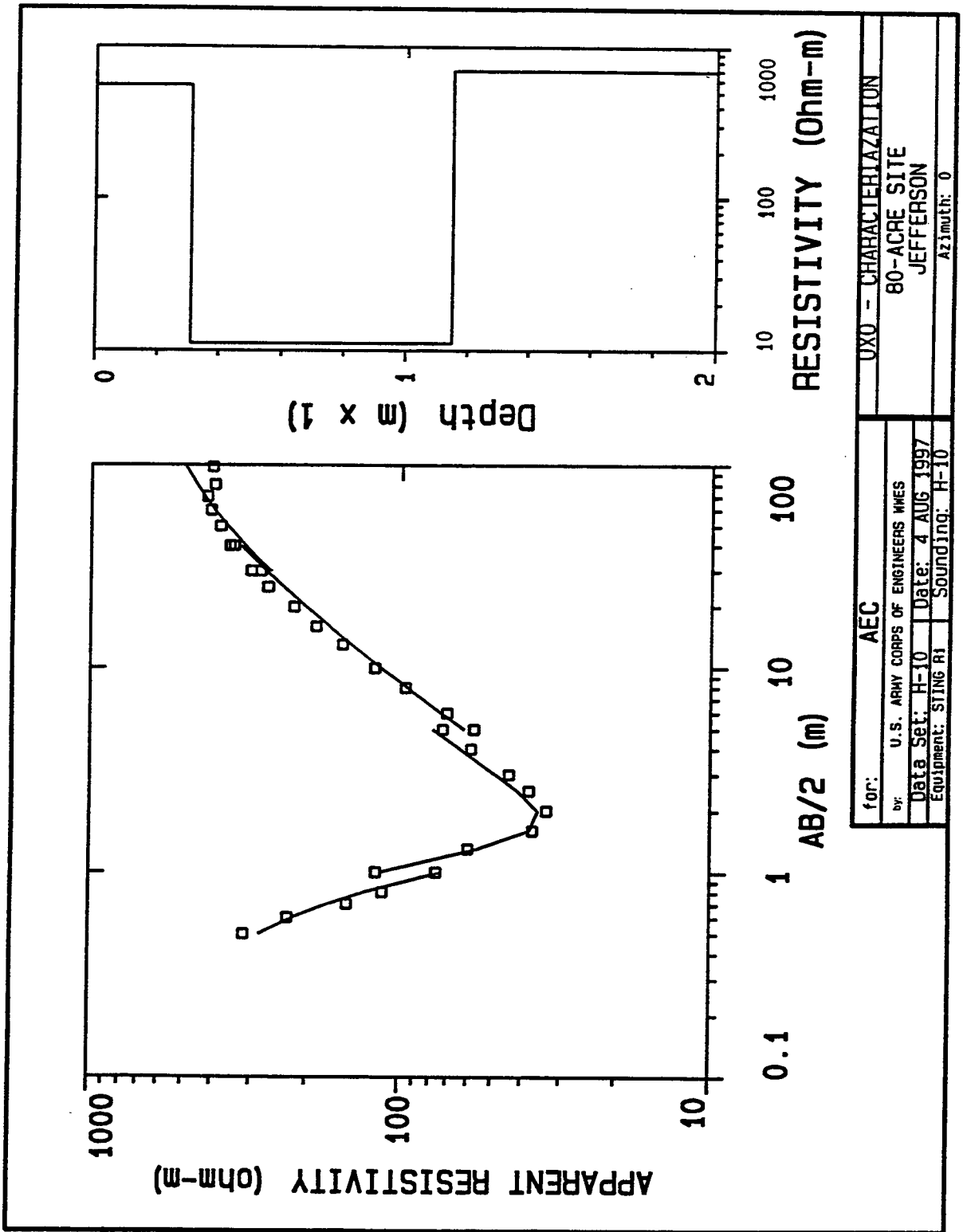
Curves: 80-acre Site

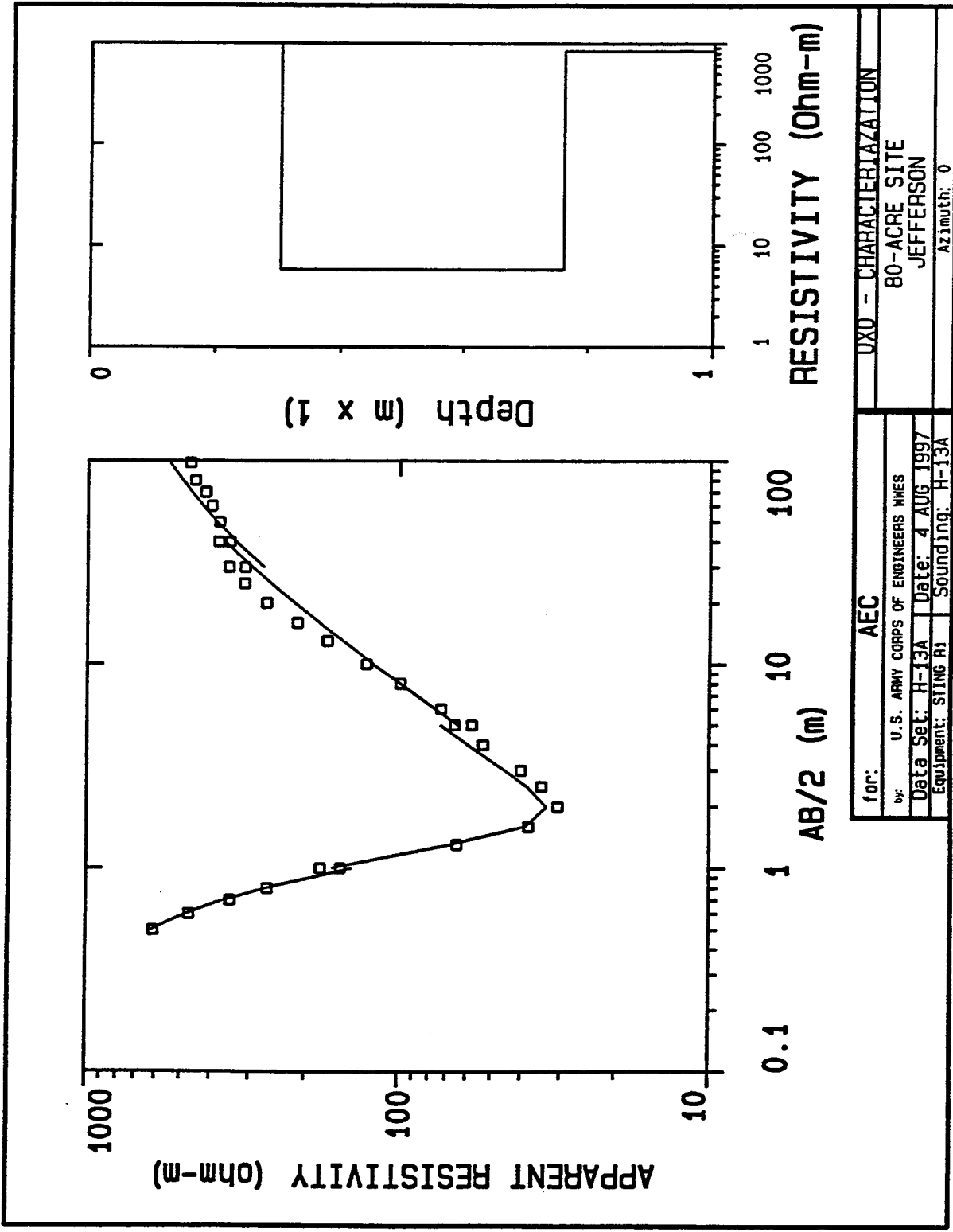


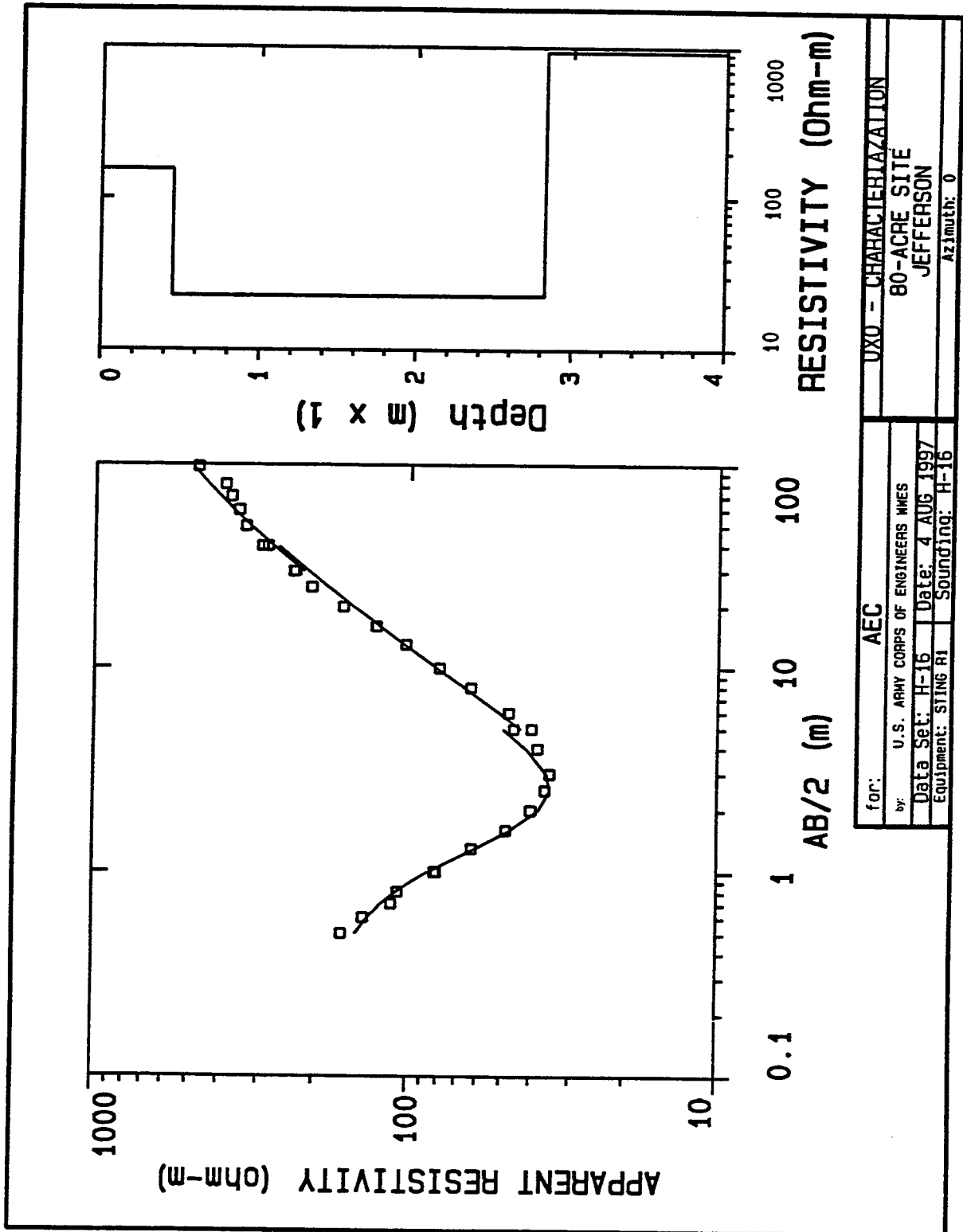


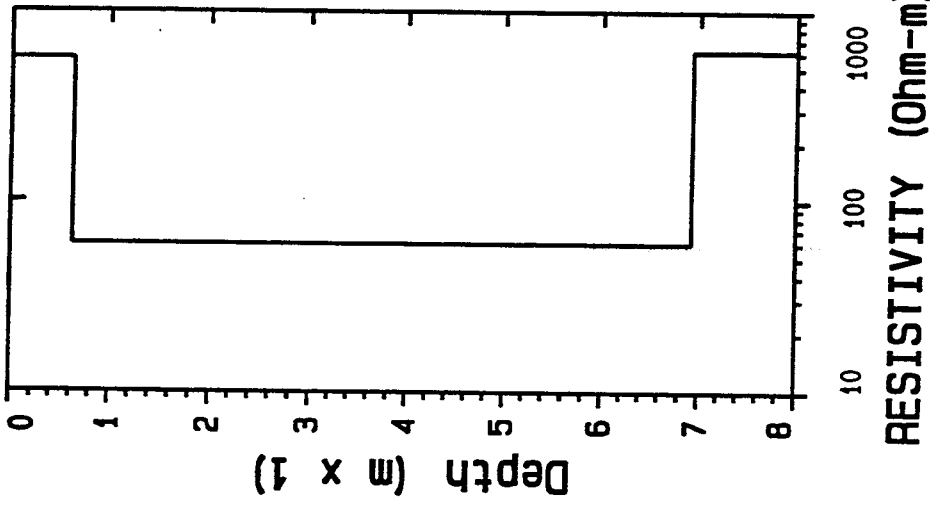
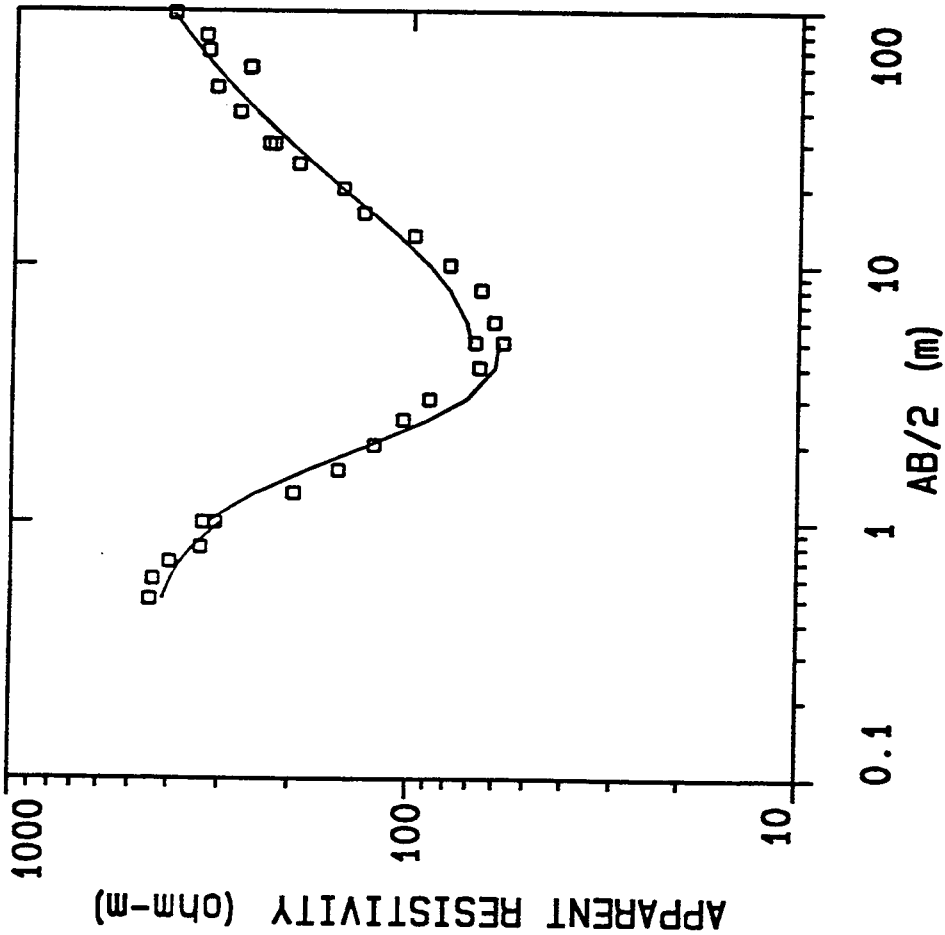


for:	AEC	UXO - CHARACTERIZATION
by:	U.S. ARMY CORPS OF ENGINEERS WMS	80-ACRE SITE
Data Set:	H-7	JEFFERSON
Equipment:	STING R1	Sounding: H-7
		Azimuth: 0

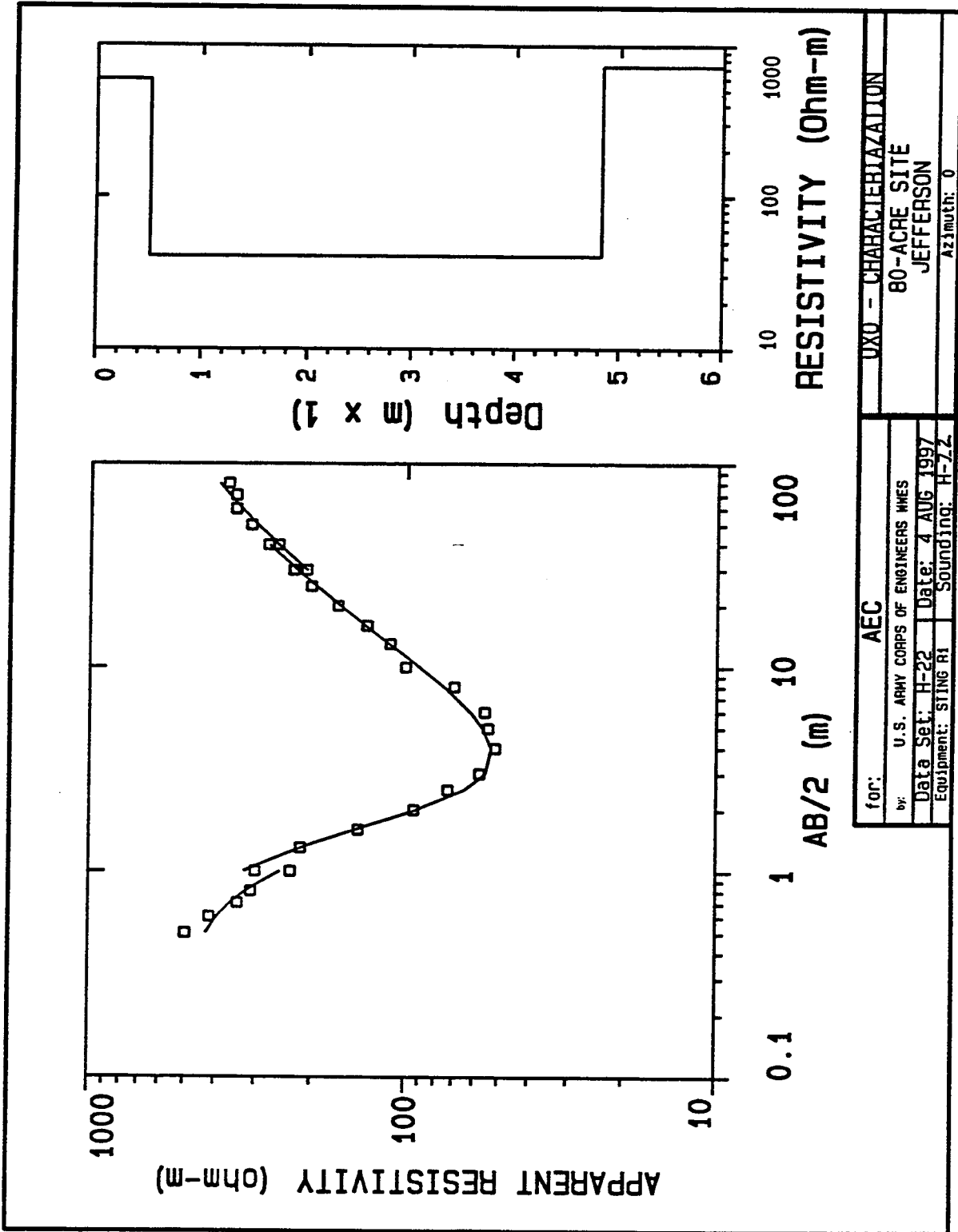




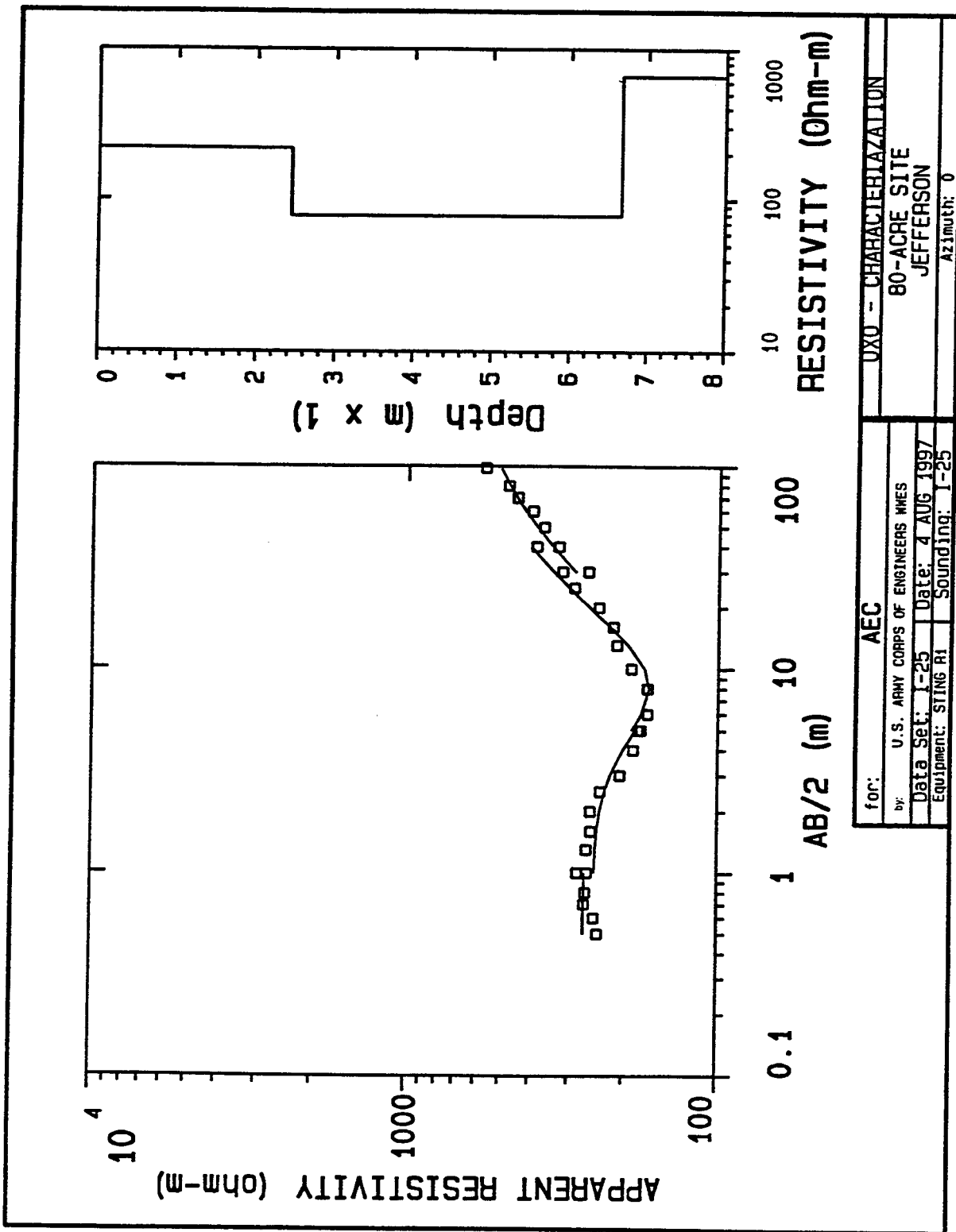


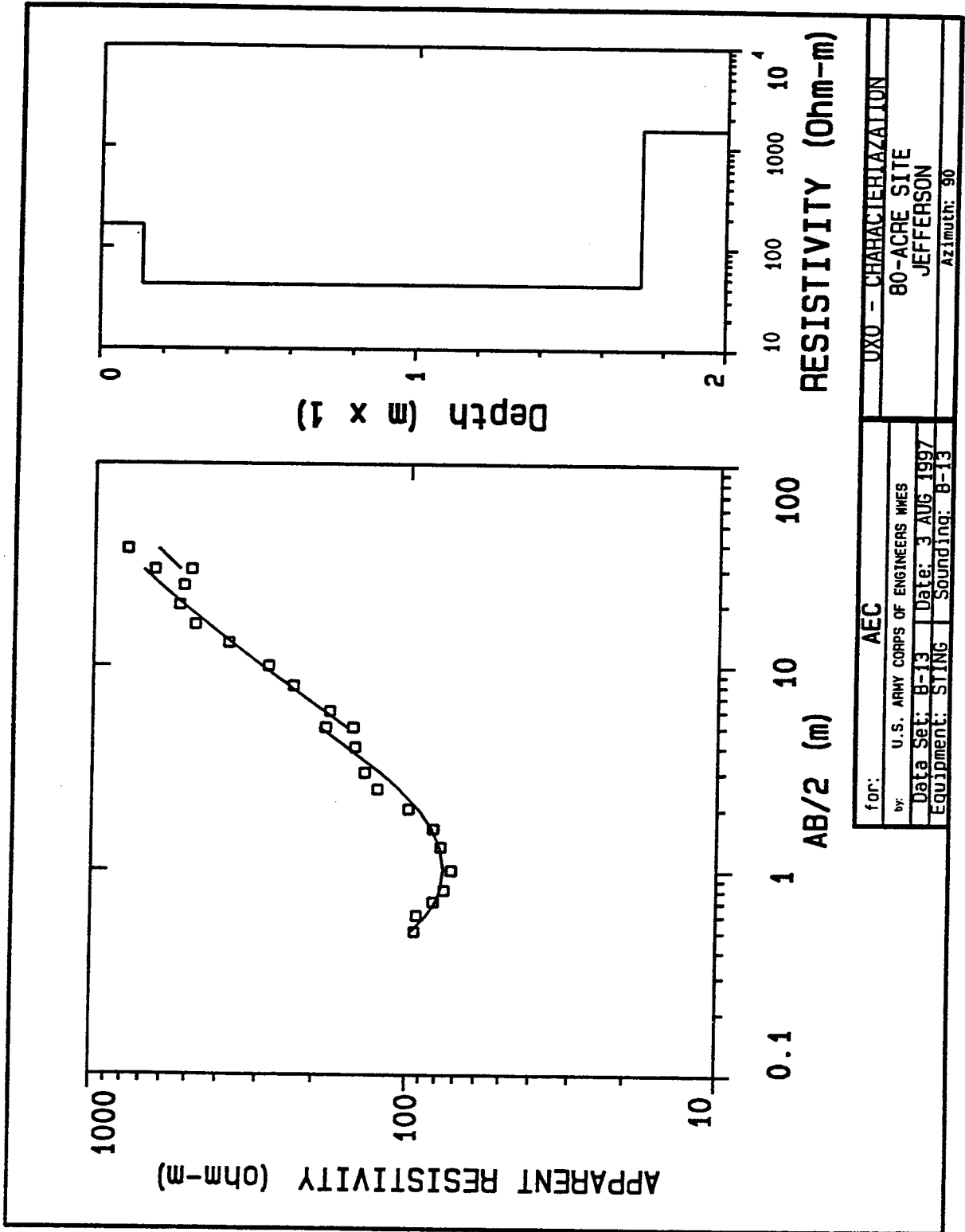


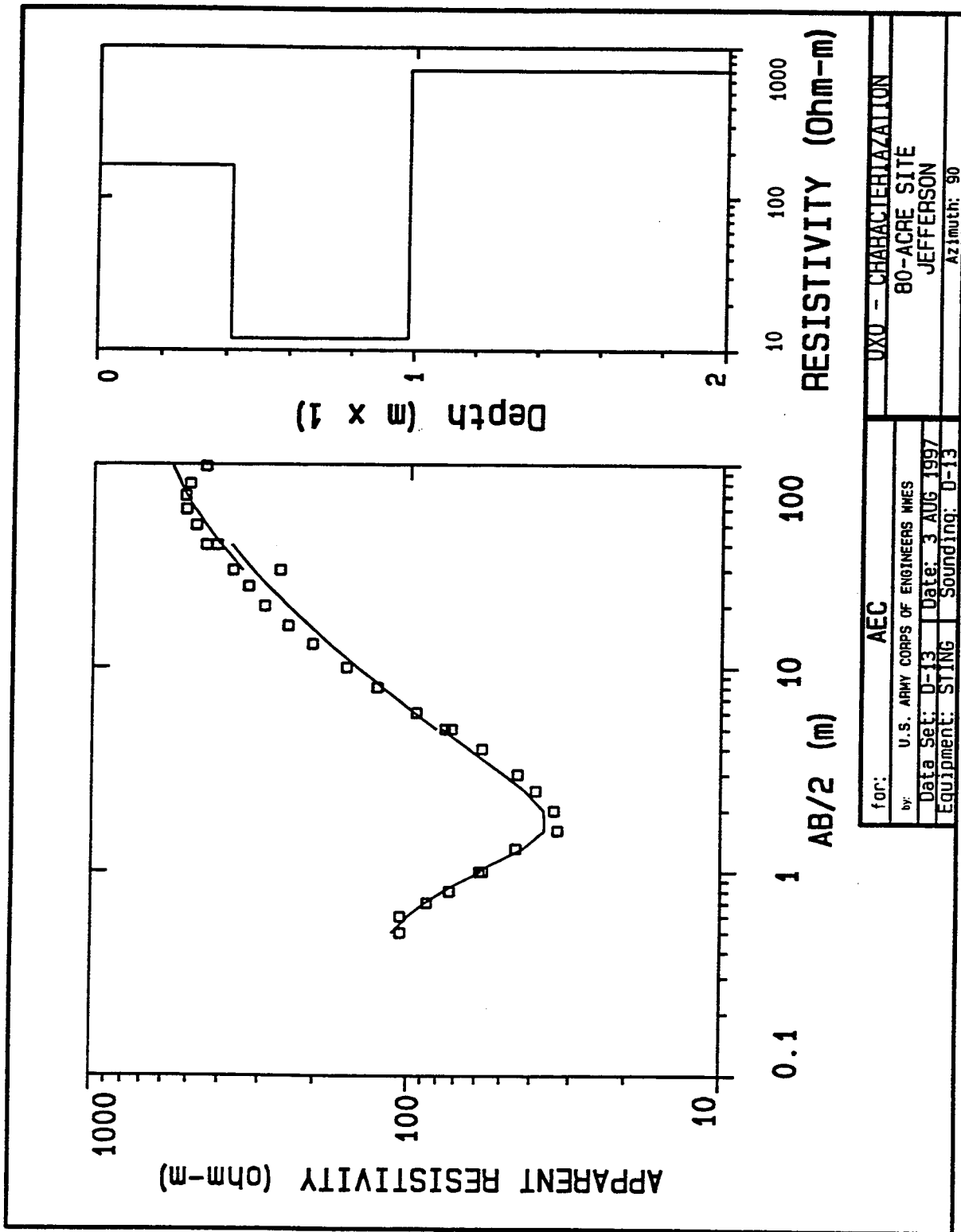
for:	AEC
by:	U.S. ARMY CORPS OF ENGINEERS WMS
Data Set:	H-19
Equipment:	STING RI
Date:	4 AUG 1997
Sounding:	H-19
Azimuth:	0
UXU - CHARACTERIZATION	
80-ACRE SITE	
JEFFERSON	

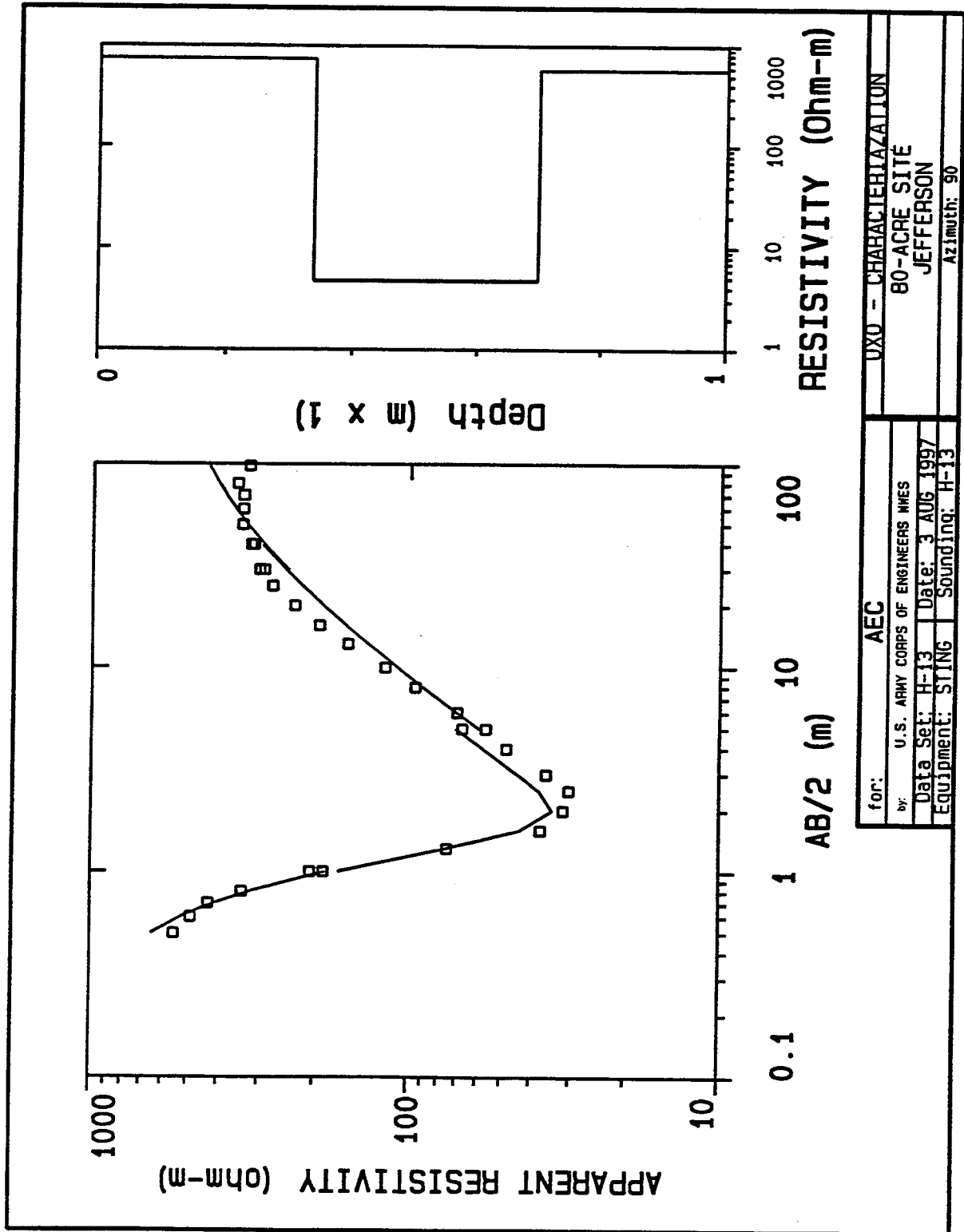


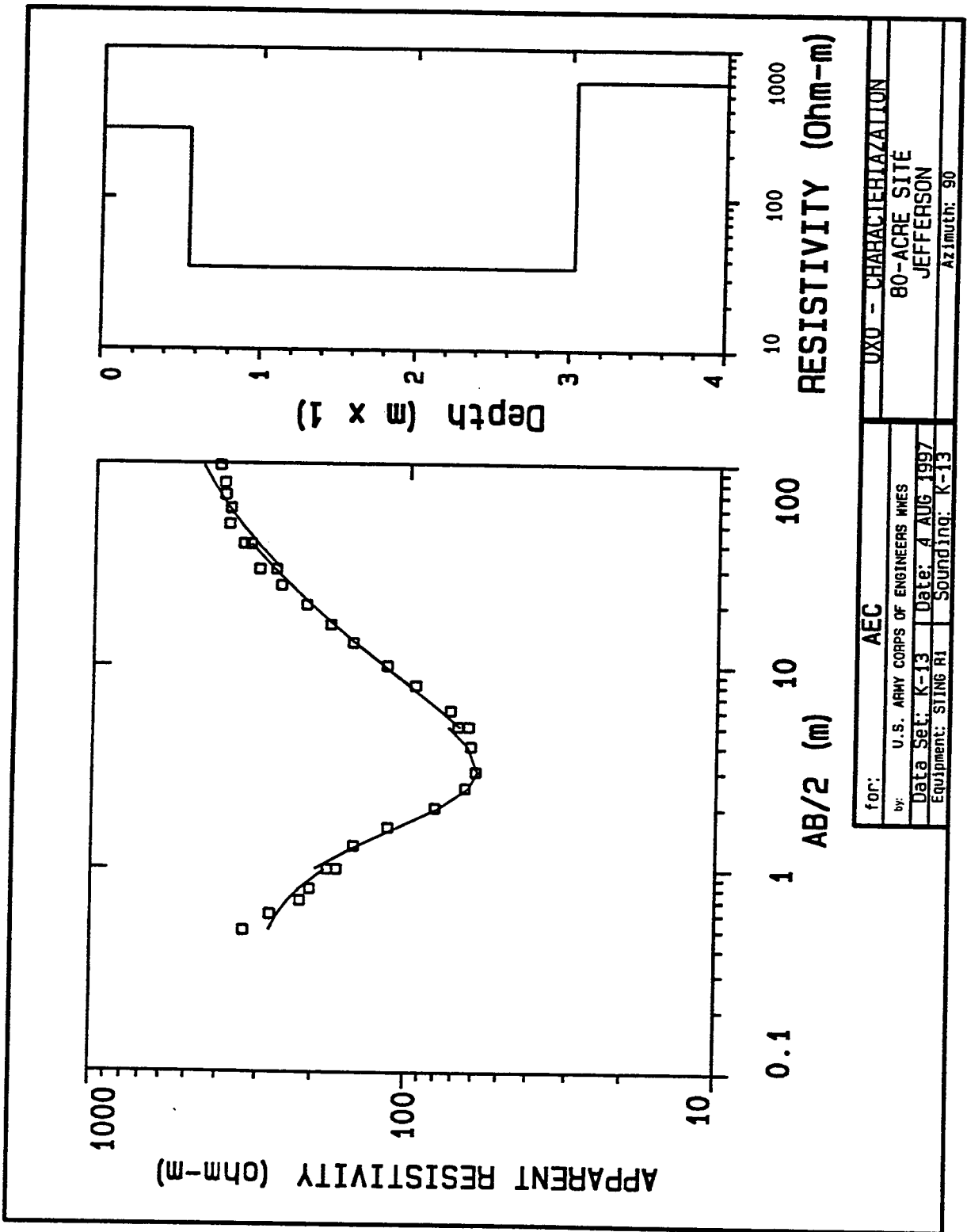
for:	AEC
by:	U.S. ARMY CORPS OF ENGINEERS WNES
Date Set:	H-22
Equipment:	STING R1
Date:	4 AUG 1997
Sounding:	H-ZZ
UXO - CHARACTERIZATION	
80-ACRE SITE	
JEFFERSON	
AZimuth: 0	

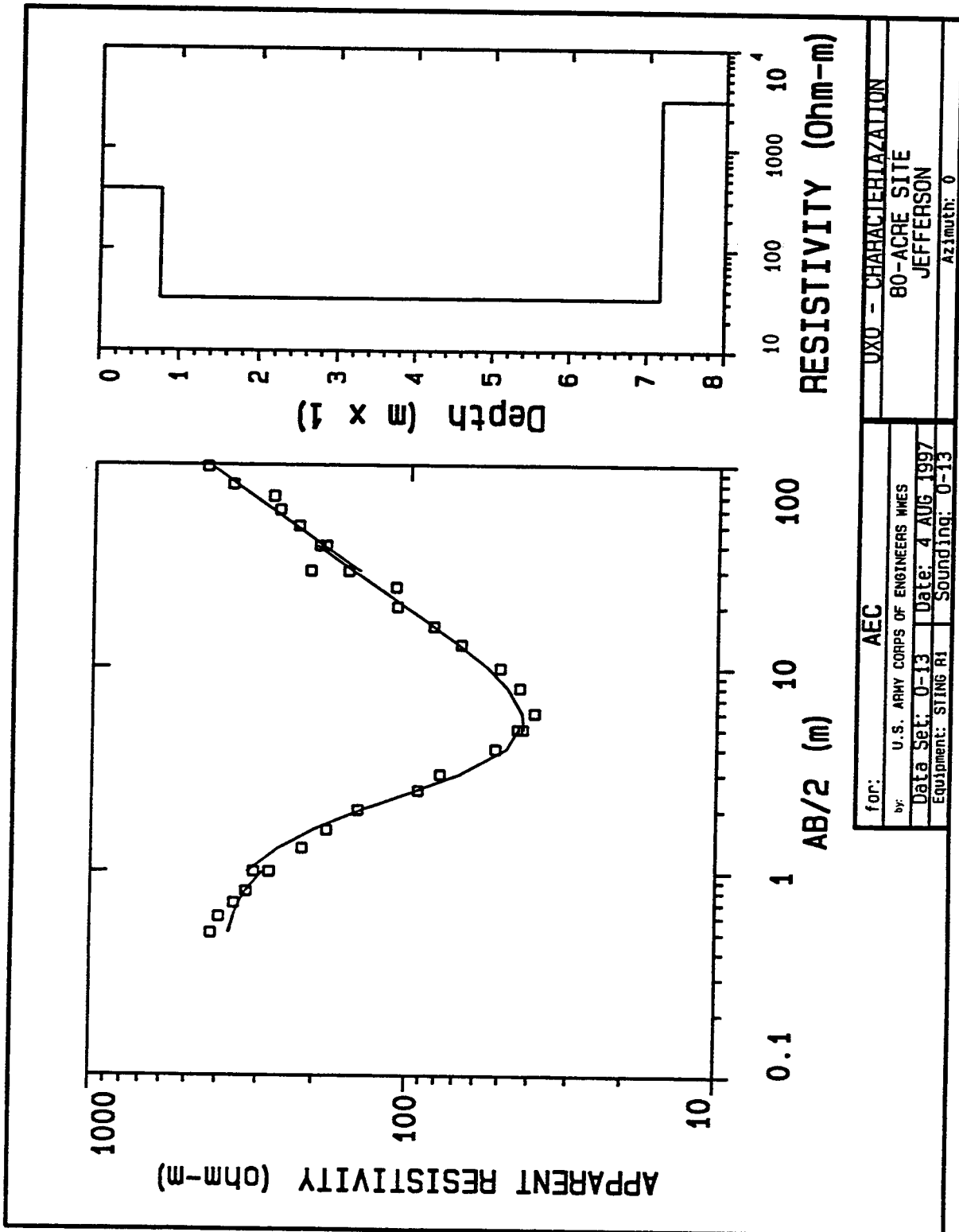








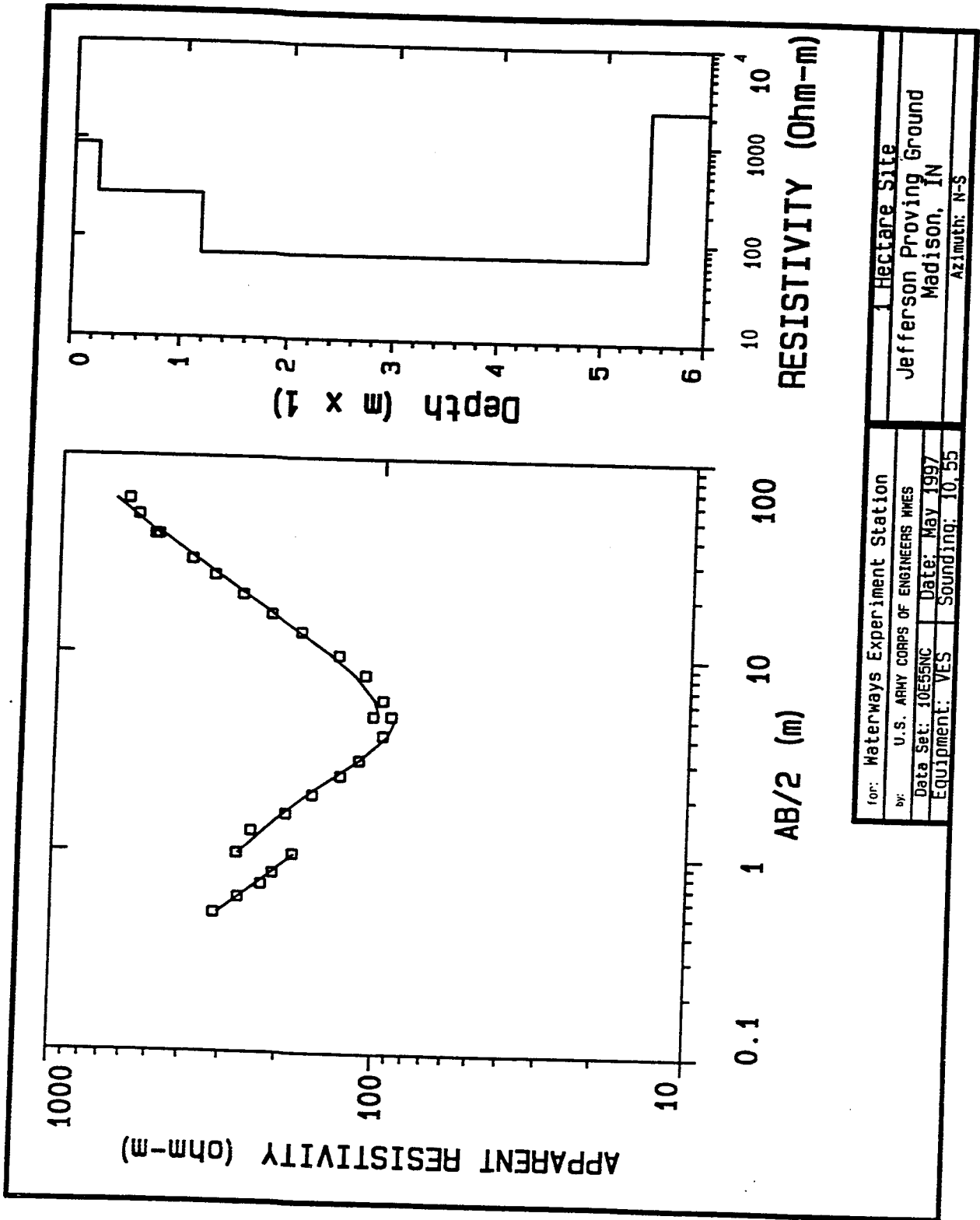


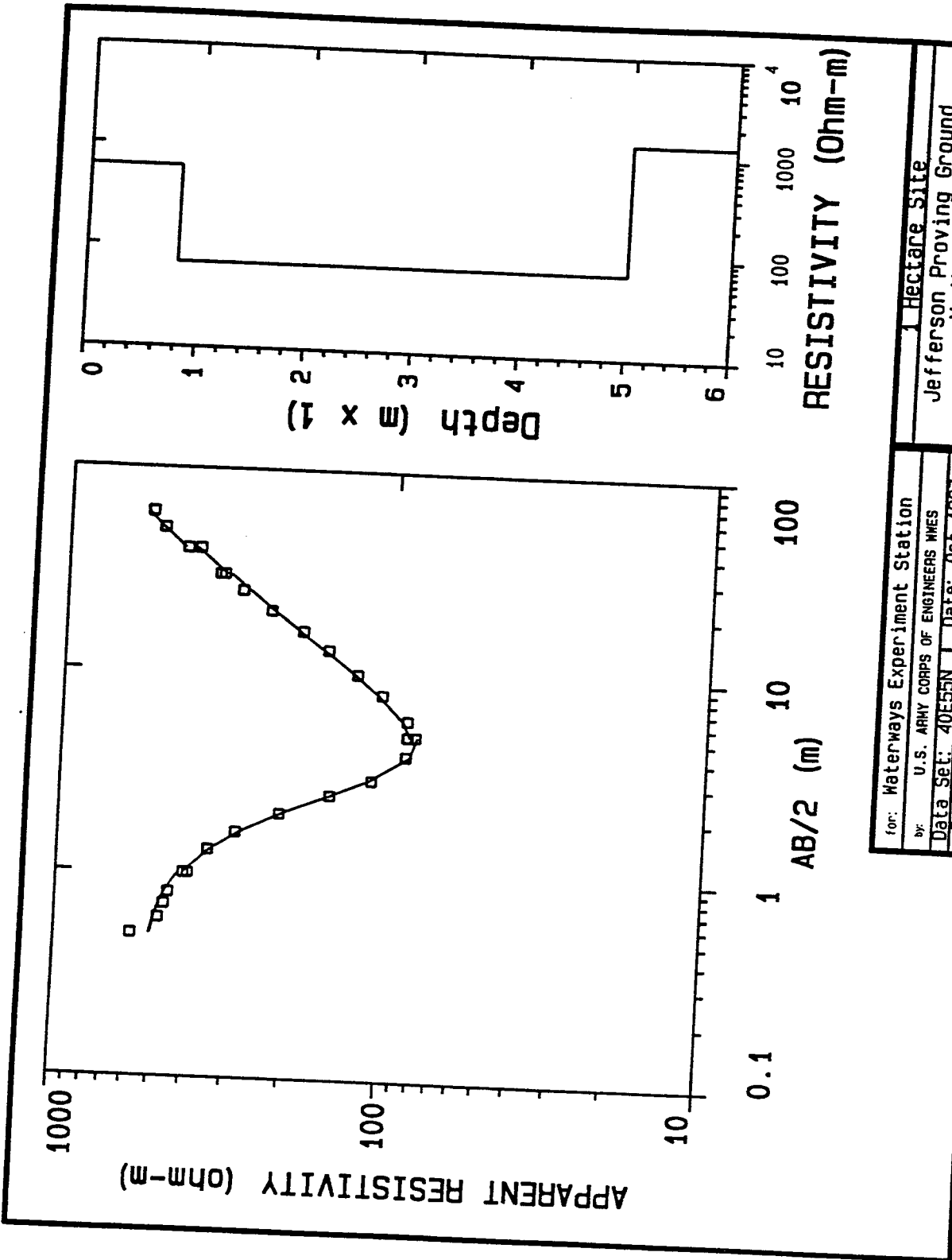


Appendix G

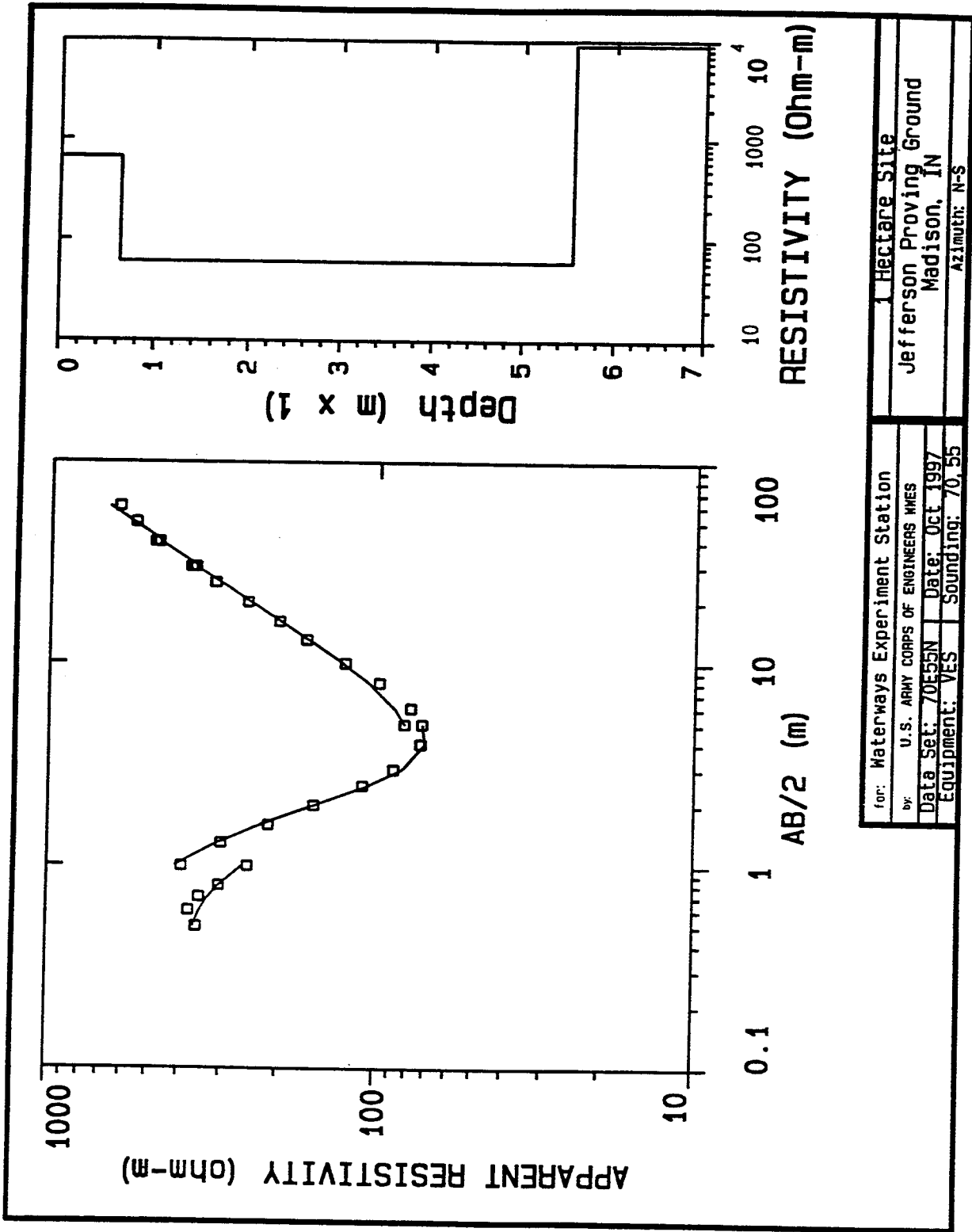
Vertical Electric Sounding

Curves: 1-hectare Site

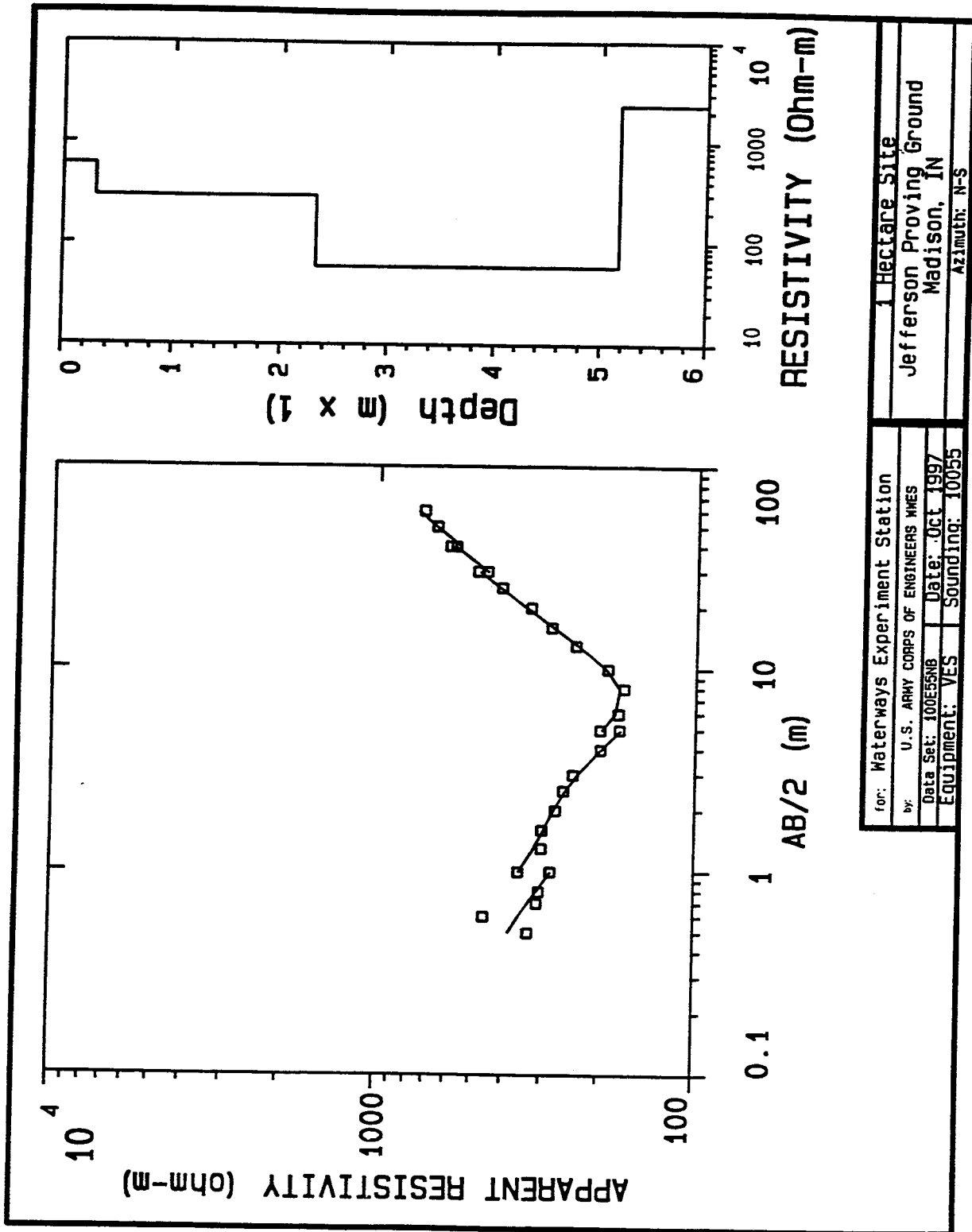


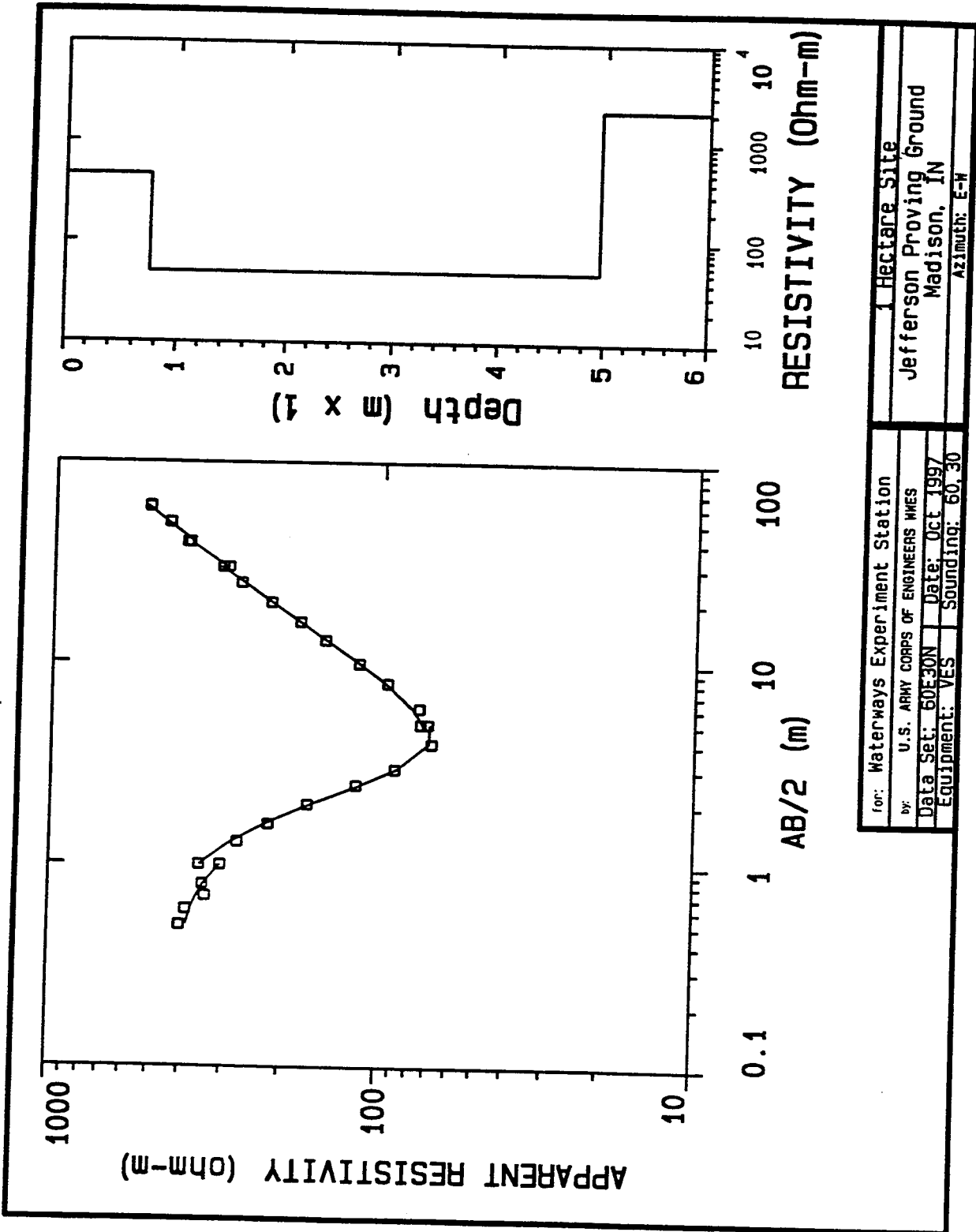


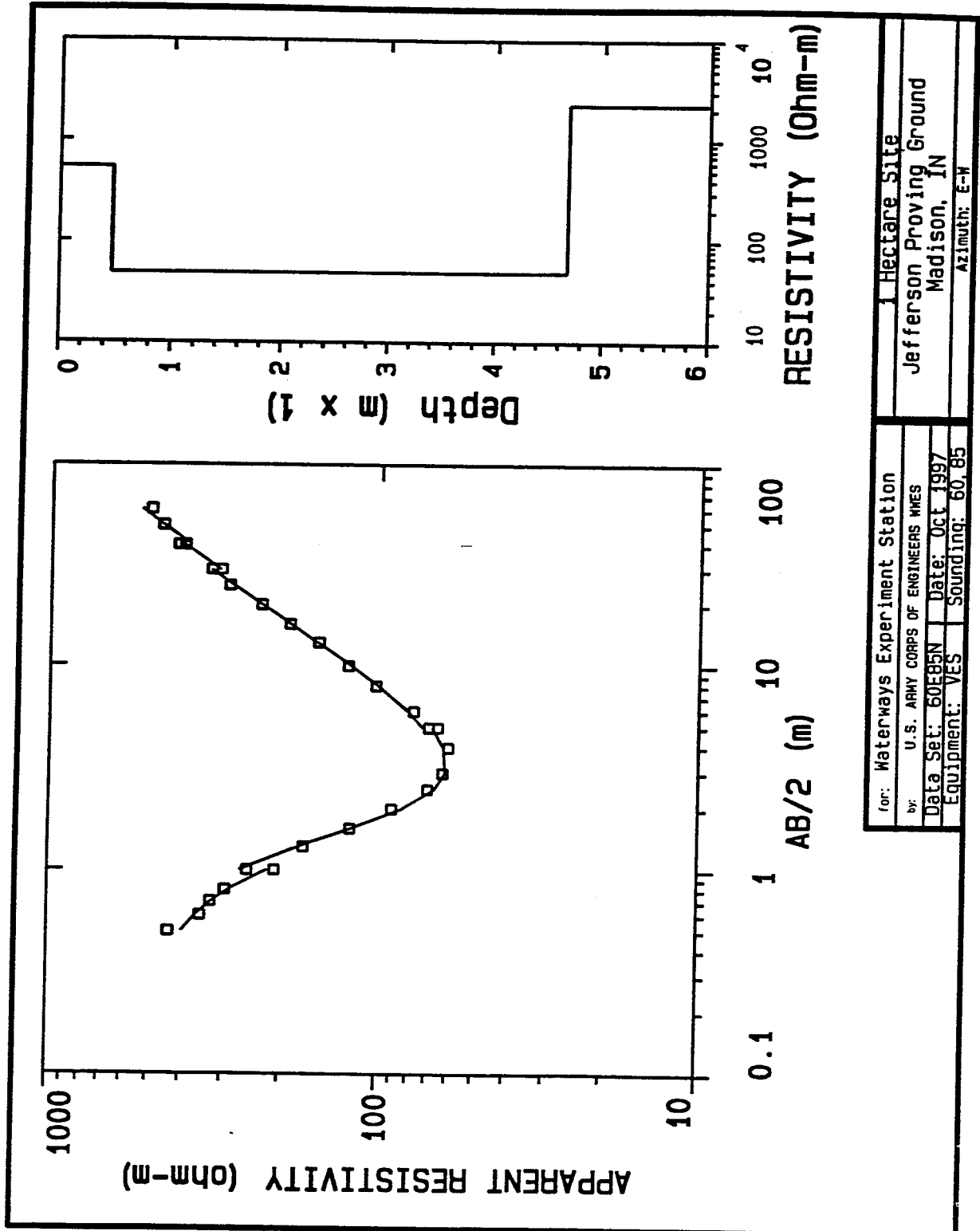
for: Waterways Experiment Station	1 Hectare Site
by: U.S. ARMY CORPS OF ENGINEERS WMS	Jefferson Proving Ground
Data Set: 40E55N	Madison, IN
Equipment: VES	Azimuth: N-S
Date: Oct 1997	
Sounding: 40.55	



for: Waterways Experiment Station
 by: U.S. ARMY CORPS OF ENGINEERS WRES
 Data Set: 70E55N Date: Oct 1997
 Equipment: VES Sounding: 70, 55
 1 Hectare Site
 Jefferson Proving Ground
 Madison, IN
 Azimuth: N-S







for:	Waterways Experiment Station
by:	U.S. ARMY CORPS OF ENGINEERS WRES
Data Set:	60E85N
Equipment:	VES
Date:	Oct 1997
Sounding:	60-85

1 Hectare Site
Jefferson Proving Ground
Madison, IN
Azimuth: E-W

Appendix H

GPR Records: 1-hectare Site

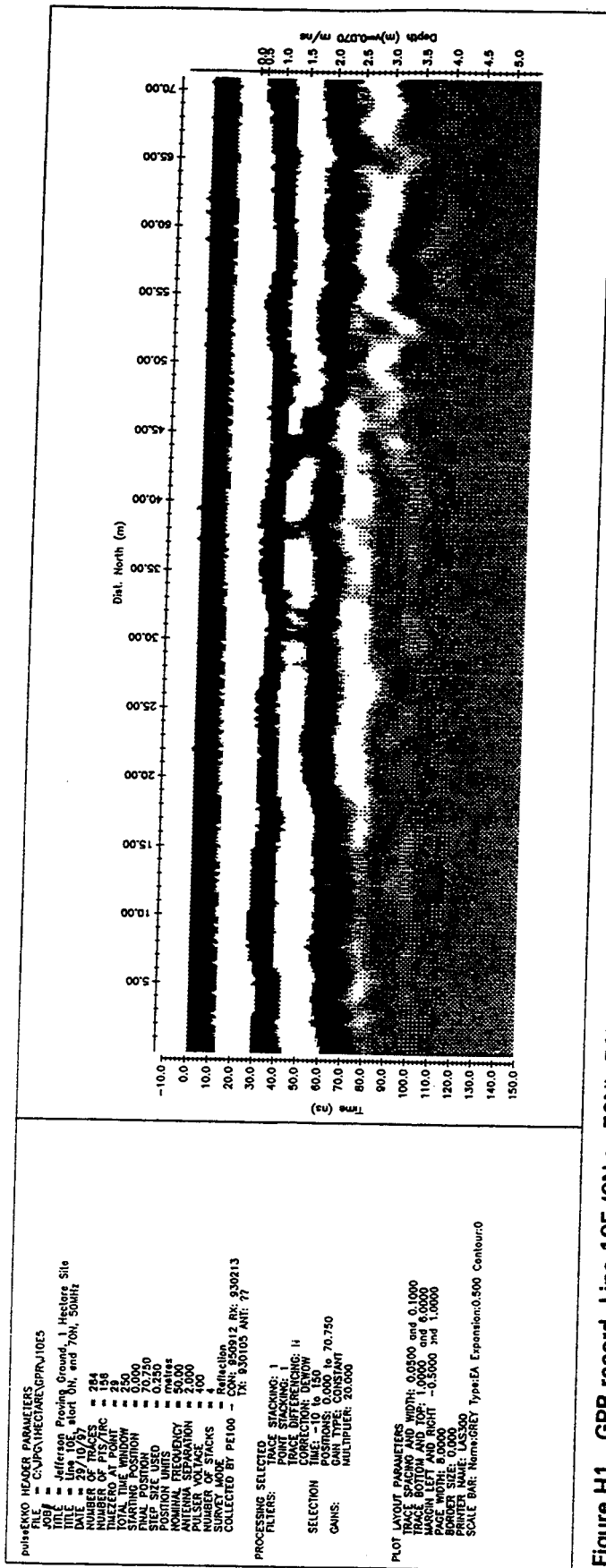


Figure H1. GPR record, Line 10E (0N to 70N), 50MHz, 1-hectare site

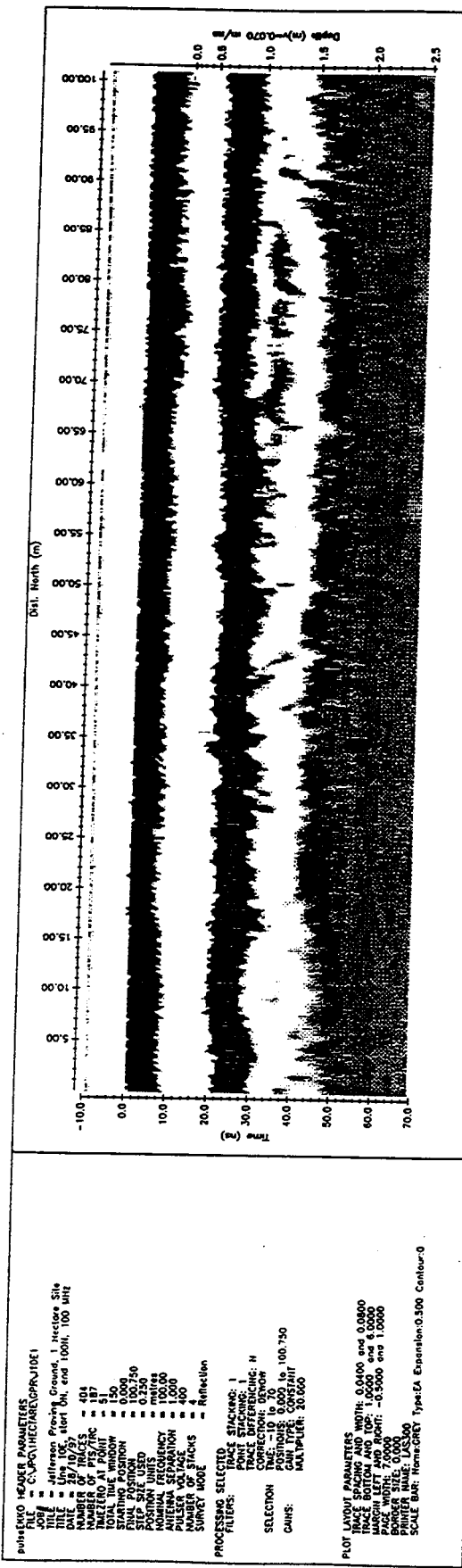


Figure H5. GPR record, Line 10E (0N to 100N), 100MHz, 1-hectare site

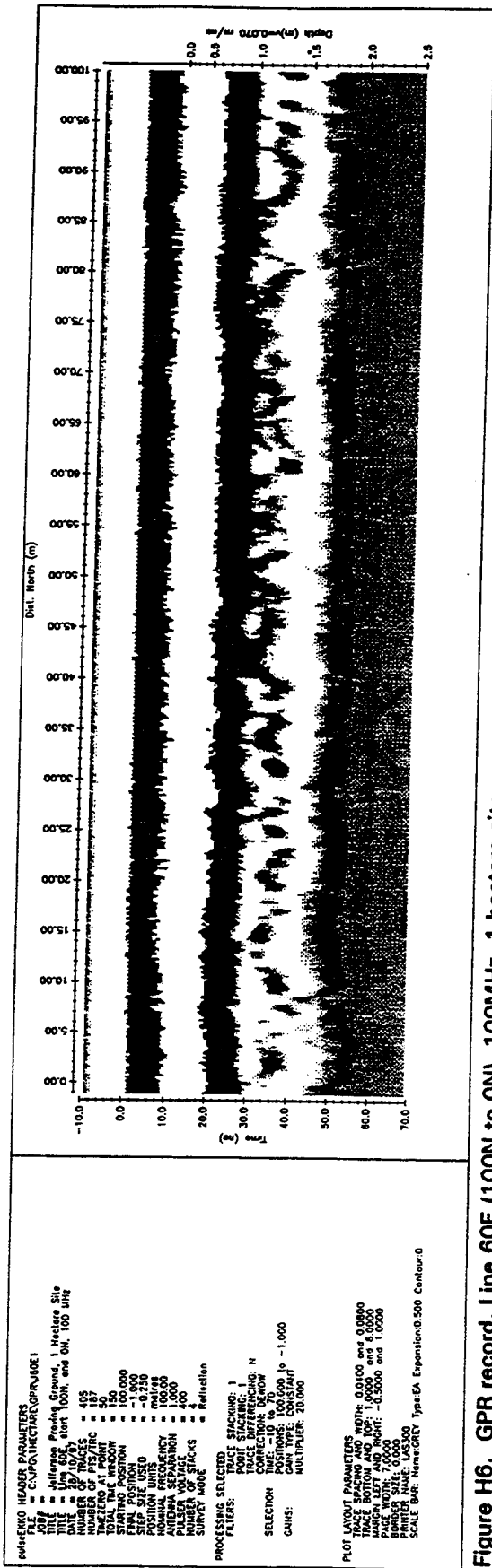


Figure H6. GPR record, Line 60E (100N to 0N), 100MHz, 1-hectare site

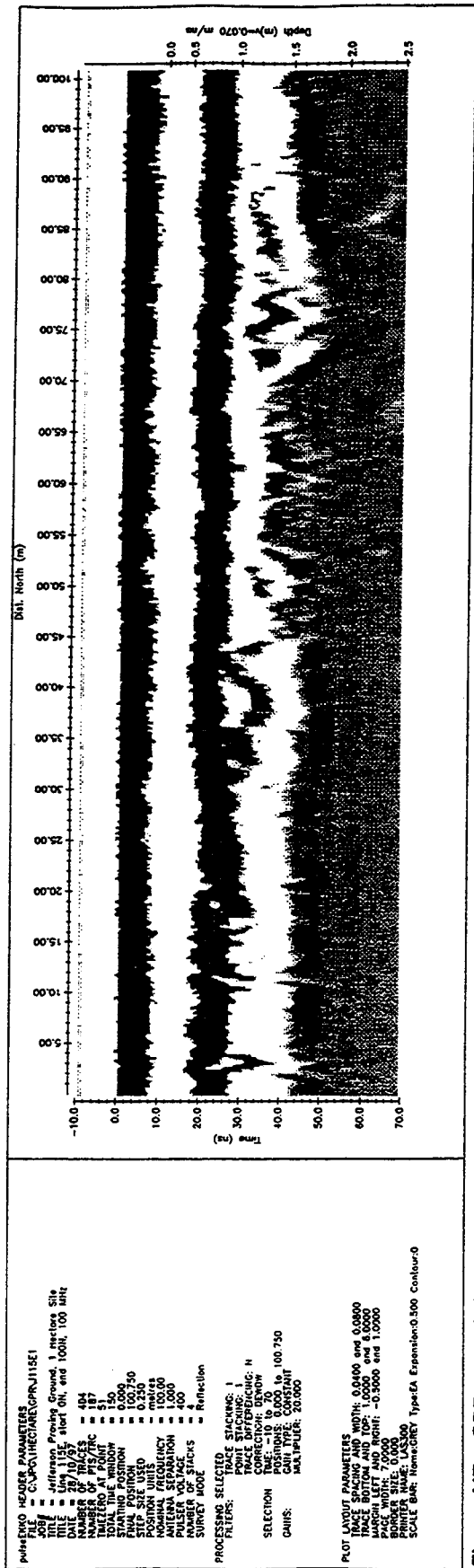


Figure H7. GPR record, Line 115E (0N to 100N), 100MHz, 1-hectare site

REPORT DOCUMENTATION PAGE

Form Approved
OMB No. 0704-0188

Public reporting burden for this collection of information is estimated to average 1 hour per response, including the time for reviewing instructions, searching existing data sources, gathering and maintaining the data needed, and completing and reviewing the collection of information. Send comments regarding this burden estimate or any other aspect of this collection of information, including suggestions for reducing this burden, to Washington Headquarters Services, Directorate for Information Operations and Reports, 1215 Jefferson Davis Highway, Suite 1204, Arlington, VA 22202-4302, and to the Office of Management and Budget, Paperwork Reduction Project (0704-0188), Washington, DC 20503.

1. AGENCY USE ONLY (Leave blank)		2. REPORT DATE September 1998	3. REPORT TYPE AND DATES COVERED Final report	
4. TITLE AND SUBTITLE Site Characterization Investigations in Support of UXO Technology Demonstrations, Jefferson Proving Ground, Indiana			5. FUNDING NUMBERS	
6. AUTHOR(S) José L. Llopis, Janet E. Simms, Dwain K. Butler, John O. Curtis, Harold W. West, Steven A. Arcone, Norbert E. Yankielum				
7. PERFORMING ORGANIZATION NAME(S) AND ADDRESS(ES) U.S. Army Engineer Waterways Experiment Station, 3909 Halls Ferry Road, Vicksburg, MS 39180-6199; U.S. Army Corps of Engineers, Cold Regions Research and Engineering Laboratory, 72 Lyne Road, Hanover, NH 03755			8. PERFORMING ORGANIZATION REPORT NUMBER Technical Report GL-98-20	
9. SPONSORING/MONITORING AGENCY NAME(S) AND ADDRESS(ES) U.S. Army Environmental Center Aberdeen Proving Ground, MD 21010			10. SPONSORING/MONITORING AGENCY REPORT NUMBER	
11. SUPPLEMENTARY NOTES Available from National Technical Information Service, 5285 Port Royal Road, Springfield, VA 22161.				
12a. DISTRIBUTION/AVAILABILITY STATEMENT Approved for public release; distribution is unlimited.			12b. DISTRIBUTION CODE	
13. ABSTRACT (Maximum 200 words) <p>Geological, geophysical, environmental, and geotechnical investigations were performed to characterize three unexploded ordnance (UXO) test sites at Jefferson Proving Ground (JPG), Indiana. The purpose of the characterization is to support: (1) Phase IV demonstrator planning and results assessment; (2) Additional assessments of Phase I-III; (3) Future use of JPG sites; and (4) Comparisons of the JPG sites with other UXO and landmine test and cleanup sites.</p> <p>Some observations made as a result of the investigations are outlined below. Soil samples collected from the three sites are classified, according to the Unified Classification System (USCS), chiefly as CH or CL and are generally characterized as clays, sandy clays, or silty clays. In the USCS, soil particles passing the No. 200 sieve are considered silt or clay. X-ray diffraction analysis indicate that these soils contain little or no clay minerals and consist chiefly of very fine-grained (silt or clay-sized) silica particles.</p> <p>Relative dielectric permittivities values generally range between 10-25 and were determined in the field and in the laboratory. Test results also indicate that the soils highly attenuate the propagation of electromagnetic waves. The depth of investigation for ground penetrating radar at the sites is limited to approximately 3.5 m.</p>				
14. SUBJECT TERMS Dielectric properties Electromagnetic Geophysics Ground penetrating radar			15. NUMBER OF PAGES 321	
			16. PRICE CODE	
17. SECURITY CLASSIFICATION OF REPORT UNCLASSIFIED		18. SECURITY CLASSIFICATION OF THIS PAGE UNCLASSIFIED	19. SECURITY CLASSIFICATION OF ABSTRACT	20. LIMITATION OF ABSTRACT